

PROJECT ADMINISTRATION DATA SHEET

ORIGINAL



REVISION NO. _____

Project No./(Center No.) E-16-601 (R6335-0A0)

GTRC/STF

DATE 7 / 8 / 87Project Director: Dr. B. T. Zinn; B. R. Daniel; J. I. Jagoda

School/XXX

AE

Sponsor: Gas Research InstituteMISCAgreement No.: Contract No. 5087-260-1466Award Period: From 1/1/87 To 12/31/89 (Performance) 4/30/90 Reports

Sponsor Amount:

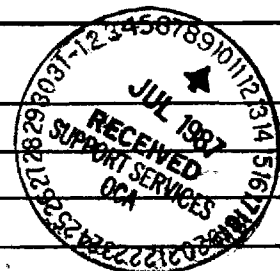
New With This ChangeTotal to DateContract Value: \$ _____ \$ 434,665Funded: \$ _____ \$ 136,985Cost Sharing No./(Center No.) E-16-323 (F6335-0A0) Cost Sharing: \$ 13,701Title: Pulsating Burner-Controlling Mechanisms and PerformanceADMINISTRATIVE DATAOCA Contact Ina R. Lashley x. 4820

1) Sponsor Technical Contact:

2) Sponsor Issuing Office:

Mr. Allen L. JordanContract AdministratorGas Research Institute8600 West Bryn Mawr Ave.Chicago, IL 60631(312) 399-8100Military Security Classification: N/AONR Resident Rep. is ACO: _____ Yes X No(or) Company/Industrial Proprietary: N/ADefense Priority Rating: N/ARESTRICTIONSSee Attached N/A Supplemental Information Sheet for Additional Requirements.

Travel: Foreign travel must have prior approval — Contact OCA in each case. Domestic travel requires sponsor approval where total will exceed greater of \$500 or 125% of approved proposal budget category.

Equipment: Title vests with GTRCCOMMENTS:This is the first year of a proposed three-year program.COPIES TO:SPONSOR'S I.D. NO. 02. [REDACTED] 87.002Project Director
Research Administrative Network
Research Property Management
AccountingProcurement/GTRI Supply Services
Research Security Services
[REDACTED]
Research CommunicationsGTRC
Library
Project File
Other _____

GEORGIA INSTITUTE OF TECHNOLOGY
OFFICE OF CONTRACT ADMINISTRATION

NOTICE OF PROJECT CLOSEOUT

Closeout Notice Date 08/02/91

Project No. E-16-601

Center No. R6335-0A0

Project Director ZINN B T

School/Lab AERO ENGR

Sponsor GAS RESEARCH INSTITUTE/

Contract/Grant No. 5087-260-1466

Contract Entity GTRC

Prime Contract No.

Title PULSATING BURNER - CONTROLLING MECHANISMS AND PERFORMANCE

Effective Completion Date 900630 (Performance) 901031 (Reports)

Closeout Actions Required:	Y/N	Date Submitted
Final Invoice or Copy of Final Invoice	Y	
Final Report of Inventions and/or Subcontracts	Y	910408
Government Property Inventory & Related Certificate	Y	
Classified Material Certificate	N	
Release and Assignment	Y	
Other	N	
Comments		

Subproject Under Main Project No.

Continues Project No.

Distribution Required:

Project Director	Y
Administrative Network Representative	Y
GTRI Accounting/Grants and Contracts	Y
Procurement/Supply Services	Y
Research Property Management	Y
Research Security Services	N
Reports Coordinator (OCA)	Y
GTRC	Y
Project File	Y
Other	N
	N

NOTE: Final Patent Questionnaire sent to PDPI

Pulsating Burners - Controlling Mechanisms and Performance

Semi Annual Report

January 1, - June 31, 1988

Prepared by

B. T. Zinn, B. R. Daniel and J. I. Jagoda

School of Aerospace Engineering

Georgia Institute of Technology

For

Gas Research Institute

Grant No. 5083-260-1466

GRI Project Manager

James A. Kezerle

Combustion

September 1988

GRI DISCLAIMER

LEGAL NOTICE: This report was prepared by the Georgia Institute of Technology as an account of work sponsored by the Gas Research Institute (GRI). Neither GRI, members of GRI, nor any person acting on behalf of either:

- a. Makes any warranty or representation, express or implied, with respect to the accuracy, completeness, or usefulness of the information contained in this report, or that the use of any apparatus, method, or process disclosed in this report may not infringe privately owned rights; or
- b. Assumes any liability with respect to the use of, or for damages resulting from the use of, any information, apparatus, method, or process disclosed in this report.

RESEARCH SUMMARY

Title: Pulsating Burners - Controlling Mechanisms and Performance

Contractor: Georgia Tech Research Institute

Contract Number: 5087-260-1466

Report Period: January - June 1988, Semi-Annual Report

Principle Investigators: B. T. Zinn, B. R. Daniel and J. I. Jagoda

Objective: It is the objective of this study to gain further insights into the physical mechanisms which control the mixing and heat release processes in pulse combustors. In addition, the acoustic driving and damping characteristics of various components and subsystems of the pulse combustor will be determined for various operating conditions. Finally, the above findings will be used to explain the performance of various combustor configurations to be tested and should be of considerable help to the designers of novel pulse combustors.

Technical Perspectives: Although gas fired pulse combustors have been on the market for a number of years, their controlling mechanisms are still not sufficiently well understood to permit the design of pulse combustors for different applications without resorting to costly trial and error development efforts. To attain pulse combustion operation, the energy supplied to the pulsations by the combustion process must be larger than the acoustic energy lost due to viscous dissipation, heat transfer, acoustic radiation and so on. Proper operation of pulse combustors also requires that mixing, cycle to cycle reignition and flame spread occur such that the oscillations of heat release be in phase with those of the pressure. In addition, the acoustics of the various components and subsystems of the pulse combustor must be matched appropriately. Thus, to develop a rational design procedure for pulse combustors, it is required that the various processes responsible for energy addition and removal to and from the pulsations be understood. Furthermore, data describing the acoustic properties of various pulse combustor components under various cold and pulse combustion operation conditions are needed. Finally, the dependence of the acoustic characteristics of the various combustor components upon the fundamental fluid mechanical, heat transfer and combustion processes must be understood. The attainment of these goals is pursued under this project.

Technical Approach:

In order to elucidate the mechanisms which control the operation of various pulse combustor configurations and determine the damping/driving characteristics of various components and subsystems of commonly used pulse combustors, the following tasks will be pursued simultaneously:

- 1) Investigation of the flow field characteristics, mixing and heat release in pulse combustors using LDV, Schlieren, mixing visualization, radical radiation (OH, CH, CC) and Rayleigh scattering measurements.
- 2) Measurements of the driving and damping characteristics of various components and subsystems which make up the pulse combustor using the impedance tube technique.
- 3) The determination of the overall driving and damping characteristics of various pulse combustor designs under different operating conditions.
- 4) Modeling of the dynamic characteristics of the flapper valve.

Results:

During the past reporting period the axial flow fields in the mixing chamber and near the transition between the combustion chamber and the tail pipe were visualized using high speed shadowgraphy. Results of the flow visualization in the mixing chamber were compared with those from LDV measurements in that part of the combustor. Shortly after the pressure passes through its maximum the fuel jet is seen to enter the mixing chamber. This is followed by the entry of the air jet which clearly dominates the flow field. A large axial recirculation zone is observed in the mixing chamber during the combustion phase of the cycle. As the pressure approaches its maximum the flow in the mixing chamber reverts back to the axial direction. The flow between the combustion chamber and the tail pipe is seen to be in phase with the pressure fluctuation. Penetration of gases from the tail pipe back into the combustion chamber is limited to a distance of a few inches.

An impedance tube technique was used to determine the admittances of the air valve, the fuel valve and the mixing chamber fitted with the fuel and air valves. The real parts of the admittances and, thus, the damping of all components is essentially zero at low driving frequencies as long as the air valve is closed. As the driving frequency is increased beyond 50 Hz the admittance of the fuel valve increases

slightly while the damping by the air valve and the mixing chamber fitted with fuel and air valve increases considerably. The real part of the admittance of the air valve also increases significantly when the valve gap is increased, i.e., when the valve is opened.

The behavior of the valve is being modeled using a linear acoustic model. Preliminary results have permitted the calculation of the variation of the real part of the admittance of the valve during a cycle. The behavior of the valve admittance is in good qualitative agreement with the admittances measured using the impedance tube. Since the model predicts the admittance of the valve plate while the measurements determined the admittance at the valve housing-mixing chamber interface, a quantitative comparison must await the determination of a transfer function which will permit the establishment of an analytical relationship between these two admittances. Such a transfer function is currently being developed. The model was also used to determine that the time required to open the air valve decreases as the frequency increases until a limiting value is reached above approximately 50 Hz. On the other hand, the valve setting appears to have little effect upon this valve opening time. It was further determined that, even at frequencies above 150 Hz, the valve opens fast enough to remain in a fully open or closed position during a significant fraction of the cycle.

OBJECTIVE

It is the objective of this study to gain further insight into the fundamental processes responsible for the operation of various pulse combustor designs. Emphasis is being placed upon obtaining practical information which will permit designers to develop new and/or larger scale pulse combustors without resorting to costly trial and error based development efforts.

The velocity and the mixing patterns in the mixing and combustion chambers will be determined both qualitatively and quantitatively. The nature of the interaction between the combustion process and the acoustics of the combustor will be established. The impedance of various components and subsystems which make up the pulse combustor will be determined under various operating conditions. In addition, the driving and damping characteristics of different pulse combustor designs will be measured under different operating conditions. Finally, the dynamic characteristics of the flapper valves will be analytically modeled.

PROGRAM PLAN

The program is divided into four major tasks as outlined below:

Task 1: Investigation of the Interaction between the Oscillatory Flow Field and Heat Release Processes in the Pulse Combustor:

- A. Laser Doppler Velocimetry: The three components of velocity will be measured at selected locations in the combustor. The period of pulsations will be divided into 36 equal time segments and the LDV counts for each segment will be stored in separate files. This will permit ensemble averaging of the velocities in each segment over many cycles. Mean velocities and turbulence intensities as well as shear stresses can then be obtained for each instant in the cycle.
- B. Schlieren Visualization: High speed Schlieren and shadowgraph cinematography will be carried out through side windows in the combustor in order to visualize the flow along the combustor axis. These shadowgrams will then be correlated with those previously obtained through a window in the end walls of the combustor. This will provide a complete picture of the three-dimensional flow field in the pulse combustor.
- C. Mixing Visualization: Mixing patterns will be recorded photographically by heavily seeding one of the reactant flows and illuminating the combustor using an expanded laser sheet. These visualizations will be carried out through the flat windows in the cylindrical walls of the mixing and combustion chambers. The use of the flat windows is expected to reduce the amount of laser light reflected by the glass. These laser light intensity losses caused problems when this technique was previously applied to the combustor through cylindrical glass walls.
- D. Spectroscopy: Local and global heat release in the pulse combustor will be determined by measuring the OH, CH and CC radical radiation emitted from the combustor. Efforts will concentrate on

measurements through the side window of the mixing chamber which will be correlated with previous results obtained through the end window of the combustor.

- E. Rayleigh Scattering: Local densities and, therefore, temperatures will be measured using Rayleigh scattering. A combination of the emission spectroscopy and the Rayleigh measurements will result in a better understanding of the location and timing of the combustion process. In addition, the Rayleigh scattering results will yield a quantitative description of the path taken by the hot combustion products in the pulse combustor.

All task I measurements will be carried out in the pulse combustor with flat windows fitted to the curved walls of the mixing and combustion chambers. The results will be correlated with each other and with the phase in the cycle at which they were obtained. This will be achieved by using the measured pressure oscillations as a clock. Only a full coordination between the flow field, the heat release and the local temperature measurements can result in a thorough understanding of the fundamental principles underlying the operation of the pulse combustor.

Task II: Impedance Measurements of Pulse Combustor Components:

The acoustic admittance of the various components and subsystems which make up the pulse combustor will be measured using an impedance tube technique. These measurements will be carried out without and with combustion and under various operating conditions and driving frequencies. These measurements will yield information on the frequency dependence of the driving provided by the various pulse combustor subsystems. In addition, the frequency dependence of the driving provided by the pulse combustion process will be determined.

Task III: Determination of Overall Driving/Damping Characteristics of Pulse Combustors:

The overall driving and damping characteristics of the pulse combustor will be determined by measuring the growth and decay rates of the combustor pressure oscillations during the start-up and shut-down phases of operation. These measurements will be carried out for various combustor configurations and for a range of operating conditions. The driving and damping for different combustor geometries, fuel/air ratios and injector configurations will be determined.

Task IV: Modeling of Flapper Valve:

The behavior of the flapper valve will be modeled using the continuity and momentum equations and the equation of motion of the flapper. In addition, a transfer function is being developed which will permit the calculation of the admittance at the air valve housing - mixing chamber interface from the calculated admittance at the valve plates.

Task V: Reporting

As per contract agreement.

TECHNICAL PROGRESS AND RESULTS

During the past reporting period the axial flow field in the pulse combustor was visualized using high speed shadow photography through the flat quartz windows in the curved side walls of the mixing and combustion chambers. Particular attention was paid to the flow field in the mixing chamber and at the downstream end of the combustion chamber where the combustor connects to the exhaust pipe. In addition, velocity measurements in the mixing chamber were continued using a two component LDV system with Bragg cells. Because the flow in the combustor is periodic, mean flow velocities and turbulence intensities at different instances during the cycle had to be determined using conditional sampling. This was achieved by dividing each cycle into 30 equal time intervals and sorting the data into the relevant bins according to their time of arrival during the cycle. Ensemble averaged mean and RMS velocities were, thus, obtained at 30 equi-spaced instances during the cycle. In Fig. 1, the images obtained by high speed shadowgraphy are compared with the LDV results in the axial and azimuthal directions at nine locations in the horizontal plane in the mixing chamber which bisects the angle between the fuel and air inlets. The pressure oscillations were used as a clock in this comparison. The orientation of the locations of the LDV measurements is shown in Fig. 2.

Since the air and fuel ports are located off axis, the flow field is not cylindrically symmetric. Shortly after the pressure passes its maximum (Fig. 1a) high speed shadowgraphy shows the fuel jet entering the mixing chamber. This fuel jet appears to have no significant effect upon the LDV measurements. Just before the pressure minimum is reached (Fig. 1b) the air jet enters the mixing chamber. The air jet drastically increases the magnitudes of the velocity vectors near the upstream end of the mixing chamber. Furthermore, the addition of air into the combustor increases the flow velocities further downstream in the mixing chamber. A little later, during the combustion phase of the cycle (Fig. 1c), a large, axial recirculation region forms in the mixing chamber which is clearly seen in the shadowgraphs. This recirculation bubble manifests itself in the vector diagram as downward pointing velocity vectors near the upstream end and upward vectors near the downstream end of the mixing chamber. As the pressure maximum is reached the flow reverts back to the downstream direction (Fig. 1d) as shown by the shadowgraph and by the velocity vector plot. Shortly thereafter, the new fuel jet enters and the cycle recommences.

High speed shadowgraphy was also carried out at the downstream end of the combustion chamber where the combustor connects to the tail pipe. As the pressure in the combustor decreases, combustion products from the tail pipe are seen to flow back into the combustion chamber. This backflow penetrates a distance of only two to three inches back into the combustor. As the acoustic pressure begins to rise again the flow reverses and reenters the tail pipe.

In another part of this investigation an impedance tube technique was used to measure the admittance of the different components which make up the pulse combustors. In this technique the component to be tested is attached to

the closed end of a long tube (see Fig. 3). An electro-pneumatic, acoustic driver is fitted to the other, open end of the tube. This driver sets up a standing pressure wave in the tube with a pressure anti-node near the closed end of the impedance tube. A piezo-electric pressure transducer mounted at the closed end of the tube measures this maximum amplitude. A second pressure transducer, mounted on the end of a long rod, is translated inside the tube to measure the location and value of the pressure minimum of the standing wave closest to the closed end of the tube.

The impedance tube technique is based upon the fact that an acoustic wave traveling down a tube is reflected by a hard termination (zero admittance) without a change in amplitude or shift in phase. The reflected wave is then exactly superimposed upon the incident wave resulting in a real pressure node (zero amplitude) at one quarter of the wavelength ($\lambda/4$) from the termination (see Fig. 4a). On the other hand, if the admittance of the termination (which is a complex quantity) is nonzero, (see Fig. 4b) the minimum pressure is non-zero and it occurs at a location other than $\lambda/4$. Physically, the termination changes the pressure amplitude of the reflected wave and introduces an apparent change in the length of the pipe by introducing a phase shift in the reflection process. From the measured values of P_{\max} - P_{\min} and the location, in the x-direction, of P_{\min} , one can determine the real and imaginary parts of the admittance of the termination and thus, of the component under investigation. A more detailed analysis shows that the real part of the admittance, which is calculated from the difference between the maximum and minimum pressures ($P_{\max} - P_{\min}$) determines the damping (or driving) by the component under investigation. Simultaneously, the imaginary part of the admittance which is a function of the axial position of the pressure minimum depends upon any phase shift and/or change in frequency of the reflected wave.

The above described technique is being used to measure the real and imaginary parts of the admittance of the different components which make up the combustor under cold and operating conditions. During this reporting period the admittances of the air valve, the fuel valve with its decoupling chamber and the mixing chamber fitted with the air and fuel valves were measured under cold flow conditions. In addition, the effect of the spacing of the air valve upon its admittance was determined. All tests were carried out at mean pressures in the impedance tube equal to the previously determined boost pressure in the combustor and acoustic driver power levels of approximately 160 dB which correspond to the typical dB level in the operating pulse combustor. Furthermore, the driving frequencies were varied between 20 and 170 Hz.

Before presenting the results obtained to date, it would be helpful to consider Fig. 5. It shows the dependence of the real part of the admittance upon ΔP ($P_{\max} - P_{\min}$). Clearly, for small admittances the value of the impedance is relatively insensitive to the accuracy of the measurement of ΔP . However, as the value of admittance increases, the sensitivity of the impedance to the measured ΔP increases rapidly. Thus, the error in the determined admittance increases with increasing value of the admittance.

The real parts of the admittances of the air valve, of the gas valve with its decoupler and of the mixing chamber with air and fuel valves are compared with that of a hard termination in Fig. 6 for frequencies between 20

and 170 Hz. The air valve and mixing chamber with fuel and air valves were tested with the air valve closed and open to .012 inches, a typical setting for the pulse combustor under normal operation. As long as the air valve is closed the admittance of all configurations is essentially zero for low frequencies. As the frequency is increased the real part of the admittance and, thus, the damping of the fuel valve slightly increases. This increase is real since it is highly repeatable and represents a relatively large measured value of ΔP (see Fig. 5). A much larger increase in damping at higher frequencies is observed for the closed air valve. The real part of the admittance is increased even further if the closed air valve along with the fuel valve is attached to the mixing chamber. This further increase in the admittance is probably not entirely due to the addition of the fuel valve. The air valve is now fitted to the side of mixing chamber instead of the end of the impedance tube (see legend of Fig. 6). The effect of this change in geometry is currently being investigated. Figure 6 also shows that opening the valve to .012 substantially increases the admittance over the entire range of frequencies investigated. The increase in the real part of the admittance with increased air valve opening is illustrated in more detail for a range of valve openings and driving frequencies in Figs. 7 and 8 for the air valve and the mixing chamber with its valves respectively.

The corresponding imaginary parts of the admittance for the above experiments are currently being analyzed and will be reported on at a later date.

Finally, work has continued on developing a linear acoustic model of the dynamics of the flapper valve. This model is based upon the integral versions of the continuity and momentum equations and the equation of motion of the flapper. Preliminary results are presented in Figs. 9-11. Figure 9 shows the variation with time of the real part of the admittance at the air valve for a valve gap of .009" for one half of the cycle at a low frequency (9 Hz). The impedance, and thus, the damping by the valve increases rapidly while the valve is opening, reaches a constant level and then drops again as the valve closes. The calculated values of the admittance for the valve in the closed and opened (.009" gap) positions are comparable to the measured admittances of the air valve for the respective valve gaps (see Fig. 7). The discrepancies between the actual calculated and measured values of the admittances are, at least partially, due to the fact that the admittance was calculated at the valve itself while the measurements determined the admittance at the interface between the valve housing and the mixing chamber. Work is, therefore, under way to develop a method to determine a transfer function which can be used to predict the admittance at the end of the valve housing from the calculated admittance at the valve plate and the geometry of the valve housing.

Figure 10 shows the calculated times required for the air valve to open as a function of frequency for four different valve spacings. Clearly, these opening times decrease as the frequency is increased until they begin to level off above about 50 Hz. On the other hand, the magnitude of the valve spacing has a relatively small effect upon the time required to open the valve.

Since the time required for the valve to open or close does no longer diminish with frequency at high frequencies it is conceivable that, at the

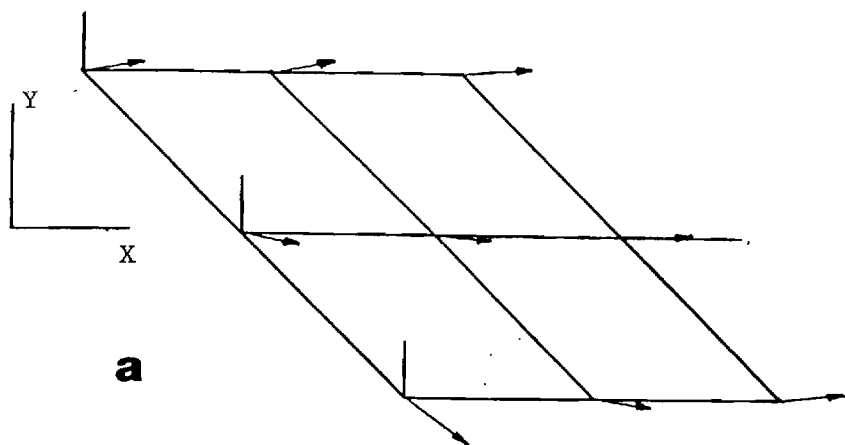
very high frequencies, there is not enough time during each cycle for the valve to open and close completely. For this reason the calculated valve opening time as a fraction of half period of the cycle was plotted against frequency in Fig. 11. This figure shows that even at frequencies of 150 Hz the valve is either open or shut during at least 30% of the duration of the cycle.

PLANNED WORK

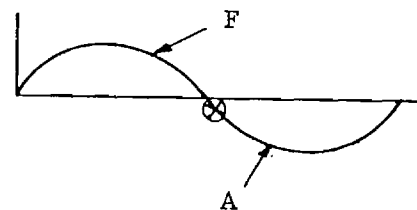
During the next reporting period the mixing patterns in the mixing chamber will be visualized using a particle seeding technique. In addition, further measurements of radiation and pressure fluctuations in the pulse combustor will be carried out near its rich limits of operation in order to confirm the reasons for the existence of this rich limit. Attention will then shift towards continuing the LDV measurements in the mixing chamber.

The impedance tube measurements will be continued. The data obtained to date will be further analyzed to determine the imaginary parts of the admittances for the valves and mixing chamber and the results will be interpreted. Further impedance measurements will be carried out under cold conditions for the remaining parts of the combustor. Work will begin to adapt the impedance tube for operation with combustion.

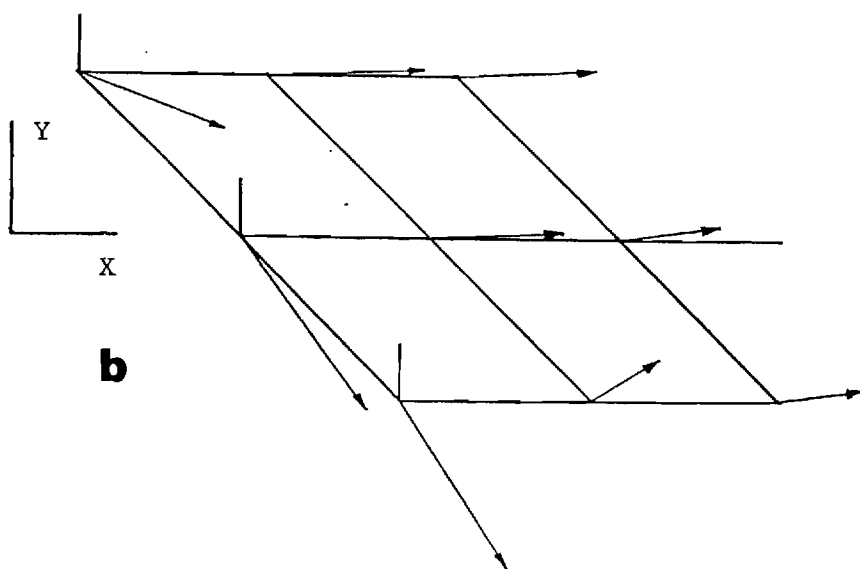
The analytical model describing the operation of the flapper valve will be extended to include non-linear acoustic effects. Work on the transfer function for determining the admittance at the interface between the valve housing and the mixing chamber from the calculated admittance at the valve plate and the geometry of the valve housing will continue.



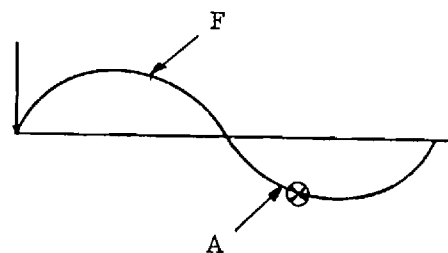
Vector Plot



Shadow Image



BVector Plot



Shadow Image

Fig. 1 Comparison of Vector Plots Obtained by LDV with High Speed Shadowgraphy Images at Four Instances During a Cycle

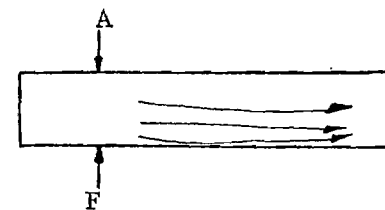
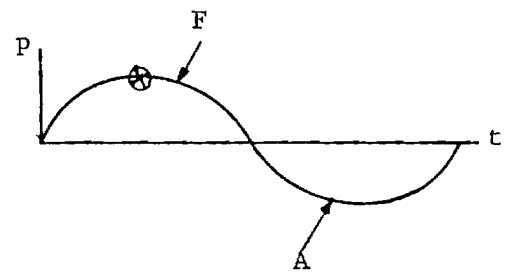
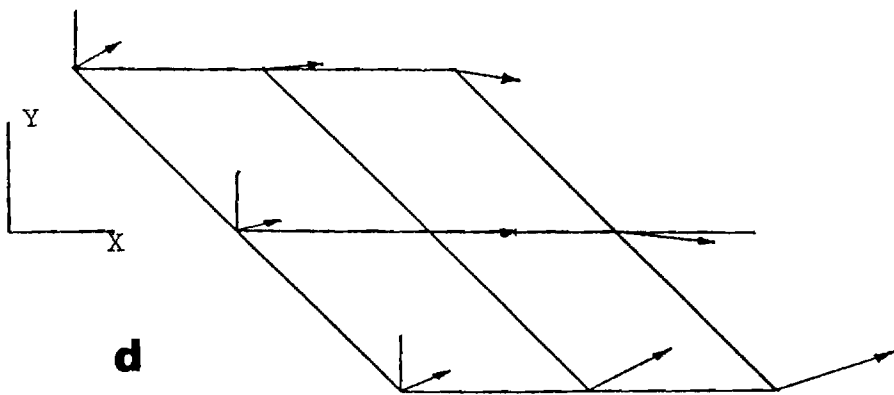
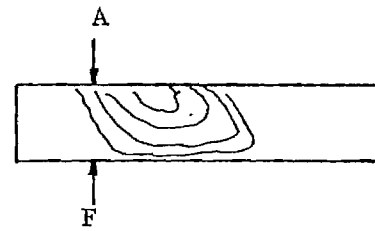
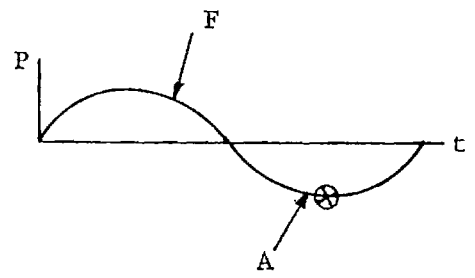
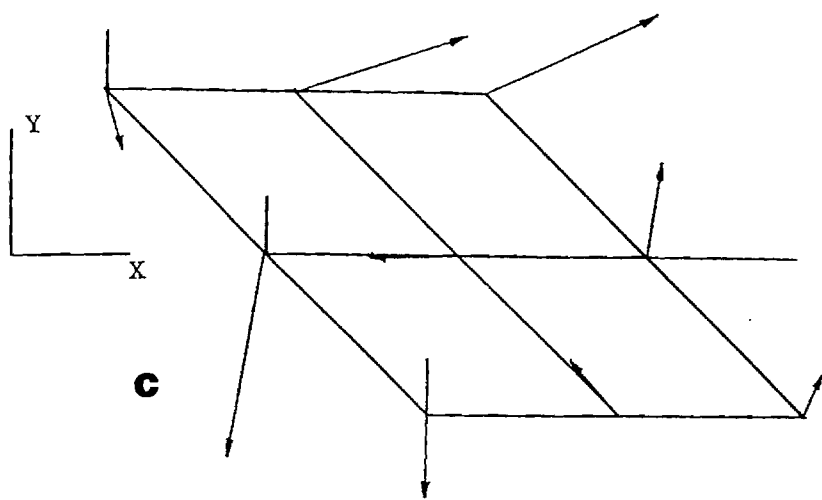
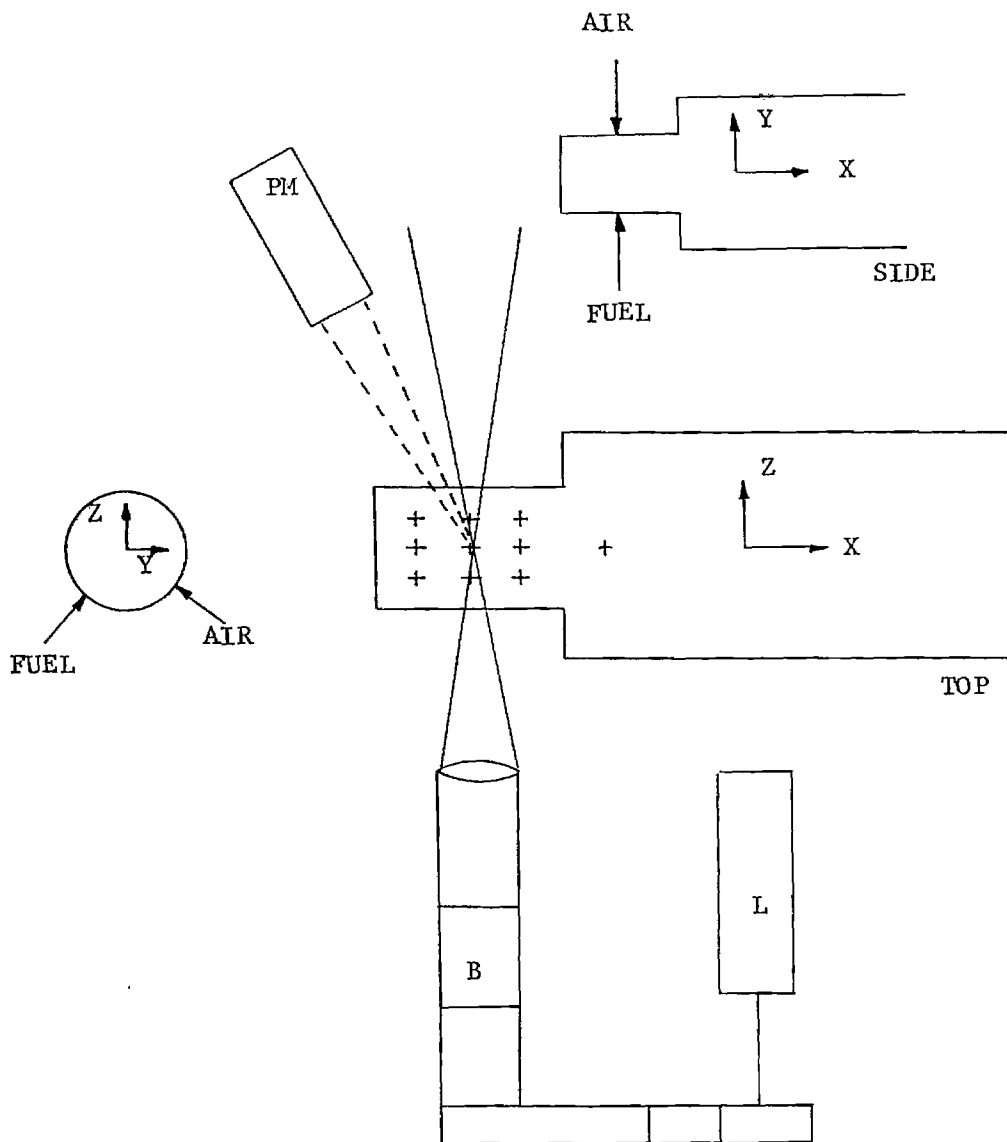


Fig. 1 Continued

LDV SCHEMATIC



VELOCITIES MEASURED IN Y & Z DIRECTIONS

Fig. 2 Location of LDV Measurements in the Mixing Chamber.

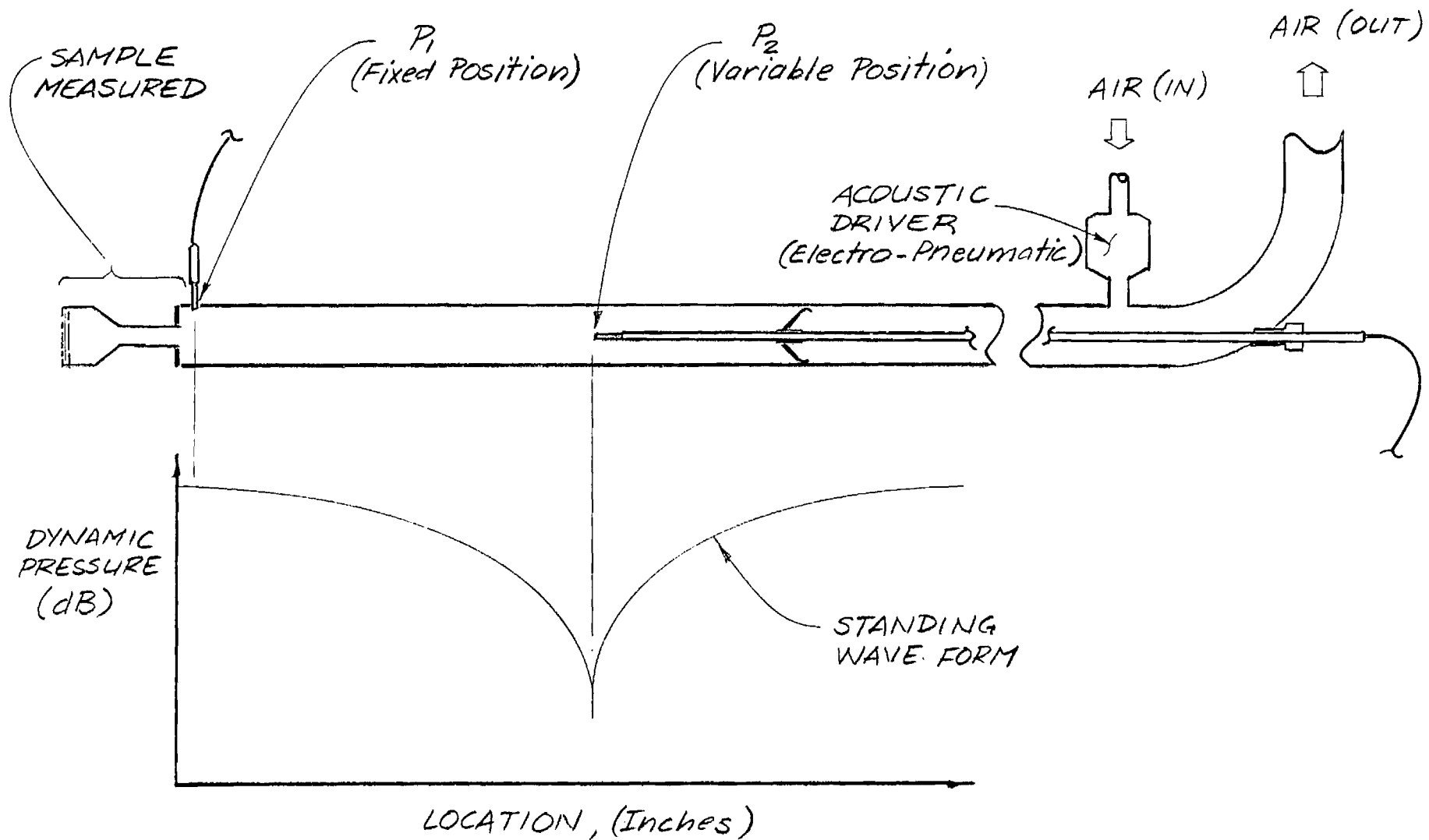


Fig. 3 Experimental Setup for Impedance Tube Measurements

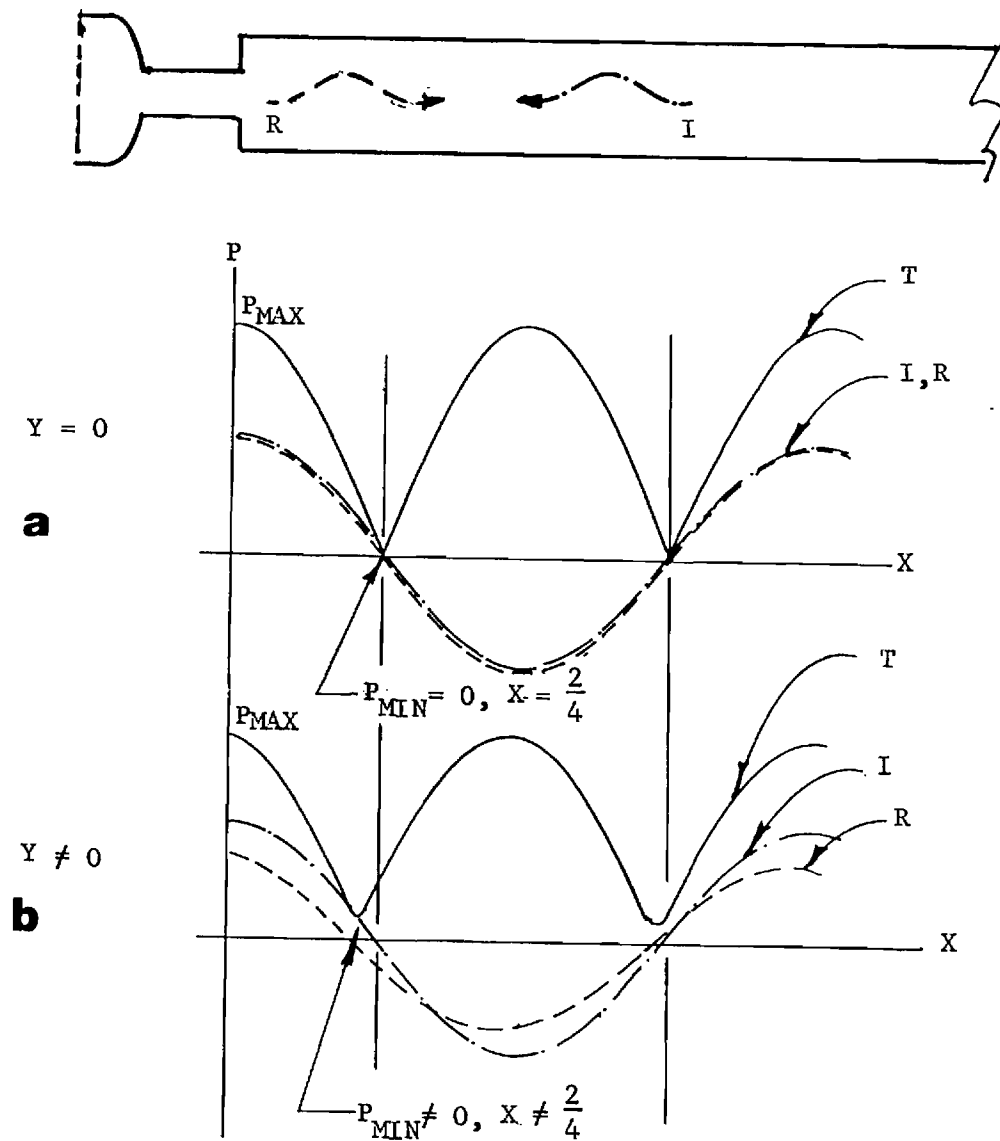


Fig. 4 Waveform of Incident (I), Reflected (R) and Total Standing Wave (T) for Hard Termination (a) and Termination with Finite Admittance (b).

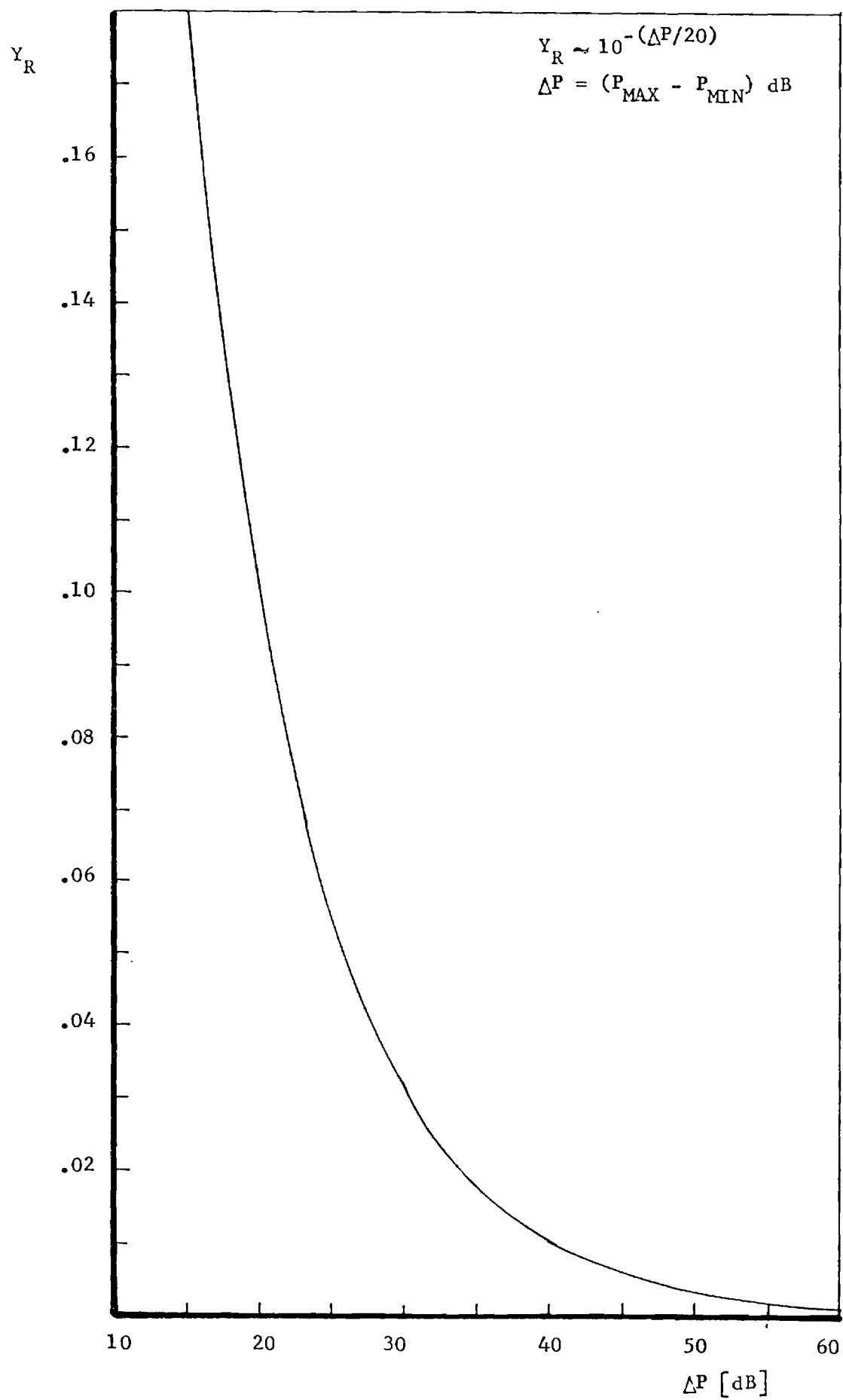


Fig. 5 Plot of ΔP vs. Real Part of Admittance (y_R)

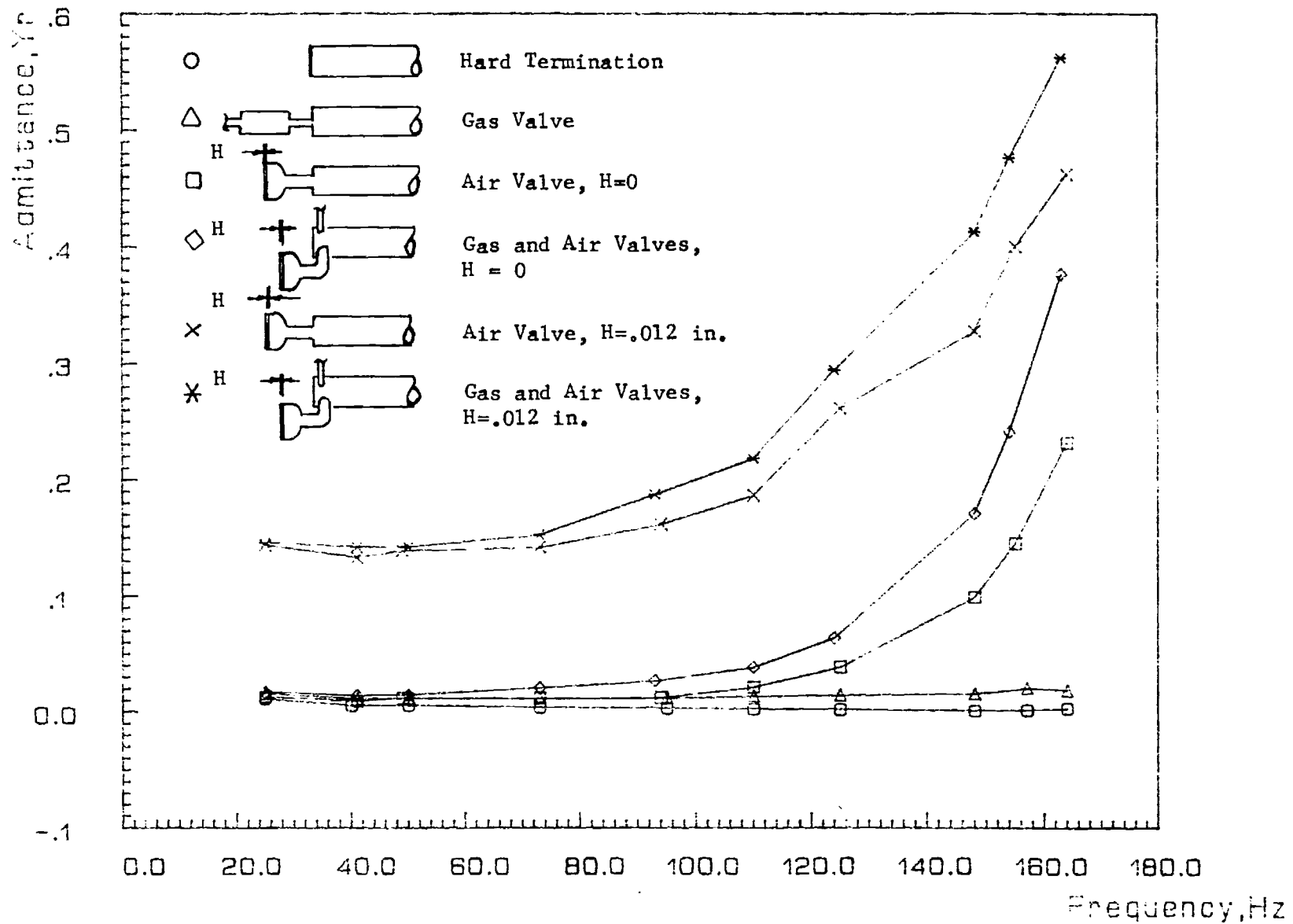


Fig. 6 Real Part of Admittance vs. Frequency for Various Impedance Tube Terminations ($H \equiv$ Air Valve Gap)

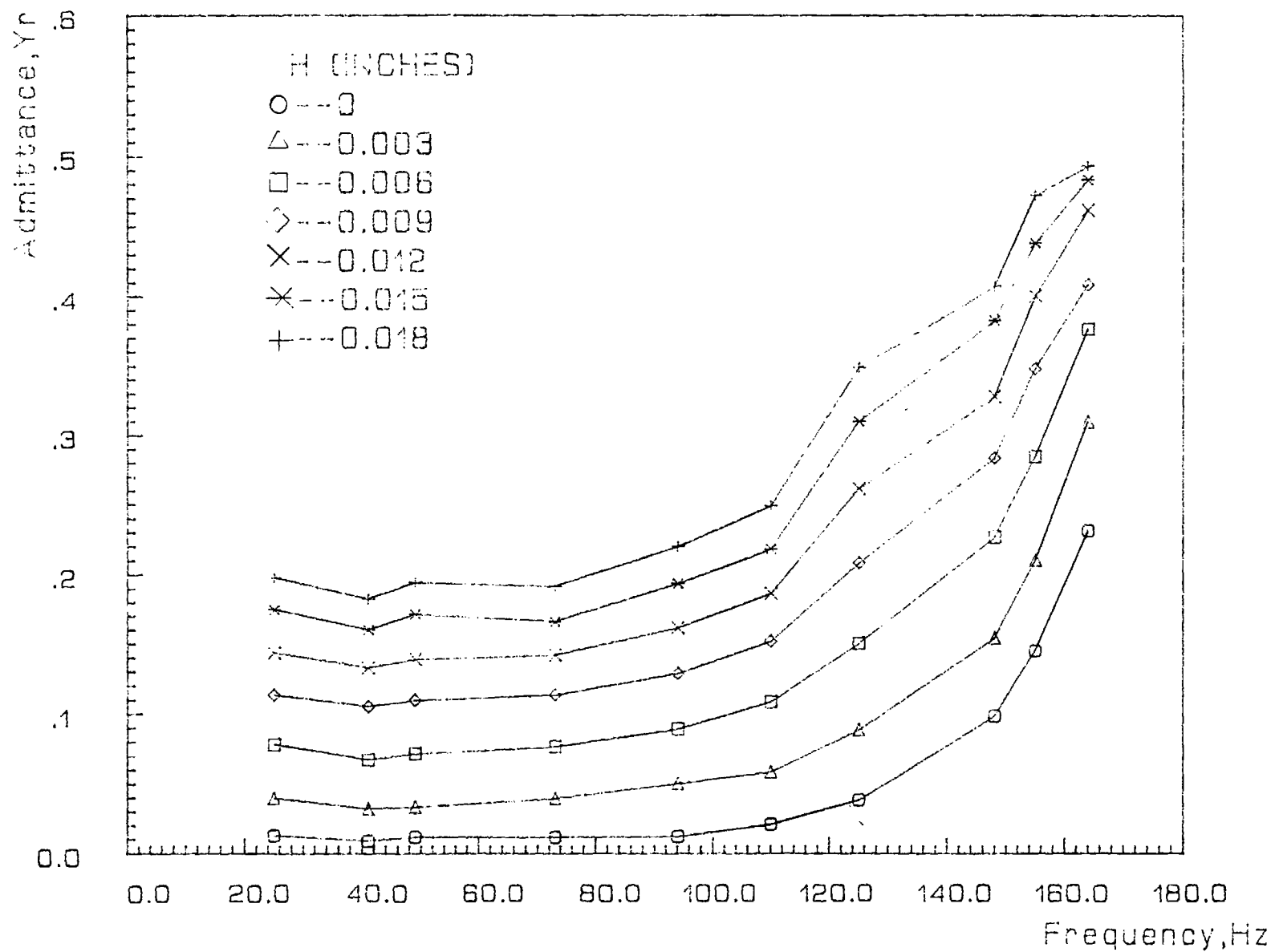


Fig. 7 Real Part of Admittance of Air Valve vs. Frequency for Different Air Valve Gap Settings (H)

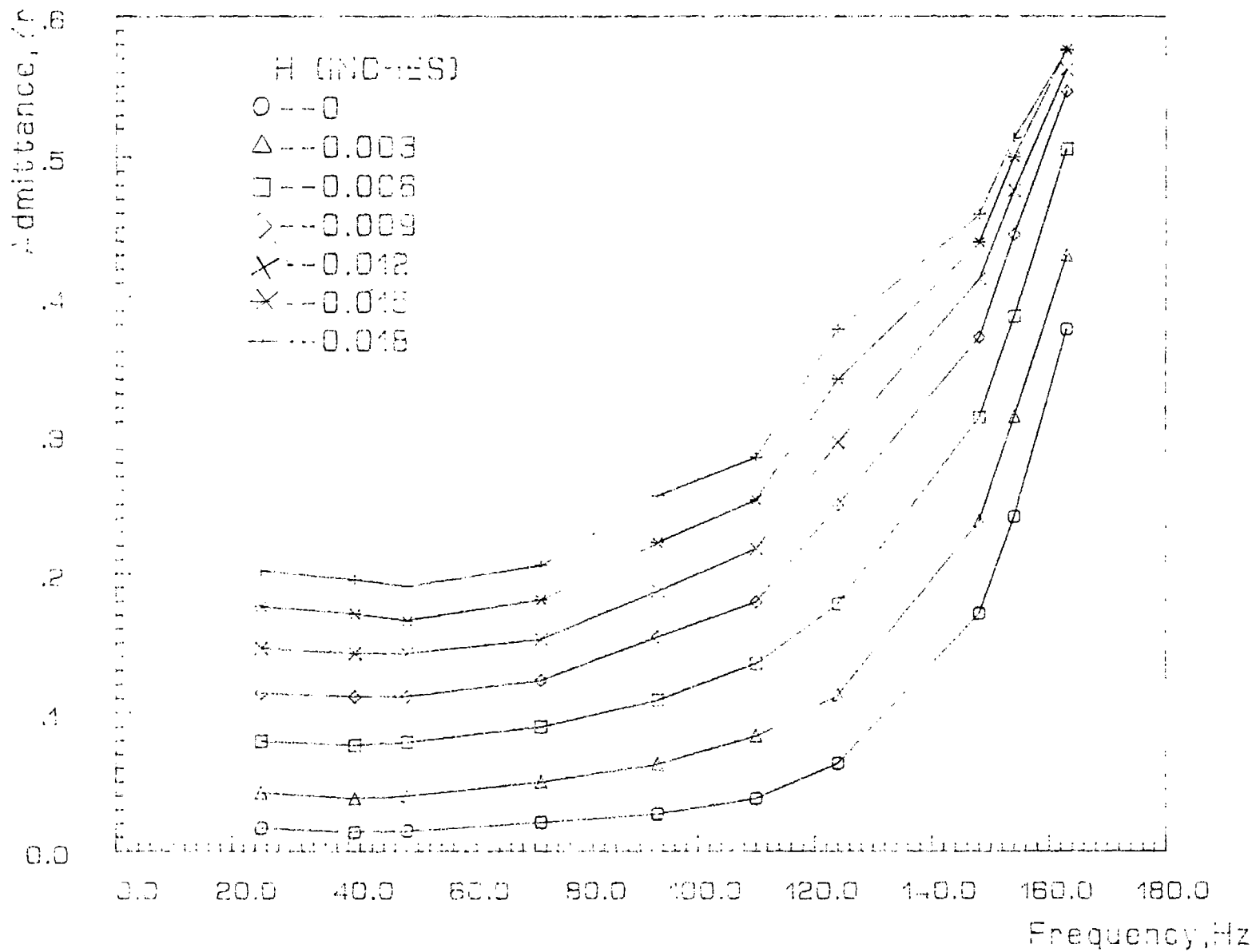


Fig. 8 Real Part of Admittance of Mixing Chamber with Air and Fuel Valves vs. Frequency for Different Air Valve Gap Settings (H)

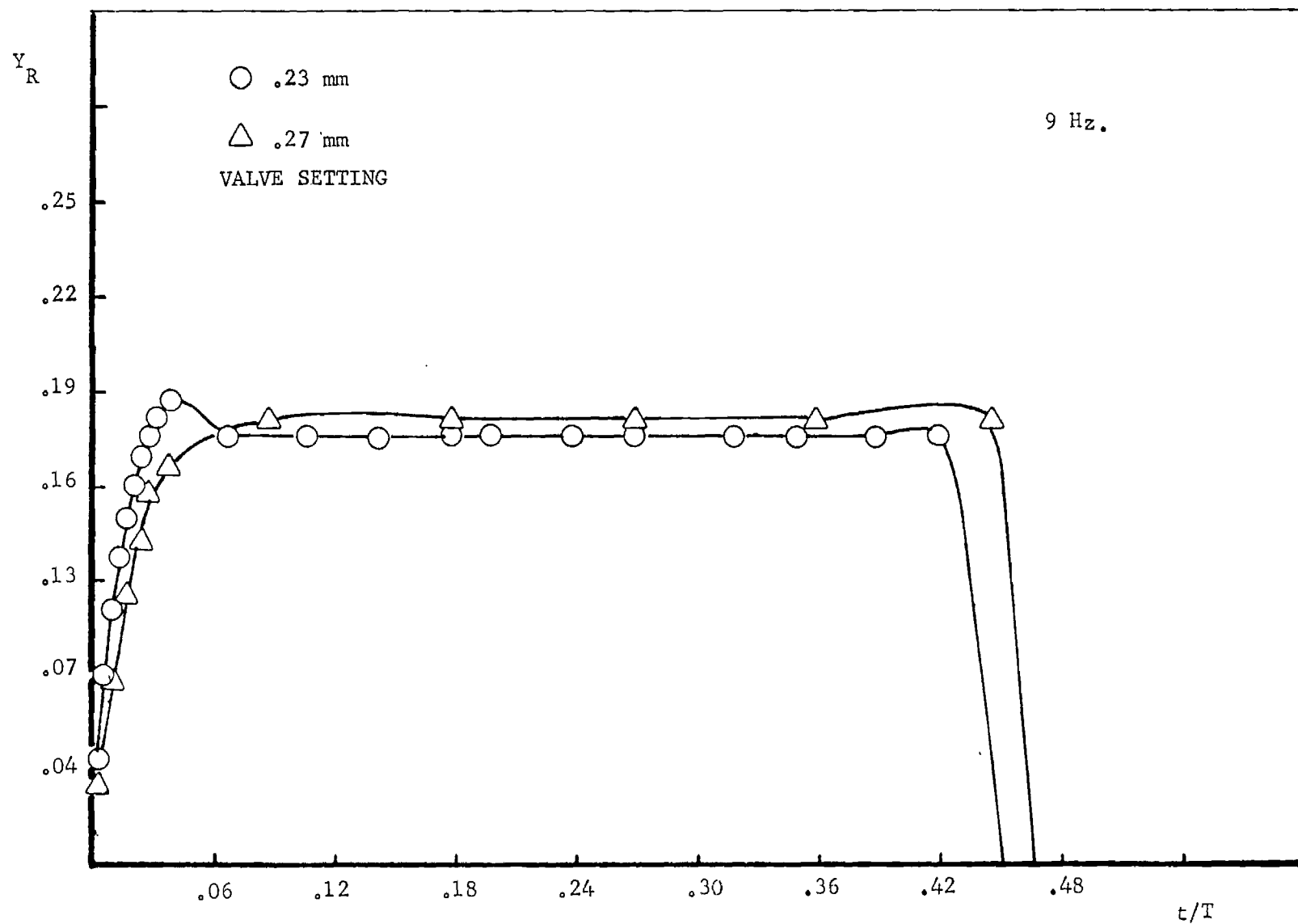


Fig. 9 Time Variation of the Calculated Real Part of the Admittance of the Air Valve for the First Half of the Cycle (Frequency: 9 Hz)

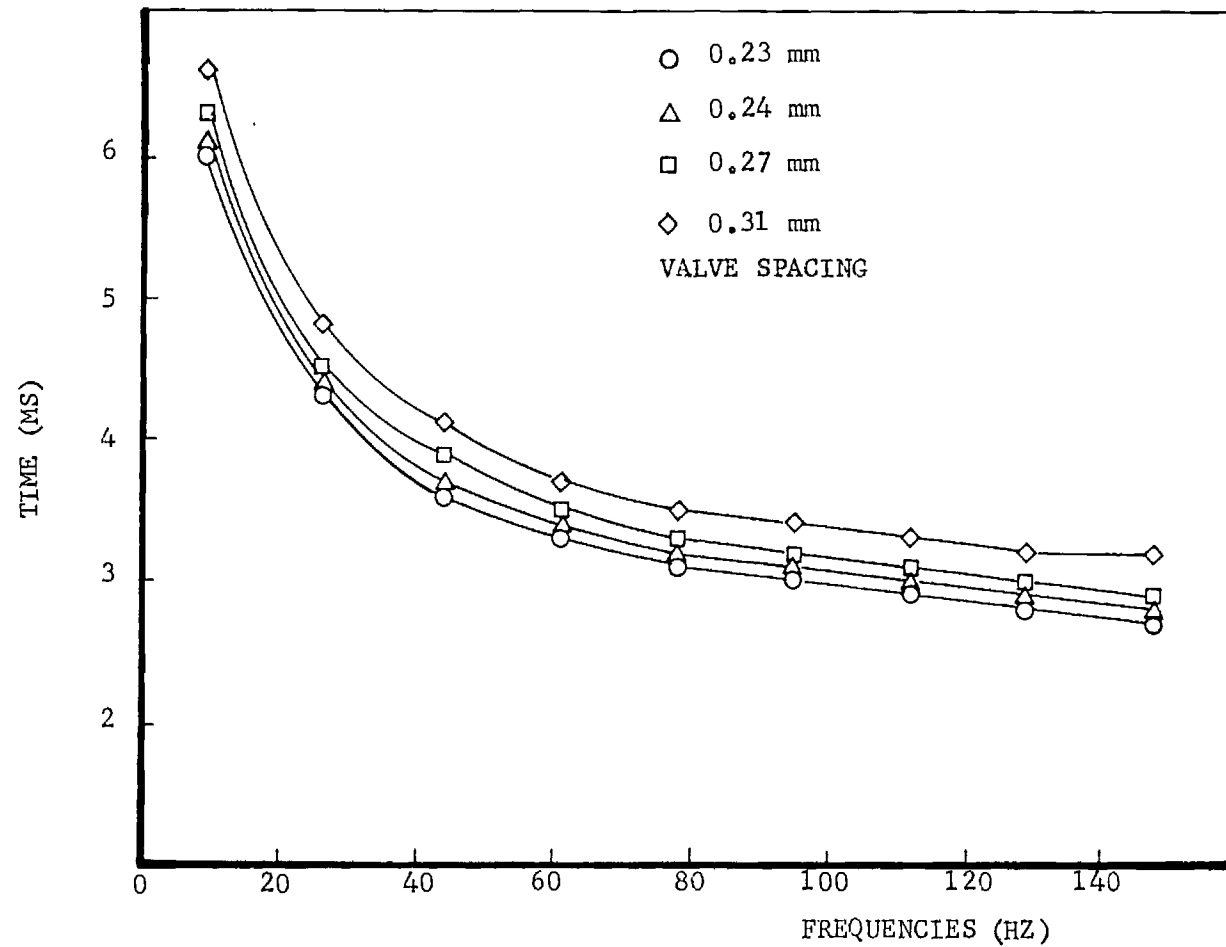


Fig. 10 Calculated Time Required to Open the Air Valve as a Function of Frequency for Different Valve Spacings

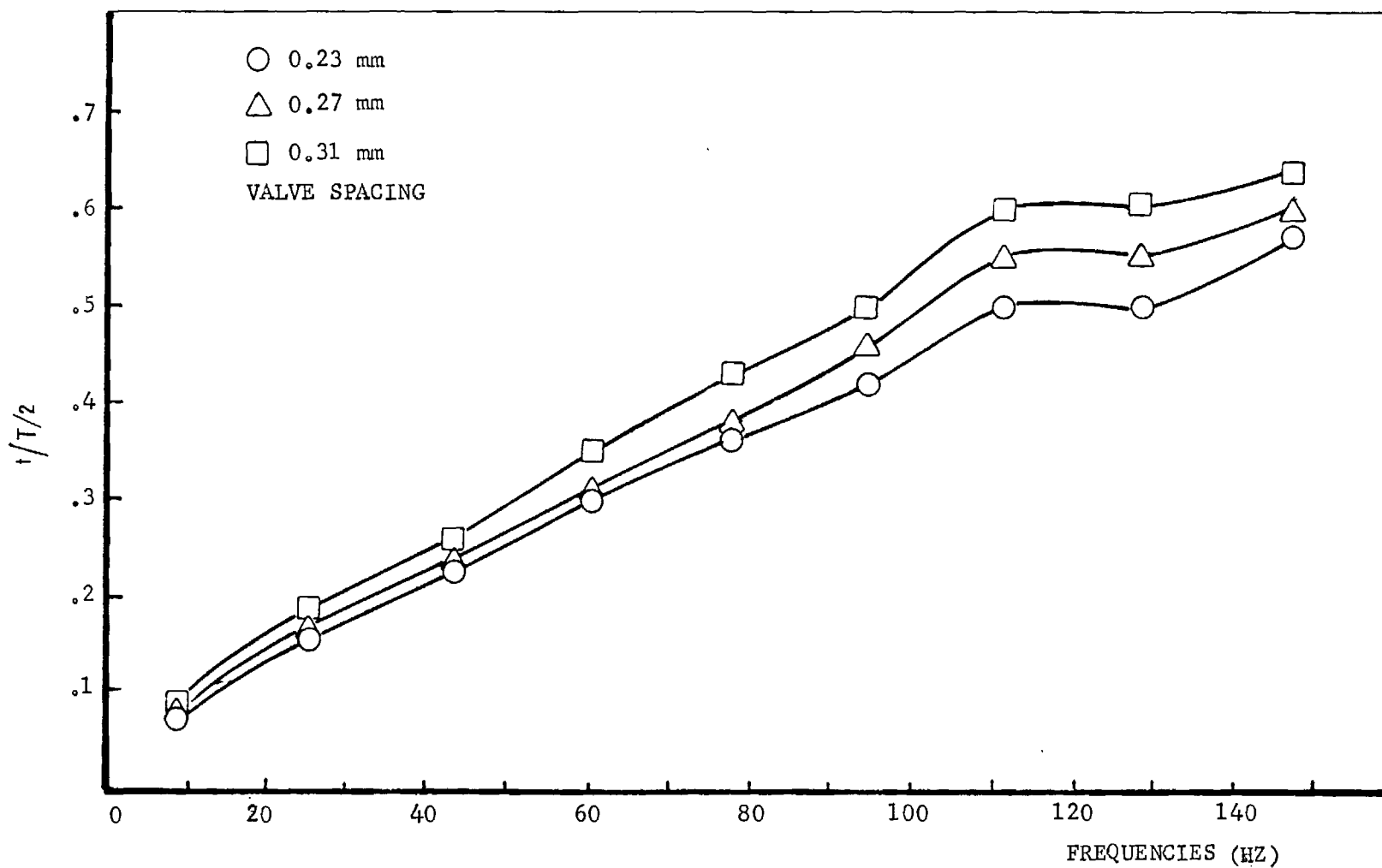


Fig. 11 Calculated Valve Opening Times as a Fraction of Half Period of the Cycle vs. Frequency for Different Valve Spacings

Pulsating Burners - Controlling Mechanisms and Performance

Semi - Annual Report

Prepared by

B. T. Zinn, B. R. Daniel and J. I. Jagoda

School of Aerospace Engineering

Georgia Institute of Technology

For

Gas Research Institute

Grant No. 5087-260-1466

GRI Project Manager

James A. Kezerle

Combustion

September 1989

RESEARCH SUMMARY

Title: Pulsating Burners - Controlling Mechanisms and Performance

Contractor: Georgia Tech Research Institute

Contract Number: 5087-260-1466

Reporting Period January - June 1989, Semi - Annual Report

Principle Investigators: B. T. Zinn, B. R. Daniel and J. I. Jagoda

Objective: To gain further insights into the physical mechanisms which control the mixing and heat release processes in pulse combustors. In addition, the acoustic driving and damping characteristics of various components and subsystems of the pulse combustor will be determined for various operating conditions.

Technical Perspective: Although gas fired pulse combustors have been on the market for a number of years, their controlling mechanisms are still not sufficiently well understood to permit their design for different applications without resorting to costly trial and error development efforts. Proper operation of pulse combustors requires that the timing of the mixing, cycle to cycle reignition and flame spread processes produce oscillatory heat release in phase with the pressure oscillations. This requires compatibility between the acoustic properties of the various components of the pulse combustor. To develop a rational design procedure for pulse combustors, it is necessary that the various processes responsible for energy

addition to and removal from the pulsations be understood. Furthermore, data describing the acoustic properties of various pulse combustor components under different operating conditions are needed. Finally, the dependence of the acoustic characteristics of the various combustor components upon the fundamental fluid mechanical, heat transfer and combustion processes must be understood.

Technical Approach: In order to elucidate the mechanisms which control the operation of various pulse combustor configurations and determine the damping/driving characteristics of different components and subsystems of commonly used pulse combustors, the following tasks are pursued simultaneously:

- 1) Investigation of the flow field characteristics, mixing and heat release in pulse combustors using LDV, Schlieren, mixing visualization, radical radiation (OH, CH, CC) and Rayleigh scattering measurements.
- 2) Measurements of the driving and damping characteristics of various components and subsystems which make up the pulse combustor using the impedance tube technique.
- 3) The determination of the overall driving and damping characteristics of various pulse combustor designs under different operating conditions.
- 4) Modeling of the dynamic characteristics of the flapper valve.

Results: During this reporting period the investigation of the admittances of the fuel and air valves and of the mixing chamber

fitted with both valves was completed. These admittances were measured using an impedance tube technique under cold flow conditions over a range of frequencies and valve openings. Similar measurements were also carried out for the entire pulse combustor without the tail pipe.

In addition, a technique was developed which permits the calculation of the real and imaginary parts of the admittance of the mixing chamber fitted with the fuel and air valves from the admittances of its component parts. The results of these calculations were found to be in excellent agreement with the measured admittances of the mixing chamber assembly over the entire ranges of frequencies and air valve settings investigated. Similar calculations for the entire combustor predicted correct trends but were quantitatively not as successful. This is, most likely, due to the stepwise expansion/contraction at the ends of the combustion chamber. The complex flow fields in the vicinity of these steps could, probably, not be correctly predicted by the one dimensional model used in these calculations.

The limits of operation of the pulse combustor were also further investigated. Previous, tests had shown that for the combustor fitted with a tail pipe of standard length (76") a rich limit of operation exists near a fuel-air ratio of one, in spite of the fact that conditions appear most favorable for driving. However, it has also been observed that this rich limit could be extended by lengthening the tailpipe. Therefore, additional measurements of pressure and heat release fluctuations and, thus, Rayleigh efficiencies, as well as Schlieren visualization were carried out in the combustor fitted with the long tail pipe. The results of these measurements were

then compared with those previously obtained for the standard combustor. It was determined that the entry of the air jet into the mixing chamber lags behind the entry of the fuel and that the time available for combustion is limited by the return of the combustion products into the mixing chamber. This strongly suggest that a rich limit of operation occurs at fuel air ratios close to one since, in the absence of air left over from the previous cycle, the ignition of the new fuel charges must await the entry of the new air jet. Insufficient time is then available to complete combustion before the reaction is quenched by the combustion products returning from the combustion chamber, unless the duration of the cycle is extended by, for example, lengthening the tail pipe.

Preliminary tests were carried out using the intensified imaging system in order to permit the graduate student to familiarize himself with its operation. A circuit was designed, built and tested which allows the imaging system to be triggered at various instants during the pressure cycle. Preliminary, two dimensional measurements of CH radiation (which is proportional to the reaction rate) have been successfully carried out.

The work on modeling the behavior of the air flapper valve has been continued. The flapper valve is highly non-linear device. First, the mass flow through the valve orifice is a non-linear function of the pressure difference across the valve. Furthermore, the valve is closed during that part of the cycle during which the pressure in the mixing chamber lies below atmospheric pressure, which introduces an additional non-linearity to the relationship between the flow rate and the pressure. This behavior was modeled by multiplying

the linearized expression describing the flow rate of air through the valve orifice as a function of pressure drop across the valve (and, therefore, of time) by a logic function which takes the form of a square wave which varies between zero and one. This modulated mass flow rate along with the pressure fluctuations near the valve permitted a theoretical determination of the non-linear admittance of the valve. This admittance along with the equation for the standing wave in the impedance tube was used to determine the frequencies and relative amplitudes of the higher harmonics as a function of the amplitude of the exciting acoustic disturbance. The power spectra calculated using a Fourier Series expansion were found to be in excellent agreement with those measured experimentally in the impedance tube. In addition, the prediction that the rectification of the air valve is primarily responsible for the existence of the higher pressure harmonics was confirmed in tests in which the pulse combustor was operated with and without the air valve. The higher harmonics present in the measured pressure signal when the combustor was operated in the valved mode were accurately predicted by the model. These higher harmonics virtually disappeared when the combustor was operated without the air flapper valve.

The remainder of this report takes the form of Topical Report entitled: "The Acoustic Characteristics of Pulse Combustor Flapper Valves and Mixing Chambers" prepared for the Thirteenth Annual Energy Resources Technology Conference, New Orleans, Jan. 14-18, 1990.

THE ACOUSTIC CHARACTERISTICS OF PULSE COMBUSTOR FLAPPER VALVES AND MIXING CHAMBERS

D. Xu, B. R. Daniel, J. I. Jagoda and B. T. Zinn

School of Aerospace Engineering

Georgia Institute of Technology

Atlanta, GA 30332

ABSTRACT

This paper reports the results of an investigation of the acoustic characteristics of the mixing chamber and flapper valves of a Helmholtz type pulse combustor. An impedance tube was used to measure the admittance of the fuel valve, the air valve and of the mixing chamber fitted with the fuel and air valves. In addition, the admittance of the mixing chamber - valves assembly was determined analytically from the measured admittances of its component parts. The flapper valve was found to be acoustically equivalent to a hard termination. The absolute value of the real part of the admittance of the air valve increases with frequency and with valve spacing while the corresponding imaginary part increases with frequency and decreases with valve opening. The trend of the admittance of the mixing chamber fitted with the fuel and air valves is similar to that of the air valve only. However, the orientation of the valve and the presence of the mixing chamber affects the magnitude of the admittance at each frequency and for each valve setting. The calculated admittances of the mixing chamber assembly are in excellent agreement with their measured values over all investigated ranges of frequencies and air valve openings. This work is currently being extended to cover the effects of the combustion chamber and of the combustion processes.

NOMENCLATURE

A	Cross sectional area
f	Frequency
H	Admittance
l	Wave length
\mathbf{n}'	Unit normal vector pointing out
p'	Pressure perturbation
\mathbf{u}'	Velocity Perturbation vector

x	Axial location
Y	Admittance

<u>Subscripts</u>	
1,2,2',3,4	Locations 1, 2, 2', 3, 4
c	Cold
h	Hot
i	Imaginary
max	Maximum
min	Minimum
v	Real
t	Tailpipe

INTRODUCTION

This paper describes an experimental investigation of the acoustic characteristics of a mixing chamber and flapper valves similar to those which have been extensively used to date in a variety of Helmholtz type pulse combustors including the immensely successful Lennox pulse furnace (Lennox Industries, Inc.). This type of pulse combustor generally consists of a mixing chamber at its upstream end, a combustion chamber in the middle, and a tail pipe at its downstream end, see Fig. 1. As its name indicates, the the mixing chamber was originally included in the system to provide a space where the fuel and air could mix prior to burning. Once formed, the combustible mixture was expected to burn inside the combustion chamber. The tail pipe had been included in the system to assure that it possessed the required acoustic properties (e.g., the appropriate frequency) and to provide heat transfer area for removing energy out of the pulse combustor and into the heated medium (e.g., air or water). It has since been shown (Reuter et al., 1986), however, that ignition and considerable burning occur inside the mixing chamber. In fact, in small scale pulse combustors, similar to those used for domestic space heating applications, the

majority of the fuel is burned inside the mixing chamber. Since the pulse combustor performance critically depends, among others, upon the characteristics of the mixing chamber, it is of utmost importance that these characteristics be understood. Specifically, it is important to understand how the mixing chamber assembly behaves under different oscillatory flow conditions (e.g., at different frequencies), how this behavior is modified by the presence of combustion and whether it is possible to predict the behavior of the mixing chamber from data which describe the properties of its component parts.

The data provided in this paper will attempt to answer some of the above questions. These data were obtained in a GRI (i.e., Gas Research Institute) sponsored research program aimed at developing a better understanding of the fundamental processes which control the operation of a variety of pulse combustors. Another goal of this research program is to obtain data which will form the foundation for the development of a rational design procedure for pulse combustors; a design procedure which is urgently needed to replace the empirical and costly, cut and try, approaches which have been used to date to develop pulse combustors. Since pulse combustors consist of subsystems which have different properties and different functions, the attainment of the above goal will require a systematic investigation of the properties of these subsystems under different operating conditions. The current paper describes the results of an investigation of the properties of a generic pulse combustor mixing chamber under cold flow operating conditions.

A typical mixing chamber, see Fig. 2, consists of a short cylindrical chamber which is closed at its upstream end, and air and fuel flapper valves attached to its walls. Each of these flapper valves is designed to open when the pressure inside the mixing chamber decreases below the pressure upstream of the flapper valve. Since the pressure upstream of the fuel flapper is generally higher than the pressure upstream of the air flapper, the fuel and air flapper valves open sequentially when the pressure inside the combustor decreases, and permit fuel and air to enter the mixing chamber. After mixing, the resulting mixture is ignited by hot combustion products, flamelets or radicals left over from the previous cycle. The energy released by the combustion process drives the combustor pulsations. As the combustor pressure starts to increase, the flapper valves close, and the combustion products are exhausted out of the system via the tail pipe.

Driving of combustor pulsations occurs if the combustion process energy is released in phase with the combustor pressure oscillations. This condition was first stated by Rayleigh (1945) and

it is generally referred to as Rayleigh's criterion. The practical implications of Rayleigh's criterion are that the mixing and combustion processes must be completed within a certain time span which is of the order of half the period of the combustor pulsations in order for the heat release and pressure oscillations to be in phase.

In addition to the above described time condition, satisfying Rayleigh's criterion also imposes a space condition upon the combustion process. This space condition states that the combustion process heat release must occur in regions of the pulse combustor where the amplitude of the pressure oscillations is large. Since significant fractions of the mixing and combustion processes occur inside the mixing chamber, the time and space conditions imposed by Rayleigh's criterion must be kept in mind when designing a mixing chamber.

In the study reported herein, an acoustic impedance tube (Scott, 1946) has been used to study the acoustic properties of a generic pulse combustor mixing chamber similar to the one shown in Fig. 2. Specifically, the impedance tube was used to determine the behavior of the flapper valves individually and the whole mixing chamber assembly at different frequencies. Next, measured data describing the behavior of the individual components was used to predict the behavior of the whole mixing chamber assembly and the predicted data are compared with the measured data. The objectives of these efforts were to determine the acoustic properties of the flapper valves and mixing chamber, and to determine whether knowledge of the acoustic properties of the individual components could be used to predict the behavior of the whole mixing chamber assembly.

BACKGROUND

The acoustic properties of various components are often described by specifying their acoustic admittances. The acoustic admittance Y is a complex quantity which is defined by

$$Y = Y_r + iY_i = u'n/p'$$

where u' , n , p' , Y_r and Y_i represent the velocity perturbation vector, the unit normal vector pointing away from the control volume boundary, the pressure perturbation and the real and imaginary parts of the admittance, respectively. The real and imaginary parts of Y provide information about the physics of the wave reflection processes at the boundary or point which is described by the given admittance. In addition, the admittance Y is used as a boundary condition in the analysis of a variety of acoustical problems.

Consider, for example, the pulse combustor configuration shown in Fig. 1 where Y_1 and Y_2 are the admittances at the interfaces between the mixing and the combustion chambers, and between the combustor and the tail pipe, respectively. The admittance Y_1 can be considered as the admittance of the mixing chamber assembly which includes everything on the left of the boundary where Y_1 is specified; that is, the short mixing chamber pipe which is closed at its upstream end, and the air and fuel flapper valves. The sign of $Y_{1,r}$ determines whether a wave incident upon this interface from the right (i.e., from the combustor) will be amplified or attenuated by the processes which take place inside the mixing chamber. When $Y_{1,r}$ is positive, the amplitude of the reflected wave is larger than that of the incident wave. This can only occur if oscillatory burning in phase with the local pressure oscillations takes place within the mixing chamber. On the other hand, when $Y_{1,r}$ is negative, acoustic energy is dissipated inside the mixing chamber and the amplitude of the reflected wave is smaller than that of the incident wave. The waves are attenuated by acoustic energy losses caused by viscous dissipation and acoustic energy radiation to the outside through the flapper valves, and if oscillatory burning out of phase with the local pressure oscillations occurs inside the mixing chamber.

The imaginary part of the admittance $Y_{1,i}$ provides information about the time delay between the instants at which an incident wave (from the right) arrives at and a reflected wave departs from the interface between the mixing and combustion chambers. This time delay is caused by the fact that a wave impinging from the right upon the interface between the combustor and mixing chambers propagates into the mixing chamber and the flapper valves before being reflected back into the combustion chamber.

Data describing the frequency dependence of the admittances of various pulse combustor components can be of considerable value to pulse combustor designers as it can be used to determine whether a given pulse combustor design will operate. Furthermore, such admittances can be used to determine the magnitude of certain processes and provide much needed boundary conditions for an analysis of the pulse combustor performance.

Consider, for example, the hypothetical frequency dependences of $Y_{r,2,h}$ and $Y_{r,2,c}$ presented in Fig. 3. They are the real parts of the admittance Y_2 (see Fig. 1) which were, presumably, measured in impedance tube experiments with and without combustion present in the system, respectively. Figure 3 shows that $Y_{2,r,h}$ is negative at low and high frequencies and positive in the center frequency range where it reaches a maximum value at a frequency f_h . This result indicates that even when

combustion occurs within the subsystem consisting of the mixing and combustion chambers, this subsystem attenuates incident waves at the high and low frequency ranges where $Y_{2,r,h}$ is negative.

Amplification of incident acoustic waves only occurs in the middle frequency range where $Y_{2,r,h}$ is positive. On the other hand, $Y_{2,r,c}$ is negative throughout the frequency range indicating that when no combustion is present in the system, acoustic energy is dissipated inside the mixing and combustion chambers at all frequencies.

Since acoustic energy losses are always present within the system, the distance H in Fig. 3, which is the difference between the real parts of the admittances measured with and without combustion present in the system, is a measure of the driving provided by the combustion process at the indicated frequency. That part of H which lies below the x-axis is needed to overcome the damping of the mixing and combustion chambers, while the part of H above the x-axis is a measure of the amount of acoustic energy available to drive pressure oscillations and overcome other dissipation processes which might be present within the system (e.g., the tail pipe). Thus, the dependence of the combustion process driving upon various system parameters (e.g., flapper valve settings) can be determined by obtaining the frequency dependences of $Y_{2,r,h}$ and $Y_{2,r,c}$ for various system configurations

Figure 3 includes a hypothetical curve $Y_{t,r}$, also assumed to have been determined from impedance tube measurements, which describes the frequency dependence of the real part of the tail pipe admittance. It lies below the x-axis because acoustic waves are always attenuated inside the tail pipe. This curve together with the one for $Y_{2,r,h}$ can be used to determine the frequencies at which a pulse combustor will operate. Since the combustion process is the only process which can drive pulsations inside a pulse combustor, and the combustion process is generally confined to the mixing and combustion chambers, the pulse combustor will operate only at those frequencies where the driving provided by the mixing and combustion chambers is larger than the damping provided by the tail pipe. Since the former is described by $Y_{2,r,h}$ and the latter by $Y_{t,r}$, the pulse combustor will operate only at those frequencies where the magnitude of $Y_{2,r,h}$ is larger than the absolute value of $Y_{t,r}$. Using the above reasoning, it follows from Fig. 3 that the hypothetical pulse combustor will operate, for example, at frequency f_1 where the driving provided by the mixing and combustion chambers is larger than the damping provided by the tail pipe. On the other hand, the pulse combustor will not operate at the frequency f_2 where the opposite occurs.

The long range objective of the study which is described in this paper is to obtain admittance data similar to that shown in Fig. 3 for various pulse combustor components. In pursuit of this

objective, this paper describes impedance tube measurements of the admittances of the mixing chamber assembly and its components under cold conditions.

EXPERIMENTAL SETUP

The impedance tube utilized in this study consists of a long pipe, 7.6 cm in diameter, which is equal to the diameter of the mixing chamber under investigation, see Fig. 4. The component whose admittance is to be measured is attached to the downstream end of the tube (i.e., $x = 0$). A Ling E-94 pneumatic acoustic driver is attached to the wall of the tube just downstream of an exhaust line that vents to the outside of the building. The length of the exhaust line can be varied to change the resonant frequency of the system consisting of the impedance tube and exhaust line. Different system lengths were used in this study in order to operate the driver at a resonant frequency of the system and, thus, increase the amplitude of the excited pulsations.

The impedance tube is instrumented with two microphones. One is permanently attached to the wall at $x = 0$ while the other is mounted on a long rod which can be translated along the axis of the impedance tube. The fixed microphone monitors the pressure amplitude at the interface between the impedance tube and the device whose admittance is to be determined. This value is usually set to 165 dB, a typical value observed inside the pulse combustor which is investigated under this program. The second microphone is used to determine the distribution of the pressure amplitude inside the impedance tube.

The outputs from the microphones are amplified, filtered and passed through an A/D converter into an HP 1000 series computer. There, the signals are Fourier analyzed and pressure spectra are calculated. These spectra are used to determine the magnitude of the amplitude of the pressure oscillation at each location. Next, these data are used to determine the maximum and minimum acoustic pressure amplitudes, and the location of the first acoustic pressure minimum from which the real and imaginary parts of the admittance at $x = 0$ are calculated using the following relationships (Scott, 1946):

$$Y_r = - \frac{[\tanh(\pi\alpha)] [1 + \tan^2(\pi\beta)]}{[\tanh(\pi\alpha) + \tan^2(\pi\beta)]} \quad (1)$$

$$\text{and } Y_i = \frac{[1 - \tanh^2(\pi\beta)] \tan(\pi\beta)}{[\tanh^2(\pi\alpha) + \tan^2(\pi\beta)]} \quad (2)$$

$$\text{where } \tanh(\pi\alpha) = 10^{-\frac{P_{\max} - P_{\min}}{20}}, \quad \beta = \frac{2 x_{\min}}{\lambda}$$

Here p_{\max} and p_{\min} , x_{\min} and λ are the maximum and minimum pressure amplitudes, the location of the pressure minimum, and the wavelength of the oscillation, respectively.

EXPERIMENTAL RESULTS

The impedance tube described above was used to measure the admittances of the fuel valve, the air valve and of the mixing chamber fitted with either the air valve only or with both, the fuel and air valves. In each case, the investigated component was attached to the downstream end of the impedance tube. These experiments were carried out over a 35-200 Hz. frequency range and air valve openings between 0 and 0.018 inches.

These tests showed that the the acoustic behavior of the fuel valve is equivalent to that of hard wall; i.e. both Y_r and Y_i were found to be essentially zero. The frequency dependences of the real and imaginary parts of the air valve admittance are shown, for different valve settings, in Figs. 5a and 5b, respectively. As expected, the real part of the admittance is always negative since under the cold flow conditions of this study the incident waves were always attenuated inside the valve. The absolute value of Y_r increases with frequency and with valve spacing. These data indicate that for a given acoustic pressure amplitude at the valve exit the air valve damping increases with increasing frequencies and valve opening. The imaginary part of the air valve admittance, Y_i , decreases with increasing valve opening and increases with frequency except at large valve settings and high frequencies where it begins to decrease again.

The real and imaginary parts of the admittance of the mixing chamber fitted with the air valve only are shown in Figs. 6a and 6b, respectively. The trends are similar to those exhibited by the admittance of the air valve on its own, see Figs. 5a and 5b. There are, however, quantitative differences between the data in Figs 5 and 6 since the orientations of the air valve in these experiments were different and because the data of Fig. 6 includes the effect of the mixing chamber.

Figures 6a and 6b also show the measured values of Y_r and Y_i for the mixing chamber fitted with both the fuel and the air valves. These data are essentially identical to those obtained with the mixing chamber fitted with the air valve only, further supporting the observation that the fuel valve is acoustically equivalent to a hard wall.

THEORETICAL RESULTS

This section discusses the analytical determination of the admittance of the mixing chamber - valves assembly from the

measured admittances of its component parts. For this purpose, the assembly was divided into five regions as shown in Fig. 7a. Next, the acoustic mass conservation equation was applied to the control volume enclosed by boundaries 1, 2, 3 and 4. Using this equation, and determined admittances at interfaces 1, 2 and 3, the admittance of interface 4 was determined. Using the known admittance at 4, a transfer function based upon the solution of the one dimensional wave equation in a duct was used to determine the admittance at the downstream end of the mixing chamber (i.e. at location 5).

In detail, a simple transfer function was used to determine the admittance of interface 1 from the known admittance (i.e., $Y_1 = Y_i = 0$) of the hard wall at the upstream end of the mixing chamber. The air flapper valve admittance at interface 2 was then determined from the measured admittance of the cross sectional area at 2' in Fig. 5. This admittance includes, however, contributions from the air flapper valve and the solid wall which connects the valve to the impedance tube. The needed air flapper valve impedance (at interface 2 in Fig. 5) was obtained from the following acoustic continuity equation:

$$A_2 u_2 = Y_2 p'_2 A_2 = A_2 u'_2 = Y'_2 p'_2 A_2 \quad (3)$$

where the A , Y and u' represent cross-sectional areas, admittances, and acoustic velocities at locations 2 and 2' in Fig. 5, respectively. Since the cross-sectional areas are known and $p'_2 = p'_2$, Y_2 can be determined from Y'_2 , using Eq. (3). The fuel valve admittance at location 3 in Fig. 7a was taken to be zero. The acoustic properties at interface 4 in Fig. 7a can now be determined from those at interfaces 1 and 2 using the following acoustic continuity equation:

$$\frac{\partial}{\partial t} (\bar{\rho}' V_D) = \bar{\rho}' u'_1 + \bar{\rho}' u'_2 - \bar{\rho}' u'_4 \quad (4)$$

where r' , $\bar{\rho}$ and V_D are the density perturbation, mean density, and the volume of the rectangular region D , respectively. Since it can be shown that the time dependent term is negligible as long as the axial dimension of volume D is small compared to the wavelength of the oscillation, and since the mean density is constant, Eq. (4) reduces to:

$$u'_1 + u'_2 = u'_4 \quad (5)$$

Since by definition $u' = Yp'$, Eq. (5) can be rewritten as:

$$Y_1 p'_1 + Y_2 p'_2 = Y_4 p'_4 \quad (6)$$

Equation 6 can now be used to calculate the admittance Y_4 from the admittances Y_1 and Y_2 which were determined by the methods discussed above, and from the acoustic pressures. Finally, the admittance at location 5 is calculated from that at location 4 using an appropriate transfer function.

It is customary in such calculations to shrink the axial dimension of the rectangular region (D) to zero (see Fig. 7b) before carrying out the acoustic mass balance and determining the admittance at location 5. In the present study, such calculations were performed for a number of air valve openings and over a range of frequencies. These results are compared in Fig. 6 with measured admittances of the mixing chamber assembly. Clearly, the agreement with the measured data is excellent.

CONCLUSIONS

The acoustic properties of a mixing chamber and its air and fuel flapper valves which are used in Helmholtz type pulse combustors have been investigated both experimentally and theoretically. The experimental efforts used an impedance tube setup to determine the frequency dependences of the admittances of the investigated devices under cold flow conditions. These studies showed that the fuel flapper valve is acoustically equivalent to a hard termination. The damping of the air flapper valve increases with increasing frequencies and flapper valve opening. Next, the acoustic continuity equation was used to determine the admittance of the mixing chamber assembly, which includes the air and fuel flapper valves, from the admittances of its components. Results of these calculations were in excellent agreement with the measured admittances of the of the mixing chamber assembly. This study is currently being extended to include the effect of the combustion chamber and combustion processes.

ACKNOWLEDGEMENT

This work is supported by the Gas Research Institute under Grant No. 5087-260-1466, monitored by Mr. J Kezerle.

REFERENCES

- "Lennox-Pulse-G14 Series Up-Flo Gas Furnaces", Engineering Data, Heating Units, Gas, published by Lennox Industries, Inc.
- Lord Rayleigh, "The Theory of Sound," Vol. II, pp. 224-235, Dover, 1945
- Reuter, D., Daniel, B.R., Jagoda, J.I., and Zinn, B.T., Combustion and Flame, Vol. 65, No. 3, pp. 281-290, 1986.
- Scott, R.A., Proceedings of the Physical Society, Vol. 58, pp. 253-264, 1946.

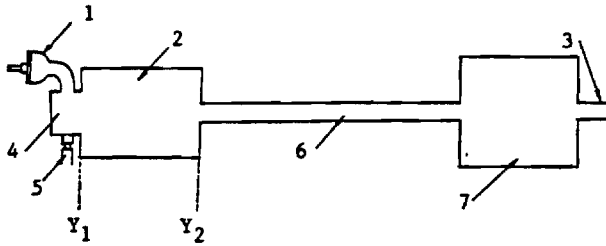


FIG. 1: SCHEMATIC OF THE HELMHOLTZ TYPE PULSE COMBUSTOR UNDER INVESTIGATION. Y_1 AND Y_2 INDICATE THE LOCATION OF THE ADMITTANCES DISCUSSED IN THE INTRODUCTION. (1-AIR VALVE, 2-COMBUSTION CHAMBER, 3-VENT PIPE, 4-MIXING CHAMBER, 5-FUEL VALVE, 6-TAIL-PIPE, 7-DECOUPLER)

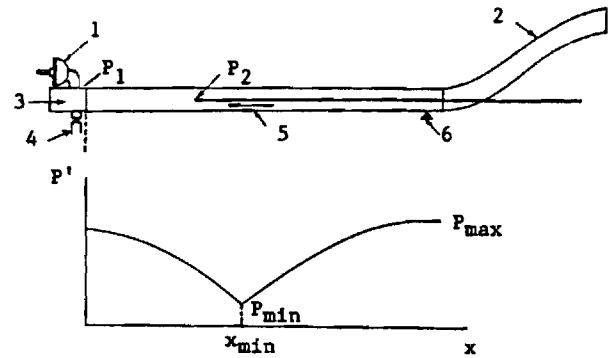


FIG. 4: SCHEMATIC OF THE IMPEDANCE TUBE WITH ATTACHED MIXING CHAMBER. P_1 AND P_2 ARE THE LOCATIONS OF THE PRESSURE TRANSDUCERS. ALSO SHOWN IS A TYPICAL DISTRIBUTION OF THE PRESSURE AMPLITUDE IN THE IMPEDANCE TUBE. (1-AIR VALVE, 2-EXHAUST LINE, 3-MIXING CHAMBER, 4-FUEL VALVE, 5-IMPEDANCE TUBE, 6-DRIVER, P_2 -TRANSLATABLE)

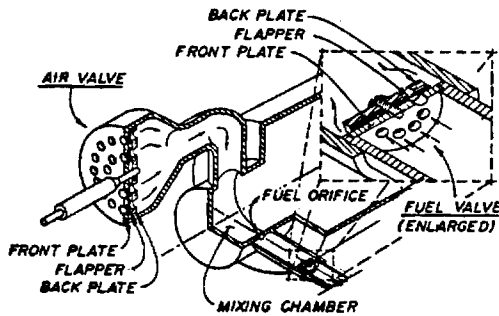


FIG. 2: SCHEMATIC OF MIXING CHAMBER WITH FUEL AND AIR VALVE ATTACHED.

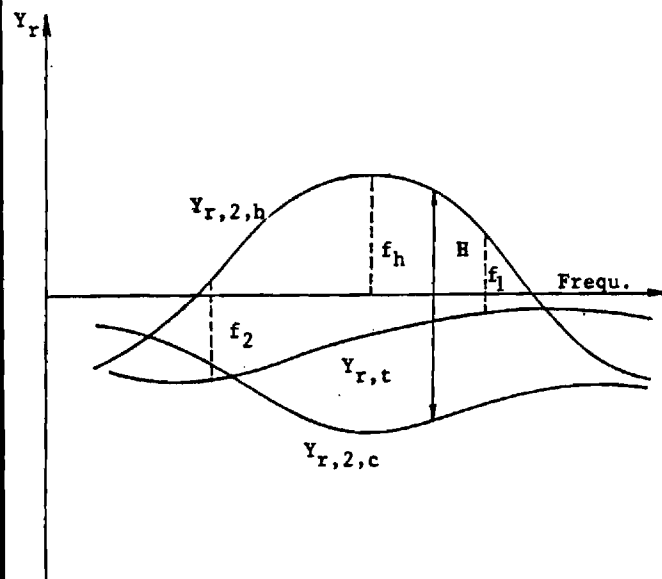


FIG. 3: HYPOTHETICAL FREQUENCY VARIATION OF THE REAL PART OF THE ADMITTANCE OF THE COMBUSTOR WITHOUT COMBUSTION ($Y_{r,2,c}$), WITH COMBUSTION ($Y_{r,2,h}$) AND OF THE TAILPIPE ($Y_{r,t}$). THE COMBUSTION PROCESS WILL DRIVE PRESSURE OSCILLATIONS AT FREQUENCY f_1 BUT NOT AT FREQUENCY f_2 .

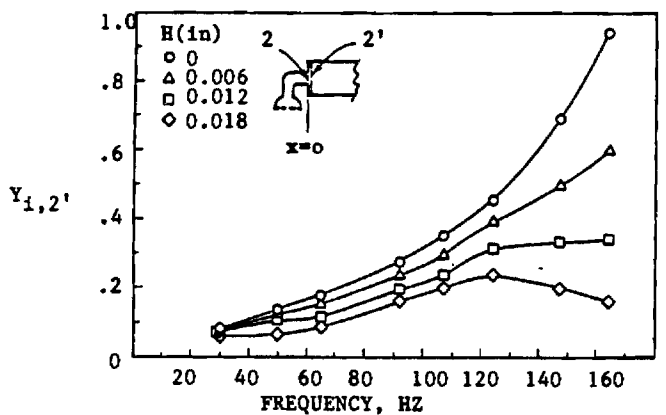
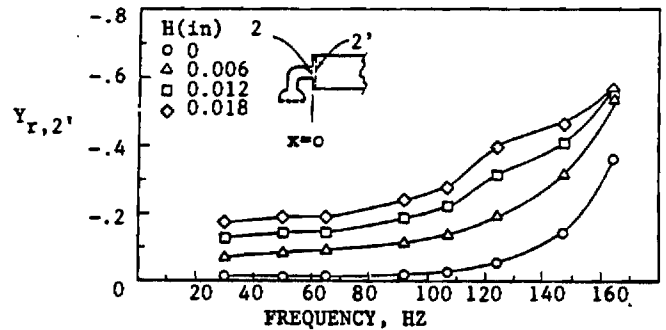


FIG. 5: VARIATION OF THE REAL (Y_r) AND IMAGINARY (Y_i) PARTS OF THE ADMITTANCE OF THE AIR VALVE WITH FREQUENCY FOR A NUMBER OF VALVE OPENINGS (H). CROSS SECTION 2' IS THAT OF THE IMPEDANCE TUBE WHILE CROSS SECTION 2 DENOTES THE EXIT AREA OF THE VALVE HOUSING.

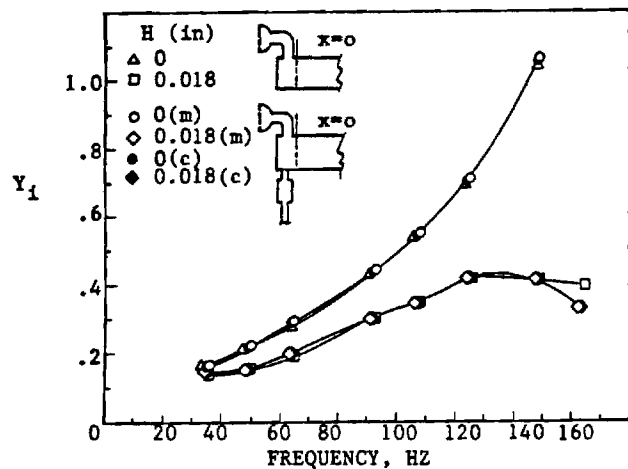
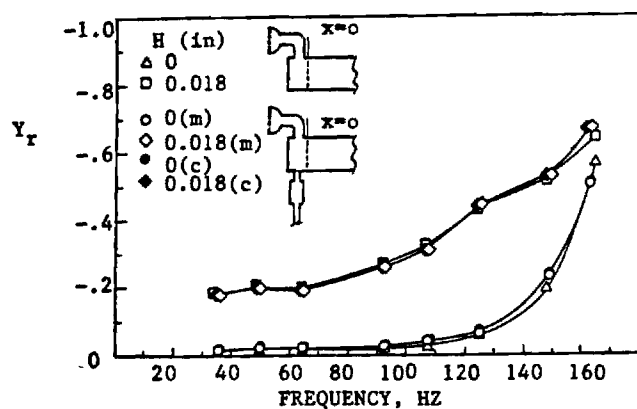


FIG. 6: VARIATION OF THE REAL (Y_r) AND THE IMAGINARY (Y_i) PARTS OF THE ADMITTANCE OF THE MIXING CHAMBER FITTED WITH (i) ONLY THE AIR VALVE AND (ii) THE FUEL AND AIR VALVES. FOR CONFIGURATION (i) ONLY MEASURED DATA ARE SHOWN WHILE FOR CONFIGURATION (ii) MEASURED (m) AND CALCULATED (c) DATA ARE COMPARED.

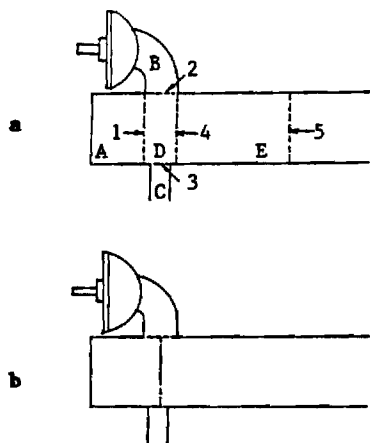


FIG. 7: SCHEMATIC OF THE MIXING CHAMBER WITH FUEL AND AIR VALVES SHOWING THE FIVE REGIONS INTO WHICH THIS ASSEMBLY HAS BEEN DIVIDED. INTERFACE 5 DENOTES THE LOCATION AT WHICH THE MIXING CHAMBER IS CONNECTED TO THE IMPEDANCE TUBE.

Pulsating Burners - Controlling Mechanisms and Performance

Semi - Annual Report

Prepared by

B. T. Zinn, B. R. Daniel and J. I. Jagoda

School of Aerospace Engineering

Georgia Institute of Technology

For

Gas Research Institute

Grant No. 5087-260-1466

GRI Project Manager

James A. Kezerle

Combustion

February 1990

RESEARCH SUMMARY

Title: Pulsating Burners - Controlling Mechanisms and Performance

Contractor: Georgia Tech Research Institute

Contract Number: 5087-260-1466

Reporting Period: July - December 1989, Semi-Annual Report

Principle Investigators: B. T. Zinn, B. R. Daniel and J. I. Jagoda

Objective: To gain further insights into the physical mechanisms which control the mixing and heat release processes in pulse combustors. In addition, the acoustic driving and damping characteristics of various components and subsystems of the pulse combustor will be determined for various operating conditions.

Technical Perspective: Although gas fired pulse combustors have been on the market for a number of years, their controlling mechanisms are still not sufficiently well understood to permit their design for different applications without resorting to costly trial and error development efforts. Proper operation of pulse combustors requires that the timing of the mixing, cycle to cycle reignition and flame spread processes produce oscillatory heat release in phase with the pressure oscillations. This requires compatibility between the acoustic properties of the various components of the pulse combustor. To develop a rational design procedure for pulse combustors, it is necessary that the various processes responsible for energy

addition to and removal from the pulsations be understood. Furthermore, data describing the acoustic properties of various pulse combustor components under different operating conditions are needed. Finally, the dependence of the acoustic characteristics of the various combustor components upon the fundamental fluid mechanical, heat transfer and combustion processes must be understood.

Technical Approach: In order to elucidate the mechanisms which control the operation of various pulse combustor configurations and determine the damping/driving characteristics of different components and subsystems of commonly used pulse combustors, the following tasks are pursued simultaneously:

1) Investigation of the flow field characteristics, mixing and heat release in pulse combustors using LDV, Schlieren, mixing visualization, radical radiation (OH, CH, CC) and Rayleigh scattering measurements.

2) Measurements of the driving and damping characteristics of various components and subsystems which make up the pulse combustor using the impedance tube technique.

3) The determination of the overall driving and damping characteristics of various pulse combustor designs under different operating conditions.

4) Modeling of the dynamic characteristics of the flapper valve.

Results: During this reporting period, use of the impedance tube technique was extended to measure the admittance of the mixing

chamber assembly in the presence of combustion. In this technique, the admittance is determined by comparing the measured shape of the standing pressure wave with the shape of the standing wave computed for different values of the admittance. This requires that the local speed of sound in impedance tube be known. As a first step, the temperature distribution in the impedance tube was mapped out using thermocouples. In addition, a long, water cooled microphone probe, which can withstand the high temperature of the combustion products, was designed and constructed. The transfer function of this probe was determined by calibration. Furthermore, the use of a two probe technique to measure admittances is being investigated. This technique would permit the determination of the admittance of the mixing chamber assembly without the need to traverse a pressure probe through the hot combustion products in the impedance tube.

In addition, the investigation into the rich limit of operation of the pulse combustor was continued. As mentioned in the last semi-annual report, a rich limit of operation of the standard pulse combustor exists near stoichiometric conditions. Since under these conditions no air from the previous cycle is available for combustion, the new fuel charges must await the late entry of the new air jet. This then appears to leave insufficient time for complete combustion of the fuel before the reaction is quenched by the returning combustion products. In order to confirm these mechanisms the entry of the air jet was further delayed by extending the duct between the air valve and the mixing chamber. As expected, this delay caused the rich limit to occur earlier. If, on the other hand, small quantities of air are

added to the combustion products before they re-enter the mixing chamber the rich limit could be, somewhat, extended.

The two dimensional imaging of the CH radiation and, thus, of the reaction rate, was continued. Images obtained at the same phase during consecutive cycles showed that the phase locked flame shapes and positions are similar but not identical for different cycles. Currently, CH radiation images are obtained at different instants during the cycle over a number of different cycles and ensemble averaged. The averaged images are sorted according to their timing during the cycle using the simultaneously recorded pressure signal as a clock. In this way, the timing and locations of cycle to cycle reignition and flame spread are obtained for a number of operating conditions.

The modification of the LDV data acquisition software which now accounts for cycle to cycle variation of operating frequency during tests has been completed. The modified software has been tested and LDV measurements in the pulse combustor are continuing.

The modeling effort has been extended to include the behavior of the entire pulse combustor. As has been previously reported, the non-linearities of the flapper valve give rise to the presence of higher harmonics in the combustor. Since the amplitudes of the higher harmonics are much smaller than those of the fundamental mode, the higher harmonics can be predicted from the fundamental mode using a linearized set of equations. Therefore, the frequency and amplitude of the fundamental mode uniquely determine the operating characteristics of the pulse combustor. The fundamental frequency and amplitude of the pulse combustor were

determined using four equations: 1. the energy equation, 2. the equation of the standing wave in the tail pipe, 3. the equation which relates the heat release to the inflow of fuel and air and 4. the linearized relation between the chamber pressure and the fuel and air flow rates. Since the pressure in the combustion chamber is uniform even though the temperature is not, the integral energy equation could be transformed into its differential form. Next, a simple model was developed which relates the heat release to the fuel flow rate via a first order delay time which accounts for the time required to mix and burn the reactants. Applying this model to the above mentioned equations revealed that the phase angle between the pressure and heat release oscillations, and, therefore, the frequency and amplitude of the fundamental mode, are strongly influenced by the fluctuating component of the heat loss to the combustor walls. The mean heat loss, on the other hand, has only a minor effect upon the characteristics of the fundamental mode. Experiments carried out using an internally insulated combustor have, indeed, shown that the insulation has a strong influence upon the operating frequency and amplitude of the pulse combustor.

The remainder of this report takes the form of a Topical Report entitled: "Controlling the Rich Limit of Operation of Pulse Combustors" accepted for presentation at the 23rd Symposium (International) on Combustion to be held in Orleans (France) July 22-27, 1990.

CONTROLLING THE RICH LIMIT OF OPERATION OF PULSE COMBUSTORS

J. -M. Tang, S. -H. Ku, B. R. Daniel, J. I. Jagoda* and B. T. Zinn

School of Aerospace Engineering
Georgia Institute of Technology
Atlanta, Georgia 30332

Subject Matter: (3) Combustion in Practical System
(17) Instability
(27) Turbulent Reacting Flows

*Corresponding author:

J. I. Jagoda

Associate Professor

School of Aerospace Engineering

Georgia Institute of Technology

Atlanta, Georgia 30332

(404) 894-3060

Word Count: 3375 words and 7 figures

ABSTRACT

This paper describes an investigation of the characteristics of the driving processes and the mechanisms which control the existence of a rich limit of operation of a gas fueled, valved, Helmholtz type, pulse combustor. Oscillating pressures and heat release rates were measured and the flow field was visualized using high speed shadowgraphy. The driving efficiency of the combustion process was quantified over a wide range of operating conditions. The results indicate that the processes which control the lean and rich limits of operation of the pulse combustor are fundamentally different. Near the lean limit of pulsations, the driving of the pulsations by the combustion process is low because of the large phase angle between the pressure and heat release oscillations. Near stoichiometric conditions, the the driving process is most efficient. Nevertheless, a rich limit is reached. This occurs because as the equivalence ratio is increased the ignition of the new fuel is delayed. A rich limit is then reached when insufficient time remains to complete the mixing and combustion of the reactants before the reaction is quenched by the backflow of combustion products. The rich limit may be extended if the time available for combustion is prolonged either through lengthening the period of oscillations or by accelerating the mixing time.

INTRODUCTION

This paper describes an investigation of the mechanisms which control the rich limit of operation of Helmholtz type, mechanically valved, non premixed, pulse combustors. Interest in developing an understanding of the mechanisms which control the operation of pulse combustors has been stimulated by the increased scope of their applications¹⁻⁴ in recent years. The increased development of pulse combustion applications has been driven by such advantages as high combustion and thermal efficiencies^{1,2}, excellent heat transfer characteristics^{5,6}, and low CO, NO_x⁷ and soot emissions. Development of new pulse combustion applications has been hampered, however, by a lack of adequate understanding of the fundamental processes which control the operation of these devices. For example, little is known about the manner in which the controlling mechanisms depend upon the scale of the pulse combustor, or the processes which control the operating ranges of these devices. Of particular interest are recent results obtained by this group and by Corliss et al.⁸ which show that gas fired, Helmholtz type, mechanically valved pulse combustors with non-premixed injection of fuel and air, possess a rich limit of operation at slightly rich operating conditions. Interestingly, this limit occurs in spite of the fact that the pulse combustor appears to be operating near its optimal conditions just before this limit is reached.

Interest in developing an understanding of the rich limit of operation of the above discussed group of pulse combustors has been stimulated by the expected need to control (e.g., extend) this limit. Capabilities for changing the rich limit will be needed if, for example, this

limit should prevent the operation future pulse combustor designs at lean operating conditions which are of interest for a specific application. Furthermore, there exist applications in, for example, metal processing where the combustor needs to be operated fuel rich, which is beyond the capabilities of the above mentioned group of pulse combustors.

Recent studies by this group⁹ have shown that the above discussed rich limit of operation of pulse combustors can be extended by lengthening the tailpipe of the combustor, which lengthens the period of the pulsations; or by injecting the combustion air under pressure, which reduces the mixing time. Furthermore, studies by Keller et al.¹⁰ have shown that a similar pulse combustor can be operated at equivalence ratios (ϕ) significantly above one as long as the fuel and air are premixed prior to injection into the combustor. In addition, Cheng et al.¹¹ have shown that increasing the temperature inside the pulse combustor by insulating the combustor walls has no measurable effect upon its rich limit of operation. Furthermore, Westbrook¹², using a kinetic model which simulates the conditions inside a pulse combustor, has concluded that "there should be no kinetically controlled rich limit near $\phi = 1$." The above observations suggest that in contrast to the premixed combustor, whose operation depends critically upon the chemical ignition delay time¹³, the rich limit for non-premixed operation is not kinetically controlled.

It is the purpose of this study to investigate the characteristics of the driving process in the pulse combustor and to elucidate the precise mechanism responsible for the existence of this rich limit. Unless this phenomenon can be satisfactorily explained, it is expected to hinder future development of pulse combustion applications.

EXPERIMENTAL SETUP

A schematic of the gas fired, valved, Helmholtz type, pulse combustor which was used in this investigation is shown in Fig. 1. It consists of a 3" long, 3" I.D., cylindrical mixing chamber; a 12.5" long, 4.4" I.D., cylindrical combustion chamber; a 76" long, 1.5" I.D., tailpipe; a 12.4" long, 12.4" I.D., decoupler; and a short vent pipe attached to the downstream end of the decoupler.

To start operation, natural gas and air are supplied through flapper valves which are attached to the curved walls of the mixing chamber at right angles to each other. After mixing, the reactants are ignited with a sparkplug. The ensuing combustion and expansion processes increase the pressure inside the mixing and combustion chambers which closes the flapper valves, and expels the hot combustion products through the tailpipe. The momentum of the exhaust gases leaving the combustor section decreases the pressure inside the mixing chamber which re-opens the valves. Fresh charges of fuel and air enter the combustor where they mix and are re-ignited by pockets of burning gases left over from the previous cycle, without the use of the sparkplug. The resulting pulse combustion process will be maintained indefinitely.

In the present study, natural gas was supplied to the combustor at five inches of water pressure while air was aspired at atmospheric or elevated pressure. The fuel and air flow rates were measured using rotameters which were separated from the flapper valves by decoupling chambers in order to eliminate flow fluctuations at the meters. While the fuel flapper valve setting was kept fixed, the air flow rate and, therefore,

the equivalence ratio could be varied by adjusting the allowed travel distance of the air flappers¹⁴. The amount of fuel entering the combustor varied between .87 and 1 SCFM as the equivalence ratio was changed since the fuel flow rate depends upon the amplitude of the pressure oscillations in the mixing chamber which, in turn, is controlled by the fuel/air ratio.

The flat wall at the upstream end of the mixing chamber and the walls of the steps between the mixing and the combustion chamber, and between the combustion chamber and the tailpipe were made out of quartz to provide optical access. In addition, flat, rectangular, longitudinal quartz windows were fitted into the mixing and combustion chamber walls as shown in Fig. 2.

The oscillating pressures in the combustor were measured using Kistler piezoelectric pressure transducers mounted in semi-infinite tube configurations several inches from the combustor. This protects the transducers from the combustor heat while providing a flat frequency response. The signals from the pressure transducers were amplified and passed through a Preston A/D converter into an HP A700 computer.

A shadowgraphy system was used to view the mixing and combustion processes along the combustor axis (see Fig. 2) as well as normal to this axis through the side windows. Along the axis, the beam through the mixing and combustion chambers was arranged to be slightly converging rather than collimated, which permitted it to exit the combustor without being obstructed by the tailpipe. All shadow images were recorded at a rate of 7000 frames per second using a HICAM high speed camera. Pressure traces from an oscilloscope were also recorded on

the film to provide a clock which was used to time the occurrences of various events with respect to the pressure cycle.

The reaction rate intensities in the pulse combustor were determined by measuring the CC radical concentration¹⁵. The radiation at 515.5 nm from the entire combustion process was focused using a large diameter lens through an interference filter and a pin hole onto a Hamamatsu R269 photomultiplier. The photomultiplier output was amplified, digitized and recorded using a computer.

A computer program was developed which acquired and analyzed the pressure and radiation data, simultaneously. The software permitted displaying of time traces of both signals and calculating their auto- and cross-correlations using FFT routines. Thus, the spectra and phase angles between the radiation and pressure signals could be determined. In addition, the radiation signals were correlated with the high speed shadowgraphy movies using the pressure signals as a clock.

RESULTS AND DISCUSSION

Generally, to attain pulse combustion operation, the energy added to the pulsations by the combustion process during the combustor startup phase must exceed the wave energy dissipated or lost due to, for example, viscous dissipation and acoustic radiation through the valves and tail pipe. Since the wave driving and damping processes are amplitude dependent, the amplitude of combustor oscillations grows until it reaches a "final", limit cycle, amplitude. The magnitude of the limit cycle amplitude is determined by the condition that the time averages of the rates of energy addition and removal from the waves, over one period of the oscillation,

equal one another. The combustor will continue to operate at this amplitude as long the balance between the energy addition and removal processes is not disturbed. A limit of the pulse combustor operation occurs when the above described relationships between the driving and damping processes fail to materialize.

According to Rayleigh's Criterion¹⁶, driving of pulsations can only occur if the the following relationship is satisfied:

$$\iint_{V_T} p(\vec{x}, t) q(\vec{x}, t) dt dV \approx |P| |Q| \cos \theta \quad (1)$$

where p , q , P , Q and θ are the amplitudes of the local oscillatory pressure, and combustion heat release rates; total pressure and total combustion heat release rates; and the phase angle between the pressure and total combustion heat release rate oscillations, respectively. Equation 1 has been derived by assuming that the instantaneous pressure is nearly uniform in the combustor and, consequently, it was taken outside the integral. Furthermore, as mentioned above, CC radiation measurements were used to determine the magnitudes of the heat release rates.

Figure 3 presents the time dependence the product of the ensemble averaged instantaneous values of p' and q' , which represent the integrand of the integral in Eq. 1 above, for several different operating conditions of the combustor shown in Fig. 1. When this product is positive, the combustion process drives the pressure oscillations, and vice versa. A measure of the net amount of driving provided by the combustor under a given operating condition can be obtained by integrating the appropriate curve in Fig. 3 over a cycle, which is equivalent to evaluating the integral

Fig 3

in Eq. 1. Another, equivalent, way to express the combustor driving is by means the dimensionless Rayleigh efficiency η which is defined by¹⁷

$$\eta = \frac{R}{C_p \bar{P} \bar{Q}} \int_0^1 p' Q' d\tau \approx \frac{|p| |Q| \cos \theta}{C_p \bar{P} \bar{Q}} \quad (2)$$

where p , Q and θ were defined below Equ. (1) above, and R , C_p , and τ are the ideal gas constant, the specific heat at constant pressure and the nondimensional time, respectively; bars, primes and brackets represent steady state, oscillating and amplitudes of the indicated quantities, respectively.

The dependences of the Rayleigh efficiencies of the combustor shown in Fig. 1, fitted with a standard (i.e., $l=76"$) and an extended tailpipe (i.e., $l=145"$), upon the equivalence ratio ϕ are presented in Fig. 4. The maximum ϕ at which each curve stops represents the rich limit of operation of that particular combustor configuration.

The data presented in Figs. 3 and 4 indicate that near the lean limit the driving is small, just enough to overcome the system damping. In contrast, near the rich limit for the combustor fitted with the standard tailpipe (i.e., near $\phi=1.1$), the driving is close to its maximum. Thus, the mechanism which controls this rich limit appears to be fundamentally different from that which controls the lean limit. However, when the tailpipe was extended, the rich limit of the combustor operation increased beyond stoichiometric conditions to a value of $\phi=1.33$. For this combustor, the Rayleigh efficiency η increases with ϕ , when ϕ is smaller than one, reaching a maximum at $\phi=.94$, and decreasing thereafter until the rich limit is reached (see Fig. 4). On the other hand, when the combustor was

Fig 4

operated without a tailpipe, pulsating operation could be only sustained when the air supply pressure was above a certain level, below which the combustion was steady.

The Rayleigh efficiencies presented in Fig. 4 were calculated, using Eq. 2, from measured ensemble averaged instantaneous values of the combustor pressure and the total CC radiation. The dependence of the pressure and radiation amplitudes, and the phase difference θ upon the equivalence ratio ϕ are presented in Figs. 5 and 6, respectively. These data show that starting at low values of ϕ , $|P|$ and $|Q|$ increase until they reach their maximum values near stoichiometric conditions. Thereafter, they decrease. On the other hand, the phase difference θ starts at a maximum value of nearly 65 degrees, and decreases as ϕ increases until it asymptotically reaches a nearly constant value which depends upon the length of the tail pipe, see Fig. 6.

In order to explain the reasons for the occurrence of the rich limit, the behavior of $|P|$, $|Q|$ and θ , in Figs 5 and 6 need to be explained. This will be done by considering how the combustor processes change as the air valve is gradually closed during a test. Before this is done, it will be helpful to consider Fig. 7 where the time dependences of the pressure and radiation oscillations, under lean and rich operating conditions, are presented. For easier comprehension, the period of oscillation and the pressure amplitude have been normalized, resulting in a single pressure trace. Arrows on the pressure curve mark the instants during the cycle at which the fuel and air jets enter the combustor. Horizontal lines at the top of the figure indicate the periods of time when the gases flow away from and towards the mixing chamber, where most of the combustion occurs.¹⁷ As discussed later, the backflow extinguishes the combustion process which

will be seen to be a major contributor to the rich limit. The data presented in Fig.7 are based upon high speed shadowgraphy, and pressure and radiation measurements conducted during experiments near the operating limits.

Keeping in mind that the re-ignition of injected fuel occurs at the instant when the magnitude of the radiation signal starts to increase after it has reached a minimum (i.e., points marked X in Fig. 7), the plots in Fig. 7 show that re-ignition under lean operating conditions occurs before the air has entered the combustor. This can occur because the fresh fuel can ignite as soon as it has mixed with the air remaining from the previous cycle. However, as ϕ is increased, less combustion air is left over from the previous cycle and the combustion process is delayed. Once stoichiometric conditions are approached, reignition must await the entry of the air jet, see Fig. 7. Since the heat release oscillations always lead the pressure oscillations, the above phenomenon explains the decrease in the phase angle θ between q' and p' as ϕ is increased, see Fig. 6.

The delay in the ignition of the new fuel charge with increasing ϕ also explains the trends in p' and q' shown in Fig. 5. The pressure p' increases as ϕ increases because of the decrease in θ , as long as the combustor is operating lean. Furthermore, because the fuel flow rate for a fixed fuel valve setting increases with increasing pressure amplitudes in the mixing chamber, the increase in p' causes a corresponding increase in q' . However, once ϕ exceeds one, q' is reduced due to incomplete combustion caused by the shortage in air. This, in turn, reduces p' . The decrease in pressure amplitudes reduces the reactant flow rates into the combustor, which lowers q' even further.

The magnitudes of p' and, therefore, of q' and η for the combustor fitted with the long tail pipe are lower than those for the combustor with the standard tailpipe, see Figs. 4, 5 and 6. This is caused by the increased acoustic damping in the longer tailpipe. The increased damping reduces p' which, in turn, reduces the fuel inflow and, thus, q' .

The rich limit of operation of the standard combustor near stoichiometric conditions can now be explained with the aid of Fig. 7. The time available for the reactants to mix and react is limited to the time interval between the instant of ignition of the fresh fuel and the instant at which the combustion is quenched by the flow of combustion products back into the mixing chamber. If reignition is delayed too long, the time period available between ignition and quenching is too short and the heat release in this time interval is insufficient to drive pulsations. This occurs at the rich limit.

When the duration of the cycle was prolonged by lengthening the tailpipe, the time available for combustion increased and the rich limit was extended to higher values of ϕ . On the other hand, when the tailpipe was removed the period of oscillations, and consequently the time available for combustion, decreased. In this case, pulsations could only be driven if ignition occurred earlier and the time required to complete the combustion process was shortened. Both effects can be achieved if the air upstream of the flapper is pressurized. Indeed, as reported earlier, pressurizing the air to above a certain threshold produced a transition between steady and pulsating operation in the pulse combustor without a tailpipe.

Also, since it has been argued that the existence of the rich limit depends critically upon the timing of the air entry into the mixing

chamber, this time was varied by changing the length of the elbow-shaped pipe that connects the air valve to the mixing chamber, see Fig. 1. Because the length of this pipe in the standard configuration is only 1-1/2", it could not be significantly shortened without affecting the overall flow pattern of the air in the mixing chamber. Consequently, the air inlet pipe was lengthened to 5", which further delayed the entry of the air into the mixing chamber. As expected, the rich limit now occurred at a fuel-air ratio below one, since even less time was available for combustion.

Finally, the hypothesis that the returning combustion products quench the combustion process was tested by injecting small quantities of air into the combustion products just downstream of the mixing chamber through a small diameter pipe. This additional air did, indeed, increase the rich limit slightly, although the effect depended critically upon the precise position of the air injection.

CONCLUSIONS

This study has shown that the mechanisms which are responsible for the lean and rich limits of operation of a gas fueled, valved, Helmholtz type, pulse combustor are fundamentally different. Near the lean limit, the driving by the combustion process barely exceeds the system damping because of the large phase angle between the pressure and heat release oscillations. On the other hand, near the rich limit of operation the driving is at its most efficient.

It has been determined that this rich limit is not kinetically controlled. Instead, it occurs when the time period between the ignition of the fresh fuel charges and the quenching of the reaction by the

combustion products flowing back into the mixing chamber is too short for the reactants to mix and burn. Not sufficient heat is then released to drive the pulsations. This is the case near stoichiometric conditions when the ignition of the fresh fuel must await the entry of the air jet. If the time available for mixing and combustion is prolonged or the time for mixing is reduced, the rich limit can be significantly extended. On the other hand, if this time is reduced, the rich limit of operation of the pulse combustor occurs at a lower equivalence ratio.

ACKNOWLEDGEMENT

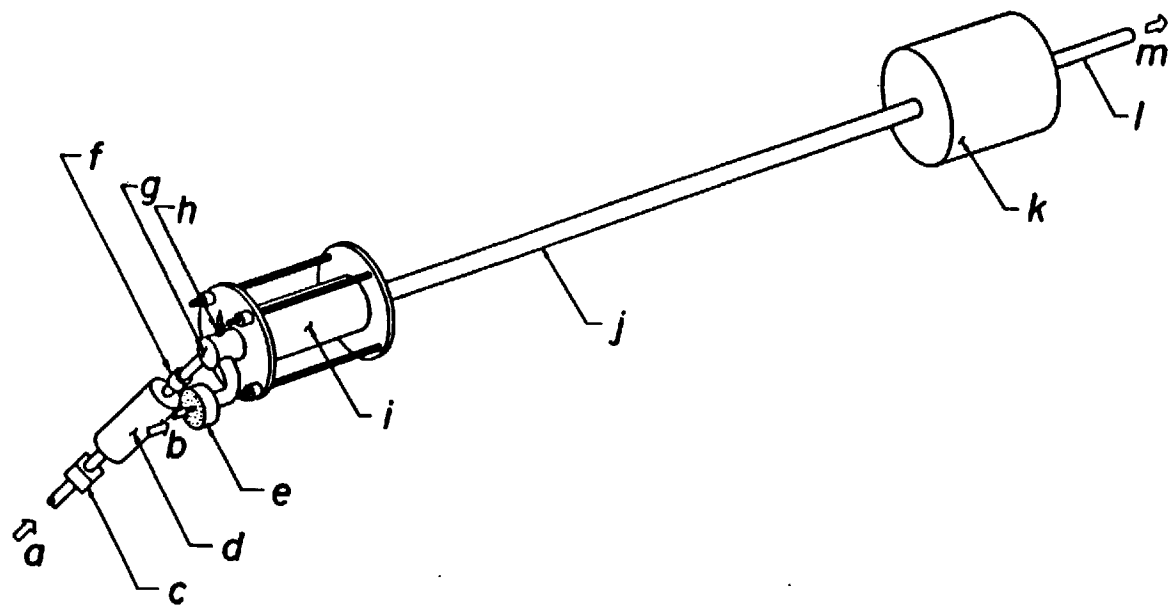
This work is supported by the Gas Research Institute under Grant No. 5087-260-1466. Mr. J. Kezerle is the monitor.

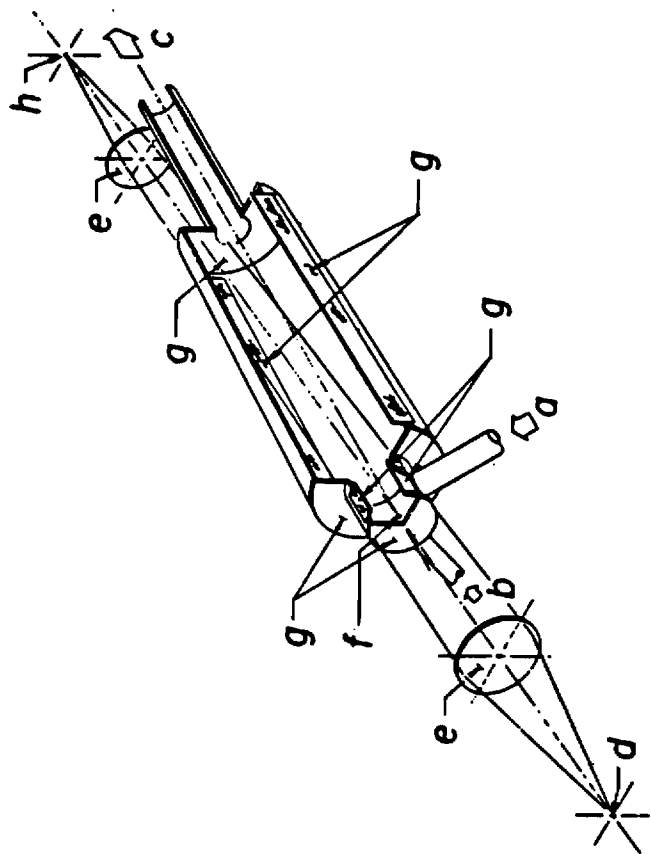
REFERENCES

1. "Lennox-Pulse-G14 Series Up-Flo Gas Furnaces," Engineering Data, Heating Units, Gas, pp. 21-24, published by Lennox Industries, Inc.
2. Hydropulse by Hydrotherm," information about pulsed combustion water hearing published by Hydrotherm, Rolfland Ave., Northvale, NJ 07647
3. Flanigan, P., AGA Laboratories: "Development of a Pulse Combustion Industrial Dryer, Phase I "Final Report to Gas Research Institute, 1987/
4. Kezerle, J., Gas Research Institute, Chicago, IL: personal communication
5. Hanby, V. I.: "Convective Heat Transfer in a Gas-Fired Pulsating Combustor," Paper No. 68-WA/FU-1 (1968).
6. Fedorov, B. N.: "Experimental Study of the Effect of Acoustic Oscillations on Heat Transfer in a Gas Flow., Juzherno-Fisicherkii Zhurnal, Vol. 32, No. 1, pp. 167-180, 1977.
7. Belles, F. E.: "R & D and Other Needs for Exploitation of Pulse-Combustion in Space-Heating Applications," Proc. of Symp. on Pulse-Combustion Technology for Heating Applications, Argonne National Laboratory, pp. 167-180, 1979.
8. Corliss, J. M, Battelle Columbus Laboratories : Annual Report, Gas Research Institute Report GRI 85/0029, April 1985.
9. Ku, S. H., Cheng, X. C., Daniel, B. R., Jagoda, J. I., and Zinn, B. T.: "Radiation Measurements in a Gas Fired Pulse Combustor," presented at the Spring Technical Meeting of the Central States Section of the Combustion Institute, Chicago, IL, 1987.
10. Dec, J. E. and Keller, J. O.: "The Effect of Fuel Burn Rate on Pulse Combustor Tailpipe Velocities," presented at the 1986 International Gas Research Conference, Toronto, Canada, September 1986.
11. Cheng, X. C., Daniel, B. R., Jagoda, J. I. and Zinn, B. T.: "Dependence of Pulse Combustion Performance upon Interior Temperature, Acoustic Losses and Combustion Time," presented at the

1989 International Gas Research Conference, Tokyo, Japan,
November 1989.

12. Westbrook, C. K.: "Successive Reignition of Fuel-Air Mixtures and Pulse Combustion," presented at the 1985 Fall Meeting of the Western States Section of the Combustion Institute, Davis, CA, October 1985.
13. Keller, J. O., Dec, J. E., Westbrook, C. K. and Bramlette, T. T.: Combustion and Flows, 75, pp. 33-44 (1989).
14. Griffiths, J. C. and Weber, E. J.: "The Design of Pulse Combustion Burners," Research Bulletin 107, American Gas Association Laboratories, June 1969.
15. Gadon, A. G. and Wolfhard, H. T.: "Flames," Chapman, R. and Hall Ltd, 1970.
16. Lord Rayleigh: "The Theory of Sound," Vol. II, pp. 224-235, Dover, 1945.
17. Reuter, D., Daniel, B. R., Jagoda, J. I. and Zinn, B. T.: Combustion and Flame, 65, pp. 281-290, (1986).





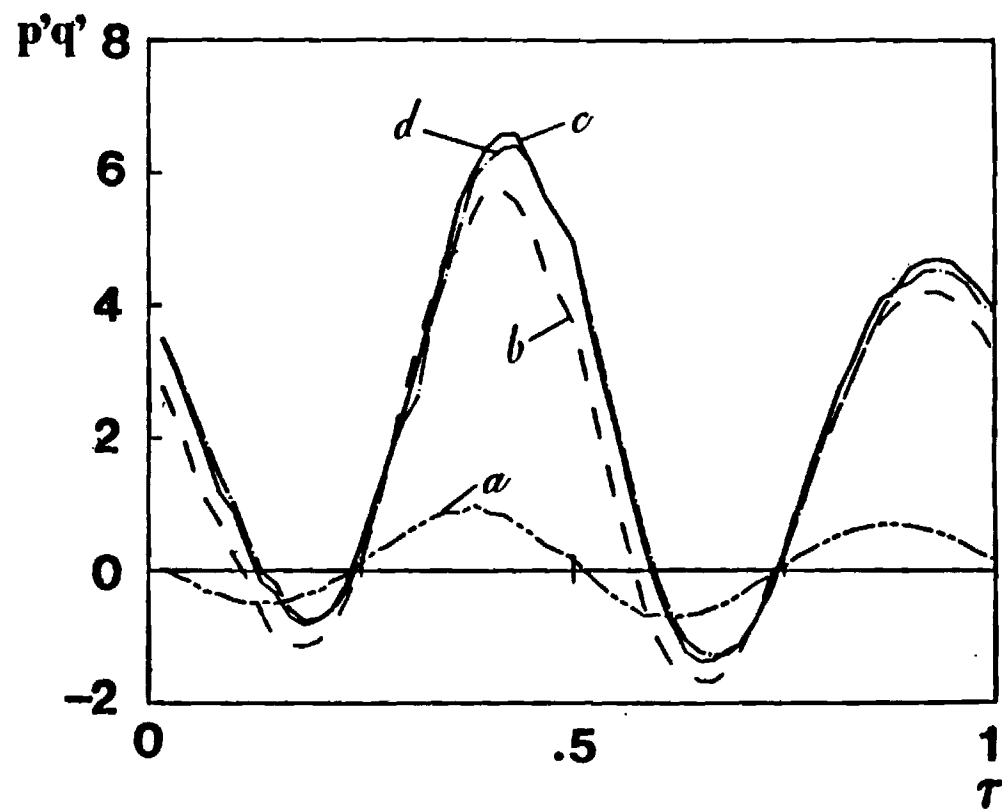
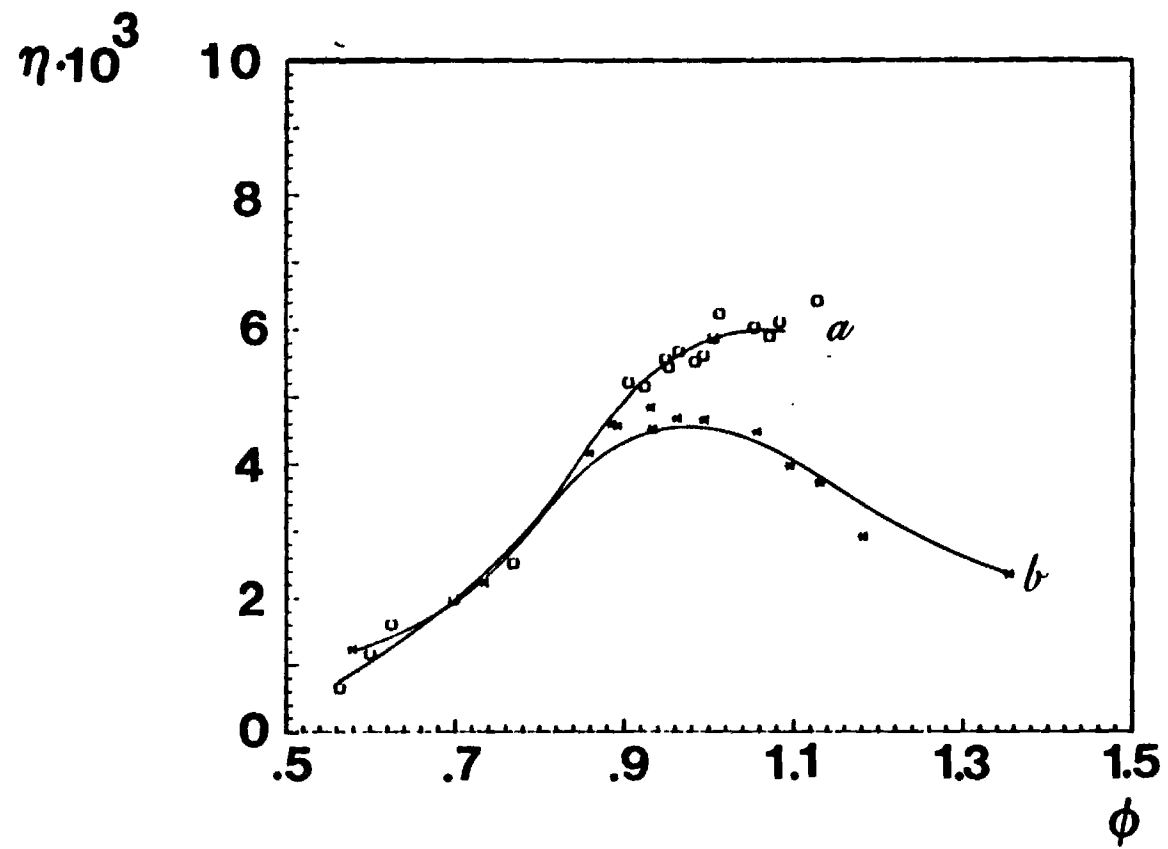


Fig. 3



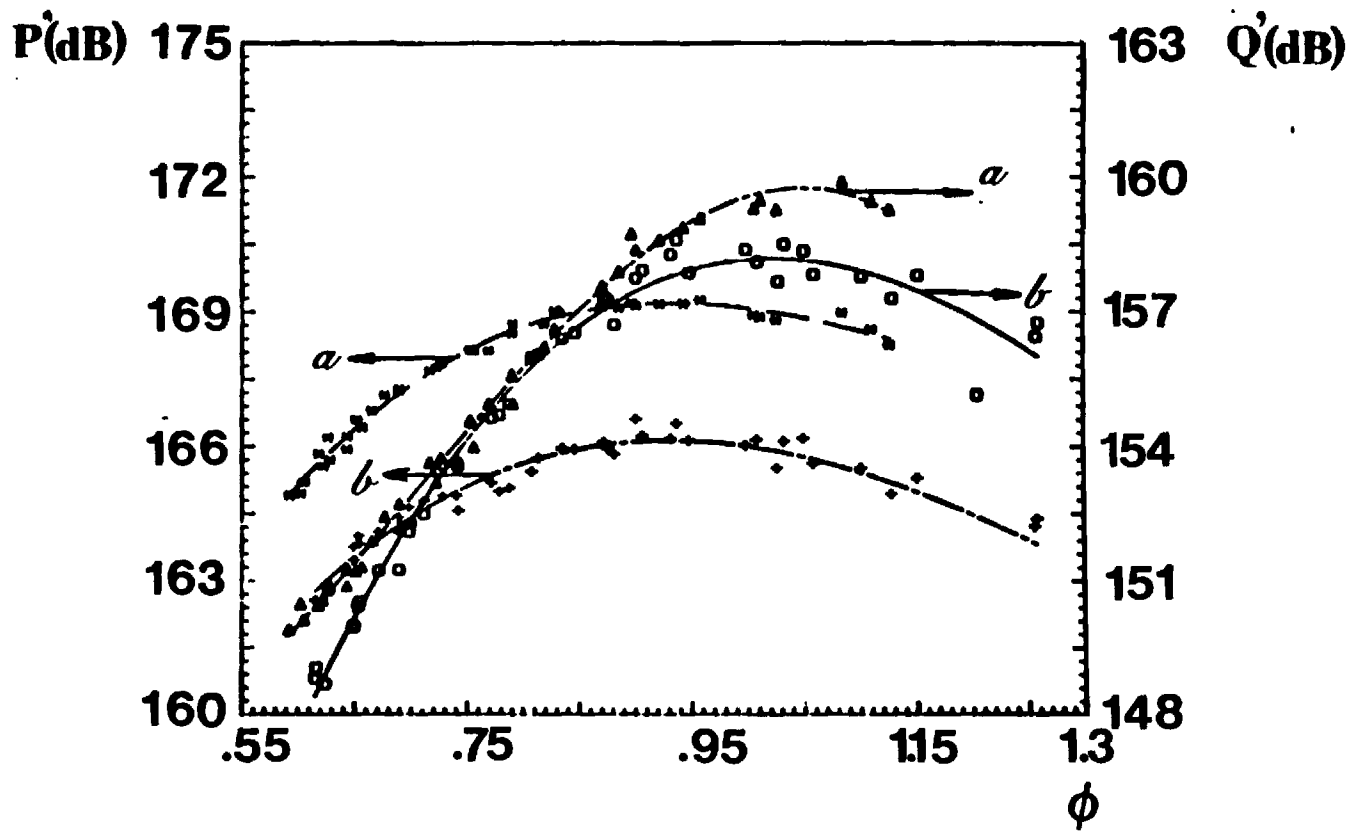
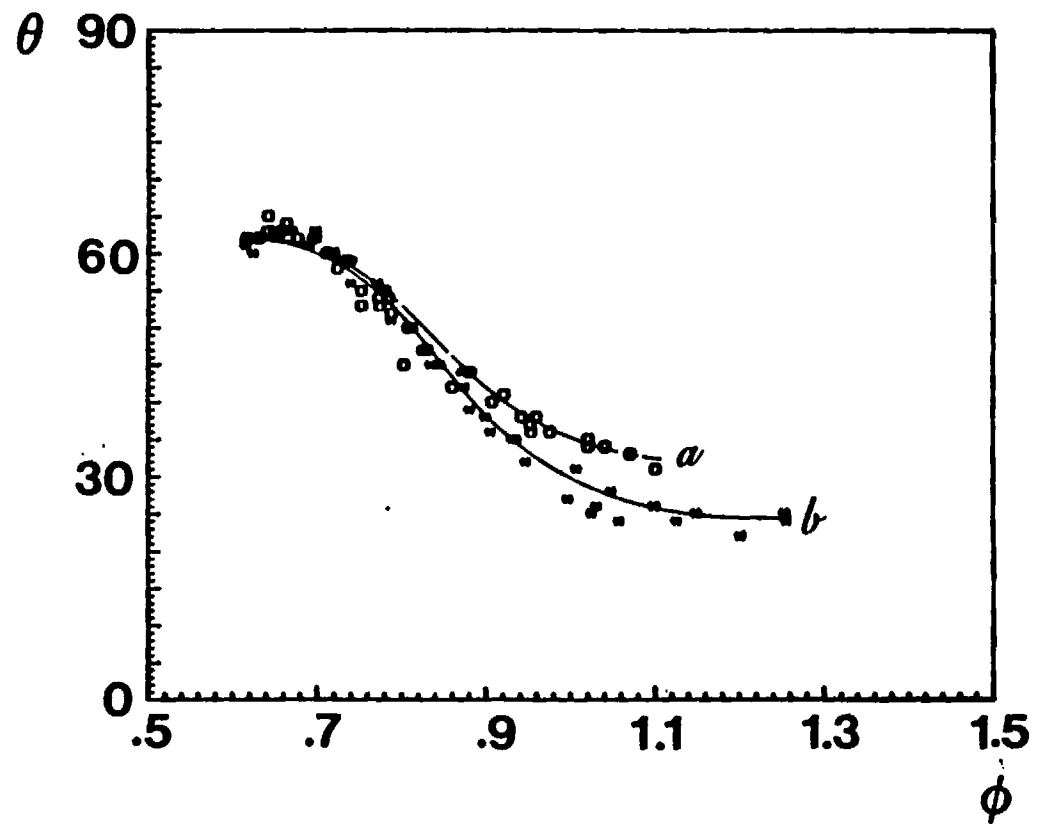


Fig 5



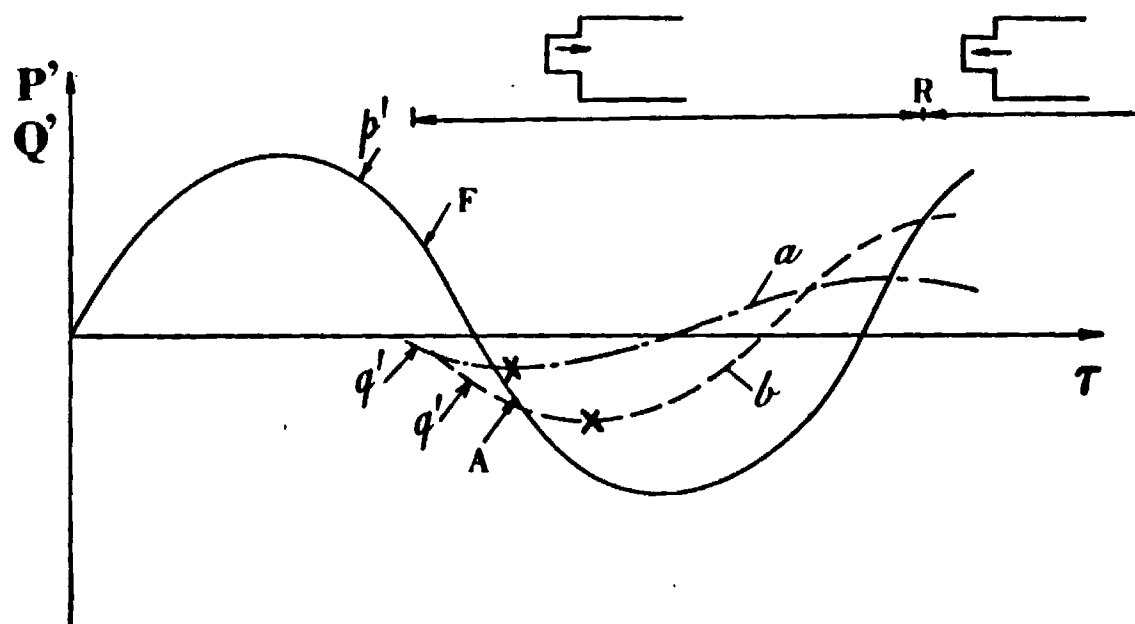


Fig. 7

FIGURE LEGENDS

Fig. 1: Schematic of the Pulse Combustor showing a) Fuel Inlet, b) Air Inlet, c) Solenoid Valve, D) Fuel Decoupler, e) Air Flapper Valve, f) Fuel Flapper Valve, g) Mixing Chamber, h) Sparkplug, i) Combustion Chamber, j) Tailpipe, k) Decoupler, l) Vent Pipe, m) Exhaust Gases.

Fig. 2: Schematic of the Pulse Combustor indicating Quartz Windows and Optical Lay-out for Axial Shadowgrams; a) Air Inlet, b) Fuel Inlet, c) Exhaust, d) Light Source, e) Collimating Lenses, f) Fuel Orifice, g) Quartz Windows, h) Focus.

Fig. 3: Instantaneous Values of $p'q'$ Over One Cycle at, a) the Lean Limit, b) $\phi = 8$, c) $\phi = 1$, d) the Rich Limit.

Fig. 4: Rayleigh Efficiency (η) vs Equivalence Ratio (ϕ) for the Combustor filled with, a) the Standard Tailpipe ($l=76''$), and b) the Extended Tailpipe ($l=145''$).

Fig. 5: Pressure (P') and Heat Release (Q') Amplitudes vs Equivalence Ratio (ϕ) for the Combustor Fitted with, a) the Standard Tailpipe ($l=76''$) and, b) the Extended Tailpipe ($l=145''$).

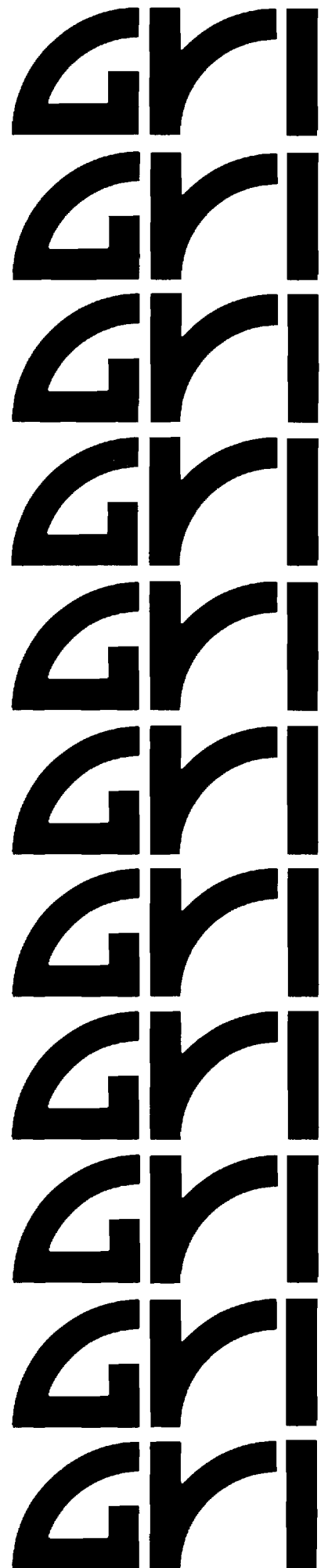
Fig. 6: Phase Angle (θ) by which the Heat Release Oscillations Lead Those of the Pressure vs Equivalence Ratio (ϕ) for the Combustor Fitted with, a) the Standard Tailpipe ($l=76''$), and b) the Extended Tailpipe ($l=145''$).

Fig. 7: Normalized Pressure (P') Cycle Showing the Relative Timing of the Heat Release Oscillations (q') Near the Lean (a) and Rich (b) Limits; Fuel Enters at F, Air enters at A, Backflow into the Mixing Chamber Starts at R; X's Denote the Instants of Reignition of Fresh Fuel Charges.

**PULSATING BURNERS
CONTROLLING MECHANISMS AND PERFORMANCE**

**ANNUAL REPORT
(January — December 1987)**

**Gas Research Institute
8600 West Bryn Mawr Avenue
Chicago, Illinois 60631**



Pulsating Burners - Controlling Mechanisms and Performance

Annual Report

January 1, 1987 - December 31, 1987

Prepared by

B. T. Zinn, B. R. Daniel and J. I. Jagoda

School of Aerospace Engineering
Georgia Institute of Technology

For

Gas Research Institute
Grant No. 5083-260-1466

GRI/88-0133

GRI Project Manager

James A. Kezerle

Combustion

January 1988

GRI DISCLAIMER

LEGAL NOTICE: This report was prepared by the Georgia Institute of Technology as an account of work sponsored by the Gas Research Institute (GRI). Neither GRI, members of GRI, nor any person acting on behalf of either:

- a. Makes any warranty or representation, express or implied, with respect to the accuracy, completeness, or usefulness of the information contained in this report, or that the use of any apparatus, method, or process disclosed in this report may not infringe privately owned rights; or
- b. Assumes any liability with respect to the use of, or for damages resulting from the use of, any information, apparatus, method, or process disclosed in this report.

REPORT DOCUMENTATION PAGE	1. REPORT NO.	2.	3. Recipient's Accession No. GRI-88/0133					
4. Title and Subtitle Pulsating Burners - Controlling Mechanism and Combustion			5. Report Date May 88 (approved)					
6. Author(s) T. Zinn, B. R. Daniel and J. I. Jagoda			7. Performing Organization Rept. No.					
8. Performing Organization Name and Address School of Aerospace Engineering Georgia Institute of Technology Atlanta, GA 30332			10. Project/Task/Work Unit No. E-16-601 11. Contract(C) or Grant(G) No. (C) 5087-260-1466 (G)					
9. Sponsoring Organization Name and Address S Research Institute 100 West Bryn Mawr Ave. Chicago, IL 60631			13. Type of Report & Period Covered Annual Jan 1,87 - Dec 31,87 14.					
15. Supplementary Notes								
16. Abstract (Limit: 200 words) This report describes the results of an ongoing investigation into the physical and chemical processes which control the operation of gas fired, valved combustors obtained during 1987. It is the aim of this investigation to develop a more rational approach towards the design of future combustors. An investigation of the importance of the duration and phase of the combustion process relative to the pressure oscillations showed that the combustor tends to pulse with a frequency whose period equals approximately, twice the characteristic combustion time. Radical radiation measurements indicated that cycle to cycle reignition occurs downstream of the plane of fuel and air injection. Local mean velocities and turbulence intensities were determined from ensemble averaged laser Doppler velocimetry measurements. The flow field is clearly dominated by the air jet which produced a large axial vortex in the mixing chamber soon after its entry into the combustor. An impedance tube technique was used to measure the admittance of the air valve. Preliminary tests showed that the admittance of and, thus, the damping by the flapper valve increase with increased valve gap. Finally, the behavior of the air valve is being modeled. The second part of the document consists of a topical report dealing with an investigation into the operational limits of the pulse combustor.								
17. Document Analysis a. Descriptors Pulse Combustor								
18. Identifiers/Open-Ended Terms Reignition, Operational Limits, Visualization, Valve Dynamics.								
<table border="1"> <tr> <td data-bbox="0 1816 777 1900" rowspan="2"> 19. OSATI Field/Group Combustion 20. Availability Statement: </td> <td data-bbox="777 1816 1162 1900"> 19. Security Class (This Report) Unclassified </td> <td data-bbox="1162 1816 1419 1900"> 21. No. of Pages </td> </tr> <tr> <td data-bbox="777 1900 1162 1959"> 20. Security Class (This Page) Unclassified </td> <td data-bbox="1162 1900 1419 1959"> 22. Price </td> </tr> </table>				19. OSATI Field/Group Combustion 20. Availability Statement:	19. Security Class (This Report) Unclassified	21. No. of Pages	20. Security Class (This Page) Unclassified	22. Price
19. OSATI Field/Group Combustion 20. Availability Statement:	19. Security Class (This Report) Unclassified	21. No. of Pages						
	20. Security Class (This Page) Unclassified	22. Price						

RESEARCH SUMMARY

Title: Pulsating Burners - Controlling Mechanisms and Performance

Contractor: Georgia Tech Research Institute

Contract Number: 5087-260-1466

Report Period: January - December 1987, Annual Report

Principle Investigators: B. T. Zinn, B. R. Daniel and J. I. Jagoda

Objective: It is the objective of this study to gain further insights into the physical mechanisms which control the mixing and heat release processes in pulse combustors. In addition, the acoustic driving and damping characteristics of various components and subsystems of the pulse combustor will be determined for various operating conditions. Finally, the above findings will be used to explain the performance of various combustor configurations to be tested and should be of considerable help to the designers of novel pulse combustors.

Technical Perspectives: Although gas fired pulse combustors have been on the market for a number of years, their controlling mechanisms are still not sufficiently well understood to permit the design of pulse combustors for different applications without resorting to costly trial and error development efforts. To attain pulse combustion operation, the energy supplied to the pulsations by the combustion process must be larger than the acoustic energy lost due to viscous dissipation, heat transfer, acoustic radiation and so on. Proper operation of pulse combustors also requires that mixing, cycle to cycle reignition and flame spread occur such that the oscillations of heat release be in phase with those of the pressure. In addition, the acoustics of the various components and subsystems of the pulse combustor must be matched appropriately. Thus, to develop a rational design procedure for pulse combustors, it is required that the various processes responsible for energy addition and removal to and from the pulsations be understood. Furthermore, data describing the acoustic properties of various pulse combustor components under various cold and pulse combustion operation conditions are needed. Finally, the dependence of the acoustic characteristics of the various combustor components upon the fundamental fluid mechanical, heat transfer and combustion processes must be understood. The attainment of these goals is pursued under this project.

Technical Approach:

In order to elucidate the mechanisms which control the operation of various pulse combustor configurations and determine the damping/driving characteristics of various components and subsystems of commonly used pulse combustors, the following tasks will be pursued simultaneously:

- 1) Investigation of the flow field characteristics, mixing and heat release in pulse combustors using LDV, Schlieren, mixing visualization, radical radiation (OH, CH, CC) and Rayleigh scattering measurements.
- 2) Measurements of the driving and damping characteristics of various components and subsystems which make up the pulse combustor using the impedance tube technique.
- 3) The determination of the overall driving and damping characteristics of various pulse combustor designs under different operating conditions.
- 4) Modeling of the dynamic characteristics of the flapper valve.

Results:

During the past year the importance of the duration and phase of the combustion process relative to the pressure oscillations was investigated. A Schmidt tube type pulse combustor was used in this study since it provided pulsations of up to 180 dB even at low frequencies. As the length of the combustor was extended the operating frequency dropped until, at a given tube length the frequency of pulsations "jumped" to a higher harmonic. However, this jump could be avoided if the time required for combustion was extended by slowing down the mixing process. This demonstrated that the combustion time must be compatible with the period of oscillations of the pulse combustor. The combustor tends to pulse with a frequency whose period equals, approximately, twice the characteristic combustion time.

Radical radiation measurements were carried out through flat windows in the curved walls of the mixing and combustion chambers. Cycle to cycle reignition was found to occur in the mixing chamber, 2.3 inches downstream of the plane of fuel and air injection. From there the flame spread in both the upstream and downstream directions.

Laser Doppler Velocimetry measurements were carried out at various locations in the mixing chamber. The LDV data were ensemble averaged in order to obtain instantaneous mean velocities and turbulence

intensities at different phases during the cycle. The flow field was clearly dominated by the air jet which produced, a large, axial vortex in the mixing chamber, soon after its entry into the combustor. The turbulence intensities were high throughout the cycle but increased further after entry of the air jet and during the combustion phase of the cycle.

The impedance tube to be used for measuring the admittances of the individual components which make up the combustor was set up and checked out. Preliminary test were carried out in which the admittance of the air valve was measured as a function of air valve spacing. It was shown that the real part of the admittance and, therefore, the damping increase when the gap in the air valve is increased.

The behavior of the air valve is being modeled by using integral versions of the appropriate continuity and momentum equations and the equation of motion of the flapper. Preliminary results indicate that the time required to open or close the valve decreases with flapping frequency. By comparing the times required to open and close the flapper valve with the duration of the cycle it was determined that even for frequencies above 150 Hz the valve is in the completely open or shut position for, at least, one third of the cycle.

The remainder of this report is a Topical Report dealing with an investigation into the operational limits of pulse combustors.

Project Implications:

The research conducted on this contract has been directed at resolving several of the remaining issues and anomalies in pulse combustion. This report attempts to explain the observed limits of operation and the physical processes that determine them. In doing so, it presents the first data on how Rayleigh's efficiency changes with "Stoichiometry" in a non-premixed pulse combustor. These results support the findings of other investigators working with premixed combustors. Additional research is needed to make this procedure predictive, and not just analytical. Further quantification of the ignition timing will be pursued during the rest of this contract, in addition to research on other aspects of the system.

Project Manager

James A. Kezerle
Manager, Combustion
Physical Sciences Department

TOPICAL REPORT

FLAME SPREAD AND LIMITS OF OPERATION OF GAS FIRED, MECHANICALLY VALVED, PULSE COMBUSTORS

S. H. Ku, B. R. Daniel, J. I. Jagoda and B. T. Zinn

School of Aerospace Engineering
Georgia Institute of Technology
Atlanta, GA 30332

ABSTRACT

This paper describes the results of an investigation of the cycle to cycle reignition process and flame spread in gas fired, mechanically valved, pulse combustors. The measured data are also used to explain the mechanisms responsible for the existence of previously observed rich and lean limits of operation of the investigated pulse combustor. High speed Schlieren cinematography, acoustic pressures and radical radiation (and, therefore, heat release rate) measurements were carried out in a combustor specifically developed for this study. Cycle to cycle reignition of the new fuel charges was observed to take place in the mixing chamber, downstream of the plane of injection of the reactants. From there, the flame spreads throughout the mixing chamber and into the combustion chamber. The instant of reignition depends upon the equivalence ratio and it occurs earlier during the cycle the lower the equivalence ratio. At low equivalence ratios, the entering fuel reacts with air supplied during the previous cycle. The lean limit of operation of the pulse combustor is reached when a substantial fraction of the fuel burns too early during the cycle causing a significant amount of combustion energy to be released out of phase with the pressure oscillations, which damps the pulsations. As the equivalence ratio increases, the amount of air from the previous cycle available for combustion is reduced causing a decrease in the phase difference between the heat release and pressure oscillations. The rich limit is reached when a shortage of air appears to reduce the amount of fuel which can react in phase with the pressure oscillation to a level which is not sufficient for driving the combustor pulsations.

INTRODUCTION

Interest in pulse combustors has been increasing rapidly in recent years. Small pulse combustors have been successfully utilized in domestic space and water heating^{1,2} and large scale units are currently under development for industrial drying³ and steam raising⁴. The advantages of pulse combustors include high combustion and thermal efficiencies^{1,2}, excellent heat transfer characteristics^{5,6}, self aspiration and low CO, NO_x and soot emissions. Yet, the physical and chemical processes which control the operation of these pulse combustors are still not fully understood. Consequently, any changes in scale or application of these devices require costly, empirical, development efforts^{3,7}. This paper describes results from an ongoing study whose overall objective is to gain an understanding of the fundamental processes which control the operation of gas fired, mechanically valved, Helmholtz type, pulse combustors similar to those which have been used as

home furnaces. Specifically, this paper describes an experimental study of the characteristics of the pulse combustion process and the mechanisms responsible for the existence of the previously observed^{8,9} low and rich limits of operation for these combustors.

The Helmholtz type pulse combustor used in this investigation is shown in Fig. 1. It consists of cylindrical mixing and combustion chambers, a tail pipe, an exhaust decoupler and a vent pipe. Natural gas and air enter the mixing chamber through two flapper valves which are welded ninety degrees apart to the curved sides of the mixing chamber. In the standard American Gas Association (AGA) pulse combustor¹⁰, which is used in this study, the combustion chamber has a volume of 183 in³, and a tail pipe length and diameter of 75 in and 1.5 in, respectively. With these dimensions, the unit pulses with a frequency of approximately 42 Hz when operated at 50,000 BTU/HR.

To start, a fuel-air mixture is admitted into the mixing chamber and ignited by a spark plug. The ensuing combustion increases the pressure inside the mixing and combustion chambers. This, in turn, closes the flapper valves. The expansion of the hot combustion products causes their expulsion through the tail pipe. The inertia of the gases leaving the combustor and cooling by heat transfer drop the pressure in the mixing chamber to below atmospheric level and results in the reopening of the valves. Fresh charges of air and fuel enter the combustor, mix and ignite without the use of the spark plug, resulting in a pulse combustion process which can be maintained indefinitely.

In previous studies^{11,12} with this combustor it was observed that the combustion process is largely confined to the mixing chamber, the frequency of pulsations decreases when the volume of the combustion chamber or the length of the tail pipe is increased, and pulse combustion operation can be attained only for equivalence ratios between 0.6 and 1.0. It was also noted¹³ that the rich limit of operation of the pulse combustor can be significantly extended if the combustor is fitted with a longer tail pipe which increases its period of pulsations. Furthermore, the combustor can be operated rich of stoichiometric if the combustion air is supplied to its flapper valve above atmospheric pressure.

In an effort to develop an understanding of the observed trends, detailed diagnostics^{11,12} of the combustion process have been initiated earlier under this program. High speed Schlieren photography carried out along the axis of the combustor clearly showed a highly turbulent fuel jet entering the mixing chamber during the early part of the cycle. This was followed by the entrance of a slower moving air jet. After the two jets mixed, combustion was seen to take place in a highly turbulent flow field. Combustion was almost completed before fuel for the next cycle entered the mixing chamber, except when the combustor was operated near its rich limit. Finally, the amplitudes of the pulsations were found to increase as the fuel-air ratio was increased⁹, within the limits of operation of the combustor.

It was the objective of the work reported herein to 1) elucidate the mechanisms responsible for the existence of the above described limits of operation and 2) investigate the location and timing of the cycle to cycle reignition of the new charges and the ensuing flame spread through the combustor.

EXPERIMENTAL SET UP

To allow high speed Schlieren and radiation measurements, a combustor similar to one shown in Fig. 1 but fitted with the required optical windows was developed, see Fig. 2. It was made out of steel except for a flat, circular quartz window at the upstream end of the mixing chamber and flat, annular, quartz windows at the transition sections between the mixing and combustion chambers and the combustion chamber and the tail-pipe. In addition, flat, rectangular, quartz windows were fitted into the curved walls of the mixing and combustion chambers. These permitted optical access into the combustion chamber along its axis and normal to it.

The pulse combustor was operated on natural gas supplied at five inches of water pressure while air could be aspirated from the atmosphere or supplied at elevated pressure. The fuel flapper valve setting was kept fixed while the air flow rate and, therefore, the fuel-air ratio could be varied by adjusting the maximum travel distance of the flappers in the air valve¹⁰.

Oscillating pressures were measured using Kistler piezoelectric transducers mounted on semi-infinite tubes several inches away from the combustor to protect the transducers from the combustor heat and provide a flat frequency response. These pressure measurements were carried out at the centers of the combustion and mixing chambers and in the pipe connecting the fuel flapper valve to the mixing chamber. The signals from the pressure transducers were amplified and passed through an A/D converter and into an HP A700 computer.

A Schlieren system was used to view the combustion process along the combustor axis, see Fig. 2. The beam through the mixing and combustion chambers was arranged to be slightly converging rather than collimated, which permitted it to exit the combustor without being obstructed by the tail pipe. The Schlieren images, along with the instantaneous pressure traces on an oscilloscope, were recorded using a HICAM high speed camera at a rate of 7000 frames per second.

The oscillating reaction rates (i.e., combustion intensities) were determined by measuring the spontaneous radiation from OH radicals through the combustor windows¹⁴. These measurements were carried out both globally and spatially resolved. For the global measurements (see Fig. 3a) the radiation from the entire combustor was focused using a large diameter, short focal length lens, through a 306 nm interference filter and a pin hole onto a Hamamatsu R269 photomultiplier. For the spatially resolved measurements, which were carried out at various locations through the end and side windows of the combustor, the focusing lens was replaced by a thin tube, fitted at both ends with small apertures (see Fig. 3b). This tube eliminated the radiation emitted from regions other than the small area under investigation. This allowed measurements of integrals of radiation signals along axes parallel to the combustor axis with a spatial resolution of 3 mm in the plane normal to the combustor axis. The output from the photomultiplier was converted to a voltage using a 10 k Ω resistor, amplified with a Neff amplifier and passed via an A/D converter into the computer.

A computer program was developed which acquired and analyzed both pressure and radiation data simultaneously. The software permitted the

display of time traces of pressure and radiation intensity and the calculation of their auto- and cross-correlations. These allowed determination of the spectra for the pressure and radiation signals and the phase angles between them. In addition, the fluctuating radiation signals were correlated with the high speed Schlieren movies using the recorded pressure oscillations as a clock.

RESULTS AND DISCUSSION

High speed Schlieren photography, spontaneous radiation, and oscillatory pressure measurements were carried out in the pulse combustor operating near its lean and rich limits of operation and under normal operating conditions. Figure 4 shows time traces of simultaneously measured pressure and global radiation fluctuations. Also indicated are the instances in the cycle at which the fuel and air jets entered the mixing chamber as determined from the high speed Schlieren records. The time in each cycle at which the radiation intensity begins to increase is denoted as the instant of reignition of the fresh fuel charge.

Figure 4 indicates that the fuel jet enters the mixing chamber before the pressure there falls below the nominal fuel supply pressure. This occurs because the pressure oscillations in the fuel line slightly lag behind those in the mixing chamber, see Fig. 5. Therefore, early in the cycle, the pressure in the fuel line is slightly higher than that in the mixing chamber, which causes the early fuel jet entry into the mixing chamber.

Figure 4 shows that the emitted radiation and, therefore, the combustion process never stop at any time during the cycle. Clearly, the fluctuations in heat release always lead those in pressure. This was expected since the pulsating combustion drives the pressure oscillations. Comparison of the data presented in Figs. 4-A,B,C further shows that the combustion of the new charges in each cycle commences earlier, the lower the fuel-air ratio. In fact, near the lean limit and under normal operating conditions ignition of the new fuel charge occurs before air for that cycle has started to enter the mixing chamber. This is possible because under fuel lean conditions the fresh fuel charge can begin its combustion process using air remaining from the previous cycle. However, as stoichiometric conditions are approached, less and less air from the previous cycle is available for combustion and the combustion of the fresh fuel charge is delayed until the air for this cycle enters the combustor.

According to Rayleigh's criterion,¹⁵ driving of the pulsations requires that a certain minimum fraction of the combustion energy be released in phase with the pressure oscillations in order to overcome the inherent losses in the system. Typical relationships between the heat addition and pressure oscillations are represented schematically in Fig. 6. The length of the vector q represents the magnitude of the integral of the heat release during a cycle. The angle θ is the phase angle between the maxima of the heat release and pressure oscillations. The latter are assumed to have zero phase (i.e., they aligned with the positive x-axis). The acoustic losses in the system (e.g., due to acoustic radiation and viscous effects) are represented by L along the negative x-axis. L does not include the damping due to the fraction of the heat release which is out of phase with the pressure oscillations since that effect is included in the determination of the phase angle

8. If the projection of q along the horizontal axis (i.e., $q \cos \theta$) exceeds L , the combustion heat release is sufficient for driving pressure oscillations. The observed delay in the occurrence of ignition, (see Fig. 4) which is caused by the unavailability of air as stoichiometric conditions are approached, apparently "produces" conditions under which only a fraction of the fuel can react during the remainder of the cycle with the available air. Thus, an unsufficient amount of energy (i.e., a reduced q) appears to be released in phase with the pressure oscillations to maintain pulsations. This is confirmed by the high speed Schlieren movies which have shown that near the rich limit the new fuel enters while the combustion process from the previous cycle is still taking place. In addition, analysis of the exhaust gases has shown that the combustion efficiency decreases near stoichiometric conditions. In terms of Fig. 6a this means that the magnitude of q is too small for $q \cos \theta$ to exceed the system losses, $-L$, in spite of the phase θ being small. This, in turn, results in stoppage of pulsations.

The observations discussed above suggest that the rich limit could be possibly extended by decreasing the frequency of oscillations and/or supplying the air at elevated pressure. The former would provide a longer period for the combustion process to take place during the cycle. The latter will cause reignition to occur earlier during the cycle (and, thus, make more air available "early" for combustion), by causing earlier entry of the air and also shorten the combustion time by increasing the mixing rate. Either could provide conditions under which Rayleigh's criterion for driving the combustor oscillations would be satisfied. Indeed, as stated above, earlier studies^{8,9} confirmed that the stated conjectures are correct. Work continues to prove conclusively that the heat release, q , is indeed reduced near the rich limit.

To further investigate the combustion process behavior under different operating conditions, spatially resolved amplitudes and phases of the radiation were measured under lean, normal and rich operating conditions, see Figs. 7 and 8. The lines of constant phase between the maximum radiation and maximum pressure signals are plotted in Figure 7. The numbers next to the lines indicate the phase angle by which the heat release leads the pressure.

Close inspection of the lean limit case shows that the early part of the combustion cycle and, therefore, of the heat release, occurs more than 90 degrees out of phase with the pressure oscillations; i.e., $\theta > 90$ in Fig. 6. According to Rayleigh's criterion, the combustion energy released during this part of the cycle damps rather than drives the pulsations. The local phase angle by which the heat release leads the pressure fluctuations and the spatially resolved dB levels of the radiation fluctuations for the lean limit case are shown in Fig. 8. This figure indicates that the part of the combustion cycle which is out of phase with the pressure oscillations exhibits large amplitude radiation fluctuations. This indicates that near the lean limit a considerable fraction of the heat release during each cycle damps rather than drives the pulsations (i.e., $q \cos \theta$ in Fig. 6b is less than $-L$). Since Fig. 7 indicates that reignition occurs earlier as the operation becomes leaner, the damping by the combustion process increases as the lean limit is approached. This is accompanied by a decrease in the amplitude of pulsations as is apparent in Figure 4. These observations strongly suggest that the lean limit of operation occurs when, due to the early combustion process, the damping provided by the heat release adds to the inherent system

acoustic losses, and the driving provided by the combustion process cannot overcome these combined damping effects. However if the frequency of pulsations is increased the lean limit of operation of the combustor should be extended. Such an effect was, indeed, observed.

In Fig. 7, the higher the phase, the earlier the occurrence of the combustion process at that location. Therefore, the location with the highest phase indicates the region of cycle to cycle reignition of fresh fuel charges. In all three cases the new fuel charges ignite in the mixing chamber opposite the fuel inlet port. However, near the rich limit a secondary reignition area is observed near the center of the mixing chamber where the air jet first impinges upon the fuel jet. From the reignition spot(s) the flame then spreads throughout the mixing chamber.

Additional radiation measurements were carried out normal to the axis of the pulse combustor along its center line. Figure 9 shows the dependence of the phase angle between the heat release and pressure oscillations upon the axial location. These data indicate that cycle to cycle reignition (i.e., the largest phase angle) occurs 2.3 inches downstream of the plane in which the fuel and air jets enter the mixing chamber for all of the tested fuel-air ratios. Furthermore, consistent with the above discussed results, ignition near the rich limit occurred later in the cycle (smaller phase angle) than for the other two cases. Figure 9 also shows that after ignition the flame quickly spreads upstream towards the mixing chamber end wall and somewhat more slowly downstream into the combustion chamber.

CONCLUSIONS

Oscillatory pressure measurements, high speed Schlieren photography and spontaneous radiation measurements were carried out in a Helmholtz type, gas fired, mechanically valved, pulse combustor. Cycle to cycle reignition of the new fuel charges was observed to occur in the mixing chamber opposite and downstream of the fuel inlet port. From there the flame spreads throughout the mixing chamber and into the combustion chamber.

The mechanisms controlling the occurrences of the lean and rich limits of operation of the pulse combustor are somewhat different. Near the lean limit of operation combustion of the new fuel charge in each cycle commences as soon as the fuel enters the mixing chamber, using excess air left over from the previous cycle. Thus, a significant fraction of the heat release occurs out of phase with the pressure oscillations, which damps the pulsations. A lean limit of operation is reached when the sum of the damping provided by the combustion process and the inherent system acoustic losses exceeds the combustion process driving. As the fuel-air ratio is increased, the heat release and pressure oscillations become more and more in phase, resulting in increased driving. Therefore, the pressure amplitudes increase as the equivalence ratio is increased.

Near stoichiometric conditions no air is left over from the previous cycle and the ignition of the new fuel is delayed until fresh air enters the mixing chamber. This, in turn, delays the beginning of the new combustion cycle and produces conditions under which the fraction of the combustion energy released in phase with the pressure oscillations does not produce

sufficient driving to overcome the system's damping. When this occurs, the rich limit of operation is reached.

Since the duration of the cycle can be changed by modifying the combustor geometry, it has been shown that the limit of operation can be extended to the fuel rich side by prolonging the period of oscillations through the use of a longer tail pipe. Alternately, the rich limit was extended by supplying the air under pressure which shortened the reignition delay and, most likely, reduced the time required for combustion by increasing the mixing rate. Both effects apparently resulted in a larger fraction of the combustion energy being released in phase with the pressure oscillations, resulting in increased driving and a lower rich limit of operation.

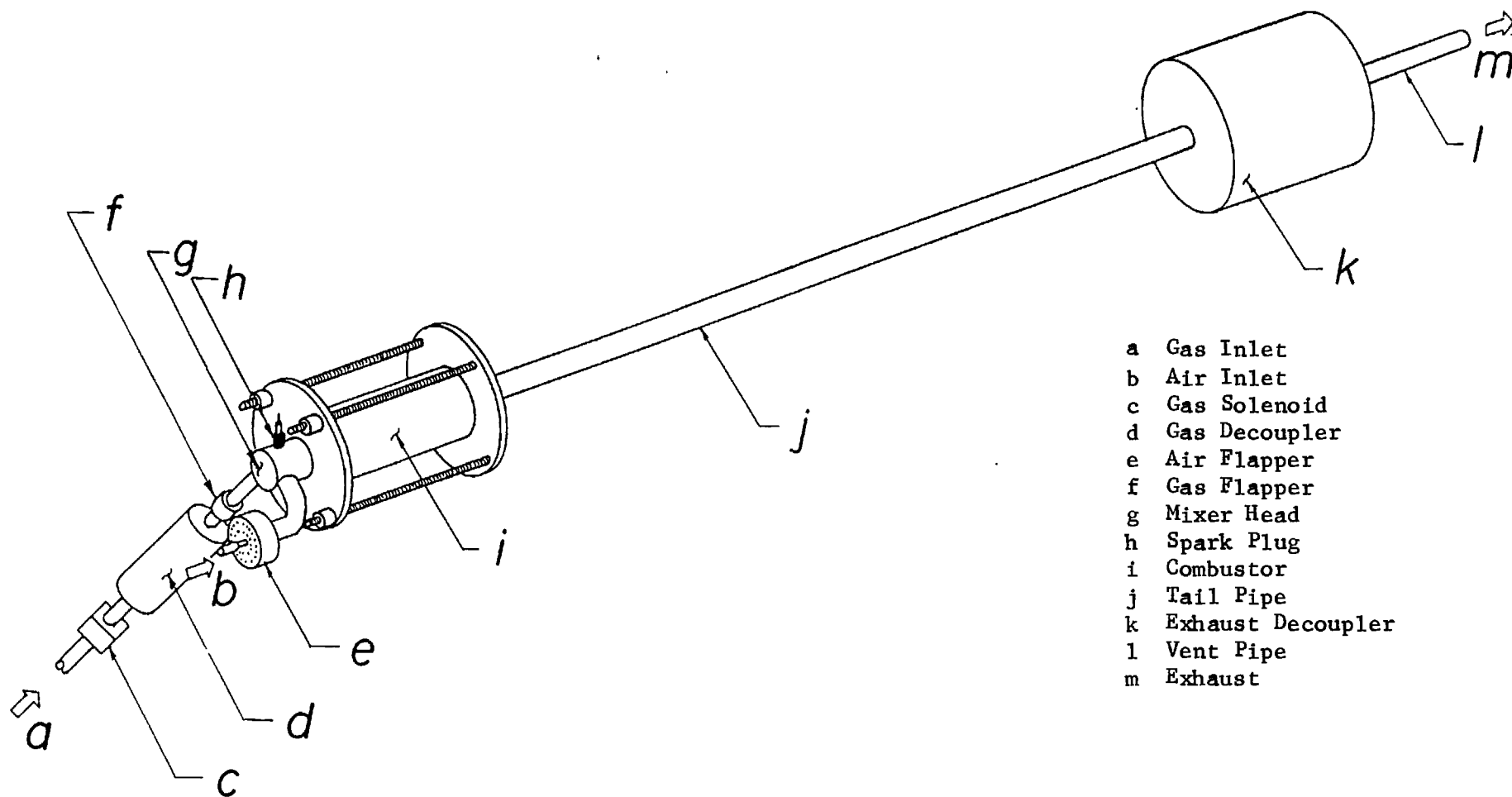
ACKNOWLEDGEMENT

This work was supported by the Gas Research Institute under Grant No. 5087-260-1466. Mr. J. Kezerle is the monitor.

REFERENCES

1. "Lennox-Pulse-G14 Series Up-Flo Gas Furnaces", Engineering Data, Heating Units, Gas, pp. 21-24, published by Lennox Industries, Inc.
2. "Hydropulse by Hydrotherm", information about pulsed combustion water heating published by Hydrotherm, Rolfland Ave., Northvale, NJ 07647.
3. Flanigan, P., AGA Laboratories "Development of a Pulse Combustion Industrial Dryer, Phase I" Final Report to Gas Research Institute, 1987.
4. Hollovell, G. T., Belles, F. E. and Kardos, P. "Development and Commercialization of Pulse Combustion Commercial Steam Boilers", Forbes Engineering Inc., Annual Report April 1986 - March 1987, GRI-87/0190.1.
5. Dec, J. E. and Keller, J. D. "Pulse Combustor Tail-Pipe Heat Transfer Dependence on Frequency, Amplitude and Mean Flow Rate", to appear in Combustion and Flame.
6. Fedorov, B. N., "Experimental Study of the Effect of Acoustic Oscillations on Heat Transfer in a Gas Flow", Juzherno-Fisicheskii Zhurnal, Vol. 32, No. 1, pp 167-180, 1977.
7. Belles, F. E., "R & D and Other Needs for Exploitation of Pulse-Combustion in Space-Heating Applications", Proc. of Symp. on Pulse-Combustion Technology for Heating Applications, Argonne National Laboratory, pp. 167-180, 1979.
8. Ku, S. H., Cheng, X. C., Daniel, B. R., Jagoda, J. I. and Zinn, B. T., "Performance Characteristics of Helmholtz Type Pulsating Combustors", presented at the Fall Technical Meeting of the Eastern States Section of the Combustion Institute, 1985.

9. Ku, S. H., Cheng, X. C., Scroubelos, G., Daniel, B. R., Jagoda, J. I. and Zinn, B. T., "Performance and Efficiency of Gas Fired Pulsating Combustors", presented at the 1986 International Gas Research Conference, Toronto, Canada, Sept. 1986.
10. Griffiths, J. C. and Weber, E. J., "The Design of Pulse Combustion Burners", Research Bulletin 107, American Gas Association Laboratories, June 1969.
11. Reuter, D., Daniel, B. R., Jagoda, J. I. and Zinn, B. T., "Periodic Mixing and Combustion Processes in Gas Fired Pulsating Combustors", presented at the Spring Joint Technical Meeting of the Central and Western States Sections of the Combustion Institute, San Antonio, TX, April 1985.
12. Reuter, D., Daniel, B. R. Jagoda, J. I. and Zinn, B. T., Combustion and Flame, Vol. 65, No. 3, pp. 281-290, 1986.
13. Ku, S. H., Cheng, X. C., Daniel, B. R., Jagoda, J. I. and Zinn, B. T., "Radiation Measurements in a Gas Fired Pulse Combustors", presented at the Spring Technical Meeting of the Central States Section of the Combustion Institute, Chicago, IL, 1987.
14. Keller, J. O. and Westbrook, C. K. Twenty first Symposium (International) on Combustion, The Combustion Institute, 1987.
15. Lord Rayleigh, "The Theory of Sound", Vol. II, pp. 224-235, Dover, 1945.



- a Gas Inlet
- b Air Inlet
- c Gas Solenoid
- d Gas Decoupler
- e Air Flapper
- f Gas Flapper
- g Mixer Head
- h Spark Plug
- i Combustor
- j Tail Pipe
- k Exhaust Decoupler
- l Vent Pipe
- m Exhaust

Fig. 1 Schematic of the Gas Fired Pulse Combustor

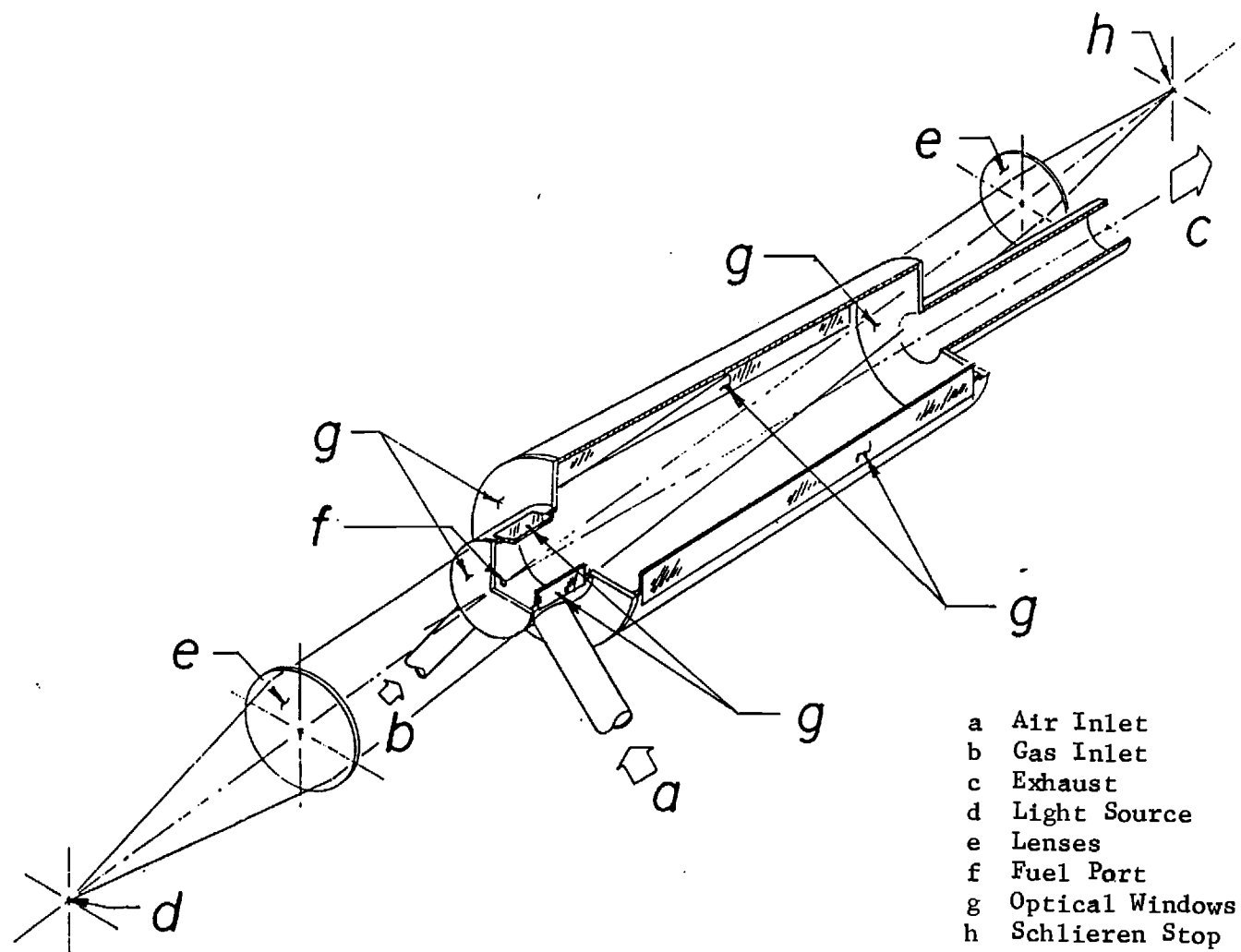


Fig. 2 Schematic of the Schlieren Set-up

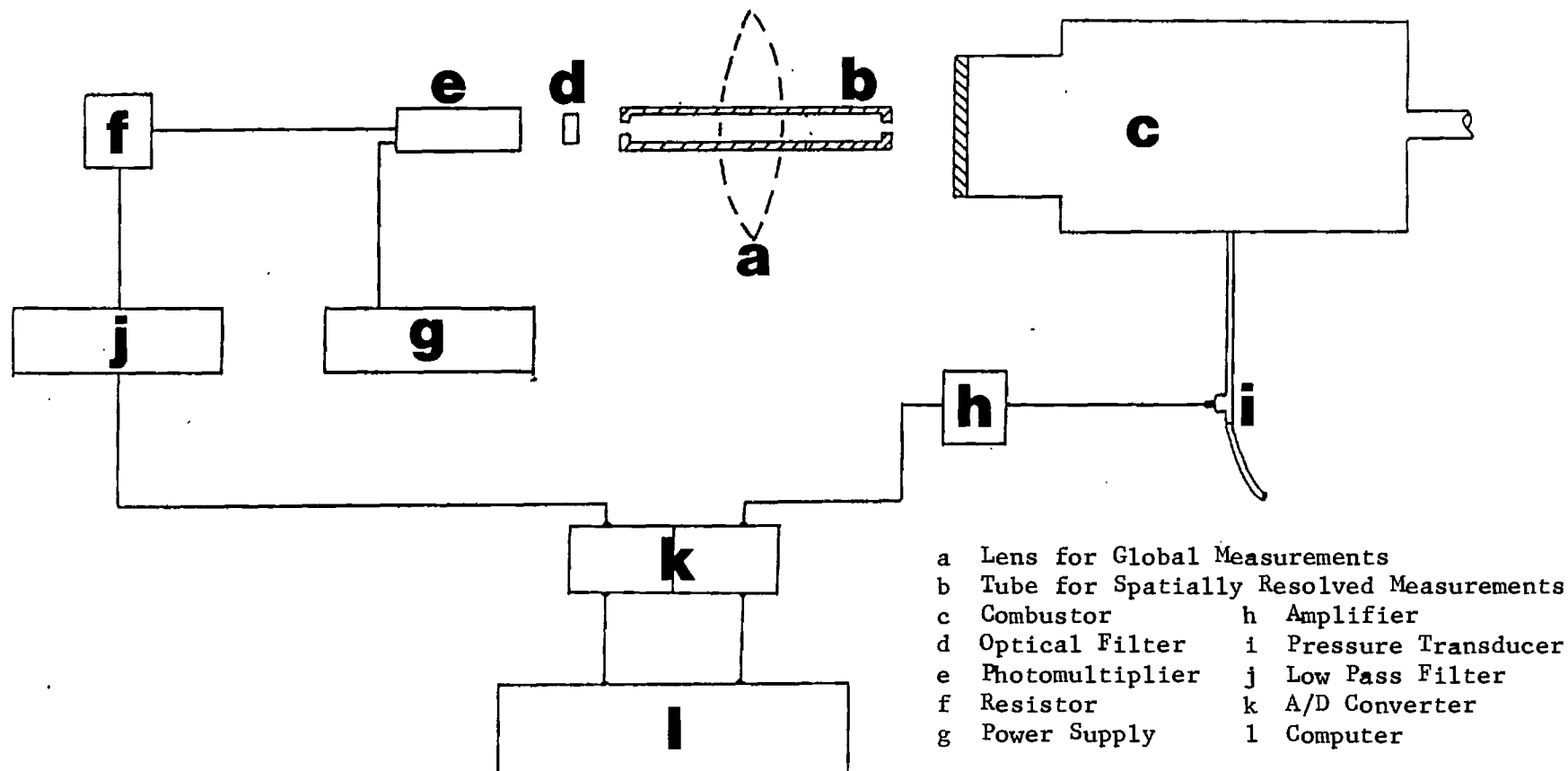


Fig. 3 Radiation/Pressure Measurement Set-up

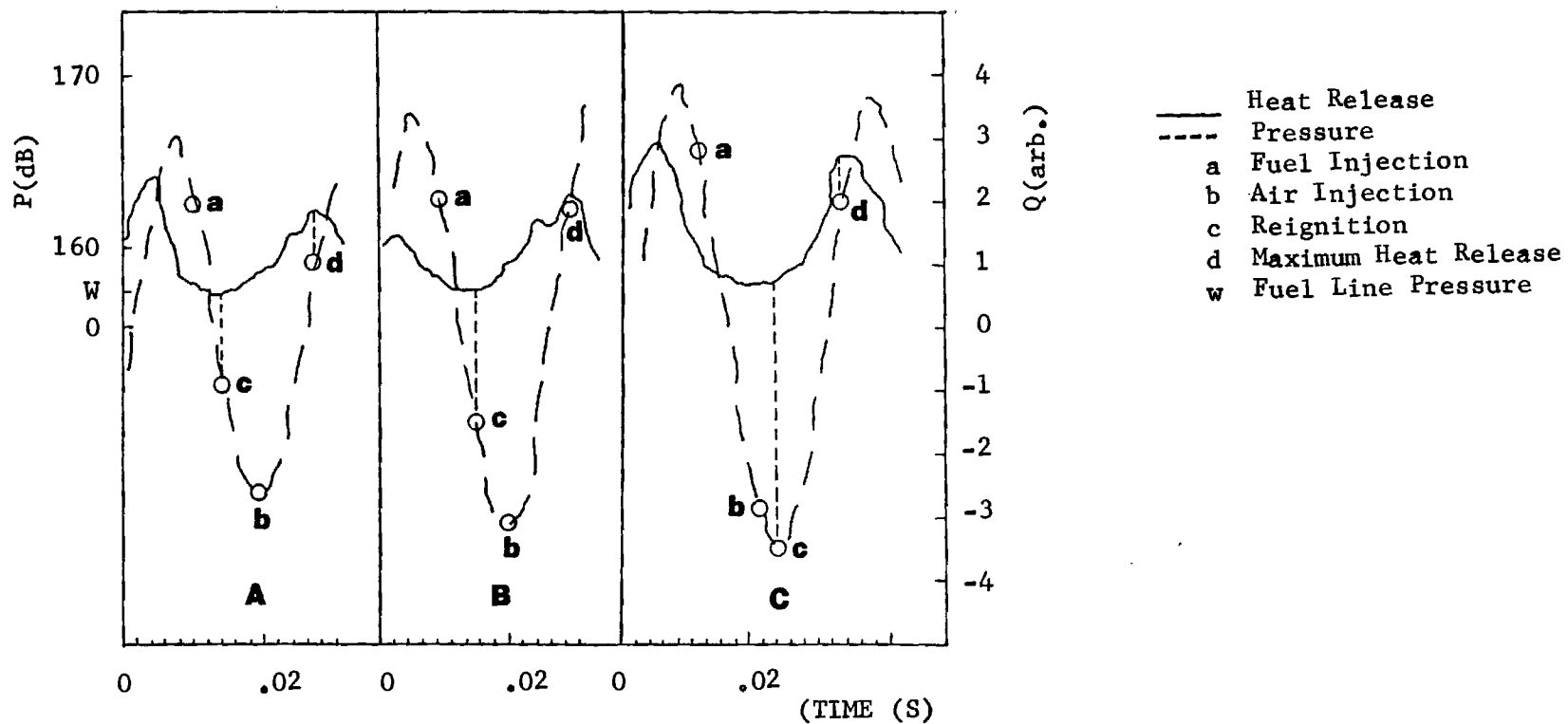
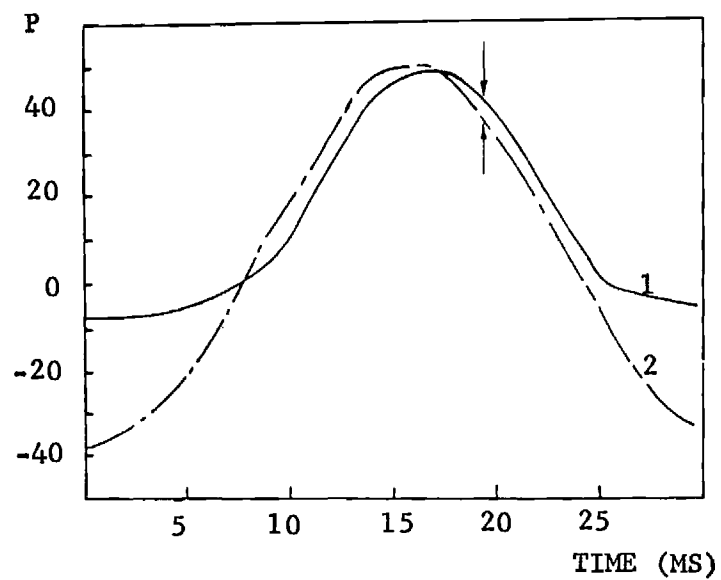
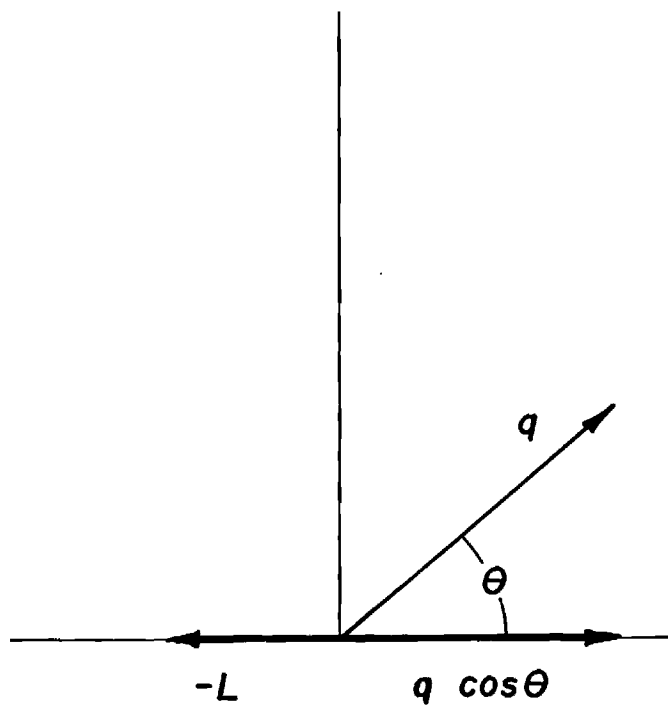


Fig. 4 Global Heat Release and Pressure Fluctuations Near Lean limit (A). for Normal Operation (B) and Near Rich Limit (C).

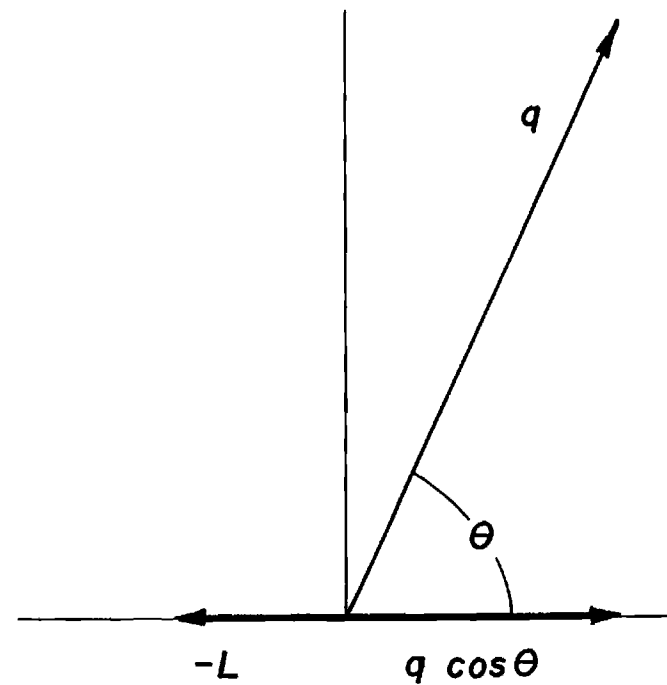


P Pressure (inches of water)
1 in Fuel Line
2 in Combustor

Fig. 5 Pressure Fluctuation vs Time in Fuel Line and Combustor



a. Near Rich Limit



b. Near Lean Limit

Fig. 6 Vector Representation of Rayleigh's Criterion

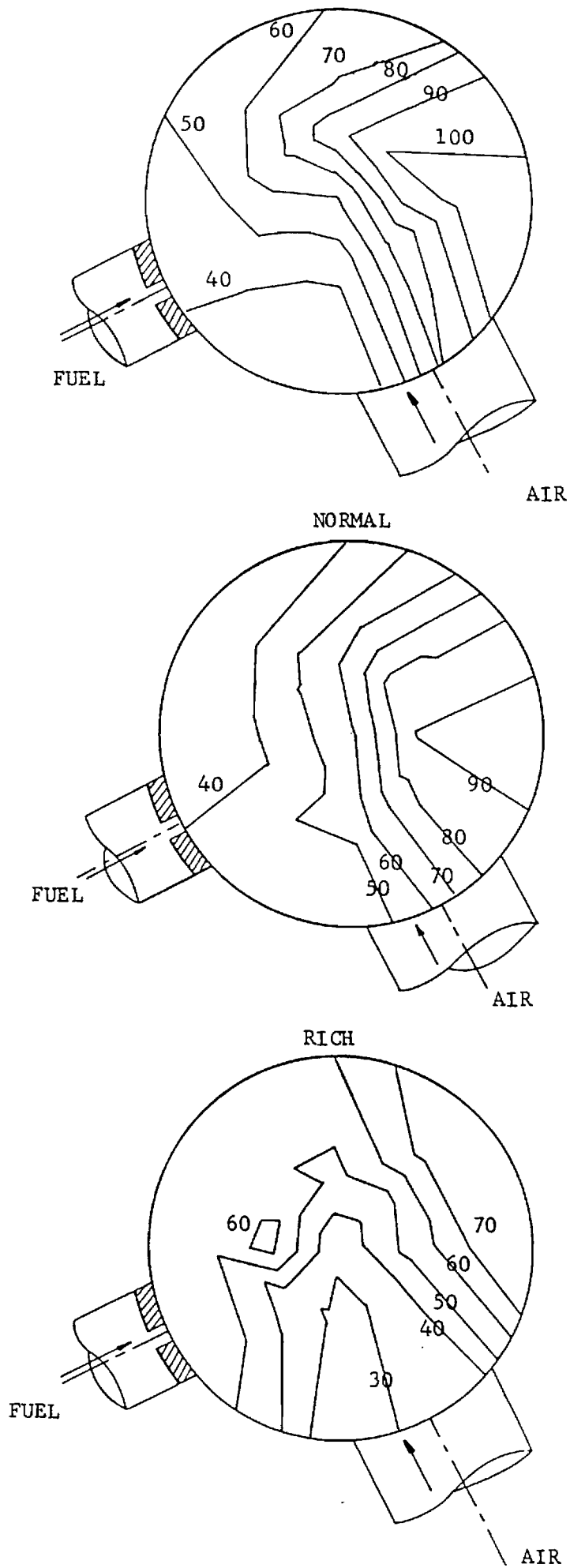


Fig. 7 Spatially Resolved Radical Radiation Measurements Through End Window Phase by which Radiation Leads Pressure.

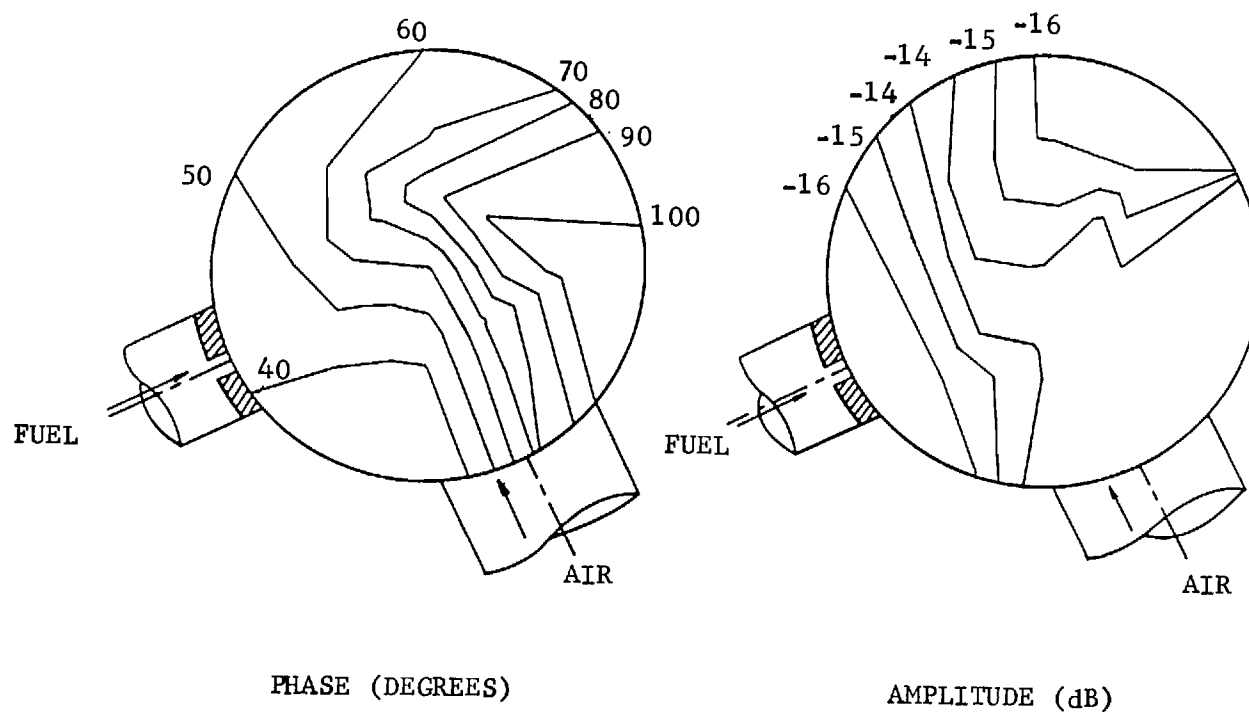


Fig. 8 Spatially Resolved Radical Radiation Measurements for Lean Conditions Through End Window: Amplitude and Phase.

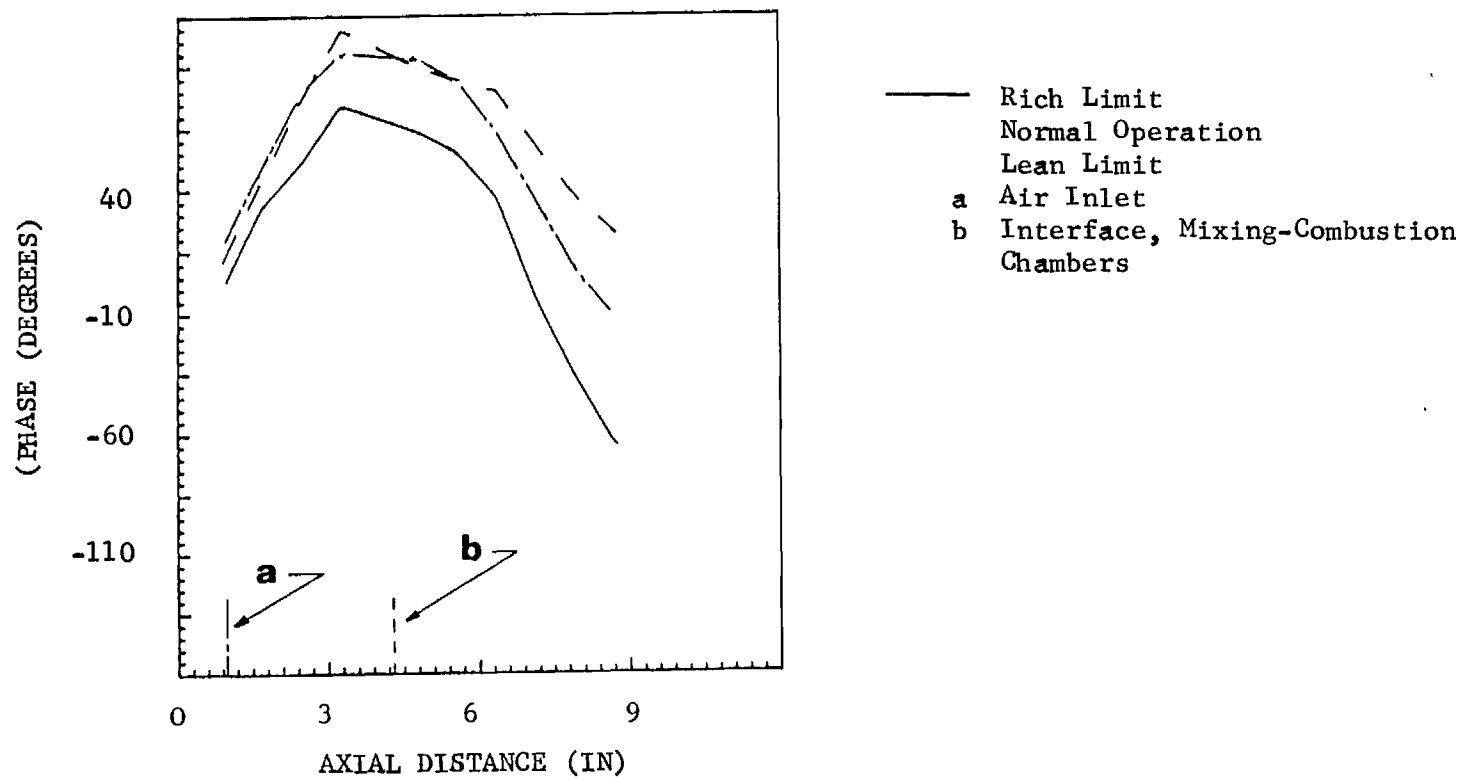


Fig. 9 Spatially Resolved Radical Radiation Measurements Through Side Windows Along the Combustor Axis; Phase by which Radiation Leads Pressure.

Pulsating Burners - Controlling Mechanisms and Performance

Annual Report

January 1, - December 31, 1988

Prepared by

B. T. Zinn, B. R. Daniel and J. I. Jagoda

School of Aerospace Engineering

Georgia Institute of Technology

For

Gas Research Institute

Grant No. 5083-260-1466

GRI Project Manager

James A. Kezerle

Combustion

January 1989
RESEARCH SUMMARY

Title: Pulsating Burners - Controlling Mechanisms and Performance

Contractor: Georgia Tech Research Institute

Contract Number: 5087-260-1466

Report Period: January - June 1988, Semi-Annual Report

Principle Investigators: B. T. Zinn, B. R. Daniel and J. I. Jagoda

Objective: It is the objective of this study to gain further insights into the physical mechanisms which control the mixing and heat release processes in pulse combustors. In addition, the acoustic driving and damping characteristics of various components and subsystems of the pulse combustor will be determined for various operating conditions. Finally, the above findings will be used to explain the performance of various combustor configurations to be tested and should be of

considerable help to the designers of novel pulse combustors.

Technical Perspectives: Although gas fired pulse combustors have been on the market for a number of years, their controlling mechanisms are still not sufficiently well understood to permit the design of pulse combustors for different applications without resorting to costly trial and error development efforts. To attain pulse combustion operation, the energy supplied to the pulsations by the combustion process must be larger than the acoustic energy lost due to viscous dissipation, heat transfer, acoustic radiation and so on. Proper operation of pulse combustors also requires that the timing of the mixing, cycle to cycle reignition and flame spread processes produce oscillatory heat release in phase with the pressure oscillations. Finally, proper operation of a pulse combustors requires compatibility between the acoustic properties of the various components of the pulse combustor. Thus, to develop a rational design procedure for pulse combustors, it is necessary that the various processes responsible for energy addition and removal to and from the pulsations be understood. Furthermore, data describing the acoustic properties of various pulse combustor components under different cold and pulse combustion operating conditions are needed. Finally, the dependence of the

acoustic characteristics of the various combustor components upon the fundamental fluid mechanical, heat transfer and combustion processes must be understood. The attainment of these goals is the main goal of this project.

Technical Approach: In order to elucidate the mechanisms which control the operation of various pulse combustor configurations and determine the damping/driving characteristics of various components and subsystems of commonly used pulse combustors, the following tasks are pursued simultaneously:

- 1) Investigation of the flow field characteristics, mixing and heat release in pulse combustors using LDV, Schlieren, mixing visualization, radical radiation (OH, CH, CC) and Rayleigh scattering measurements.
- 2) Measurements of the driving and damping characteristics of various components and subsystems which make up the pulse combustor using the impedance tube technique.
- 3) The determination of the overall driving and damping characteristics of various pulse combustor designs under different operating conditions.

- 4) Modeling of the dynamic characteristics of the flapper valve.

Results:

During the past year the axial flow fields in the mixing chamber and near the interface between the combustion chamber and the tail pipe were visualized using high speed shadowgraphy. Results of the flow visualization in the mixing chamber were compared with those from LDV measurements in that part of the combustor. These show that the fuel jet enters the mixing chamber shortly after the pressure there passes through its maximum. This is followed by the entry of the air jet which clearly dominates the flow field. A large, axial recirculation zone is observed in the mixing chamber during the combustion phase of the cycle. As the pressure approaches its maximum the flow in the mixing chamber becomes axial again. The level of turbulence intensity in the mixing chamber is high throughout the cycle, and it increases significantly immediately after the air enters the mixing chamber. The pressure oscillations cause periodic gas movement between the combustion chamber and the tail pipe with the gases in the tail pipe penetrating a distance of several inches into the combustion chamber.

An impedance tube technique was used to determine the admittances of the air valve, the fuel valve and the mixing chamber fitted with the air valve only and with both the fuel and air valves. The real and imaginary parts of the admittance (i.e., Y_r , Y_i) describe the damping/driving and phase delay experienced by an acoustic wave upon reflection of the surface whose admittance Y is being measured, respectively. The measurements show that the real parts of the admittances (i.e., damping) of all components are essentially zero at low driving frequencies as long as the air valve is closed. As the frequency increases beyond 50 Hz the real part of the admittance of the fuel valve increases slightly while the damping by the air valve and the mixing chamber fitted with fuel and air valve increases considerably. Y_r of the air valve also depends upon the geometry of the pipe connecting the valve housing to the mixing chamber but is not affected by the presence of the fuel valve. Y_r of the air valve increases significantly when the valve opening is increased. The imaginary parts of the admittance of all of the investigated components are practically zero at low frequencies as long as the air valve is closed. Y_i of the fuel valve remains zero as the frequency increases. On the other hand, Y_i of the closed air valve increases from zero as the frequency increases. Y_i of the air valve decreases, however, as the air valve is opened.

Y_j of the air valve admittance is finite because an incident wave must travel inside the valve housing before it is reflected off the valve plates. Y_j decreases as the air valve is opened because opening the air valve moves the pressure antinode and, therefore, the pressure node away from the valve. Y_j of the mixing chamber - air valve assembly exhibits trends similar to those of the air alone. Finally, adding the fuel valve to mixing chamber - air valve assembly has no significant effect upon the system's admittance.

The behavior of the valve is being modeled using a linear acoustic model. The variation of the real part of the admittance of the valve during a cycle has been calculated. The predicted behavior of the valve admittance is in good qualitative agreement with the measured impedance tube data. However, since the model predicts the admittance of the valve itself and the measurements determined the admittance at the valve housing-mixing chamber interface, a precise comparison must await the determination of the transfer function which will relate these two admittances. The model predictions also indicate that the time required to open the air valve decreases as the frequency increases until a limiting value is reached above approximately 50 Hz. Furthermore, the valve setting appears to have little effect upon the

valve opening time. It was also determined that even at frequencies above 150 Hz the valve opening and closing times are small fractions of the periods during which the valve is either fully open or closed.

OBJECTIVES

It is the objective of this study to gain further insight into the fundamental processes responsible for the operation of various pulse combustor designs. Emphasis is being placed upon obtaining practical information which will permit designers to develop new and/or larger scale pulse combustors without resorting to costly trial and error based development efforts.

The velocity and the mixing patterns in the mixing and combustion chambers will be determined both qualitatively and quantitatively. The nature of the interaction between the combustion process and the acoustics of the combustor will be established. The impedance of various components and subsystems which make up the pulse combustor will be determined under various operating conditions. In addition, the driving and damping characteristics of different pulse combustor designs will be measured under different operating conditions. Finally, the dynamic characteristics of the flapper valves will be analytically modeled.

PROGRAM PLAN

The program is divided into four major tasks as outlined below:

Task 1: Investigation of the Interaction between the Oscillatory Flow Field and Heat Release Processes in the Pulse Combustor:

A. Laser Doppler Velocimetry: The three components of velocity will be measured at selected locations in the combustor. The period of

pulsations will be divided into a number of equal time segments and the LDV counts for each segment will be stored in separate files. This will permit ensemble averaging of the velocities in each segment over many cycles. Mean velocities and turbulence intensities as well as shear stresses can then be obtained for each instant in the cycle.

- B. Schlieren Visualization: High speed Schlieren and shadowgraph cinematography will be carried out through side windows in the combustor in order to visualize the flow along the combustor axis. These shadowgrams will then be correlated with those previously obtained through windows in the end walls of the combustor. This will provide a complete picture of the three-dimensional flow field in the pulse combustor.
- C. Mixing Visualization: Mixing patterns will be recorded photographically by heavily seeding one of the reactant flows and illuminating the combustor using an expanded laser sheet. These visualizations will be carried out through the flat windows in the cylindrical walls of the mixing and combustion chambers. The use of the flat windows is expected to reduce the amount of laser light reflected by the glass. These laser light intensity losses caused problems when this technique was previously applied to the combustor through cylindrical glass walls.
- D. Spectroscopy: Local and global heat release in the pulse combustor will be determined by measuring the OH, CH and CC radical radiation emitted from the combustor. Efforts will concentrate on

measurements through the side windows of the mixing chamber which will be correlated with previous results obtained through the end window of the combustor. A recently acquired intensified CCD system will help to increase spatial resolution of these measurements by an order of magnitude when it becomes operational.

- E. Rayleigh Scattering: Local densities and, therefore, temperatures will be measured using Rayleigh scattering. A combination of the emission spectroscopy and the Rayleigh measurements will result in a better understanding of the location and timing of the combustion process. In addition, the Rayleigh scattering results will yield a quantitative description of the path taken by the hot combustion products in the pulse combustor.

All task I measurements will be carried out in the pulse combustor with flat windows fitted to the curved walls of the mixing and combustion chambers. The results will be correlated with each other and with the phase in the cycle at which they were obtained. This will be achieved by using the measured pressure oscillations as a clock. Only a full coordination between the flow field, the heat release and the local temperature measurements can result in a thorough understanding of the fundamental processes which control the operation of the pulse combustor.

Task II: Impedance Measurements of Pulse Combustor Components:

The acoustic admittance of the various components and subsystems which make up the pulse combustor will be measured using an

impedance tube technique. These measurements will be carried out without and with combustion and under various operating conditions and frequencies. These measurements will yield information on the frequency dependence of the acoustic properties of various pulse combustor subsystems. In addition, the frequency dependence of the driving provided by the pulse combustion process will be investigated.

Task III: Determination of Overall Driving/Damping Characteristics of Pulse Combustors:

The overall driving and damping characteristics of the pulse combustor will be determined by measuring the growth and decay rates of the combustor pressure oscillations during the start-up and shut-down phases of operation. These measurements will be carried out for various combustor configurations and for a range of operating conditions. The driving and damping for different combustor geometries, fuel/air ratios and injector configurations will be determined.

Task IV: Modeling of Flapper Valve:

The behavior of the flapper valve will be modeled using the continuity and momentum equations and the equation of motion of the flapper. In addition, a transfer function which will permit the calculation of the admittance at the air valve housing-mixing chamber interface from the calculated admittance at the valve plate will be developed.

Task V: Reporting

As per contract agreement.

TECHNICAL PROGRESS AND RESULTS

During the past year the axial flow field in the pulse combustor was visualized using high speed shadow photography through the flat quartz windows in the curved side walls of the mixing and combustion chambers. Particular attention was paid to the flow field in the mixing chamber and in the vicinity of the combustion chamber-tail pipe interface. In addition, velocity measurements in the mixing chamber were continued using a two component LDV system with Bragg cells. Because the flow in the combustor is periodic, mean flow velocities and turbulence intensities at different instances during the cycle had to be determined using conditional sampling. This was achieved by dividing each cycle into 30 equal time intervals and sorting the data into the relevant bins according to their time of arrival during the cycle. Ensemble averaged mean and RMS velocities were, thus, obtained at 30 equi-spaced instances during the cycle. The orientation of the locations of the LDV measurements are shown in Fig. 1. Images obtained by high speed shadowgraphy are compared with the axial and azimuthal LDV data measured at nine locations in the horizontal plane in the mixing chamber which bisects the angle between the fuel and air inlets in Fig. 2. The pressure oscillations were used as a clock in this comparison.

Since the air and fuel ports are located off axis, the flow field is not cylindrically symmetric. The high speed shadowgraphy shows (Fig. 2a) that the fuel jet enters the mixing chamber shortly after the pressure there passes through its maximum. This fuel jet appears to have no significant effect upon the LDV measurements. Just before the pressure minimum is reached (Fig. 2b) the air jet enters the mixing chamber. The air jet drastically increases the magnitudes of the velocity vectors near the upstream end of the mixing chamber. Furthermore, the addition of air into the combustor increases the flow velocities further downstream in the mixing chamber. A little later, during the combustion phase of the cycle (Fig. 2c), a large, axial recirculation region forms in the mixing chamber which is clearly seen in the shadowgraphs. This recirculation bubble manifests itself in the vector diagram as downward pointing velocity vectors near the upstream end and upward vectors near the downstream end of the mixing chamber. As the pressure maximum is reached the flow becomes axial again (Fig. 2d) as shown by the shadowgraph and the velocity vector plot. Shortly thereafter, the new fuel jet enters and the cycle repeats itself.

The variation of the turbulence intensity with time during the cycle at a number of representative locations is shown in Fig. 3. The apparent level of turbulence, as measured by the RMS value of the conditionally sampled velocity, is rather high throughout the cycle. However, only a part of this RMS is due to true turbulence. Since the values of the velocity fluctuations were obtained by ensemble averaging, there are also contributions due to: 1) the finite width of the slots into which each cycle was divided; 2) the slight differences in the flow field from cycle to cycle; and 3) slight variations in the combustor frequency during the experiment. Nevertheless, a significant increase in the intensity of

turbulence can be observed in the mixing chamber immediately after the entry of the air. The LDV data acquisition software is currently being modified to eliminate the effect due to the slight variations in pulse frequency. Once completed, the pulse duration for each cycle will be determined from the actual pressure oscillations measured during the experiment rather than from a previously determined mean frequency as is presently the case.

High speed shadowgraphy was also carried out at the downstream end of the combustion chamber where the combustor connects with the tail pipe. As the pressure in the combustor decreases, combustion products from the tail pipe are seen to flow back into the combustion chamber. This backflow penetrates a distance of only two to three inches back into the combustor. As the acoustic pressure begins to rise again the flow reverses and reenters the tail pipe.

In another part of this investigation the impedance tube technique was used to measure the admittances (i.e., the complex ratio of the acoustic velocity normal to the surface and the local pressure) of different pulse combustor components. In this technique, the investigated component is attached to the upstream end of a long tube, see Fig. 4, and an electro-pneumatic, acoustic driver is attached to the wall just upstream of the opposite end of the tube. The acoustic driver is used to excite an incident acoustic wave which moves towards the tested component. The interaction of this wave with the investigated sample produces a reflected wave with modified amplitude and phase. The incident and reflected waves combine to establish a standing wave in the impedance tube. A piezo-electric pressure transducer mounted near the tested sample measures the amplitude at the upstream end of the tube. A second pressure transducer,

mounted at the end of a long rod, is translated inside the tube to measure the axial variation of the standing wave amplitude along the impedance tube.

When measuring the admittance of a hard termination (i.e., zero admittance), the incident wave is reflected without a change in amplitude or shift in phase. In this case the combination of incident and reflected waves produces a standing wave with a zero amplitude pressure minimum located one quarter of the wavelength ($\lambda/4$) from the hard termination, see Fig. 5a. On the other hand, if the complex admittance of the termination is nonzero, see Fig. 5b, the minimum pressure amplitude is non-zero and it occurs at a location other than $\lambda/4$ from the tested sample. Physically, the termination changes the pressure amplitude of the reflected wave and introduces an apparent change in the length of the pipe by introducing a phase shift in the reflection process. The measured values of P_{\max} , P_{\min} and the distance of P_{\min} from the tested sample can be used to determine the real and imaginary parts of the admittance of the termination and, thus, of the component under investigation. A more detailed analysis shows that the real part of the admittance, which is calculated from the difference between the maximum and minimum pressure amplitudes (i.e., $P_{\max} - P_{\min}$) determines the damping (or driving) provided by the component under investigation. On the other hand, the imaginary part of the admittance provides information which affects the frequency of the system which utilizes the tested component.

The above described technique is being used to measure the real and imaginary parts of the admittances of different pulse combustor components under cold and "hot" operating conditions. To date, the admittances of the air valve, the fuel valve with its decoupling chamber and the mixing chamber fitted with the air valve and with both the air and fuel valves were measured under

cold flow conditions. In addition, the effect of the spacing of the air valve upon its admittance was determined. All tests were carried out at mean pressures in the impedance tube equal to the previously determined boost pressure in the pulse combustor and acoustic driver power levels of approximately 160 dB which correspond to typical dB levels in the pulse combustor. Furthermore, the driving frequencies were varied between 20 and 170 Hz.

Before presenting the obtained results, it would be helpful to consider Fig. 6. It shows the dependence of the real part of the admittance upon ΔP (i.e., $P_{\max} - P_{\min}$). Clearly, when the magnitude of the real part of the admittance (i.e., Y_r) is small, the value of Y_r is relatively insensitive to the accuracy of the measurement of ΔP . However, as the magnitude of Y_r increases, the sensitivity of the Y_r to the measured ΔP increases rapidly. Thus, the error in the determined Y_r increases with increasing value Y_r . In addition, while the real part of the admittance depends largely upon the value of ΔP , the value of the imaginary part of the admittance is largely determined by the location of P_{\min} . Since the standing pressure wave has a relatively flat minimum, especially at low frequencies, it was easier to determine the value of the minimum than its location. The real parts of the admittances were, therefore, measured with better accuracy than their imaginary parts.

The admittances were measured under cold flow conditions for the following configurations: (1) a hard termination at the end of the impedance tube (2) the gas valve and its decoupler at the end of the tube; (3) the air valve at the end of the tube; (4) the mixing chamber fitted with the air valve only; and (5) the mixing chamber fitted with both the fuel and the air valves. The air valve opening was varied between 0 and .018 inches for configurations 3, 4 and 5.

The real parts of the admittances for the above configurations with the air valve (when included) closed and open (to .012 inches) measured over a 20 - 170 Hz frequency range are shown in Fig. 7. An air valve opening of .012 inches was selected since it corresponds to a typical setting of a pulse combustor under normal operating conditions. As long as the air valve is closed Y_r is essentially zero at low frequencies for all of the tested configurations. As the frequency is increased, Y_r and, thus, the damping of the air valve slightly increases. A much larger increase in damping at higher frequencies is observed for the closed air valve. The real part of the admittance is increased even further if the closed air valve is attached to the mixing chamber. Thus, adding the mixing chamber and the "elbow" connection between the air valve and the mixing chamber increases the real part of the admittance measurably. On the other hand, adding the fuel valve to the mixing chamber - air valve assembly has no significant effect upon the real part of the admittance at any investigated frequency. Figure 7 also shows that opening the air valve substantially increases the real part of the admittance over the entire range of investigated frequencies. Once again, the effect of attaching the air valve housing to the side of the mixing chamber is significantly greater than adding the fuel valve to the mixing chamber - air valve assembly. The increase in the real part of the admittance with increasing air valve opening is illustrated in more detail in Fig. 8 for a range of valve openings and driving frequencies for the mixing chamber fitted with both valves.

The measured imaginary parts of the admittance (i.e., Y_i) for these configurations over the 20 to 170 Hz frequency range are shown in Fig. 9. Once again, Y_i is zero for the hard termination as well as for the fuel valve only.

However, once the closed air valve was added to any of the three investigated configurations the imaginary part of the admittance increased substantially. The latter effect increased with increasing frequency. This occurred because adding the valve assembly moves the termination, in the form of the valve plates, further away from the end of the impedance tube, see Fig. 10. The minimum of the standing pressure wave in the impedance tube was, therefore, moved upstream resulting in an increase in Y_i . Because of the size of the mixing chamber and the elbow that connects the air valve to it this effect is more pronounced for the valve - mixing chamber assembly than for the air valve alone.

Once the air valve is opened the pressure anti-node moves away from the valve plates towards the driver end of the impedance tube, see Fig. 10. (If the valve plates are completely removed the resulting open end corresponds to a pressure node). This causes the decrease in the magnitude of Y_i observed in Fig. 9. Because of the difficulty of determining the precise location of the minimum of the standing pressure wave, discussed above, no clear difference between the imaginary part of the impedance of the air valve only and that of the valve - mixing chamber assembly could be established. However, Fig. 11 clearly shows that the magnitude of Y_i decreases as the opening of the air valve increases. This effect is particularly pronounced at higher frequencies. The lack of smoothness of the curves is, once again, due to the difficulty in determining the precise location of the flat minimum of the standing wave.

Finally, work has continued on developing a linear acoustic model of the dynamics of the flapper valve. This model is based upon integral formulations of the continuity and momentum equations and the equation of motion of the

flapper. Some results are presented in Figs. 12-14. Figure 12 shows the variation with time of the real part of the admittance of the air valve for a valve gap of .009" for one half of the cycle at a low frequency (i.e., 9 Hz). Y_r and, thus, the valve damping increases rapidly while the valve is opening. Y_r reaches a constant level and it drops again as the valve closes. The calculated values of Y_r for the valve in the closed and opened (.009" gap) positions are comparable to the measured admittances of the air valve for the respective valve gaps (see Fig. 7). The discrepancies between the actual calculated and measured values of the admittances are (at least partially) due to the fact that the admittance was calculated at the valve itself while the measurements determined the admittance at the interface between the valve housing and the impedance tube. In addition, the calculate admittances are instantaneous values while the admittance measurements integrate over a large number of cycles.

Figure 13 shows the calculated times required for the air valve to open as a function of frequency for four different valve gaps. Clearly, these opening times decrease as the frequency is increased until they begin to level off above about 50 Hz. On the other hand, the magnitude of the valve spacing has a relatively small effect upon the time required to open the valve.

Since the time required for the valve to open or close does no longer diminish with frequency at high frequencies it is conceivable that at the very high frequencies there is not enough time during each cycle for the valve to open and close completely. For this reason the calculated valve opening time as a fraction of half period of the cycle was plotted against frequency in Fig. 14. This figure shows that even at frequencies of 150 Hz the valve is either open or shut during at least 30% of the duration of the cycle.

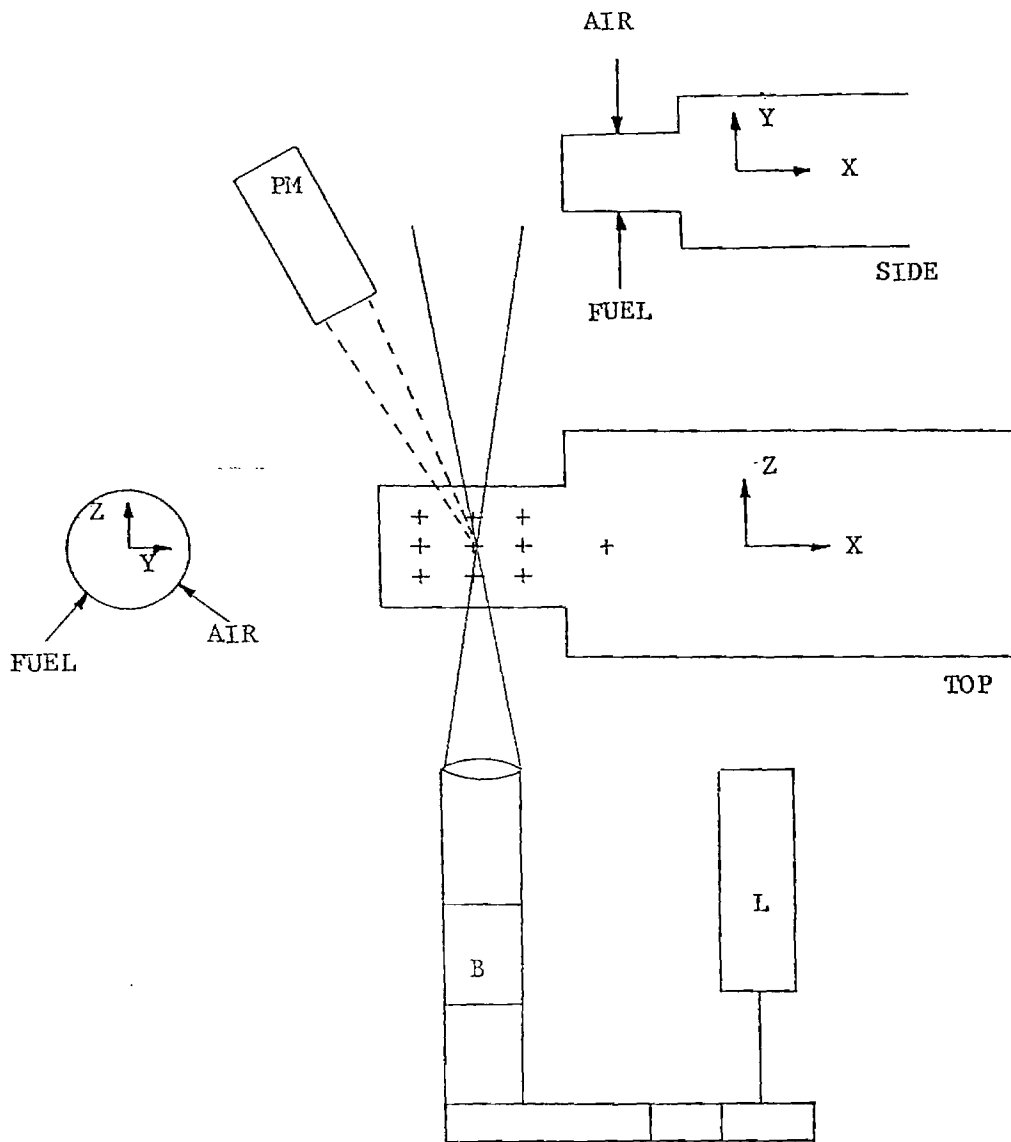
PLANNED WORK

During the next reporting period the LDV software modification will be completed and velocity measurements will continue. In addition, local densities and, therefore, temperatures will be determined using molecular Rayleigh scattering. Furthermore, the recent arrival of an intensified CCD imaging system will permit radiation measurements to be carried out efficiently and with much improved resolution (128 x 128 pixles).

Impedance tube measurements of the combustor components under cold flow will be completed and this effort will move on to measuring the admittances of the combustor with combustion.

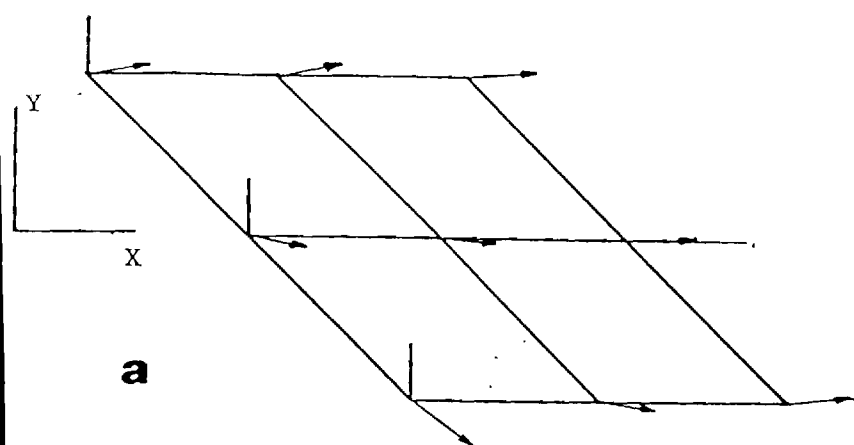
The modeling of the air flapper valve will continue and selected experiments will be carried out in order to confirm the model's predictions.

LDV SCHEMATIC

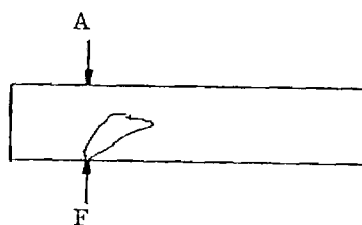
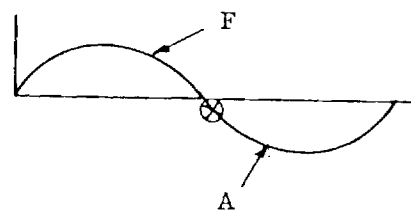


VELOCITIES MEASURED IN Y & Z DIRECTIONS

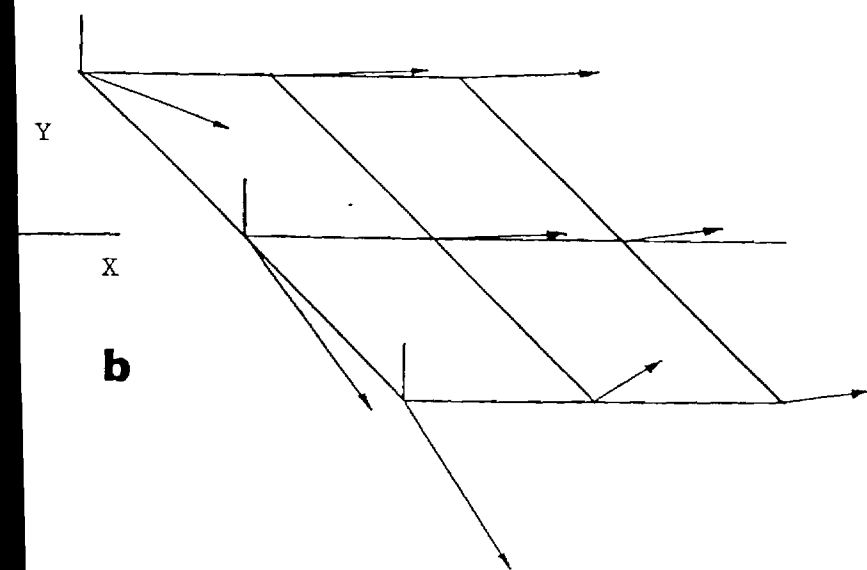
Fig. 1 Location of LDV Measurements in the Mixing Chamber.



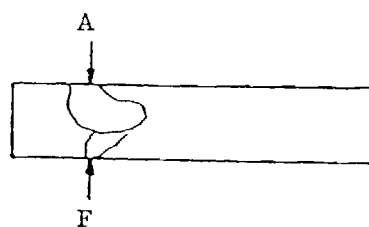
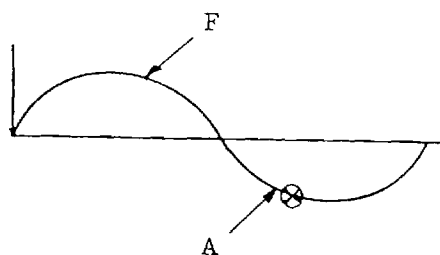
Vector Plot



Shadow Image



BVector Plot



Shadow Image

Fig. 2 Comparison of Vector Plots Obtained by LDV with High Speed Shadowgraphy Images at Four Instances During a Cycle

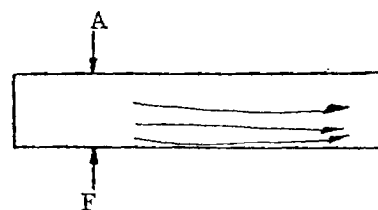
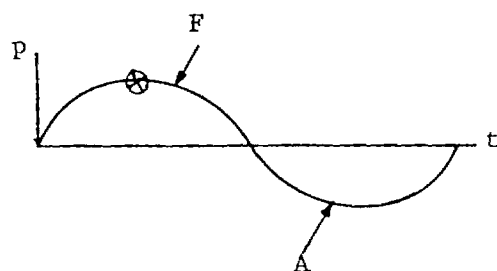
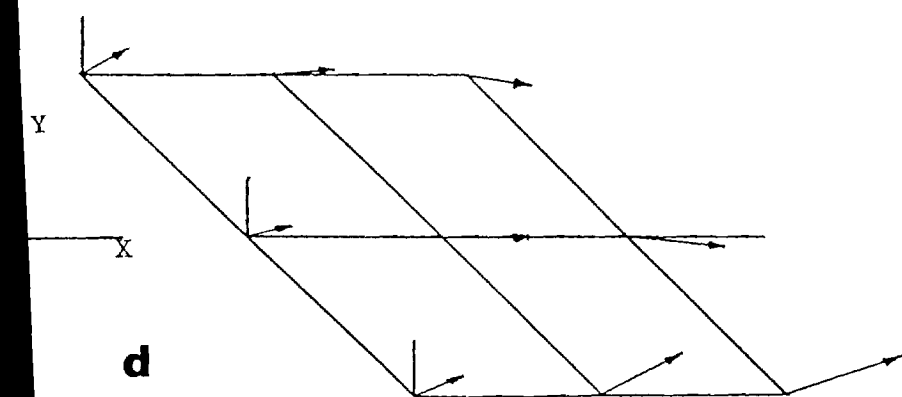
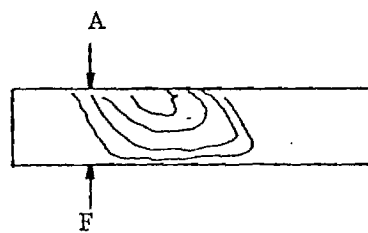
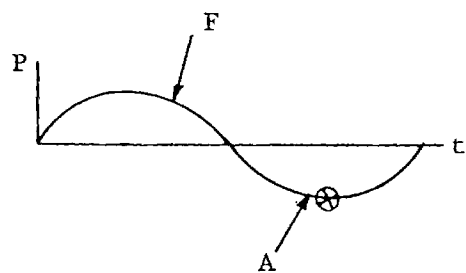
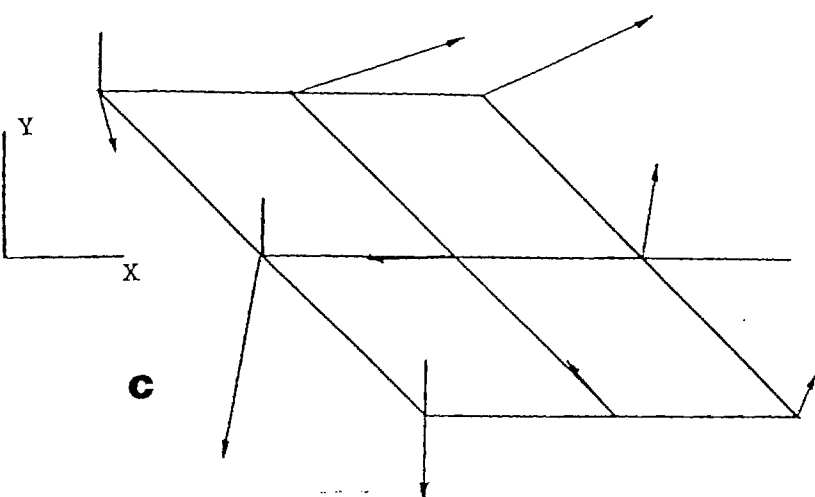


Fig. 2 Continued

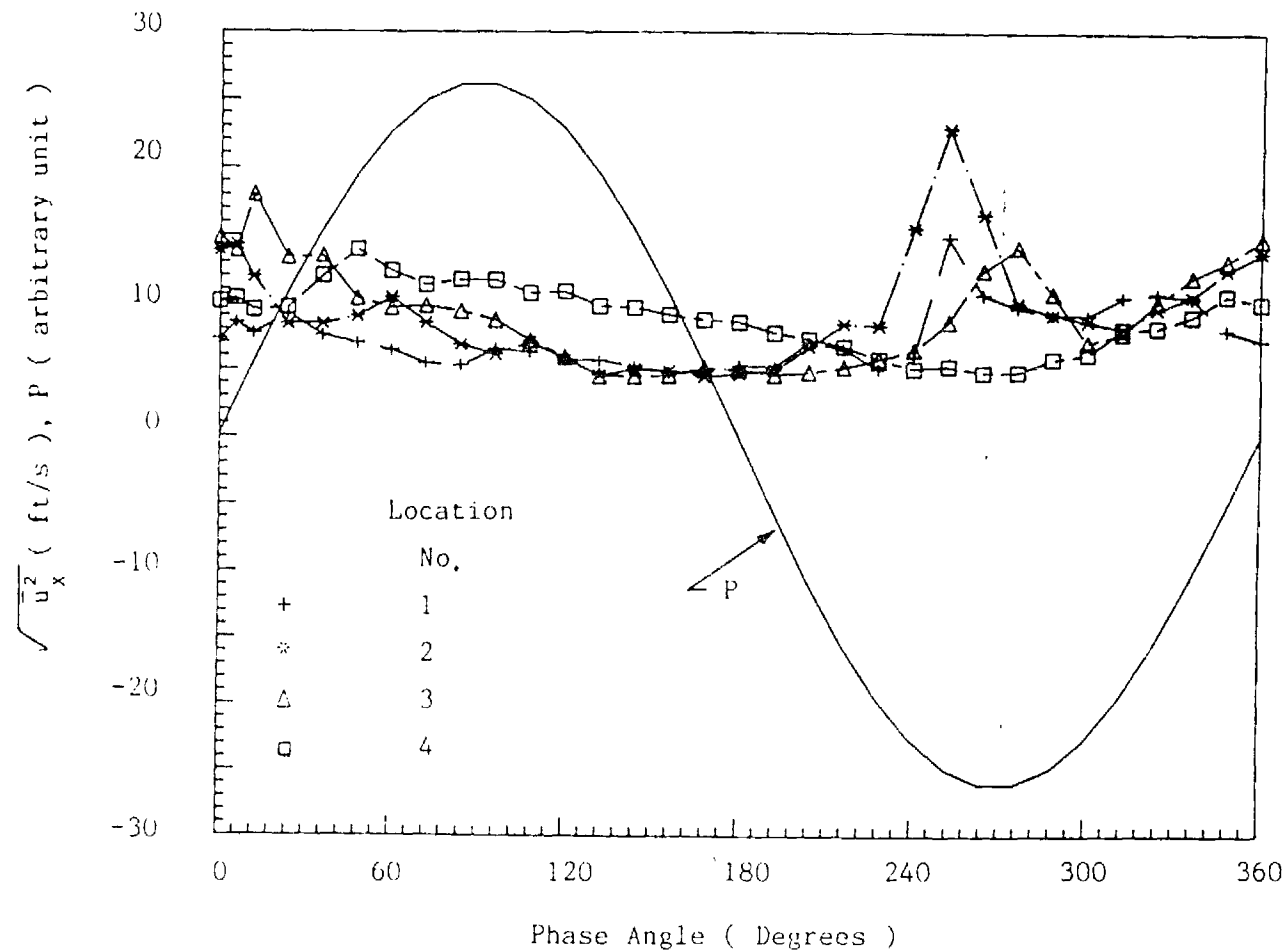


Fig. 3 Variation of RMS Values of Axial Velocities during Cycle at four different locations. Locations 1, 2 and 3 in the Mixing Chamber, Location 4 in the Combination Chamber. The Pressure Cycle is shown for Reference.

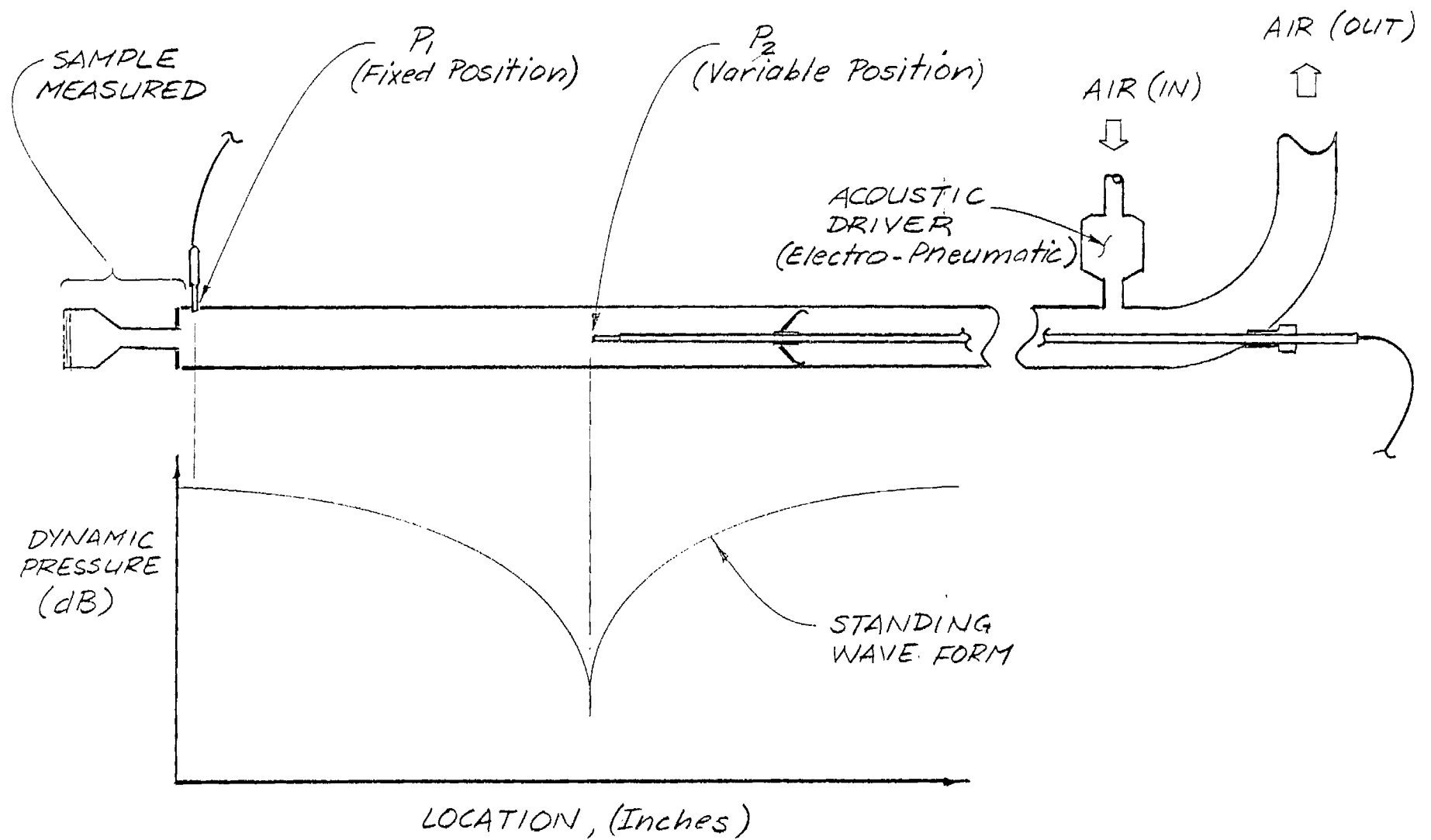


Fig. 4 Experimental Setup for Impedance Tube Measurements

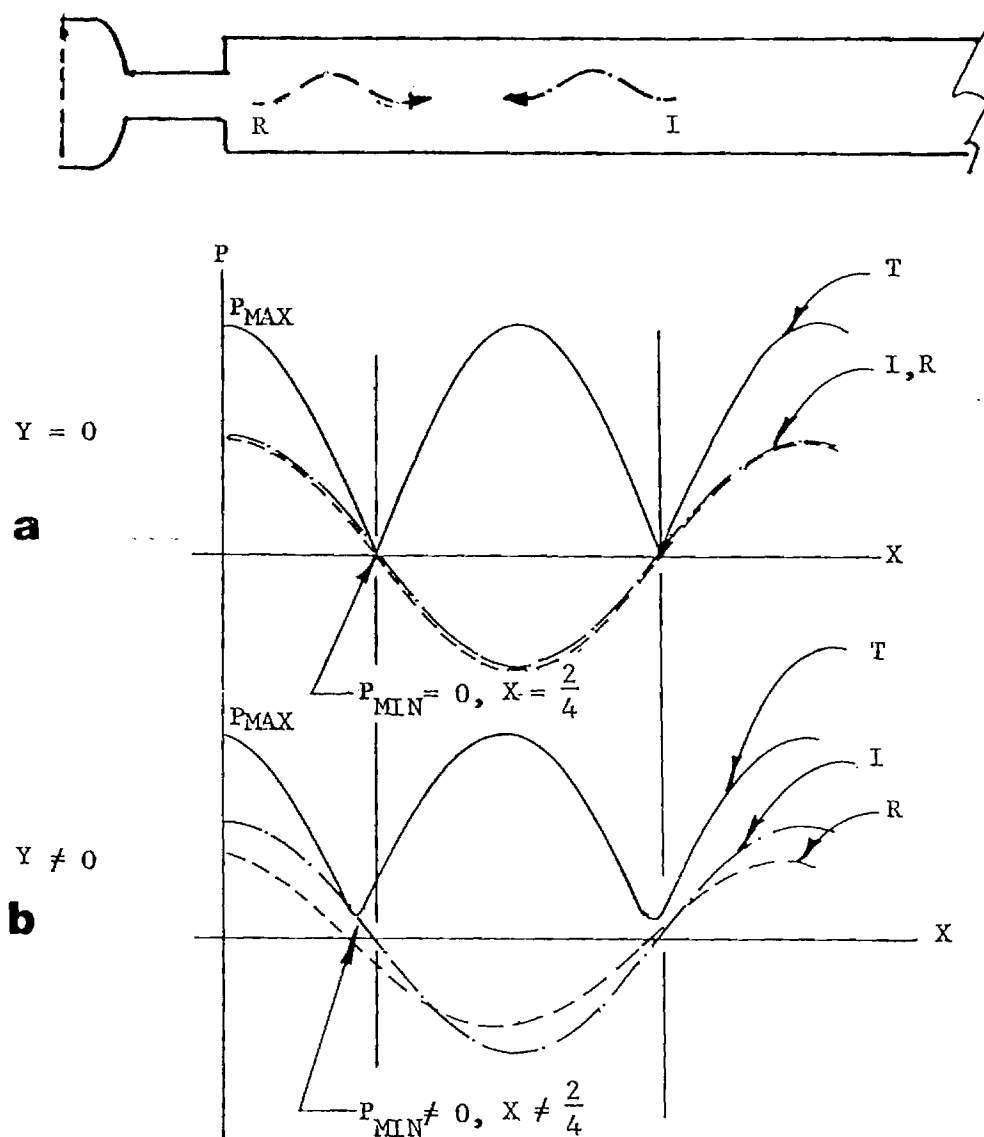


Fig. 5 Waveform of Incident (I), Reflected (R) and Total Standing Wave (T) for Hard Termination (a) and Termination with Finite Admittance (b).

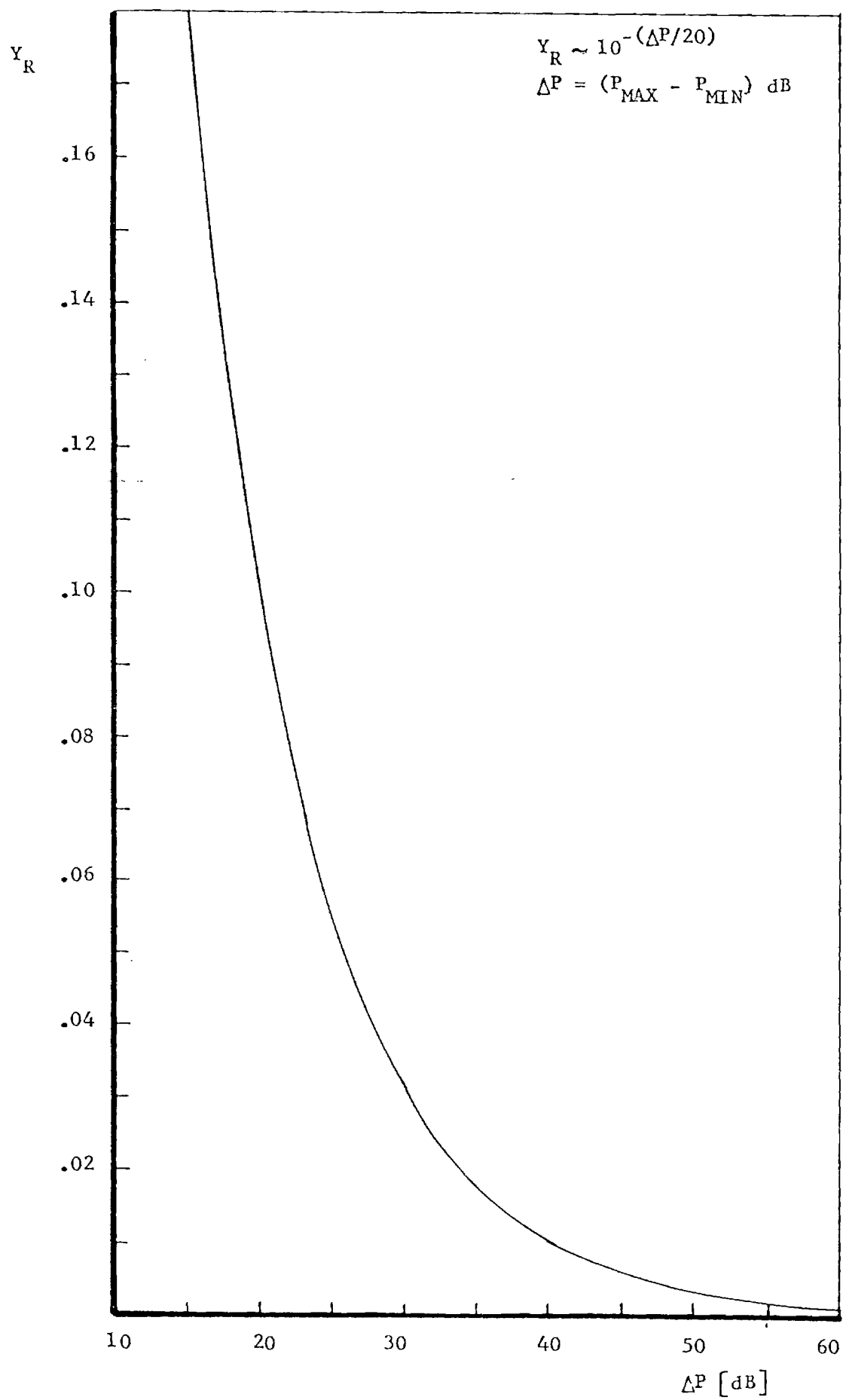


Fig. 6 Plot of ΔP vs. Real Part of Admittance (y_R)

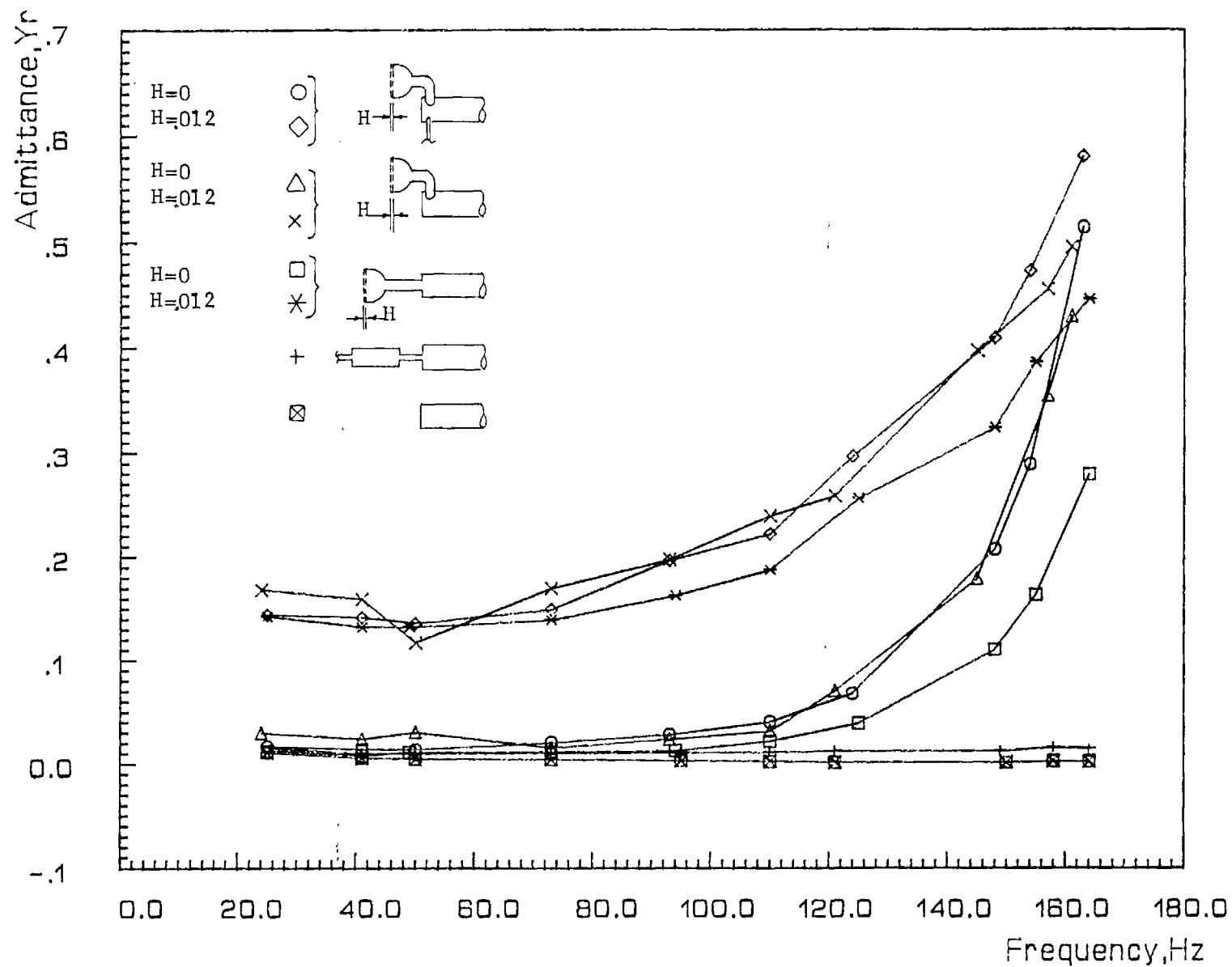


Fig. 7 Real Part of Admittance vs. Frequency for various Impedance Tube Terminations. (H=Air Valve Gap in inches)

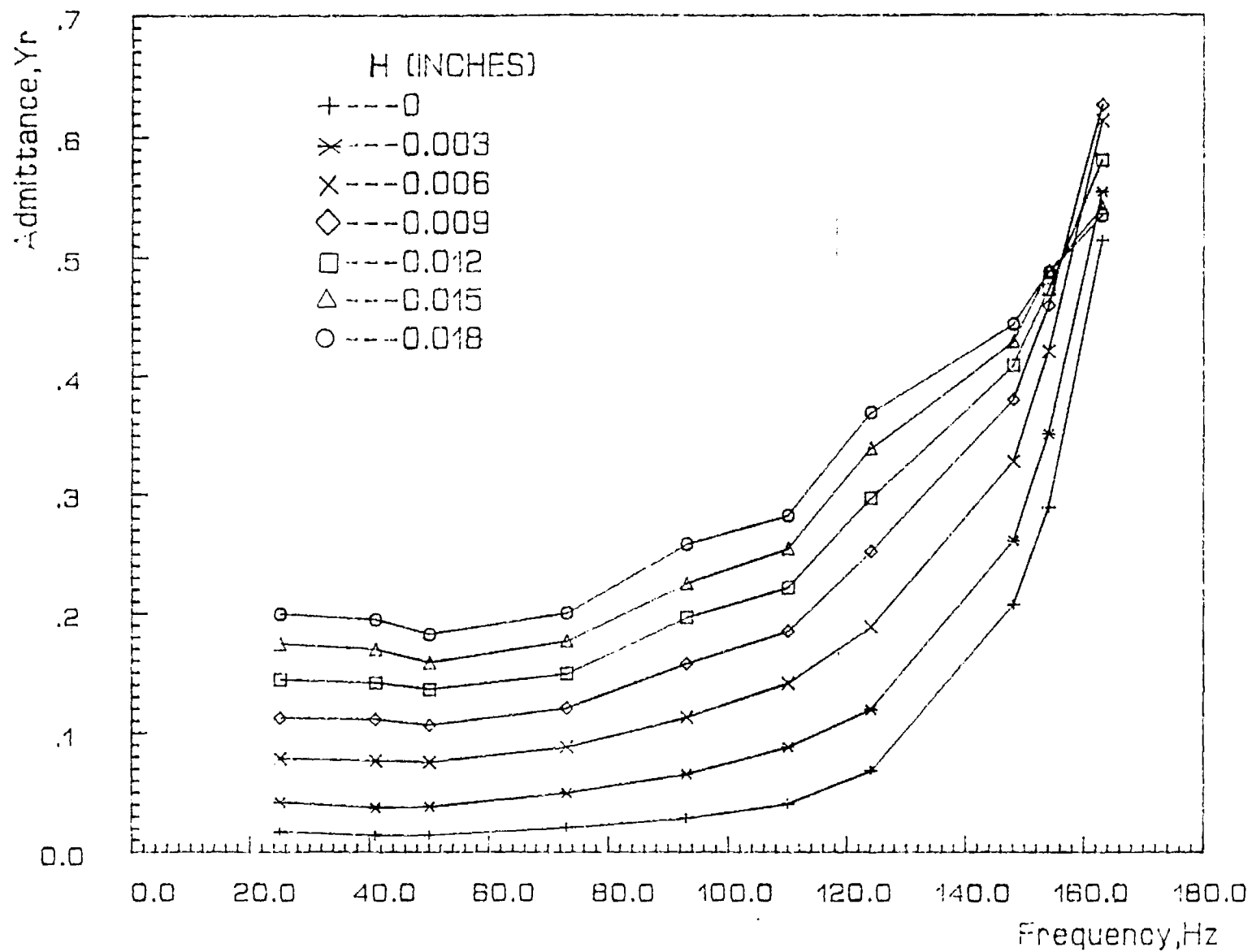


Fig. 8 Real part of Admittance of Mixing Chamber with Fuel and Air Valves vs. Frequency for different Air Valve Gap Settings (H).

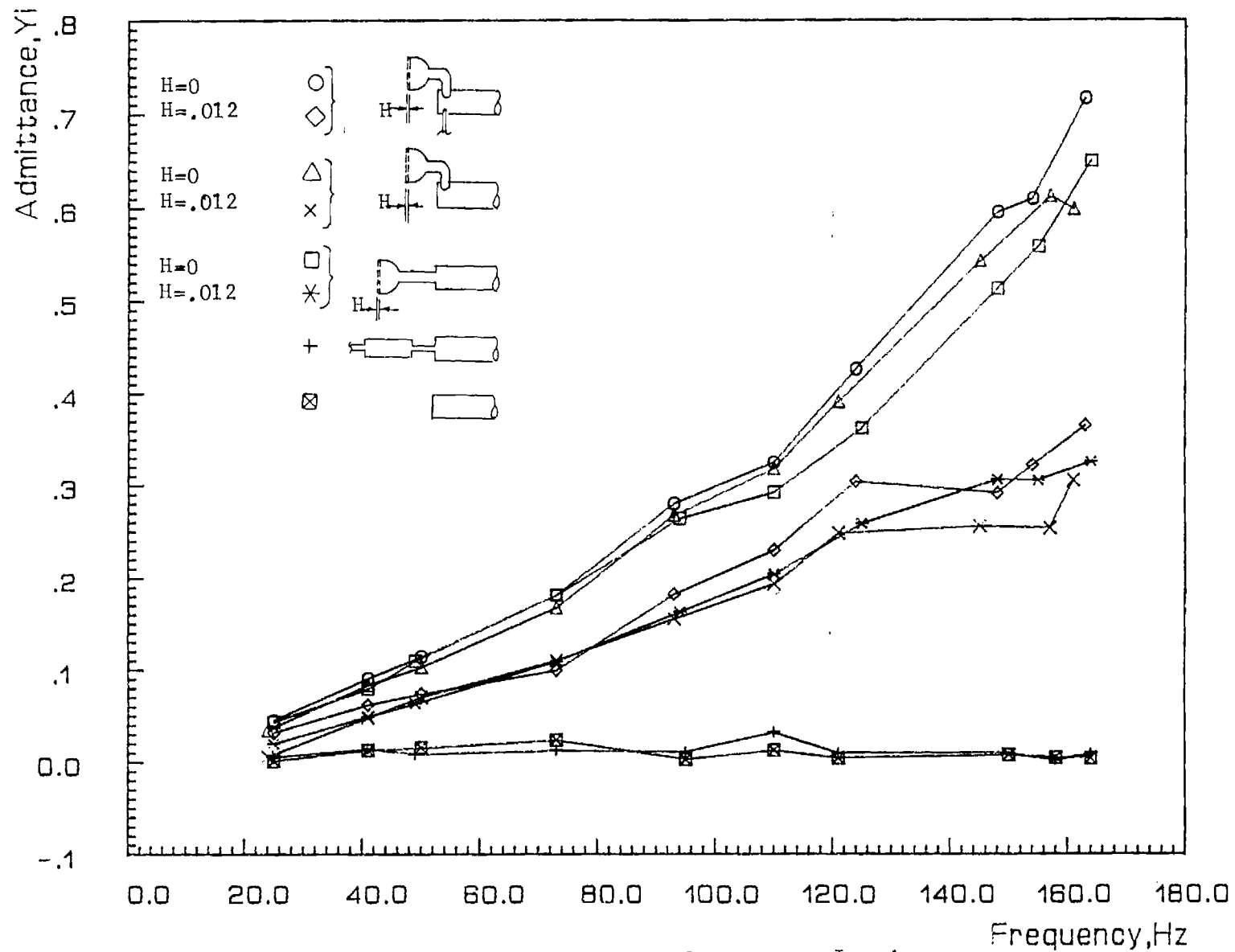
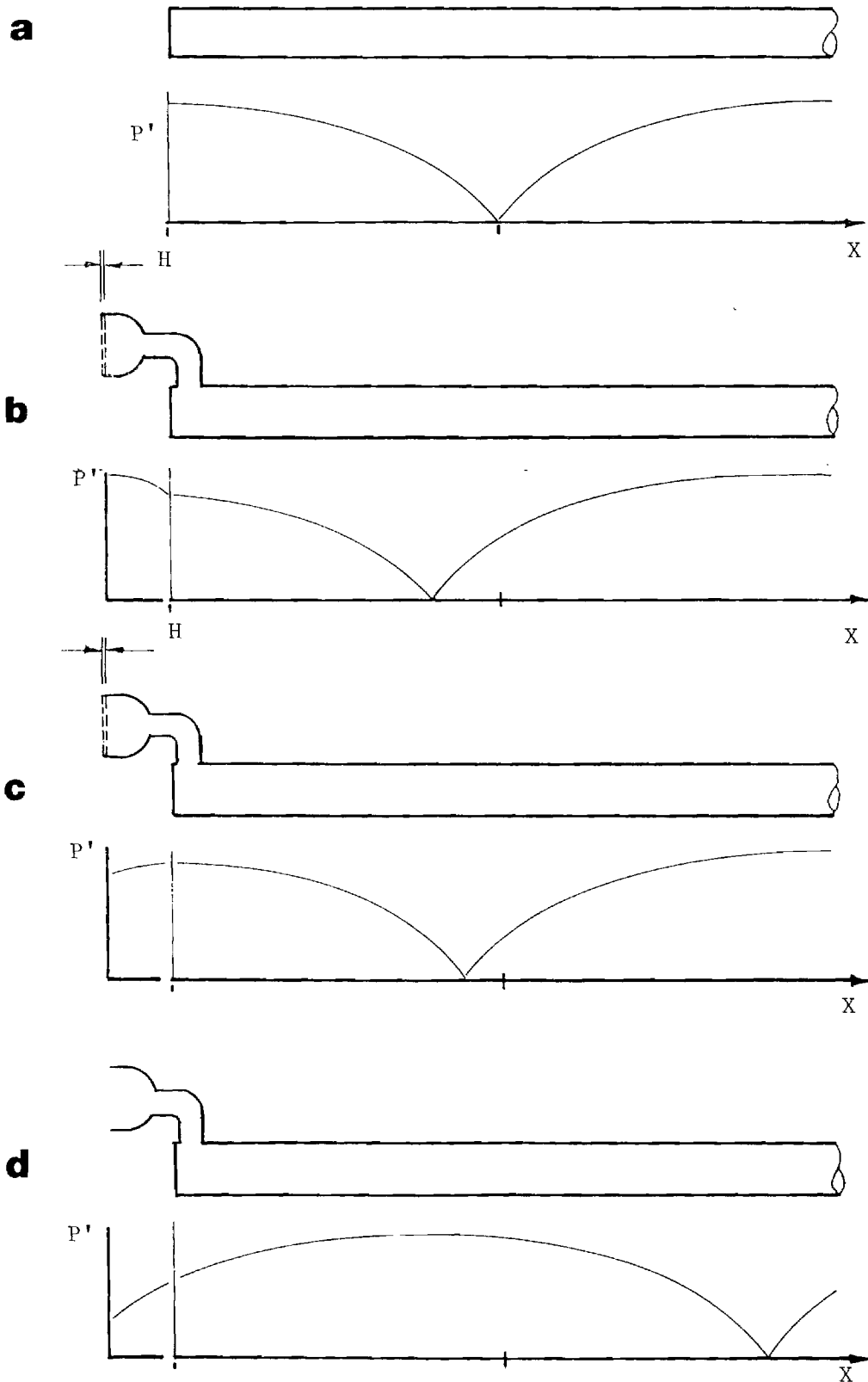


Fig. 9 Imaginary Part of Admittance vs. Frequency for various Impedance Tube Terminations (H =Air Valve Gap in inches)



10 Schematic of Standing Wave Pattern in Impedance Tube Fitted with a) Hard Termination, b) Closed Valve ($H=0$), c) Open Valve ($H \neq 0$) and d) Valve Housing but Valve Plates Removed. Actual Measured Standing Wave more Complex in the Valve Housing due to its Geometry.

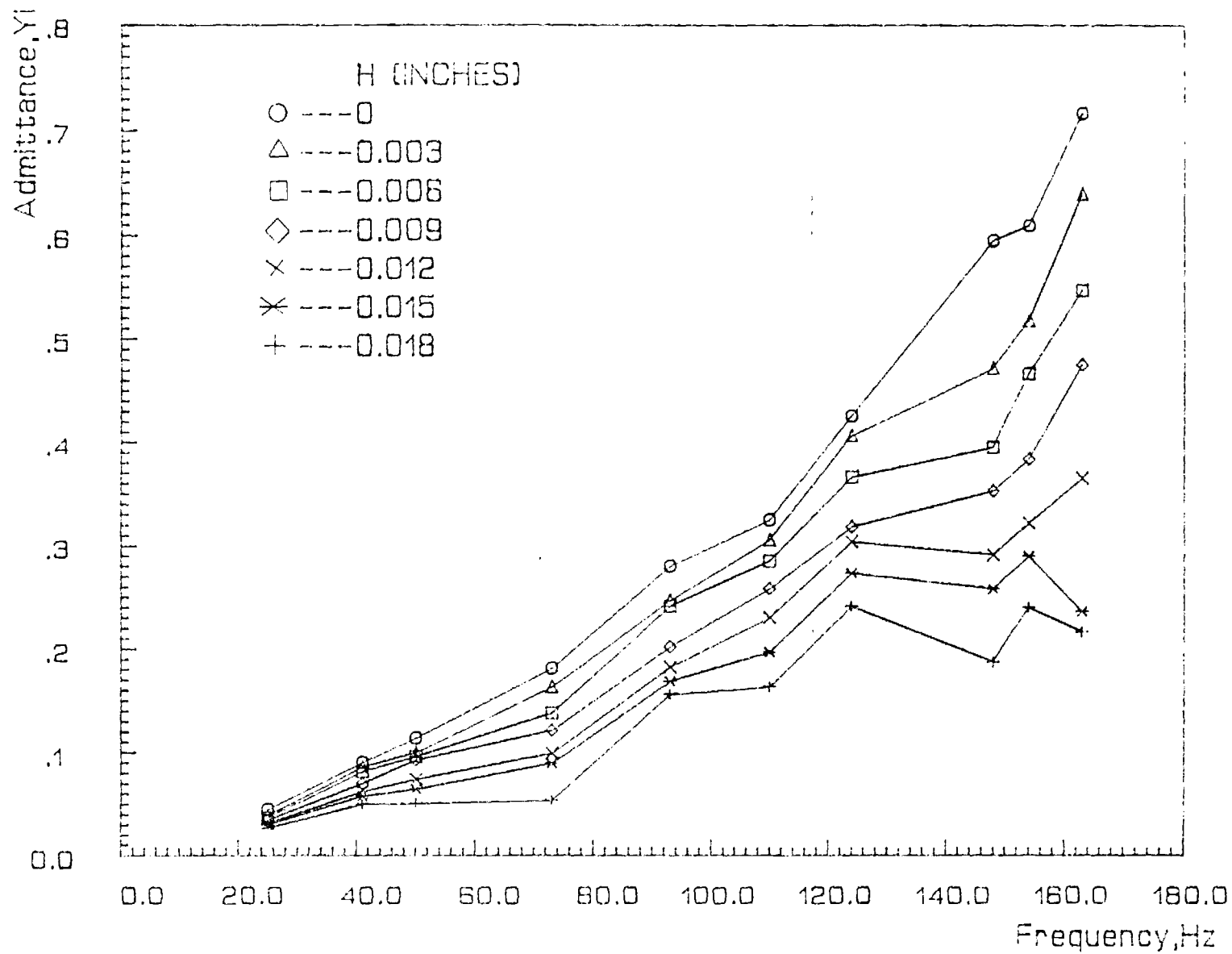


Fig. 11 Imaginary Part of Admittance of Mixing Chamber with Fuel and Air Valves vs. Frequency for different Air Valve Gap Settings (H).

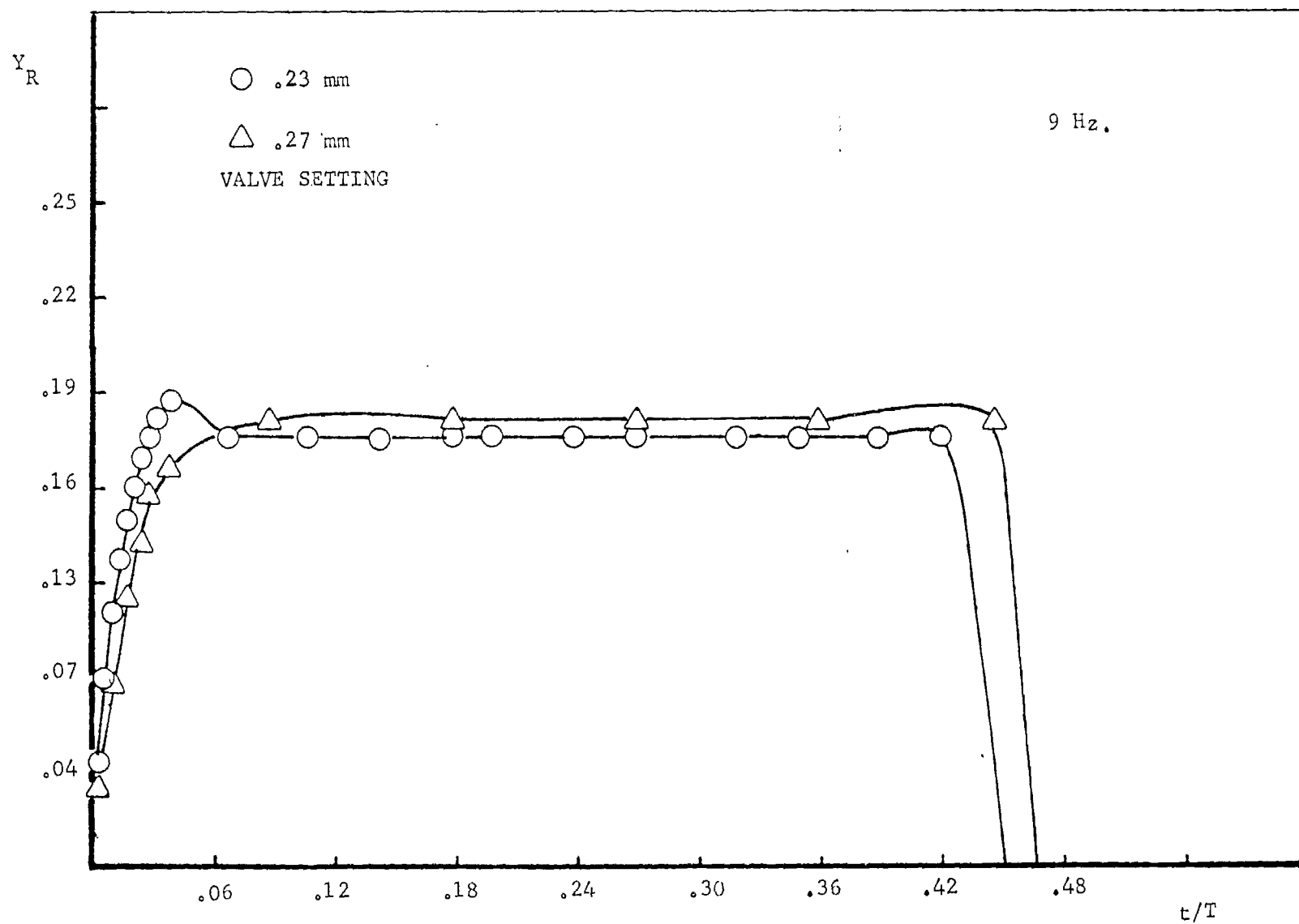


Fig. 12 Time Variation of the Calculated Real Part of the Admittance of the Air Valve for the First Half of the Cycle (Frequency: 9 Hz)

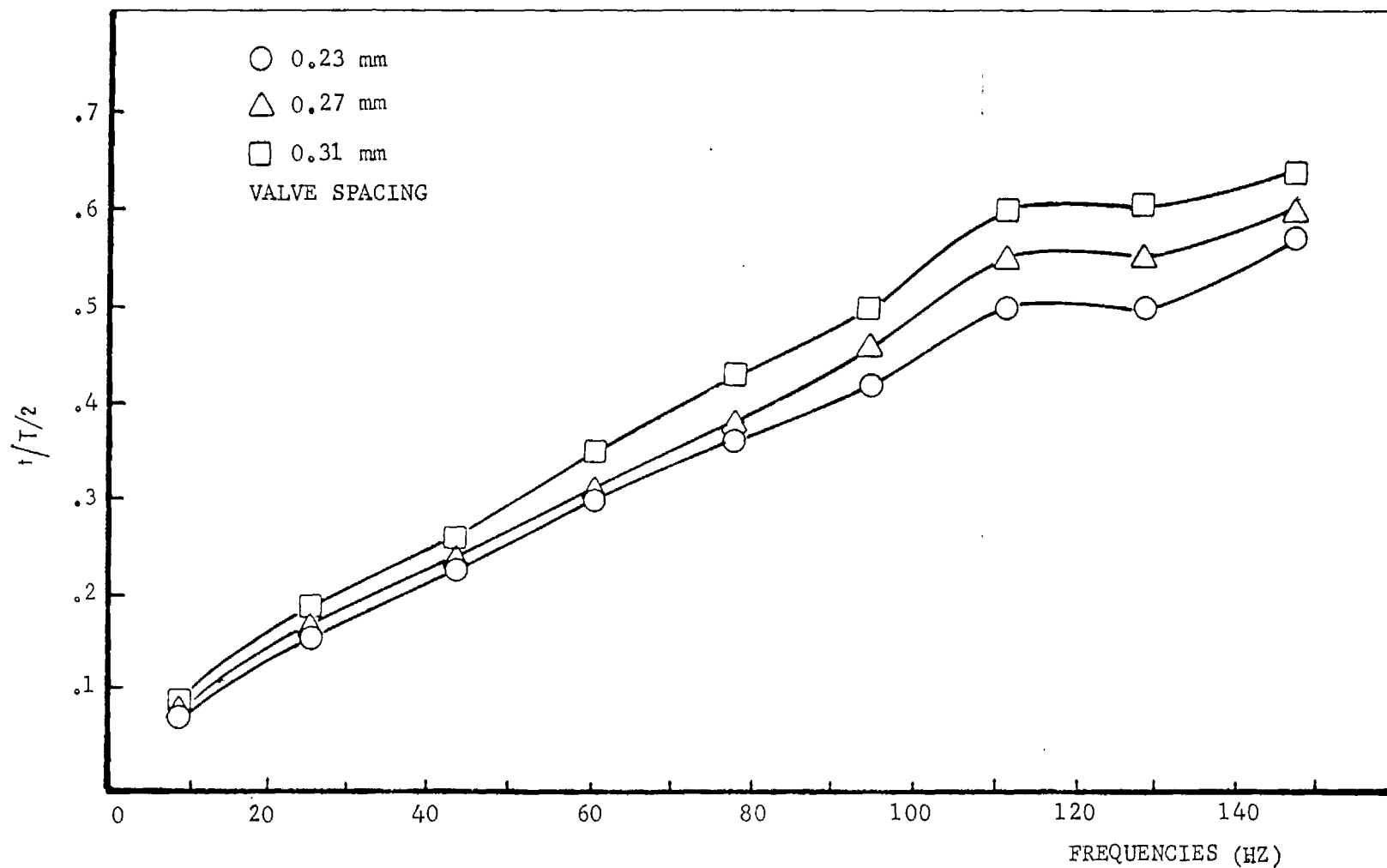
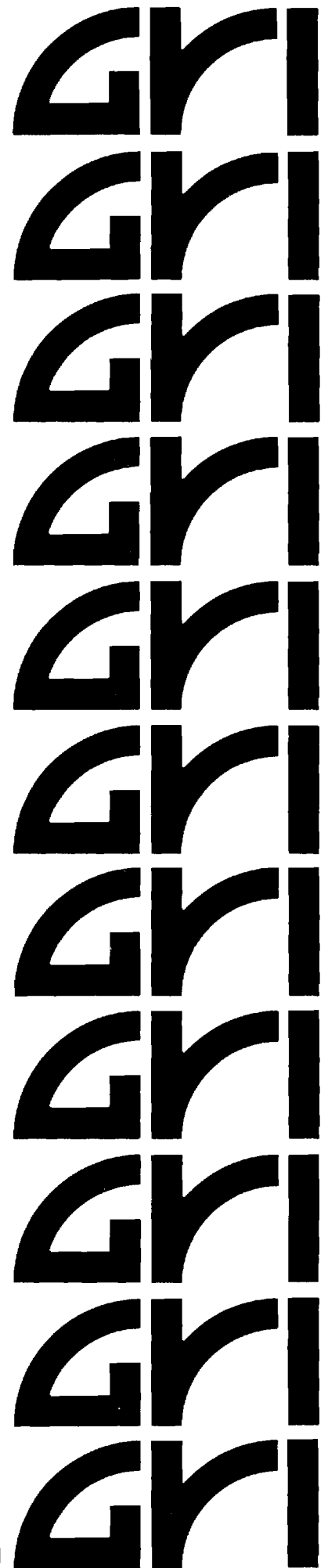


Fig. 14 Calculated Valve Opening Times as a Fraction of Half Period of the Cycle vs. Frequency for Different Valve Spacings

**PULSATING BURNERS
CONTROLLING MECHANISMS AND PERFORMANCE**

**ANNUAL REPORT
(January — December 1988)**

**Gas Research Institute
8600 West Bryn Mawr Avenue
Chicago, Illinois 60631**



Pulsating Burners - Controlling Mechanisms and Performance

Annual Report

January 1, - December 31, 1988

Prepared by

B. T. Zinn, B. R. Daniel and J. I. Jagoda

School of Aerospace Engineering

Georgia Institute of Technology

For

Gas Research Institute

Grant No. 5087-260-1466

GRI Project Manager

James A. Kezerle

Combustion

January, 1989

GRI DISCLAIMER

LEGAL NOTICE: This report was prepared by the Georgia Institute of Technology as an account of work sponsored by the Gas Research Institute (GRI). Neither GRI, members of GRI, nor any person acting on behalf of either:

- a: Makes any warranty or representation, express or implied, with respect to the accuracy, completeness, or usefulness of the information contained in this report, or that the use of any apparatus, method, or process disclosed in this report may not infringe privately owned rights; or
- b. Assumes any liability with respect to the use of, or for damages resulting from the use of, any information, apparatus, method, or process disclosed in this report.

REPORT DOCUMENTATION PAGE		1. REPORT NO.	2.	3. Recipient's Accession No. GRI 89/0191
4. Title and Subtitle PULSATING BURNERS - CONTROLLING MECHANISMS AND PERFORMANCE				5. Report Date OCTOBER '89 (APPROVED)
7. Author(s) B.T.ZINN, B.R.DANIEL AND J.I.JAGODA				6. Performing Organization Rept. No.
9. Performing Organization Name and Address SCHOOL OF AEROSPACE ENGINEERING GEORGIA INSTITUTE OF TECHNOLOGY ATLANTA, GEORGIA 30332				10. Project/Task/Work Unit No. E-16-601
				11. Contract(s) or Grant(s) No. (C) 5087-260-1466 (G)
12. Sponsoring Organization Name and Address GAS RESEARCH INSTITUTE 8600 WEST BRYN MAWR AVENUE CHICAGO, IL 60631				13. Type of Report & Period Covered ANNUAL JAN.1, '88-DEC.31, '88
15. Supplementary Notes				14.
16. Abstract (Limit: 300 words) This report describes the results of an ongoing investigation of the physical and chemical processes which control the operation of gas fired, valved pulse combustors. Results of flow visualization experiments were compared with LDV measurements in the mixing chamber. They show that the flow field is dominated by the entry of the air jet. A large, axial recirculation zone occupies most of the mixing chamber during the combustion phase of the cycle, and the flow is extremely turbulent. Finally, backflow from the tailpipe penetrates several inches into the combustion chamber and it does not reach the combustion region. The admittance of various components which make up the pulse combustor were measured using an impedance tube technique. The real and imaginary parts of the admittances of the fuel valve, the air valve and the mixing chamber fitted with the fuel and air valves were determined over a range of frequencies and for a range of air valve openings. A linear model of the air valve was developed and used to calculate the instantaneous damping by this valve during the cycle. These calculated results are in good qualitative agreement with experimental observations. In addition, the model predicts the times required to open and close the air valve as a function of frequency.				
17. Document Analysis a. Descriptors PULSE COMBUSTION				
b. Identifiers/Open-Ended Terms				
c. COSATI Field/Group COMBUSTION				
18. Availability Statement:		20. Security Class (This Report) Unclassified	21. No. of Pages	
		20. Security Class (This Page) Unclassified	22. Price	

RESEARCH SUMMARY

Title: Pulsating Burners - Controlling Mechanisms and Performance

Contractor: Georgia Tech Research Institute

Contract Number: 5087-260-1466

Reporting Period January - December 1988, Annual Report

Principle Investigators: B. T. Zinn, B. R. Daniel and J. I. Jagoda

Objective: It is the objective of this study to gain further insights into the physical mechanisms which control the mixing and heat release processes in pulse combustors. In addition, the acoustic driving and damping characteristics of various components and subsystems of the pulse combustor will be determined for various operating conditions.

Technical Perspectives: Although gas fired pulse combustors have been on the market for a number of years, their controlling mechanisms are still not sufficiently well understood to permit the design of pulse combustors for different applications without resorting to costly trial and error

development efforts. Proper operation of pulse combustors requires that the timing of the mixing, cycle to cycle reignition and flame spread processes produce oscillatory heat release in phase with the pressure oscillations, which results from compatibility between the acoustic properties of the various components of the pulse combustor. To develop a rational design procedure for pulse combustors, it is necessary that the various processes responsible for energy addition to and removal from the pulsations be understood. Furthermore, data describing the acoustic properties of various pulse combustor components under different cold and pulse combustion operating conditions are needed. Finally, the dependence of the acoustic characteristics of the various combustor components upon the fundamental fluid mechanical, heat transfer and combustion processes must be understood.

Technical Approach: In order to elucidate the mechanisms which control the operation of various pulse combustor configurations and determine the damping/driving characteristics of various components and subsystems of commonly used pulse combustors, the following tasks are pursued simultaneously:

- 1) Investigation of the flow field characteristics, mixing and heat release in pulse combustors using

LDV, Schlieren, mixing visualization, radical radiation (OH, CH, CC) and Rayleigh scattering measurements.

2) Measurements of the driving and damping characteristics of various components and subsystems which make up the pulse combustor using the impedance tube technique.

3) The determination of the overall driving and damping characteristics of various pulse combustor designs under different operating conditions.

4) Modeling of the dynamic characteristics of the flapper valve.

Results:

Results of the flow visualization in the mixing chamber were compared with those from LDV measurements in that part of the combustor. These show that the fuel jet enters the mixing chamber shortly after the pressure there passes through its maximum. This is followed by the entry of the air jet which clearly dominates the flow field. A large, axial recirculation zone is observed in the mixing chamber during the combustion phase of the cycle. The level of turbulence intensity in the mixing chamber is high throughout the cycle, and it increases significantly immediately after the air enters the mixing chamber. The pressure oscillations cause periodic gas movement between the combustion chamber and the tail pipe

with the gases in the tail pipe penetrating a distance of several inches into the combustion chamber.

An impedance tube technique was used to determine the admittances of the air valve, the fuel valve and the mixing chamber fitted with the air valve only and with both the fuel and air valves. The measurements show that the real parts, Y_r , of the admittances (i.e., damping) of all components are essentially zero at low driving frequencies as long as the air valve is closed. As the frequency increases beyond 50 Hz the real part of the admittance of the fuel valve increases slightly while the damping by the air valve and the mixing chamber fitted with fuel and air valve increases considerably. Y_r of the air valve also depends upon the geometry of the pipe connecting the valve housing to the mixing chamber but is not affected by the presence of the fuel valve. Y_r of the air valve increases significantly when the valve opening is increased. The imaginary parts of the admittance, Y_i , of all of the investigated components are practically zero at low frequencies as long as the air valve is closed. Y_i of the fuel valve remains zero as the frequency increases. On the other hand, Y_i of the closed air valve increases from zero as the frequency increases. Y_i of the air valve decreases, however, as the air valve is opened. Y_i of the mixing chamber - air valve assembly exhibits trends similar to those of the air valve alone. Finally,

adding the fuel valve to mixing chamber - air valve assembly has no significant effect upon the system's admittance.

The behavior of the valve is being modeled using a linear acoustic model. The variation of the instantaneous real part of the admittance of the valve during a cycle has been calculated. The predicted behavior of the valve admittance is in good qualitative agreement with the measured impedance tube data. The model predictions indicate that the time required to open the air valve decreases as the frequency increases until a limiting value is reached above approximately 50 Hz. Furthermore, the valve setting appears to have little effect upon the valve opening time. It was also determined that even at frequencies above 150 Hz the valve opening and closing times are small fractions of the periods during which the valve is either fully open or closed.

Project Implementations: This research seeks to build on the results of recent fundamental research on pulse combustion and eliminate the remaining roadblocks to a rational design procedure. Flow measurements and visualization, measurements of acoustic properties, and modeling of the flapper valves are the three activities that are being pursued. Progress has been made on each, as summarized in this report. In the

third year of this contract, the contractor will conduct experiments that assure the dependability and generality of the results. GRI will require that the results of all three activities are put in a form that is useful to other organizations conducting research and development of pulse combustion devices. This contract will not be renewed. Further research on pulse combustion will be done through a Pulse Combustion Research Laboratory (PCRL), which will emphasize interaction with manufactures.

James A. Kezerle
Manager, Combustion
Physical Sciences Department

OBJECTIVES

It is the objective of this study to gain further insight into the fundamental processes responsible for the operation of various pulse combustor designs. Emphasis is being placed upon obtaining practical information which will permit designers to develop new and/or larger scale pulse combustors without resorting to costly trial and error based development efforts.

The velocity and the mixing patterns in the mixing and combustion chambers will be determined both qualitatively and quantitatively. The nature of the interaction between the combustion process and the acoustics of the combustor will be established. The impedance of various components and subsystems which make up the pulse combustor will be determined under various operating conditions. In addition, the driving and damping characteristics of different pulse combustor designs will be measured under different operating conditions. Finally, the dynamic characteristics of the flapper valves will be analytically modeled.

PROGRAM PLAN

The program is divided into four major tasks as outlined below:

Task 1: Investigation of the Interaction between the Oscillatory Flow Field and Heat Release Processes in the Pulse Combustor:

A. Laser Doppler Velocimetry: The three components of velocity will be measured at selected locations in the combustor. The period of

pulsations will be divided into a number of equal time segments and the LDV counts for each segment will be stored in separate files. This will permit ensemble averaging of the velocities in each segment over many cycles. Mean velocities and turbulence intensities as well as shear stresses can then be obtained for each instant in the cycle.

- B. Schlieren Visualization: High speed Schlieren and shadowgraph cinematography will be carried out through side windows in the combustor in order to visualize the flow along the combustor axis. These shadowgrams will then be correlated with those previously obtained through windows in the end walls of the combustor. This will provide a complete picture of the three-dimensional flow field in the pulse combustor.
- C. Mixing Visualization: Mixing patterns will be recorded photographically by heavily seeding one of the reactant flows and illuminating the combustor using an expanded laser sheet. These visualizations will be carried out through the flat windows in the cylindrical walls of the mixing and combustion chambers. The use of the flat windows is expected to reduce the amount of laser light reflected by the glass. These laser light intensity losses caused problems when this technique was previously applied to the combustor through cylindrical glass walls.
- D. Spectroscopy: Local and global heat release in the pulse combustor will be determined by measuring the OH, CH and CC radical radiation emitted from the combustor. Efforts will concentrate on

measurements through the side windows of the mixing chamber which will be correlated with previous results obtained through the end window of the combustor. A recently acquired intensified CCD system will help to increase spatial resolution of these measurements by an order of magnitude when it becomes operational.

- E. Rayleigh Scattering: Local densities and, therefore, temperatures will be measured using Rayleigh scattering. A combination of the emission spectroscopy and the Rayleigh measurements will result in a better understanding of the location and timing of the combustion process. In addition, the Rayleigh scattering results will yield a quantitative description of the path taken by the hot combustion products in the pulse combustor.

All task I measurements will be carried out in the pulse combustor with flat windows fitted to the curved walls of the mixing and combustion chambers. The results will be correlated with each other and with the phase in the cycle at which they were obtained. This will be achieved by using the measured pressure oscillations as a clock. Only a full coordination between the flow field, the heat release and the local temperature measurements can result in a thorough understanding of the fundamental processes which control the operation of the pulse combustor.

Task II: Impedance Measurements of Pulse Combustor Components:

The acoustic admittance of the various components and subsystems which make up the pulse combustor will be measured using an

impedance tube technique. These measurements will be carried out without and with combustion and under various operating conditions and frequencies. These measurements will yield information on the frequency dependence of the acoustic properties of various pulse combustor subsystems. In addition, the frequency dependence of the driving provided by the pulse combustion process will be investigated.

Task III: Determination of Overall Driving/Damping Characteristics of Pulse Combustors:

The overall driving and damping characteristics of the pulse combustor will be determined by measuring the growth and decay rates of the combustor pressure oscillations during the start-up and shut-down phases of operation. These measurements will be carried out for various combustor configurations and for a range of operating conditions. The driving and damping for different combustor geometries, fuel/air ratios and injector configurations will be determined.

Task IV: Modeling of Flapper Valve:

The behavior of the flapper valve will be modeled using the continuity and momentum equations and the equation of motion of the flapper. In addition, a transfer function, which will permit the calculation of the admittance at the air valve housing-mixing chamber interface from the calculated admittance at the valve plate, will be developed.

Task V: Reporting

As per contract agreement.

TECHNICAL PROGRESS AND RESULTS

TASK I

During the past year the axial flow field in the pulse combustor was visualized using high speed shadow photography through the flat quartz windows in the curved side walls of the mixing and combustion chambers. Particular attention was paid to the flow field in the mixing chamber and in the vicinity of the combustion chamber-tail pipe interface. In addition, velocity measurements in the mixing chamber were continued using a two component LDV system with Bragg cells. Because the flow in the combustor is periodic, mean flow velocities and turbulence intensities at different instances during the cycle had to be determined using conditional sampling. This was achieved by dividing each cycle into 30 equal time intervals and sorting the data into the relevant bins according to their time of arrival during the cycle. Ensemble averaged mean and RMS velocities were, thus, obtained at 30 equi-spaced instances during the cycle. The orientation of the locations of the LDV measurements are shown in Fig. 1. Images obtained by high speed shadowgraphy are compared with the axial and azimuthal LDV data measured at nine locations in the horizontal plane in the mixing chamber which bisects the angle between the fuel and air inlets in Fig. 2. The pressure oscillations were used as a clock in this comparison.

Since the air and fuel ports are located off axis, the flow field is not cylindrically symmetric. The high speed shadowgraphy shows (Fig. 2a) that the fuel jet enters the mixing chamber shortly after the pressure there passes through its maximum. This fuel jet appears to have no significant effect upon the LDV measurements. Just before the pressure minimum is reached (Fig. 2b) the air jet enters the mixing chamber. The air jet drastically increases the magnitudes of the velocity vectors near the upstream end of the mixing chamber. Furthermore, the addition of air into the combustor increases the flow velocities further downstream in the mixing chamber. A little later, during the combustion phase of the cycle (Fig. 2c), a large, axial recirculation region forms in the mixing chamber which is clearly seen in the shadowgraphs. This recirculation bubble manifests itself in the vector diagram as downward pointing velocity vectors near the upstream end and upward vectors near the downstream end of the mixing chamber. As the pressure maximum is reached the flow becomes axial again (Fig. 2d) as shown by the shadowgraph and the velocity vector plot. Shortly thereafter, the new fuel jet enters and the cycle repeats itself.

The variation of the turbulence intensity with time during the cycle at a number of representative locations is shown in Fig. 3. The apparent level of turbulence, as measured by the RMS value of the conditionally sampled velocity, is considerably higher than that observed in other turbulent flows, (e.g. in the turbulent shear layer behind a backward facing step). However, only a part of this RMS is due to true turbulence. Since the values of the velocity fluctuations were obtained by ensemble averaging, there are also contributions due to: 1) the finite width of the slots into which each cycle was divided; 2) the slight differences in the flow field from cycle to cycle; and 3) slight variations in the

combustor frequency during the experiment. Nevertheless, a significant increase in the intensity of turbulence can be observed in the mixing chamber immediately after the entry of the air. The LDV data acquisition software is currently being modified to eliminate the effect due to the slight variations in pulse frequency. Once completed, the pulse duration for each cycle will be determined from the actual pressure oscillations measured during the experiment rather than from a previously determined mean frequency as is presently the case.

High speed shadowgraphy was also carried out at the downstream end of the combustion chamber where the combustor connects with the tail pipe. As the pressure in the combustor decreases, combustion products from the tail pipe are seen to flow back into the combustion chamber. This backflow penetrates a distance of only two to three inches back into the combustor. As the acoustic pressure begins to rise again the flow reverses and reenters the tail pipe.

TASK II

In this task, the impedance tube technique was used to measure the admittances (i.e., the complex ratio of the acoustic velocity normal to the surface and the local pressure) of different pulse combustor components. In this technique, the investigated component is attached to the upstream end of a long tube, see Fig. 4, and an electro-pneumatic, acoustic driver is attached to the wall just upstream of the opposite end of the tube. The acoustic driver is used to excite an incident acoustic wave which moves towards the tested component. The interaction of this wave with the investigated sample produces a reflected wave with modified amplitude and phase. The incident and reflected waves combine to establish a standing wave in the impedance tube. A piezo-electric pressure

transducer mounted near the tested sample measures the amplitude at the upstream end of the tube. A second pressure transducer, mounted at the end of a long rod, is translated inside the tube to measure the axial variation of the standing wave amplitude along the impedance tube.

When measuring the admittance of a hard termination (i.e., zero admittance), the incident wave is reflected without a change in amplitude or shift in phase. In this case the combination of incident and reflected waves produces a standing wave with a zero-amplitude pressure minimum located one quarter of the wavelength ($1/4$) from the hard termination, see Fig. 5a. On the other hand, if the complex admittance of the termination is non-zero, see Fig. 5b, the minimum pressure amplitude is non-zero and it occurs at a location other than $1/4$ from the tested sample. Physically, the termination changes the pressure amplitude of the reflected wave and introduces an apparent change in the length of the pipe by introducing a phase shift in the reflection process. The measured values of P_{\max} , P_{\min} and the distance of P_{\min} from the tested sample can be used to determine the real and imaginary parts of the admittance of the termination and, thus, of the component under investigation. A more detailed analysis shows that the real part of the admittance, which is calculated from the difference between the maximum and minimum pressure amplitudes (i.e., $P_{\max} - P_{\min}$) determines the damping (or driving) provided by the component under investigation. On the other hand, the imaginary part of the admittance provides information which affects the frequency of the system which utilizes the tested component.

The above described technique is being used to measure the real and imaginary parts of the admittances of different pulse combustor components

under cold and "hot" operating conditions. To date, the admittances of the air valve, the fuel valve with its decoupling chamber, and the mixing chamber fitted with the air valve and with both the air and fuel valves were measured under cold flow conditions. In addition, the effect of the spacing of the air valve upon its admittance was determined. All tests were carried out at mean pressures in the impedance tube equal to the previously determined boost pressure in the pulse combustor and acoustic driver power levels of approximately 160 dB which correspond to typical dB levels in the pulse combustor. Furthermore, the driving frequencies were varied between 20 and 170 Hz.

Before presenting the obtained results, it would be helpful to consider Fig. 6. It shows the dependence of the real part of the admittance upon ΔP (i.e., $P_{\max} - P_{\min}$). Clearly, when the magnitude of the real part of the admittance (i.e., Y_r) is small, the value of Y_r is relatively insensitive to the accuracy of the measurement of ΔP . However, as the magnitude of Y_r increases, the sensitivity of the Y_r to the measured ΔP increases rapidly. Thus, the error in the determined Y_r increases with increasing value Y_r . In addition, while the real part of the admittance depends largely upon the value of ΔP , the value of the imaginary part of the admittance is largely determined by the location of P_{\min} . Since the standing pressure wave has a relatively flat minimum, especially at low frequencies, it was easier to determine the value of the minimum than its location. The real parts of the admittances were, therefore, measured with better accuracy than their imaginary parts.

The admittances were measured under cold flow conditions for the following configurations: (1) a hard termination at the end of the impedance tube (2) the gas valve and its decoupler at the end of the tube; (3) the air valve at

the end of the tube; (4) the mixing chamber fitted with the air valve only; and (5) the mixing chamber fitted with both the fuel and the air valves. The air valve opening was varied between 0 and .018 inches for configurations 3, 4 and 5.

The real parts of the admittances for the above configurations with the air valve (when included) closed and open (to .012 inches) measured over a 20 - 170 Hz frequency range are shown in Fig. 7. An air valve opening of .012 inches was selected since it corresponds to a typical setting of a pulse combustor under normal operating conditions. As long as the air valve is closed Y_r is essentially zero at low frequencies for all of the tested configurations. As the frequency is increased, Y_r and, thus, the damping of the air valve slightly increases. A much larger increase in damping at higher frequencies is observed for the closed air valve. The real part of the admittance is increased even further if the closed air valve is attached to the mixing chamber. Thus, adding the mixing chamber and the "elbow" connection between the air valve and the mixing chamber increases the real part of the admittance measurably. On the other hand, adding the fuel valve to the mixing chamber - air valve assembly has no significant effect upon the real part of the admittance at any investigated frequency. Figure 7 also shows that opening the air valve substantially increases the real part of the admittance over the entire range of investigated frequencies. Once again, the effect of attaching the air valve housing to the side of the mixing chamber is significantly greater than adding the fuel valve to the mixing chamber - air valve assembly. The increase in the real part of the admittance with increasing air valve opening is illustrated in more detail in Fig. 8 for a range of valve openings and driving frequencies for the mixing chamber fitted with both valves.

The measured imaginary parts of the admittance (i.e., Y_i) for these configurations over the 20 to 170 Hz frequency range are shown in Fig. 9. Once again, Y_i is zero for the hard termination as well as for the fuel valve only. However, once the closed air valve was added to any of the three investigated configurations the imaginary part of the admittance increased substantially. The latter effect increased with increasing frequency. This occurred because adding the valve assembly moves the termination, in the form of the valve plates, further away from the end of the impedance tube, see Fig. 10. The minimum of the standing pressure wave in the impedance tube was, therefore, moved upstream resulting in an increase in Y_i . Because of the size of the mixing chamber and the elbow that connects the air valve to it this effect is more pronounced for the valve - mixing chamber assembly than for the air valve alone.

Once the air valve is opened the pressure anti-node moves away from the valve plates towards the driver end of the impedance tube, see Fig. 10. (If the valve plates are completely removed the resulting open end corresponds to a pressure node). This causes the decrease in the magnitude of Y_i observed in Fig. 9. Because of the difficulty of determining the precise location of the minimum of the standing pressure wave, discussed above, no clear difference between the imaginary part of the impedance of the air valve only and that of the valve - mixing chamber assembly could be established. However, Fig. 11 clearly shows that the magnitude of Y_i decreases as the opening of the air valve increases. This effect is particularly pronounced at higher frequencies. The lack of smoothness of the curves is, once again, due to the difficulty in determining the precise location of the flat minimum of the standing wave.

TASK III

No activity during this reporting period.

TASK IV

Work has continued on developing a linear acoustic model of the dynamics of the flapper valve. This model is based upon integral formulations of the continuity and momentum equations and the equation of motion of the flapper. Some results are presented in Figs. 12-14. Figure 12 shows the variation with time of the instantaneous, real part of the admittance of the air valve for a valve gap of .009" for one half of the cycle at a low frequency (i.e., 9 Hz). Y_r and, thus, the valve damping increases rapidly while the valve is opening. Y_r reaches a constant level and it drops again as the valve closes. The calculated values of Y_r for the valve in the closed and opened (.009" gap) positions are comparable to the measured admittances of the air valve for the respective valve gaps (see Fig. 7). The discrepancies between the actual calculated and measured values of the admittances are (at least partially) due to the fact that the admittance was calculated at the valve itself while the measurements determined the admittance at the interface between the valve housing and the impedance tube. In addition, the calculated admittances are instantaneous values while the admittance measurements integrate over a large number of cycles.

Figure 13 shows the calculated times required for the air valve to open as a function of frequency for four different valve gaps. Clearly, these opening times decrease as the frequency is increased until they begin to level off above about 50 Hz. On the other hand, the magnitude of the valve spacing has a relatively small effect upon the time required to open the valve.

Since the time required for the valve to open or close no longer diminishes with frequency at high frequencies, it is conceivable that at very high frequencies there is not enough time during each cycle for the valve to open and close completely. For this reason the calculated valve opening time as a fraction of half period of the cycle was plotted against frequency in Fig. 14. This figure shows that even at frequencies of 150 Hz the valve is either open or shut during at least 30% of the duration of the cycle.

PROBLEMS

Four problems related to the work described above were encountered during the past year.

1) The fluctuations in the measured local LDV data are caused not only by turbulent velocity fluctuations but also contain effects due to: a) the finite width of the time slots used for conditional sampling; b) small differences in the flow field from cycle to cycle; and c) slight variations in the combustor frequency during each run. The LDV data acquisition technique is, therefore, being refined to minimize these effects. The velocity measurements at each location are successively ensemble averaged using different slot sizes. The resulting RMS values of the velocities can then be extrapolated to zero slot width. In addition, the data reduction software has been modified to measure actual cycle durations from the recorded positive zero-crossings of the pressure signal for each cycle. The use of those measured cycle durations rather than those calculated from the mean frequency of operation of the combustor eliminates the effect of frequency variations upon the ensemble averaging procedure.

2) The determination of the imaginary part of the admittance, Y_i requires accurate determination of the location of the pressure minimum of the standing wave in the impedance tube (see Fig. 5). Since this pressure minimum is relatively flat, its precise location was difficult to establish. The following technique was developed to maximize the accuracy with which the P_{\min} location is determined. First, an approximate location of P_{\min} is found by translating the pressure transducer along the impedance tube axis and observing the transducer output on an RMS meter. The transducer is then positioned at a number of locations in the vicinity of the approximate P_{\min} location and the the pressure transducer output is entered into the computer. Pressure spectra at each of these locations are calculated and a precise sound pressure level is determined at each point by in an accurately reproducible P_{\min} location.

3) Streaklines and mixing visualizations were attempted by injecting small particles into the mixing chamber through the air valve and illuminating the resulting flow pattern with a thin laser light sheet. The stream of particles was clearly seen entering the mixing chamber along with the flow from the air valve. However, as soon as the particle-laden combustion products from the previous cycle reentered the mixing chamber, the visualization pattern became "washed out". In addition, the intensity of light scattered by the particles was insufficient to clearly mark the film at a framing rate of 5000 frames/sec, the minimum required to freeze the improvement over the shadowgraph visualizations, it was abandoned.

4) The driving and damping characteristics of the combustor were to be determined by measuring the exponential growth and decay rates of the

pressure oscillations during start-up and shut-down of the combustor. Because of the low operating frequency of the pulse combustor only three to four cycles were required to reach either full operational amplitudes or conditions of zero pressure fluctuations. Thus, only three to four points were available to plot the exponential pressure growth and decay curves. Because of the resulting lack in accuracy it was decided to concentrate our efforts on the impedance tube measurements which, to date, have yielded superior data describing the damping of the various combust components.

CONCLUSIONS:

During the past year, flow visualization by high speed shadowgraphy was completed and compared with the results from the LDV measurements. It was determined that the entry of the fuel jet is followed by that of the air jet which largely dominates the flow field. A large, axial recirculation zone occupies most of the mixing chamber during the phase of high combustion intensity during the cycle. The flow is extremely turbulent at all times with additional turbulence being generated by the entry of the air jet. Backflow from the tailpipe was seen to penetrate several inches into the combustion chamber as the pressure in the combustion chamber decreased. This backflow does not interact directly with the reacting gases.

The admittances of several combustor components were measured over a range of frequencies using the impedance tube technique. It was determined that the fuel valve assembly acts like a hard termination in all of the investigated configurations and at all frequencies. The damping by the air valve, described by the real part of the admittance Y_R , increases with frequency for a given

valve spacing, and with valve opening at each frequency. The phase shift of the wave reflected off the air valve, which is described by Y_I , increases with frequency. However, this increase in Y_I can be compensated for by opening the air valve. The geometry of the pipe connecting the air valve housing to the impedance tube was found to have only a minor effect upon either component of the valve admittance.

A linear model was developed which describes the behavior of the air valve. This model was used to calculate the instantaneous real part of the air valve admittance during the cycle. The predicted behavior of Y_R was found to be in good qualitative agreement with the results of the impedance tube measurements. Calculations based upon this model showed that the times required to open or close the air valve are independent of the valve setting. In addition, it was determined that these valve opening and closing times are independent of frequency for operational frequencies above 50 Hz. Nevertheless, the valve opening and closing times remain only a small fraction of the duration of the cycle, even at high frequencies. Thus, for most of the cycle the valve is either fully open or fully closed.

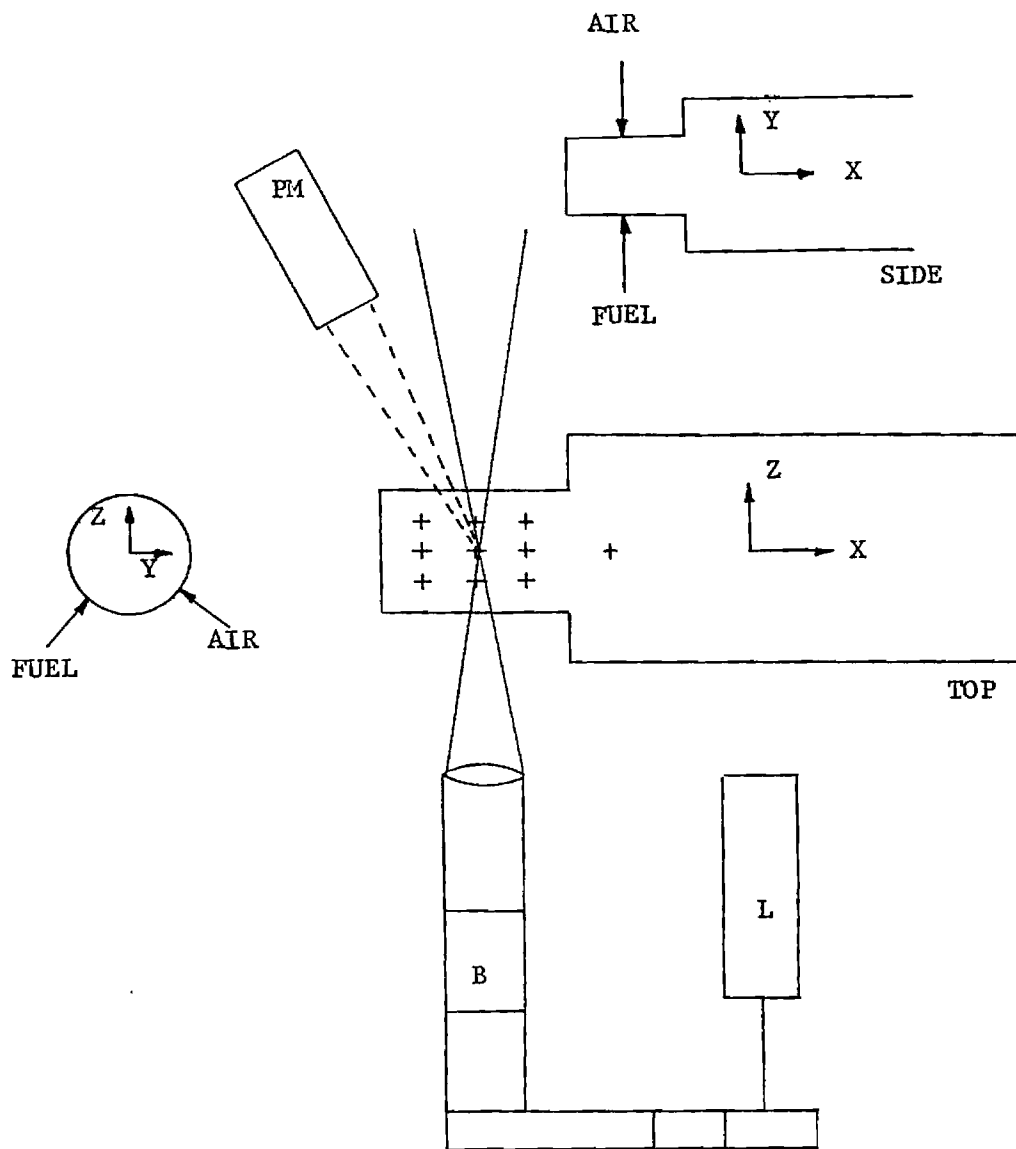
PLANNED WORK

During the next reporting period the LDV software modification will be completed and velocity measurements will continue. Local densities and, therefore, temperatures will be determined using molecular Rayleigh scattering. Furthermore, the recent arrival of an intensified CCD imaging system will permit radiation measurements to be carried out efficiently and with much improved resolution (128 x 128 pixels).

Impedance tube measurements of the combustor components under cold flow will be completed and this effort will move on to measuring the admittances of the combustor with combustion.

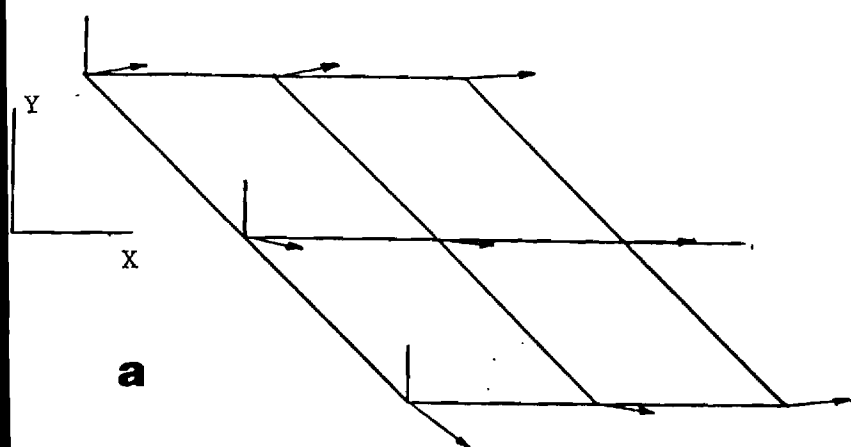
The modeling of the air flapper valve will continue and selected experiments will be carried out in order to confirm the model's predictions.

LDV SCHEMATIC



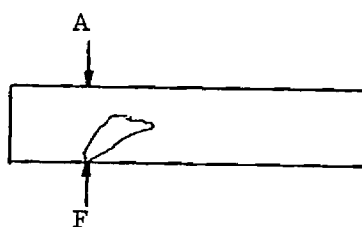
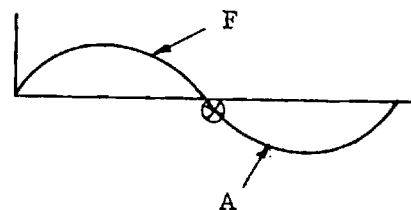
VELOCITIES MEASURED IN Y & Z DIRECTIONS

Fig. 1 Location of LDV Measurements in the Mixing Chamber.

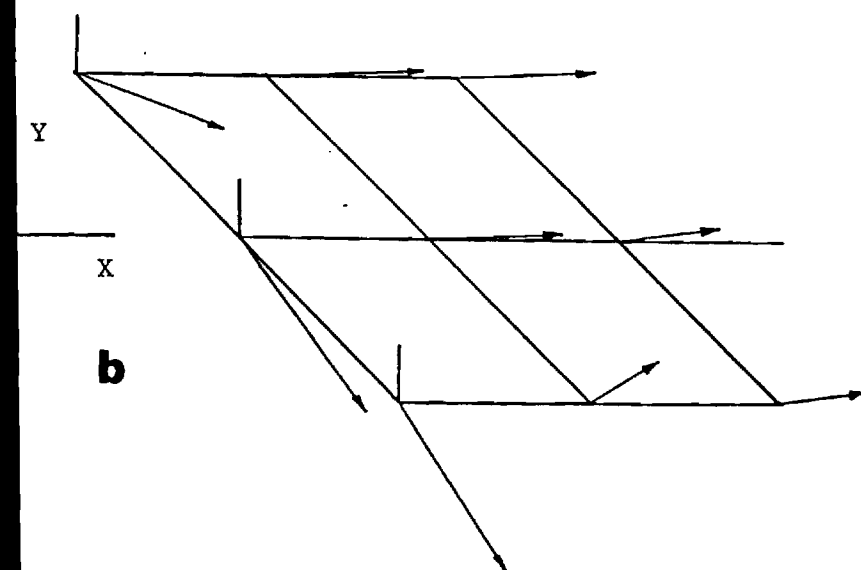


a

Vector Plot

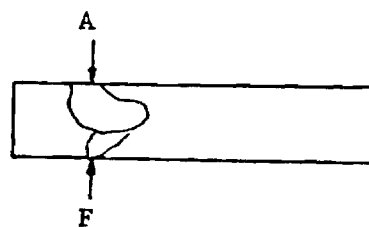
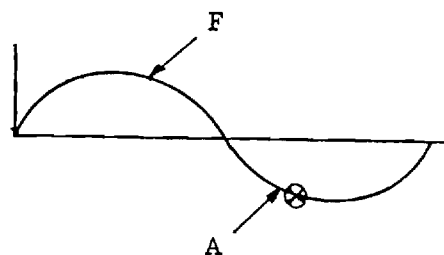


Shadow Image



b

BVector Plot



Shadow Image

Fig. 2 Comparison of Vector Plots Obtained by LDV with High Speed Shadowgraphy Images at Four Instances During a Cycle

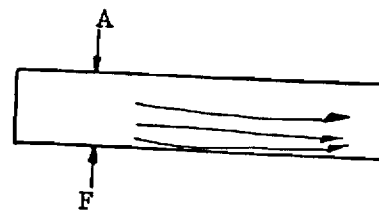
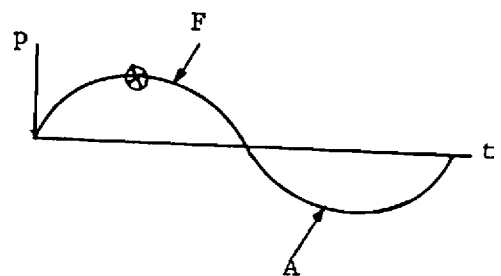
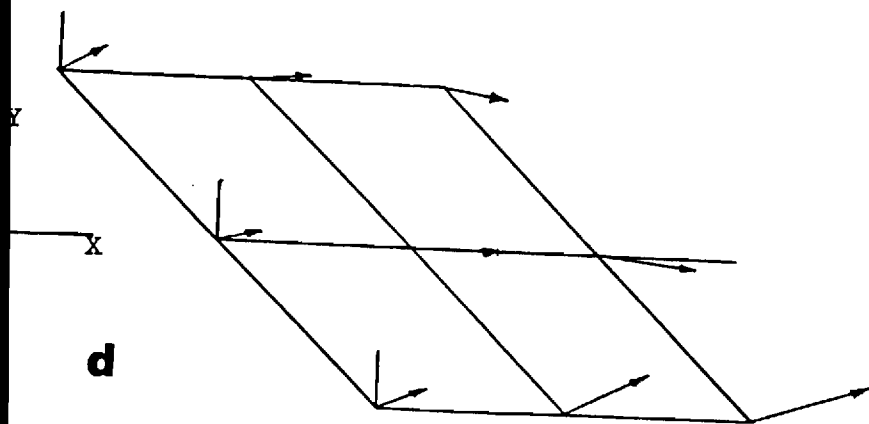
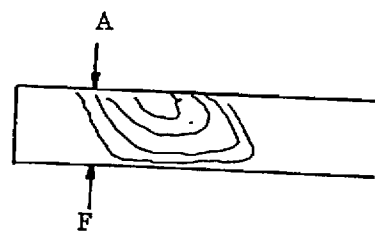
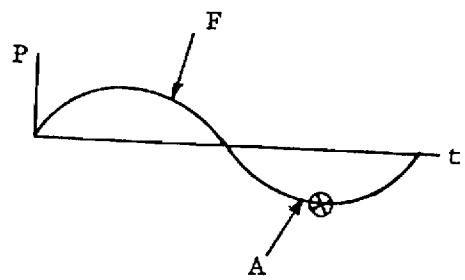
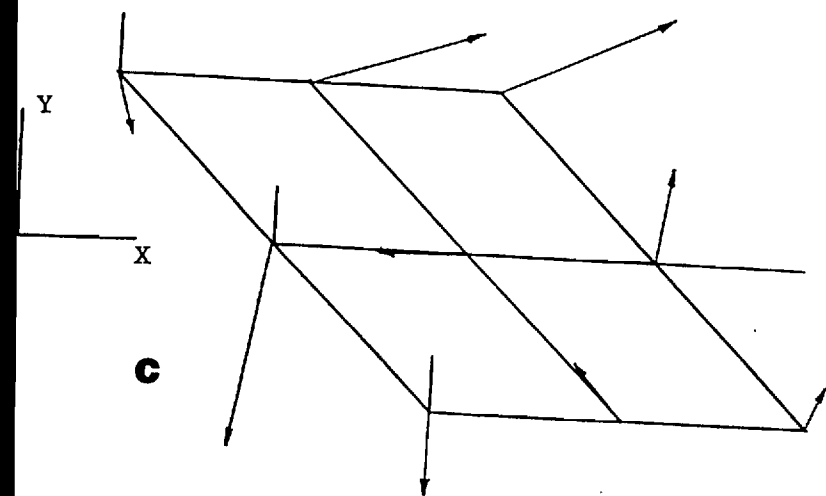


Fig. 2 Continued

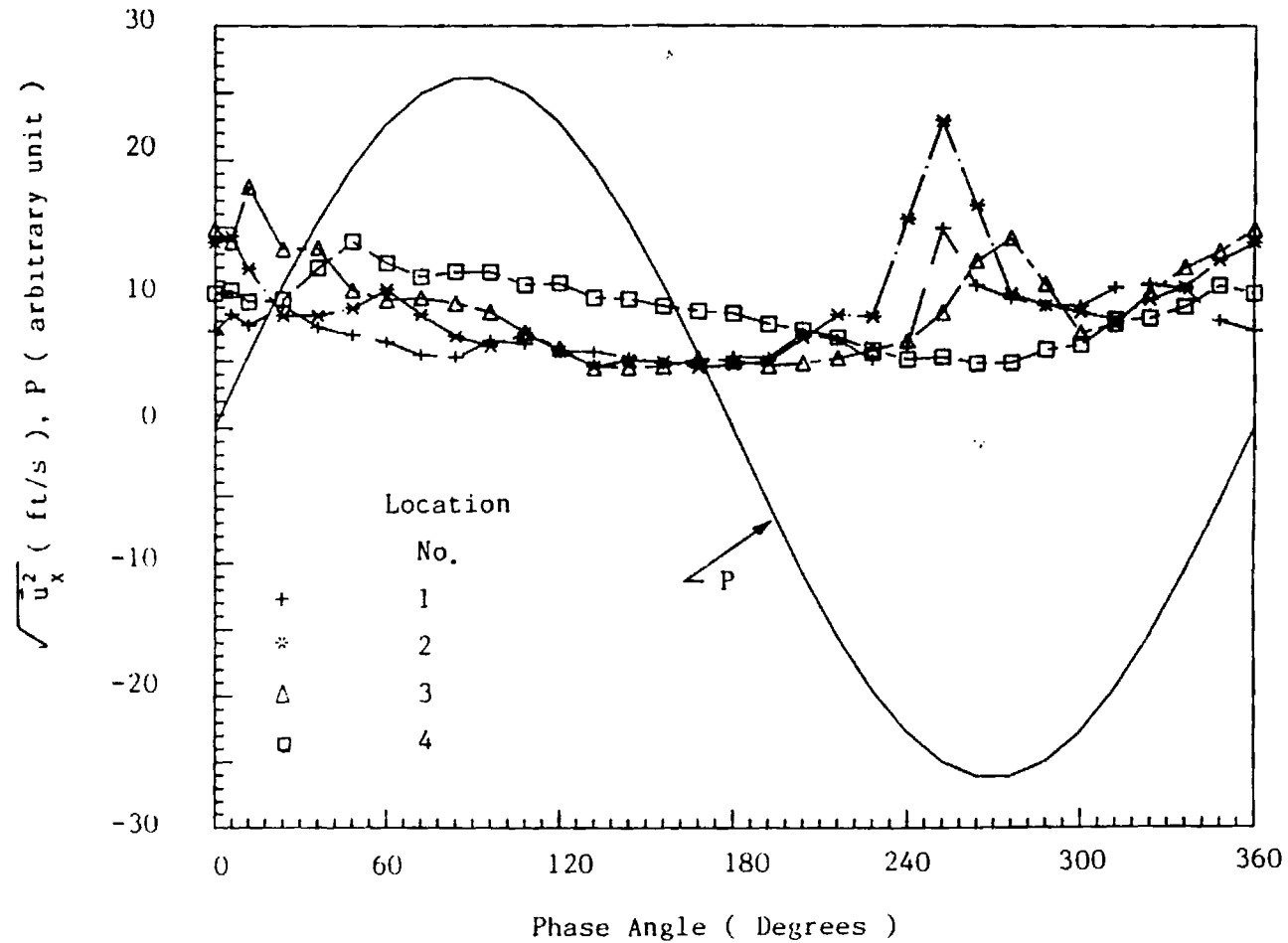


Fig. 3 Variation of RMS Values of Axial Velocities during Cycle at four different locations. Locations 1, 2 and 3 in the Mixing Chamber, Location 4 in the Combination Chamber. The Pressure Cycle is shown for Reference.

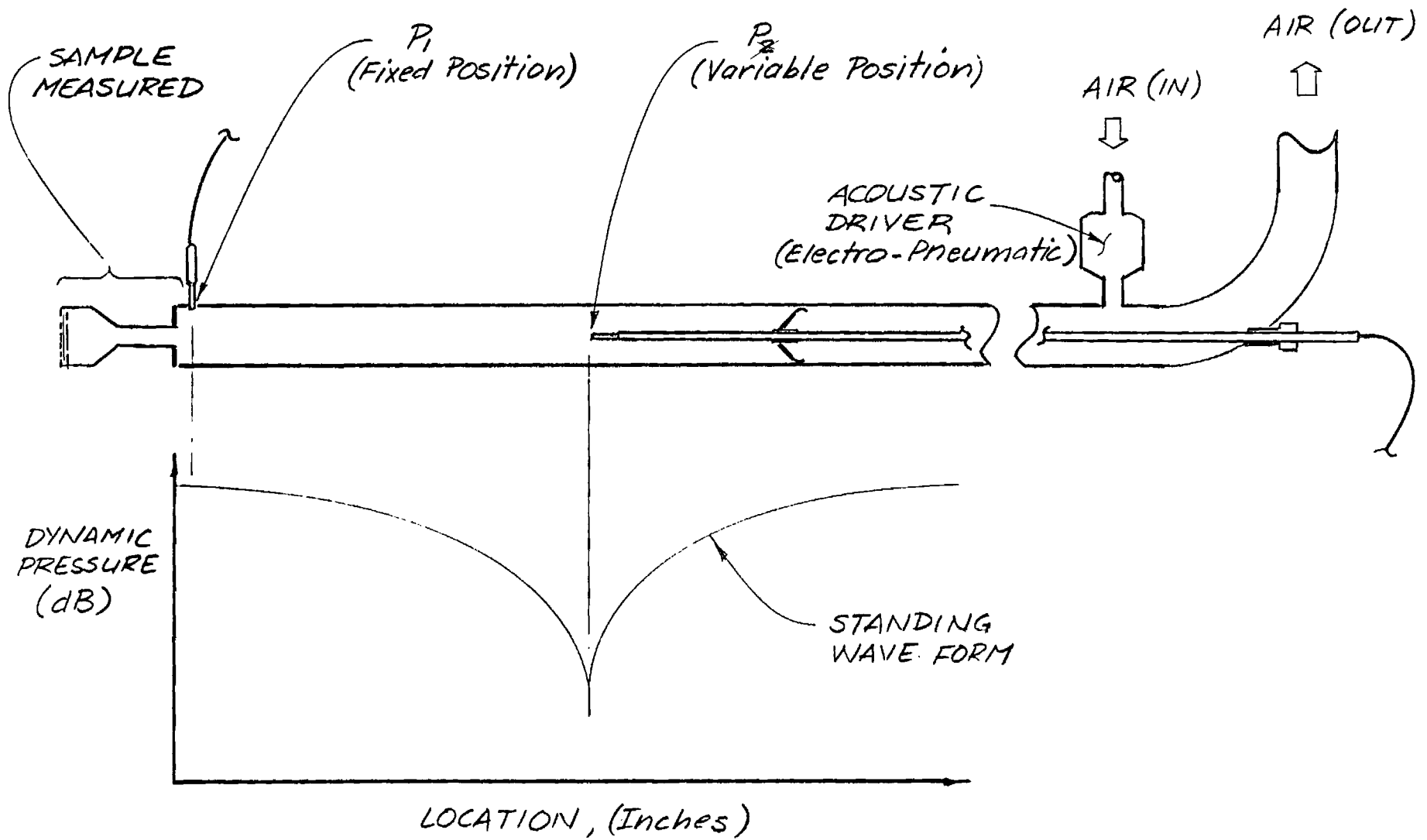


Fig. 4 Experimental Setup for Impedance Tube Measurements

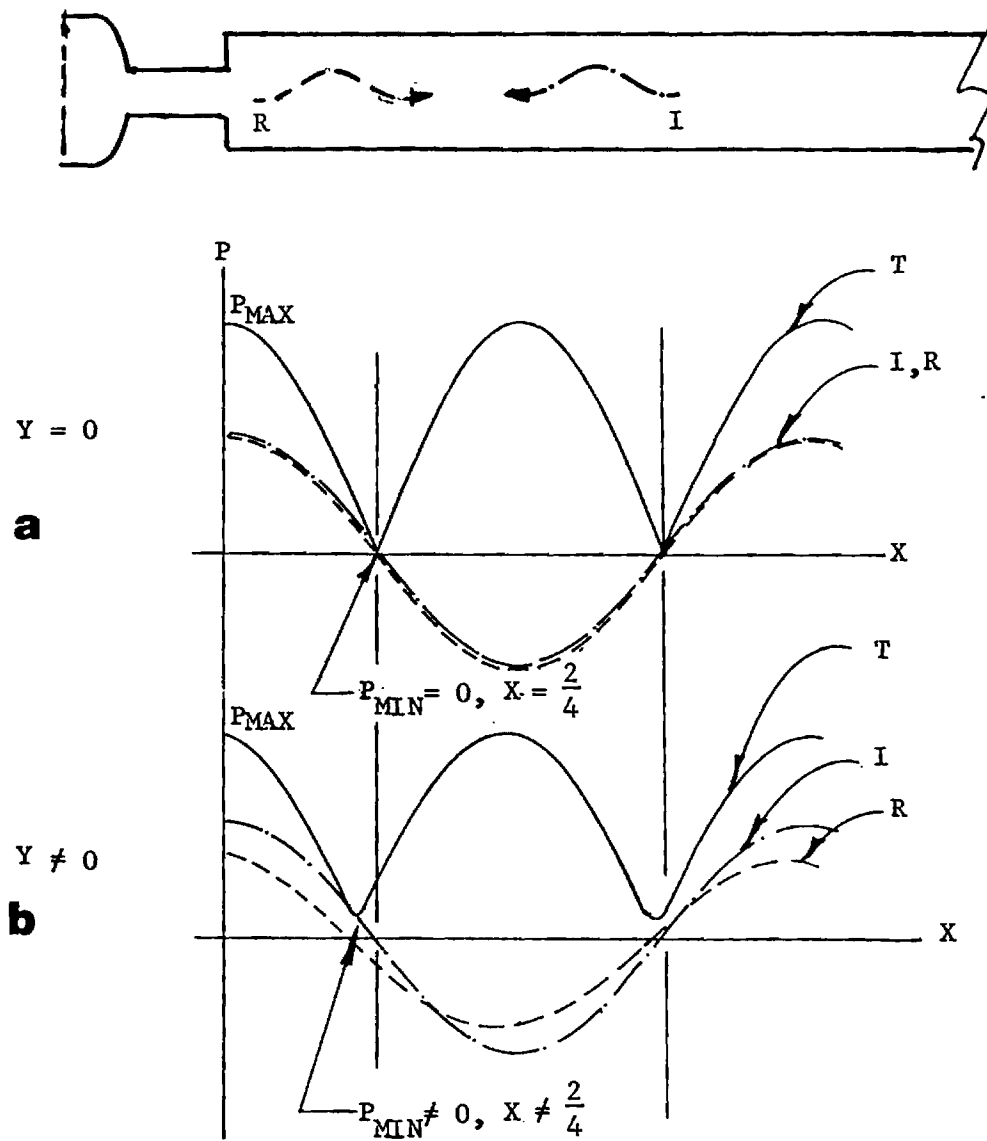


Fig. 5 Waveform of Incident (I), Reflected (R) and Total Standing Wave (T) for Hard Termination (a) and Termination with Finite Admittance (b).

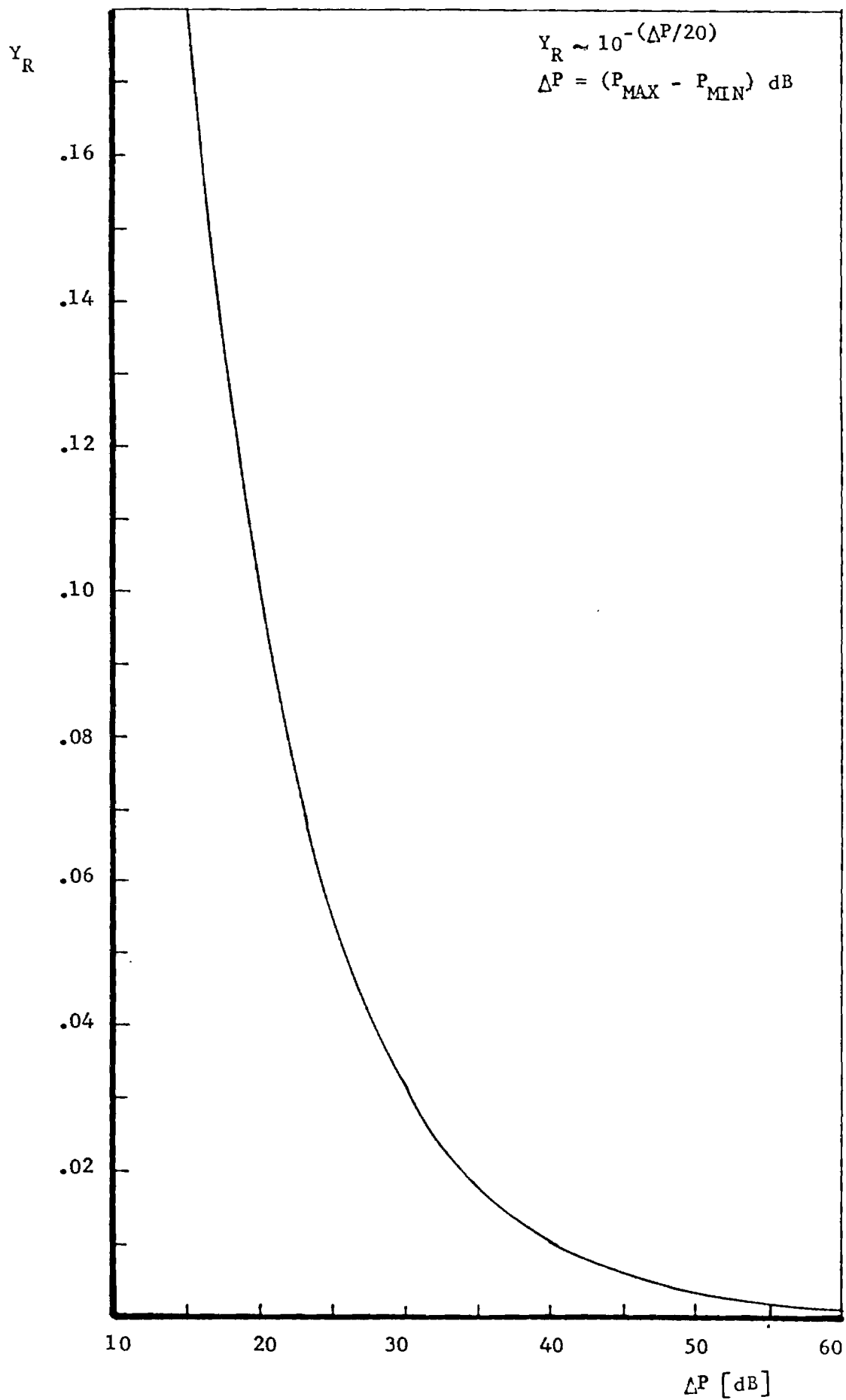


Fig. 6 Plot of ΔP vs. Real Part of Admittance (y_R)

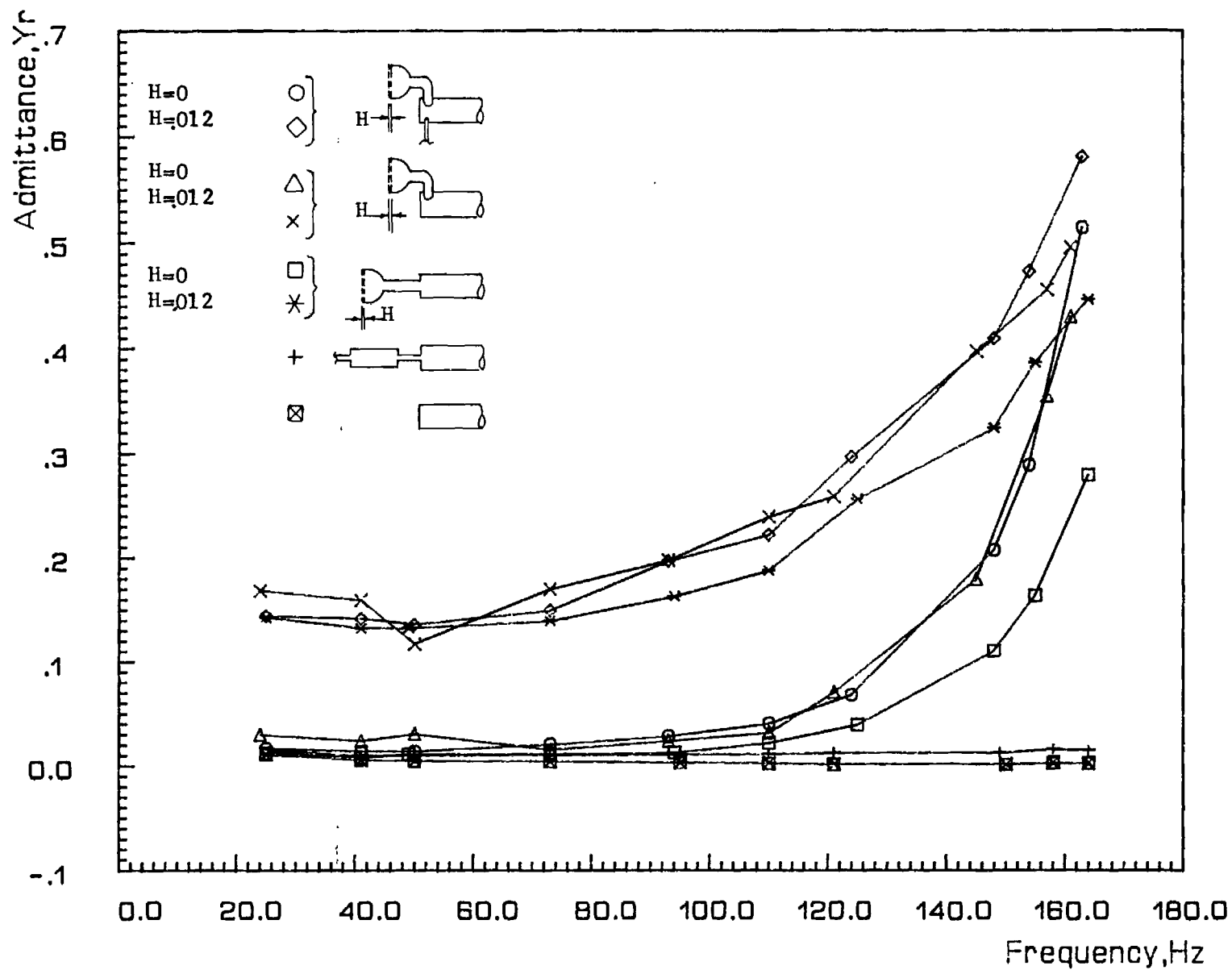


Fig. 7 Real Part of Admittance vs. Frequency for various Impedance Tube Terminations. (H =Air Valve Gap in inches)

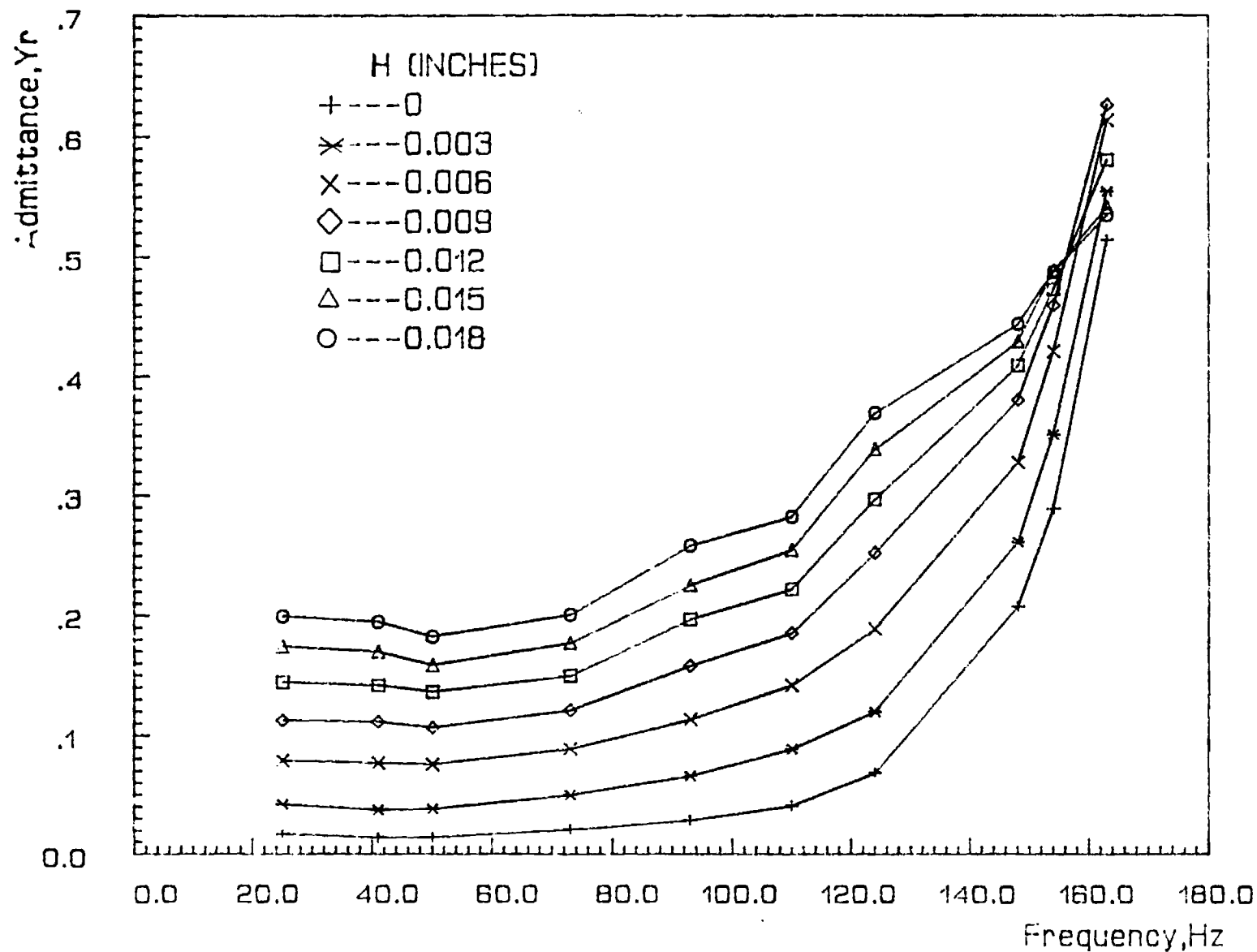


Fig. 8 Real part of Admittance of Mixing Chamber with Fuel and Air Valves vs. Frequency for different Air Valve Gap Settings (H).

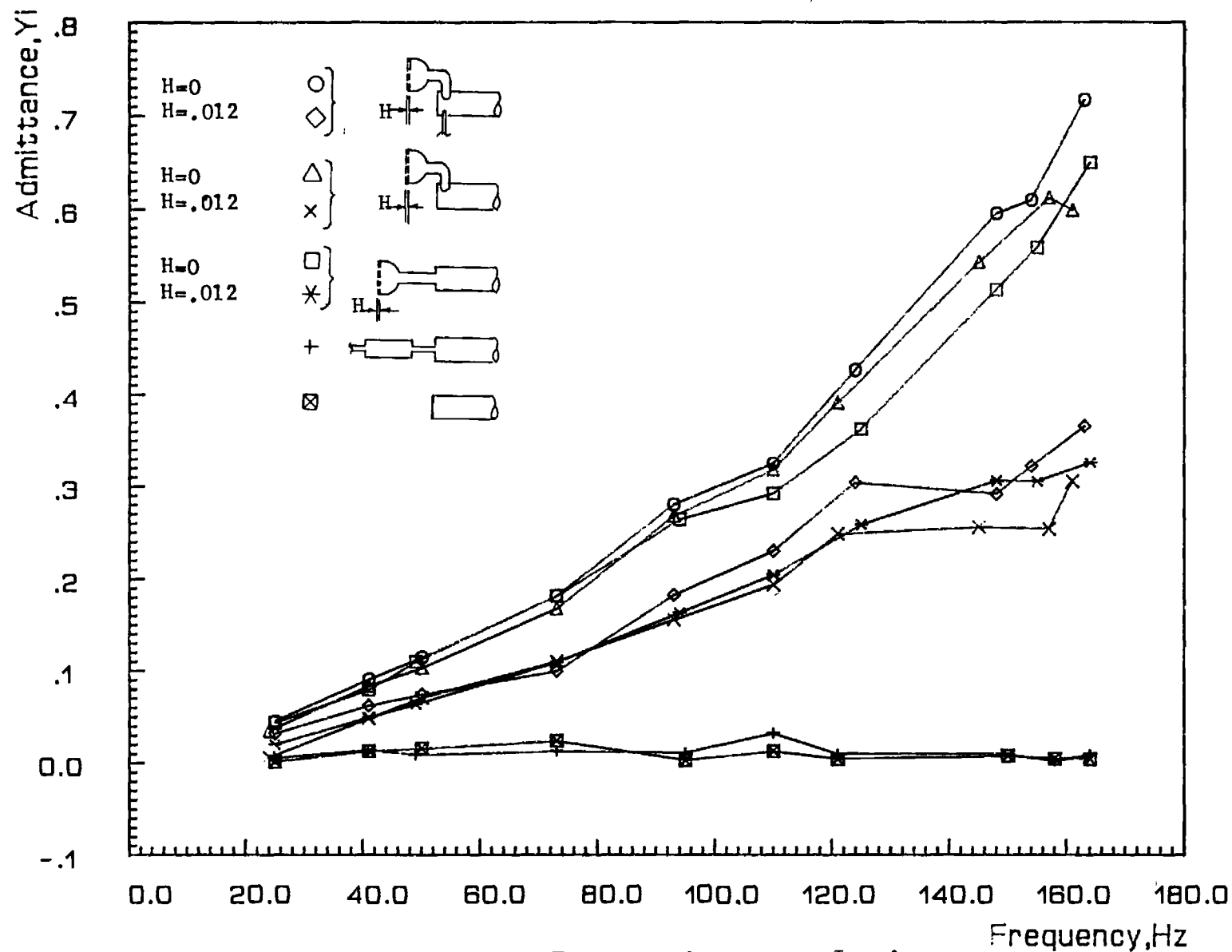
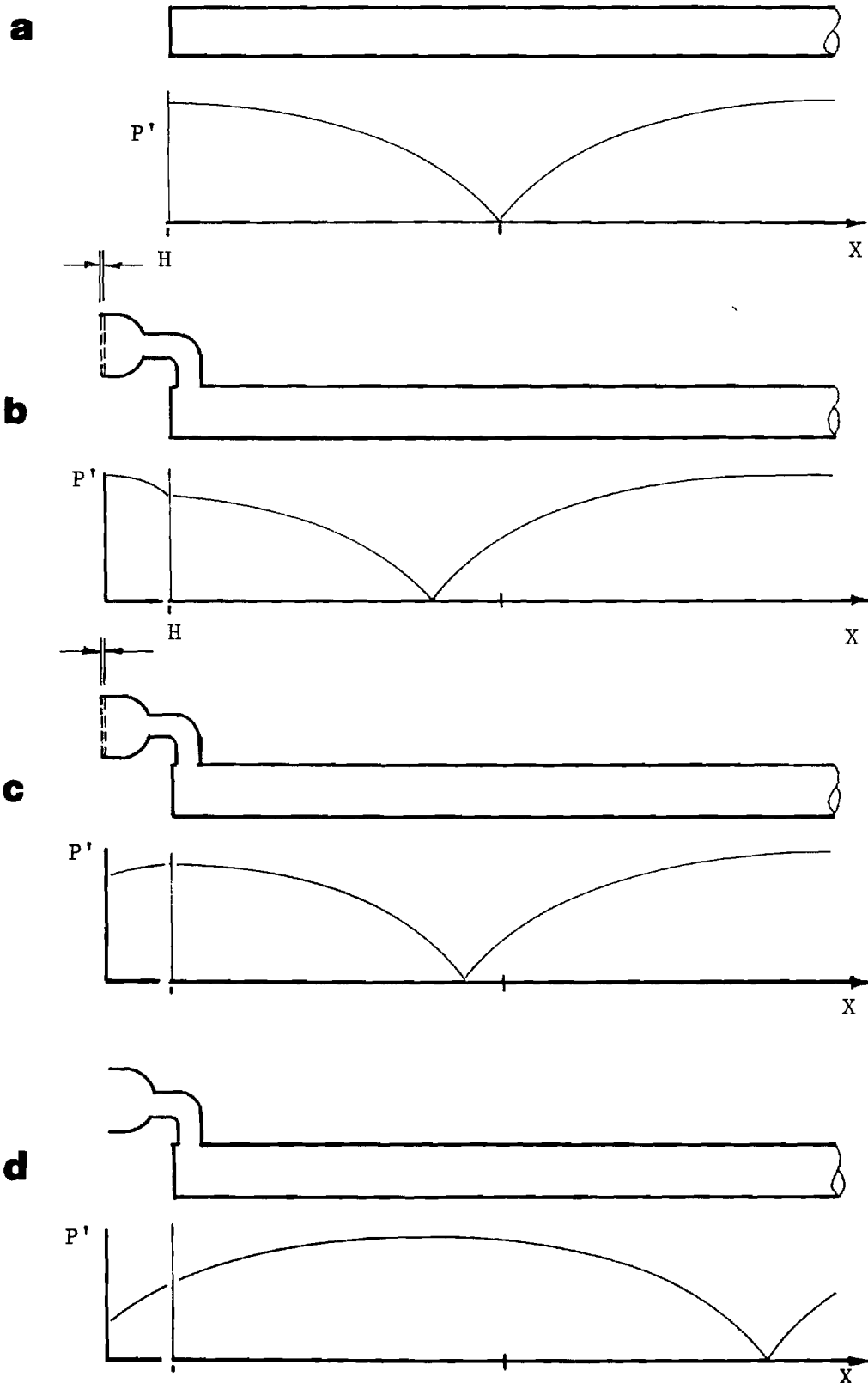


Fig. 9 Imaginary Part of Admittance vs. Frequency for various Impedance Tube Terminations (H =Air Valve Gap in inches)



10 Schematic of Standing Wave Pattern in Impedance Tube Fitted with a) Hard Termination, b) Closed Valve ($H=0$), c) Open Valve ($H \neq 0$) and d) Valve Housing but Valve Plates Removed. Actual Measured Standing Wave more Complex in the Valve Housing due to its Geometry.

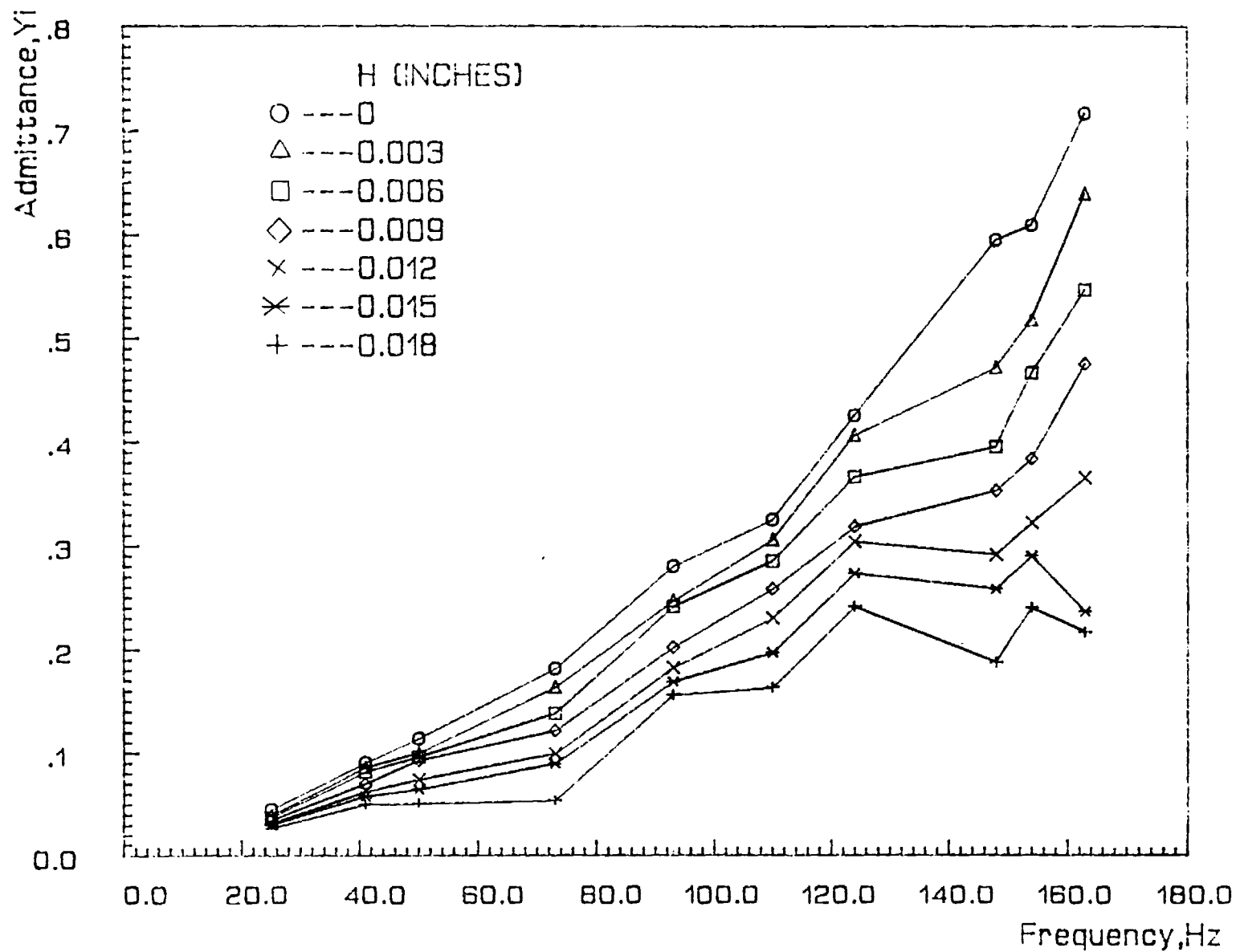


Fig. 11 Imaginary Part of Admittance of Mixing Chamber with Fuel and Air Valves vs. Frequency for different Air Valve Gap Settings (H).

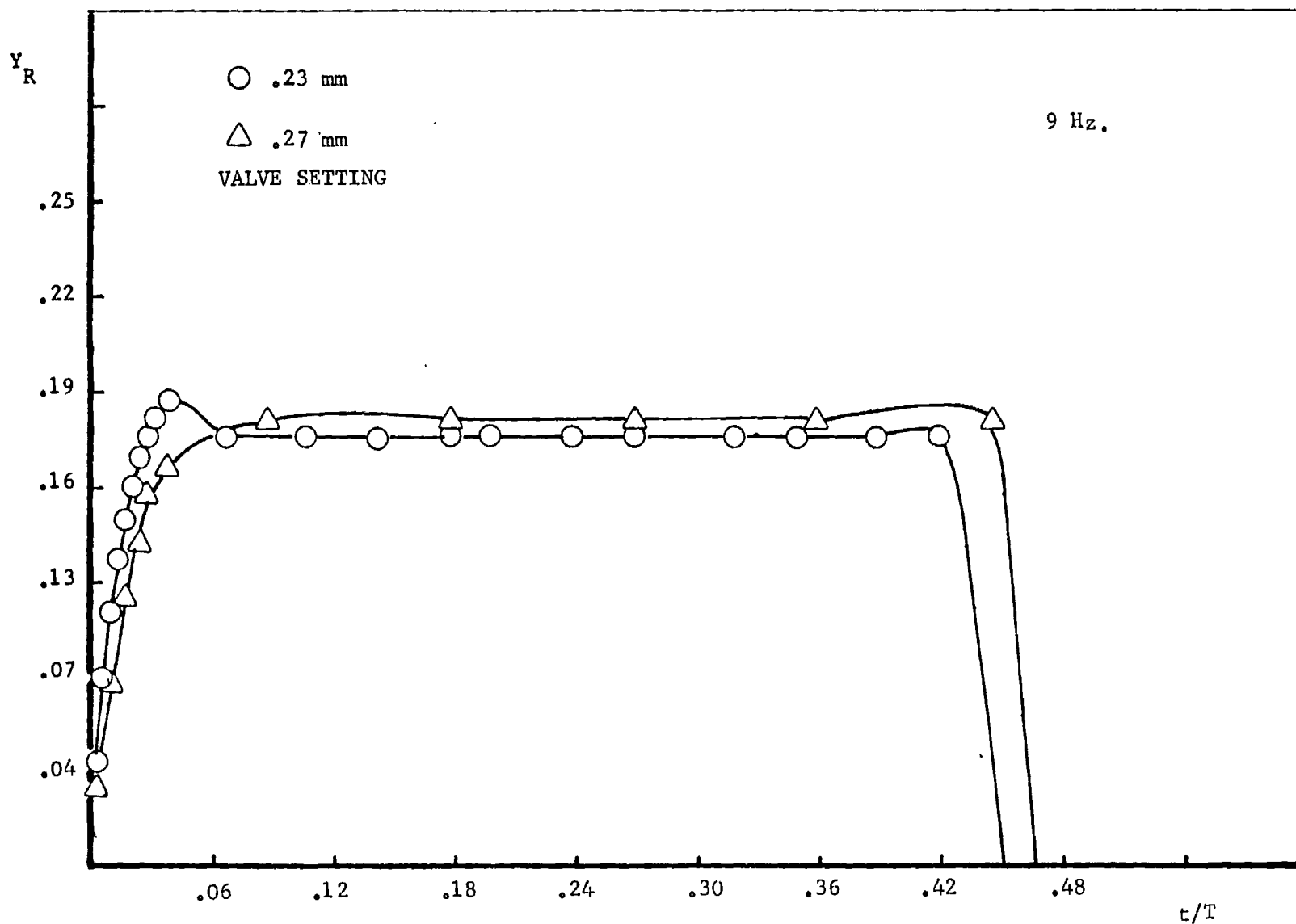


Fig. 12 Time Variation of the Calculated Real Part of the Admittance of the Air Valve for the First Half of the Cycle (Frequency: 9 Hz)

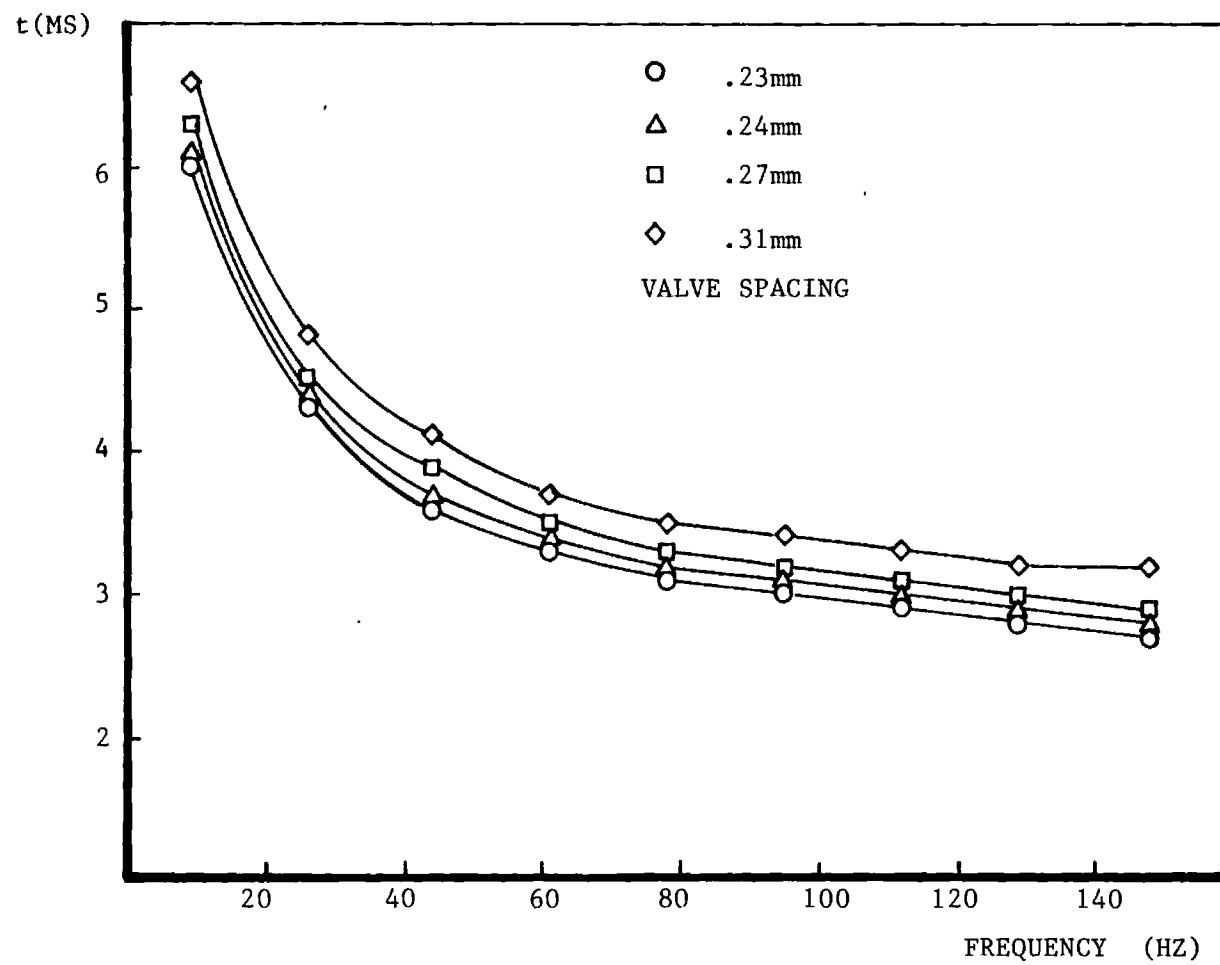


Fig. 13 Calculated Valve Opening Times vs Frequency for Different Valve Spacings.

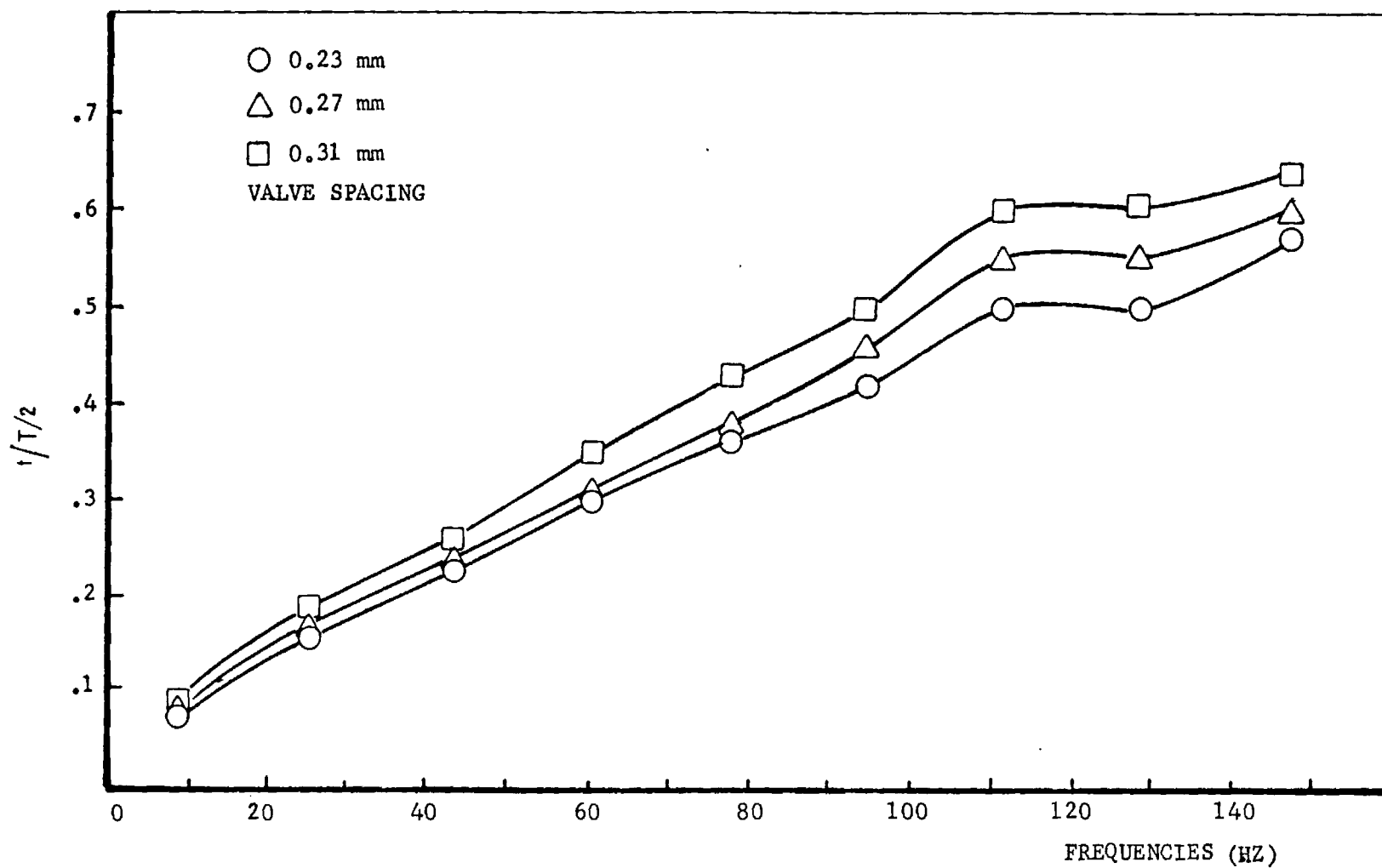


Fig. 14 Calculated Valve Opening Times as a Fraction of Half Period of the Cycle vs. Frequency for Different Valve Spacings

**GAS RESEARCH INSTITUTE
ACCOMPLISHMENT REPORT**

GRI Contract No. 5083-260-0873 / 5087-260-1466

Principal Investigator B. T. Zinn, B. R. Daniel and J. I. Jagoda

Firm Aerospace Engineering / Georgia Tech.

Telephone 404 /894-3060 **Ext.**

1. **Please list all publications in 1987 resulting from GRI-funded research.**
"Radiation Measurements in a Gas Fired Pulse Combustor" S. H. Ku, X. C. Cheng, B. R. Daniel, J. I. Jagoda and B. T. Zinn, Proceedings of the 1987 Spring Technical Meeting, Central States Section of The Combustion Institute, Chicago, IL, May 1987.

2. **Please list any manuscripts submitted but not yet published in 1987, based on GRI-funded research.**
"Flame Spread and Limits of Operation of Gas Fired, Mechanically Valved, Pulse Combustors," S. H. Ku, B. R. Daniel, J. I. Jagoda and B. T. Zinn, Submitted to the 22nd Symposium (International) on Combustion to be held in Seattle, WA, Aug. 1988.

3. **Please list all papers given, symposia presentations, and other presentations and publications, based on GRI-funded research in 1987.**
"Radiation Measurements in a Gas Fired Pulse Combustor," Presented at the 1987 Spring Technical Meeting of the Central States Section, The Combustion Institute, Chicago, IL, May 11-12, 1987.

4. **Please list any honors or special recognition of your research work.**
None

University Researchers: Please complete the following information.

5. A) How many undergraduate students participated in this research?

None

B) How many candidates for advanced degrees participated in this research?

Three

C) Please list any post-doctoral students who participated in this research.

None

D) Please list all students awarded degrees based on this project and indicate degrees earned and dates awarded.

<u>NAME</u>	<u>DEGREE</u>	<u>DATE</u>
None in 1987		

GAS RESEARCH INSTITUTE - PHYSICAL SCIENCES DEPARTMENT
1988 ACCOMPLISHMENT REPORT

GRI Contract No. 5087-260-1466

Principal Investigator B. T. Zinn, J. I. Jagoda and B. R. Daniel

Mailing Address School of Aerospace Engineering
Georgia Institute of Technology
Atlanta, GA 30332

Telephone: (404) 894-3033 Ext.

PLEASE NOTE: A publication must include certain minimum data: for journals-author(s), manuscript title, journal title, year of publication, volume number, and initial page of cited article (the complete span is better); for books or proceedings - overall author or editor, book title, publisher, city of publication, and year of publication.

1. Please list all retrievable publications in 1988 resulting from GRI funded research. This would include journals and books.

"Pulsating Burners - Controlling Mechanisms and Performance" B. T. Zinn, B.R. Daniel and J. I. Jagoda. GRI Annual Report, Grant No. 5083-260-1466, January 1988.

2. List any manuscripts submitted but not yet published in 1988 which were based on GRI funded research.

"Dependence of Pulse Combustor Performance upon Interior Temperature, Acoustic Losses and Combustion Time," X. C. Cheng, J. I. Jagoda and B. T. Zinn, submitted to the 1989 International Gas Research Conference, Tokyo, Japan, November 1989.

3. Please list all papers given, symposia or conferences presentations in which a retrievable publication has been published, e.g., a proceeding document, based on GRI funded research in 1988.

4. Please list all papers given, symposia or conferences presentations in which a retrievable publication has not been published.

"Pulsating Burners - Controlling Mechanisms and Performance," B. R. Daniel, J. I. Jagoda and B. T. Zinn, presented at Sandia - GRI Pulse Combustion Workshop, Sandia National Lab, Livermore, CA, April 25, 1988.

"Flame Spread and Limits of Operation of Gas Fired, Mechanically Valved Pulse Combustor," S. H. Ku, B. R. Daniel, J. J. Jagoda and B. T. Zinn, presented at the 22nd Symposium (International) on Combustion, Seattle, WA (August 14-19, 1988).

"Frequency Modeling and Velocity Measurements in Gas Fired, Valved Pulse Combustors," X. C. Cheng, B. R. Daniel, J. I. Jagoda and B. T. Zinn, presented at the 1988 Fall Technical Meeting, The Eastern Section, Combustion Institute, Clearwater Beach, FL, December 5-7, 1988.

5. Please list any honors or special recognition of your research work.

University Researcher: Please complete the following information.

6. A) How many undergraduate students participated in this research?

None

- B) How many candidates for advanced degrees participated in this research?

2

- C) Please list any post-doctoral students on this research.

1

- D) Please list all students awarded degrees based on this project and indicate degree earned and date awarded.

<u>NAME</u>	<u>DEGREE</u>	<u>DATE</u>
S. H. Ku	Ph.D	Sept. 1988
J. M. Tang	M. S.	Dec. 1988

RESEARCH SUMMARY

Title: Pulsating Burners - Controlling Mechanisms and Performance

Contractor: Georgia Tech Research Institute

Contract Number: 5087-260-1466

Report Period: January - June 1987, Semi-Annual Report

Principle Investigators: B. T. Zinn, B. R. Daniel and J. I. Jagoda

Objective: It is the objective of this study to gain further insights into the physical mechanisms which control the mixing and heat release processes in pulse combustors. In addition, the acoustic driving and damping characteristics of various components and subsystems of the pulse combustor will be determined for various operating conditions. Finally, the above findings will be used explain the performance of various combustor configurations to be tested and should be of considerable help to the designers of novel pulse combustors.

Technical Perspective: Although gas fired pulse combustors have been on the market for a number of years, their controlling mechanisms are still not sufficiently well understood to permit the design of pulse combustors for different applications without resorting to costly trial and error development efforts. To attain pulse combustion operation, the energy supplied to the pulsations by the combustion process must be larger than the acoustic energy lost due to viscous dissipation, heat transfer, acoustic

radiation and so on. Proper operation of pulse combustors also requires that mixing, cycle to cycle reignition and flame spread occur such that the oscillations of heat release be in phase with those of the pressure. In addition, the acoustics of the various components and subsystems of the pulse combustor must be matched appropriately. Thus, to develop a rational design procedure for pulse combustors, it is required that the various processes responsible for energy addition and removal to and from the pulsations be understood. Furthermore, data describing the acoustic properties of various pulse combustor components under various cold and pulse combustion operating conditions are needed. Finally, the dependence of the acoustic characteristics of the various combustor components upon the fundamental fluid mechanical, heat transfer and combustion processes must be understood. The attainment of these goals is pursued under this project.

Technical Approach:

In order to elucidate the mechanisms which control the operation of various pulse combustor configurations and determine the damping/driving characteristics of various components and subsystems of commonly used pulse combustors, the following tasks will be pursued simultaneously:

- 1) Investigation of the flow field characteristics, mixing and heat release in pulse combustors using LDV, Schlieren, mixing visualization, radical radiation (OH, CH, CC) and Rayleigh scattering measurements.

- 2) Measurements of the driving and damping characteristics of various components and subsystems

which make up the pulse combustor using the impedance tube technique.

3) The determination of the overall driving and damping characteristics of various pulse combustor designs under different operating conditions.

Results:

During the past reporting period the importance of the duration and phase of the combustion process (including mixing, ignition delay and reaction) relative to that of the pulse combustor pressure oscillations was investigated. For this purpose, the period of pulsation of the combustor was extended by increasing the volume of the combustion chamber and by lengthening the tail pipe of the Helmholtz combustor. This resulted, however, in increased damping and, therefore, an unacceptably low dB level in the combustor. In addition, the combustion efficiency was seriously reduced. Better combustion efficiencies were obtained with a Schmidt (quarter wave) type pulse combustor. Furthermore, because of its lower damping pulsations of the order of 170 dB could be obtained in the Schmidt combustor even at low frequencies. As the length of the Schmidt tube was increased the frequency of pulsations was reduced until a given tube length was reached at which the frequency of pulsations suddenly "jumped" to that of the next harmonic of the combustor. Further increase in combustor length then caused the frequency to decrease once again. This frequency "jump" to a higher harmonic could, however, be avoided if the combustion time was extended by slowing down the mixing process through modification of the reactant injection system. These results demonstrate that the combustion time must be "compatible" with the period of pulsations of the

pulse combustor. It appears that the combustor will pulsate with a frequency whose period equals, approximately, twice the length of the characteristic combustion time. In addition, the Schmidt combustion was found to be more suitable for pulse combustion operation at low frequencies.

Radical radiation measurements were continued during this period. Measurements were carried out using the combustor with flat windows fitted to the curved walls of the mixing and combustion chambers. The position of cycle to cycle reignition was found to be in the mixing chamber 2.3 inches downstream of the plane where fuel and air first mix. The flame was then seen to spread in the upstream and downstream directions. The maximum combustion intensity was observed upstream of the ignition location. These measurements are continuing and their results are being correlated with radiation data measured through a window in the upstream end of the combustor using the pressure signals as a clock. The LDV has been readied for operation and checked out. A seeder has been designed, constructed and installed upstream of the air flapper valve. Velocity measurements along the central axis of the combustor have commenced.

Objective

It is the objective of this study to gain further insight into the fundamental processes responsible for the operation of various pulse combustor designs. Emphasis is being placed upon obtaining practical information which will permit designers to develop new and/or larger scale pulse combustors without resorting to costly trial and error based development efforts.

The velocity and the mixing patterns in the mixing and combustion chambers will be determined both qualitatively and quantitatively. The nature of the interaction between the combustion process and the acoustics of the combustor will be established. The impedance of various components and subsystems which make up the pulse combustor will be determined under various operating conditions. In addition, the driving and damping characteristics of different pulse combustor designs will be measured under different operating conditions.

PROGRAM PLAN

The program is divided into four major tasks as outlined below:

Task I: Investigation of the Interaction between the Oscillatory Flow Field and Heat Release Processes in the Pulse Combustor:

- A. Laser Doppler Velocimetry: The three components of velocity will be measured at selected locations in the combustor. The period of pulsations will be divided into 36 equal time segments and the LDV counts for each segment will be stored in separate files. This will permit ensemble averaging of the velocities in each segment over many cycles. Mean velocities and turbulence intensities as well as shear stresses can then be obtained for each instant in the cycle.
- B. Schlieren Visualization: High speed Schlieren and shadowgraph cinematography will be carried out through side windows in the

combustor (henceforth to be denoted "side on", Fig. 1) in order to visualize the flow along the combustor axis. These shadowgrams will then be correlated with those previously obtained through a window in the end walls of the combustor (to be denoted "end on", Fig. 1) using the pressure oscillations as a clock. This will provide a complete picture of the three-dimensional flow field in the pulse combustor.

- C. Mixing Visualization: Mixing patterns will be recorded photographically by heavily seeding one of the reactant flows and illuminating the combustor using an expanded laser sheet. These visualizations will be carried out through the flat windows in the cylindrical walls of the mixing and combustion chambers. The use of the flat windows is expected to reduce the amount of laser light reflected by the glass. These laser light intensity losses caused problems when this technique was previously applied to the combustor with cylindrical glass walls.
- D. Spectroscopy: Local and global heat release in the pulse combustor will be determined by measuring the OH, CH and CC radical radiation emitted from the combustor. Efforts will concentrate on the "side on" measurements which will be correlated with previously obtained "end on" results using the measured pressure oscillations as a clock.
- E. Rayleigh Scattering: Local densities and, therefore, temperatures will be measured using Rayleigh scattering. A combination of the emission spectroscopy and the Rayleigh measurements will result in a better understanding of the location and timing of the combustion process. In addition, the Rayleigh scattering results will yield a quantitative description of the path taken by the hot combustion products in the pulse combustor.

All Task I measurements will be carried out in the pulse combustor with flat windows fitted to the curved walls of the mixing and combustion chambers. The results will be correlated with each other and with the phase in the cycle at which they were obtained. This will be achieved by using the measured pressure oscillations as a clock. Only a full coordination between the flow field, the heat release and the local temperature measurements can result in a thorough understanding of the fundamental principles underlying the operation of the pulse combustor.

Task II: Impedance Measurements of Pulse Combustor Components:

The acoustic impedance of the various components and subsystems which make up the pulse combustor will be measured using the impedance tube technique. These measurements will be carried out without and with combustion and under various operating conditions and driving frequencies. These measurements will yield information on the frequency dependence of the damping provided by the various pulse combustor subsystems. In addition, the frequency dependence of the driving provided by the pulse combustion process will be determined.

Task III: Determination of Overall Driving/Damping Characteristics of Pulse Combustors:

The overall driving and damping characteristics of the pulse combustor will be determined by measuring the growth and decay rates of the combustor pressure oscillations during the start-up and shut-down phases of operation. These measurements will be carried out for various combustor configurations and for a range of operating conditions. The driving and damping for different combustor geometries, fuel/air ratios and injector configurations will be determined.

Task IV: Reporting

As per contract agreement.

TECHNICAL PROGRESS AND RESULTS

During this reporting period the effect of the timing and duration of the combustion process upon the pulse combustor operation was investigated. For this purpose, the combustion process was defined as the combined duration of the mixing, ignition delay and chemical kinetic processes. In order to increase the period of pulsation of the Helmholtz type combustor while attempting to keep the combustion time constant the volume of the combustion chamber was increased and the tailpipe was lengthened. This resulted, however, in a substantial decrease in the pulsation amplitudes. Measurements of the decay rate of the pressure oscillations during the shut down phase of this combustor indicated that this was caused by a significantly increased damping factor. In addition, the combustion efficiency of the enlarged combustor was appreciably reduced.

For the reasons indicated above, the investigation of the effect of combustion time upon the performance of the pulse combustor was shifted to a Schmidt (quarter wave) type combustor. The damping of the Schmidt combustor was measured to be only one half of that of Helmholtz combustor of equal pulsation frequency. Acoustic pulsations of up to 170 dB were obtained for this combustor. In addition, the combustor efficiency was found to be close to one even for very long Schmidt tubes. As the length of the Schmidt combustor was increased the frequency of pulsations decrease until, at a specific length, the pulsations frequency "jumped" to that of the next acoustic harmonic (see Fig.2). When the tube length was further increased, the frequency, once again, started to decrease. This "jump" in frequency is a result of the period of pressure pulsations trying to adjust itself, within the limits set by the combustor geometry, to a value which equals, as close as possible, twice the characteristic combustion time which accounts for the duration of the flow, mixing and chemical kinetic processes.

In the next step of this study the duration of the combustion process was extended by slowing down the mixing of the reactants. Early attempts to delay mixing by installing a separator plate between the fuel and air jets in the mixing chamber were unsuccessful. The separator plate apparently interfered with the driving processes resulting in very low pulsation amplitudes. In addition, the combustion efficiency was considerably lower. Better results were obtained if, after ignition, the fuel injection location

was moved to a position three inches downstream of the location of air injection (see Fig. 3). This resulted in slower mixing and, thus, a longer combustion time. With this configuration the frequency of pulsations did not jump to the next acoustic harmonic when the combustor length was extended beyond a value for which the frequency jump occurred with the original configuration.

When the air flapper valve was removed from the Schmidt tube and the combustor was operated with air supplied at slightly above atmospheric pressure the frequency increased while the dB level somewhat decreased. Pressure measurements along the axis of the combustor indicated that the combustor no longer seemed to operate as a quarter wave tube but, instead, behaved like a Rijke tube as shown in Fig. 4. The drop in the dB level was, most likely, caused by losses in the air supply ducts. In addition, the heat release did not occur at exactly at a distance of $L/4$ from the air inlet which would be required to achieve optimum driving in a Rijke tube. Removal of the fuel valve resulted in a reduced dB level because of a 30% reduction in fuel intake.

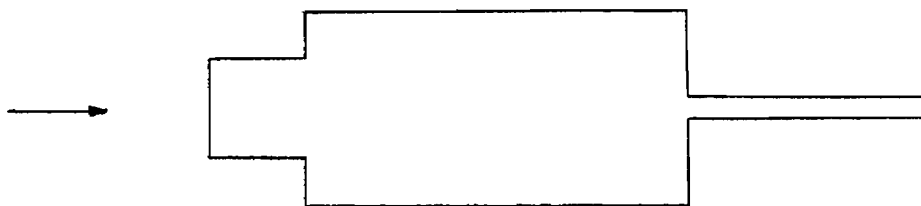
Radical radiation measurements were carried out in the "side on" position along the centerline of a Helmholtz type combustor. These measurements were made using a combustor fitted with flat windows in the curved side walls of both, the mixing and combustion chambers. Cycle to cycle reignition was observed to occur 2.3 inches downstream of the plane in which the fuel and air jets first enter the mixing chamber for all the tested fuel/air ratios (Fig. 5). Once again, near the fuel rich limit (i.e., equivalence ratio = 1) ignition was observed to take place later than for normal operating conditions and near the fuel lean limit. After ignition the flame spread quickly upstream towards the mixing chamber end wall and somewhat more slowly downstream into the combustion chamber. The maximum combustion intensity (Fig. 6) was observed about one half inch upstream of the location of first ignition for the lean limit case and one and one half inches upstream for the normal and rich limit cases. These measurements are continuing and are being correlated with the radiation measurements made through a window in the upstream end of the combustor using the pressure signal as a clock.

The laser Doppler velocimeter (LDV) has been readied for operation. A seeder has been designed, constructed and installed upstream of the air

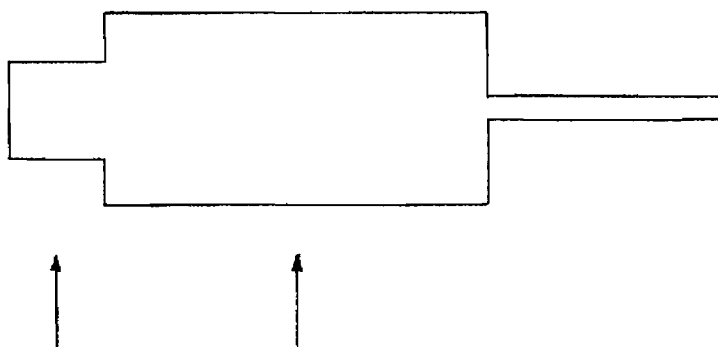
flapper valve. Cold flow tests in the combustor have been started. In these tests a seeded air flow is sucked through the air flapper valve into the combustor by applying a partial vacuum to the tail pipe. The resulting flow velocity in the mixing chamber is measured using the LDV. This permits a proper alignment of the optics and an optimization of the frequency shift and filter settings of the LDV data reduction system.

PLANNED WORK:

- During the next reporting period the work on the LDV will progress to measurements under combusting conditions. Mean axial velocities and turbulence intensities will be measured at selected points along the centerline of the combustor. In addition, the swirl velocity will be determined by moving the probe volume off the central axis and measuring the vertical velocity components.
- The measurement of the damping characteristics of various components and subsystems which make up the pulse combustor will commence. The impedance tube technique will be used in these measurements. A new visiting scientist who has recently joined the group has been charged with these tests.
- Finally, the "side on" radical radiation measurements will continue to the extent to which they do not interfere with the LDV work. A new graduate student joining the program will take over this part of the work.



a) "end on" position



b) "side on" position

Figure 1: Measurement Orientations.

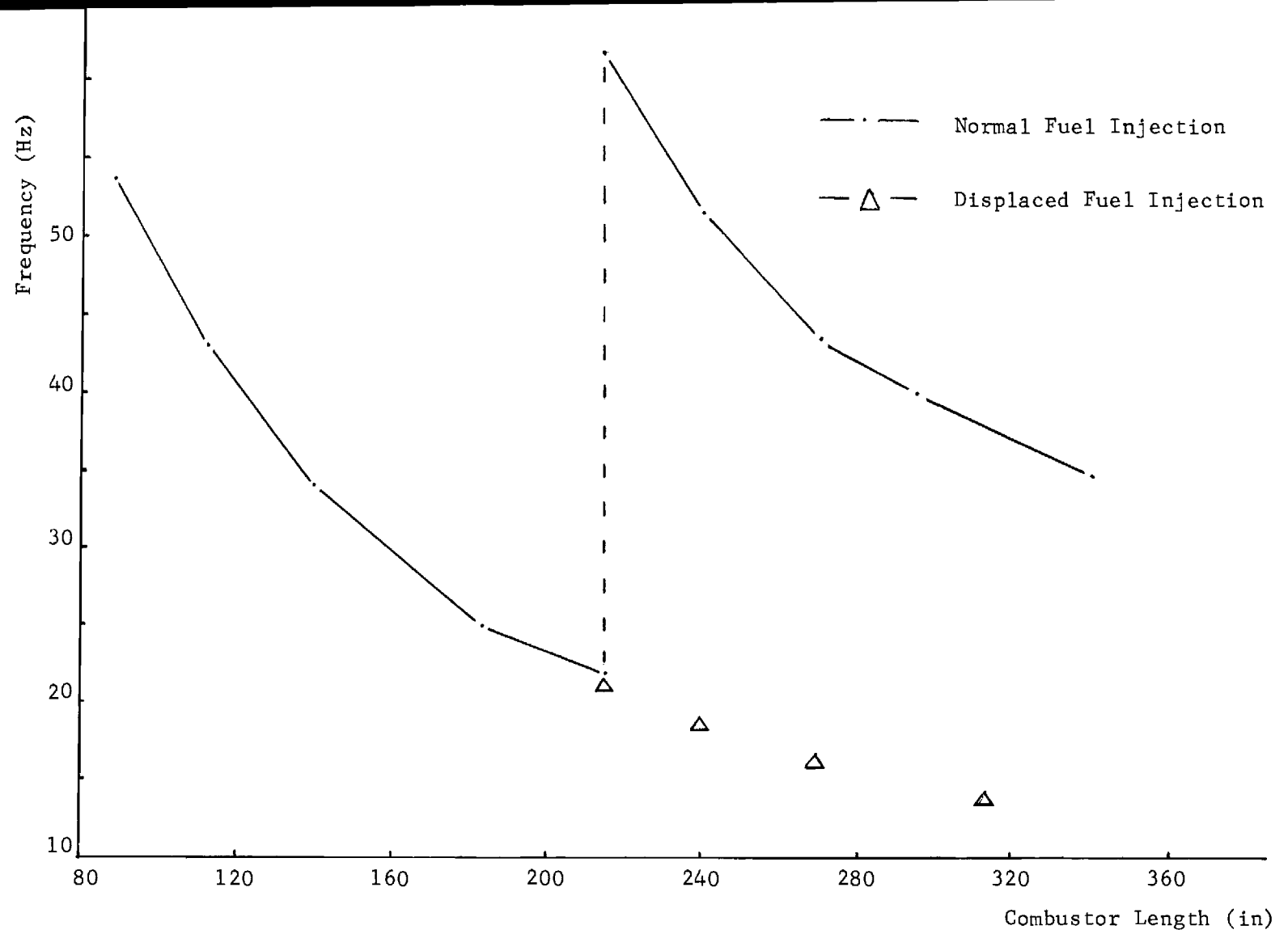


Figure 2: Frequency vs Combustor Length for Schmidt Tube Type Pulse Combustor.

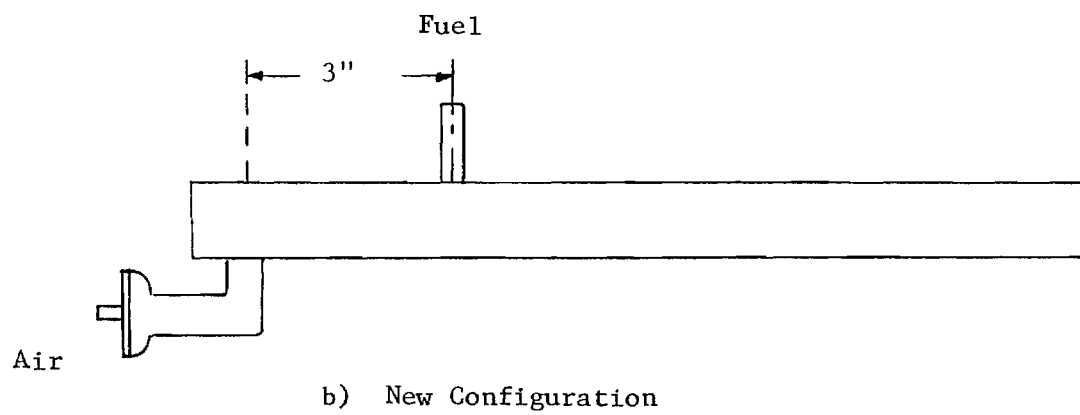
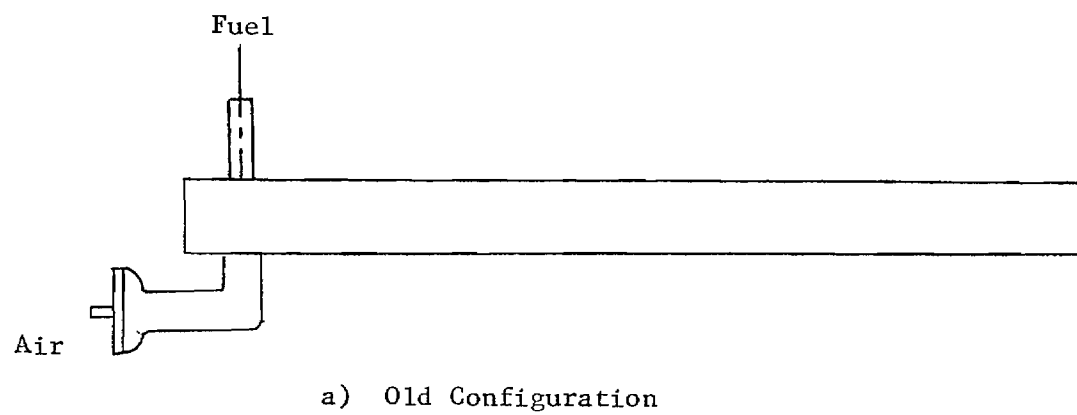
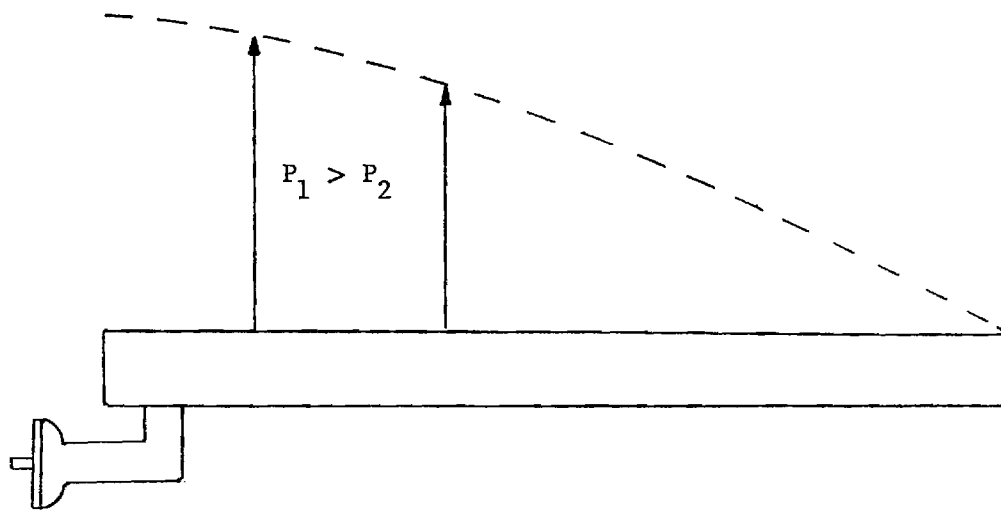
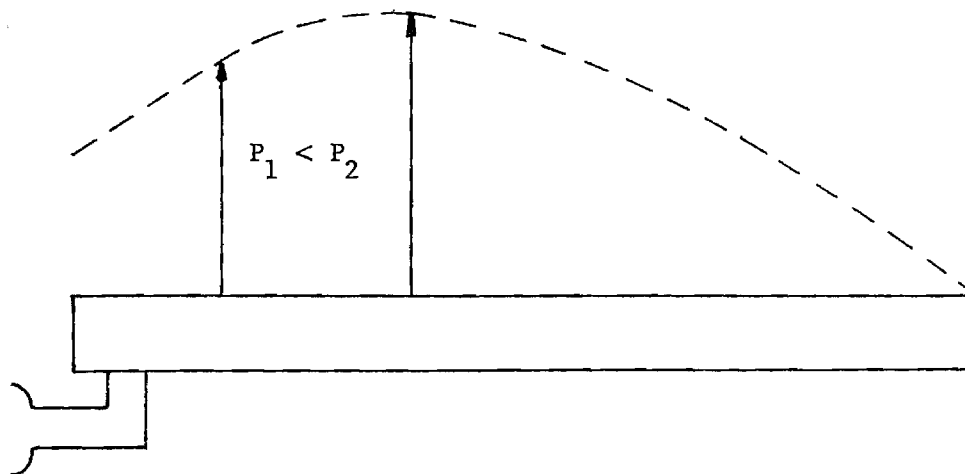


Figure 3: Fuel Injection Positions in Schmidt Combustor.



a) With Air Valve



b) Without Air Valve

Figure 4: Pressure Distributions in Schmidt Combustor. With and Without Air Flapper Valve (Arrows Denote Measured Pressures, Dotted Line Denotes Pressure Wave Form).

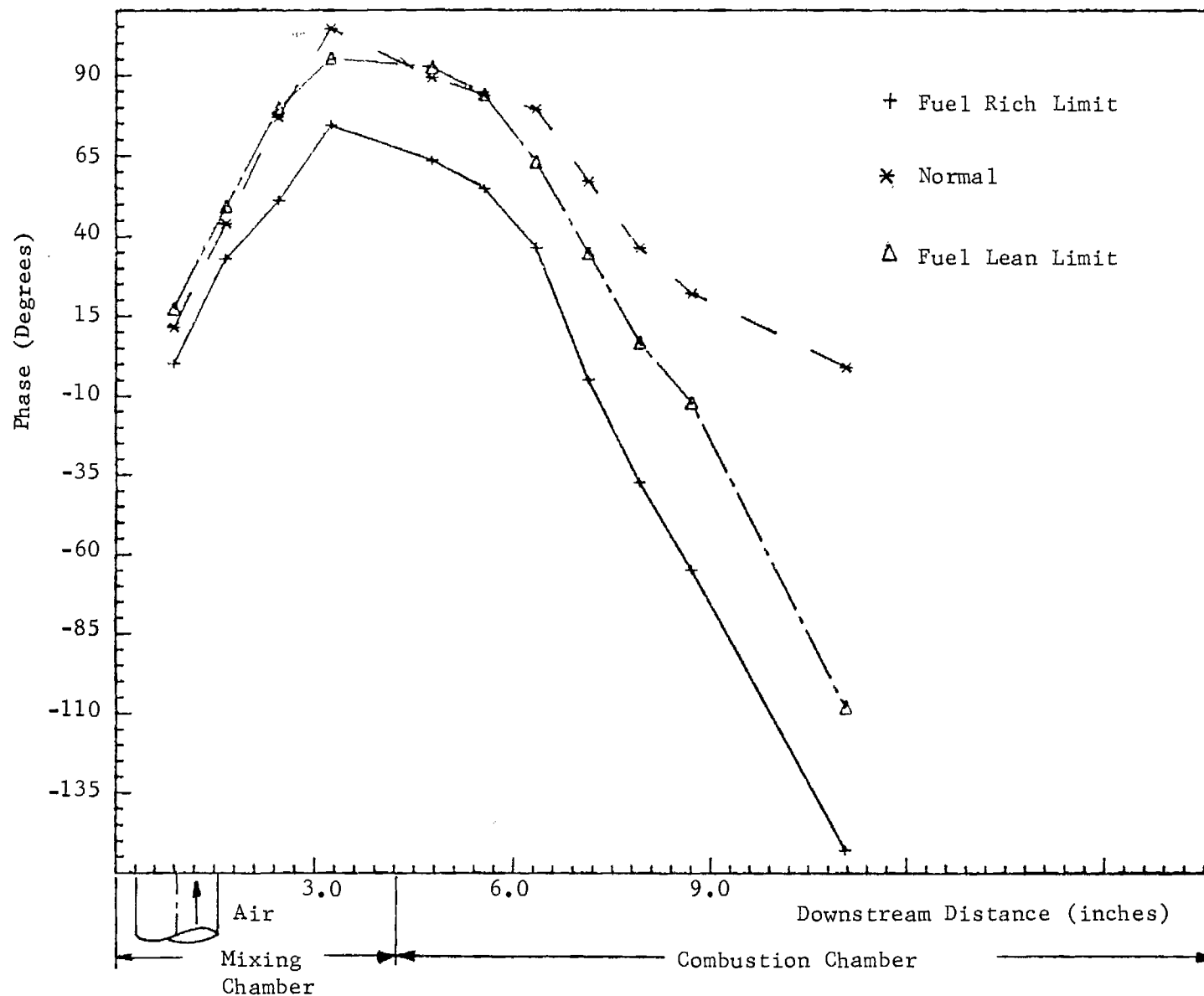


Figure 5: Phase Angle Between Heat Release and Pressure Oscillations as a Function of Axial Distance.

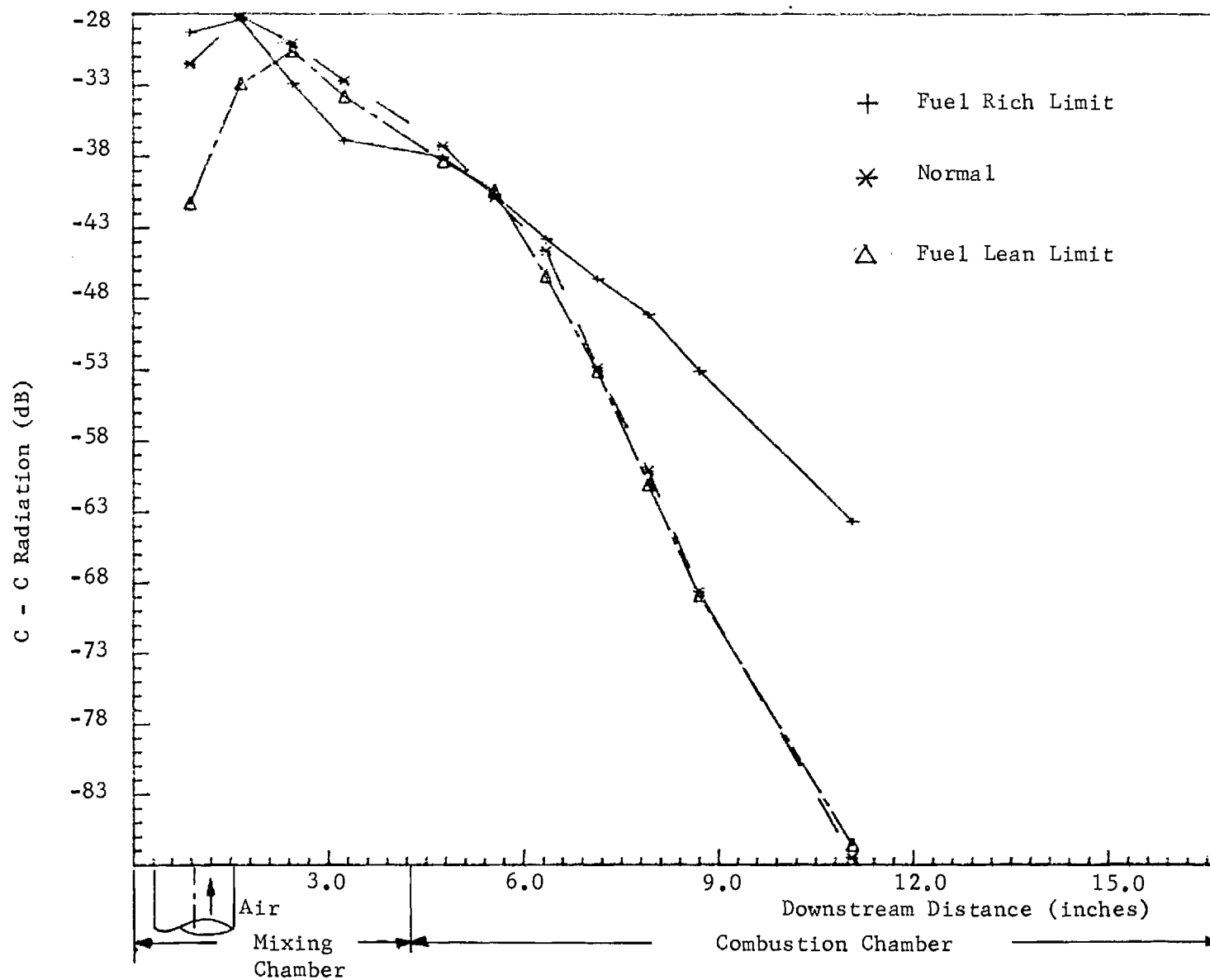


Figure 6: Combustion Intensity vs. Axial Position.

"Submitted to the 22nd Symposium (International) on Combustion"

FLAME SPREAD AND LIMITS OF OPERATION OF GAS FIRED,
MECHANICALLY VALVED, PULSE COMBUSTORS

S. H. Ku, B. R. Daniel, J. I. Jagoda* and B. T. Zinn

School of Aerospace Engineering
Georgia Institute of Technology
Atlanta, GA 30332

Subject Matter: (3) Combustion in Practical Systems
(30) Turbulent Reacting Flows
(15) Ignition

ABSTRACT

This paper describes the results of an investigation of the cycle to cycle reignition process and flame spread in gas fired, mechanically valved, pulse combustors. The measured data are also used to explain the mechanisms responsible for the existence of previously observed rich and lean limits of operation of the investigated pulse combustor. High speed Schlieren cinematography, acoustic pressures and radical radiation (and, therefore, heat release rate) measurements were carried out in a combustor specifically developed for this study. Cycle to cycle reignition of the new fuel charges was observed to take place in the mixing chamber, downstream of the plane of injection of the reactants. From there, the flame spreads throughout the mixing chamber and into the combustion chamber. The instant of reignition depends upon the equivalence ratio and it occurs earlier during the cycle the lower the equivalence ratio. At low equivalence ratios, the entering fuel reacts with air supplied during the previous cycle. The lean limit of operation of the pulse combustor is reached when a substantial fraction of the fuel burns too early during the cycle causing a significant amount of combustion energy to be released out of phase with the pressure oscillations, which damps the pulsations. As the equivalence ratio increases, the amount of air from the previous cycle available for combustion is reduced causing a decrease in the phase difference between the heat release and pressure oscillations. The rich limit is reached when a shortage of air reduces the amount of fuel which can react in phase with the pressure oscillation to a level which is not sufficient for driving the combustor pulsations.

*Corresponding Author:

Dr. J. I. Jagoda
Associate Professor
School of Aerospace Engineering
Georgia Institute of Technology
Atlanta, GA 30332

INTRODUCTION

Interest in pulse combustors has been increasing rapidly in recent years. Small pulse combustors have been successfully utilized in domestic space and water heating^{1,2} and large scale units are currently under development for industrial drying³ and steam raising⁴. The advantages of pulse combustors include high combustion and thermal efficiencies^{1,2}, excellent heat transfer characteristics^{5,6}, self aspiration and low CO, NO_x⁷ and soot emissions. Yet, the physical and chemical processes which control the operation of these pulse combustors are still not fully understood. Consequently, any changes in scale or application of these devices require costly, empirical, development efforts^{3,7}. This paper describes results from an ongoing study whose overall objective is to gain an understanding of the fundamental processes which control the operation of gas fired, mechanically valved, Helmholtz type, pulse combustors similar to those which have been used as home furnaces. Specifically, this paper describes an experimental study of the characteristics of the pulse combustion process and the mechanisms responsible for the existence of the previously observed^{8,9} low and rich limits of operation for these combustors.

The Helmholtz type pulse combustor used in this investigation is shown in Fig. 1. It consists of cylindrical mixing and combustion chambers, a tail pipe, an exhaust decoupler and a vent pipe. Natural gas and air enter the mixing chamber through two flapper valves which are welded ninety degrees apart to the curved sides of the mixing chamber. In the standard American Gas Association (AGA) pulse combustor¹⁰, which is used in this study, the combustion chamber has a volume of 183 in³, and a tail pipe length and diameter of 75 in and 1.5 in, respectively. With these dimensions, the unit

1
CFD

pulses with a frequency of 42 Hz. The design loading for this combustor is 50,000 BTU/HR.

To ignite, a fuel-air mixture is admitted into the mixing chamber and ignited by a spark plug. The ensuing combustion increases the pressure inside the mixing and combustion chambers. This, in turn, closes the flapper valves. The expansion of the hot combustion products causes their expulsion through the tail pipe. The inertia of the gases leaving the combustor drops the pressure in the mixing chamber to below atmospheric level and results in the reopening of the valves. Fresh charges of air and fuel enter the combustor, mix and ignite without the use of the spark plug, resulting in a pulse combustion process which can be maintained indefinitely.

In previous studies^{11,12} with this AGA combustor it was observed that the combustion process is largely confined to the mixing chamber, the frequency of pulsations decreases when the volume of the combustion chamber or the length of the tail pipe is increased, and pulse combustion operation can be attained only for equivalence ratios between 0.6 and 1.0. It was also noted¹³ that the rich limit of operation of the pulse combustor can be significantly extended if the combustor is fitted with a longer tail pipe which increases its period of pulsations. Furthermore, the combustor can be operated rich of stoichiometric if the combustion air is supplied to its flapper valve at above atmospheric pressure.

In an effort to develop an understanding of the observed trends, detailed diagnostics of the combustion process have been initiated earlier under this program^{11,12}. High speed Schlieren photography carried out along the axis of the combustor clearly showed a highly turbulent fuel jet entering the mixing chamber during the early part of the cycle. This was followed by the entrance of a slower moving air jet. After the two jets mixed,

combustion was seen to take place in a highly turbulent flow field. Combustion was almost completed before fuel for the next cycle entered the mixing chamber, except when the combustor was operated near its rich limit. Finally, the amplitudes of the pulsations were found to increase as the fuel-air ratio was increased⁹, within the limits of operation of the combustor.

It was the objective of the work reported herein to elucidate the mechanisms responsible for the existence of the above described limits of operation and investigate the location and timing of the cycle to cycle reignition of the new charges and the ensuing flame spread through the combustor.

EXPERIMENTAL SET UP

To allow high speed Schlieren and radiation measurements, a combustor similar to one shown in Fig. 1 but fitted with the required optical windows was developed, see Fig. 2. It was made out of steel except for a flat, circular quartz window at the upstream end of the mixing chamber and flat, annular, quartz windows at the transition sections between the mixing and combustion chambers and the combustion chamber and the tail-pipe. In addition, flat, rectangular, quartz windows were fitted into the curved walls of the mixing and combustion chambers. These permitted optical access into the combustion chamber along its axis and normal to it.

The pulse combustor was operated on natural gas supplied at five inches of water pressure while air could be aspirated from the atmosphere or supplied at elevated pressure. The fuel flapper valve setting was kept fixed while the air flow rate and, therefore, the fuel-air ratio could be varied by adjusting the maximum travel distance of the flappers in the air valve¹⁰.

Oscillating pressures were measured using Kistler piezoelectric transducers mounted on semi-infinite tubes several inches away from the

combustor to protect the transducers from the combustor heat and provide a flat frequency response. These pressure measurements were carried out at the centers of the combustion and mixing chambers and in the pipe connecting the fuel flapper valve to the mixing chamber. The signals from the pressure transducers were amplified and passed through an A/D converter and into an HP A700 computer.

A Schlieren system was used to view the combustion process along the combustor axis, see Fig. 2. The beam through the mixing and combustion chambers was arranged to be slightly converging rather than collimated which permitted it to exit the combustor without being obstructed by the tail pipe. The Schlieren images along with the instantaneous pressure traces on an oscilloscope were recorded using a HICAM high speed camera at a rate of 7000 frames per second.

The oscillating reaction rates (i.e., combustion intensities) were determined by measuring the spontaneous radiation from OH radicals through the combustor windows¹⁴. These measurements were carried out both, globally and spatially resolved. For the global measurements (see Fig. 3a) the radiation from the entire combustor was focused, using a large diameter, short focal length lens, through a 306 nm interference filter and a pin hole onto a Hamamatsu R269 photomultiplier. For the spatially resolved measurements, which were carried out at various locations through the end and side windows of the combustor, the focusing lens was replaced by a thin tube, fitted at both ends with small apertures (see Fig. 3b). This tube eliminated the radiation emitted from regions other than the small area under investigation. This allowed measurements of integrals of radiation signals along axes parallel to the combustor axis with a spatial resolution of 3 mm in the plane normal to the combustor axis. The output from the

Fig³

photomultiplier was converted to a voltage using a 10 k Ω resistor, amplified with a Neff amplifier and passed via an A/D converter into the computer.

A computer program was developed which acquired and analyzed both pressure and radiation data simultaneously. The software permitted the display of time traces of pressure and radiation intensity and the calculation of their auto- and cross-correlations. These allowed determination of the spectra for the pressure and radiation signals and the phase angles between them. In addition, the fluctuating radiation signals were correlated with the high speed Schlieren movies using the recorded pressure oscillations as a clock.

RESULTS AND DISCUSSION

High speed Schlieren photography, spontaneous radiation and oscillatory pressure measurements were carried out in the pulse combustor operating near its lean and rich limits of operation and under normal operating conditions. Figure 4 shows time traces of simultaneously measured pressure and global radiation fluctuations. Also indicated are the instances in the cycle at which the fuel and air jets entered the mixing chamber as determined from the high speed Schlieren records. The time in each cycle at which the radiation intensity begins to increase is denoted as the instant of reignition of the fresh fuel charge. 4

Figure 4 indicates that the fuel jet enters the mixing chamber before the pressure there falls below the nominal fuel supply pressure. This occurs because the pressure oscillations in the fuel line slightly lag behind those in the mixing chamber, see Fig. 5. Therefore, early in the cycle, the pressure in the fuel line is slightly higher than that in the mixing chamber, which causes the early fuel jet entry into the mixing chamber. 5

Figure 4 shows that the emitted radiation and, therefore, the combustion process never stop at any time during the cycle. Clearly, the fluctuations in heat release always lead those in pressure. This was expected since the pulse combustion drives the pressure oscillations. Comparison of the data presented in Figs. 4-A,B,C further shows that the combustion of the new charges in each cycle commences earlier, the lower the fuel-air ratio. In fact, near the lean limit and under normal operating conditions ignition of the new fuel charge occurs before air for that cycle has started to enter the mixing chamber. This is possible because under fuel lean conditions the fresh fuel charge can begin its combustion process using air remaining from the previous cycle. However, as stoichometric conditions are approached, less and less air from the previous cycle is available for combustion and the combustion of the fresh fuel charge is delayed until the air for this cycle enters the combustor.

According to Rayleigh's criterion,¹⁵ driving of the pulsations requires that a certain minimum fraction of the combustion energy be released in phase with the pressure oscillations, in order to overcome the inherent losses in the system. Typical relationships between the heat addition and pressure oscillations are represented schematically in Fig. 6 where the length of the vector q represents the magnitude of the heat release and θ is the phase angle with respect to the pressure oscillations which are always aligned with the positive axis. If the projection of q along the horizontal axis (i.e., $q \cos \theta$) exceeds the systems losses, represented by $-L$, the combustion heat release is sufficient to drive pressure oscillations. The observed delay in the occurrence of ignition, which is caused by the unavailability of air as stoichometric conditions are approached, apparently "produces" conditions under which the amount of fuel which reacts in phase with the available air

Fig. 6

does not release a "sufficient" amount of energy in phase with the pressure oscillations. This is confirmed by the high speed Schlieren movies which have shown that near the rich limit the new fuel enters while the combustion process from the previous cycle is still taking place. In terms of Fig. 6a this means that the magnitude of q is too small for $q \cos \theta$ to exceed the system losses, $-L$, in spite of the phase θ being small. This, in turn, results in stoppage of pulsations.

The above discussed observations suggest that the rich limit could be possibly extended by decreasing the frequency of oscillations and/or supplying the air at elevated pressure. The former would provide a longer period for the combustion process to take place during the cycle. The latter will cause reignition to occur earlier during the cycle (and, thus, make more air available "early" for combustion), by causing earlier entry of the air and also shorten the combustion time by increasing the mixing rate. Either could provide conditions under which Rayleigh's criterion for driving the combustor oscillations would be satisfied. Indeed, as stated above, earlier studies^{8,9} confirmed that the stated conjectures are correct.

To further investigate the combustion process behavior under different operating conditions, spatially resolved amplitudes and phases of the radiation were measured under lean, normal and rich operating conditions, see Figs. 7 and 8. The lines of constant phase between the maximum radiation and maximum pressure signals are plotted in Figure 7. The numbers next to the lines indicate the phase angle by which the heat release leads the pressure.

Close inspection of the lean limit case shows that the early part of the combustion cycle and, therefore, of the heat release, occurs more than 90 degrees out of phase with the pressure oscillations; i.e., $\theta > 90$ in Fig. 6. According to Rayleigh's criterion, the combustion energy released during this

fig 7
fig 8

part of the cycle damps rather than drives the pulsations. The local phase angle by which the heat release leads the pressure fluctuations and the spatially resolved dB levels of the radiation fluctuations for the lean limit case are shown in Fig. 8. This figure indicates that the part of the combustion cycle which is out of phase with the pressure oscillations exhibits large amplitude radiation fluctuations. This indicates that near the lean limit a considerable fraction of the heat release during each cycle damps rather than drives the pulsations (i.e., $q \cdot \cos\theta$ in Fig. 6b is less than $-L$). Since Fig. 7 indicates that reignition occurs earlier as the operation becomes leaner, the damping by the combustion process increases as the lean limit is approached. This is accompanied by a decrease in the amplitude of pulsations as is apparent in Figure 4. These observations strongly suggest that the lean limit of operation occurs when due to the early combustion process the damping provided by the heat release adds to the inherent system acoustic losses and the driving provided by the combustion process cannot overcome these combined damping effects.

In Fig. 7, the higher the phase, the earlier the occurrence of the combustion process at that location. Therefore, the location with the highest phase indicates the region of cycle to cycle reignition of fresh fuel charges. In all three cases the new fuel charges ignite in the mixing chamber opposite the fuel inlet port. However, near the rich limit a secondary reignition area is observed near the center of the mixing chamber where the air jet first impinges upon the fuel jet. From the reignition spot(s) the flame then spreads throughout the mixing chamber.

Additional radiation measurements were carried out normal to the axis of the pulse combustor along its center line. Figure 9 shows the dependence of the phase angle between the heat release and pressure oscillations upon the

Fig. 9

axial location. These data indicate that cycle to cycle reignition (i.e., the largest phase angle) occurs 2.3 inches downstream of the plane in which the fuel and air jets enter the mixing chamber for all of the tested fuel-air ratios. Consistent with the above discussed results, ignition near the rich limit occurred later than for the other two cases. Figure 9 also shows that after ignition the flame quickly spreads upstream towards the mixing chamber end wall and somewhat more slowly downstream into the combustion chamber.

CONCLUSIONS

Oscillatory pressure measurements, high speed Schlieren photography and spontaneous radiation measurements were carried out in a Helmholtz type, gas fired, mechanically valved, pulse combustor. Cycle to cycle reignition of the new fuel charges was observed to occur in the mixing chamber opposite and downstream of the fuel inlet port. From there the flame spreads throughout the mixing chamber and into the combustion chamber.

The mechanisms controlling the occurrences of the lean and rich limits of operation of the pulse combustor are fundamentally different. Near the lean limit of operation combustion of the new fuel charge in each cycle commences as soon as the fuel enters the mixing chamber using excess air left over from the previous cycle. Thus, a significant fraction of the heat release occurs out of phase with the pressure oscillations which damps the pulsations. A lean limit of operation is reached when the sum of the damping provided by the combustion process and the inherent system acoustic losses exceeds the combustion process driving. As the fuel-air ratio is increased, the heat release and pressure oscillations become more and more in phase, resulting in increased driving. Therefore, the pressure amplitudes increase as the equivalence ratio is increased. Near stoichiometric conditions no air is left over from the previous cycle and the ignition of the new fuel is

delayed until fresh air enters the mixing chamber. This, in turn, delays the beginning of the new combustion cycle and produces conditions under which the fraction of the combustion energy released in phase with the pressure oscillations does not produce sufficient driving to overcome the system's damping. When this occurs, the rich limit of operation is reached. Since the duration of the cycle can be changed by modifying the combustor geometry, it has been shown that the limit of operation can be extended to the fuel rich side by prolonging the period of oscillations through the use of a longer tail pipe. Alternately, the rich limit was extended by supplying the air under pressure which shortened the reignition delay and, most likely, reduced the time required for combustion by increasing the mixing rate. Both effects apparently resulted in a larger fraction of the combustion energy being released in phase with the pressure oscillations, resulting in increased driving and a lower rich limit of operation.

ACKNOWLEDGEMENT

This work was supported by the Gas Research Institute under Grant No. 5083-260-0873. Mr. J. Kezerle is the monitor.

REFERENCES

1. "Lennox-Pulse-G14 Series Up-Flo Gas Furnaces," Engineering Data, Heating Units, Gas, pp. 21-24, published by Lennox Industries, Inc.
2. "Hydropulse by Hydrotherm," information about pulsed combustion water heating published by Hydrotherm, Rolfland Ave., Northvale, NJ 07647.
3. Flanigan, P., AGA Laboratories "Development of a Pulse Combustion Industrial Dryer, Phase I" Final Report to Gas Research Institute, 1987.
4. Kezerle, J., Gas Research Institute, Chicago, IL, personal communication.

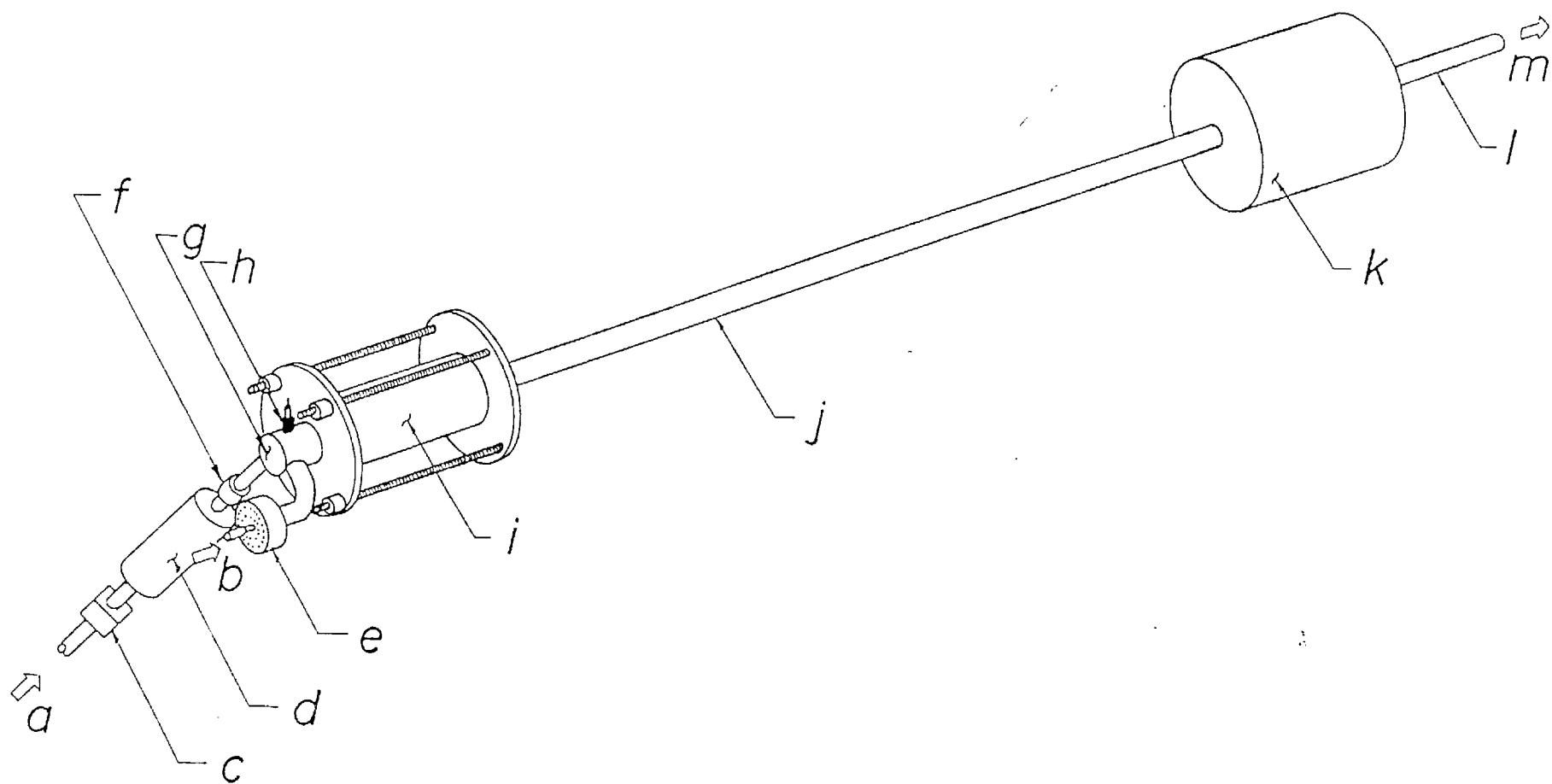
5. Hanby, V. I., "Convective Heat Transfer in a Gas-Fired Pulsating Combustor," Paper No. 68-WA/FU-1 (1968).
6. Fedorov, B. N., "Experimental Study of the Effect of Acoustic Oscillations on Heat Transfer in a Gas Flow," *Juzherno-Fisicheskii Zhurnal*, Vol. 32, No. 1, pp 167-180, 1977.
7. Belles, F. E., "R & D and Other Needs for Exploitation of Pulse-Combustion in Space-Heating Applications," *Proc. of Symp. on Pulse-Combustion Technology for Heating Applications*, Argonne National Laboratory, pp. 167-180, 1979.
8. Ku, S. H., Cheng, X. C., Daniel, B. R., Jagoda, J. I. and Zinn, B. T., "Performance Characteristics of Helmholtz Type Pulsating Combustors" presented at the Fall Technical Meeting of the Eastern States Section of the Combustion Institute, 1985.
9. Ku, S. H., Cheng, X. C., Scroubelos, G., Daniel, B. R., Jagoda, J. I. and Zinn, B. T., "Performance and Efficiency of Gas Fired Pulsating Combustors" presented at the 1986 International Gas Research Conference, Toronto, Canada, Sept. 1986.
10. Griffiths, J. C. and Weber, E. J., "The Design of Pulse Combustion Burners," *Research Bulletin 107*, American Gas Association Laboratories, June 1969.
11. Reuter, D., Daniel, B. R., Jagoda, J. I. and Zinn, B. T., "Periodic Mixing and Combustion Processes in Gas Fired Pulsating Combustors" presented at the Spring Joint Technical Meeting of the Central and Western States Sections of the Combustion Institute, San Antonio, TX, April 1985.
12. Reuter, D., Daniel, B. R., Jagoda, J. I. and Zinn, B. T., Combustion and Flame, Vol. 65, No. 3, pp. 281-290, 1986.

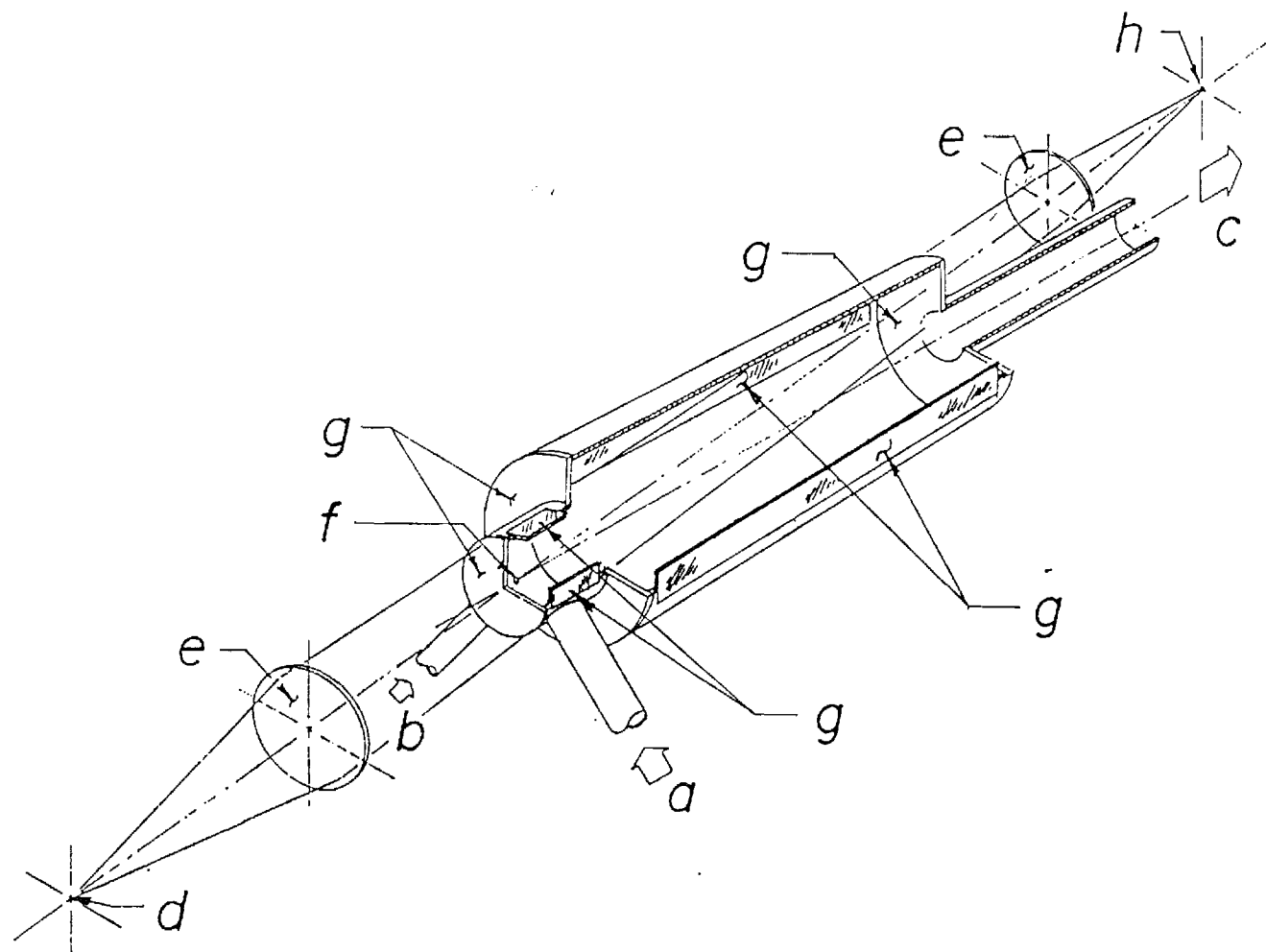
13. Ku, S. H., Cheng, X. C., Daniel, B. R., Jagoda, J. I. and Zinn, B. T., "Radiation Measurements in a Gas Fired Pulse Combustors" presented at the Spring Technical Meeting of the Central States Section of the Combustion Institute, Chicago, IL, 1987.
14. Keller, J. O. and Westbrook, C. K. Twenty first Symposium (International) on Combustion, The Combustion Institute, 1987.
15. Lord Rayleigh, "The Theory of Sound," Vol. II, pp. 224-235, Dover, 1945.

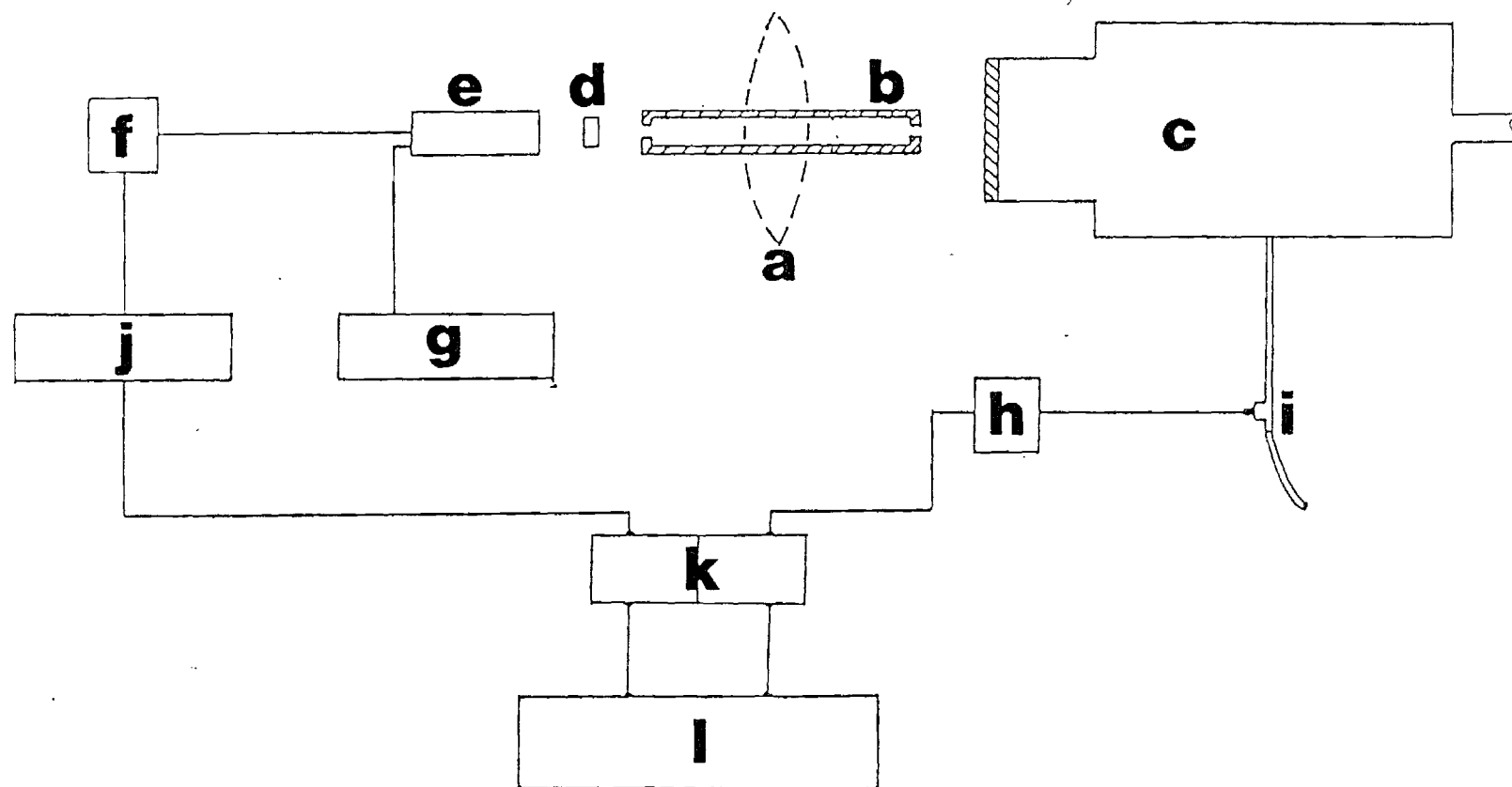
FIGURE CAPTIONS

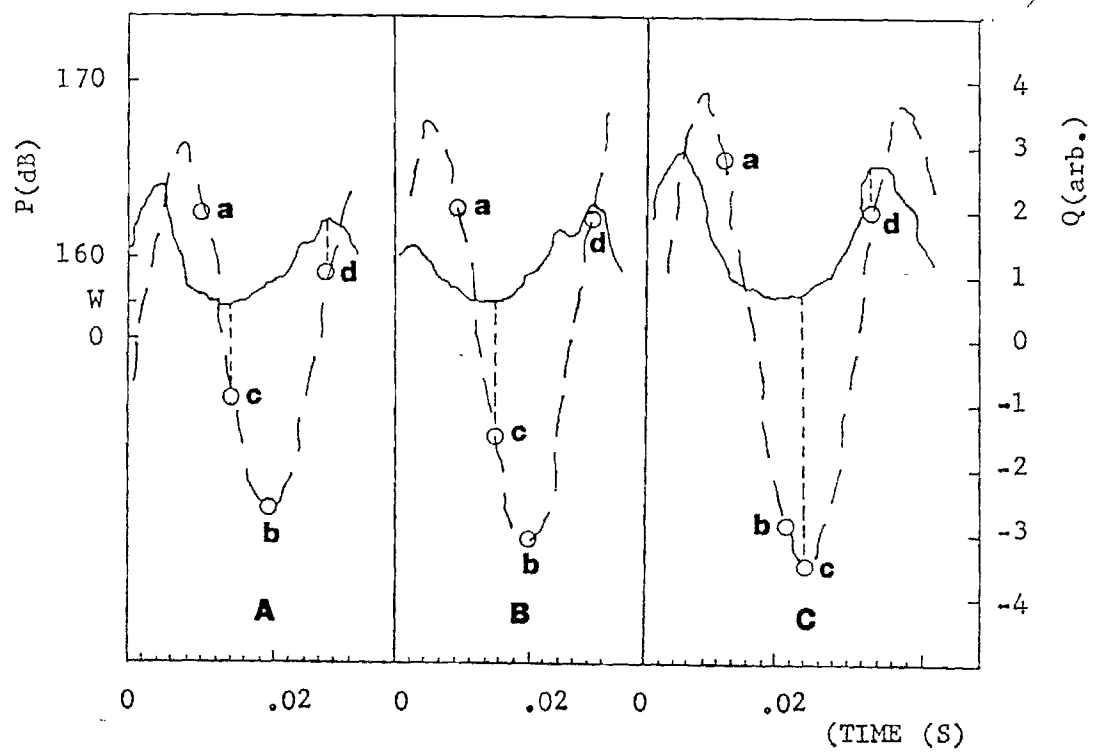
1. Schematic of the Gas Fired Pulse Combustor;
(a) Gas Inlet, (b) Air Inlet, (c) Gas Solenoid, (d) Gas Decoupler,
(e) Air Flapper, (f) Gas Flapper, (g) Mixer Head, (h) Spark Plug,
(i) Combustor, (j) Tail Pipe, (k) Exhaust Decoupler, (l) Vent Pipe and
(m) Exhaust.
2. Schematic of Schlieren Set-up;
(a) Air Inlet, (b) Gas Inlet, (c) Exhaust, (d) Light Source, (e) Lenses,
(f) Fuel Port, (g) Optical Windows and (h) Schlieren Stop.
3. Radiation / Pressure Measurement Set-up;
(a) Lens for Global Radiation Measurements, (b) Tube for Spatially
Resolved Radiation Measurements, (c) Combustor, (d) Optical Filter, (e)
Photomultiplier, (f) Resistor, (g) Power Supply, (h) Amplifier, (i)
Kistler Piezoelectric Pressure Transducer, (j) Low Pass Filter, (k) A/D
Converter and (l) Computer.
4. Global Heat Release (Q) in Arbitrary Units (—) and Pressure
Fluctuations (P) in dB (---) Near the Lean Limit (A), for Normal
Operation (B) and Near the Rich Limit (C);
(a) Fuel Injection, (b) Air Injection, (c) Reignition and (d) Maximum
Heat Release; W Corresponds to Fuel Line Pressure.
5. Pressure Fluctuations (P) in Inches of Water vs. Time in (1) Fuel Line,
(2) Combustor.
6. Vector Representation of Rayleigh's Criterion;
(a) Near the Rich Limit, (b) Near the Lean Limit.
7. Spatially Resolved Radical Radiation Measurements Through End Window:
Phase by which Radiation Leads Pressure.

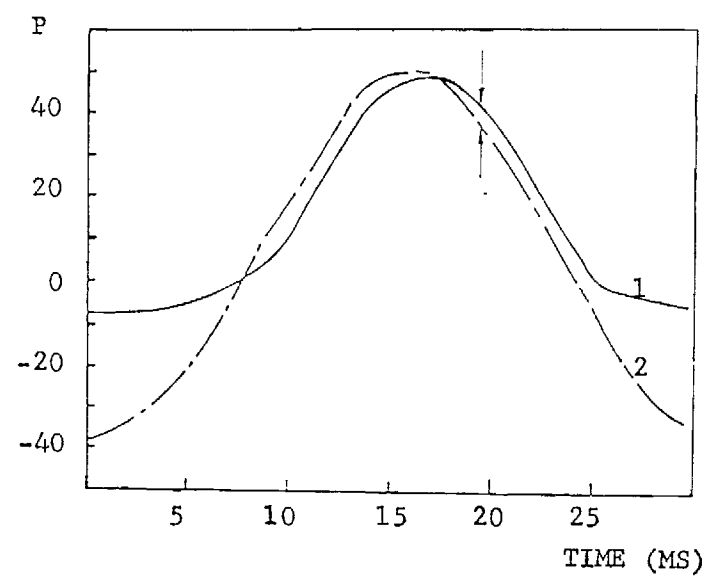
8. Spatially Resolved Radical Radiation Measurements for Lean Conditions Through End Window: Amplitude and Phase.
9. Spatially Resolved Radical Radiation Measurements Through Side Windows Along the Combustor Axis for (——) Fuel Rich Limit, (— — —) Normal Operation and (- — —) Fuel Lean Limit; Phase by which Radiation Leads Pressure;
(a) Air Inlet, (b) Interface Between Mixing and Combustion Chambers.

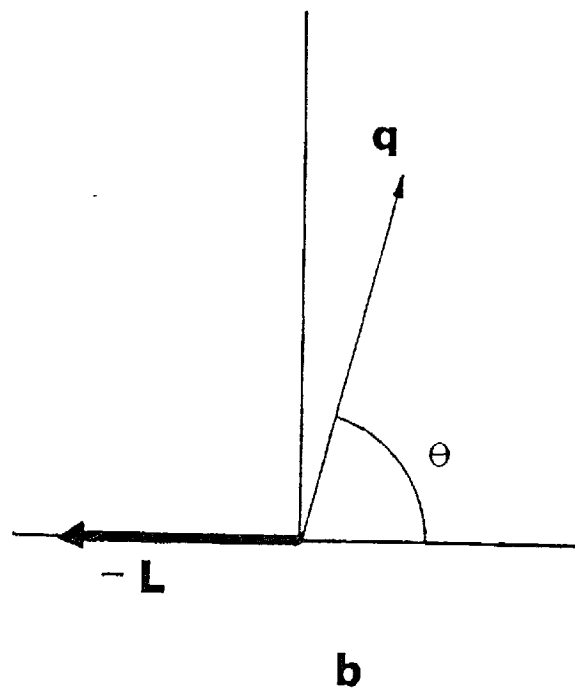
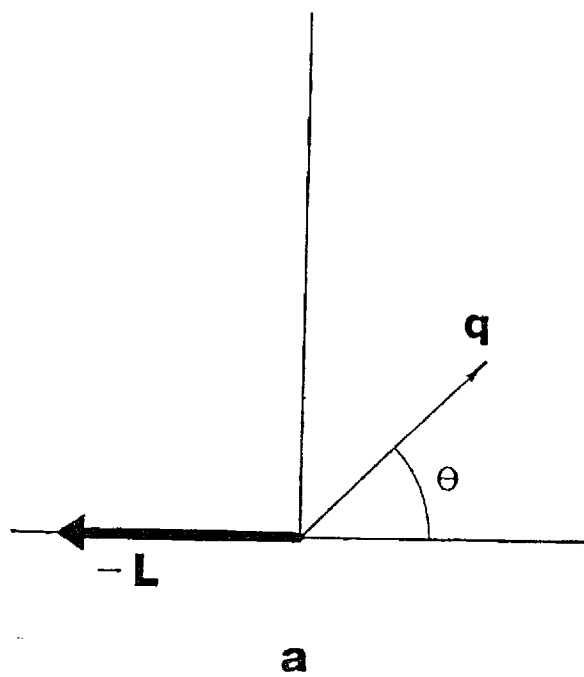


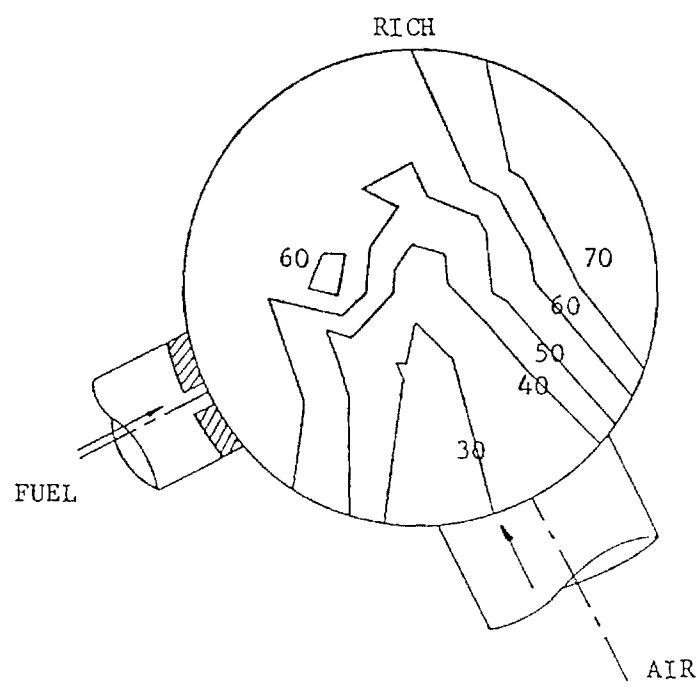
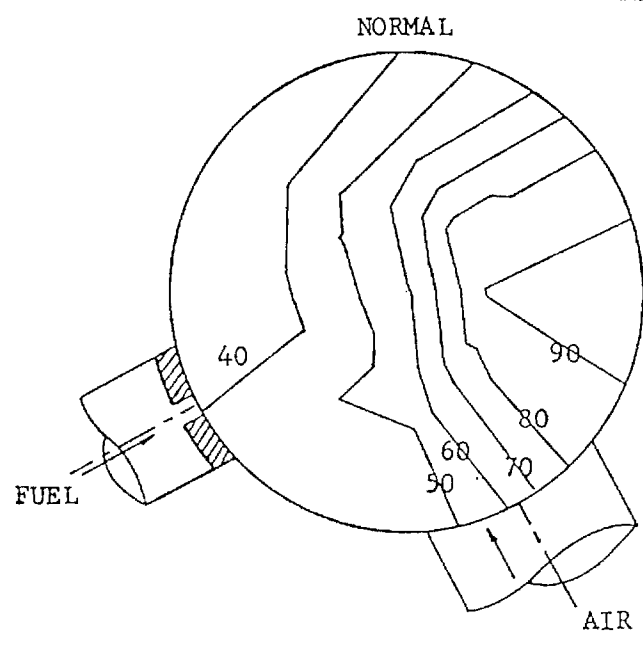
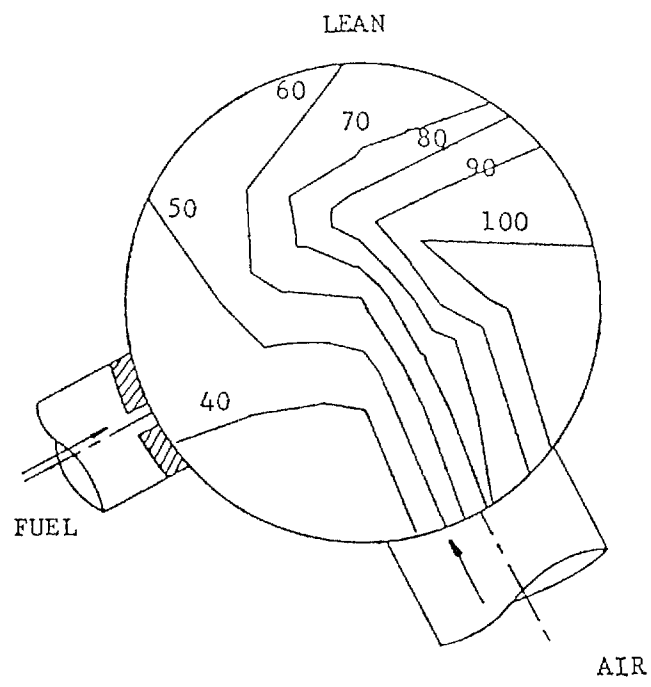


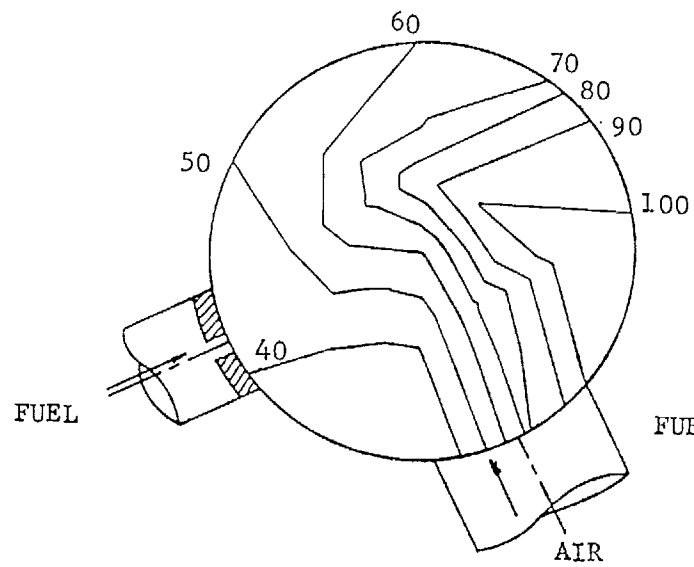




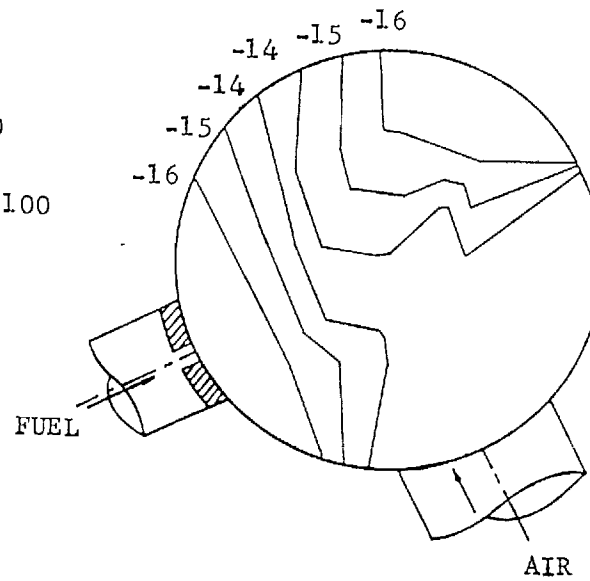




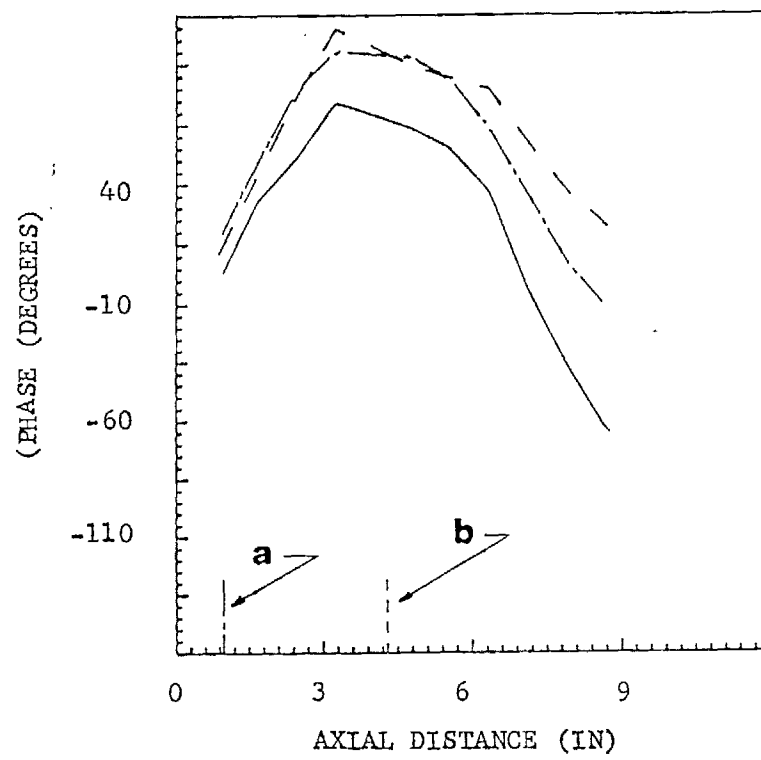




PHASE (DEGREES)



AMPLITUDE (dB)



Pulsating Burners - Controlling Mechanisms and Performance

Final Report

January 1, 1987 - June 30, 1990

Prepared by

J.I. Jagoda, B.R. Daniel and B.T. Zinn

School of Aerospace Engineering

Georgia Institute of Technology

For

Gas Research Institute

Grant No. 5087-260-1466

GRI Project Managers

James A. Kezerle and Thomas R. Roose, Ph. D.

Combustion

January 1991

GRI DISCLAIMER

LEGAL NOTICE: This report was prepared by the Georgia Institute of Technology as an account of work sponsored by the Gas Research Institute (GRI). Neither GRI, members of GRI, nor any person acting on behalf of either:

- a. Makes any warranty or representation, express or implied, with respect to the accuracy, completeness, or usefulness of the information contained in this report, or that the use of any apparatus, method, or process disclosed in this report may not infringe privately owned rights; or
- b. Assume any liability with respect to the use of, or for damages resulting from the use of, any information, apparatus, method, or process disclosed in this report.

REPORT DOCUMENTATION PAGE		1. REPORT NO.	2.	3. Recipient's Accession No.
4. Title and Subtitle "Pulsating Burners - Controlling Mechanism and Performance"				5. Report Date January 1991
7. Author(s) J.I.Jagoda, B.R.Daniel and B.T.Zinn				6.
9. Performing Organization Name and Address School of Aerospace Engineering Georgia Institute of Technology Atlanta, Georgia 30332				8. Performing Organization Rept. No.
12. Sponsoring Organization Name and Address Gas Research Institute 8600 West Bryn Mawr Avenue Chicago, IL 60631				10. Project/Task/Work Unit No. E-16-601
				11. Contract(C) or Grant(G) No. (C) 5087-260-1466 (G)
				13. Type of Report & Period Covered Final Jan.'87-June '90
15. Supplementary Notes				14.
16. Abstract (Limit: 200 words) The objective of this study was to increase our understanding of the physical processes which control the mixing and heat release processes in valved, natural gas fired, pulse combustors. The effects of combustor geometry and heat transfer upon the performance of the pulse combustor were investigated. The flow and flame spread in the pulse combustor were visualized using high speed shadowgraphy and radical imaging, respectively. In addition, the flow field has been quantified using laser Doppler velocimetry. The resulting data were used to explain the dependence of the pulse combustor's performance upon the timing of the entry of the reactants and the complex interaction between the fuel and air jets. Furthermore, the reasons for the existence of lean and rich limits of operation were determined. Under a separate task, the acoustic characteristics of the various parts which make up a pulse combustor were determined using an impedance tube technique. Finally, an analytical scheme was developed which allows the calculation of the admittance of entire sections of the pulse combustor from measured admittances of its component parts.				
17. Document Analysis a. Descriptors Pulse Combustion				
b. Identifiers/Open-Ended Terms Performance, Flow Visualization, Reignition, Flame Spread, Limits of Operation, Admittance Measurements.				
c. COSATI Field/Group Combustion				
18. Availability Statement: Distribution Unlimited		19. Security Class (This Report) unclassified		21. No. of Pages
		20. Security Class (This Page) unclassified		22. Price

RESEARCH SUMMARY

Title: Pulsating Burners - Controlling Mechanisms and Performance

Contractor: Georgia Tech Research Corporation

Contract Number: 5087-260-1466

Reporting Period January 1987- June 1990, Final Report

Principle Investigators: B. T. Zinn, B. R. Daniel and J. I. Jagoda

Objective: The objectives of this study were to gain further insights into the detailed physical mechanisms which control the mixing and heat release processes in pulse combustors. In addition, the acoustic damping characteristics of various components and subsystems of the pulse combustor were to be determined over a range of operating conditions.

Technical Perspective: Natural gas fired pulse combustors have been on the market for a number of years. Nevertheless, their controlling mechanisms are still not sufficiently well understood to permit the design

of pulse combustors for different applications without resorting to costly trial and error development efforts. Proper operation of pulse combustors requires that the timing of the mixing, cycle to cycle reignition and flame spread processes produce oscillatory heat release in phase with the pressure oscillations. In addition, the thus generated driving must be sufficient to overcome the damping by the pulse combustor. To develop a rational design procedure for pulse combustors, it is necessary that the various processes responsible for energy addition to and removal from the pulsations be understood. Furthermore, data describing the acoustic properties of various pulse combustor components under different operating conditions are needed. Finally, the interaction between the acoustic characteristics of the various combustor components and the fundamental fluid mechanical, heat transfer and combustion processes must be understood.

Technical Approach: In order to elucidate the mechanisms which control the operation of a natural gas fired, Helmholtz type, pulse combustor and to determine the acoustic characteristics of different components and

subsystems which make up this pulse combustor, the following tasks were performed:

- 1) The flow field characteristics, mixing and heat release distributions in the pulse combustor were investigated using LDV, Schlieren, mixing visualization and radical radiation imaging.
- 2) The acoustic characteristics of various components and subsystems which make up the pulse combustor were measured using the impedance tube technique.

Results:

A natural gas fired, valved, Helmholtz type, pulse combustor based upon an AGA design was studied. High speed shadowgraphy showed that the injection of the fuel jet leads the entry of the air jet. The latter creates large axial and transverse vortices in the mixing chamber. Comparison of the flow field with spatially and time resolved heat release measurements indicated that the order in which the reactants enter the combustor is critical to the spread of the combustion process through the mixing chamber. While the fuel jet begins to react with air left over from the previous cycle as soon as it enters the mixing chamber, the main ignition of the new fuel occurs near the combustor wall opposite of the fuel port. Combustion is then convected by the leading edge vortex of the air jet through the remainder of the mixing chamber. It is

this complex interaction between the fuel and air jets which stabilizes the combustion process in the mixing chamber. An increase in the combustor temperature was found to lower the lean limit of operation of the pulse combustor. However, the period of pulsations had to be extended or combustion air had to be supplied under pressure to extend its rich limit. This rich limit occurs near stoichiometric conditions because no air is left over from the previous cycle. The combustion process is then confined to the time interval between the entry of the new air jet and the quenching of the reaction by the combustion products returning to the mixing chamber. For the standard AGA combustor this time is too short to permit sufficient heat release to drive the pressure oscillations. Further investigation of the importance of the timing between the heat release and the pressure oscillations revealed that at low operating frequencies the combustion process can excite higher pressure harmonics in the combustor unless the timing of the heat release is delayed. Furthermore, reduction of heat transfer to the combustor walls was found to significantly reduce the operating frequency of the device. The results of ensemble averaged mean velocity and turbulence intensity measurements are used to

qualitatively describe the complex, turbulent flow field in the mixing chamber at various instants during the cycle. These measurements are currently being completed by the graduate student as part of his Ph. D. thesis work. Under a separate task, an impedance tube technique was used to measure the acoustic characteristics (i.e., the admittance) of the fuel and air valves and of the mixing chamber fitted with both valves. These measurements indicated that, while the fuel valve behaves acoustically like a hard termination, the damping by the air valve increases with increasing frequency and valve opening and decreases with increasing pressure amplitude. Comparisons of the admittance measurements of the mixing chamber with those of the entire combustor showed that the damping by the Helmholtz volume formed by the combustion chamber overshadows the effect of the damping by the air flapper valve for the pulse combustor configuration under investigation. In addition to these measurements, an analytical scheme was developed which permits the determination of the admittance of the entire mixing chamber - valve assembly from the measured admittances of its component parts.

Project Implications: To be completed by the GRI technical manager.

TABLE OF CONTENTS

Title	Page No.
Introduction	1
Objectives	2
Program Plan	3
Technical Progress and Results	5
Task I	5
Performance Evaluation	5
Effect of Combustor Geometry	6
Effect of Temperature upon Performance	7
Effect of Heat release Duration and Timing	8
Shadow Visualization	10
Mixing Visualization	11
Spectroscopy	12
Laser Doppler Velocimetry	16
Rich Limit of Pulse Combustor Operation	20
Task II	24
Task III	31
Conclusions	32

LIST OF FIGURES

Fig. #	Title
1.	Schematic of the Helmholtz Type Pulse Combustor.
2.	Schematic of the Mixing Chamber showing the Fuel and Air Flapper Valves.
3.	Operational Frequency of the a) Helmholtz and b) Schmidt Combustors as a Function of Tailpipe or Combustor Length Respectively.
4.	Schematic of Relative Timing of Heat Release (Q') and Pressure (P') Oscillations for a) High Frequencies, b) Low Frequencies with Standard Fuel Injection and c) Low Frequencies with Displaced Fuel Injection Leading to Delayed Heat Release.
5.	Standing Wave Pattern along Schmidt Combustor a) with Air Valve and b) without Air Valve.
6.	Schematic of the Schlieren Set-up along the Combustor Axis.
7.	Schematic of Selected Frames from the High Speed Shadow Movie Showing the Flow Field at Different Instances during the Cycle as Seen along the Combustor Axis.
8.	Schematic of the Schlieren Set-up normal to the Combustor Axis.
9.	Comparison of the Flow Field and the Heat Release Distribution as Seen along the Combustor Axis at Four Instants during the Cycle.
10.	Contour Plot of Phase Angle by which the Heat Release Oscillations Lead the Pressure Oscillations.

11. Locations at which the Laser Doppler Velocimeter Results Shown in Figures 12 through 29 were Obtained. Each Location is Labeled (m,n).
12. Variation of the Vertical Mean Velocity During a Cycle for Locations along the Line $m = 1$. The Top Plot includes the Pressure Trace for Reference.
13. Variation of the Vertical Mean Velocity During a Cycle for Locations along the Line $m = 2$. The Top Plot includes the Pressure Trace for Reference.
14. Variation of the Vertical Mean Velocity During a Cycle for Locations along the Line $m = 3$. The Top Plot includes the Pressure Trace for Reference.
15. Variation of the Axial Mean Velocity During a Cycle for Locations along the Line $m = 1$. The Top Plot includes the Pressure Trace for Reference.
16. Variation of the Axial Mean Velocity During a Cycle for Locations along the Line $m = 2$. The Top Plot includes the Pressure Trace for Reference.
17. Variation of the Axial Mean Velocity During a Cycle for Locations along the Line $m = 3$. The Top Plot includes the Pressure Trace for Reference.
18. Variation of the Vertical Turbulence Intensity During a Cycle for Locations along the Line $m = 1$. The Top Plot includes the Pressure Trace for Reference.
19. Variation of the Vertical Turbulence Intensity During a Cycle for Locations along the Line $m = 2$. The Top Plot includes the Pressure Trace for Reference.

20. Variation of the Vertical Turbulence Intensity During a Cycle for Locations along the Line $m = 3$. The Top Plot includes the Pressure Trace for Reference.
21. Variation of the Axial Turbulence Intensity During a Cycle for Locations along the Line $m = 1$. The Top Plot includes the Pressure Trace for Reference.
22. Variation of the Axial Turbulence Intensity During a Cycle for Locations along the Line $m = 2$. The Top Plot includes the Pressure Trace for Reference.
23. Variation of the Vertical Turbulence Intensity During a Cycle for Locations along the Line $m = 3$. The Top Plot includes the Pressure Trace for Reference.
24. Three Dimensional Plot of Vertical Mean Velocities during a Cycle for Locations along the Line $m = 1$.
25. Three Dimensional Plot of Vertical Mean Velocities during a Cycle for Locations along the Line $m = 2$.
26. Three Dimensional Plot of Vertical Mean Velocities during a Cycle for Locations along the Line $m = 3$.
27. Three Dimensional Plot of Axial Mean Velocities during a Cycle for Locations along the Line $m = 1$.
28. Three Dimensional Plot of Axial Mean Velocities during a Cycle for Locations along the Line $m = 2$.
29. Three Dimensional Plot of Axial Mean Velocities during a Cycle for Locations along the Line $m = 3$.
30. Rayleigh Efficiency as a Function of Equivalence Ratio for the Combustor Fitted with the Standard and Long Tailpipes.

31. Pressure and Heat Release Fluctuations as a Function of Equivalence Ratio for the Combustor Fitted with the Standard and Long Tailpipes.
32. Phase Angle by which the Heat Release Leads the Pressure as a function of Equivalence Ratio for the Combustor Fitted with the Standard and Long Tailpipes.
33. Normalized Pressure (P') Cycle Showing the Timing of the Heat Release Oscillations (Q') for a) Lean and b) Rich Limits of Operation; Fuel Enters at "F", Air Enters at "A", Backflow into the Mixing Chamber Starts at "R"; the "X"s Denote the Instants of Reignition of the Fresh Fuel Charges.
34. Schematic of the Impedance Tube Experiment.
35. Wave Form of the Incident (I), Reflected (R) and Total (T) Standing Wave for a) Hard Termination and b) Termination with Finite Admittance.
36. Sensitivity of the Real Part of the Admittance to the Measured Pressure Difference between the Pressure Maximum and the Pressure Minimum.
37. Real Part of the Admittance as a Function of Frequency for Various Impedance Tube Terminations. H Denotes the Valve Gap Setting in Inches.
38. Real Part of the Admittance of the Mixing Chamber Assembly as a Function of Frequency for Different Air Valve Gap Settings (H).
39. Imaginary Part of the Admittance as a Function of Frequency for Various Impedance Tube Terminations. H Denotes the Valve Gap Setting in Inches.

40. Comparison of Standing Wave Pattern in the Impedance Tube Fitted with a) Hard Termination, b) Closed Air Valve, c) Open Valve and d) Valve Housing with Valve Plates Removed. The Actual Wave Pattern in the Valve Housing is more Complex due to the Geometry of the Housing.
41. Imaginary Part of the Admittance of the Mixing Chamber Assembly as a Function of Frequency for Different Air Valve Gap Settings (H).
42. Comparison of the Real Part of the Admittance as a Function of Pressure Amplitude for the the Mixing Chamber Assembly only and for the Entire Helmholtz Combustor.
43. Schematic Showing the Five Regions into which the Mixing Chamber Assembly has been Divided.
44. Comparison between the Measured (m) and Calculated (c) Real Parts of the Admittance of the Mixing Chamber Assembly over a Range of Frequencies.
45. Comparison between the Measured (m) and Calculated (c) Imaginary Parts of the Admittance of the Mixing Chamber Assembly over a Range of Frequencies.

INTRODUCTION

A recent increase in interest in pulse combustors has been driven by such advantages as high combustion and thermal efficiencies, excellent heat transfer characteristics and low CO, NO_x and soot emissions. Development of new pulse combustor applications has been hampered, however, by a lack of adequate understanding of the fundamental processes which control the operation of these devices. It was the purpose of this program to shed new light upon the mechanisms which control the operation of pulse combustors and to provide the designer with additional insight which would help him in the development of new and the scaling of existing pulse combustion devices.

The natural gas fired, valved, Helmholtz type, pulse combustor whose operating characteristics were investigated in this program is based upon an AGA design. It is shown schematically in Fig. 1. The combustor consists of cylindrical mixing and combustion chambers, a tailpipe, a cylindrical decoupling chamber and a short vent pipe. Natural gas and air enter the combustor at right angle to each other through separate flapper valves attached to the curved side wall of the mixing chamber. During start up, the reactants are allowed to mix and are ignited using a spark plug. As the natural gas burns (a process which has previously been shown to take place primarily in the mixing chamber) the pressure in the combustor rises. This closes the flapper valves which prevents further reactants from entering the mixing chamber. This pressure rise also pushes the combustion products out through the tail pipe. The momentum of the

expelled exhaust gases causes the pressure in the mixing chamber to drop which reopens the flapper valves. New reactants now enter the combustor where they mix and are ignited by burning pockets of gas left over from the previous cycle. The cycle now repeats itself. Thus, pulse combustion operation can be maintained indefinitely without the use of the spark plug.

The gap in the fuel flapper valve is fixed while that in the air valve can be adjusted using a micrometer, see Fig. 2. The overall equivalence ratio in the pulse combustor is, therefore, varied by adjusting the air flapper valve setting which changes the air flow rate.

OBJECTIVES

It was the objective of this study to gain further insight into the fundamental processes responsible for the operation of pulse combustors in general and natural gas fired, valved, Helmholtz type, pulse combustors in particular. Emphasis was placed upon obtaining practical information which will permit designers to develop new and/or larger scale pulse combustors without resorting to costly trial and error based development efforts.

More specifically, the goal was to determine the effect of the combustor geometry and temperature upon its performance. In addition, the velocity, mixing and heat release distributions in the mixing and combustion chambers were measured both qualitatively and quantitatively and used to establish the nature of the interaction between

the combustion process and the acoustics of the combustor. This would lead to a physical explanation of the operating characteristics of the natural gas fired, valved, Helmholtz type, pulse combustor. In addition, the admittance of various components and subsystems which make up the pulse combustor were to be determined under a variety of operating conditions.

PROGRAM PLAN

The program is divided into three major tasks as outlined below:

Task I: Investigation of the Oscillatory Flow and Heat Release Fields and their Interaction in the Pulse Combustor

- A. Performance Evaluation A limited number of measurements were carried out in modified, gas fired, valved, Helmholtz and Schmidt type pulse combustors in order to complement the performance studies carried out under a previous contract.
- B. Shadow Visualization High speed shadowgraph cinematography was carried out parallel and normal to the axis of the combustor. These shadowgrams were then correlated in order to obtain a complete picture of the three-dimensional flow field in the pulse combustor.

- C. Mixing Visualization An attempt was made to visualize mixing patterns photographically by heavily seeding one of the reactant flows and illuminating the combustor using an expanded laser sheet.
- D. Spectroscopy Local and global heat release in the pulse combustor were determined by measuring the radical radiation emitted from the combustor. Instantaneous readings were ensemble averaged using the pressure signal as a clock. Planar spectroscopy using an intensified CCD camera resulted in local heat release measurements with excellent spatial and temporal resolution.
- E. Laser Doppler Velocimetry Velocities were measured in the periodically varying, turbulent flow field at selected locations in the combustor. These velocities were then ensemble averaged which permitted the determination of mean velocities and turbulence intensities at various locations, at each instant during the cycle.

All Task I measurements were carried out in a pulse combustor whose mixing and combustion chambers were fitted with flat windows. The results from the different investigations outlined above were then correlated with each other and with the phase in the cycle at which they were obtained using the pressure oscillation as a clock. Such a coordination between the pressure, flow field and heat release measurements was

necessary to shed further light upon the fundamental processes which control the operation of the pulse combustor.

Task II: Admittance Measurements of Pulse Combustor Components

The acoustic admittances of various components and subsystems which make up a natural gas fired, valved, Helmholtz type, pulse combustor were measured using an impedance tube technique. These measurements yielded information on the frequency and amplitude dependances of the damping caused by the various pulse combustor subsystems. In addition, a methodology was developed which permits the designer to predict the damping in the pulse combustor from the acoustic properties of its component parts.

Task III: Reporting

As per contract agreement.

TECHNICAL PROGRESS AND RESULTS

Task I

Performance Evaluation:

This part of the study dealt with the investigation of the dependence of the performance of the pulse combustor upon the combustor geometry, the temperature in the combustion chamber and the relative duration and phase between the heat release and pressure oscillations.

Effect of the Combustor Geometry. The AGA based pulse combustor design consists of a small diameter mixing chamber attached to a larger diameter combustion chamber, see Fig. 1 . This introduces a step at the interface between the mixing and combustion chambers which has long been assumed to be critical for stabilizing the combustion process. This hypothesis was tested by constructing a pulse combustor with the same combustion chamber volume but without the step; i.e., a combustor whose mixing and combustion chamber diameters are equal. Tests revealed that the performance characteristics of the stepless pulse combustor are identical to those of the standard combustor. The combustion process in this type of pulse combustor is, therefore, not stabilized by the flow behind the backward facing step but by the complex interaction between the fuel and air jets in the mixing chamber.

Investigations under a previous contract have shown that the Helmholtz type pulse combustor fitted with a standard tailpipe (i.e., 183 cm long) operates well for equivalence ratios between 0.61 and 1.03. When the tailpipe of the Helmholtz combustor was extended to 366 cm the rich limit of operation increased to an equivalence ratio 1.43. On the other hand, when the tailpipe was shortened to 69 cm the lean limit of operation was lowered to an equivalence ratio of 0.56. For tailpipes shorter than 69 cm the air supply had to be significantly pressurized in order to maintain the pulsation. If the pressurization was reduced the combustor switched from a pulsating to a non-pulsating mode of operation. The reasons for the existence of the limits of operation mentioned above will be addressed later.

Effect of Temperature upon Combustor Performance. The temperature in the pulse combustor was increased by insulating its mixing and combustion chambers either externally or internally. When the combustor was externally insulated the temperature increased by approximately 30 °K. Nevertheless, the kinetics of the combustion process were noticeably affected. For example, the CO level in the exhaust increased by 15%. However, the amplitude of the pressure pulsations remained unchanged. More importantly, the addition of thermal insulation lowered the lean limit of operation from an equivalence ratio of 0.64 to 0.55. The rich limit of operation was not affected by the increase in temperature. This suggests that the lean limit of operation of the pulse combustor is, at least in part, kinetically controlled. A more detailed explanation of the reason for the existence of the rich limit will be given later.

The temperature in the pulse combustor was more significantly increased by insulating the combustor internally using high temperature ceramic padding. However, the acoustic losses caused by this insulating material significantly decreased the amplitude of the pulsations. Since the mass flow rates of the reactants through the flapper valves depend upon the pressure amplitudes, the operating range of the pulse combustor was decreased. In some cases it was necessary to increase the gap in the air flapper valve and/or to pressurize the air supply to maintain the pulsations. In addition, it was noted that the internal insulation decreased the frequency of the pulsations. An analytical model currently being developed under a new program does, indeed, predict a dependence of

the frequency of pulsation upon the rate of heat transfer to the walls of the combustor. More details of the effect of temperature upon the operating characteristics of the pulse combustor are given in Ref. 1.

Effect of Heat Release Duration and Timing. The effect of the relative timing between the heat release and pressure oscillations were investigated by changing the duration of the pressure cycle. Both the Helmholtz and a Schmidt tube pulse combustors were used in this investigation. The Schmidt (or quarter wave) pulse combustor used the same fuel and air injection system as the Helmholtz pulse combustor. However, the mixing chamber, the combustion chamber and the tail pipe were replaced by a single, constant diameter pipe.

Tests showed that lengthening of the tailpipe of the Helmholtz combustor caused a decrease in the pulsating frequency until a tailpipe length of 550 cm was reached. Then the operating frequency of the combustor "jumped" to the tailpipe's first harmonic, see Fig. 3a. If the tailpipe was further lengthened, the frequency continued to decrease. A similar trend was observed when the Schmidt pulse combustor was lengthened, as shown in Fig. 3b. It should be noted that a "jump" to the higher harmonic of the Helmholtz combustor's tailpipe and of the Schmidt pulse combustor causes a doubling and tripling of the frequencies, respectively. However, if the mixing of the reactants and, therefore, the heat release process was delayed with respect to the pressure oscillations this frequency jump could be avoided. Such a delay could be introduced by moving the fuel injection port 7.5 cm downstream of its normal location.

The above phenomena can be explained using Rayleigh's criterion which states that an oscillating heat release will drive pressure fluctuations if both are in phase. The timing and duration of the heat release due to the combustion process are determined by the injection of the reactants and their mixing. At relatively high frequencies (i.e., short cycle durations) the heat release is primarily in phase with the fundamental mode of the combustor, as is shown schematically in Fig. 4a. If the frequency of pulsations is decreased the cycle duration lengthens. The heat release is then confined to the early part of the fundamental pressure fluctuation (see Fig. 4b). However, the same figure also shows that the heat release is now more in phase with the first harmonic of the pressure oscillation. Therefore, it is this harmonic that is excited. Finally, if the combustion process is delayed the heat release is, once again, in phase with the fundamental pressure oscillation, see Fig. 4c. This causes the fundamental mode to be excited. This work is described in more detail in Refs. 1 and 2.

Finally, pressure amplitude measurements along the axis of the Schmidt pulse combustor indicated that as long as the air valve is in place this pulse combustor behaves like a true quarter wave tube, see Fig. 5. However, once the air valve is removed the standing wave pattern is closer to that characteristic of a Rijke tube. In that configuration the combustor is open at both ends, at the valve housing and at the downstream end, both of which are pressure nodes. Combustion takes place at approximately one quarter of the combustor length from the air inlet. Since in the Rijke tube the length of the combustor represents one

half of the acoustic wavelength, compared with one quarter of the wavelength in the Schmidt tube, the frequency of pulsations increases once the air valve is removed. This is discussed in more detail in Ref. 2.

Shadow Visualization

During a previous contract, the flow in the mixing chamber was visualized using high speed shadowgraphy through flat quartz walls at the end of the mixing chamber and the quartz transition between the combustion chamber and the tailpipe, see Fig 6. Briefly, a fast moving, highly turbulent fuel jet was seen to enter the mixing chamber followed by a wider, slower moving air jet, see Fig. 7. The air jet impinges upon the fuel jet at approximately the same instant at which the latter reaches the mixing chamber wall opposite the fuel port. The leading edge vortex of the air jet then rapidly "scoops up" the fuel and sets up two, counter rotating vortices in the mixing chamber. Combustion occurs under conditions of intense, small scale turbulence and is nearly completed when the fuel for the next cycle enters the mixing chamber. Some of these shadow visualizations were repeated under different operating conditions during the present contract period. These tests indicated that the entry of the air jet is delayed as the fuel - air ratio in the combustor is increased.

In addition, the axial flow field in the pulse combustor was visualized using high speed shadow photography through the flat quartz windows in the curved side walls of the mixing and combustion chambers, see Fig. 8. Particular attention was focused on the flow field in the mixing chamber and in the vicinity of the combustion chamber - tail pipe interface.

Since the air and fuel ports are located off axis, the flow field is not cylindrically symmetric. Once again, the high speed shadowgraphy showed that the fuel jet enters the mixing chamber shortly after the pressure there has passed through its maximum. Just before the pressure minimum is reached the air jet enters the mixing chamber. The addition of this air into the combustor increases the axial flow velocities further downstream in the mixing chamber. A little later, during the combustion phase of the cycle, a large, axial recirculation region forms in the mixing chamber. As the pressure maximum is reached the flow becomes axial again. Shortly thereafter, the new fuel jet enters and the cycle repeats itself.

High speed shadowgraphy was also carried out at the downstream end of the combustion chamber where the combustor connects with the tail pipe. As the pressure in the combustor decreases, combustion products from the tail pipe are seen to flow back into the combustion chamber. This backflow penetrates a distance of only two to three inches back into the combustor. As the acoustic pressure begins to rise again the flow reverses and reenters the tail pipe.

Mixing Visualization

Attempts were made to visualize the mixing process between the fuel and air as they enter the mixing chamber. For this purpose, the air jet was heavily seeded with micron sized titanium dioxide particles while the fuel jet was left unseeded. As the reactants entered the mixing chamber, slices through this chamber were illuminated using vertical sheets of light produced by expanding the beam from a five watt argon ion laser using a

cylindrical lens. The resulting light scattered by the particles in the flow was then recorded using a high speed camera capable of framing rates of up to 11,000 frames per second.

These visualization experiments were not very successful. In spite of mirror generated, multiple traverses by the laser sheet through the mixing chamber not enough light was scattered by the particles to mark the film at framing rates above 2,500 frames per second. At these framing rates it was difficult to freeze the fast moving flow. In addition, seed particles remaining in the mixing chamber from previous cycles tended to obscure the details of the mixing flow field of the newly entering reactants. It was, therefore, decided to abandon this part of the investigation, at least until a more powerful pulsed laser, such as a copper vapor becomes available at this laboratory.

Spectroscopy

This investigation makes use of the fact that the intensity of spontaneously emitted CH, CC or OH radiation has been shown to be a measure of the local reaction rate. Under a previous contract the temporal oscillations of the overall reaction rate in the combustor were compared with those of the pressure. It was shown that the global radiation from the combustor fluctuates with the same frequency as the combustor pressure. The heat release fluctuations lead those of the pressure by a phase angle which decreases as the equivalence ratio in the combustor is increased. As predicted by Rayleigh's criterion, this leads to an increase in sound pressure level in the combustor when the equivalence ratio is

increased. At the same time it was shown that the combustion process never stops entirely during the cycle.

Under the present contract these experiments were extended to cover spatially as well as temporally resolved radiation measurements. A newly acquired intensified imaging system was used in these experiments. The radiation from the combustor is allowed to pass through a quartz window in the combustor wall before being focused through an interference filter onto an image intensifier. The intensifier is connected via an optical fiber bundle to the face plate of an 128 x 128 pixel CCD array. The array is read by an Omnicomp frame grabber and the data are transferred to the memory of a MicroVAX II workstation. The workstation is equipped with a 200 Mbite disk and a tape drive. The image intensifier can be gated which results in exposure times down to 50 nanoseconds, faster than necessary to freeze the fast, highly turbulent flow in the combustor. Images can be read and transferred at a rate of 200 frames per second from the array to the computer. In addition, up to four channels of scalars can be recorded simultaneously with the images. In these studies, the acoustic pressure signal was recorded and used to identify the instant during the cycle at which the image was obtained.

Once the images have been obtained they can be manipulated using a wide range of software. Images can be sorted, added, subtracted and averaged, contrasts can be enhanced and contour maps can be plotted using false colors. Furthermore, the intensities recorded by selected, individual pixels during consecutive frames can be plotted versus time. The frequency of any oscillations in these signals can be determined by

Fourier analysis and the phase angle between the fluctuations in the pixel intensities and the pressure signal can be calculated. This allows the determination of the local driving of the pulsations by the combustion process using Rayleigh's criterion.

Local radical radiation and, therefore, heat release rates in the combustor were measured by imaging CC radiation through the flat quartz window at the upstream end of the mixing chamber. Images obtained at the same instants during consecutive cycles indicate that while the overall features of the flame shape are very similar at given instants during the cycle, the precise path over which the flame has spread varies somewhat from cycle to cycle. Figure 9 shows four frames which indicate the locations of the ignition and flame spread during one cycle in the pulse combustor. Each "frame" actually represents the average of 128 separate images obtained at the same phase during different cycles. The mechanism of flame spread is best illustrated by comparing the instantaneous flow fields and heat release distributions in Fig. 9. Early in the cycle (Fig. 9a), as the fuel jet enters the mixing chamber, it begins to react weakly with the air left over from the previous cycle. Main ignition of the new fuel occurs at the time and location where the fuel jet impinges upon the opposite wall, as shown in Fig. 9b. At that instant the new air jet has just reached the center of the mixing chamber. Shortly thereafter, the upper part of the leading mushroom vortex of the air jet entrains the reacting fuel which intensifies the combustion process and spreads it throughout the upper part of the mixing chamber (Fig. 9c). Only after a pair of counter-rotating vortices have established themselves does

the flame spread throughout the entire mixing chamber, as shown in Fig. 9d.

In order to quantify the flame spread in the mixing chamber, software was developed which permits the calculation of the phase angle between the maximum heat release rate at every location and the maximum pressure. The distribution of these phase angles then gives an indication of the instantaneous shape of the flame and of its spread through the combustor. Figure 10 shows a contour plot obtained using this technique. The numbers indicate the phase by which the local heat release leads the pressure. The flame, thus, spreads from the upper left hand side of the mixing chamber, opposite the fuel port, towards the lower left hand side and, finally, towards the right hand side of the mixing chamber into the region between the fuel and air ports.

These results indicate that, for the present valve configuration, it is essential that the fuel enter the mixing chamber prior to the air jet. Otherwise the momentum of the air jet would prevent the fuel jet from penetrating significantly into the mixing chamber. This would result in poor mixing of the fuel and air. At the same time, a different fuel and air port configuration or dual fuel inlets would, probably, result in a quicker, more uniform distribution of the combustion process in the mixing chamber. The results of these heat release measurements are discussed further in Refs. 3 and 4.

Laser Doppler Velocimetry

Velocity measurements in the mixing chamber were carried out using a two component LDV system based on a five watt argon ion laser. The results of the flow visualization experiments had indicated that reverse flow exists in the mixing chamber. Therefore, Bragg cells were incorporated into both components of the system. Because the flow in the combustor is periodic, mean flow velocities and turbulence intensities at different instances during the cycle had to be determined using conditional sampling. This was achieved by detecting the start of each cycle which was taken to be the positive zero crossing of the pressure signal. Each cycle was then divided into 60 equal time intervals based upon the previously obtained operational frequency of the combustor. Finally, the data were sorted into the relevant bins according to their time of arrival during the cycle. Ensemble averaged mean and RMS velocities were, thus, obtained at 60 equi-spaced instances during the cycle.

Early tests of the performance of the LDV indicated that the system and its data reduction software produced reproducible mean velocities which were in good agreement with quantitative observations from the flow visualization, see Ref. 5. However, the apparent level of turbulence, as measured by the RMS value of the conditionally sampled velocities, was considerably higher than that observed in other turbulent flows, (e.g. in the turbulent shear layer behind a backward facing step). It is important to realize that it is possible that only a part of this RMS may be due to true turbulence. Since the values of the velocity fluctuations were obtained by ensemble averaging, they may contain contributions due to 1) the finite width of the slots into which each cycle was divided; 2) the

slight variations in the flow field from cycle to cycle; and 3) slight variations in the combustor frequency during the experiment. In order to eliminate at least the effect of variations in the operating frequency of the combustor the data reduction software was modified. In the updated data reduction routine the pulse duration for each cycle was determined from the actual pressure oscillations measured during the experiment rather than from a previously determined mean frequency.

Typical spatially and temporally resolved mean velocity and turbulence intensity data in the axial (u) and vertical (v) directions are shown in Figs. 11 through 29. Figure 11 shows the locations at which these LDV data were obtained. All measurement points lie in a plane which bisects the right angle between the fuel and air injection ports, equi-spaced along lines which are normal to the axis of the combustor. Each measurement location is labeled (m,n) where m represents the number of the line counting from the flat end of the mixing chamber and n denotes the point number on this line counting from the curved wall of the chamber opposite to the fuel and air ports.

Each of the velocity and turbulence intensity figures represents one cycle starting at the negative zero crossing of the pressure signal; i.e., at an instant after the fuel has started to enter but before the air has entered the mixing chamber. Figures 12 through 23 represent velocity and turbulence intensity traces at each of the ten points along one measurement line; i.e., along a given value of m. In order to avoid having ten data traces superimposed upon each other each of these figures consists of three plots one of which also shows the pressure signal for

reference. Figures 24 through 29 show a different representation of the same data which is more qualitative but conveys a better physical picture of the variation of the complex flow field in the mixing chamber during a cycle. These are three - dimensional "carpet plots" in which one axis represents the location of the measurement station along a given measurement line, the second axis represents the normalized time (i.e., 0 to 1 for one cycle) and the third axis shows either the u or v components of the velocity. This results in two carpet plots (one for u and one for v) for each value of m.

Figures 24, 25 and 26 show the carpet plots of the vertical velocities for the three measurement lines closest to the closed, upstream end of the mixing chamber. These are best analyzed in conjunction with the instantaneous velocity vs. time plots in Figs. 12, 13 and 14. Large positive (upward) velocity peaks are seen early in the cycle along all three lines. At $m = 3$, which lies in the paths of the fuel and air jets, (Fig. 26) the maximum occurs very early in the cycle, near the center of the mixing chamber ($n = 4$ to 7). Further upstream, at $m = 1$ and 2 (Figs 24 and 25), the peaks occur later, and are confined to locations $n = 9$ and 10 , which lie close to the curved mixing chamber wall between the fuel and air ports. Immediately following the peak at $m = 3$ and coincident with the peaks at $m = 1$ and 2 , deep, wide and wide valleys (downward velocities) are seen near the center of all three measurement lines. The early peak at $m = 3$ is caused by the entry of the fuel jet which results in an upward component of velocity. The valley observed later in the cycle is due to the downward component of the velocity of the entering air jet. Since the positive peaks along $m = 1$ and 2 occur at the same instant in the cycle as the valley they

must be due to the leading edge vortex of the air jet observed in the flow visualization. Later in the cycle the flow near the wall opposite to the inlet ports is generally upward while that near the ports is directed downward. This suggests the existence of a large vortex in the plane normal to the axis of the combustor.

The time dependence of the instantaneous axial velocities and their carpet plots at the same locations are shown in Figs. 15 through 17 and 27 through 29, respectively. Early in the cycle, when the fuel jet enters the mixing chamber, a significant downstream velocity directed towards the combustion chamber is observed. These positive velocity peaks are particularly large along lines $m = 2$ and 3 (Figs. 16 and 17), where the effect of the fuel jet is felt most strongly. It is also confined to the area near the curved mixing chamber wall opposite the injection ports. This wall deflects the incoming jet. In addition, the initial combustion process and the associated expansion of the combustion products are concentrated in this area. Shortly thereafter, the air jet enters the mixing chamber. It has very little effect upon the axial velocities along the line $m = 3$ which coincides with the centerline of the jet. However, at locations $m = 1$ and 2 large valleys representing upstream velocities can be seen. These are formed by the leading edge vortex of the incoming air jet which has an upstream component of velocity. After this vortex has passed, a small upstream velocity continues to be observed. This flow causes the acoustic pressure in the mixing chamber to increase. As the acoustic pressure approaches its maximum the flow reverses direction and the combustion products exhaust towards the combustion chamber for the remainder of the cycle.

The instantaneous turbulence intensities for all measurement lines are plotted versus phase in the cycle in Figs. 18 through 23. Early in the cycle the turbulence levels at all locations are relatively low. At the central locations ($n = 3, 4, 5$ and 6) along the lines $m = 2$ and 3 , which lie directly in the path of the fuel jet, the turbulence intensity increases as soon as this jet enters the mixing chamber. At all other locations the turbulence intensity does not significantly increase until the entry of the air jet is detected in the mean velocities. The turbulence levels then remain elevated for part of the cycle and then slowly drop to their initial values.

These LDV measurements are presently continuing as part of the Ph.D. thesis work of the graduate student responsible for this work. Velocity measurements in the mixing chamber will be completed and velocity measurements at the combustion chamber - tailpipe interface will be added. The complete set of velocity results will then be submitted for publication to a suitable journal and as a "Topical Report" to GRI.

Rich Limit of Pulse Combustor Operation

As mentioned in the section dealing with performance measurements, the Helmholtz type pulse combustor fitted with the standard, 163 cm long tail pipe has a rich limit of operation at an equivalence ratio of 1.03. This limit exists even though the pulse combustor appears to be operating near its optimal condition immediately before this limit is reached. This operational limit can, however, be extended if the tail pipe is lengthened; i.e., the period of the pulsations is prolonged, or if the combustion air is supplied under pressure. Based

upon the results of the measurements discussed above, the following mechanism appears to control this rich limit.

In order to attain pulse combustion, the driving of the pulsations by the combustion process must overcome the acoustic damping due to, for example, viscous dissipation and acoustic radiation from the combustor. A limit of operation of the pulse combustor occurs if this balance between the driving and damping processes fails to materialize. According to Rayleigh's criterion, the driving by the combustion process can be quantified by the Rayleigh efficiency η which is defined by

$$\eta = \frac{R}{C_p \bar{P} \bar{Q}} \int_0^1 P' Q d\tau \approx \frac{|P| |Q| \cos \theta}{C_p \bar{P} \bar{Q}}$$

where P and Q are the total pressure and combustion heat release rate, θ is the phase angle between the pressure and the heat release rate oscillations, R and C_p are the ideal gas constant and the specific heat at constant pressure, respectively, and τ is the time normalized by the duration of one cycle. Bars, primes and brackets represent the steady state, oscillating components and amplitudes of the indicated quantities, respectively.

Figure 30 shows the variation of the Rayleigh efficiency of the combustor fitted with a standard tailpipe and an extended tailpipe as a function of equivalence ratio, ϕ . The maximum ϕ at which each curve stops represent the rich limit of operation for each configuration. Clearly, near the lean limit the driving is small, just enough to overcome the damping

in the system. In contrast, near the rich limit for the combustor fitted with a standard tailpipe the driving is close to its maximum. Thus, the mechanism which controls this rich limit appears fundamentally different from that which is responsible for the lean limit.

The Rayleigh efficiencies presented in Fig. 30 were calculated from the measured fluctuations of pressure and heat release and the phase angle between them. The dependences of these three variables upon the equivalence ratio in the combustor are shown in Figs. 31 and 32. The amplitudes of both, the pressure and heat release fluctuations reach their maxima near stoichiometric conditions. The phase angle by which the heat release leads the pressure, on the other hand, decreases with increasing equivalence ratio until it asymptotically reaches a constant value which depends upon the length of the tailpipe.

In order to understand the combustor behavior described above, it is helpful to consider the relative phases of the pressure and radiation oscillations and the instants of fuel and air injection. Figure 33 shows one normalized period of oscillation for both rich and lean operating conditions. The arrows indicate the instants at which fuel and air jets enter the mixing chamber. Horizontal lines at the top of the figure indicate those parts of the cycle when the combustion products move away from or towards the mixing chamber where most of the combustion process occurs. Finally, the points marked "X" indicate the instants at which the new fuel charges reignite, as indicated by the increase in the radiation signal. All this information is based upon the high speed shadowgrams, pressure and CC radiation measurements described above.

Figure 33 indicates that for lean operation the new fuel ignites before the new air enters the mixing chamber. This is possible since there is air left over from the previous cycle. As the equivalence ratio is increased, less air is available from the previous cycle and ignition is delayed until, under stoichiometric conditions, ignition of the fuel jet must await the entry of the air jet. Since the oscillations of heat release always lead those of pressure, the phase angle between the two decreases as the equivalence ratio is decreased, see Fig. 32. Since with decreasing phase angle the pressure and heat release fluctuations are more in phase, the Rayleigh criterion causes the pressure amplitudes in the combustor increase with increasing equivalence ratio, as observed in Fig. 31.

The rich limit of operation can now be explained with the aid of Fig. 33. The time available for the reactants to mix and burn is limited to the time interval between the instants when the new fuel charge ignites and when the reaction is quenched by the combustion products returning from the combustion chamber to the mixing chamber. If ignition is delayed this time interval is too short and not enough heat is released to drive the pulsations. This occurs at the rich limit.

When the duration of the cycle is prolonged by extending the tailpipe the time available for combustion is increased and the rich limit is significantly extended. A similar result is obtained if ignition of the new fuel is advanced by forcing the air to enter earlier or if mixing is improved by injecting the air jet under pressure. Conversely, delaying the entry of the air jet by, for example, extending the pipe which connects the air valve to the mixing chamber reduced the rich limit to an equivalence

ratio of less than one. A more detailed description of this part of the work is given in Refs. 6 and 7.

Task II

In this task, the impedance tube technique was used to measure the admittances (i.e., the complex ratio between the acoustic velocity and pressure) of different pulse combustor components. The admittance is a complex quantity which describes the acoustic behavior of the system. As discussed later, the magnitude of the real part of the admittance describes whether the system drives or damps the acoustic pressure oscillations. All components which make up the pulse combustor damp the pressure oscillations in the absence of combustion. Therefore, the measured, real part of the admittance of the cold combustor provides an indication of how much driving the combustion process will have to provide to assure pulse operation.

In the impedance tube set-up, the investigated component is attached to one end of a long tube, see Fig. 34. An electro-pneumatic, acoustic driver is attached to the wall just upstream of the opposite, open end of the tube. The acoustic driver is used to excite an incident acoustic wave which moves towards the tested component. The interaction of this wave with the investigated sample produces a reflected wave with modified amplitude and phase. The incident and reflected waves combine to establish a standing wave in the impedance tube. A piezo-electric pressure transducer mounted near the tested sample measures the acoustic pressure amplitude at the upstream end of the tube. A second

pressure transducer, mounted at the end of a long rod, is translated inside the tube to measure the axial variation of the standing wave pressure amplitude along the impedance tube.

When measuring the admittance of a hard termination (i.e., zero admittance), the incident wave is reflected without a change in amplitude or a shift in phase. In this case, the combination of incident and reflected waves produces a standing wave with a zero-amplitude pressure minimum located one quarter of the wavelength ($\lambda/4$) from the hard termination, see Fig. 35a. On the other hand, if the complex admittance of the termination is non-zero, see Fig. 35b, the minimum pressure amplitude is non-zero and it occurs at a location other than $\lambda/4$ from the tested sample. Physically, the termination changes the pressure amplitude of the reflected wave and introduces an apparent change in the length of the pipe by introducing a phase shift in the reflection process. The measured values of P_{\max} , P_{\min} and the distance of P_{\min} from the tested sample can be used to determine the real and imaginary parts of the admittance of the termination and, thus, of the component under investigation. A more detailed analysis shows that the real part of the admittance, which is calculated from the difference between the maximum and minimum pressure amplitudes (i.e., $P_{\max} - P_{\min}$) determines the damping (or driving) provided by the component under investigation. On the other hand, the imaginary part of the admittance provides information which affects the frequency of the system which utilizes the tested component.

The above described technique was used to measure the real and imaginary parts of the admittances of different pulse combustor components under cold and "hot" operating conditions. Admittance measurements under cold conditions were completed as part of this project. The system was also prepared for measurements with combustion under the present program but most actual measurements were carried out under a new contract.

The admittances were measured under cold flow conditions for the following configurations: (1) a hard termination at the end of the impedance tube; (2) the gas valve and its decoupler at the end of the tube; (3) the air valve at the end of the tube; (4) the mixing chamber fitted with the air valve only; and (5) the mixing chamber fitted with both the fuel and the air valves. The air valve opening was varied between 0 and .018 inches for configurations 3, 4 and 5. In these tests the acoustic driver was set to generate sound pressure levels of approximately 160 dB near the tested component. This corresponds to typical dB levels in pulse combustors. Furthermore, the driving frequencies were varied between 20 and 170 Hz. In addition, the admittance of the air flapper valve and of the entire pulse combustor including valves, mixing and combustion chambers were measured as a function of amplitude. All tests were carried out at mean pressures in the impedance tube equal to the previously determined boost pressure in the pulse combustor.

Before presenting the obtained results, it would be helpful to consider Fig. 36. It shows the dependence of the real part of the admittance upon ΔP (i.e., $P_{\max} - P_{\min}$). Clearly, when the magnitude of

the real part of the admittance (i.e., Y_r) is small, the value of Y_r is relatively insensitive to the accuracy of the measurement of ΔP . However, as the magnitude of Y_r increases, the sensitivity of the Y_r to the measured ΔP increases rapidly. Thus, the error in the determined Y_r increases with increasing value Y_r . In addition, while the real part of the admittance depends largely upon the value of ΔP , the value of the imaginary part of the admittance is primarily determined by the location of P_{min} . Since the standing pressure wave has a relatively flat minimum, especially at low frequencies, it was easier to determine the value of the minimum than its location. The real parts of the admittances were, therefore, measured with better accuracy than their imaginary parts.

The real parts of the admittances for the above configurations with the air valve (when included) closed and open (to .012 inches) measured over a 20 to 170 Hz frequency range are shown in Fig. 37. An air valve opening of .012 inches was selected since it corresponds to a typical setting for the pulse combustor under normal operating conditions. Both, the hard termination and the fuel flapper valve with its decoupling chamber showed no damping over the entire range of investigated frequencies (i.e., $Y_r = 0$). This indicates that the fuel valve orifice behaves, essentially, like a solid surface.

For all of the tested configurations which contain an air flapper valve Y_r is essentially zero at low frequencies as long as the air valve is closed. As the frequency is increased, Y_r and, thus, the damping by the air valve and its housing increases until it becomes quite significant at high

frequencies. The real part of the admittance is increased even further if the closed air valve is attached via an elbow to the mixing chamber. On the other hand, adding the fuel valve to the mixing chamber - air valve assembly has no significant effect upon the admittance at any investigated frequency. This provides further indication that the fuel valve behaves like a solid surface.

Figure 37 also shows that opening the air valve substantially increases the real part of the admittance over the entire range of investigated frequencies. Once again, the effect of attaching the air valve housing to the side of the mixing chamber is significantly greater than adding the fuel valve to the mixing chamber - air valve assembly. The increase in the real part of the admittance with increasing air valve opening is illustrated in more detail in Fig. 38 for a range of valve openings and driving frequencies for the mixing chamber fitted with both valves.

The variation of the measured imaginary part of the admittance (i.e., Y_i) for these configurations over the 20 to 170 Hz frequency range are shown in Fig. 39. Once again, Y_i is zero for the hard termination as well as for the fuel valve only. However, once the closed air valve was added to any of the three investigated configurations the imaginary part of the admittance increased substantially. The latter effect increased with increasing frequency. This occurred because adding the valve assembly moves the termination, in the form of the valve plates, further away from the end of the impedance tube, see Fig. 40. The minimum of the standing pressure wave in the impedance tube was, therefore, moved upstream

resulting in an increase in Y_i . Because of the size of the mixing chamber and the elbow that connects the air valve to it, this effect is more pronounced for the valve - mixing chamber assembly than for the air valve alone.

Once the air valve is opened the pressure anti-node moves away from the valve plates towards the driver end of the impedance tube, see Fig. 40. (If the valve plates are completely removed the resulting open end corresponds to a pressure node). This causes the decrease in the magnitude of Y_i observed in Fig. 39. Because of the above discussed difficulty in determining the precise location of the minimum of the standing pressure wave, no clear difference between the imaginary part of the impedance of the air valve only and that of the valve - mixing chamber assembly could be established. However, Fig. 41 clearly shows that the magnitude of Y_i decreases as the opening of the air valve increases. This effect is particularly pronounced at higher frequencies. The lack of smoothness of the curves is, once again, due to the difficulty in determining the precise location of the flat minimum of the standing wave.

Additional admittance measurements were carried out in which either the mixing chamber with its valves or the entire combustor consisting of mixing and combustion chambers and the flapper valves were attached to the impedance tube. In these tests, the admittances were measured as a function of applied sound pressure level for a given air valve opening. Figure 42 shows that for the mixing chamber assembly only the damping decreases with increasing sound pressure level. Since it

has been shown that the only significant acoustic losses in the mixing chamber assembly occur in the air flapper valve it can be concluded that it is the damping in the air valve that decreases with increasing acoustic excitation. However, the damping of the entire combustor (including the combustion chamber) increases with increased applied sound pressure level, as shown in Fig. 42. This suggests that the damping in the Helmholtz volume formed by the combustion chamber overshadows the effect of the damping in the air flapper valve for this pulse combustor configuration.

In addition to the above detailed measurements an analytical scheme was developed which permits the determination of the admittance of the entire mixing chamber - valve assembly from the measured admittances of its component parts. As shown in Fig. 43, the assembly was divided into five sections. The admittance at location "1" was calculated from that of the solid wall ($Y = 0$) which closes the upstream end of the mixing chamber using a transfer function. The admittance at "2" was determined from the measured admittance values of the valve. The admittance at "3" was taken to be zero since the fuel valve had been shown to behave like a solid surface. The acoustic mass conservation equation was then applied to the control volume bounded by interfaces 1,2,3 and 4 to calculate the admittance at "4" from the admittances at the other interfaces. Finally, the admittance at "5" was calculated from that at "4" using a transfer function. Details of these calculations are given in Ref. 8. The results of these calculations for different valve openings and over a range of frequencies are compared with the experimentally measured values of the real and imaginary parts of the admittance of the mixing chamber - valve assembly in Figs. 44 and 45. Clearly, the agreement is excellent.

At the end of this contract the impedance tube set up was modified to accommodate tests with combustion. Because of heat transfer to the impedance tube wall a temperature gradient existed along the axis of the impedance tube. A measurement technique was developed to determine the temperature gradient using thermocouples and the classical impedance tube theory was modified to account for it. The actual measurement of the driving by the unsteady combustion process was initiated and completed under a new contract.

Task III

Apart from the semiannual and annual reports specified in the contract, the following papers were presented and published during the contract period. They are listed in the order in which they are referenced in the above text:

1. "Dependence of Pulse Combustion Performance upon Interior Temperature, Acoustic Losses and Combustion Time", X.C. Cheng, B.R. Daniel, J.I. Jagoda and B.T. Zinn, International Gas Research Conference, Tokyo, Japan, November, 1989.
2. "Dependence of Pulse Combustor Frequency upon Combustion Process Timing", X.C. Cheng, B.R. Daniel, J.I. Jagoda and B.T. Zinn, Twelfth Annual Energy Sources Technology Conference and Exhibition, Fossil Fuels Combustion Symposium, PD-Vol. 25, pp 39-42, Houston, TX, January, 1989.
3. "Radiation Measurements in a Gas Fired Pulse Combustor", S.H. Ku, X.C. Cheng, B.R. Daniel and B.T. Zinn, Proceedings of the Spring Technical

Meeting, Central States Section of The Combustion Institute, Chicago, IL, May, 1987.

4. "The Interaction between Fluid Mechanics and Combustion in a Helmholtz Type Pulse Combustor", J.M. Tang, B.R. Daniel, J.I. Jagoda and B.T. Zinn, Fall Technical Meeting, Eastern Section of The Combustion Institute, Orlando, FL, December, 1990.
5. "Frequency Modeling and Velocity Measurements in Gas Fired, Valved Pulse Combustors", Fall Technical Meeting, Eastern Section of The Combustion Institute, Clearwater Beach, FL, December, 1988.
6. "Flame Spread and Limits of Operation of Gas Fired, Mechanically Valved Pulse Combustor", S.H. Ku, B.R. Daniel, J.I. Jagoda and B.T. Zinn, Poster at the Twenty-Second Symposium (International) on Combustion, Seattle, WA, August, 1988.
7. "Controlling the Rich Limit of Operation of Pulse Combustors", J.M. Tang, S.H. Ku, B.R. Daniel, J.I. Jagoda and B.T. Zinn, Twenty-Third Symposium (International) on Combustion, Orleans, France, August 1990, (in print).
8. "The Acoustic Characteristics of Pulse Combustor Flapper Valves and Mixing Chambers", D. Xu, B.R. Daniel, J.I. Jagoda and B.T. Zinn, Thirteenth Annual Energy Sources Technology Conference and Exhibition, Fossil Fuel Combustion Symposium, PD-Vol. 30, pp 21-28, New Orleans, LA, January, 1990.

CONCLUSIONS

The physical mechanisms which control the performance of a natural gas fired, valved Helmholtz type pulse combustor were investigated. Comparison of flow and flame spread visualization indicated that the fuel

jet enters the mixing chamber ahead of the air jet. Under lean operating conditions the fuel begins to react as soon as it enters the combustor. Main ignition occurs once the fuel is scooped up by the leading edge vortex of the air jet. Combustion then spreads by the convection of this vortex throughout the mixing chamber. It is this complex interaction between the fuel and air jets entering the mixing chamber which stabilizes the combustion process. The lean limit of operation of the pulse combustor could be extended by reducing the heat losses to the combustor walls while its rich limit was increased by reducing the pulsation frequency or supplying the combustion air under pressure. The rich limit of operation near stoichiometric conditions exists because of the limited time available for combustion during the cycle if no air from the previous cycle is available for early ignition. In addition to the visualization experiments the flow field is currently being quantified by laser Doppler velocimetry.

Under a separate task the acoustic characteristics of the air flapper valve were determined by an impedance tube technique. In addition, an analytical scheme was developed which allows the determination of the admittance of entire sections of a pulse combustor from the measured admittances of its component parts.

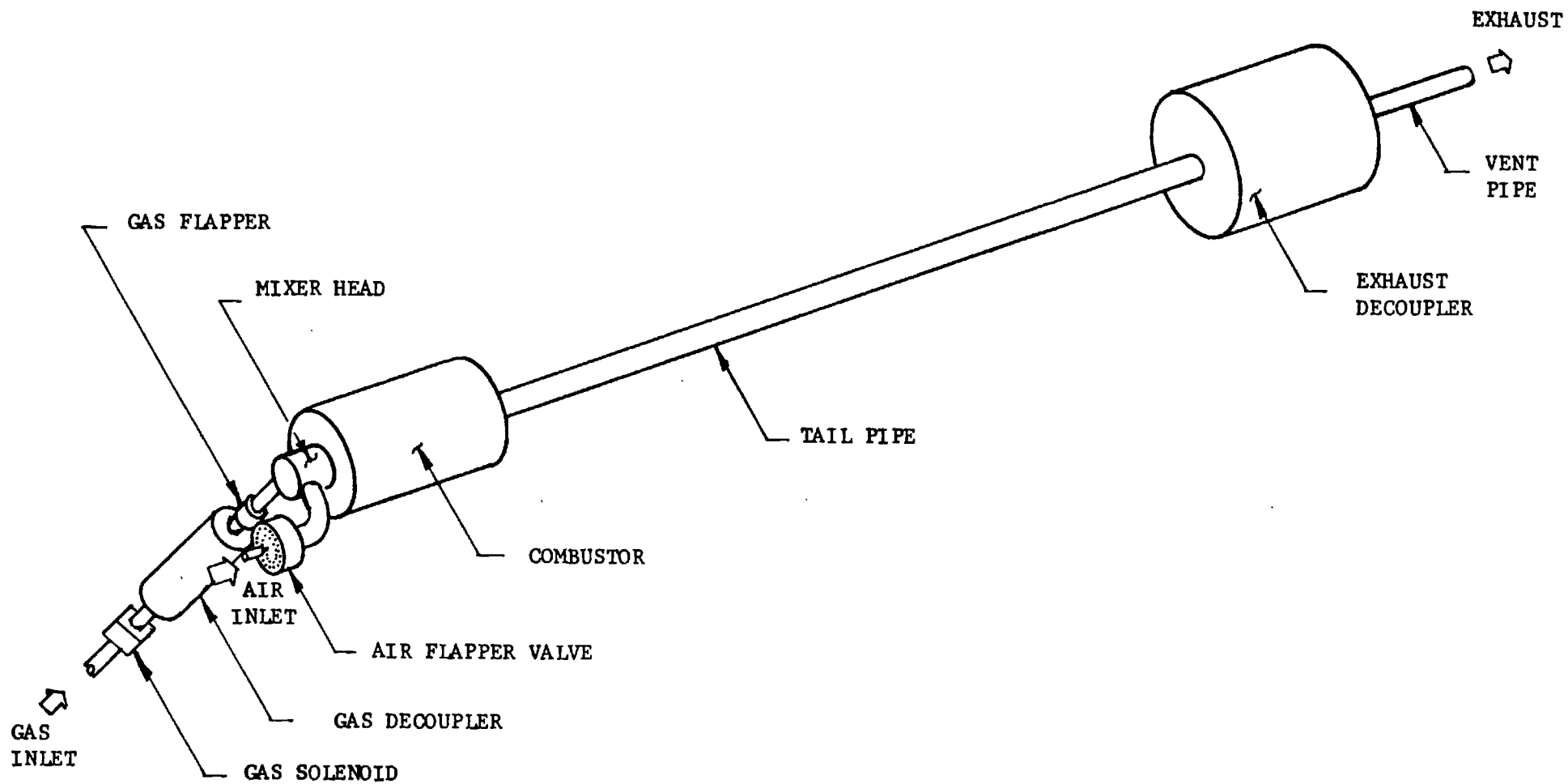


Fig. 1 Schematic of the Helmholtz Type Pulse Combustor

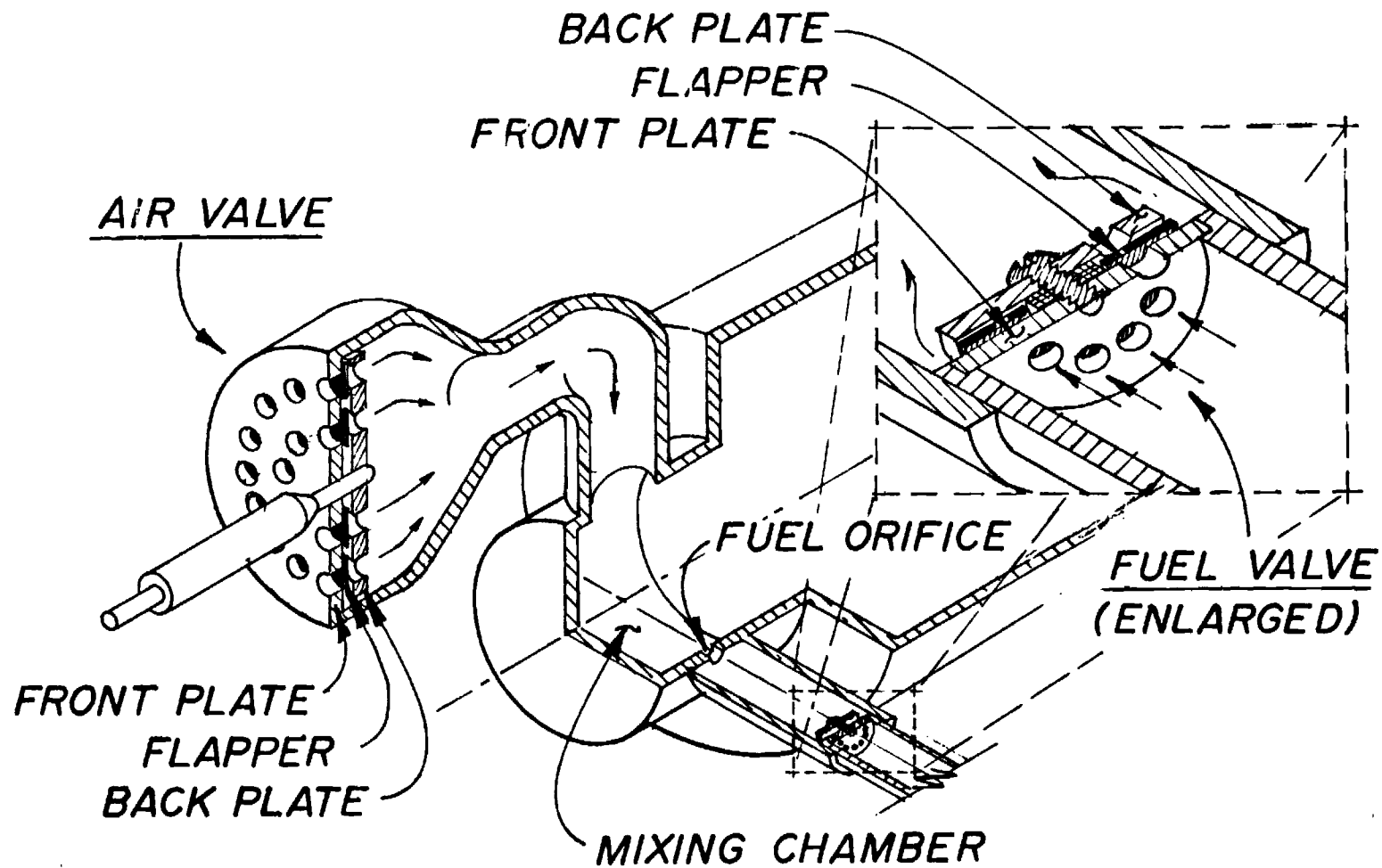
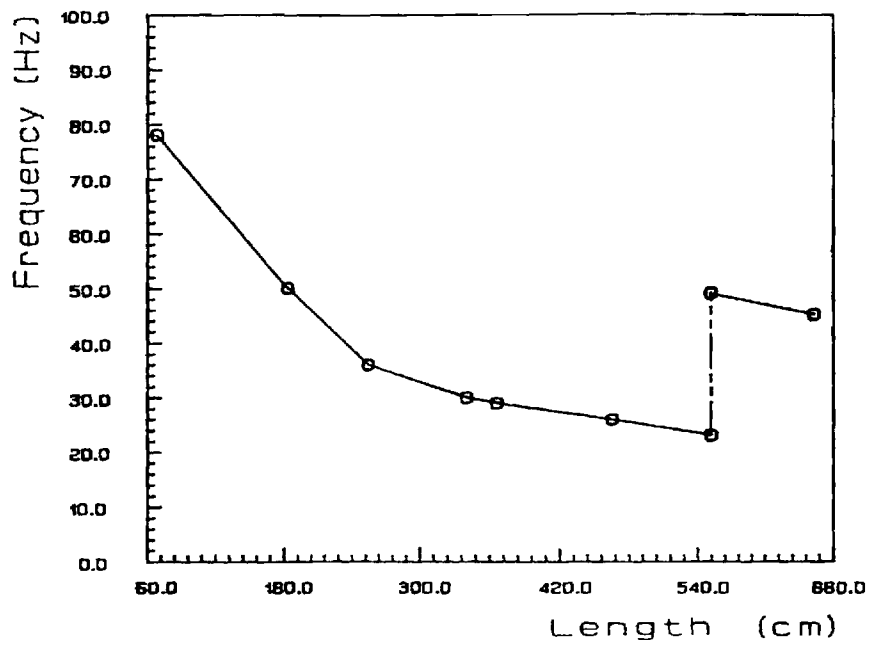
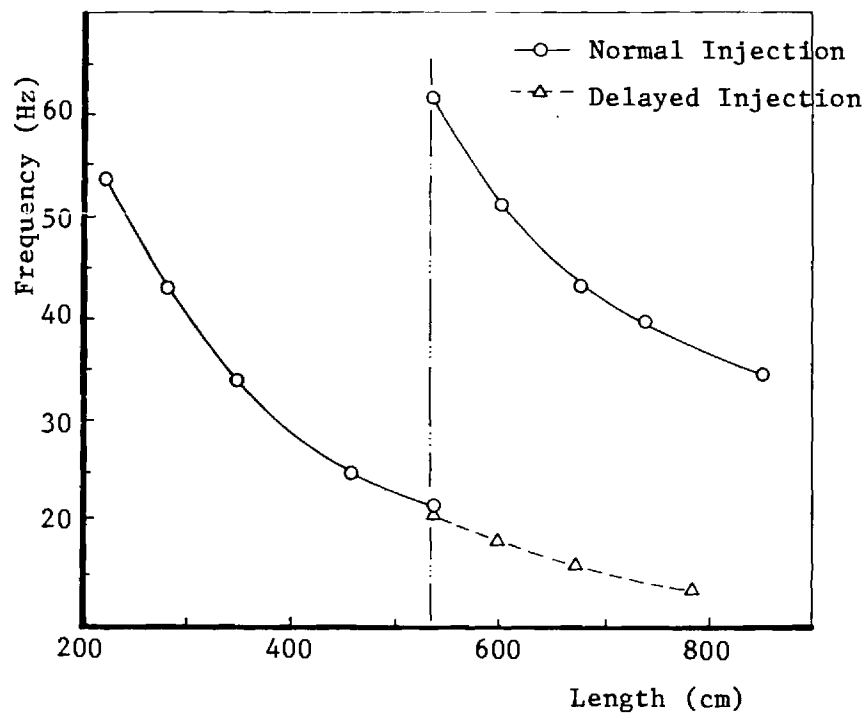


Fig. 2 Schematic of the Mixing Chamber Showing the Fuel and Air Flapper Valves



a



b

Fig. 3 Operational Frequency of the a) Helmholtz and b) Schmidt Combustors as a Function of Tailpipe or Combustor Length Respectively.

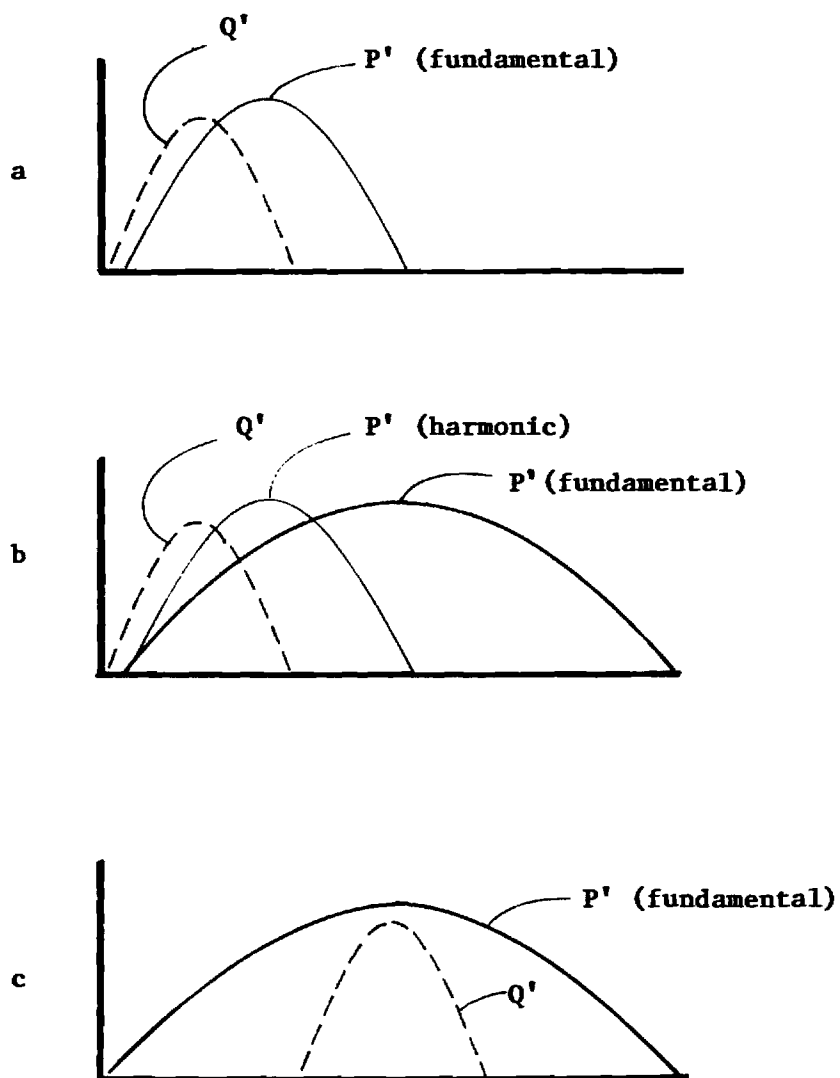


Fig. 4 Schematic of Relative Timing of Heat Release (Q') and Pressure (P') Oscillations for a) High Frequencies, b) Low Frequencies with Standard Fuel Injection and c) Low Frequencies with Displaced Fuel Injection Leading to Delayed Heat Release.

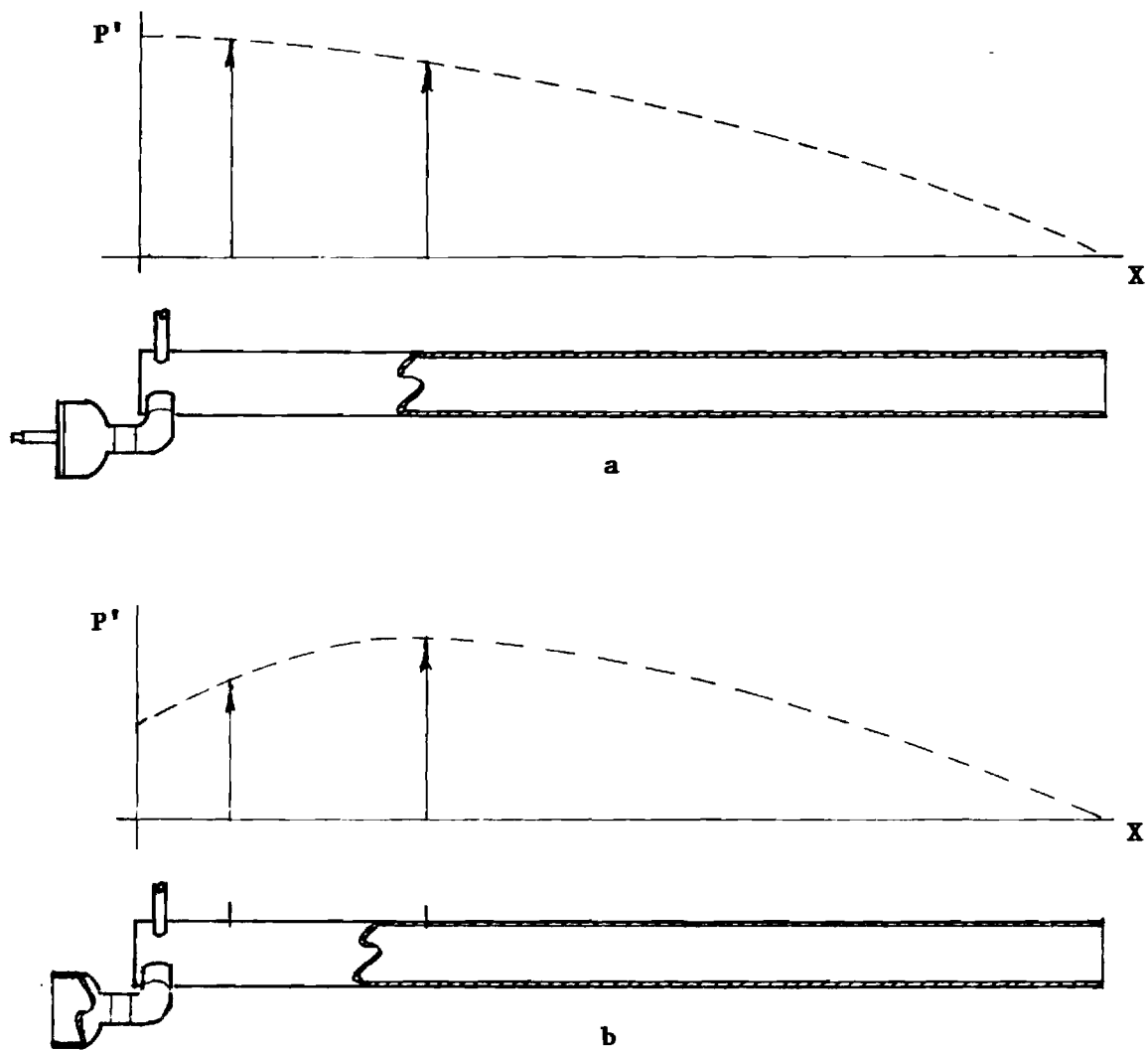


Fig. 5 Standing Wave Pattern along Schmidt Combustor a) with Air Valve and b) without Air Valve.

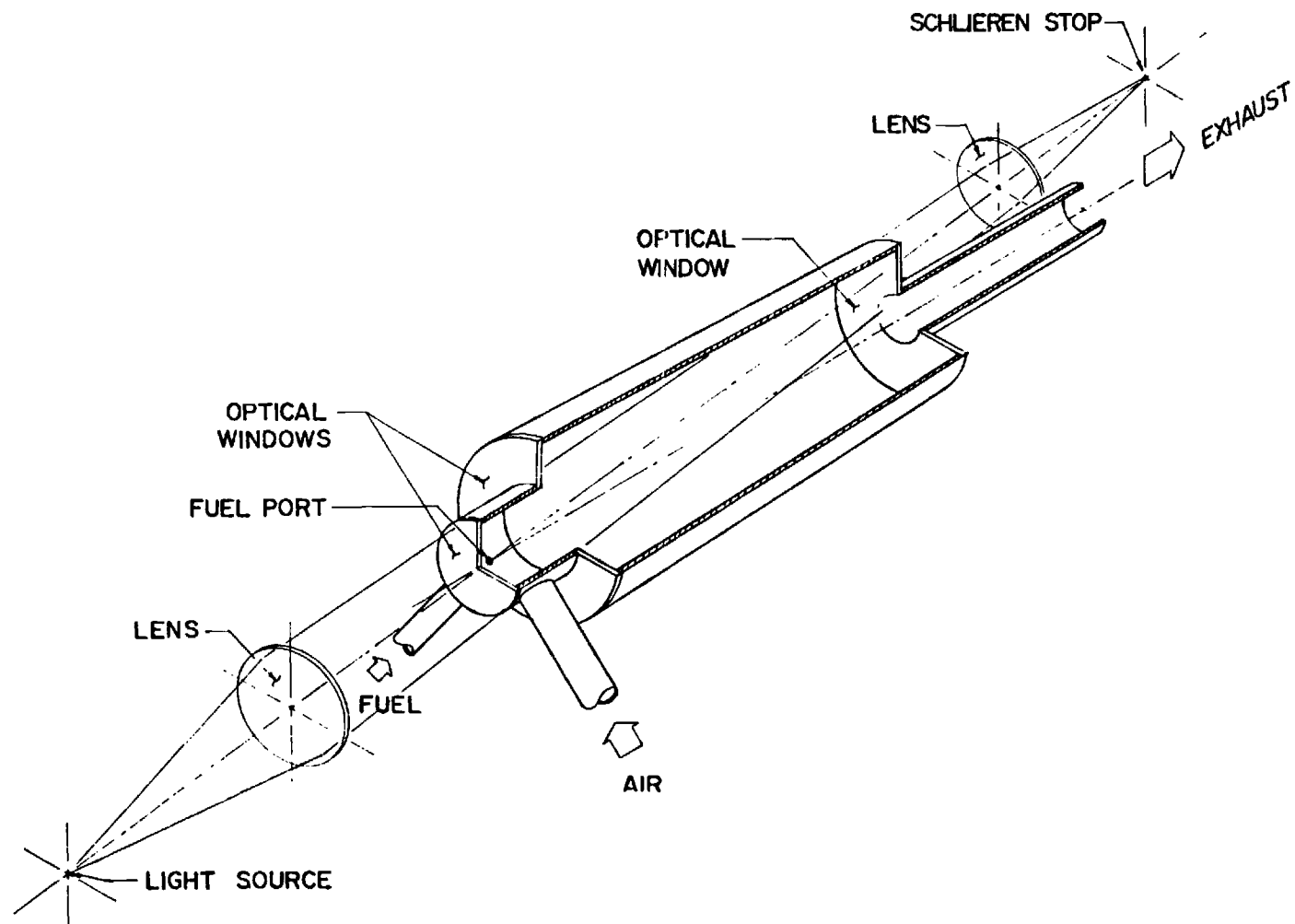


Fig. 6 Schematic of the Schlieren Set-up along the Combustor Axis

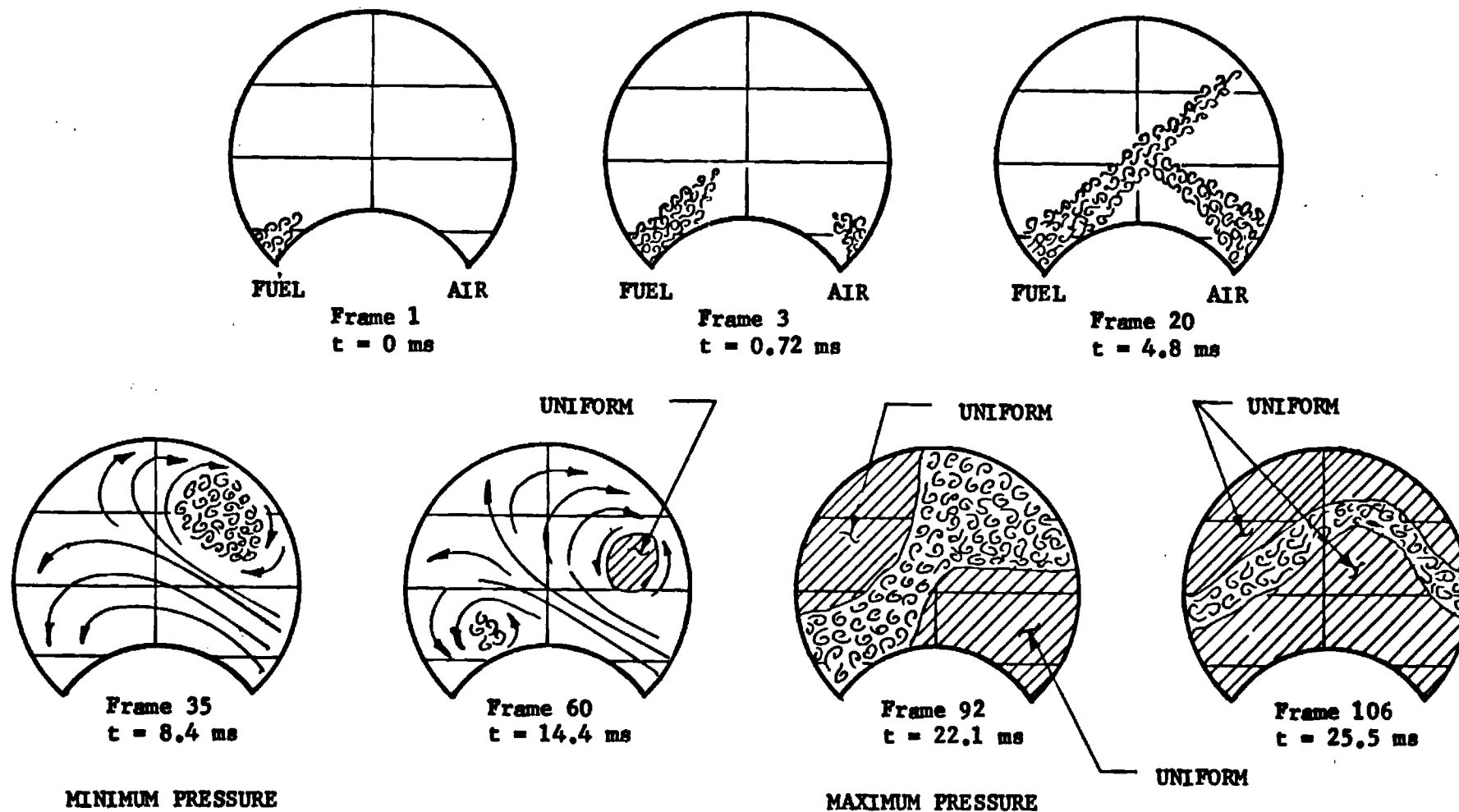


Fig. 7 Schematic of Selected Frames from the High Speed Shadow Movie Showing the Flow Field at Different Instances during the Cycle as Seen along the Combustor Axis

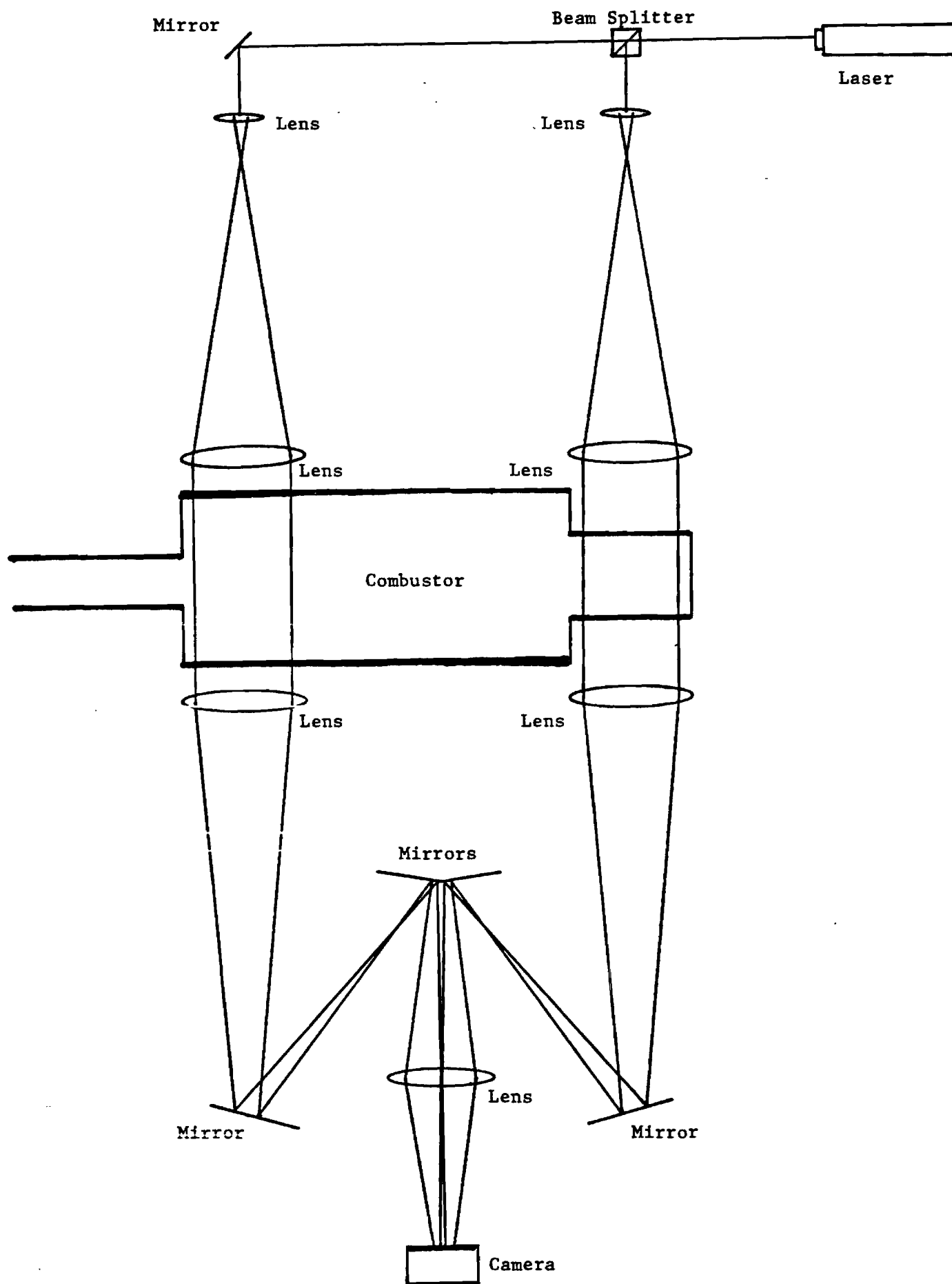


Fig. 8 Schematic of the Schlieren Set-up normal to the Combustor Axis

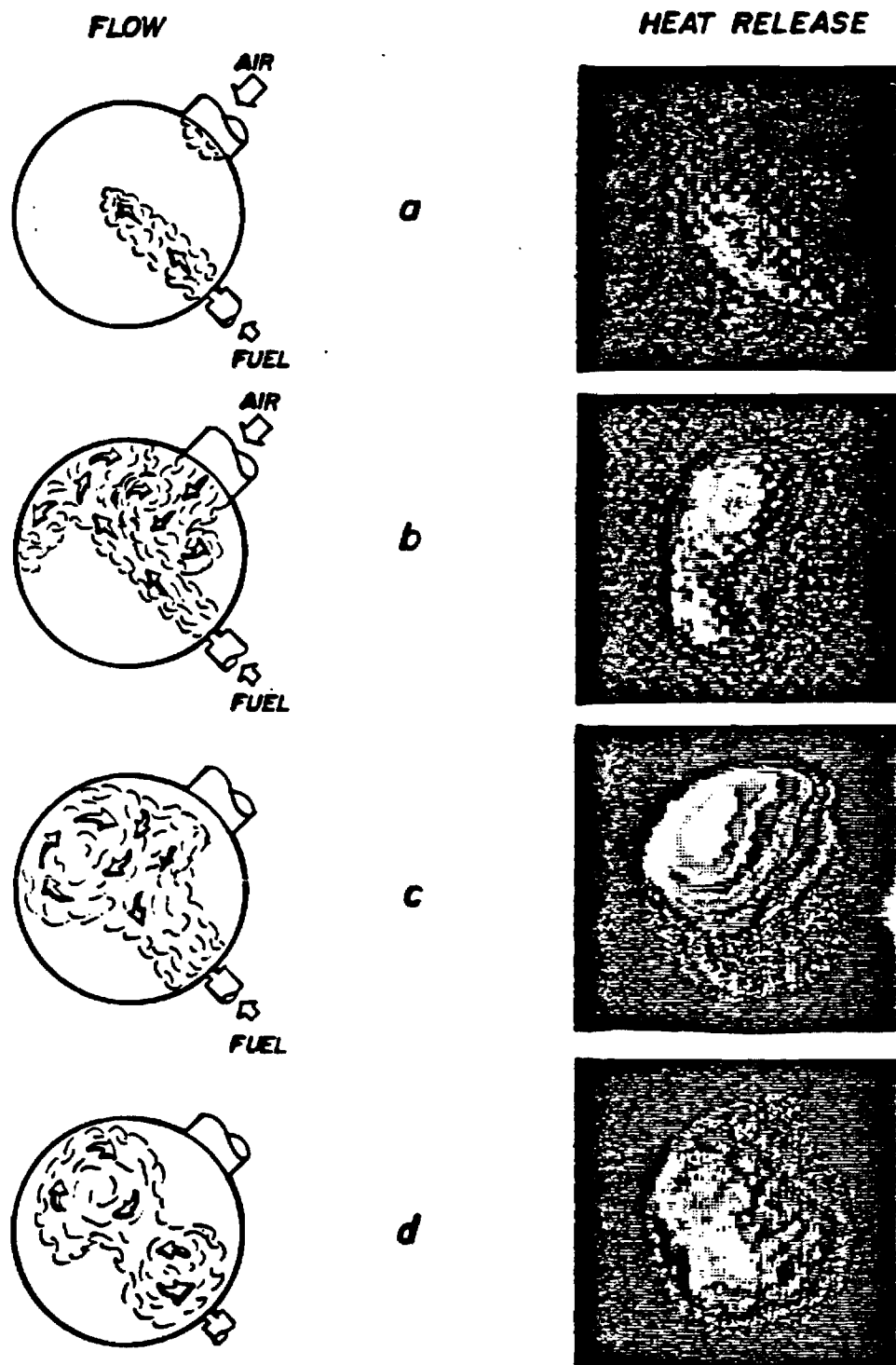


Fig. 9 Comparison of the Flow Field and the Heat Release Distribution as Seen along the Combustor Axis at Four Instants during the Cycle.

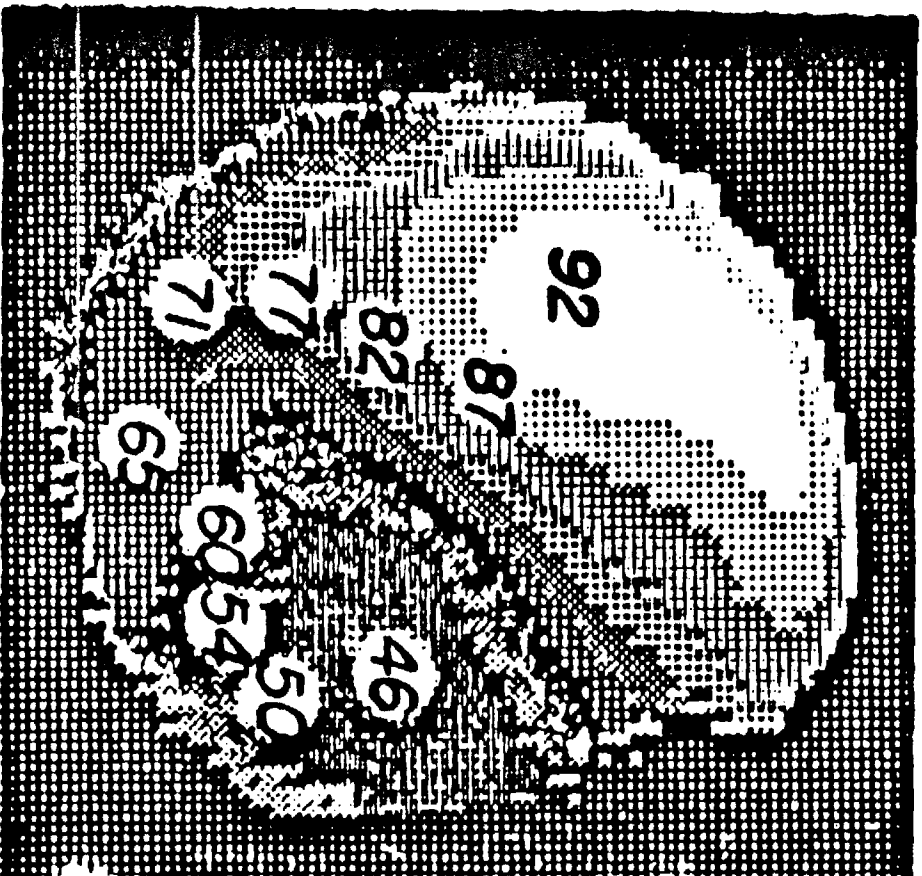


Fig. 10 Contour Plot of Phase Angle by which the Heat Release Oscillations Lead the Pressure Oscillations.

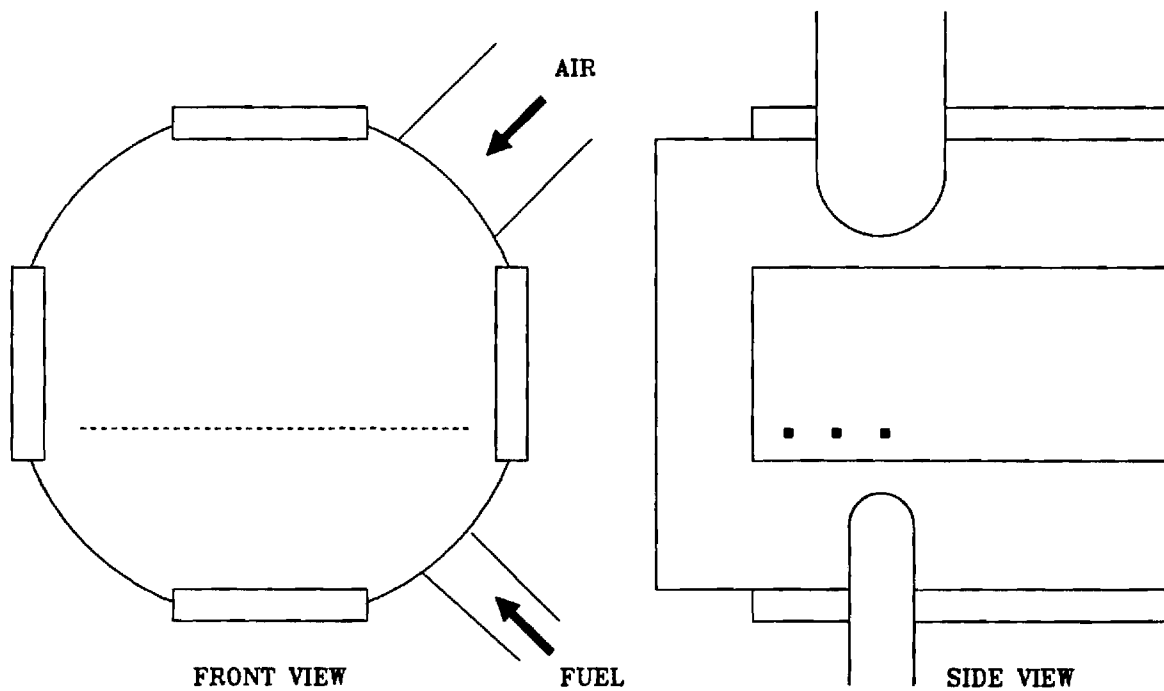
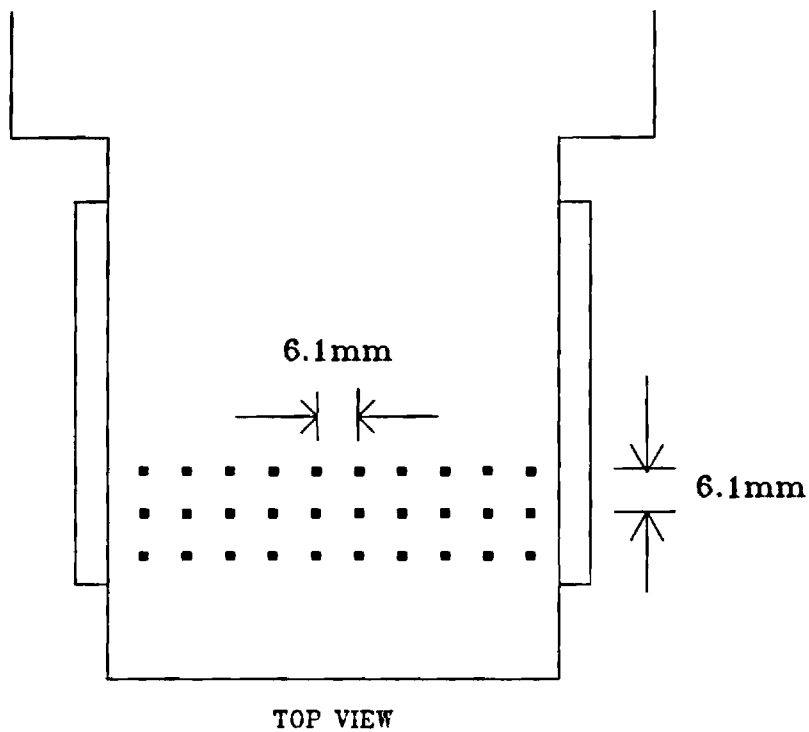


Fig. 11 Locations at which the Laser Doppler Velocimeter Results Shown in Figures 12 through 29 were Obtained. Each Location is Labeled (m,n).

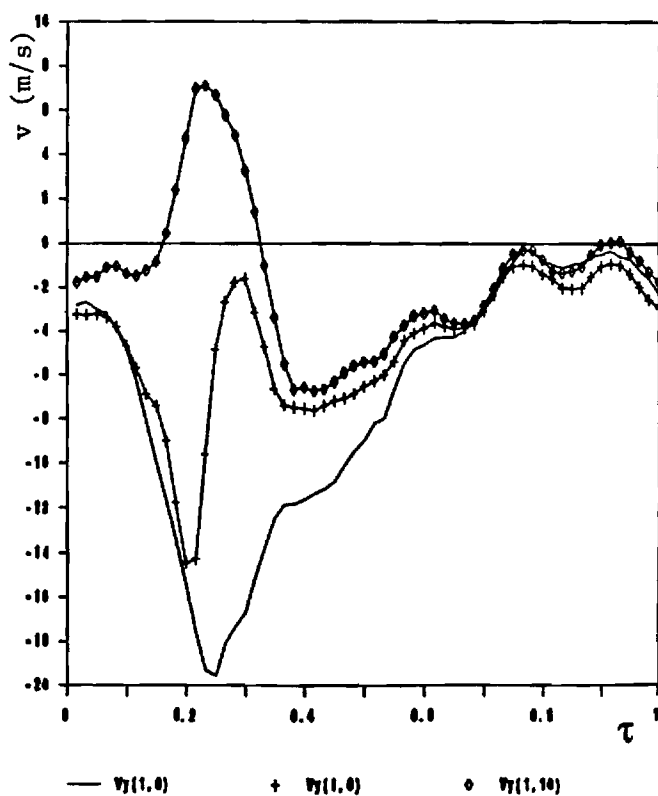
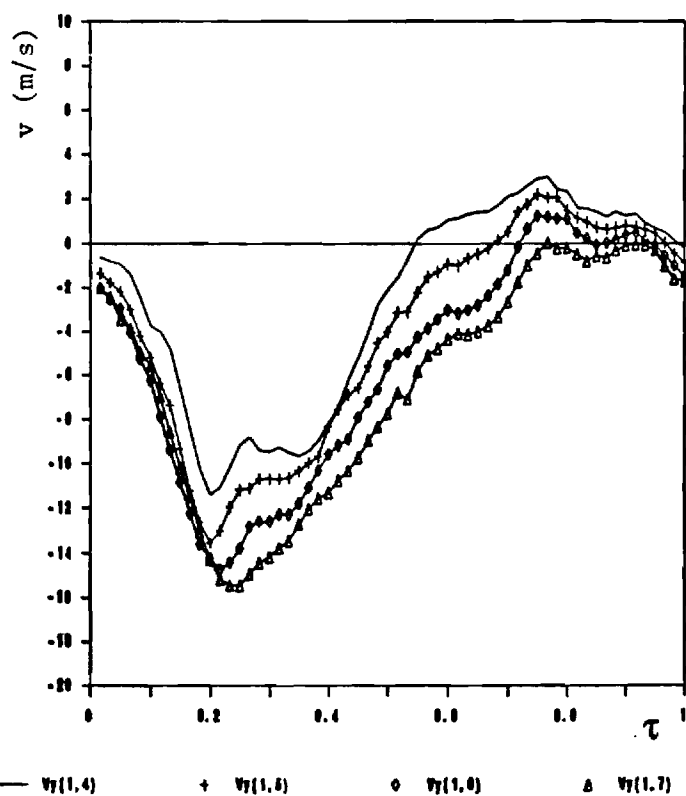
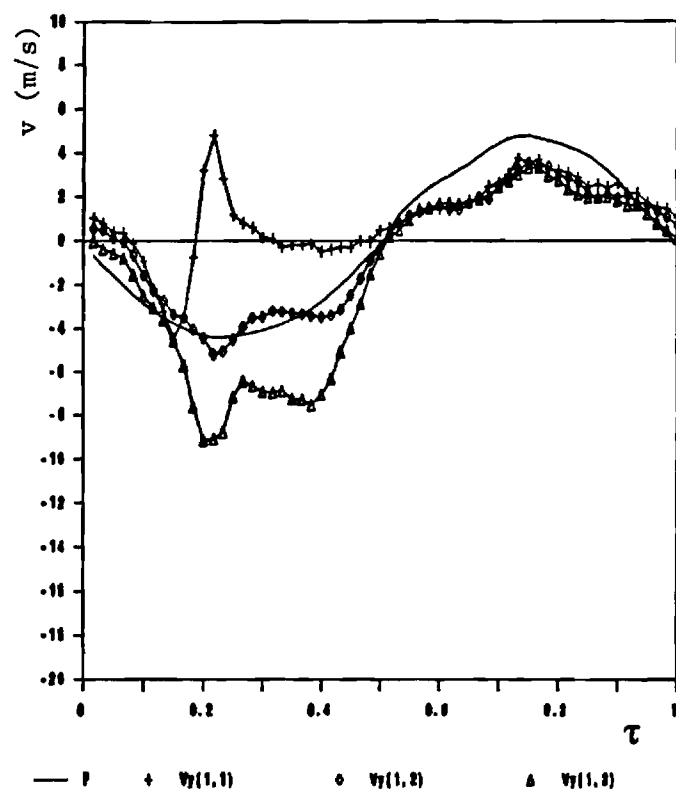


Fig. 12 Variation of the Vertical Mean Velocity During a Cycle for Locations along the Line $m = 1$. The Top Plot includes the Pressure Trace for Reference.

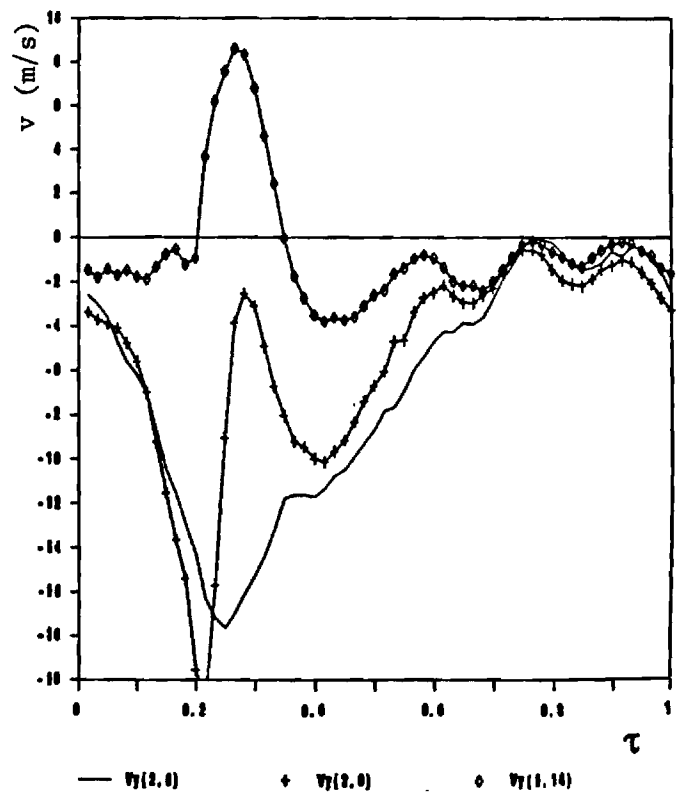
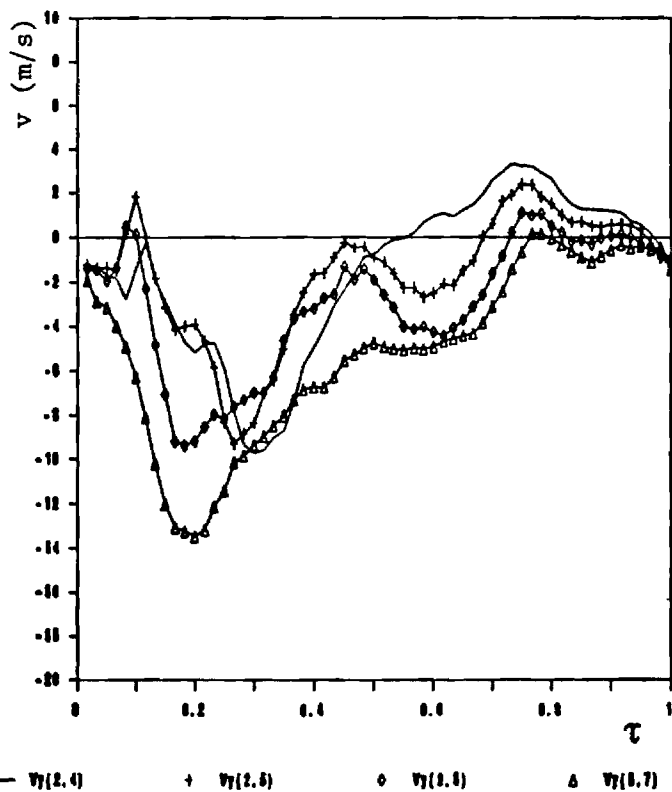
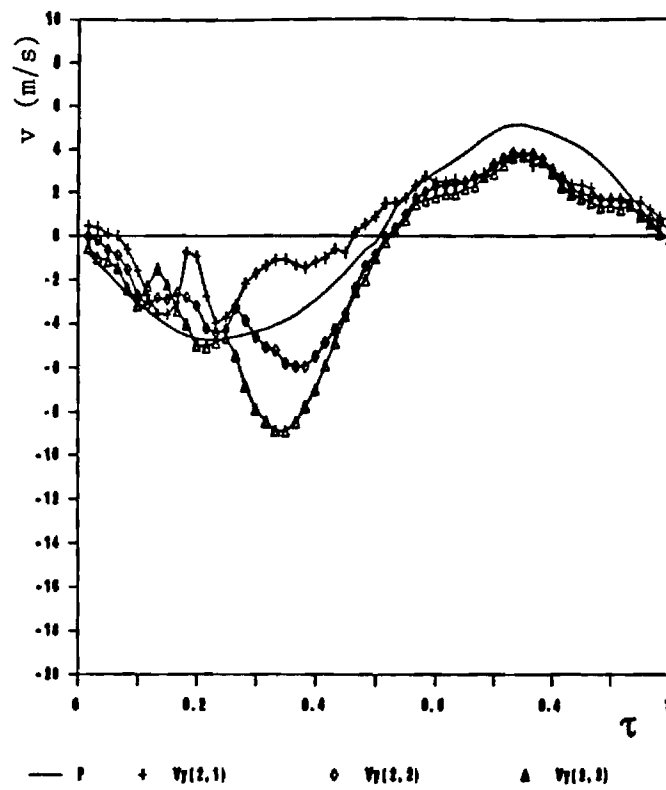


Fig. 13 Variation of the Vertical Mean Velocity During a Cycle for Locations along the Line $m = 2$. The Top Plot includes the Pressure Trace for Reference.

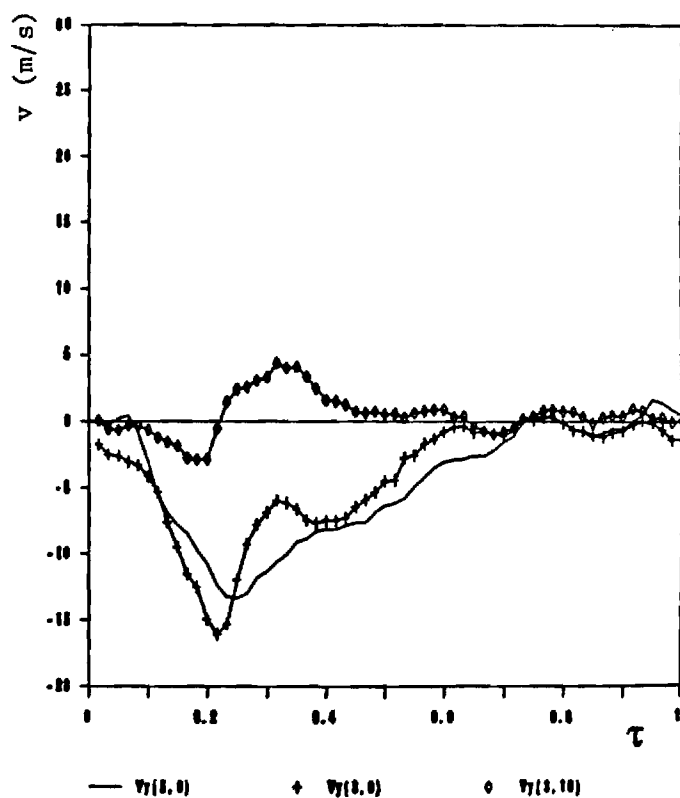
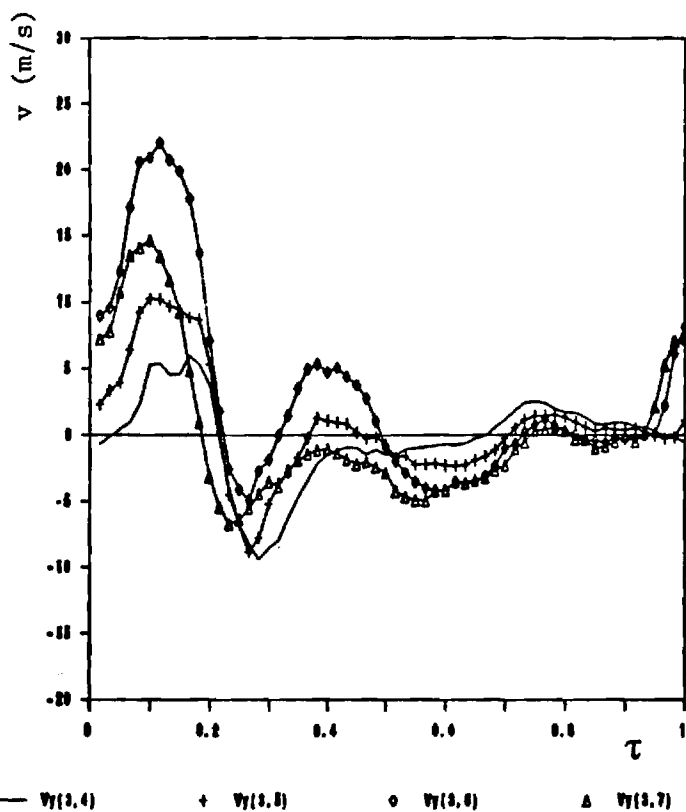
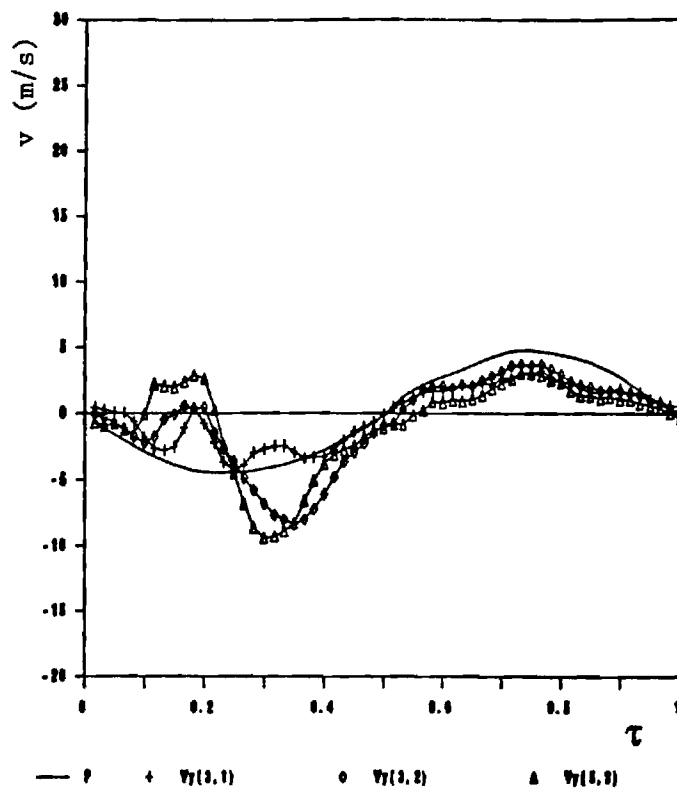


Fig. 14 Variation of the Vertical Mean Velocity During a Cycle for Locations along the Line $m = 3$. The Top Plot includes the Pressure Trace for Reference.

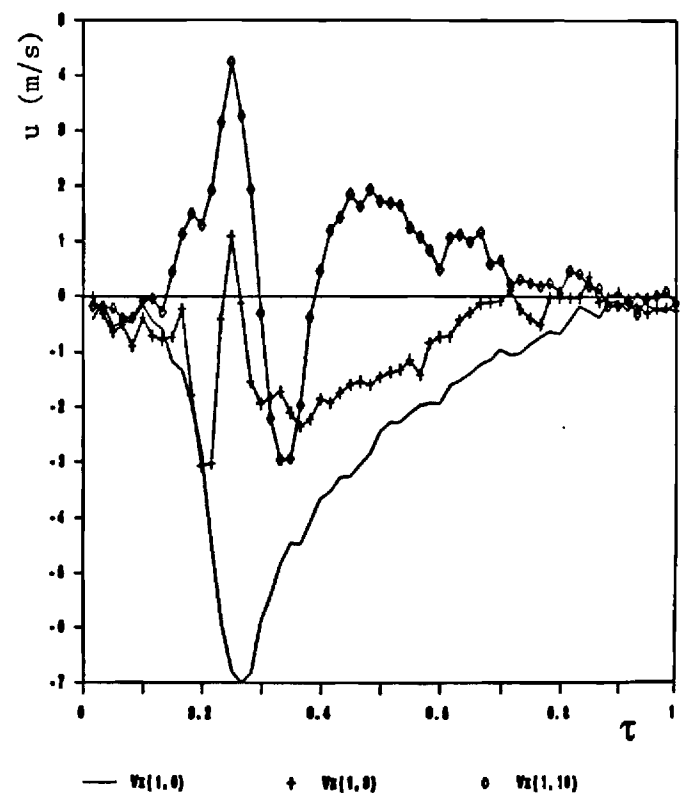
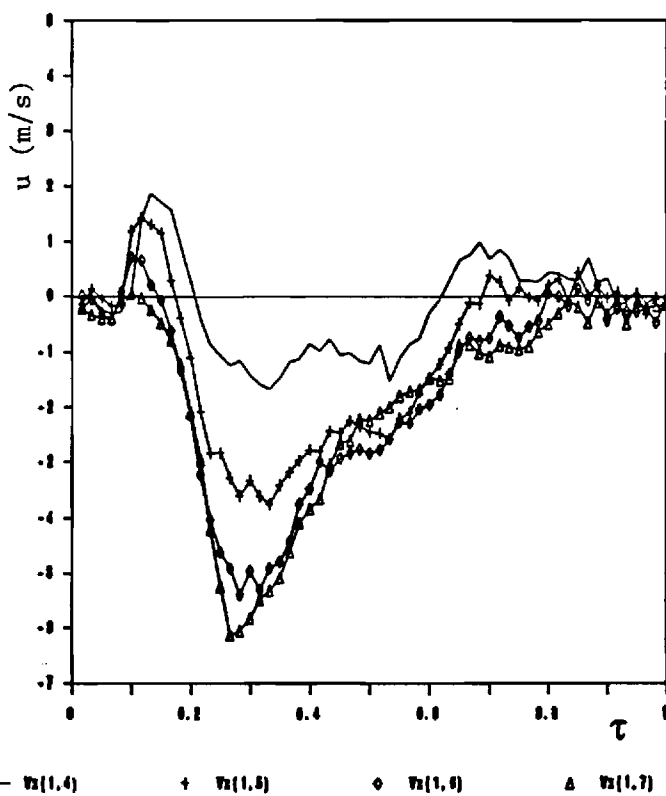
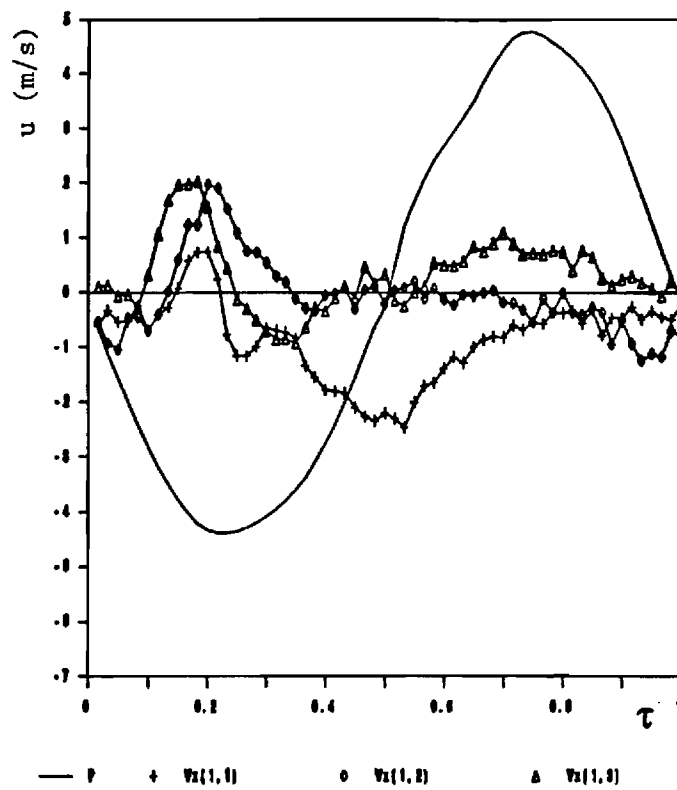


Fig. 15 Variation of the Axial Mean Velocity During a Cycle for Locations along the Line $m = 1$. The Top Plot includes the Pressure Trace for Reference.

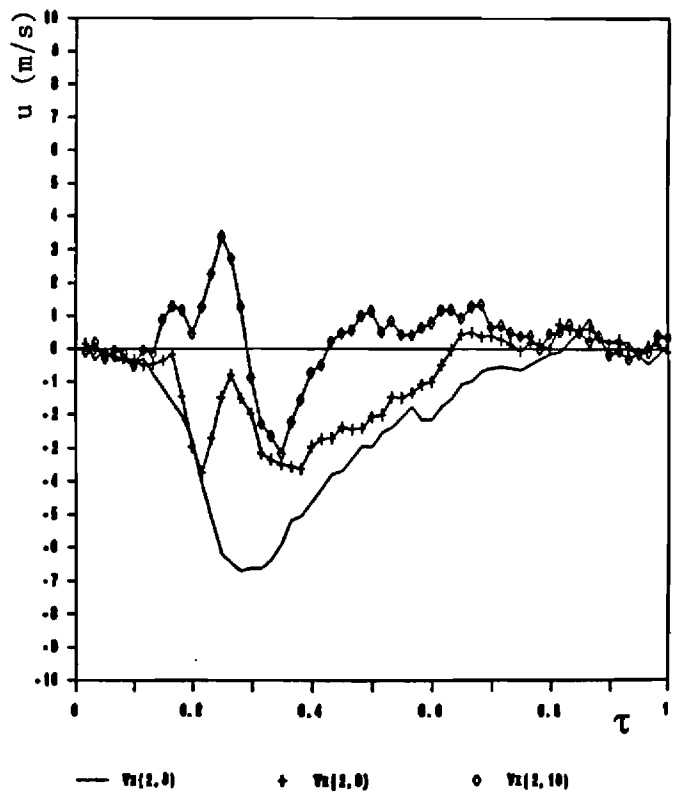
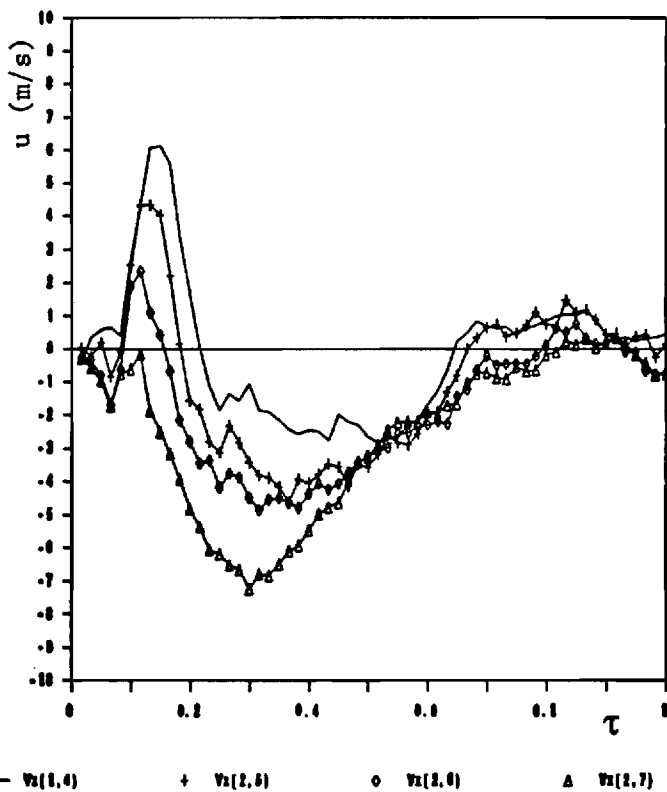
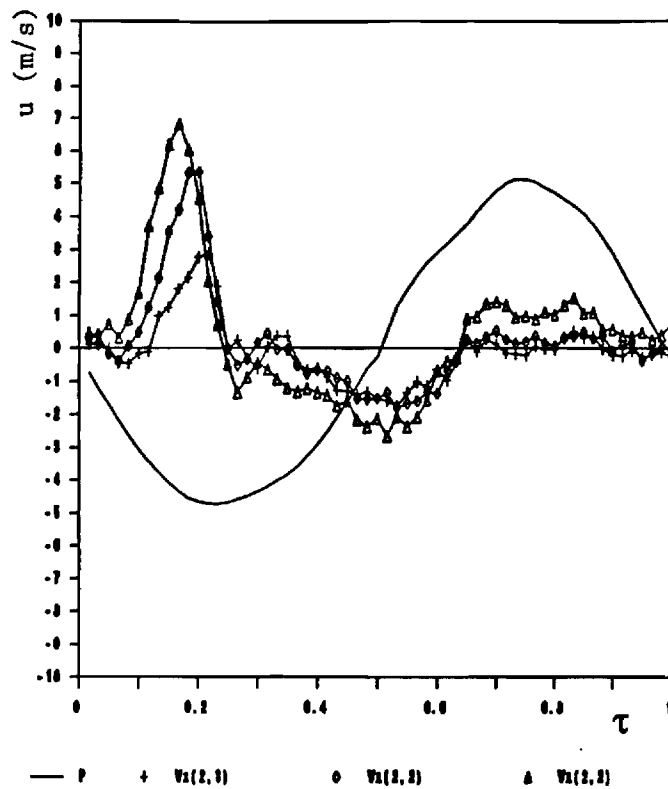


Fig. 16 Variation of the Axial Mean Velocity During a Cycle for Locations along the Line $m = 2$. The Top Plot includes the Pressure Trace for Reference.

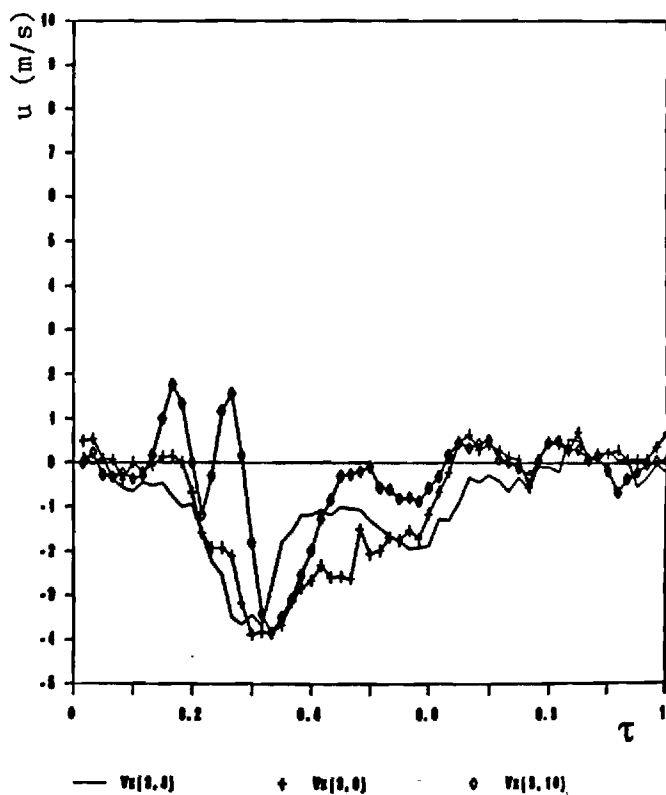
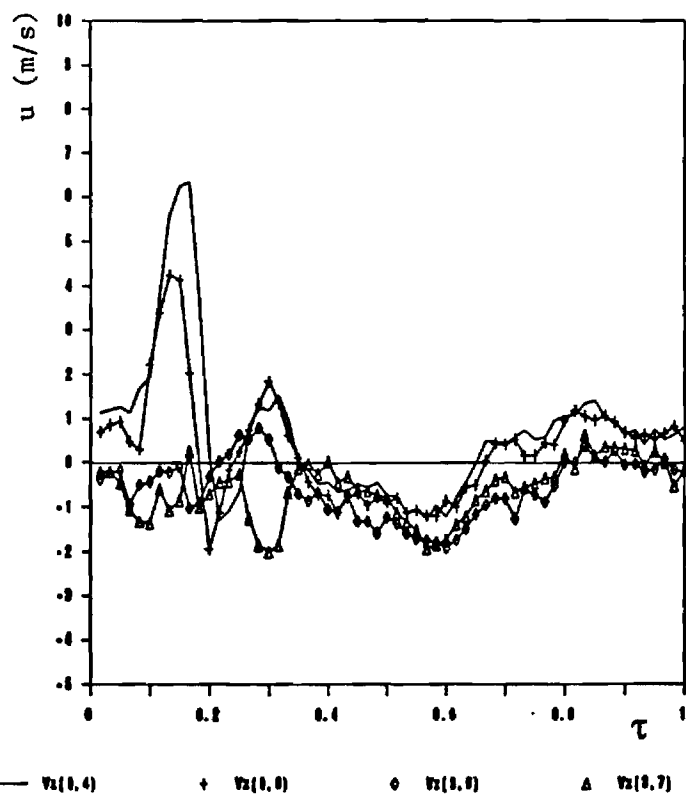
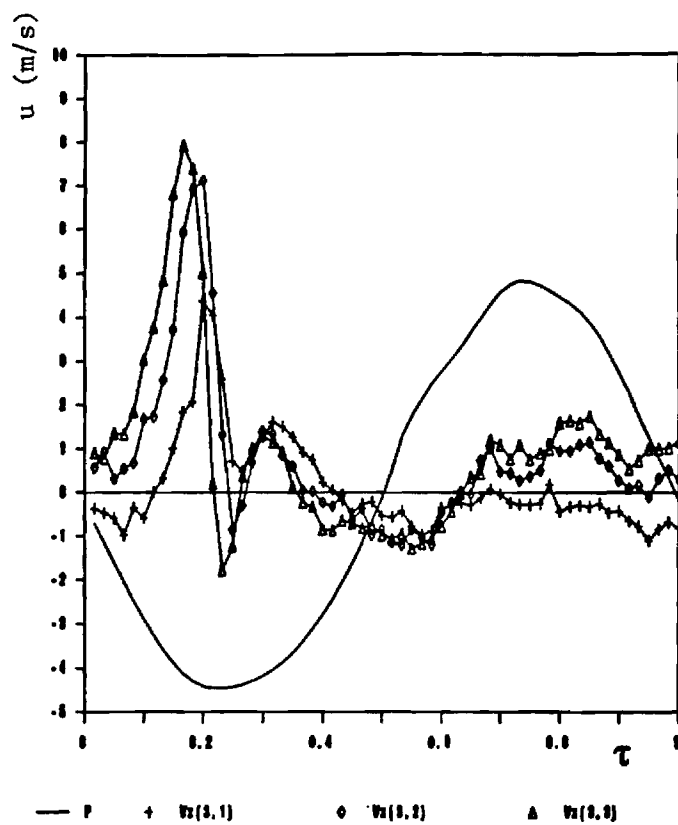


Fig. 17 Variation of the Axial Mean Velocity During a Cycle for Locations along the Line $m = 3$. The Top Plot includes the Pressure Trace for Reference.

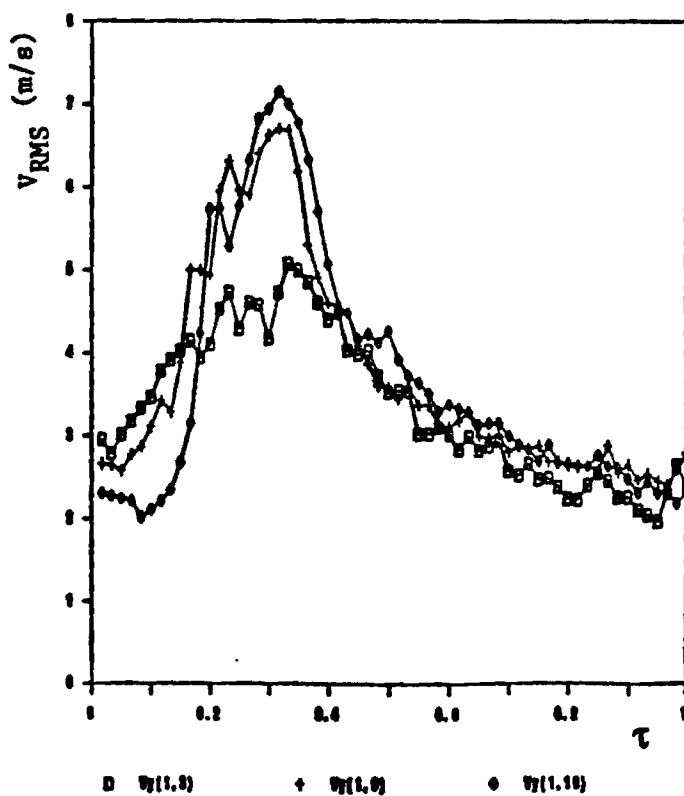
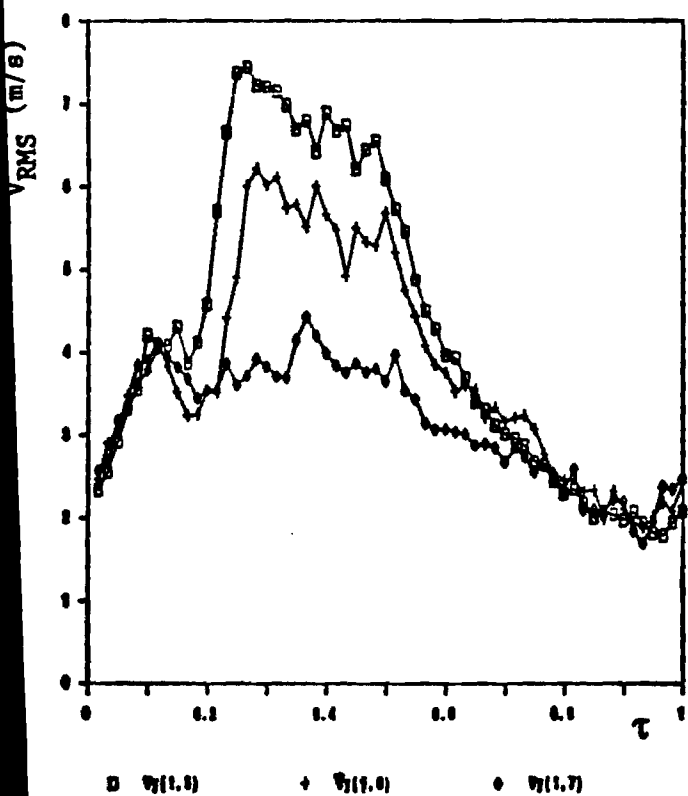
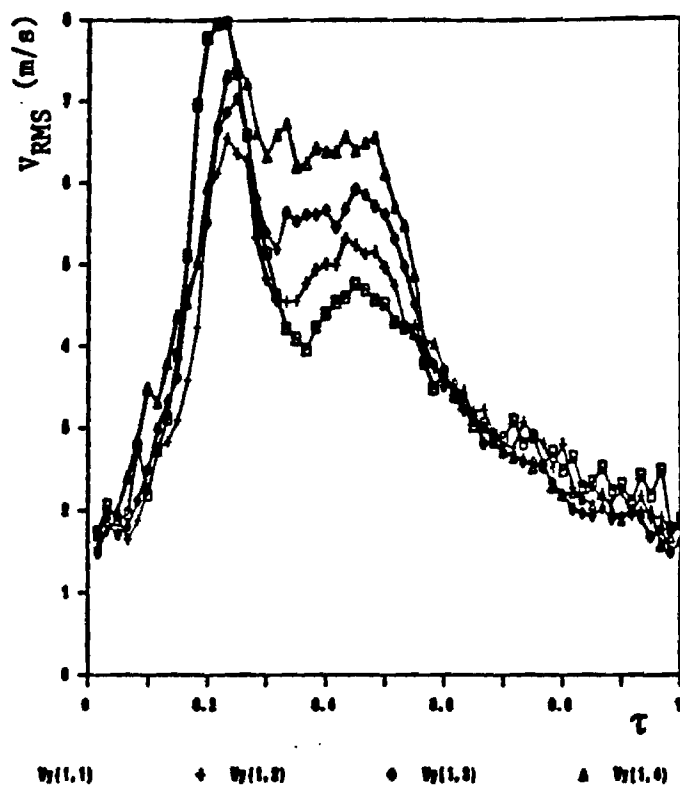


Fig. 18 Variation of the Vertical Turbulence Intensity During a Cycle for Locations along the Line $m = 1$.

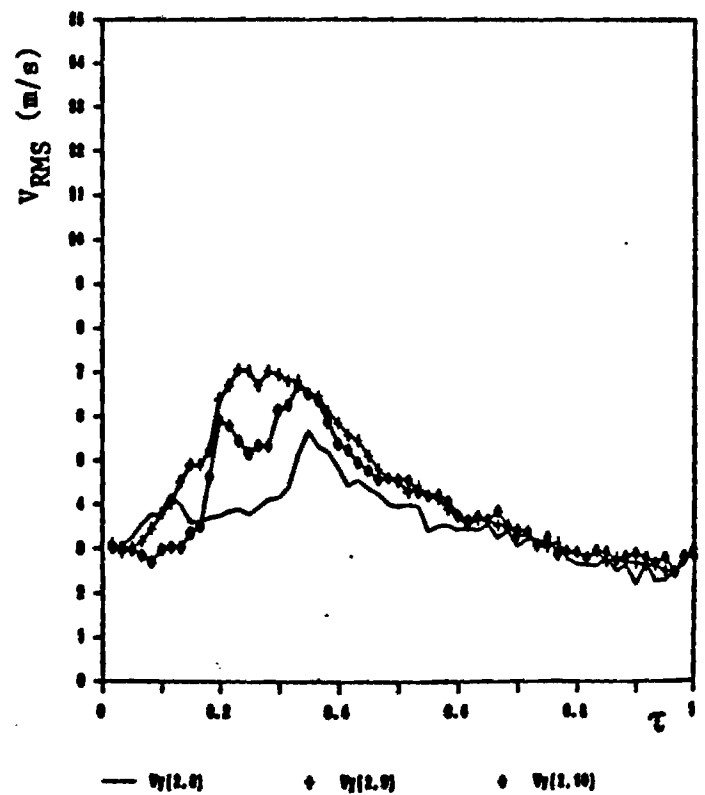
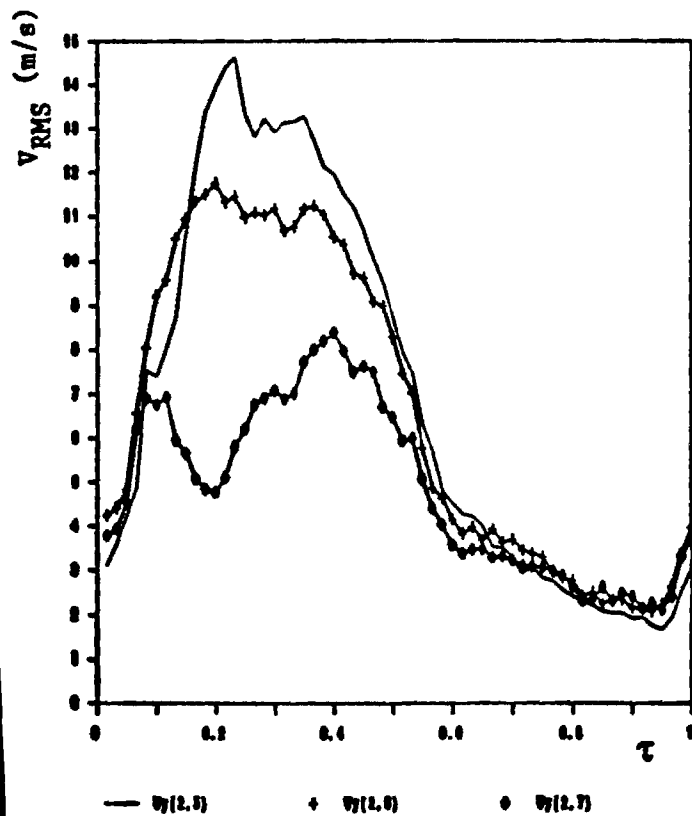
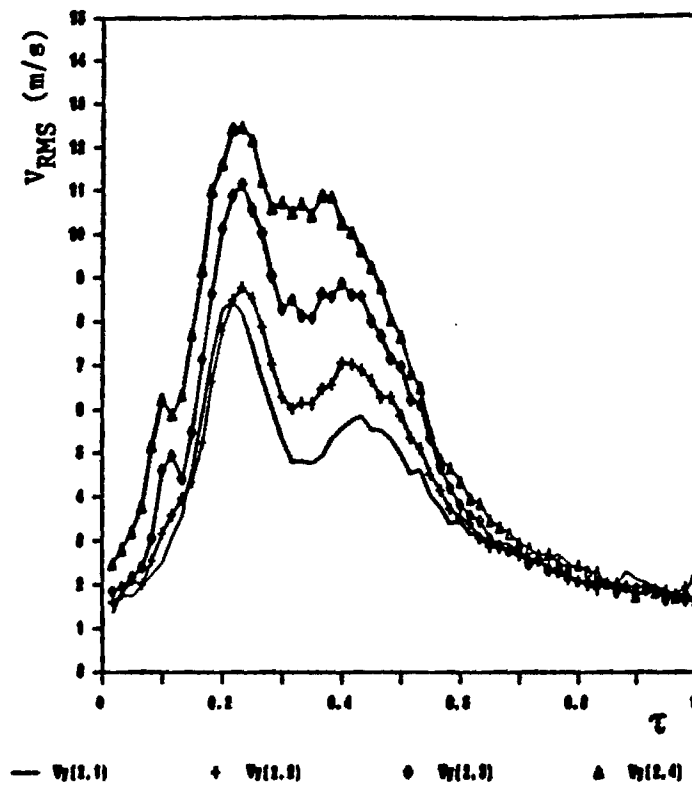


Fig. 19 Variation of the Vertical Turbulence Intensity During a Cycle for Locations along the Line $m = 2$.

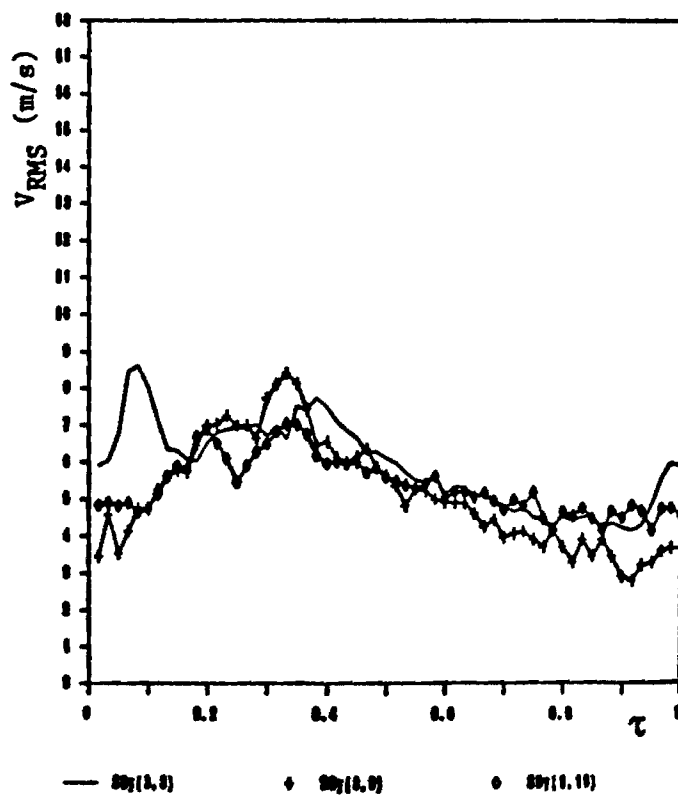
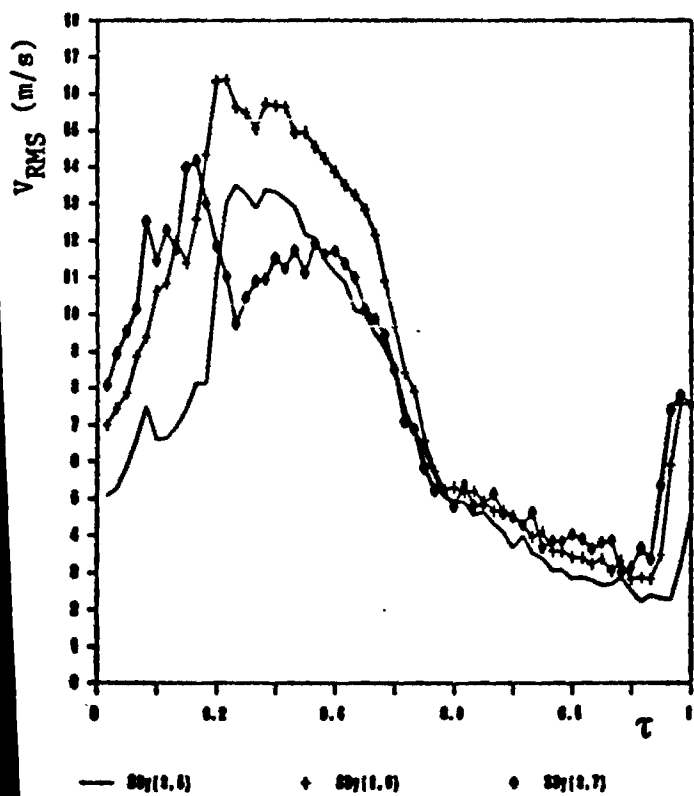
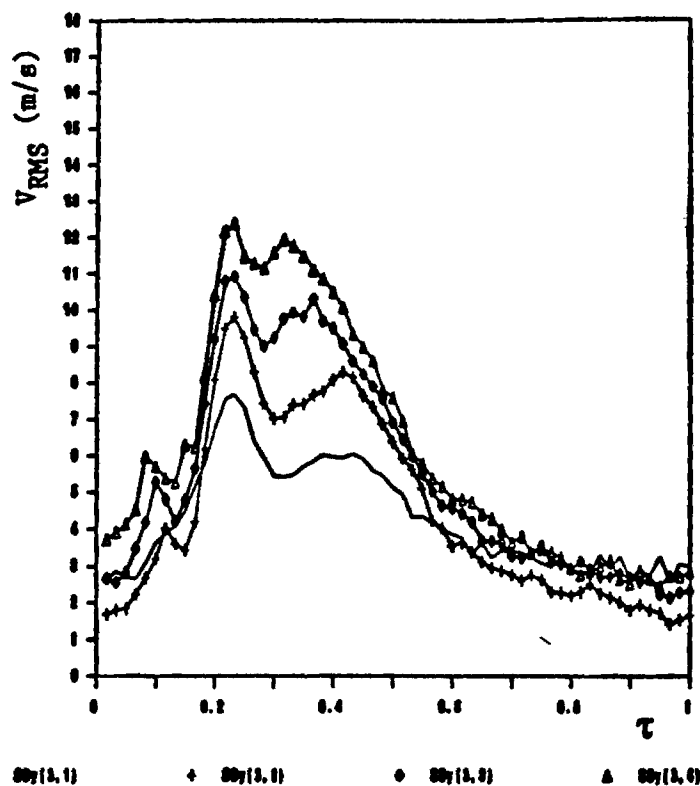


Fig. 20 Variation for the Vertical Turbulence Intensity During a Cycle for Locations along the Line $m = 3$.

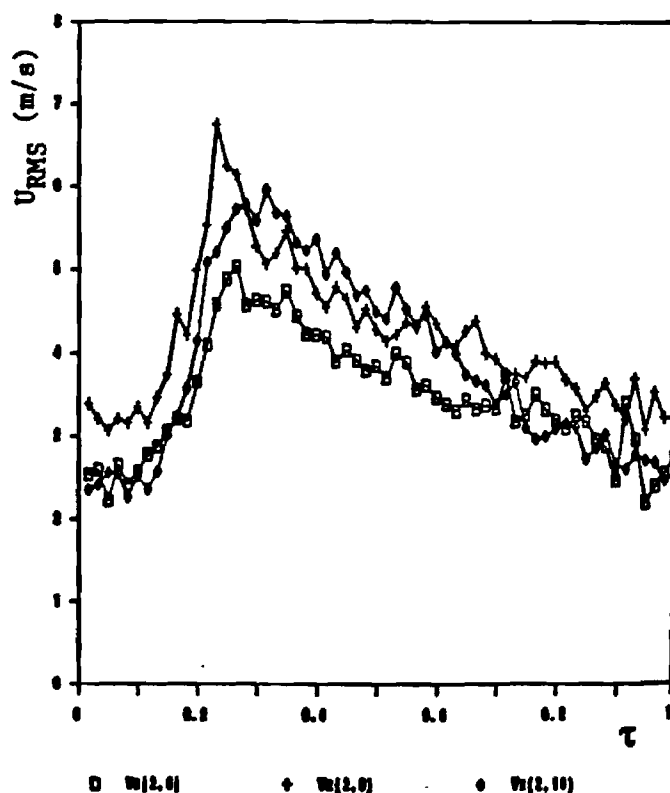
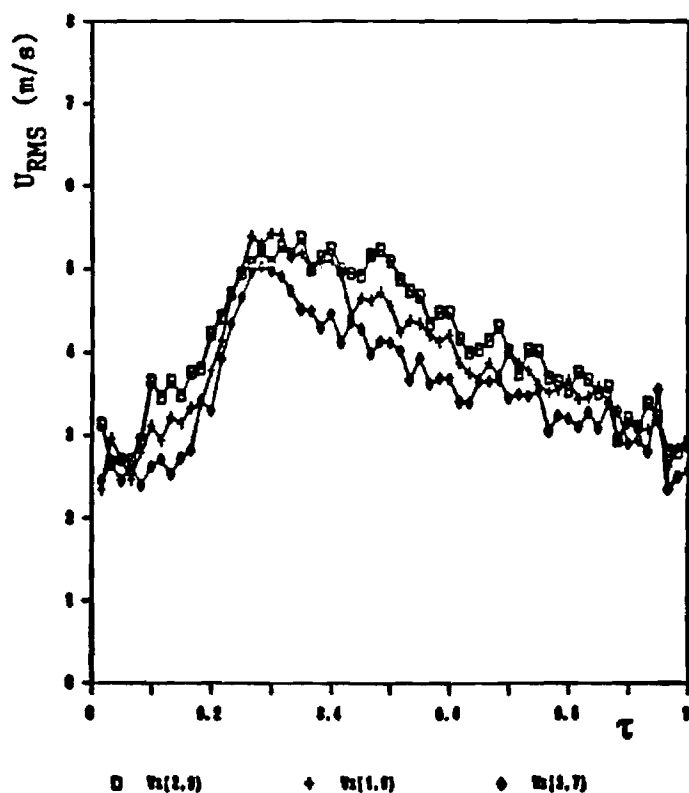
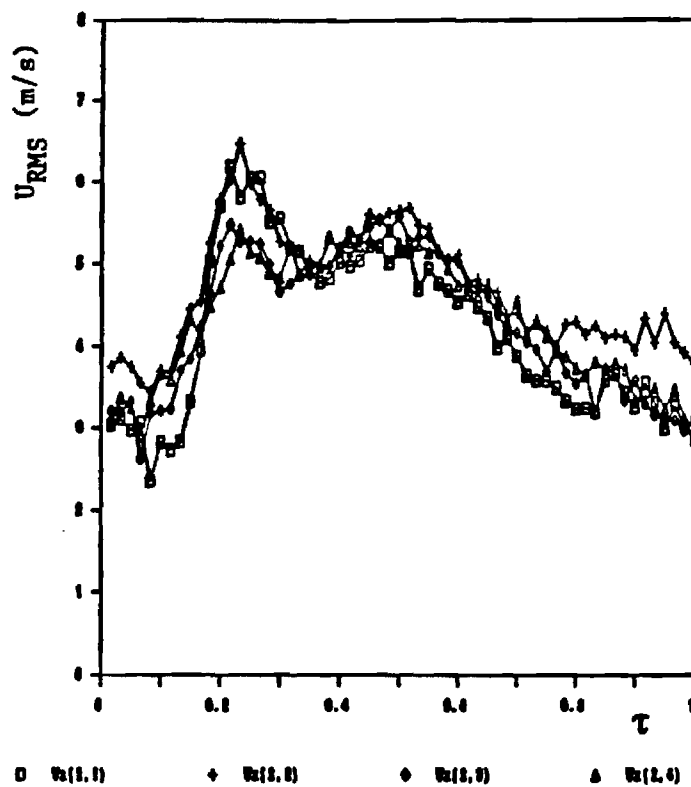


Fig. 21 Variation of the Axial Turbulence Intensity During a Cycle for Locations along the Line $m = 1$.

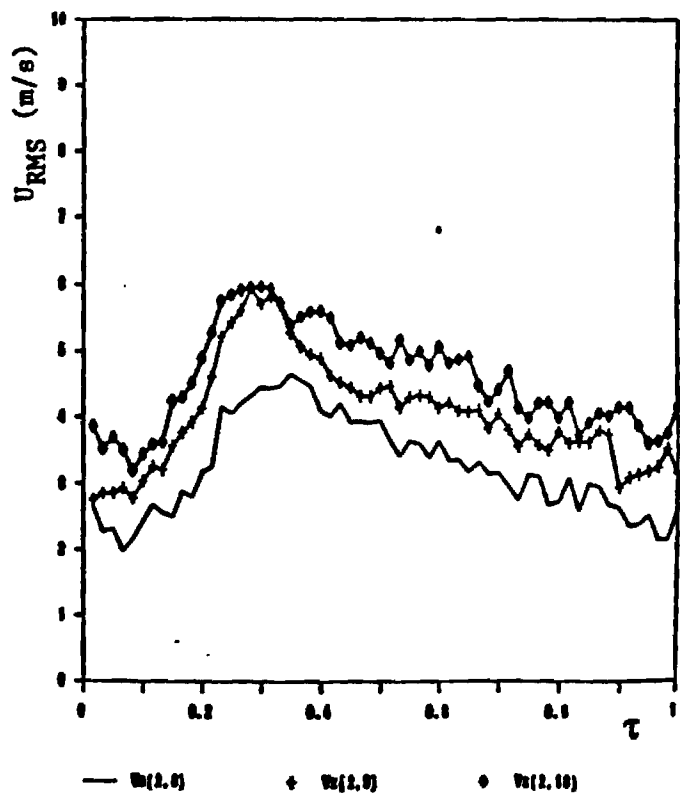
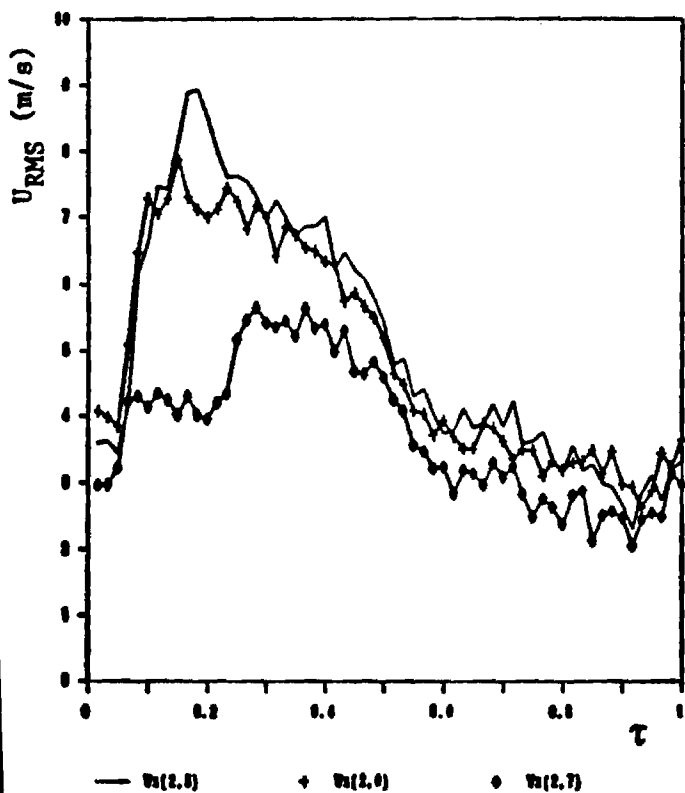
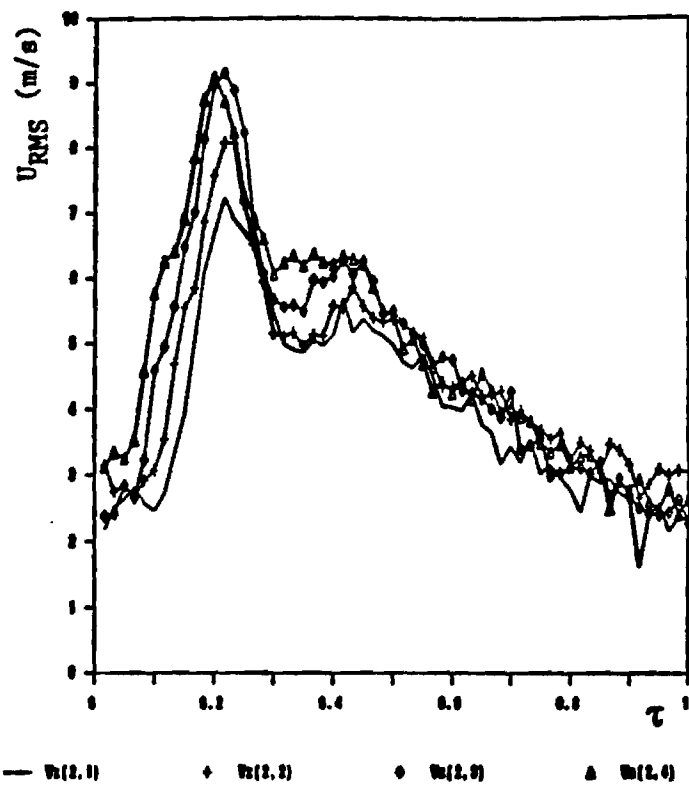


Fig. 22 Variation of the Axial Turbulence Intensity During a Cycle for Locations along the Line $m = 2$.

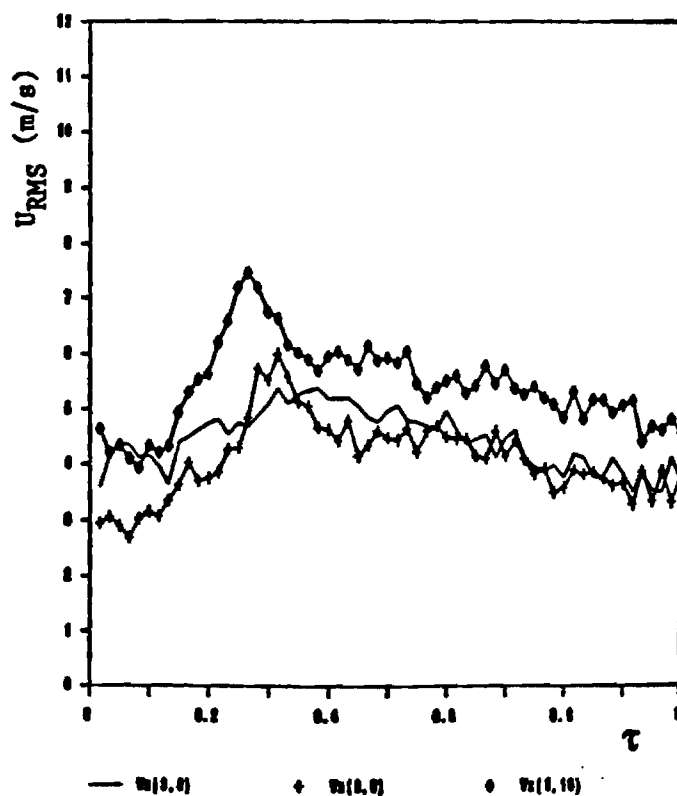
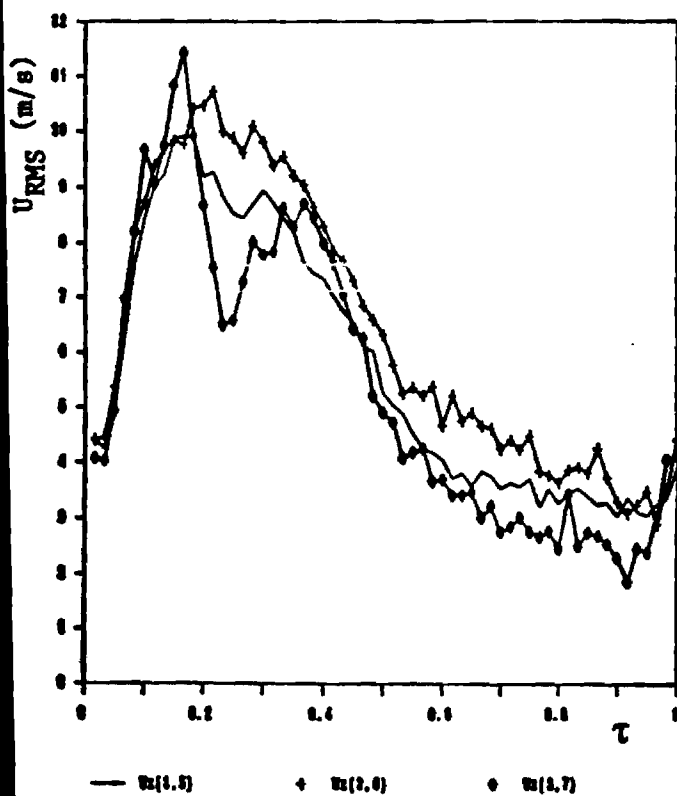
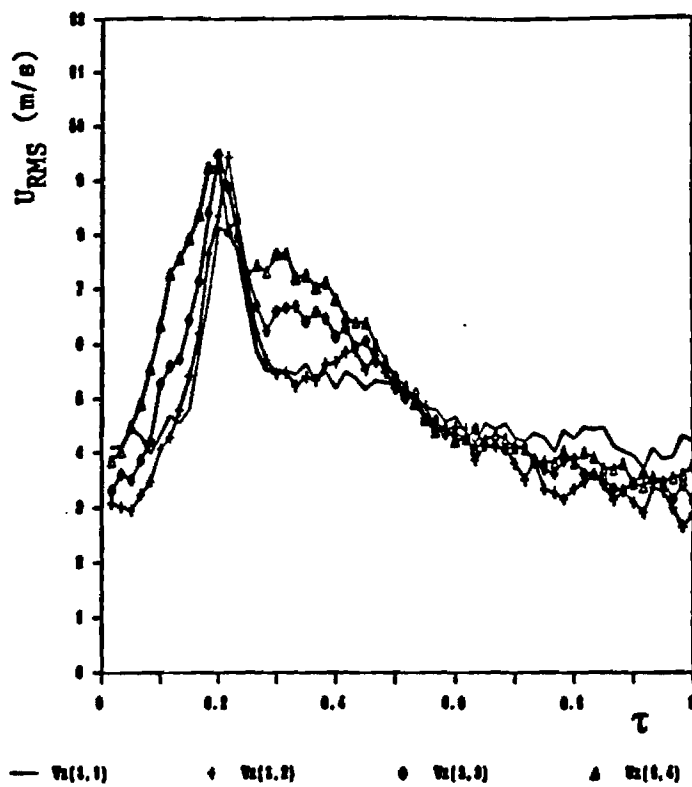


Fig. 23 Variation of the Vertical Turbulence Intensity During a Cycle for Locations along the Line $m = 3$.

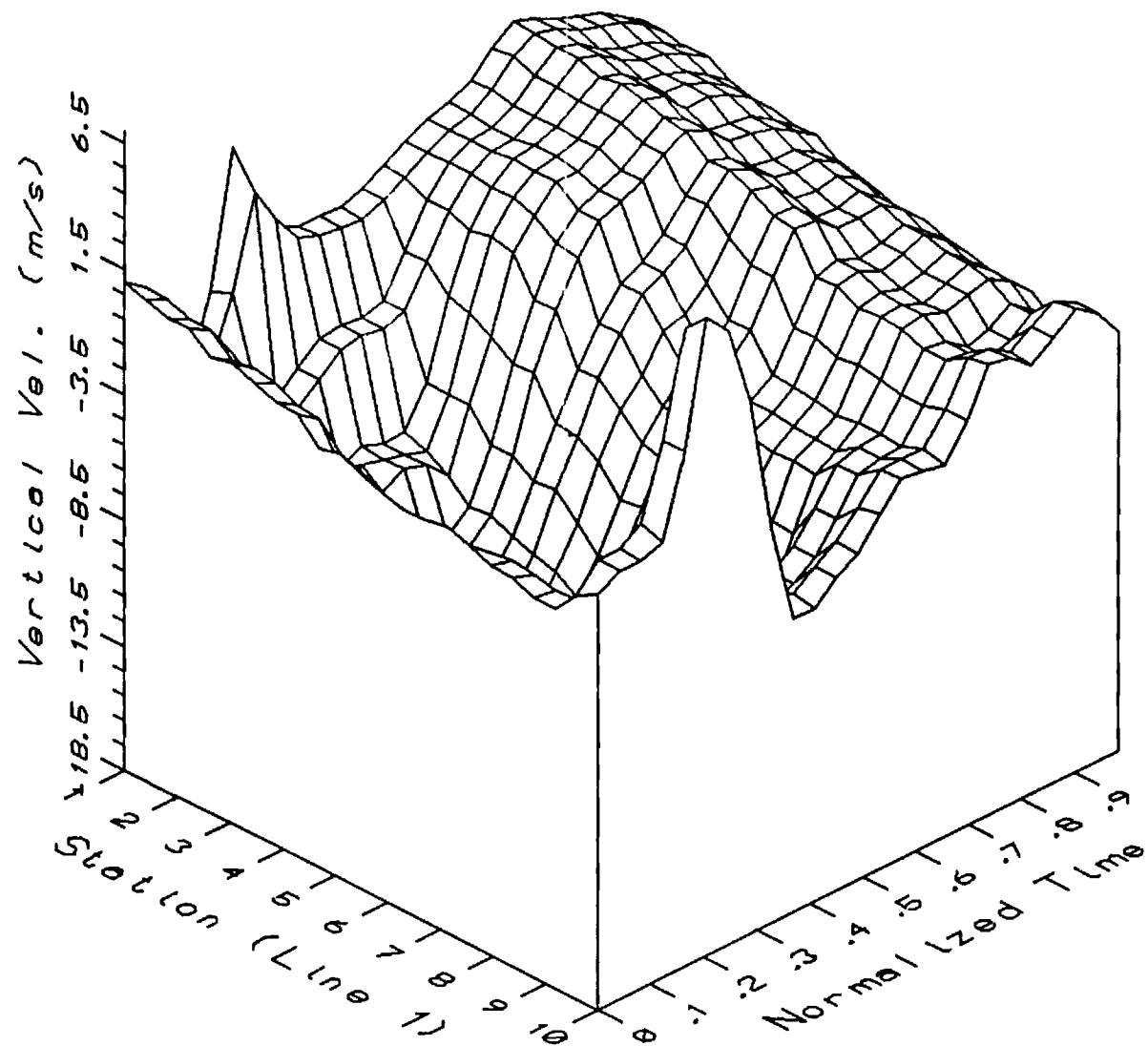


Fig. 24 Three Dimensional Plot of Vertical Mean Velocities during a Cycle for Locations along the Line $m = 1$.

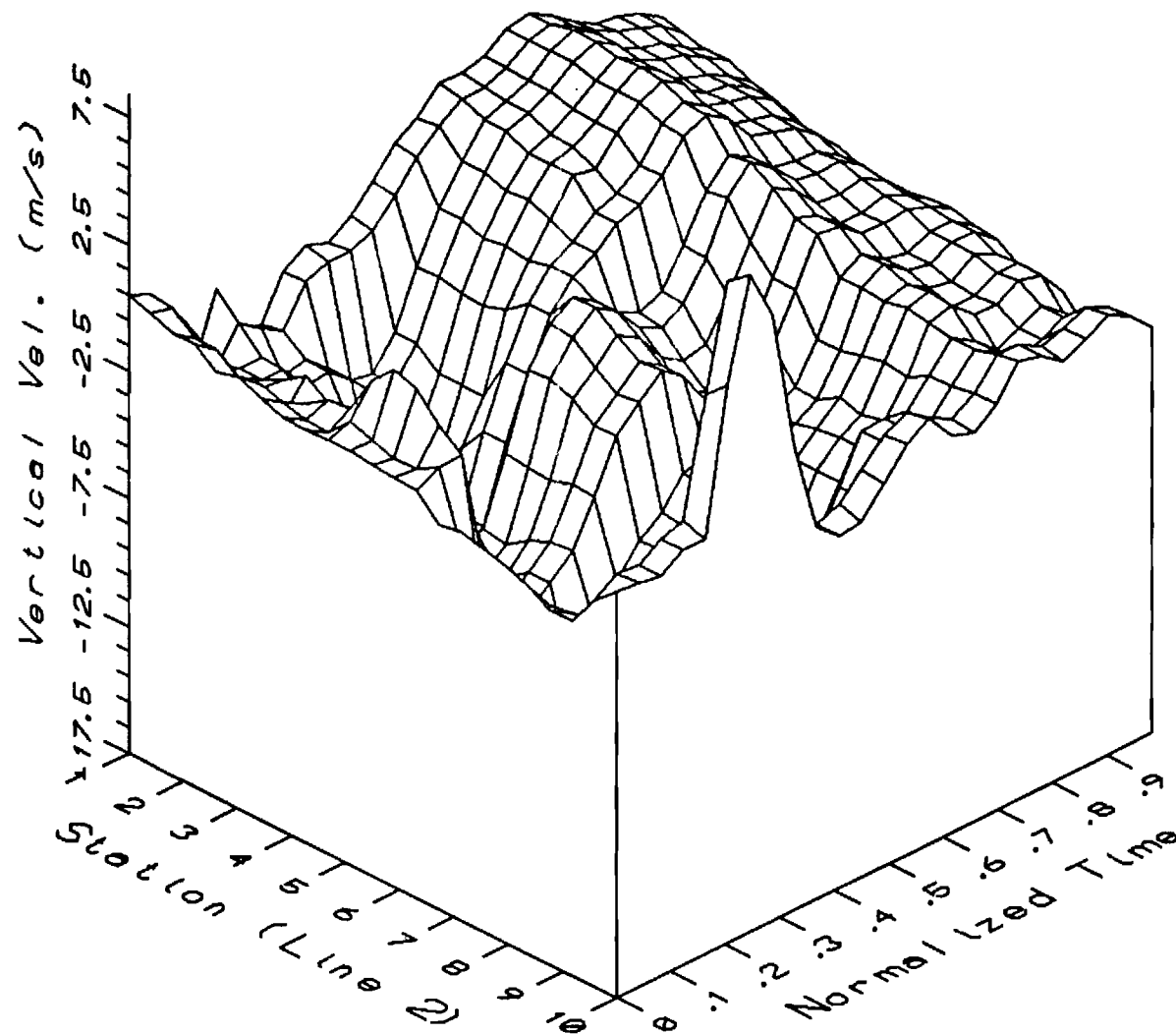


Fig. 25 Three Dimensional Plot of Vertical Mean Velocities during a Cycle for Locations along the Line $m = 2$.

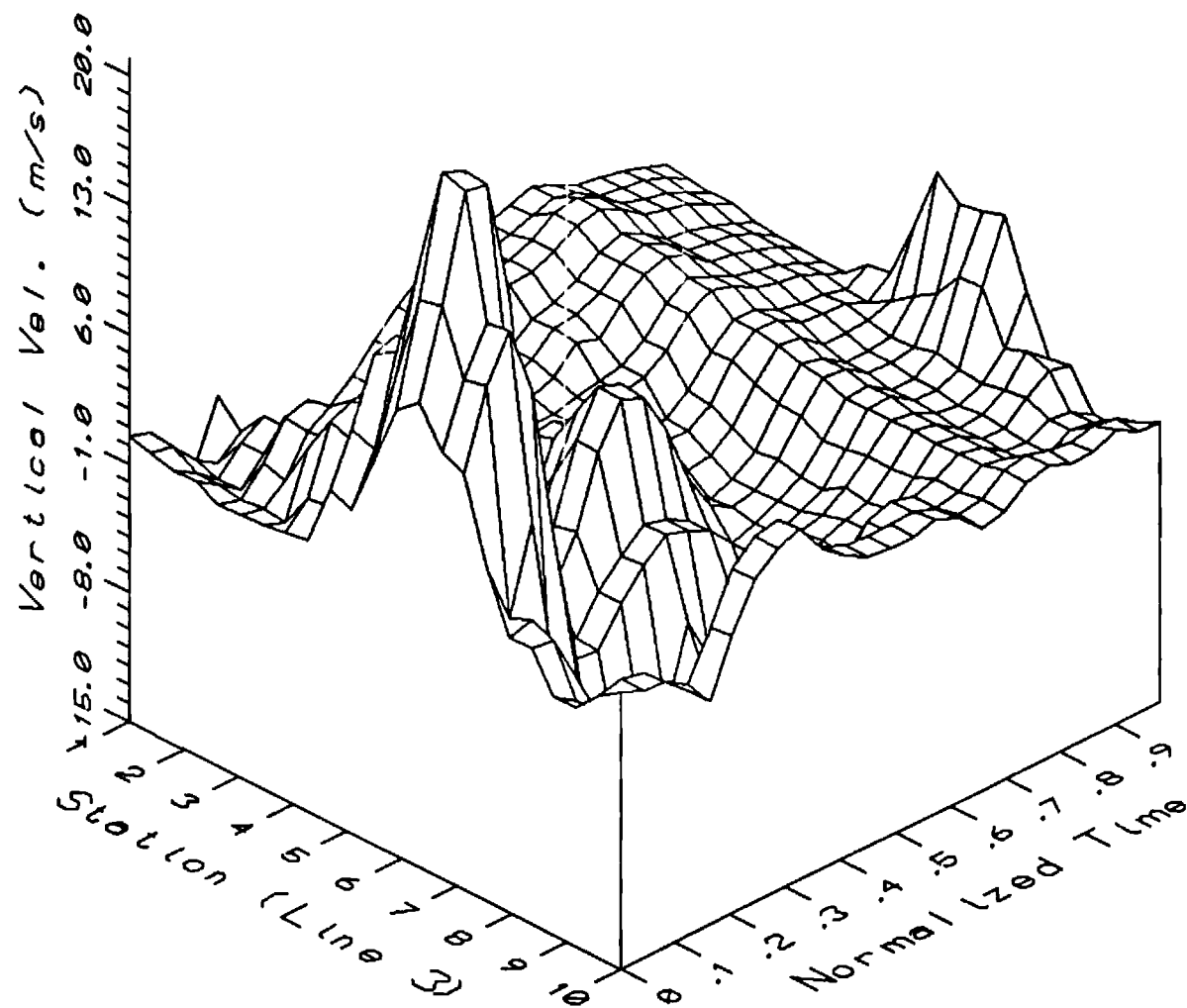


Fig. 26 Three Dimensional Plot of Vertical Mean Velocities during a Cycle for Locations along the Line $m = 3$.

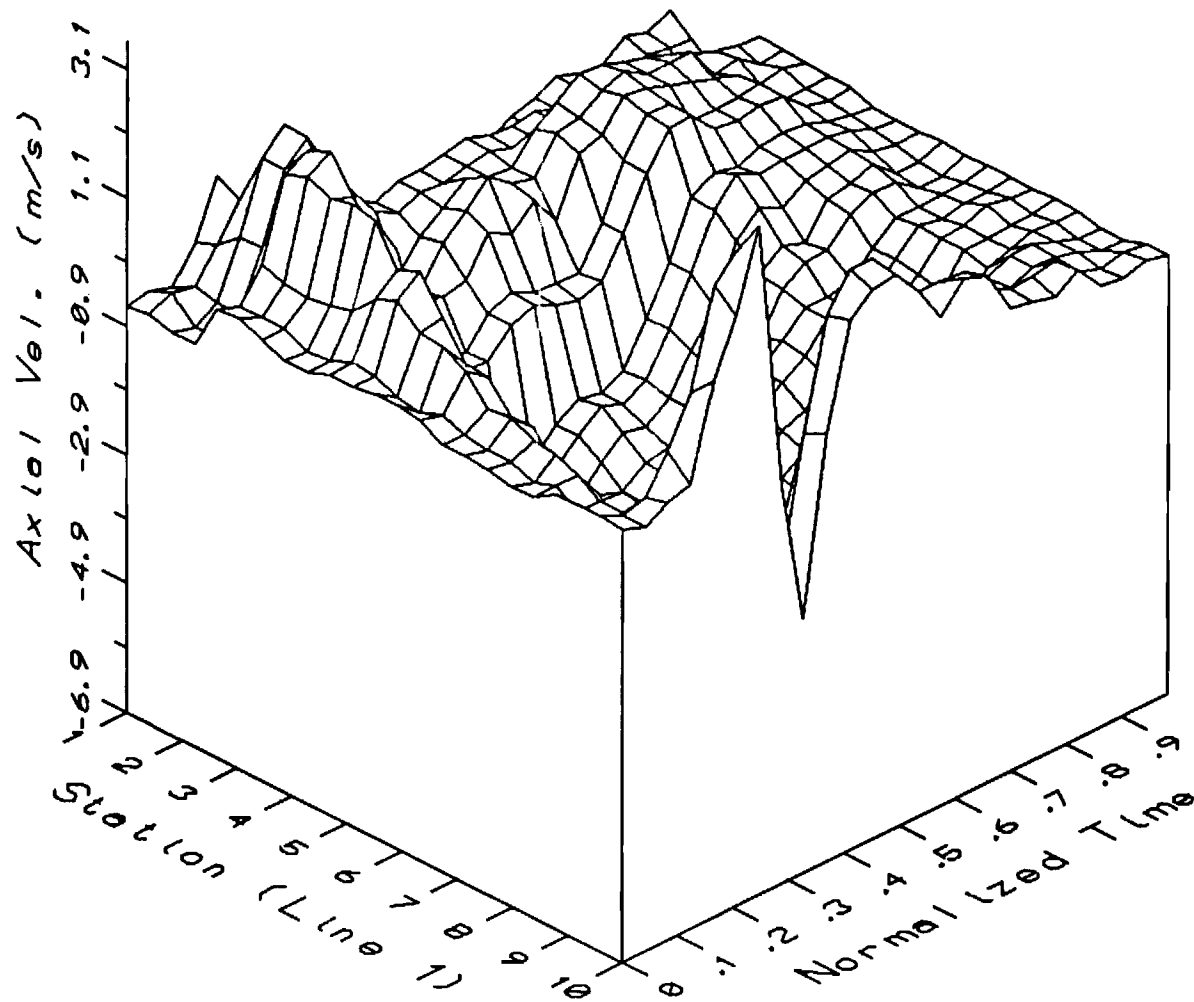


Fig. 27 Three Dimensional Plot of Axial Mean Velocities during a Cycle for Locations along the Line $m = 1$.

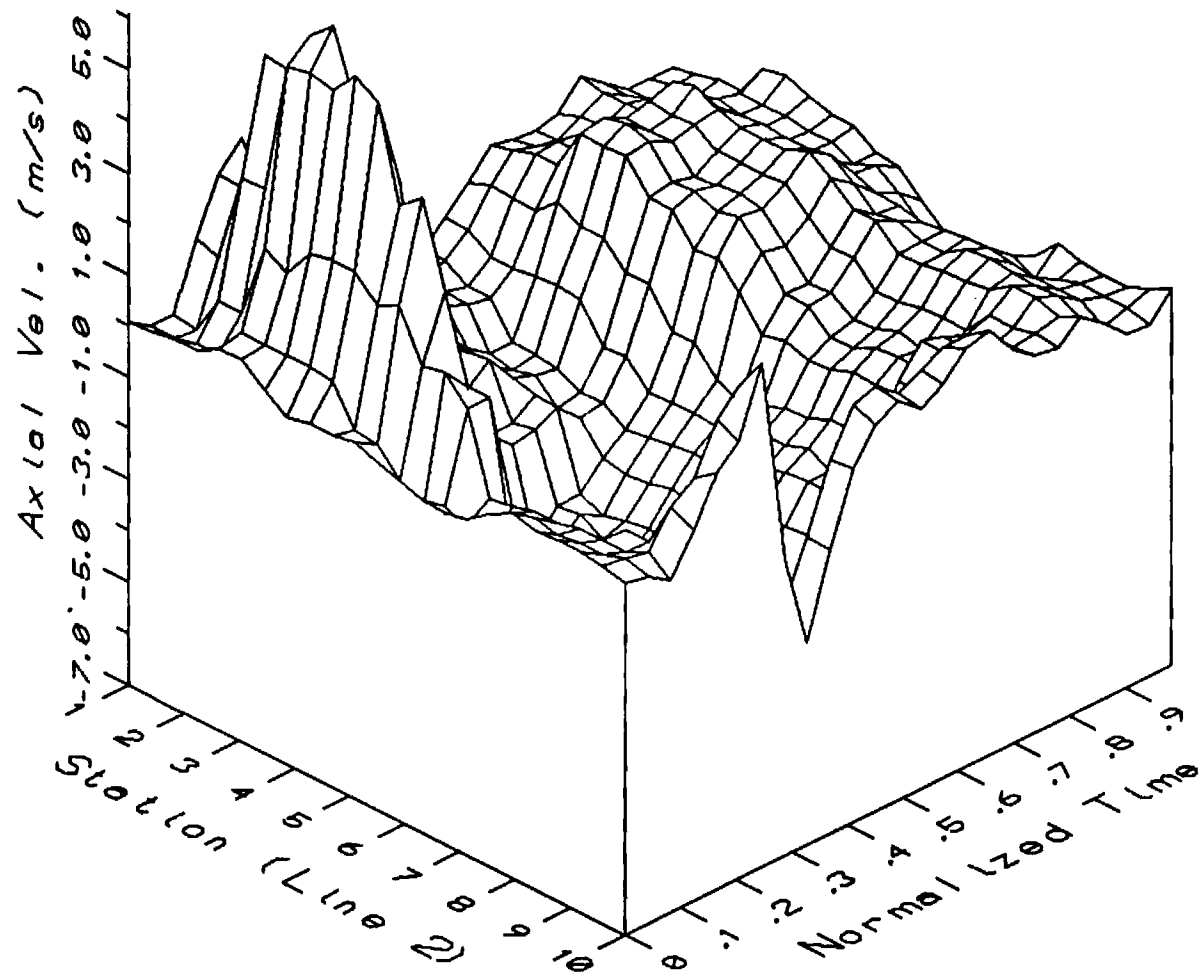


Fig. 28 Three Dimensional Plot of Axial Mean Velocities during a Cycle for Locations along the Line $m = 2$.

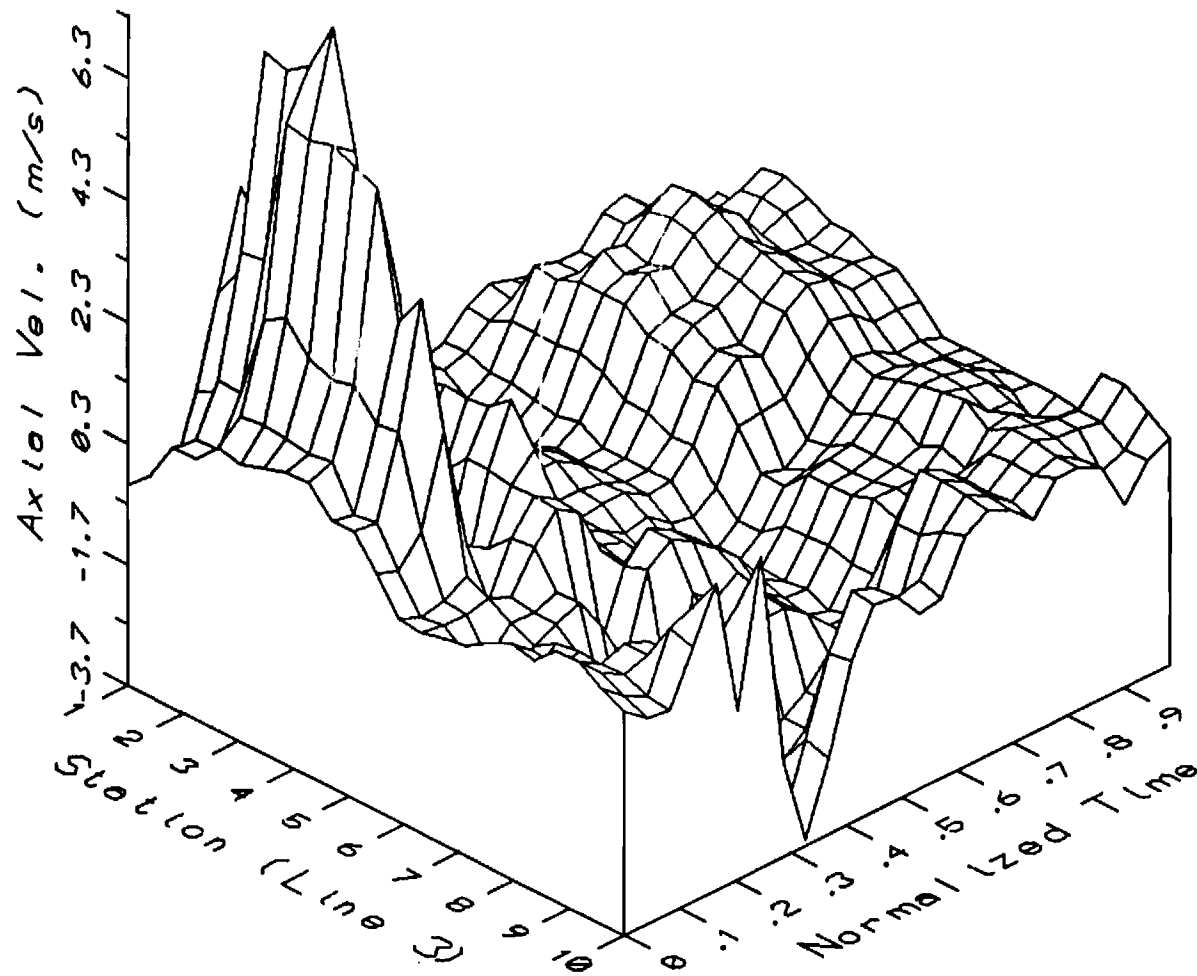


Fig. 29 Three Dimensional Plot of Axial Mean Velocities during a Cycle for Locations along the Line $m = 3$.

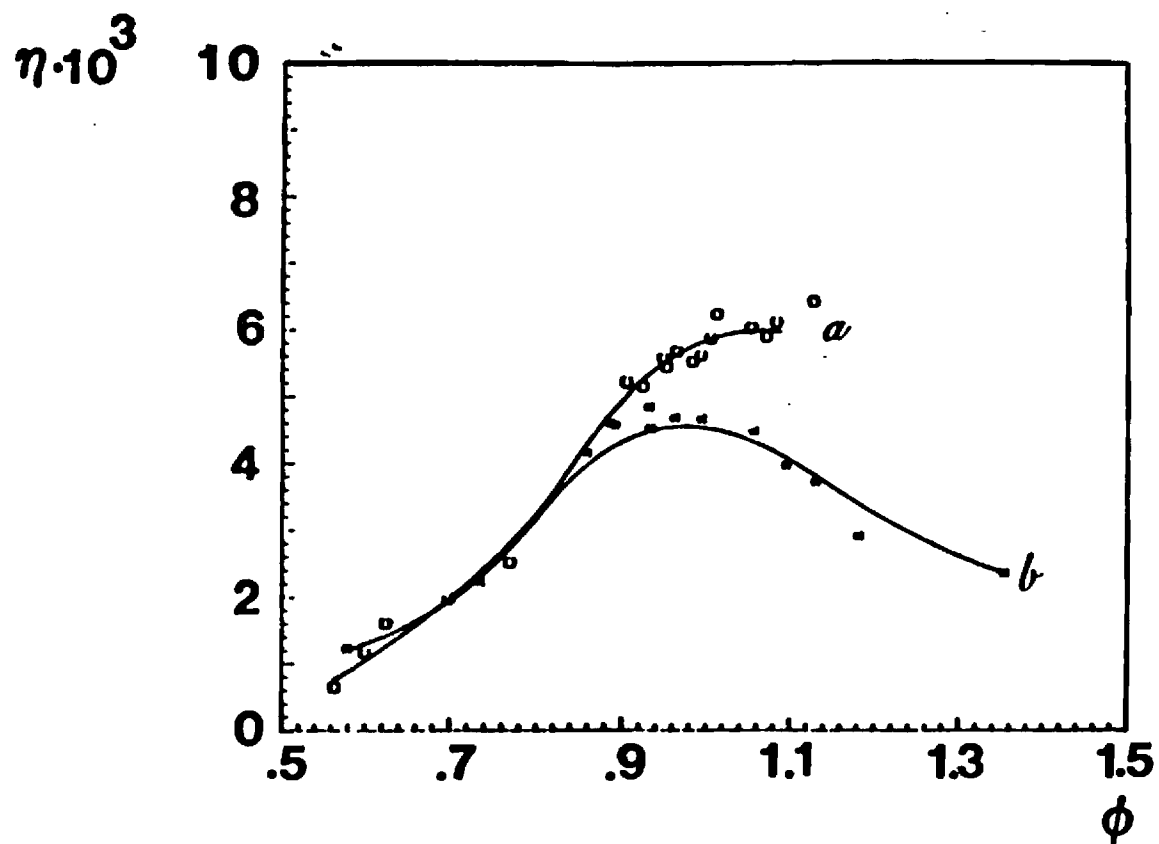


Fig. 30 Rayleigh Efficiency as a Function of Equivalence Ratio for The Combustor Fitted with the a) Standard and b) Long Tail-pipes.

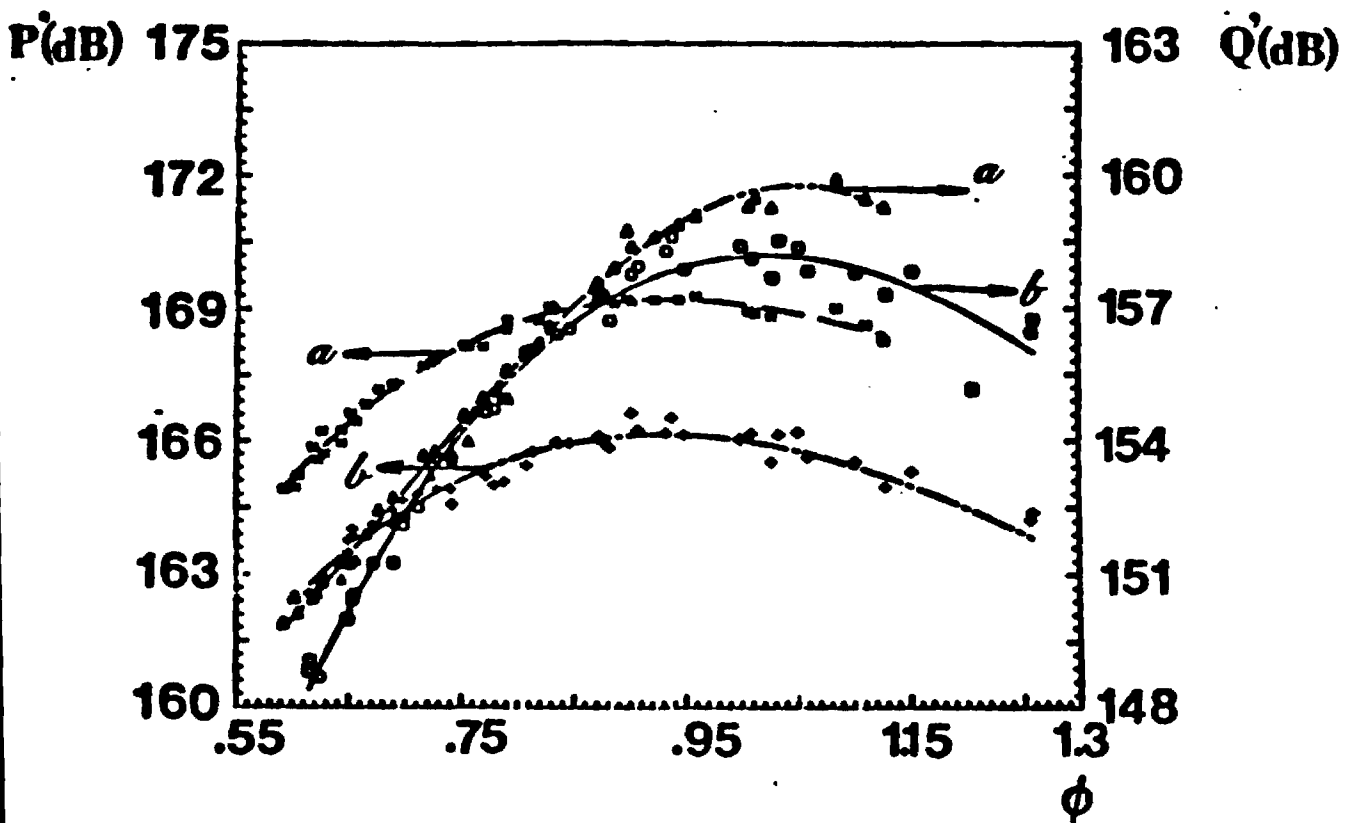


Fig. 31 Pressure and Heat Release Fluctuations as a Function of Equivalence Ratio for the Combustor Fitted with the Standard (a) and Long (b) Tailpipes.

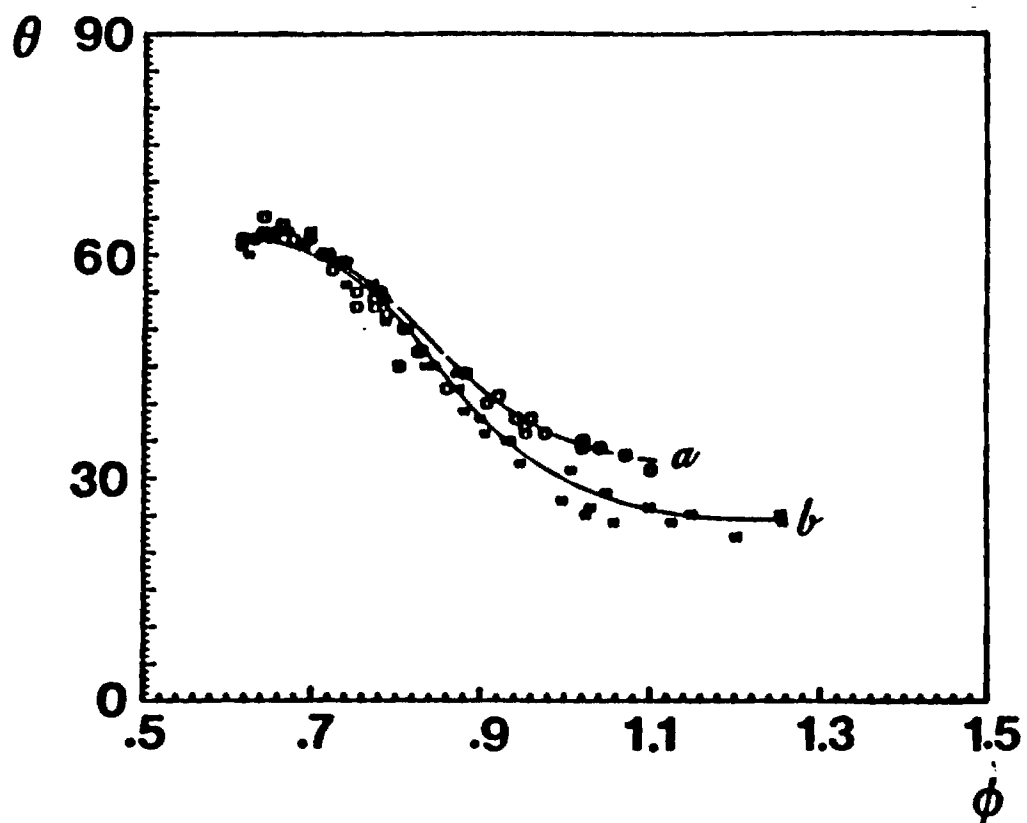


Fig. 32 Phase Angle by which the Heat Release Leads the Pressure as a Function of Equivalence Ratio for the Combustor Fitted with the a) Standard and b) Long Tailpipes.

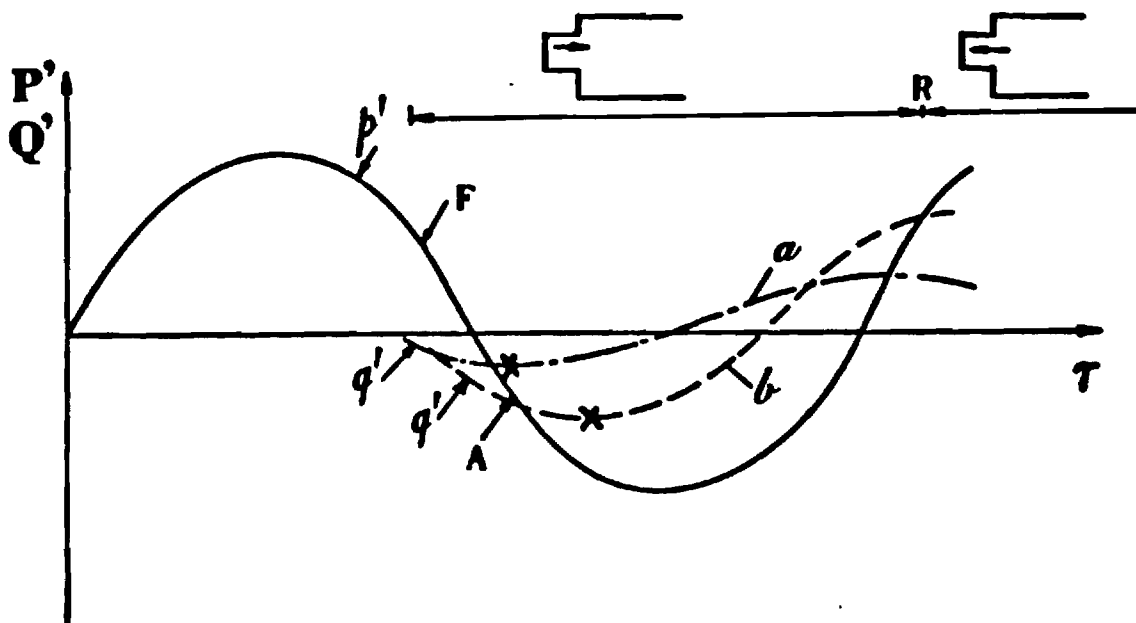


Fig. 33 Normalized Pressure (P') Cycle Showing the Timing of the Heat Release Oscillations (Q') for a) Lean and b) Rich Limits of Operation; Fuel Enters at "F", Air Enters at "A", Backflow into the Mixing Chamber Starts at "R"; the "X"s Denote the Instants of Reignition of the Fresh Fuel Charges.

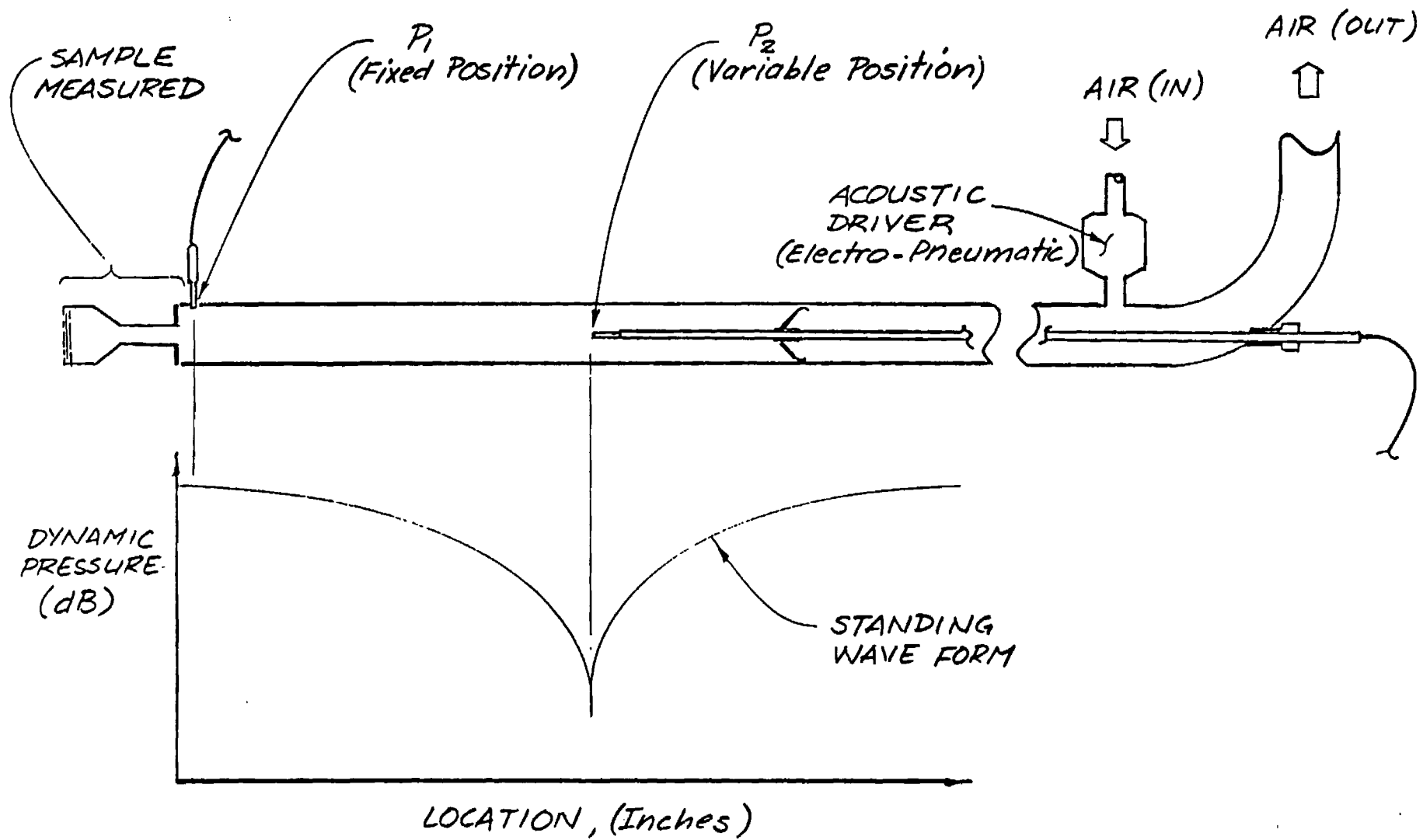


Fig. 34 Schematic of the Impedance Tube Experiment.

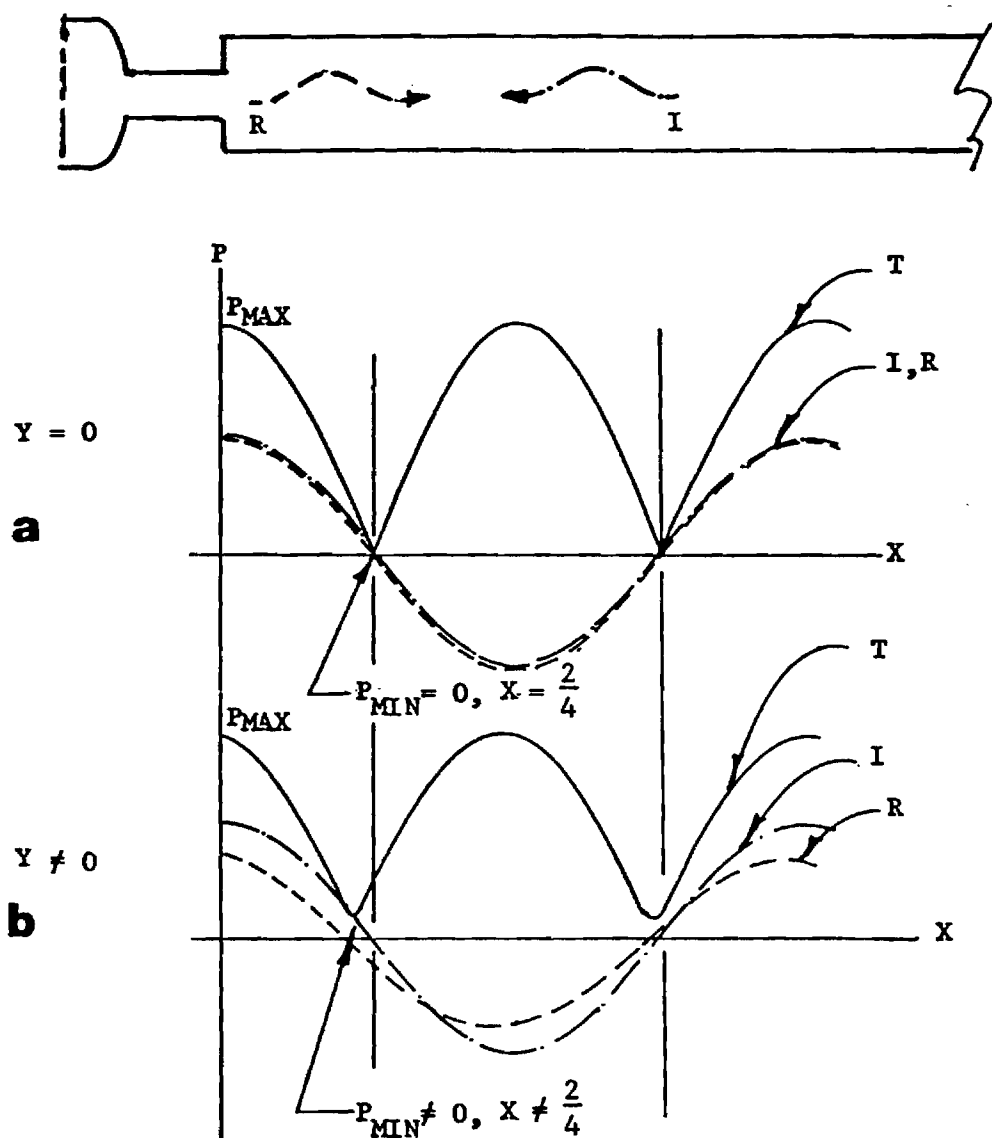


Fig. 35 Wave Form of the Incident (I), Reflected (R) and Total (T) Standing Wave for a) Hard Termination and b) Termination with Finite Admittance.

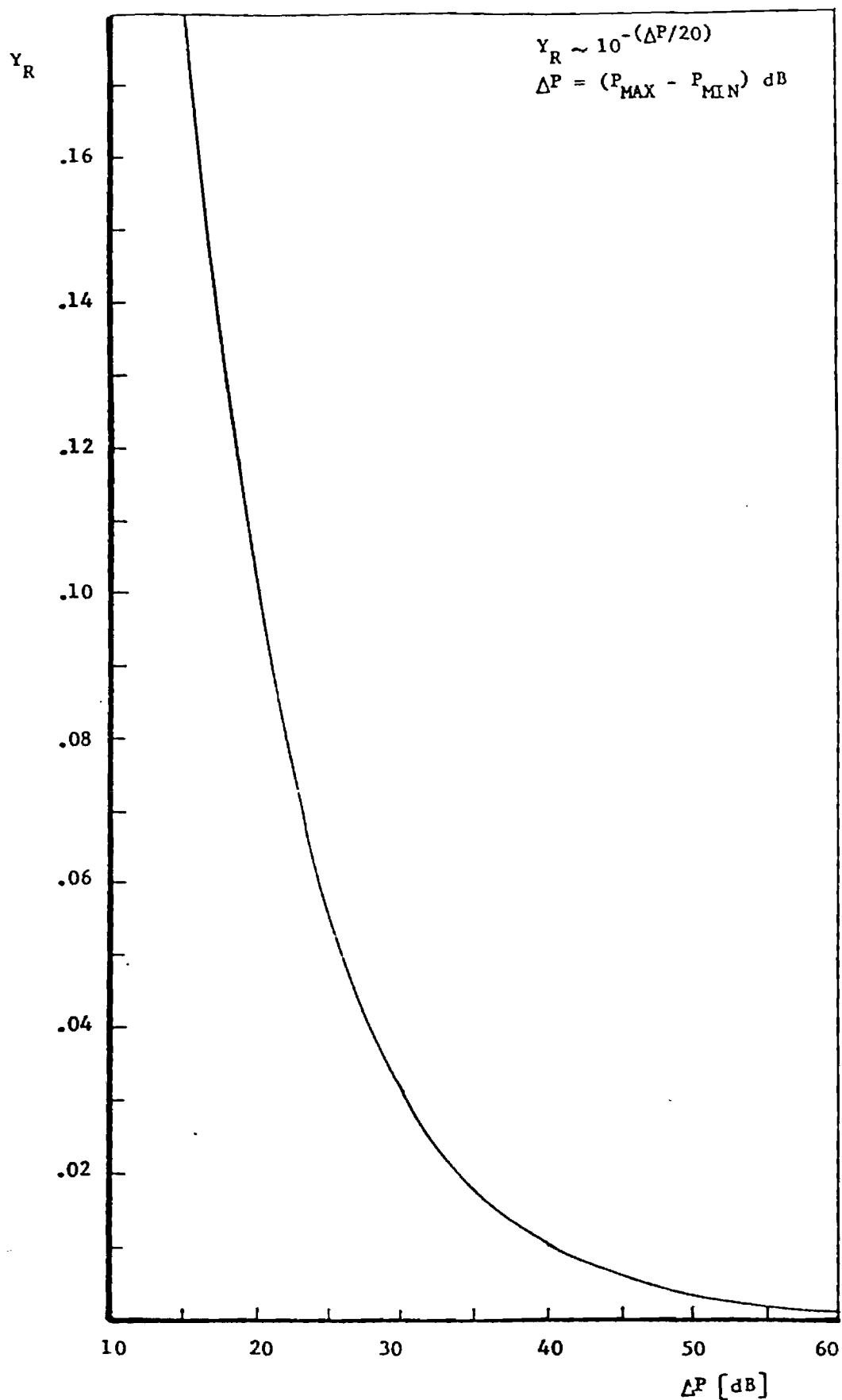


Fig. 36 Sensitivity of the Real Part of the Admittance to the Measured Pressure Difference between the Pressure Maximum and the Pressure Minimum.

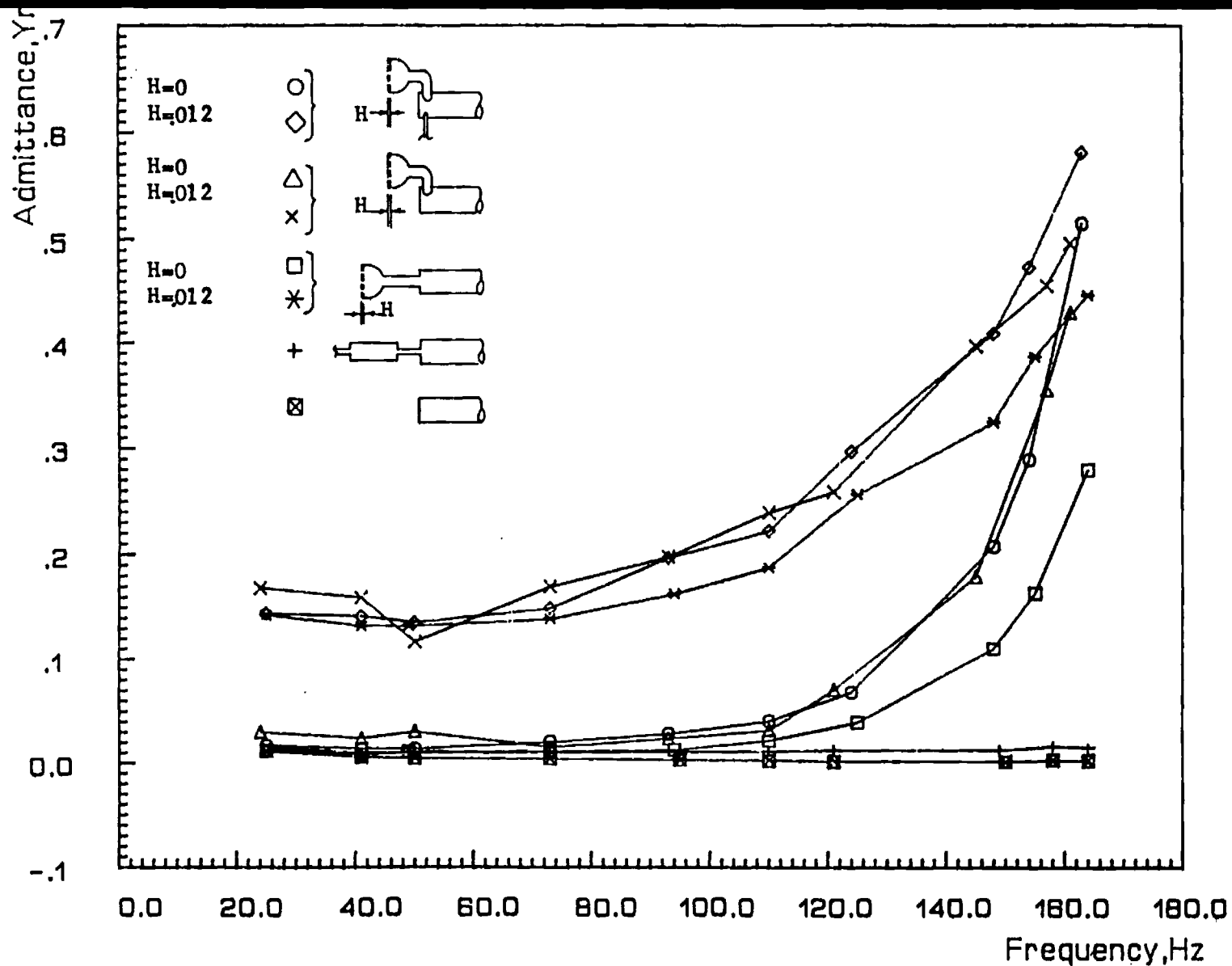


Fig. 37 Real Part of the Admittance as a Function of Frequency for Various Impedance Tube Terminations. H Denotes the Valve Gap Setting in Inches.

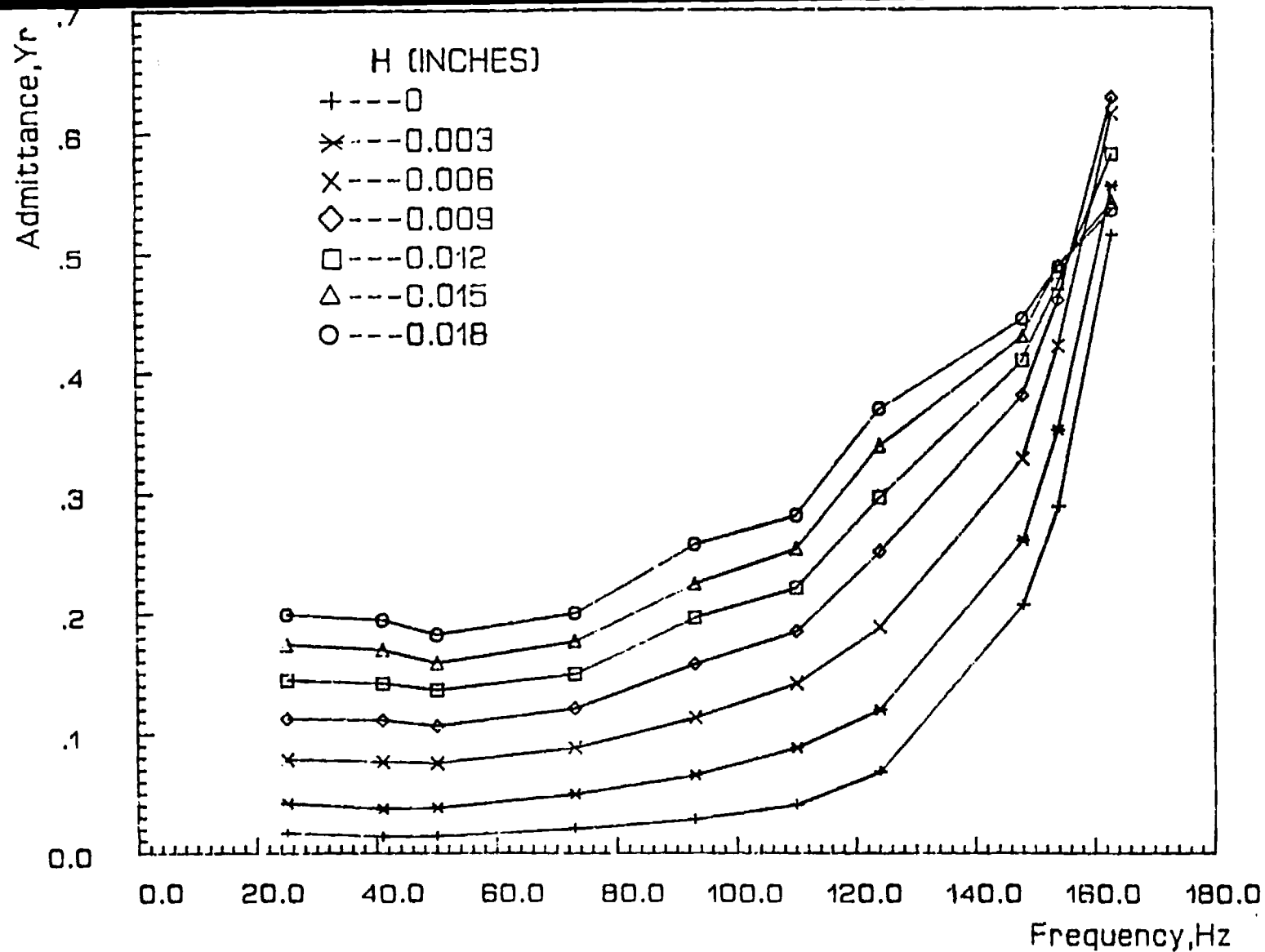


Fig. 38 Real Part of the Admittance of the Mixing Chamber Assembly as a Function of Frequency for Different Air Valve Gap Settings (H).

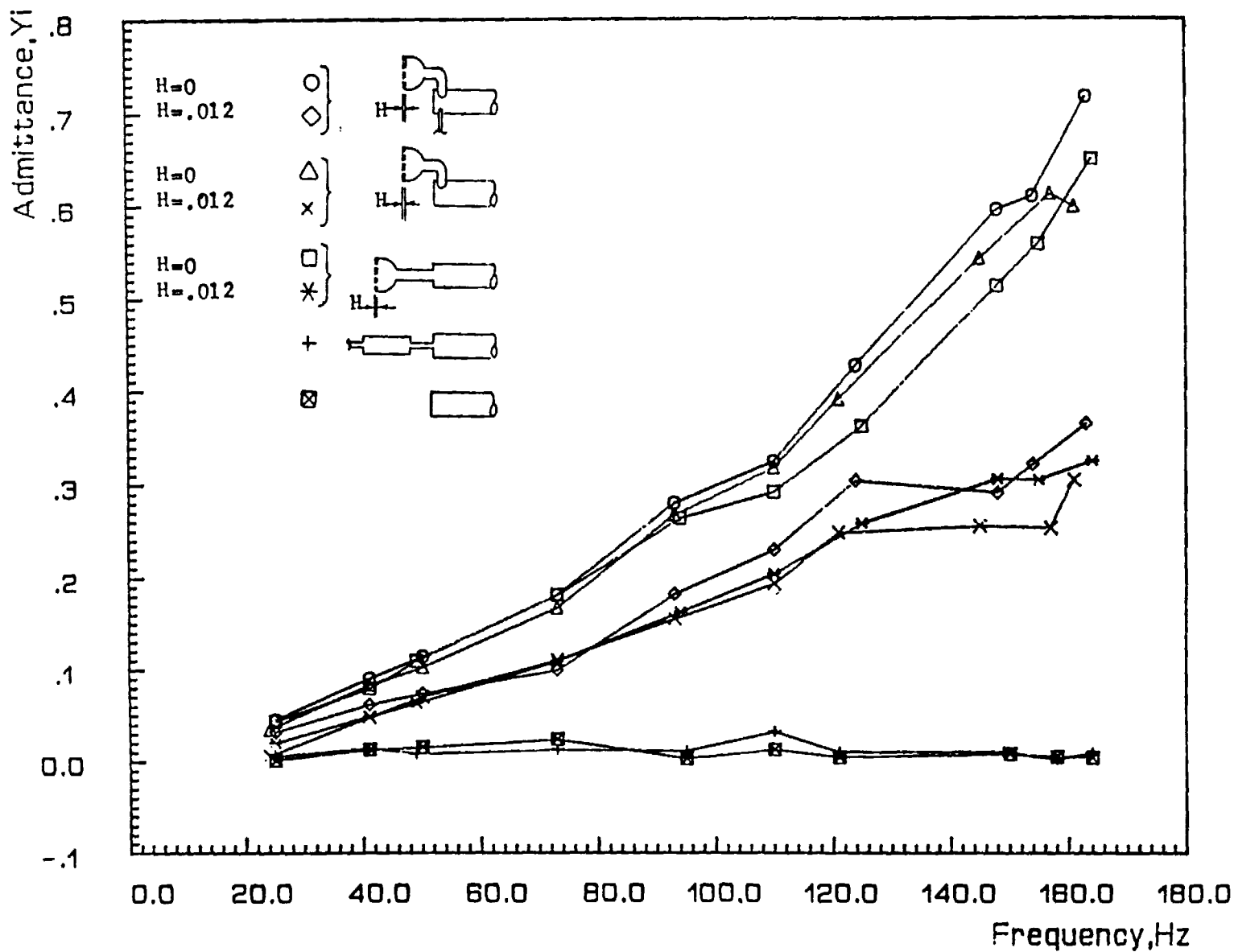


Fig. 39 Imaginary Part of the Admittance as a Function of Frequency for Various Impedance Tube Terminations. H Denotes the Valve Gap Setting in Inches.

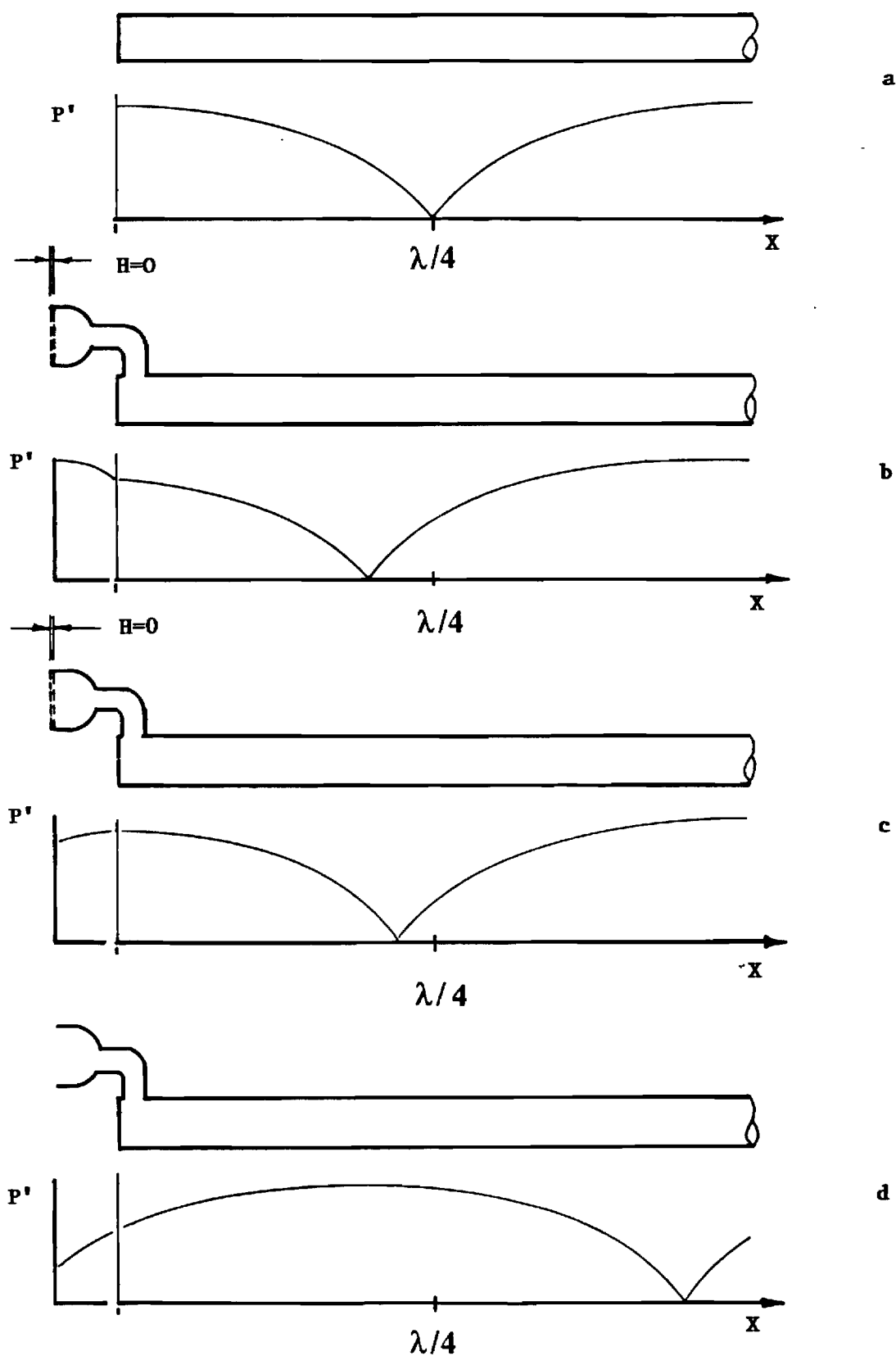


Fig. 40 Comparison of Standing Wave Pattern in the Impedance Tube Fitted with a) Hard Termination, b) Closed Air Valve, c) Open Valve and d) Valve Housing with Valve Plates Removed. The Actual Wave Pattern in the Valve Housing is More Complex Due to the Geometry of the Housing.

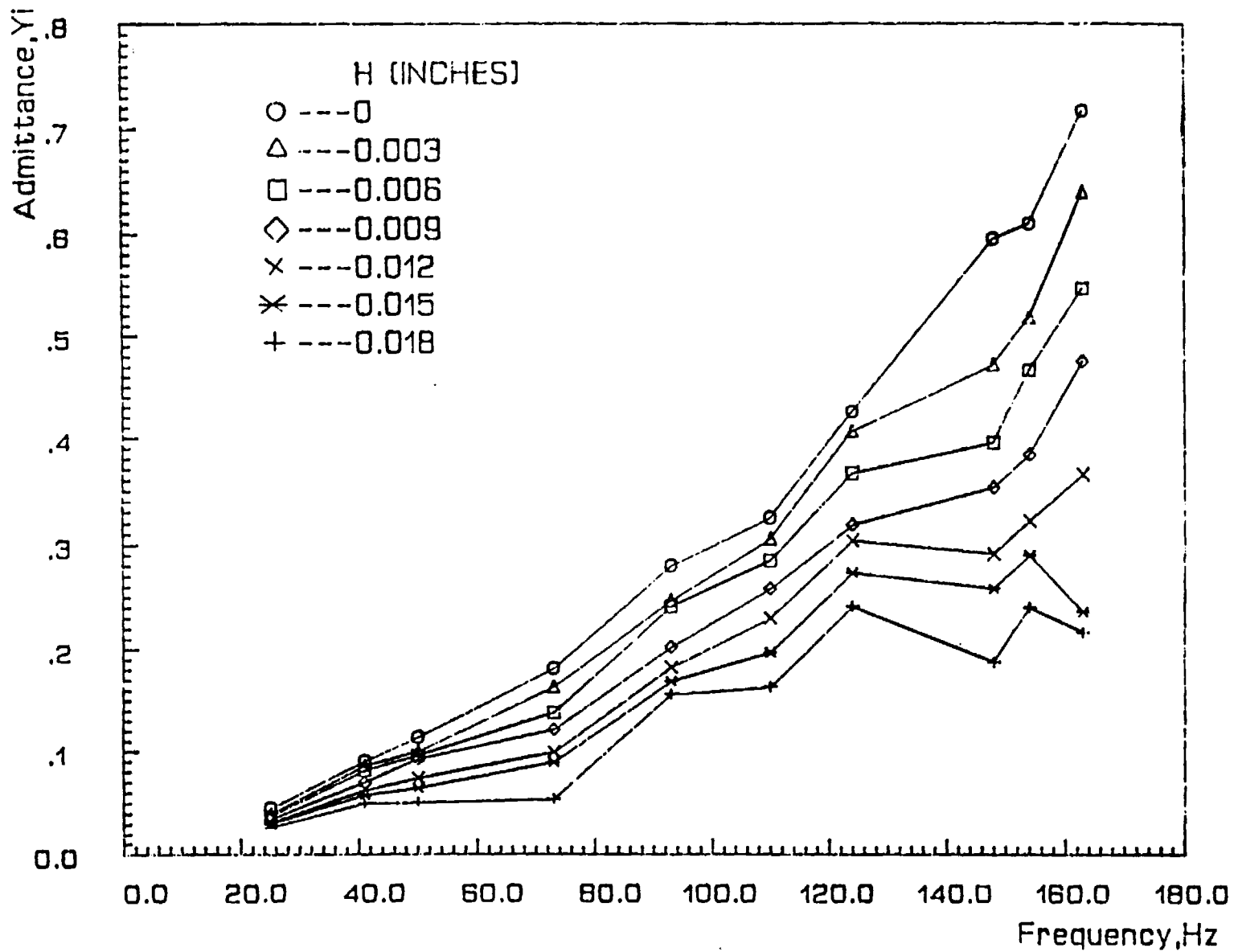


Fig. 41 Imaginary Part of the Admittance of the Mixing Chamber Assembly as a Function of Frequency for Different Air Valve Gap Settings (H).

Frequency = 38 Hz

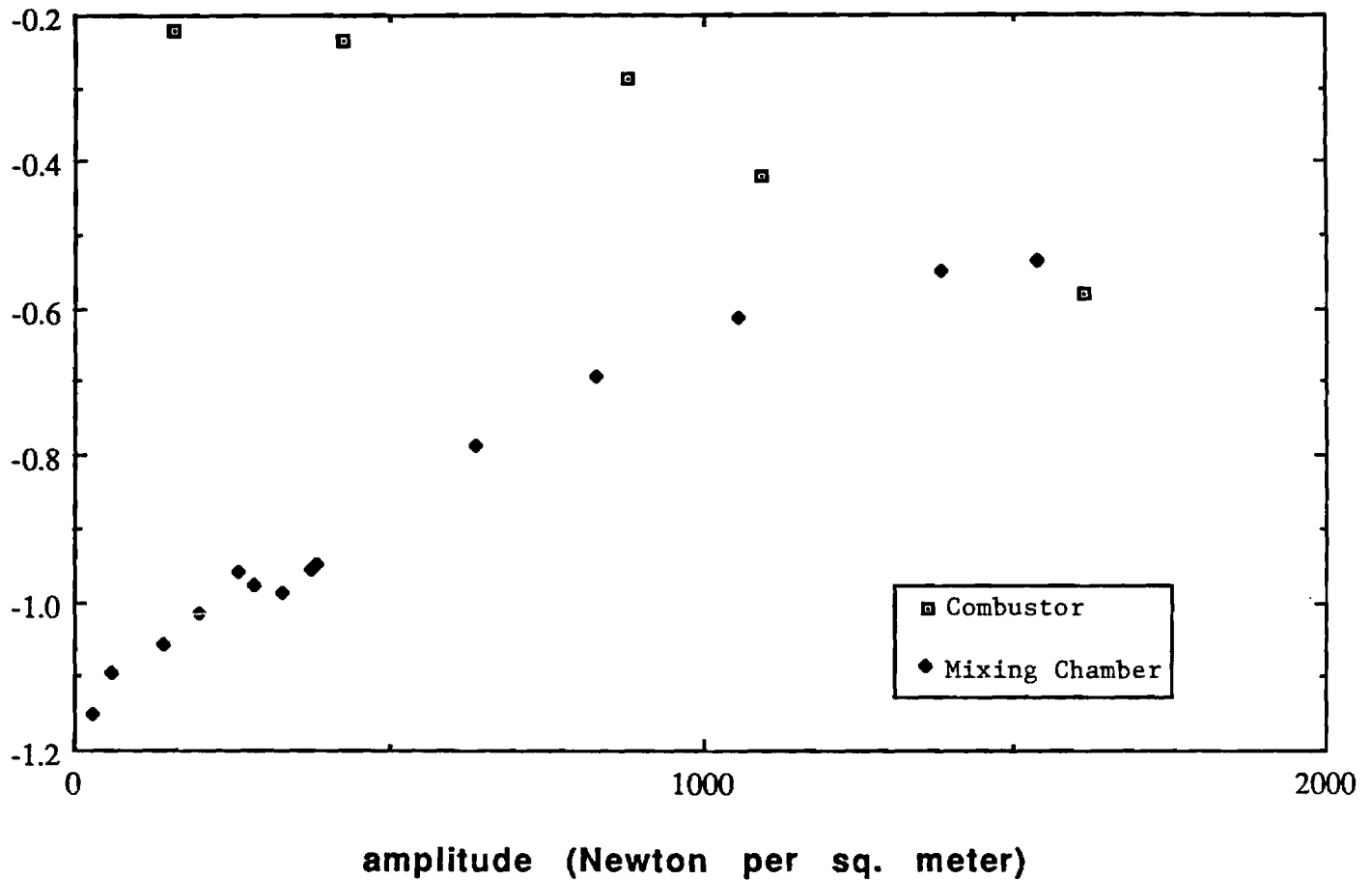


Fig. 42 Comparison of the Real Part of the Admittance as a Function of Pressure Amplitude for the Mixing Chamber Assembly only and for the Entire Helmholtz Combustor.

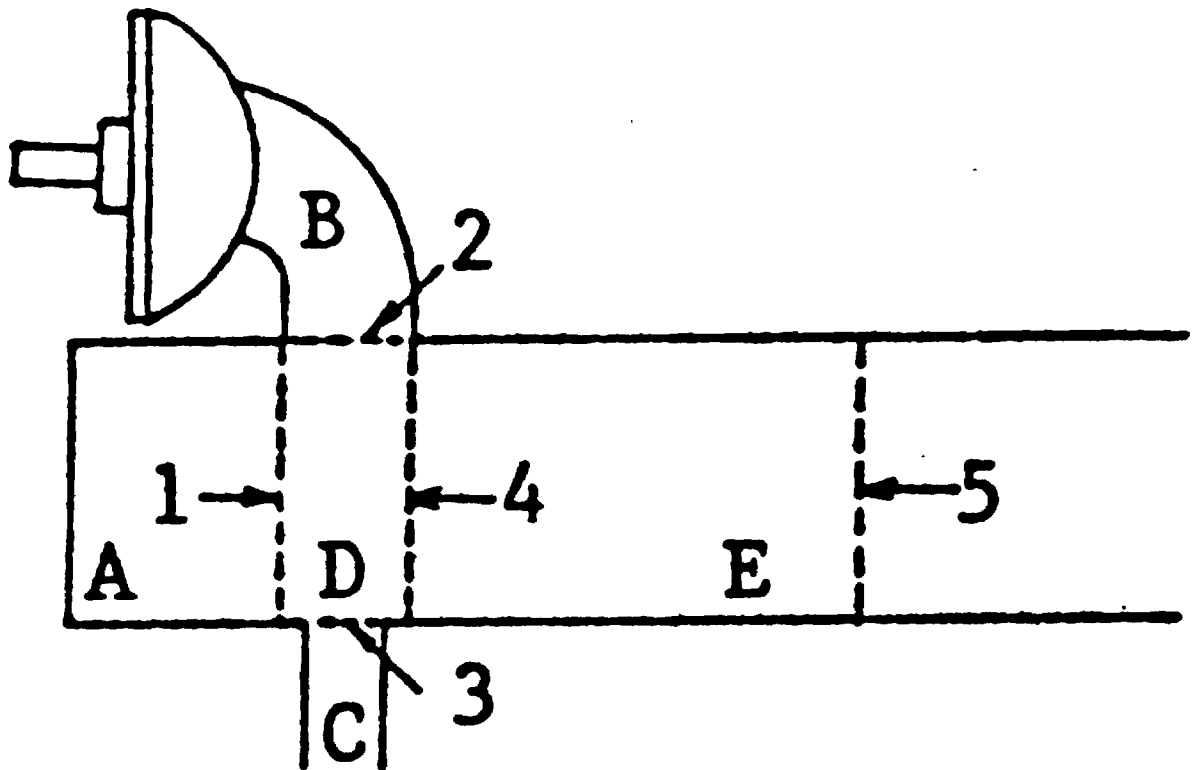


Fig. 43 Schematic Showing the Five Regions into which the Mixing Chamber Assembly has been Divided.

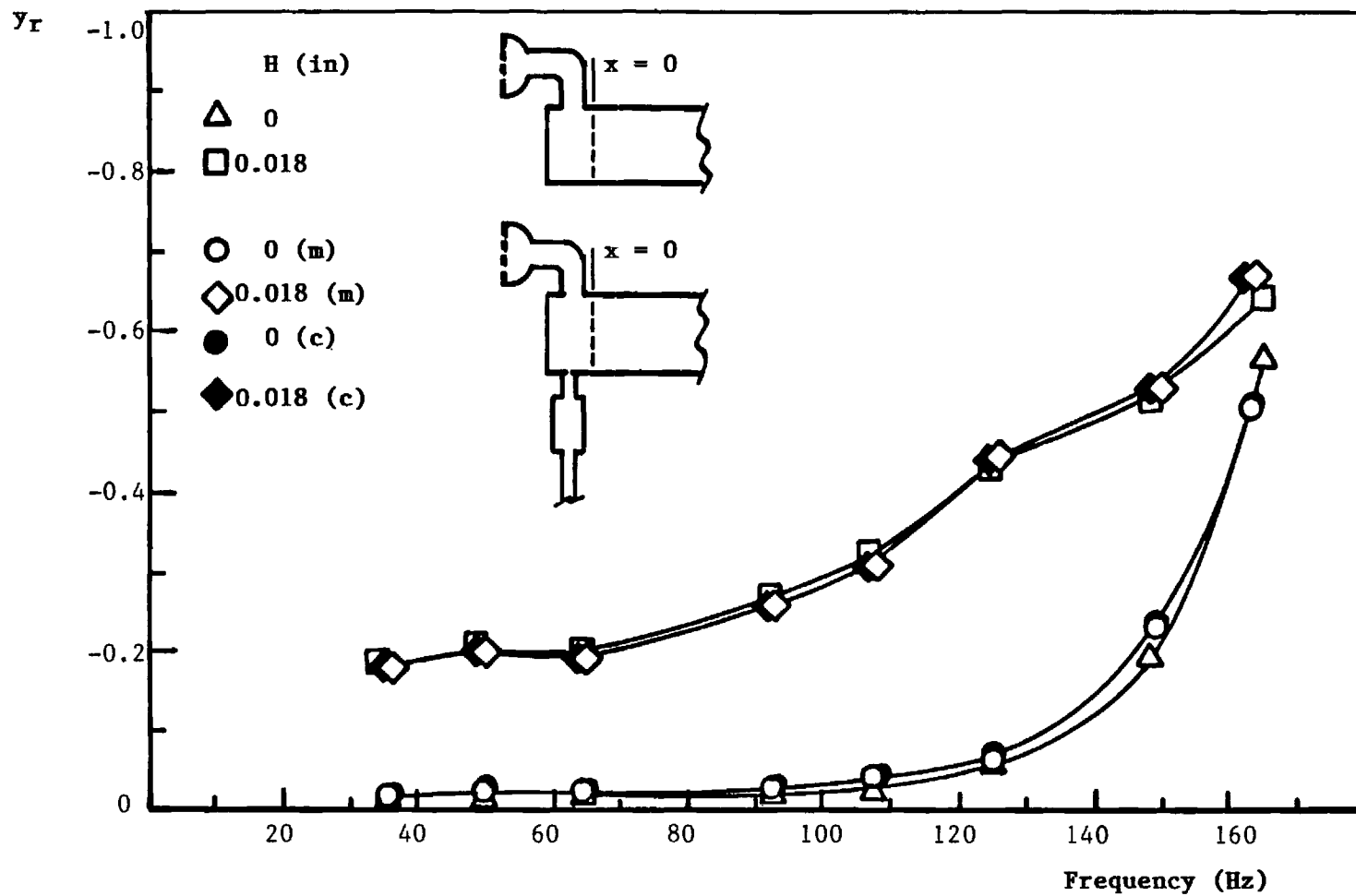


Fig. 44 Comparison between the Measured (m) and Calculated (c) Real Parts of the Admittance of the Mixing Chamber Assembly over a Range of Frequencies.

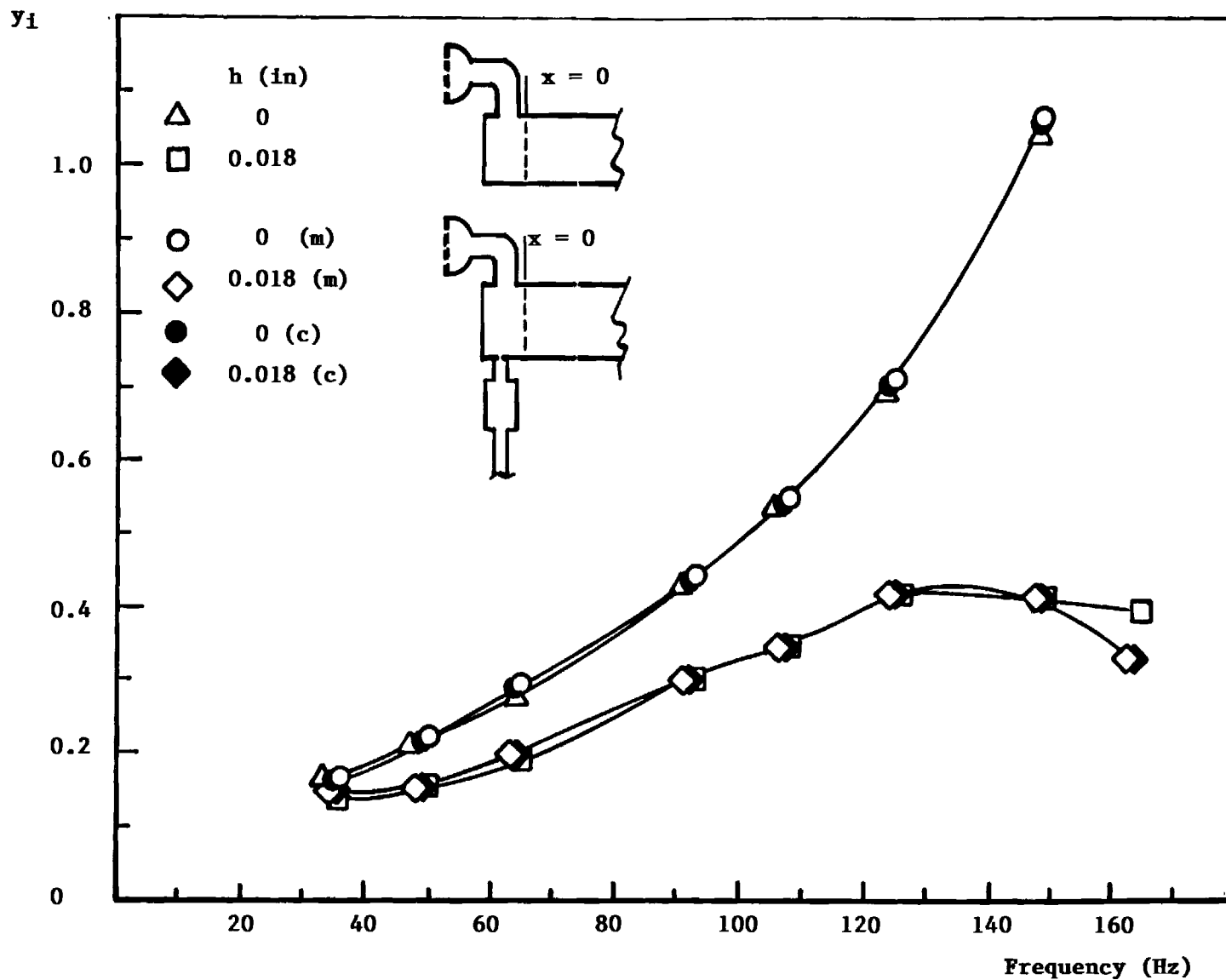
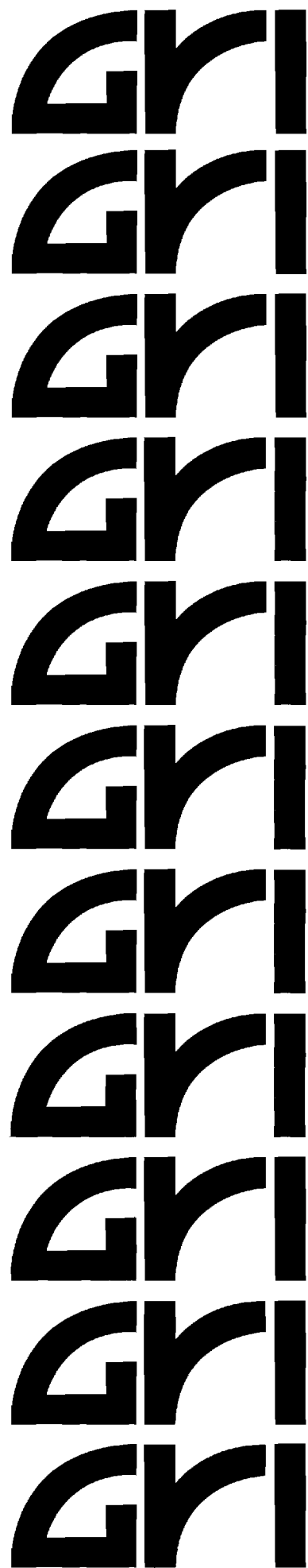


Fig. 45 Comparison between the Measured (m) and Calculated (c) Imaginary Parts of the Admittance of the Mixing Chamber Assembly over a Range of Frequencies.

**PULSATING BURNERS
CONTROLLING MECHANISMS AND PERFORMANCE**

**FINAL REPORT
(January 1, 1987 - June 30, 1991)**

**Gas Research Institute
8600 West Bryn Mawr Avenue
Chicago, Illinois 60631**



Pulsating Burners - Controlling Mechanisms and Performance

Final Report

January 1, 1987 - June 30, 1991

Prepared by

J.I. Jagoda, B.R. Daniel and B.T. Zinn

School of Aerospace Engineering

Georgia Institute of Technology

For

Gas Research Institute

Grant No. 5087-260-1466

GRI Project Managers

James A. Kezerle and Thomas R. Roose

Combustion

June 1991

GRI DISCLAIMER

LEGAL NOTICE: This report was prepared by the Georgia Institute of Technology as an account of work sponsored by the Gas Research Institute (GRI). Neither GRI, members of GRI, nor any person acting on behalf of either:

- a. Makes any warranty or representation, express or implied, with respect to the accuracy, completeness, or usefulness of the information contained in this report, or that the use of any apparatus, method, or process disclosed in this report may not infringe privately owned rights; or
- b. Assume any liability with respect to the use of, or for damages resulting from the use of, any information, apparatus, method, or process disclosed in this report.

REPORT DOCUMENTATION PAGE		1. REPORT NO. GRI-91/0105	2.	3. Recipient's Accession No.
4. Title and Subtitle "Pulsating Burners - Controlling Mechanism and Performance"			5. Report Date January 1991	
7. Author(s) J.I.Jagoda, B.R.Daniel and B.T.Zinn			6.	
9. Performing Organization Name and Address School of Aerospace Engineering Georgia Institute of Technology Atlanta, Georgia 30332			8. Performing Organization Rept. No. -	
			10. Project/Task/Work Unit No. E-16-601	
			11. Contract(C) or Grant(G) No. (C) 5087-260-1466 (G)	
12. Sponsoring Organization Name and Address Gas Research Institute 8600 West Bryn Mawr Avenue Chicago, IL 60631			13. Type of Report & Period Covered Final Jan.'87-June '91	
14.				
15. Supplementary Notes				
16. Abstract (Limit: 200 words) The objective of this study was to increase our understanding of the physical processes which control the mixing and heat release processes in valved, natural gas fired, pulse combustors. The effects of combustor geometry and heat transfer upon the performance of the pulse combustor were investigated. The flow and flame spread in the pulse combustor were visualized using high speed shadowgraphy and radical imaging, respectively. In addition, the flow field has been quantified using laser Doppler velocimetry. The resulting data were used to explain the dependence of the pulse combustor's performance upon the timing of the entry of the reactants and the complex interaction between the fuel and air jets. Furthermore, the reasons for the existence of lean and rich limits of operation were determined. Under a separate task, the acoustic characteristics of the various parts which make up a pulse combustor were determined using an impedance tube technique. Finally, an analytical scheme was developed which allows the calculation of the admittance of entire sections of the pulse combustor from measured admittances of its component parts.				
17. Document Analysis a. Descriptors Pulse Combustion				
b. Identifiers/Open-Ended Terms Performance, Flow Visualization, Reignition, Flame Spread, Limits of Operation, Admittance Measurements.				
c. COSATI Field/Group Combustion				
18. Availability Statement: Distribution Unlimited		19. Security Class (This Report) unclassified		21. No. of Pages
		20. Security Class (This Page) unclassified		22. Price

RESEARCH SUMMARY

Title: Pulsating Burners - Controlling Mechanisms and Performance

Contractor: Georgia Tech Research Corporation

Contract Number: 5087-260-1466

Reporting Period January 1987- June 1990, Final Report

Principle Investigators: B. T. Zinn, B. R. Daniel and J. I. Jagoda

Objective: The objective of this study was to gain further insights into the detailed physical mechanisms which control the mixing and heat release processes in pulse combustors. In addition, the acoustic damping characteristics of various components and subsystems of the pulse combustor were to be determined over a range of operating conditions.

Technical Perspective: Natural gas fired pulse combustors have been on the market for a number of years. Nevertheless, their controlling mechanisms are still not sufficiently well understood to permit the design

of pulse combustors for different applications without resorting to costly trial and error development efforts. Proper operation of pulse combustors requires that the timing of the mixing, cycle to cycle reignition and flame spread processes produce oscillatory heat release in phase with the pressure oscillations. In addition, the thus generated driving must be sufficient to overcome the damping by the pulse combustor. To develop a rational design procedure for pulse combustors, it is necessary that the various processes responsible for energy addition to and removal from the pulsations be understood. Furthermore, data describing the acoustic properties of various pulse combustor components under different operating conditions are needed. Finally, the interaction between the acoustic characteristics of the various combustor components and the fundamental fluid mechanical, heat transfer and combustion processes must be understood.

Technical Approach: In order to elucidate the mechanisms which control the operation of a natural gas fired, Helmholtz type, pulse combustor and to determine the acoustic characteristics of different components and

subsystems which make up this pulse combustor, the following tasks were performed:

- 1) The flow field characteristics, mixing and heat release distributions in the pulse combustor were investigated using LDV, Schlieren, mixing visualization and radical radiation imaging.
- 2) The acoustic characteristics of various components and subsystems which make up the pulse combustor were measured using the impedance tube technique.

Results:

A natural gas fired, valved, Helmholtz type, pulse combustor based upon an AGA design was studied. High speed shadowgraphy showed that the injection of the fuel jet leads the entry of the air jet by one quarter of a cycle. The latter creates large axial and transverse vortices in the mixing chamber. Comparison of the flow field with spatially and time resolved heat release measurements indicated that the order in which the reactants enter the combustor is critical to the spread of the combustion process through the mixing chamber. While the fuel jet begins to react with air left over from the previous cycle as soon as it enters the mixing chamber, the main ignition of the new fuel occurs near the combustor wall opposite of the fuel port. Combustion is then convected by the leading edge vortex of the air jet through the remainder of

the mixing chamber. It is this complex interaction between the fuel and air jets which stabilizes the combustion process in the mixing chamber. An increase in the combustor temperature by 30°K (54°F) was found to lower the lean limit of operation of the pulse combustor from a fuel air ratio (ϕ) of 0.64 to 0.55. However, the period of pulsations had to be extended or combustion air had to be supplied under pressure to extend its rich limit from $\phi = 1$ to 1.3. This rich limit occurs near stoichiometric conditions because no air is left over from the previous cycle. The combustion process is then confined to the time interval between the entry of the new air jet and the quenching of the reaction by the combustion products returning to the mixing chamber. For the standard AGA combustor this time is too short to permit sufficient heat release to drive the pressure oscillations. Further investigation of the importance of the timing between the heat release and the pressure oscillations revealed that at low operating frequencies (less than 25 Hz) the combustion process can excite higher pressure harmonics in the combustor unless the timing of the heat release is delayed. Furthermore, reduction of heat transfer to the combustor walls was found to significantly reduce the operating frequency of the device. The

results of ensemble averaged mean velocity and turbulence intensity measurements are used to qualitatively describe the complex, turbulent flow field in the mixing chamber at various instants during the cycle. These measurements are currently being completed by the graduate student as part of his Ph.D. thesis work. Under a separate task, an impedance tube technique was used to measure the acoustic characteristics (i.e., the admittance) of the fuel and air valves and of the mixing chamber fitted with both valves. These measurements indicated that, while the fuel valve behaves acoustically like a hard termination, the damping by the air valve increases with increasing frequency and valve opening and decreases with increasing pressure amplitude. Comparisons of the admittance measurements of the mixing chamber with those of the entire combustor showed that the damping by the Helmholtz volume formed by the combustion chamber overshadows the effect of the damping by the air flapper valve for the pulse combustor configuration under investigation. In addition to these measurements, an analytical scheme was developed which permits the determination of the admittance of the entire mixing chamber - valve assembly from the measured admittances of its component parts.

In summary:

- The detailed interactions between the flow field, the reignition and the flame spread during the cycle were determined
- The importance of the relative timing between the heat release and pressure fluctuations was investigated.
- The reasons for the existence of lean and rich operating limits for the Helmholtz type pulse combustor were established.
- The ensemble averaged velocity and turbulence intensity fields were quantified using laser Doppler velocimetry.
- The acoustic behavior of the pulse combustor and its component parts were determined.
- An analytic technique for predicting the acoustic damping by different combustor configurations from the acoustic characteristic of its component parts was developed.

Project Implications: This research has obtained important results and insights pertaining to pulse combustion. The knowledge gained in this contract is important to moving pulse combustion from an "art" to a science. The results explain the dependence of the pulse combustor's performance upon the timing of the reactant entry and the interaction among the fuel and air jets. Important fundamental data

characterizing the acoustics of pulse combustor components was obtained. These results will be used in models which are underway to describe pulse combustion. Additional pulse combustion research is being done at the Georgia Institute of Technology and at Forbes Energy Engineering, Inc. as part of the work scope for GRI's Pulse Combustion Engineering Research Laboratories. Pulse combustion continues to offer the potential for high efficiency with low NO_x emissions.

Thomas R. Roose

Principal Scientist, Engineering Sciences

Physical Sciences Department

TABLE OF CONTENTS

Title	Page No.
Introduction	1
Objectives	2
Program Plan	3
Technical Progress and Results	5
Task I	5
Performance Evaluation	5
Effect of Combustor Geometry	6
Effect of Temperature upon Performance	7
Effect of Heat release Duration and Timing	8
Shadow Visualization	10
Mixing Visualization	11
Spectroscopy	12
Laser Doppler Velocimetry	16
Rich Limit of Pulse Combustor Operation	20
Task II	24
Publications	31
Conclusions	32
References	

LIST OF FIGURES

Fig. #	Title	Page
1.	Schematic of the Helmholtz Type Pulse Combustor.	39
2.	Schematic of the Mixing Chamber showing the Fuel and Air Flapper Valves.	40
3.	Operational Frequency of the a) Helmholtz and b) Schmidt Combustors as a Function of Tailpipe or Combustor Length Respectively.	41
4.	Schematic of Relative Timing of Heat Release (Q') and Pressure (P') Oscillations for a) High Frequencies, b) Low Frequencies with Standard Fuel Injection and c) Low Frequencies with Displaced Fuel Injection Leading to Delayed Heat Release.	42
5.	Standing Wave Pattern along Schmidt Combustor a) with Air Valve and b) without Air Valve.	43
6.	Schematic of the Schlieren Set-up along the Combustor Axis.	44
7.	Schematic of Selected Frames from the High Speed Shadow Movie Showing the Flow Field at Different Instances during the Cycle as Seen along the Combustor Axis.	45
8.	Schematic of the Schlieren Set-up normal to the Combustor Axis.	46
9.	Comparison of the Flow Field and the Heat Release Distribution as Seen along the Combustor Axis at	47

Four Instants during the Cycle.

10.	Contour Plot of Phase Angle by which the Heat Release Oscillations Lead the Pressure Oscillations.	48
11.	Locations at which the Laser Doppler Velocimeter Results Shown in Figures 12 through 29 were Obtained. Each Location is Labeled (m,n).	49
12.	Variation of the Vertical Mean Velocity During a Cycle for Locations along the Line $m = 1$. The Top Plot includes the Pressure Trace for Reference.	50
13.	Variation of the Vertical Mean Velocity During a Cycle for Locations along the Line $m = 2$. The Top Plot includes the Pressure Trace for Reference.	51
14.	Variation of the Vertical Mean Velocity During a Cycle for Locations along the Line $m = 3$. The Top Plot includes the Pressure Trace for Reference.	52
15.	Variation of the Axial Mean Velocity During a Cycle for Locations along the Line $m = 1$. The Top Plot includes the Pressure Trace for Reference.	53
16.	Variation of the Axial Mean Velocity During a Cycle for Locations along the Line $m = 2$. The Top Plot includes the Pressure Trace for Reference.	54
17.	Variation of the Axial Mean Velocity During a Cycle for Locations along the Line $m = 3$. The Top Plot includes the Pressure Trace for Reference.	55
18.	Variation of the Vertical Turbulence Intensity During a Cycle for Locations along the Line $m = 1$. The Top Plot includes the Pressure Trace for Reference.	56

19.	Variation of the Vertical Turbulence Intensity During a Cycle for Locations along the Line $m = 2$. The Top Plot includes the Pressure Trace for Reference.	57
20.	Variation of the Vertical Turbulence Intensity During a Cycle for Locations along the Line $m = 3$. The Top Plot includes the Pressure Trace for Reference.	58
21.	Variation of the Axial Turbulence Intensity During a Cycle for Locations along the Line $m = 1$. The Top Plot includes the Pressure Trace for Reference.	59
22.	Variation of the Axial Turbulence Intensity During a Cycle for Locations along the Line $m = 2$. The Top Plot includes the Pressure Trace for Reference.	60
23.	Variation of the Vertical Turbulence Intensity During a Cycle for Locations along the Line $m = 3$. The Top Plot includes the Pressure Trace for Reference.	61
24.	Three Dimensional Plot of Vertical Mean Velocities during a Cycle for Locations along the Line $m = 1$.	62
25.	Three Dimensional Plot of Vertical Mean Velocities during a Cycle for Locations along the Line $m = 2$.	63
26.	Three Dimensional Plot of Vertical Mean Velocities during a Cycle for Locations along the Line $m = 3$.	64
27.	Three Dimensional Plot of Axial Mean Velocities during a Cycle for Locations along the Line $m = 1$.	65
28.	Three Dimensional Plot of Axial Mean Velocities during a Cycle for Locations along the Line $m = 2$.	66
29.	Three Dimensional Plot of Axial Mean Velocities during a Cycle for Locations along the Line $m = 3$.	67

30.	Rayleigh Efficiency as a Function of Equivalence Ratio for the Combustor Fitted with the Standard and Long Tailpipes.	68
31.	Pressure and Heat Release Fluctuations as a Function of Equivalence Ratio for the Combustor Fitted with the Standard and Long Tailpipes.	69
32.	Phase Angle by which the Heat Release Leads the Pressure as a function of Equivalence Ratio for the Combustor Fitted with the Standard and Long Tailpipes.	70
33.	Normalized Pressure (P') Cycle Showing the Timing of the Heat Release Oscillations (Q') for a) Lean and b) Rich Limits of Operation; Fuel Enters at "F", Air Enters at "A", Backflow into the Mixing Chamber Starts at "R"; the "X"s Denote the Instants of Reignition of the Fresh Fuel Charges.	71
34.	Schematic of the Impedance Tube Experiment.	72
35.	Wave Form of the Incident (I), Reflected (R) and Total (T) Standing Wave for a) Hard Termination and b) Termination with Finite Admittance.	73
36.	Sensitivity of the Real Part of the Admittance to the Measured Pressure Difference between the Pressure Maximum and the Pressure Minimum.	74
37.	Real Part of the Admittance as a Function of Frequency for Various Impedance Tube Terminations. H Denotes the Valve Gap Setting in Inches.	75
38.	Real Part of the Admittance of the Mixing Chamber Assembly as a Function of Frequency for Different	76

Air Valve Gap Settings (H).

- | | | |
|-----|--|----|
| 39. | Imaginary Part of the Admittance as a Function of Frequency for Various Impedance Tube Terminations.
H Denotes the Valve Gap Setting in Inches. | 77 |
| 40. | Comparison of Standing Wave Pattern in the impedance Tube Fitted with a) Hard Termination, b) Closed Air Valve, c) Open Valve and d) Valve Housing with Valve Plates Removed. The Actual Wave Pattern in the Valve Housing is more Complex due to the Geometry of the Housing. | 78 |
| 41. | Imaginary Part of the Admittance of the Mixing Chamber Assembly as a Function of Frequency for Different Air Valve Gap Settings (H). | 79 |
| 42. | Comparison of the Real Part of the Admittance as a Function of Pressure Amplitude for the the Mixing Chamber Assembly only and for the Entire Helmholtz Combustor. | 80 |
| 43. | Schematic Showing the Five Regions into which the Mixing Chamber Assembly has been Divided. | 81 |
| 44. | Comparison between the Measured (m) and Calculated (c) Real Parts of the Admittance of the Mixing Chamber Assembly over a Range of Frequencies. | 82 |
| 45. | Comparison between the Measured (m) and Calculated (c) Imaginary Parts of the Admittance of the Mixing Chamber Assembly over a Range of Frequencies. | 83 |

INTRODUCTION

A recent increase in interest in pulse combustors has been driven by such advantages as high combustion and thermal efficiencies^{1,2}, excellent heat transfer characteristics^{3,4} and low CO, NO_x⁵ and soot emissions. Development of new pulse combustor applications has been hampered, however, by a lack of adequate understanding of the fundamental processes which control the operation of these devices. It was the purpose of this program to shed new light upon the mechanisms which control the operation of pulse combustors and to provide the designer with additional insight which would help him in the development of new and the scaling of existing pulse combustion devices.

The natural gas fired, valved, Helmholtz type, pulse combustor whose operating characteristics were investigated in this program is based upon an AGA design⁶. It is shown schematically in Fig. 1. The combustor consists of cylindrical mixing and combustion chambers, a tailpipe, a cylindrical decoupling chamber and a short vent pipe. Natural gas and air enter the combustor at right angle to each other through separate flapper valves attached to the curved side wall of the mixing chamber. During start up, the reactants are allowed to mix and are ignited using a spark plug. As the natural gas burns (a process which has previously been shown to take place primarily in the mixing chamber) the pressure in the combustor rises. This closes the flapper valves which prevents further reactants from entering the mixing chamber. This pressure rise also pushes the combustion products out through the tail pipe. The momentum

of the expelled exhaust gases causes the pressure in the mixing chamber to drop which reopens the flapper valves. New reactants now enter the combustor where they mix and are ignited by burning pockets of gas left over from the previous cycle. The cycle now repeats itself. Thus, pulse combustion operation can be maintained indefinitely without the use of the spark plug.

The gap in the fuel flapper valve is fixed while that in the air valve can be adjusted using a micrometer, see Fig. 2. The overall equivalence ratio in the pulse combustor is, therefore, varied by adjusting the air flapper valve setting which changes the air flow rate.

OBJECTIVES

It was the objective of this study to gain further insight into the fundamental processes responsible for the operation of pulse combustors in general and natural gas fired, valved, Helmholtz type, pulse combustors in particular. Emphasis was placed upon obtaining practical information which will permit designers to develop new and/or larger scale pulse combustors without resorting to costly trial and error based development efforts.

More specifically, the goal was to determine the effect of the combustor geometry and temperature upon its performance. In addition, the velocity, mixing and heat release distributions in the mixing and combustion chambers were measured both qualitatively and quantitatively and used to establish the nature of the interaction between

the combustion process and the acoustics of the combustor. This would lead to a physical explanation of the operating characteristics of the natural gas fired, valved, Helmholtz type, pulse combustor. In addition, the admittance of various components and subsystems which make up the pulse combustor were to be determined under a variety of operating conditions.

PROGRAM PLAN

The program is divided into two major tasks as outlined below:

Task I: Investigation of the Oscillatory Flow and Heat Release Fields and their Interaction in the Pulse Combustor

- A. Performance Evaluation A limited number of measurements were carried out in modified, gas fired, valved, Helmholtz and Schmidt type pulse combustors in order to complement the performance studies carried out under a previous contract.
- B. Shadow Visualization High speed shadowgraph cinematography was carried out parallel and normal to the axis of the combustor. These shadowgrams were then correlated in order to obtain a complete picture of the three-dimensional flow field in the pulse combustor.

- C. Mixing Visualization An attempt was made to visualize mixing patterns photographically by heavily seeding one of the reactant flows and illuminating the combustor using an expanded laser sheet.
- D. Spectroscopy Local and global heat release in the pulse combustor were determined by measuring the radical radiation emitted from the combustor. Instantaneous readings were ensemble averaged using the pressure signal as a clock. Planar spectroscopy using an intensified CCD camera resulted in local heat release measurements with excellent spatial and temporal resolution.
- E. Laser Doppler Velocimetry Velocities were measured in the periodically varying, turbulent flow field at selected locations in the combustor. These velocities were then ensemble averaged which permitted the determination of mean velocities and turbulence intensities at various locations, at each instant during the cycle.

All Task I measurements were carried out in a pulse combustor whose mixing and combustion chambers were fitted with flat windows. The results from the different investigations outlined above were then correlated with each other and with the phase in the cycle at which they were obtained using the pressure oscillation as a clock. Such a coordination between the pressure, flow field and heat release measurements was

necessary to shed further light upon the fundamental processes which control the operation of the pulse combustor.

Task II: Admittance Measurements of Pulse Combustor Components

The acoustic admittances of various components and subsystems which make up a natural gas fired, valved, Helmholtz type, pulse combustor were measured using an impedance tube technique. These measurements yielded information on the frequency and amplitude dependances of the damping caused by the various pulse combustor subsystems. In addition, a methodology was developed which permits the designer to predict the damping in the pulse combustor from the acoustic properties of its component parts.

TECHNICAL PROGRESS AND RESULTS

Task I

Performance Evaluation:

This part of the study dealt with the investigation of the dependence of the performance of the pulse combustor upon the combustor geometry, the temperature in the combustion chamber and the relative duration and phase between the heat release and pressure oscillations.

Effect of the Combustor Geometry. The AGA based pulse combustor design⁶ consists of a small diameter mixing chamber attached to a larger diameter combustion chamber, see Fig. 1 . This introduces a

step at the interface between the mixing and combustion chambers which has long been assumed to be critical for stabilizing the combustion process. This hypothesis was tested by constructing a pulse combustor with the same combustion chamber volume but without the step; i.e., a combustor whose mixing and combustion chamber diameters are equal. Tests revealed that the performance characteristics of the stepless pulse combustor are identical to those of the standard combustor. The combustion process in this type of pulse combustor is, therefore, not stabilized by the flow behind the backward facing step but by the complex interaction between the fuel and air jets in the mixing chamber.

Investigations under a previous contract⁷ have shown that the Helmholtz type pulse combustor fitted with a standard tailpipe (i.e., 183 cm long) operates well for equivalence ratios between 0.61 and 1.03. When the tailpipe of the Helmholtz combustor was extended to 366 cm the rich limit of operation increased to an equivalence ratio 1.43. On the other hand, when the tailpipe was shortened to 69 cm the lean limit of operation was lowered to an equivalence ratio of 0.56. For tailpipes shorter than 69 cm the air supply had to be significantly pressurized in order to maintain the pulsation. If the pressurization was reduced the combustor switched from a pulsating to a non-pulsating mode of operation. The reasons for the existence of the limits of operation mentioned above will be addressed later.

Effect of Temperature upon Combustor Performance. The temperature in the pulse combustor was increased by insulating its

mixing and combustion chambers either externally or internally. When the combustor was externally insulated the temperature increased by approximately 30 °K (54 °F). Nevertheless, the kinetics of the combustion process were noticeably affected. For example, the CO level in the exhaust increased by 15%. However, the amplitude of the pressure pulsations remained unchanged. More importantly, the addition of thermal insulation lowered the lean limit of operation from an equivalence ratio of 0.64 to 0.55. The rich limit of operation was not affected by the increase in temperature. This suggests that the lean limit of operation of the pulse combustor is, at least in part, kinetically controlled. A more detailed explanation of the reason for the existence of the rich limit will be given later.

The temperature in the pulse combustor was increased by an additional 50 °K (90 °F) when the combustor was internally insulated using high temperature ceramic padding. However, the acoustic losses caused by this insulating material significantly decreased the amplitude of the pulsations. Since the mass flow rates of the reactants through the flapper valves depend upon the pressure amplitudes, the operating range of the pulse combustor was decreased. In some cases it was necessary to increase the gap in the air flapper valve and/or to pressurize the air supply to maintain the pulsations. In addition, it was noted that the internal insulation decreased the frequency of the pulsations. An analytical model currently being developed under a new program does, indeed, predict a dependence of the frequency of pulsation upon the rate of heat transfer to the walls of the combustor. More details of the effect of temperature upon the operating characteristics of the pulse combustor are given in Ref. 8.

Effect of Heat Release Duration and Timing. The effect of the relative timing between the heat release and pressure oscillations were investigated by varying the duration of the pressure cycle between 12 msec. and 67 msec. Both the Helmholtz and a Schmidt tube pulse combustors were used in this investigation. The Schmidt (or quarter wave) pulse combustor used the same fuel and air injection system as the Helmholtz pulse combustor. However, the mixing chamber, the combustion chamber and the tail pipe were replaced by a single, constant diameter pipe.

Tests showed that lengthening of the tailpipe of the Helmholtz combustor from 60 cm to 550 cm (24 in. to 217 in.) caused the pulsating frequency to decrease from 80 Hz to 24 Hz. At that point, the operating frequency of the combustor "jumped" to the tailpipe's first harmonic, i.e., 48 Hz, see Fig. 3a. If the tailpipe was further lengthened to 660 cm (260 in.), the frequency, once again, decreased from 48 Hz to 45 Hz. A similar trend was observed when the Schmidt pulse combustor was lengthened from 200 cm to 800 cm (79 in. to 315 in.) At 520 cm (205 in.) the frequency jumped from 20 Hz to 60 Hz, as shown in Fig. 3b. It should be noted that a "jump" to the higher harmonic of the Helmholtz combustor's tailpipe and of the Schmidt pulse combustor causes a doubling and tripling of the frequencies, respectively. However, if the mixing of the reactants and, therefore, the heat release process was delayed with respect to the pressure oscillations this frequency jump could be avoided. Such a delay could be introduced by moving the fuel injection port 7.5 cm (3 in.) downstream of its normal location.

The above phenomena is explained using Rayleigh's criterion which states that an oscillating heat release will drive pressure fluctuations if both are in phase. The timing and duration of the heat release due to the combustion process are determined by the injection of the reactants and their mixing. At relatively high frequencies, above 25 Hz, (i.e., short cycle durations) the heat release is primarily in phase with the fundamental mode of the combustor, as is shown schematically in Fig. 4a. If the frequency of pulsations is decreased below 20 Hz the cycle duration lengthens. The heat release is then confined to the early part of the fundamental pressure fluctuation (see Fig. 4b). However, the same figure also shows that the phase angle between the heat release and the first harmonic of the pressure oscillation is now closer to zero. Therefore, it is this harmonic that is excited. Finally, if the combustion process is delayed the phase angle between the heat release and the fundamental pressure oscillation is, once again, close to zero, see Fig. 4c. This causes the fundamental mode to be excited. This work is described in more detail in Refs. 8 and 9.

Finally, pressure amplitude measurements along the axis of the Schmidt pulse combustor indicated that as long as the air valve is in place this pulse combustor behaves like a true quarter wave tube even when the flapper valve gap is fully opened, see Fig. 5. However, once the air valve is completely removed the standing wave pattern is closer to that characteristic of a Rijke tube¹⁰. In that configuration the combustor is open at both ends, at the valve housing and at the downstream end, both of which are pressure nodes. Combustion takes place at approximately

one quarter of the combustor length from the air inlet. Since in the Rijke tube the length of the combustor represents one half of the acoustic wavelength, compared with one quarter of the wavelength in the Schmidt tube, the frequency of pulsations increases once the air valve is removed. This is discussed in more detail in Ref. 9.

Shadow Visualization

During a previous contract⁷, the flow in the mixing chamber was visualized using high speed shadowgraphy through flat quartz walls at the end of the mixing chamber and the quartz transition between the combustion chamber and the tailpipe, see Fig 6. Briefly, a fast moving, highly turbulent fuel jet was seen to enter the mixing chamber followed by a wider, slower moving air jet, see Fig. 7. (Precise velocities will be discussed in the section on laser Doppler velocimetry.) The air jet impinges upon the fuel jet at approximately the same instant at which the latter reaches the mixing chamber wall opposite the fuel port. The leading edge vortex of the air jet then rapidly "scoops up" the fuel and sets up two, counter rotating vortices in the mixing chamber. Combustion occurs under conditions of intense, small scale turbulence and is nearly completed when the fuel for the next cycle enters the mixing chamber. Some of these shadow visualizations were repeated under different operating conditions during the present contract period. These tests indicated that the entry of the air jet is delayed as the fuel - air ratio in the combustor is increased.

In addition, the axial flow field in the pulse combustor was visualized using high speed shadow photography through the flat quartz windows in

the curved side walls of the mixing and combustion chambers, see Fig. 8. Particular attention was focused on the flow field in the mixing chamber and in the vicinity of the combustion chamber - tail pipe interface.

Since the air and fuel ports are located off axis, the flow field is not cylindrically symmetric. Once again, the high speed shadowgraphy showed that the fuel jet enters the mixing chamber shortly after the pressure there has passed through its maximum. Just before the pressure minimum is reached the air jet enters the mixing chamber. The addition of this air into the combustor increases the axial flow velocities further downstream in the mixing chamber. A little later, during the combustion phase of the cycle, a large, axial recirculation region forms in the mixing chamber. As the pressure maximum is reached the flow becomes axial again. Shortly thereafter, the new fuel jet enters and the cycle repeats itself.

High speed shadowgraphy was also carried out at the downstream end of the combustion chamber where the combustor connects with the tail pipe. As the pressure in the combustor decreases, combustion products from the tail pipe are seen to flow back into the combustion chamber. This backflow penetrates a distance of only two to three inches back into the combustor. As the acoustic pressure begins to rise again the flow reverses and reenters the tail pipe.

Mixing Visualization

Attempts were made to visualize the mixing process between the fuel and air as they enter the mixing chamber. For this purpose, the air jet

was heavily seeded with micron sized titanium dioxide particles while the fuel jet was left unseeded. As the reactants entered the mixing chamber, slices through this chamber were illuminated using vertical sheets of light produced by expanding the beam from a five watt argon ion laser using a cylindrical lens. The resulting light scattered by the particles in the flow was then recorded using a high speed camera capable of framing rates of up to 11,000 frames per second.

Unfortunately, the particle streak images obtained were not very clear. In spite of mirror generated, multiple traverses by the laser sheet through the mixing chamber not enough light was scattered by the particles to mark the film at framing rates above 2,500 frames per second. At these framing rates it was difficult to freeze the fast moving flow. In addition, seed particles remaining in the mixing chamber from previous cycles tended to obscure the details of the mixing flow field of the newly entering reactants. It was, therefore, decided to abandon this part of the investigation, at least until a more powerful pulsed laser, such as a copper vapor becomes available at this laboratory.

Spectroscopy

This investigation makes use of the fact that the intensity of spontaneously emitted CH, CC or OH radiation has been shown to be a measure of the local reaction rate¹¹. Under a previous contract⁷ the temporal oscillations of the overall reaction rate in the combustor were compared with those of the pressure. It was shown that the global radiation from the combustor fluctuates with the same frequency as the combustor pressure. The heat release fluctuations lead those of the

pressure by a phase angle which decreases as the equivalence ratio in the combustor is increased. As predicted by Rayleigh's criterion¹², this leads to an increase in sound pressure level in the combustor when the equivalence ratio is increased. At the same time it was shown that the combustion process never stops entirely during the cycle.

Under the present contract these experiments were extended to cover spatially as well as temporally resolved radiation measurements. A newly acquired intensified imaging system was used in these experiments. The radiation from the combustor is allowed to pass through a quartz window in the combustor wall before being focused through an interference filter onto an image intensifier. The intensifier is connected via an optical fiber bundle to the face plate of an 128 x 128 pixel CCD array. The array is read by an Omnicomp frame grabber and the data are transferred to the memory of a MicroVAX II workstation. The workstation is equipped with a 200 Mbyte disk and a tape drive. The image intensifier can be gated which results in exposure times down to 50 nanoseconds, faster than necessary to freeze the fast, highly turbulent flow in the combustor. Images can be read and transferred at a rate of 200 frames per second from the array to the computer. In addition, up to four channels of scalars can be recorded simultaneously with the images. In these studies, the acoustic pressure signal was recorded and used to identify the instant during the cycle at which the image was obtained.

Once the images have been obtained they are manipulated using a wide range of software. Images are sorted, added, subtracted and averaged, contrasts are enhanced and contour maps are plotted using

false colors. Furthermore, the intensities recorded by selected, individual pixels during consecutive frames are plotted versus time. The frequency of any oscillations in these signals are determined by Fourier analysis and the phase angle between the fluctuations in the pixel intensities and the pressure signal are calculated. This allows the determination of the local driving of the pulsations by the combustion process using Rayleigh's criterion.

Local radical radiation and, therefore, heat release rates in the combustor were measured by imaging CC radiation through the flat quartz window at the upstream end of the mixing chamber. Images obtained at the same instants during consecutive cycles indicate that while the overall features of the flame shape are very similar at given instants during the cycle, the precise path over which the flame has spread varies somewhat from cycle to cycle. Figure 9 shows four frames which indicate the locations of the ignition and flame spread during one cycle in the pulse combustor. Each "frame" actually represents the average of 128 separate images obtained at the same phase during different cycles. The mechanism of flame spread is best illustrated by comparing the instantaneous flow fields and heat release distributions in Fig. 9. Early in the cycle (Fig. 9a), as the fuel jet enters the mixing chamber, it begins to react weakly with the air left over from the previous cycle. Main ignition of the new fuel occurs at the time and location where the fuel jet impinges upon the opposite wall, as shown in Fig. 9b. At that instant the new air jet has just reached the center of the mixing chamber. Shortly thereafter, the upper part of the leading mushroom vortex of the air jet entrains the reacting fuel which intensifies the combustion process and

spreads it throughout the upper part of the mixing chamber(Fig. 9c). Only after a pair of counter-rotating vortices have established themselves does the flame spread throughout the entire mixing chamber, as shown in Fig. 9d.

In order to quantify the flame spread in the mixing chamber, software was developed which permits the calculation of the phase angle between the maximum heat release rate at every location and the maximum pressure. The distribution of these phase angles then gives an indication of the instantaneous shape of the flame and of its spread through the combustor. Figure 10 shows a contour plot obtained using this technique. The numbers indicate the phase by which the local heat release leads the pressure. The flame, thus, spreads from the upper left hand side of the mixing chamber, opposite the fuel port, towards the lower left hand side and, finally, towards the right hand side of the mixing chamber into the region between the fuel and air ports.

These results indicate that, for the present valve configuration, it is essential that the fuel enter the mixing chamber prior to the air jet. Otherwise the momentum of the air jet would prevent the fuel jet from penetrating significantly into the mixing chamber. This would result in poor mixing of the fuel and air. At the same time, a different fuel and air port configuration or dual fuel inlets would, probably, result in a quicker, more uniform distribution of the combustion process in the mixing chamber. The results of these heat release measurements are discussed further in Refs. 13 and 14.

Laser Doppler Velocimetry

Velocity measurements in the mixing chamber were carried out using a two component LDV system based on a five watt argon ion laser. The results of the flow visualization experiments had indicated that reverse flow exists in the mixing chamber. Therefore, Bragg cells were incorporated into both components of the system. Because the flow in the combustor is periodic, mean flow velocities and turbulence intensities at different instances during the cycle had to be determined using conditional sampling. This was achieved by detecting the start of each cycle which was taken to be the positive zero crossing of the pressure signal. Each cycle was then divided into 60 equal time intervals based upon the previously obtained operational frequency of the combustor. Finally, the data were sorted into the relevant bins according to their time of arrival during the cycle. Ensemble averaged mean and RMS velocities were, thus, obtained at 60 equally spaced instances during the cycle.

Early tests of the performance of the LDV indicated that the system and its data reduction software produced reproducible mean velocities which were in good agreement with quantitative observations from the flow visualization¹⁵. However, the apparent level of turbulence, as measured by the RMS value of the conditionally sampled velocities, was considerably higher than that observed in other turbulent flows, (e.g. in the turbulent shear layer behind a backward facing step). It is important to realize that it is possible that only a part of this RMS may be due to true turbulence. Since the values of the velocity fluctuations were obtained by ensemble averaging, they may contain contributions due to 1) the finite width of the slots into which each cycle was divided; 2) the

slight variations in the flow field from cycle to cycle; and 3) slight variations in the combustor frequency during the experiment. In order to eliminate at least the effect of variations in the operating frequency of the combustor the data reduction software was modified. In the updated data reduction routine the pulse duration for each cycle was determined from the actual pressure oscillations measured during the experiment rather than from a previously determined mean frequency.

Typical spatially and temporally resolved mean velocity and turbulence intensity data in the axial (u) and vertical (v) directions are shown in Figs. 11 through 29. Figure 11 shows the locations at which these LDV data were obtained. All measurement points lie in a plane which bisects the right angle between the fuel and air injection ports, equi-spaced along lines which are normal to the axis of the combustor. Each measurement location is labeled (m,n) where m represents the number of the line counting from the flat end of the mixing chamber and n denotes the point number on this line counting from the curved wall of the chamber opposite to the fuel and air ports.

Each of the velocity and turbulence intensity figures represents one cycle starting at the negative zero crossing of the pressure signal; i.e., at an instant after the fuel has started to enter but before the air has entered the mixing chamber. Figures 12 through 23 represent velocity and turbulence intensity traces at each of the ten points along one measurement line; i.e., along a given value of m. For greater clarity, each of these figures consists of three plots one of which also shows the pressure signal for reference. Figures 24 through 29 show a different

representation of the same data which is more qualitative but conveys a better physical picture of the variation of the complex flow field in the mixing chamber during a cycle. These are three - dimensional "carpet plots" in which one axis represents the location of the measurement station along a given measurement line, the second axis represents the normalized time (i.e., 0 to 1 for one cycle) and the third axis shows either the u or v components of the velocity. This results in two carpet plots (one for u and one for v) for each value of m.

Figures 24, 25 and 26 show the carpet plots of the vertical velocities for the three measurement lines closest to the closed, upstream end of the mixing chamber. These are best analyzed in conjunction with the instantaneous velocity vs. time plots in Figs. 12, 13 and 14. Large positive (upward) velocity peaks are seen early in the cycle along all three lines. At $m = 3$, which lies in the paths of the fuel and air jets, (Fig. 26) the maximum velocity is 22 m/s (73 ft/s) which occurs very early in the cycle, near the center of the mixing chamber ($n = 4$ to 7). Further upstream, at $m = 1$ and 2 (Figs 24 and 25), the velocities peak at 8 m/s (26 ft/s). These maxima occur later, and are confined to locations $n = 9$ and 10, which lie within 12 mm (0.5 in.) of the curved mixing chamber wall between the fuel and air ports. Immediately following the peak at $m = 3$ and coincident with the peaks at $m = 1$ and 2, deep, wide and wide valleys (downward velocities) are seen near the center of all three measurement lines. The early peak at $m = 3$ is caused by the entry of the fuel jet which results in an upward component of velocity, close to 22 m/s (73 ft/s). The valley observed later in the cycle is due to the downward component of velocity of 18 m/s (59 ft/s) caused by the entering air jet.

Since the positive peaks along $m = 1$ and 2 occur at the same instant in the cycle as the valley they must be due to the leading edge vortex of the air jet observed in the flow visualization. Later in the cycle the flow near the wall opposite to the inlet ports is generally upward while that near the ports is directed downward. This suggests the existence of a large vortex in the plane normal to the axis of the combustor.

The time dependence of the instantaneous axial velocities and their carpet plots at the same locations are shown in Figs. 15 through 17 and 27 through 29, respectively. Early in the cycle, when the fuel jet enters the mixing chamber, a significant downstream velocity directed towards the combustion chamber is observed. These positive velocity peaks are particularly large, up to 8 m/s (26 ft/s), along lines $m = 2$ and 3 (Figs. 16 and 17), where the effect of the fuel jet is felt most strongly. It is also confined to an area within 20 mm ($.8 \text{ in.}$) of the curved mixing chamber wall opposite the injection ports. This wall deflects the incoming jet. In addition, the initial combustion process and the associated expansion of the combustion products are concentrated in this area. Shortly thereafter, the air jet enters the mixing chamber. It has very little effect upon the axial velocities along the line $m = 3$ which coincides with the centerline of the jet. However, at locations $m = 1$ and 2 large valleys representing upstream velocities of up to 7 m/s (23 ft/s) can be seen. These are formed by the leading edge vortex of the incoming air jet which has an upstream component of velocity. After this vortex has passed, a small upstream velocity, of the order of 2 m/s (7 ft/s), continues to be observed. This flow causes the acoustic pressure in the mixing chamber to increase. As the acoustic pressure approaches its maximum the flow

reverses direction and the combustion products exhaust towards the combustion chamber for the remainder of the cycle.

The instantaneous turbulence intensities for all measurement lines are plotted versus phase in the cycle in Figs. 18 through 23. Early in the cycle the turbulence levels at all locations are relatively low ($u_{RMS} = 3$ m/s, 10 ft/s). At the central locations ($n = 3, 4, 5$ and 6) along the lines $m = 2$ and 3 , which lie directly in the path of the fuel jet, the turbulence intensity increases as soon as this jet enters the mixing chamber to a value of u_{RMS} close to 8 m/s (26 ft/s). At all other locations the turbulence intensity does not significantly increase until the entry of the air jet is detected in the mean velocities. The turbulence levels then remain close to $u_{RMS} = 6$ m/s (20 ft/s) for part of the cycle and then slowly drop to their initial values.

These LDV measurements are presently continuing as part of the Ph.D. thesis work of the graduate student responsible for this work. Velocity measurements in the mixing chamber will be completed and velocity measurements at the combustion chamber - tailpipe interface will be added. The complete set of velocity results will then be submitted for publication to a suitable journal and as a "Topical Report" to GRI.

Rich Limit of Pulse Combustor Operation

As mentioned in the section dealing with performance measurements, the Helmholtz type pulse combustor fitted with the standard, 163 cm (64.2 in.) long tail pipe has a rich limit of operation at an equivalence ratio of 1.03. This limit exists even though the pulse combustor appears to be operating near its optimal condition immediately before this limit is reached. This operational limit can, however, be

extended if the tail pipe is lengthened; i.e., the period of the pulsations is prolonged, or if the combustion air is supplied under pressure¹³. Based upon the results of the measurements discussed above, the following mechanism appears to control this rich limit.

In order to attain pulse combustion, the driving of the pulsations by the combustion process must overcome the acoustic damping due to, for example, viscous dissipation and acoustic radiation from the combustor. A limit of operation of the pulse combustor occurs if this balance between the driving and damping processes fails to materialize. According to Rayleigh's criterion, the driving by the combustion process can be quantified by the Rayleigh efficiency¹⁶ η which is defined by

$$\eta = \frac{R}{C_p \bar{P} \bar{Q}} \int_0^1 P' Q \, d\tau \approx \frac{|P| |Q| \cos \theta}{C_p \bar{P} \bar{Q}}$$

where P and Q are the total pressure and combustion heat release rate, θ is the phase angle between the pressure and the heat release rate oscillations, R and C_p are the ideal gas constant and the specific heat at constant pressure, respectively, and τ is the time normalized by the duration of one cycle. Bars, primes and brackets represent the steady state, oscillating components and amplitudes of the indicated quantities, respectively.

Figure 30 shows the variation of the Rayleigh efficiency of the combustor fitted with a standard tailpipe and an extended tailpipe as a function of equivalence ratio, ϕ . The maximum ϕ at which each curve stops

represent the rich limit of operation for each configuration. Clearly, near the lean limit, at $\phi = 0.55$, the driving is small, just enough to overcome the damping in the system. In contrast, near the rich limit for the combustor fitted with a standard tailpipe, at $\phi = 1.03$, the driving is close to its maximum. Thus, the mechanism which controls this rich limit appears fundamentally different from that which is responsible for the lean limit.

The Rayleigh efficiencies presented in Fig. 30 were calculated from the measured fluctuations of pressure and heat release and the phase angle between them. The dependences of these three variables upon the equivalence ratio in the combustor are shown in Figs. 31 and 32. The amplitudes of both, the pressure and heat release fluctuations reach their maxima near stoichiometric conditions, at $\phi = 0.98$. The phase angle by which the heat release leads the pressure, on the other hand, decreases with increasing equivalence ratio until it asymptotically reaches a constant value which depends upon the length of the tailpipe.

In order to understand the combustor behavior described above, it is helpful to consider the relative phases of the pressure and radiation oscillations and the instants of fuel and air injection. Figure 33 shows one normalized period of oscillation for both rich and lean operating conditions. The arrows indicate the instants at which fuel and air jets enter the mixing chamber. Horizontal lines at the top of the figure indicate those parts of the cycle when the combustion products move away from or towards the mixing chamber where most of the combustion process occurs. Finally, the points marked "X" indicate the instants at which the new fuel charges reignite, as indicated by the increase in the radiation

signal. All this information is based upon the high speed shadowgrams, pressure and CC radiation measurements described above.

Figure 33 indicates that for lean operation the new fuel ignites before the new air enters the mixing chamber. This is possible since there is air left over from the previous cycle. As the equivalence ratio is increased, less air is available from the previous cycle and ignition is delayed until, under stoichometric conditions, ignition of the fuel jet must await the entry of the air jet. Since the oscillations of heat release always lead those of pressure, the phase angle between the two decreases from 60° to 30° as the equivalence ratio is decreased, see Fig. 32. Since with decreasing phase angle the pressure and heat release fluctuations are more in phase, the Rayleigh criterion causes the pressure amplitudes in the combustor increase from 165 dB to 169 dB when the equivalence ratio is increased from 0.55 to 0.98, as observed in Fig. 31.

The rich limit of operation can now be explained with the aid of Fig. 33. The time available for the reactants to mix and burn is limited to the time interval between the instants when the new fuel charge ignites and when the reaction is quenched by the combustion products returning from the combustion chamber to the mixing chamber. If ignition is sufficiently delayed this time interval is too short and not enough heat is released to drive the pulsations. This occurs at the rich limit.

When the duration of the cycle is prolonged by extending the tailpipe the time available for combustion is increased and the rich limit is extended beyond $\phi = 1.3$. A similar result is obtained if ignition of the new

fuel is advanced by forcing the air to enter earlier or if mixing is improved by injecting the air jet under pressure. Conversely, delaying the entry of the air jet by, for example, extending the pipe which connects the air valve to the mixing chamber reduced the rich limit to an equivalence ratio of less than one. A more detailed description of this part of the work is given in Refs. 6 and 7.

Task II

In this task, the impedance tube technique¹⁹ was used to measure the admittances (i.e., the complex ratio between the acoustic velocity and pressure) of different pulse combustor components. The admittance is a complex quantity which describes the acoustic behavior of the system. As discussed later, if the real part of the admittance is positive the system drives the acoustic pressure oscillations, if it is negative the system damps. All components which make up the pulse combustor damp the pressure oscillations in the absence of combustion. Therefore, the measured, real part of the admittance of the cold combustor provides an indication of how much driving the combustion process will have to provide to assure pulse operation.

In the impedance tube set-up, the investigated component is attached to one end of a long tube, see Fig. 34. An electro-pneumatic, acoustic driver is attached to the wall just upstream of the opposite, open end of the tube. The acoustic driver is used to excite an incident acoustic wave which moves towards the tested component. The interaction of this wave with the investigated sample produces a reflected wave with

modified amplitude and phase. The incident and reflected waves combine to establish a standing wave in the impedance tube. A piezo-electric pressure transducer mounted near the tested sample measures the acoustic pressure amplitude at the upstream end of the tube. A second pressure transducer, mounted at the end of a long rod, is translated inside the tube to measure the axial variation of the standing wave pressure amplitude along the impedance tube.

When measuring the admittance of a hard termination (i.e., zero admittance), the incident wave is reflected without a change in amplitude or a shift in phase. In this case, the combination of incident and reflected waves produces a standing wave with a zero-amplitude pressure minimum located one quarter of the wavelength ($\lambda/4$) from the hard termination, see Fig. 35a. On the other hand, if the complex admittance of the termination is non-zero, see Fig. 35b, the minimum pressure amplitude is non-zero and it occurs at a location other than $\lambda/4$ from the tested sample. Physically, the termination changes the pressure amplitude of the reflected wave and introduces an apparent change in the length of the pipe by introducing a phase shift in the reflection process. The measured values of P_{\max} , P_{\min} and the distance of P_{\min} from the tested sample can be used to determine the real and imaginary parts of the admittance of the termination and, thus, of the component under investigation. A more detailed analysis shows that the real part of the admittance, which is calculated from the difference between the maximum and minimum pressure amplitudes (i.e., $P_{\max} - P_{\min}$) determines the damping (or driving) provided by the component under investigation. On the other hand, the imaginary part of the admittance

provides information which affects the frequency of the system which utilizes the tested component.

The above described technique was used to measure the real and imaginary parts of the admittances of different pulse combustor components under cold and "hot" operating conditions. Admittance measurements under cold conditions were completed as part of this project. The system was also prepared for measurements with combustion under the present program but most actual measurements were carried out under a new contract.

The admittances were measured under cold flow conditions for the following configurations: (1) a hard termination at the end of the impedance tube; (2) the gas valve and its decoupler at the end of the tube; (3) the air valve at the end of the tube; (4) the mixing chamber fitted with the air valve only; and (5) the mixing chamber fitted with both the fuel and the air valves. The air valve opening was varied between 0 and .018 inches for configurations 3, 4 and 5. In these tests the acoustic driver was set to generate sound pressure levels of approximately 160 dB near the tested component. This corresponds to typical dB levels in pulse combustors. Furthermore, the driving frequencies were varied between 20 and 170 Hz. In addition, the admittance of the air flapper valve and of the entire pulse combustor including valves, mixing and combustion chambers were measured as a function of amplitude. All tests were carried out at mean pressures in the impedance tube equal to the previously determined boost pressure in the pulse combustor.

Before presenting the obtained results, it would be helpful to consider Fig. 36. It shows the dependence of the real part of the admittance upon ΔP (i.e., $P_{\max} - P_{\min}$). Clearly, when the magnitude of the real part of the admittance (i.e., Y_r) is small, the value of Y_r is relatively insensitive to the accuracy of the measurement of ΔP . However, as the magnitude of Y_r increases, the sensitivity of the Y_r to the measured ΔP increases rapidly. Thus, the error in the determined Y_r increases with increasing value Y_r . In addition, while the real part of the admittance depends largely upon the value of ΔP , the value of the imaginary part of the admittance is primarily determined by the location of P_{\min} . Since the standing pressure wave has a relatively flat minimum at 40 Hz, which is the operational frequency for the pulse combustor under investigation, it was easier to determine the value of the minimum than its location. The real parts of the admittances were, therefore, measured with better accuracy than their imaginary parts.

The real parts of the admittances for the above configurations with the air valve (when included) closed and open (to .012 inches) measured over a 20 to 170 Hz frequency range are shown in Fig. 37. An air valve opening of .012 inches was selected since it corresponds to a typical setting for the pulse combustor under normal operating conditions. Both, the hard termination and the fuel flapper valve with its decoupling chamber showed no damping over the entire range of investigated frequencies (i.e., $Y_r = 0$). This indicates that the fuel valve orifice behaves, essentially, like a solid surface.

For all of the tested configurations which contain an air flapper valve Y_r is essentially zero at low frequencies as long as the air valve is closed. As the frequency is increased, Y_r and, thus, the damping by the air valve and its housing increases until it becomes quite significant at high frequencies. The real part of the admittance is increased even further if the closed air valve is attached via an elbow to the mixing chamber. On the other hand, adding the fuel valve to the mixing chamber - air valve assembly has no significant effect upon the admittance at any investigated frequency. This provides further indication that the fuel valve behaves like a solid surface.

Figure 37 also shows that opening the air valve substantially increases the real part of the admittance over the entire range of investigated frequencies. Once again, the effect of attaching the air valve housing to the side of the mixing chamber is significantly greater than adding the fuel valve to the mixing chamber - air valve assembly. The increase in the real part of the admittance with increasing air valve opening is illustrated in more detail in Fig. 38 for a range of valve openings and driving frequencies for the mixing chamber fitted with both valves.

The variation of the measured imaginary part of the admittance (i.e., Y_i) for these configurations over the 20 to 170 Hz frequency range are shown in Fig. 39. Once again, Y_i is zero for the hard termination as well as for the fuel valve only. However, once the closed air valve was added to any of the three investigated configurations the imaginary part of the admittance increased substantially. The latter effect increased with

increasing frequency. This occurred because adding the valve assembly moves the termination, in the form of the valve plates, further away from the end of the impedance tube, see Fig. 40. The minimum of the standing pressure wave in the impedance tube was, therefore, moved upstream resulting in an increase in Y_i . Because of the size of the mixing chamber and the elbow that connects the air valve to it, this effect is more pronounced for the valve - mixing chamber assembly than for the air valve alone.

Once the air valve is opened the pressure anti-node moves away from the valve plates towards the driver end of the impedance tube, see Fig. 40. (If the valve plates are completely removed the resulting open end corresponds to a pressure node). This causes the decrease in the magnitude of Y_i observed in Fig. 39. Because of the above discussed difficulty in determining the precise location of the minimum of the standing pressure wave, no clear difference between the imaginary part of the impedance of the air valve only and that of the valve - mixing chamber assembly could be established. However, Fig. 41 clearly shows that the magnitude of Y_i decreases as the opening of the air valve increases. This effect is particularly pronounced at higher frequencies. The lack of smoothness of the curves is, once again, due to the difficulty in determining the precise location of the flat minimum of the standing wave. More details of these results are given in Ref. 20.

Additional admittance measurements were carried out in which either the mixing chamber with its valves or the entire combustor consisting of mixing and combustion chambers and the flapper valves

were attached to the impedance tube. In these tests, the admittances were measured as a function of applied sound pressure level for a given air valve opening. Figure 42 shows that for the mixing chamber assembly only the damping decreases with increasing sound pressure level. Since it has been shown that the only significant acoustic losses in the mixing chamber assembly occur in the air flapper valve it can be concluded that it is the damping in the air valve that decreases with increasing acoustic excitation. However, the damping of the entire combustor (including the combustion chamber) increases with increased applied sound pressure level, as shown in Fig. 42. This suggests that the damping in the Helmholtz volume formed by the combustion chamber overshadows the effect of the damping in the air flapper valve for this pulse combustor configuration.

In addition to the above detailed measurements an analytical scheme was developed which permits the determination of the admittance of the entire mixing chamber - valve assembly from the measured admittances of its component parts. As shown in Fig. 43, the assembly was divided into five sections. The admittance at location "1" was calculated from that of the solid wall ($Y = 0$) which closes the upstream end of the mixing chamber using a transfer function. The admittance at "2" was determined from the measured admittance values of the valve. The admittance at "3" was taken to be zero since the fuel valve had been shown to behave like a solid surface. The acoustic mass conservation equation was then applied to the control volume bounded by interfaces 1,2,3 and 4 to calculate the admittance at "4" from the admittances at the other interfaces. Finally, the admittance at "5" was calculated from that at "4" using a transfer function. Details of these calculations are given in Ref. 20. The results of these

calculations for different valve openings and over a range of frequencies are compared with the experimentally measured values of the real and imaginary parts of the admittance of the mixing chamber - valve assembly in Figs. 44 and 45. Clearly, the agreement is excellent.

At the end of this contract the impedance tube set up was modified to accommodate tests with combustion. Because of heat transfer to the impedance tube wall a temperature gradient existed along the axis of the impedance tube. A measurement technique was developed to determine the temperature gradient using thermocouples and the classical impedance tube theory was modified to account for it. The actual measurement of the driving by the unsteady combustion process was initiated and completed under a new contract.

Publications

Apart from the semiannual and annual reports specified in the contract, the following papers were presented and published during the contract period:

"Dependence of Pulse Combustion Performance upon Interior Temperature, Acoustic Losses and Combustion Time", X.C. Cheng, B.R. Daniel, J.I. Jagoda and B.T. Zinn, International Gas Research Conference, Tokyo, Japan, November, 1989.

"Dependence of Pulse Combustor Frequency upon Combustion Process Timing", X.C. Cheng, B.R. Daniel, J.I. Jagoda and B.T. Zinn, Twelfth Annual Energy Sources Technology Conference and Exhibition, Fossil Fuels Combustion Symposium, PD-Vol. 25, pp 39-42, Houston, TX, January, 1989.

- "Radiation Measurements in a Gas Fired Pulse Combustor", S.H. Ku, X.C. Cheng, B.R. Daniel, J.I. Jagoda and B.T. Zinn, Proceedings of the Spring Technical Meeting, Central States Section of The Combustion Institute, Chicago, IL, May, 1987.
- "The Interaction between Fluid Mechanics and Combustion in a Helmholtz Type Pulse Combustor", J.M. Tang, B.R. Daniel, J.I. Jagoda and B.T. Zinn, Fall Technical Meeting, Eastern Section of The Combustion Institute, Orlando, FL, December, 1990.
- "Frequency Modeling and Velocity Measurements in Gas Fired, Valved Pulse Combustors", S.H. Ku, B.R. Daniel, J.I. Jagoda and B.T. Zinn, Fall Technical Meeting, Eastern Section of The Combustion Institute, Clearwater Beach, FL, December, 1988.
- "Flame Spread and Limits of Operation of Gas Fired, Mechanically Valved Pulse Combustor", S.H. Ku, B.R. Daniel, J.I. Jagoda and B.T. Zinn, Poster at the Twenty-Second Symposium (International) on Combustion, Seattle, WA, August, 1988.
- "Controlling the Rich Limit of Operation of Pulse Combustors", J.M. Tang, S.H. Ku, B.R. Daniel, J.I. Jagoda and B.T. Zinn, Twenty-Third Symposium (International) on Combustion, Orleans, France, August 1990, (in print).
- "The Acoustic Characteristics of Pulse Combustor Flapper Valves and Mixing Chambers", D. Xu, B.R. Daniel, J.I. Jagoda and B.T. Zinn, Thirteenth Annual Energy Sources Technology Conference and Exhibition, Fossil Fuel Combustion Symposium, PD-Vol. 30, pp 21-28, New Orleans, LA, January, 1990.

CONCLUSIONS

The physical mechanisms which control the performance of a natural gas fired, valved Helmholtz type pulse combustor were investigated. Comparison of flow and flame spread visualization indicated that the fuel jet enters the mixing chamber ahead of the air jet. Under lean operating conditions the fuel begins to react as soon as it enters the combustor. Main ignition occurs once the fuel is scooped up by the leading edge vortex of the air jet. Combustion then spreads by the convection of this vortex throughout the mixing chamber. It is this complex interaction between the fuel and air jets entering the mixing chamber which stabilizes the combustion process. The lean limit of operation of the pulse combustor could be extended by reducing the heat losses to the combustor walls while its rich limit was increased by reducing the pulsation frequency or supplying the combustion air under pressure. The rich limit of operation near stoichiometric conditions exists because of the limited time available for combustion during the cycle if no air from the previous cycle is available for early ignition. In addition to the visualization experiments the flow field is currently being quantified by laser Doppler velocimetry.

Under a separate task the acoustic characteristics of the air flapper valve were determined by an impedance tube technique. In addition, an analytical scheme was developed which allows the determination of the admittance of entire sections of a pulse combustor from the measured admittances of its component parts.

In summary:

- The detailed interactions between the flow field, the reignition and the flame spread during the cycle were determined
- The importance of the relative timing between the heat release and pressure fluctuations was investigated.
- The reasons for the existence of lean and rich operating limits for the Helmholtz type pulse combustor were established.
- The ensemble averaged velocity and turbulence intensity fields were quantified using laser Doppler velocimetry.
- The acoustic behavior of the pulse combustor and its component parts were determined.
- An analytic technique for predicting the acoustic damping by different combustor configurations from the acoustic characteristic of its component parts was developed.

REFERENCES

1. "Lennox-Pulse-G14 Series Up-Flo Gas Furnaces," Engineering Data, Heating Units, Gas, pp. 21-24, published by Lennox Industries, Inc.
2. Hydropulse by Hydrotherm," information about pulsed combustion water heating published by Hydrotherm, Rolfland Ave., Northvale, NJ 07647
3. Hanby, V. I.: "Convective Heat Transfer in a Gas-Fired Pulsating Combustor," Paper No. 68-WA/FU-1, 1968.
4. Fedorov, B. N.: "Experimental Study of the Effect of Acoustic Oscillations on Heat Transfer in a Gas Flow", Juzherno-Fisicheskii Zhurnal, 32, No. 1, pp. 167-180, 1977.
5. Belles, F. E.: "R & D and Other Needs for Exploitation of Pulse-Combustion in Space-Heating Applications," Proceedings of the Symposium on Pulse Combustion Technology for Heating Applications, Argonne National Laboratory, pp. 167-180, 1979.
6. Corliss, J. M, Battelle Columbus Laboratories : Annual Report, Gas Research Institute Report GRI 85/0029, April, 1985.
7. Reuter, D., Daniel, B. R., Jagoda, J. I. and Zinn, B. T.: Combustion and Flame, 65, pp. 281-290, 1986.

8. Cheng, X.C., Daniel, B.R., Jagoda, J.I. and B.T. Zinn, B.T.: "Dependence of Pulse Combustion Performance upon Interior Temperature, Acoustic Losses and Combustion Time", presented at the International Gas Research Conference, Tokyo, Japan, November, 1989.
9. Cheng, X.C., Daniel, B.R., Jagoda, J.I. and B.T. Zinn, B.T.: "Dependence of Pulse Combustor Frequency upon Combustion Process Timing", presented at the Twelfth Annual Energy Sources Technology Conference and Exhibition, Fossil Fuels Combustion Symposium, PD-Vol. 25, pp 39-42, Houston, TX, January, 1989.
10. Miller, N., Carvalho, J.A., Daniel, B.R. and Zinn, B.T.: Proceedings of the Nineteenth Symposium (International) on Combustion, pp. 1197-1203, 1982.
11. Gaydon, A. G. and Wolfhard, H. T.: "Flames," Chapman, R. and Hall Ltd, 1970.
12. Lord Rayleigh: "The Theory of Sound," Vol. II, pp. 224-235, Dover, 1945.
13. Ku, S.H., Cheng, X.C., Jagoda, J.I., Daniel B.R. and Zinn B.T.: "Radiation Measurements in a Gas Fired Pulse Combustor", Proceedings of the Spring Technical Meeting, Central States Section of The Combustion Institute, Chicago, IL, May, 1987.

14. Tang, J.M., Daniel, B.R., Jagoda, J.I., and Zinn B.T.: "The Interaction between Fluid Mechanics and Combustion in a Helmholtz Type Pulse Combustor", presented at the Fall Technical Meeting, Eastern Section of The Combustion Institute, Orlando, FL, December, 1990.
15. Ku, S.H., Daniel, B.R., Jagoda, J.I., and Zinn B.T.: "Frequency Modeling and Velocity Measurements in Gas Fired, Valved Pulse Combustors", presented at the Fall Technical Meeting, Eastern Section of The Combustion Institute, Clearwater Beach, FL, December, 1988.
16. Keller, J. O., Dec, J. E., Westbrook, C. K. and Bramlette, T. T.:
Combustion and Flame, 75, pp. 33-44, 1989.
17. Ku, S.H., Daniel, B.R., Jagoda, J.I., and Zinn B.T.: "Flame Spread and Limits of Operation of Gas Fired, Mechanically Valved Pulse Combustor", Poster at the Twenty-Second Symposium (International) on Combustion, Seattle, WA, August, 1988.
18. Tang, J.M. Ku, S.H., Daniel, B.R., Jagoda, J.I., and Zinn B.T., "Controlling the Rich Limit of Operation of Pulse Combustors", Twenty-Third Symposium (International) on Combustion, Orleans, France, August 1990, (in print).
19. Scott, R.A.: Proceedings of the Physical Society, 58, pp. 253-264, 1946.

20. Xu, D., Daniel, B.R., Jagoda, J.I. and Zinn, B.T.: "The Acoustic Characteristics of Pulse Combustor Flapper Valves and Mixing Chambers", presented at the Thirteenth Annual Energy Sources Technology Conference and Exhibition, Fossil Fuel Combustion Symposium, PD-Vol. 30, pp 21-28, New Orleans, LA, January, 1990.

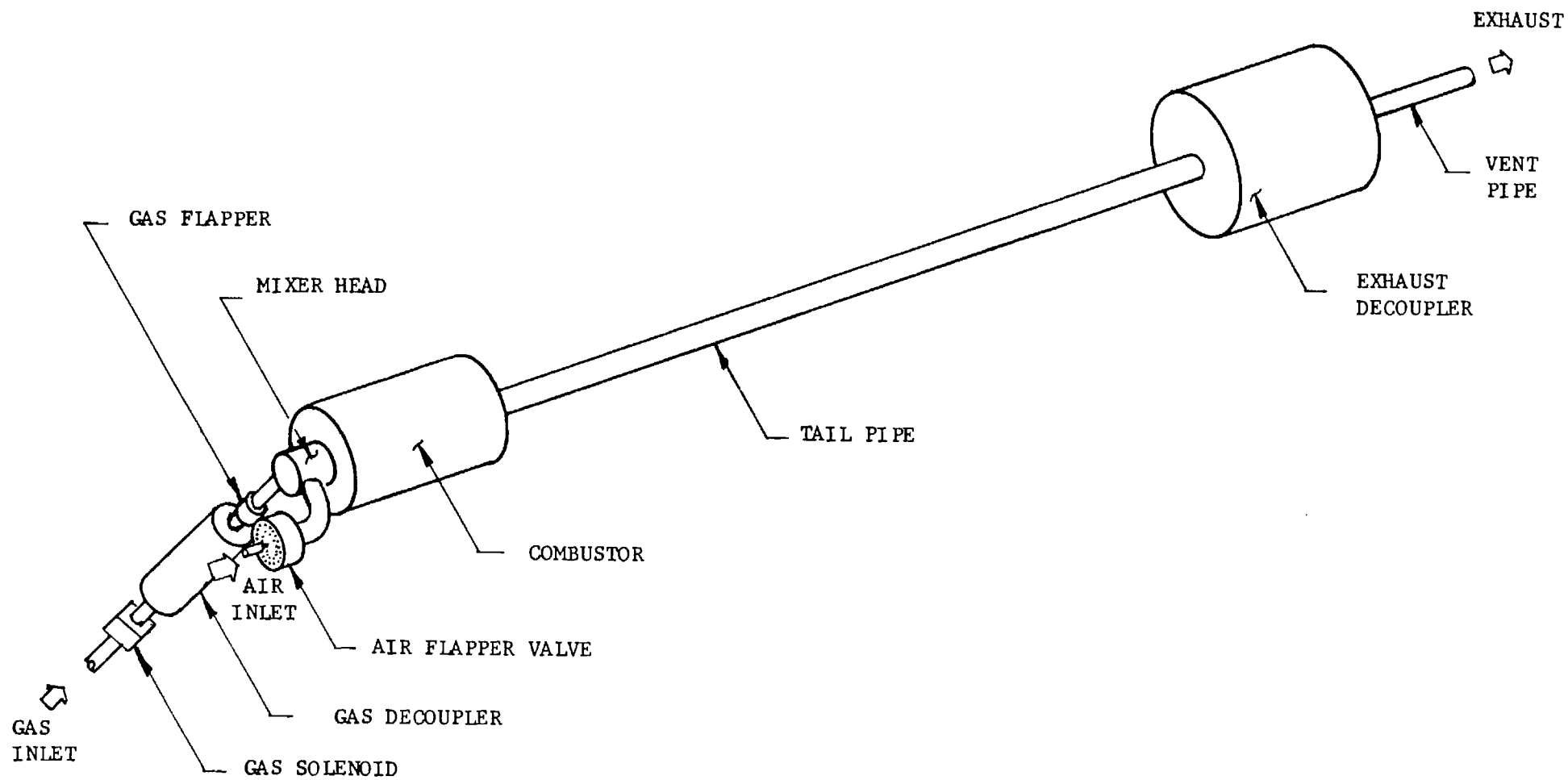


Fig. 1 Schematic of the Helmholtz Type Pulse Combustor

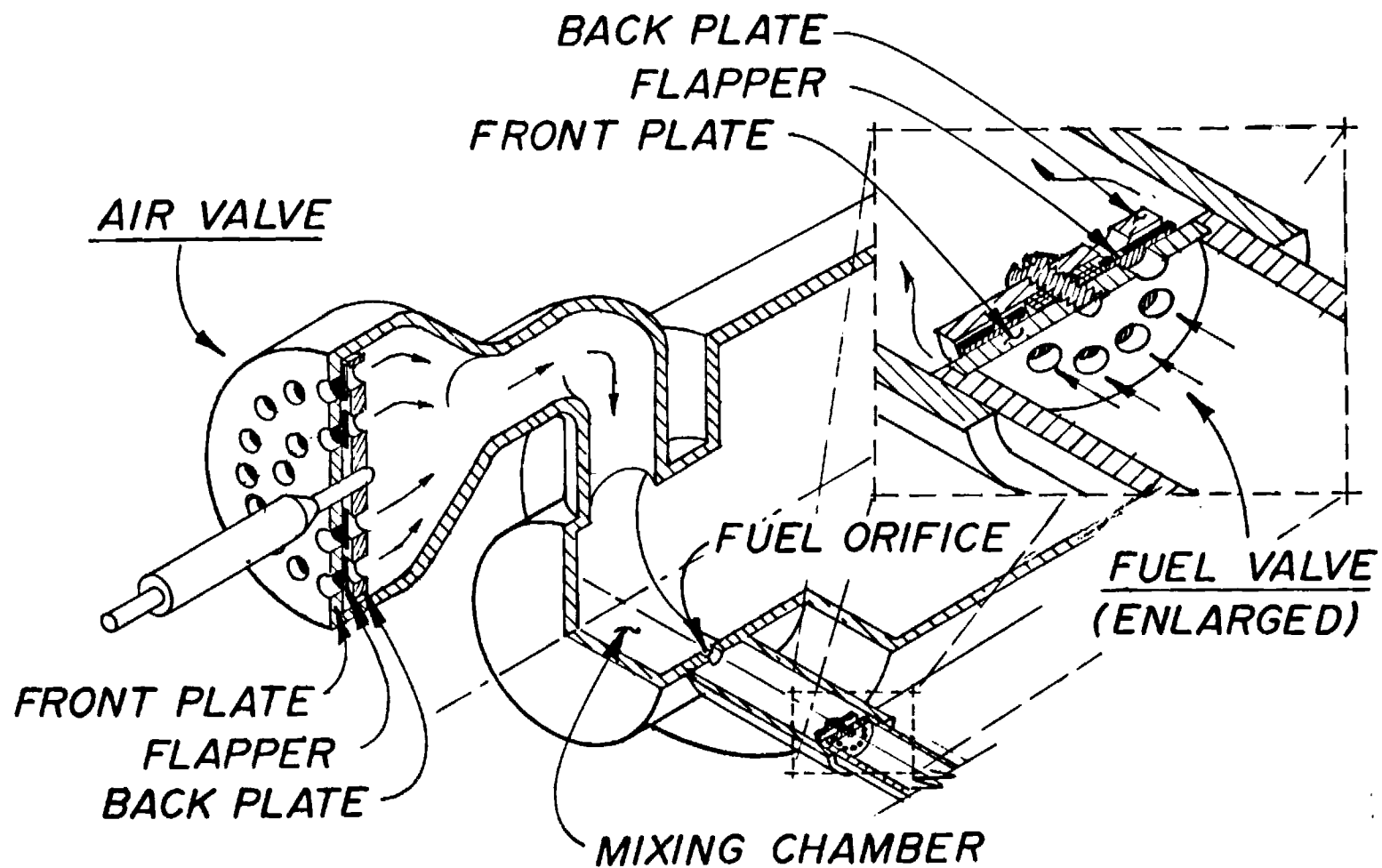


Fig. 2 Schematic of the Mixing Chamber Showing the Fuel and Air Flapper Valves

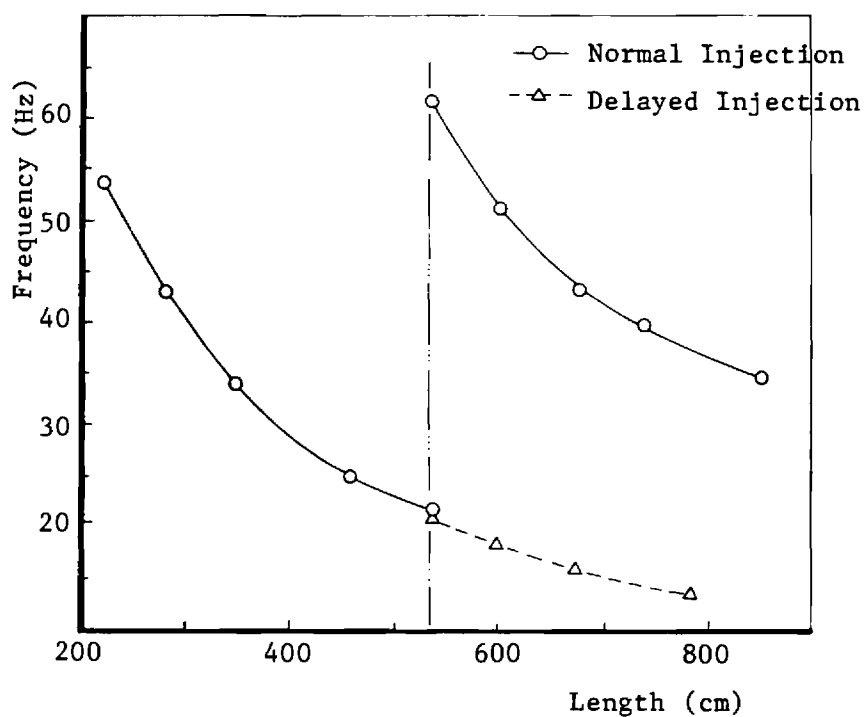
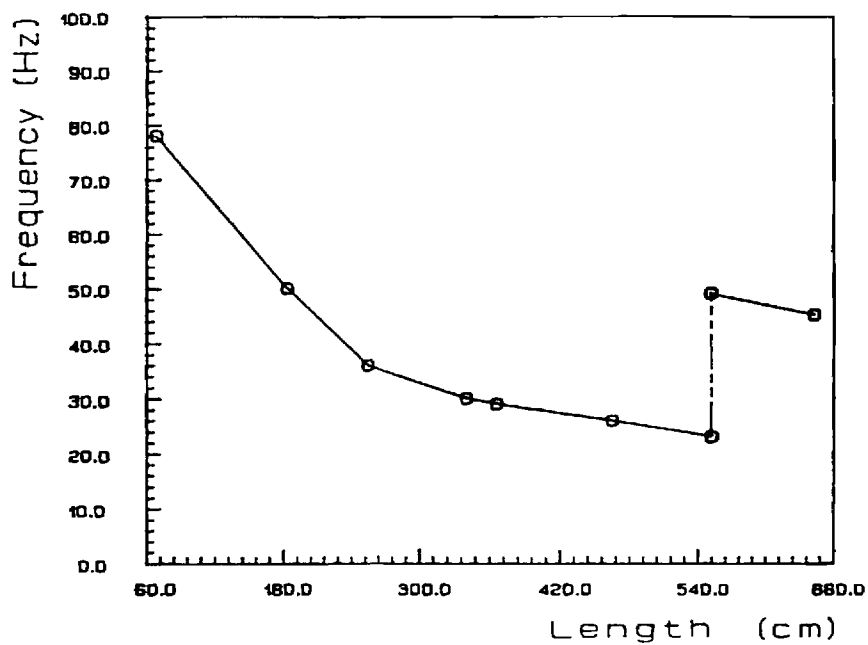


Fig. 3 Operational Frequency of the a) Helmholtz and b) Schmidt Combustors as a Function of Tailpipe or Combustor Length Respectively.

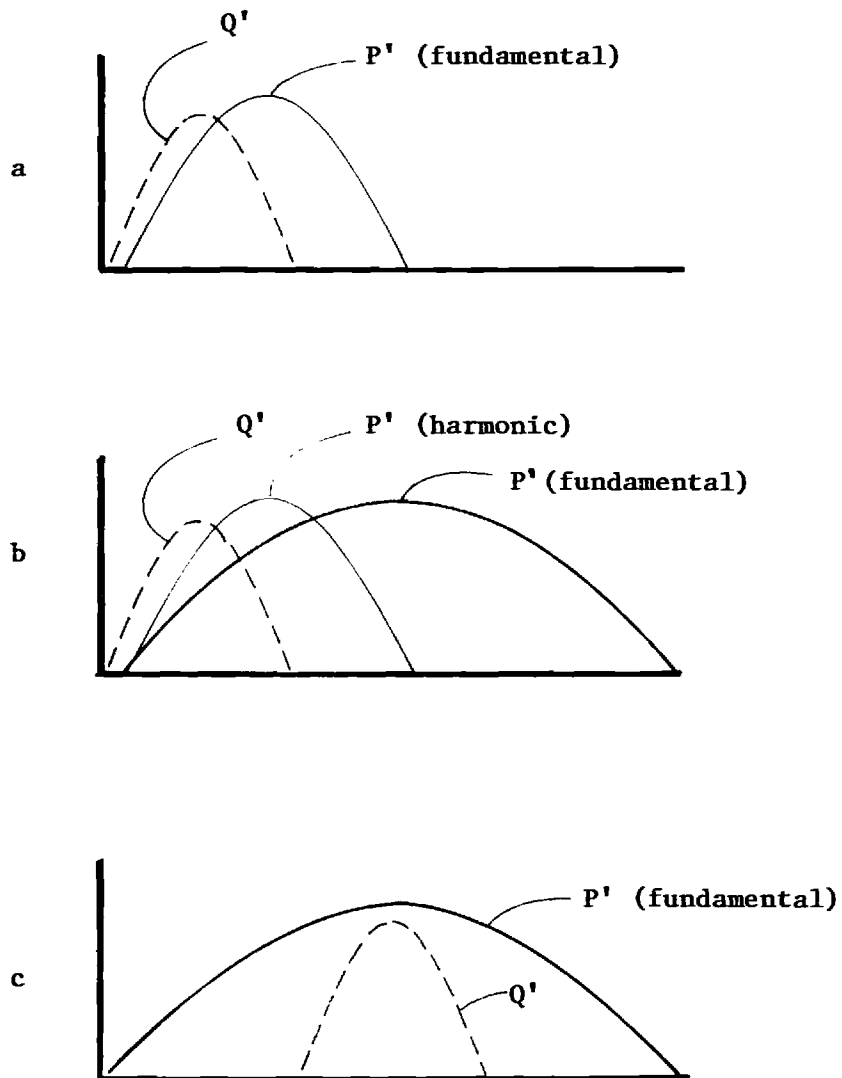


Fig. 4 Schematic of Relative Timing of Heat Release (Q') and Pressure (P') Oscillations for a) High Frequencies, b) Low Frequencies with Standard Fuel Injection and c) Low Frequencies with Displaced Fuel Injection Leading to Delayed Heat Release.

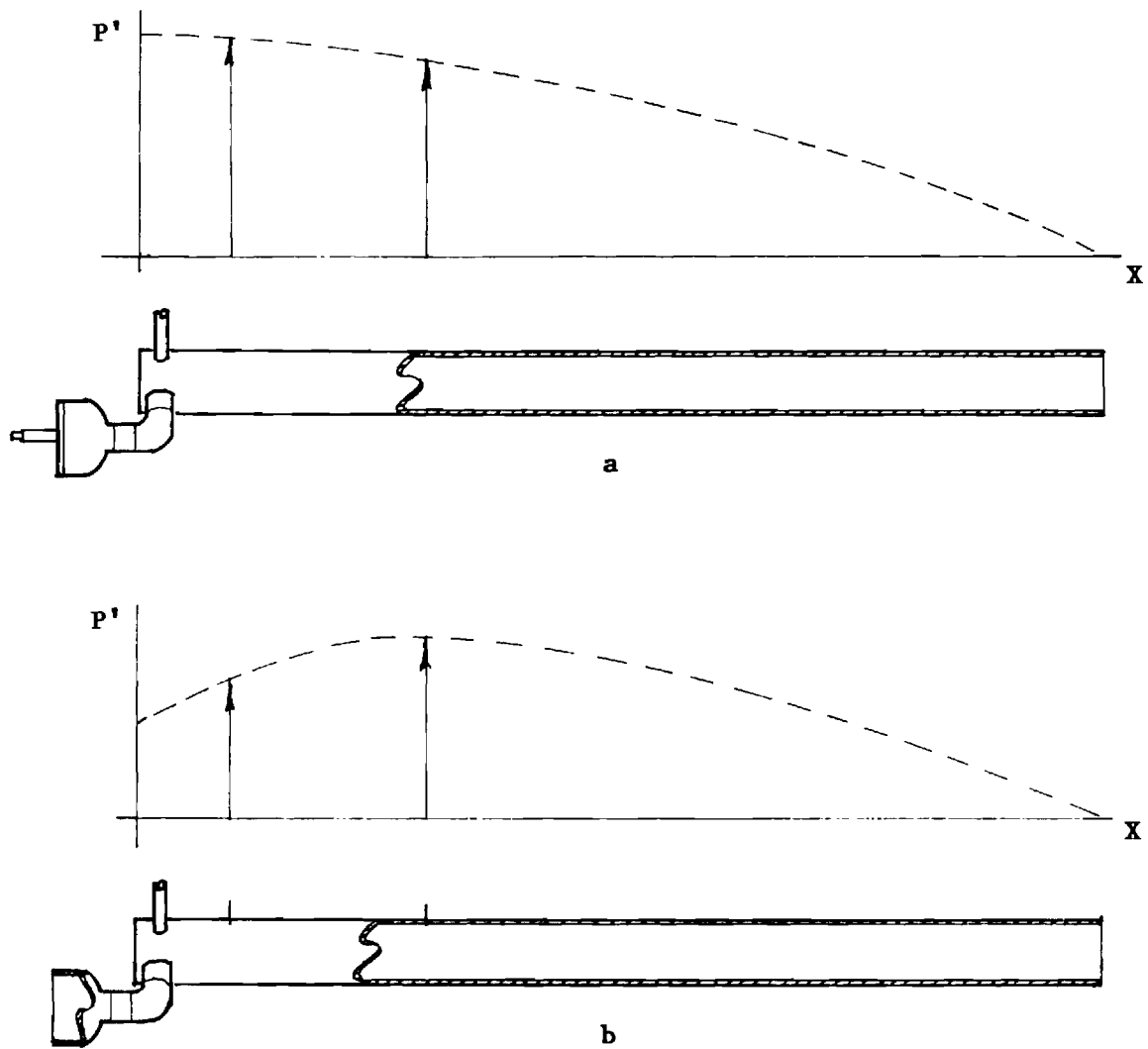


Fig. 5 Plot of Pressure Amplitude (P') vs. Axial Distance along the Combustor (X) Showing Standing Wave Pattern along Schmidt Combustor a) with Air Valve and b) without Air Valve.

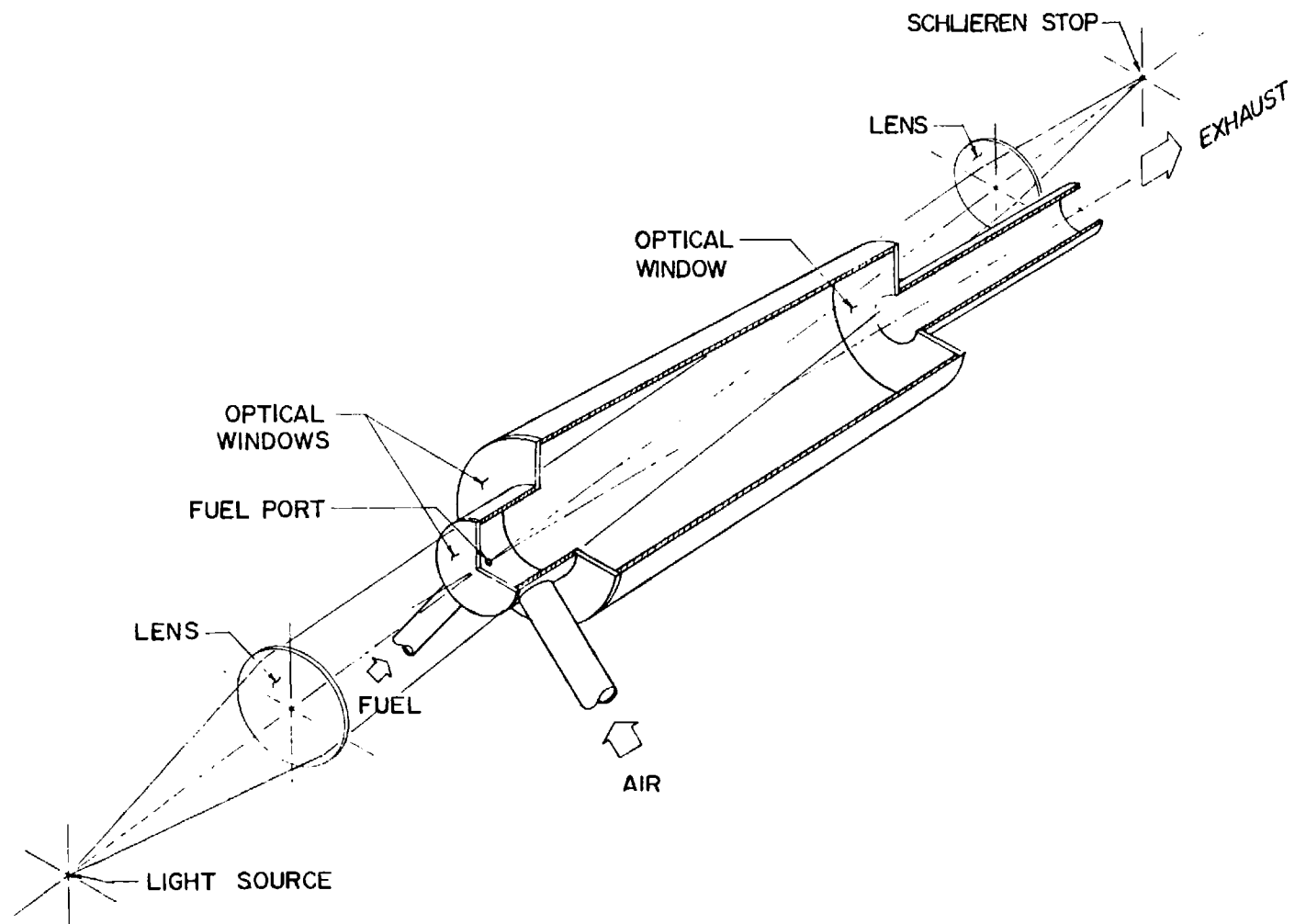


Fig. 6 Schematic of the Schlieren Set-up along the Combustor Axis

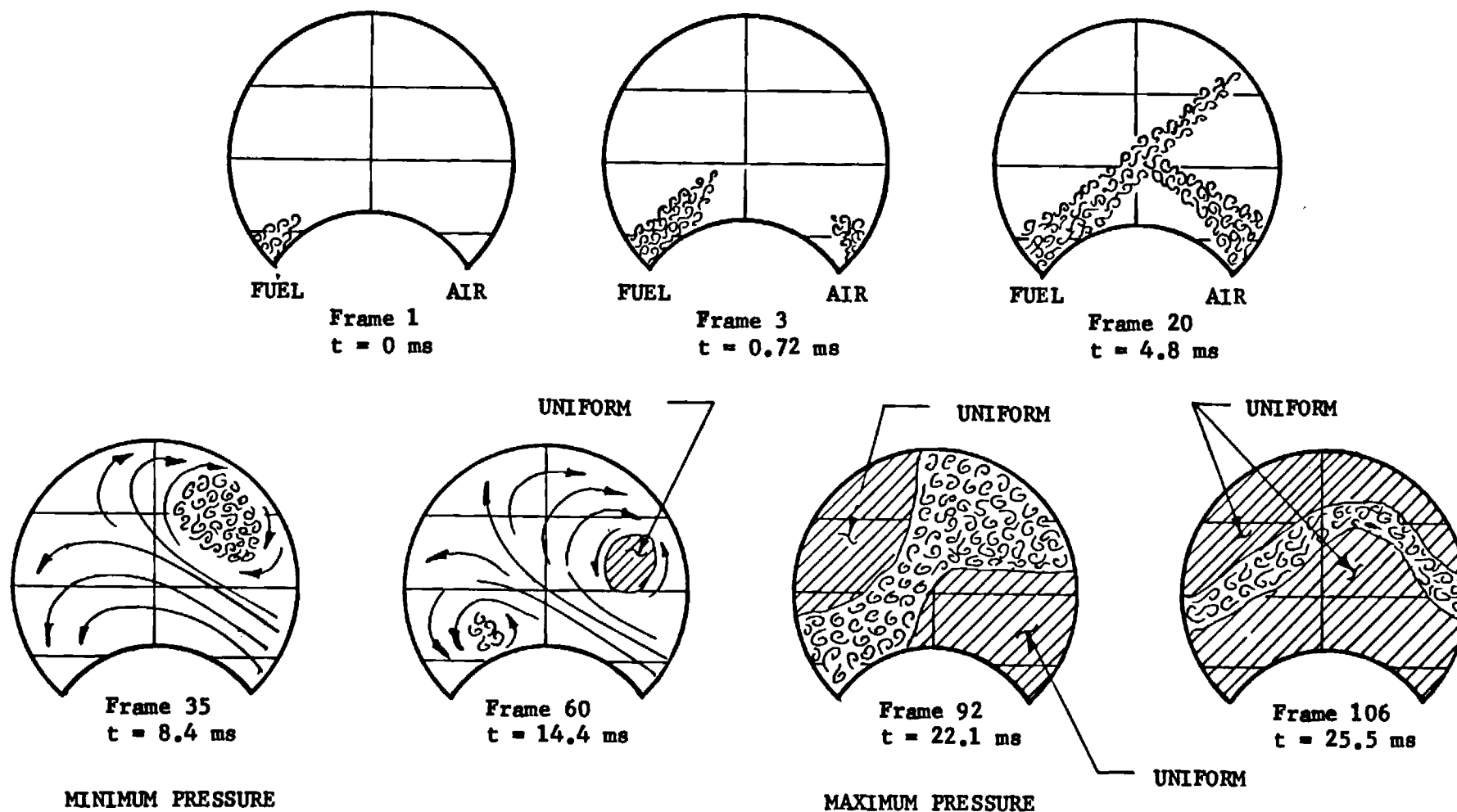


Fig. 7 Schematic of Selected Frames from the High Speed Shadow Movie Showing the Flow Field at Different Instances during the Cycle as Seen along the Combustor Axis

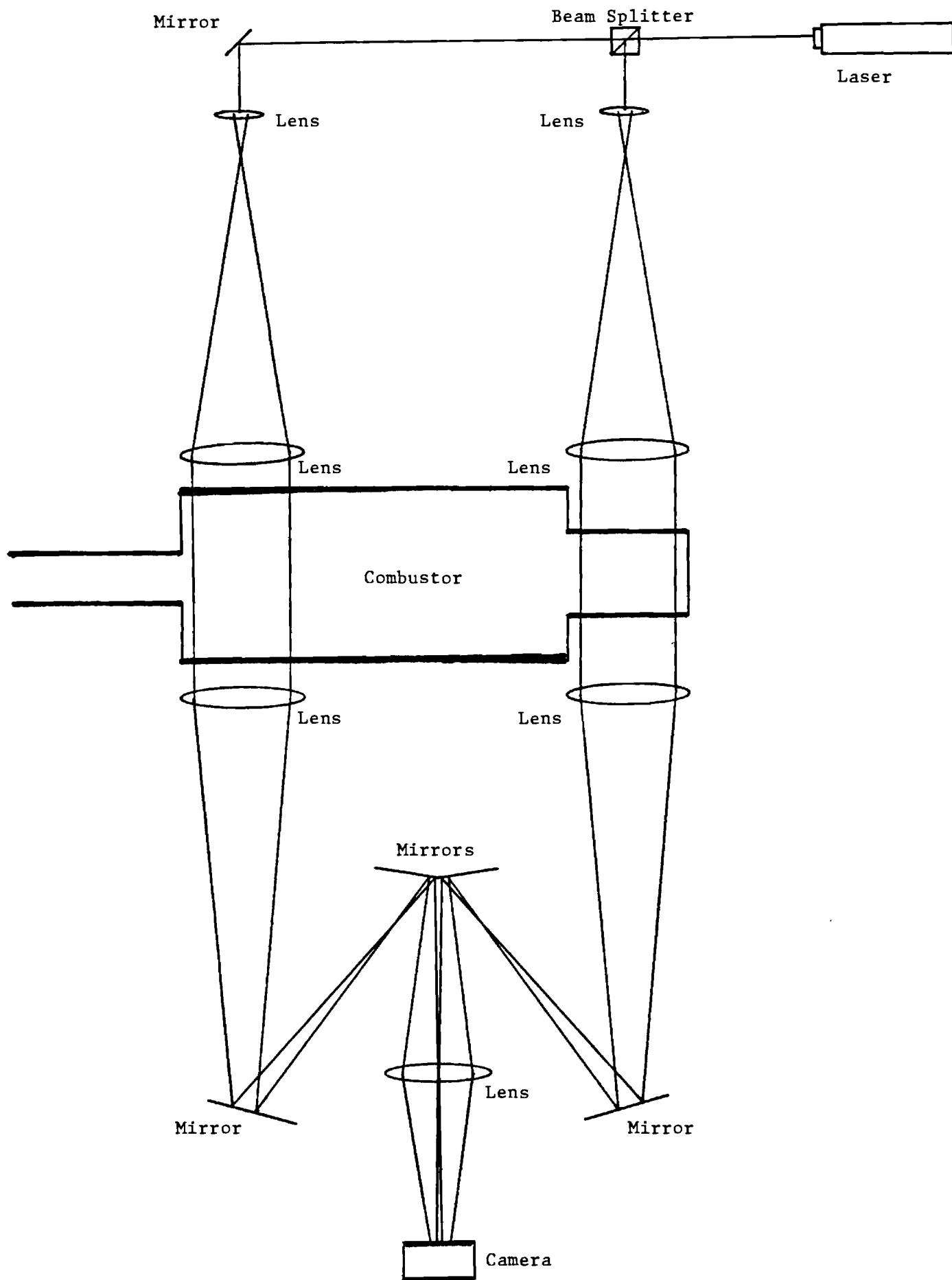


Fig. 8 Schematic of the Schlieren Set-up normal to the Combustor Axis

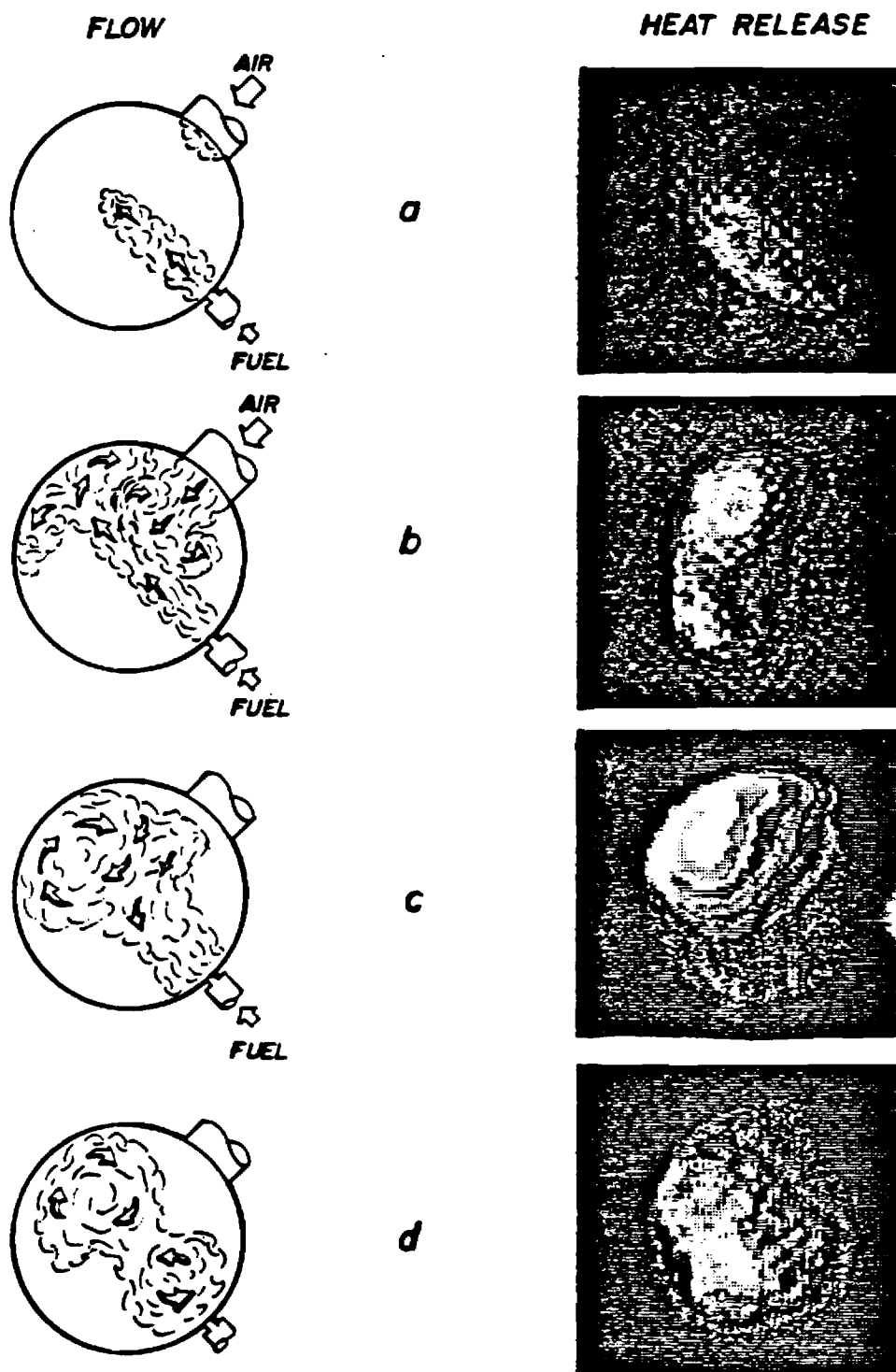


Fig. 9 Comparison of the Flow Field and the Heat Release Distribution as Seen along the Combustor Axis at Four Instants during the Cycle.

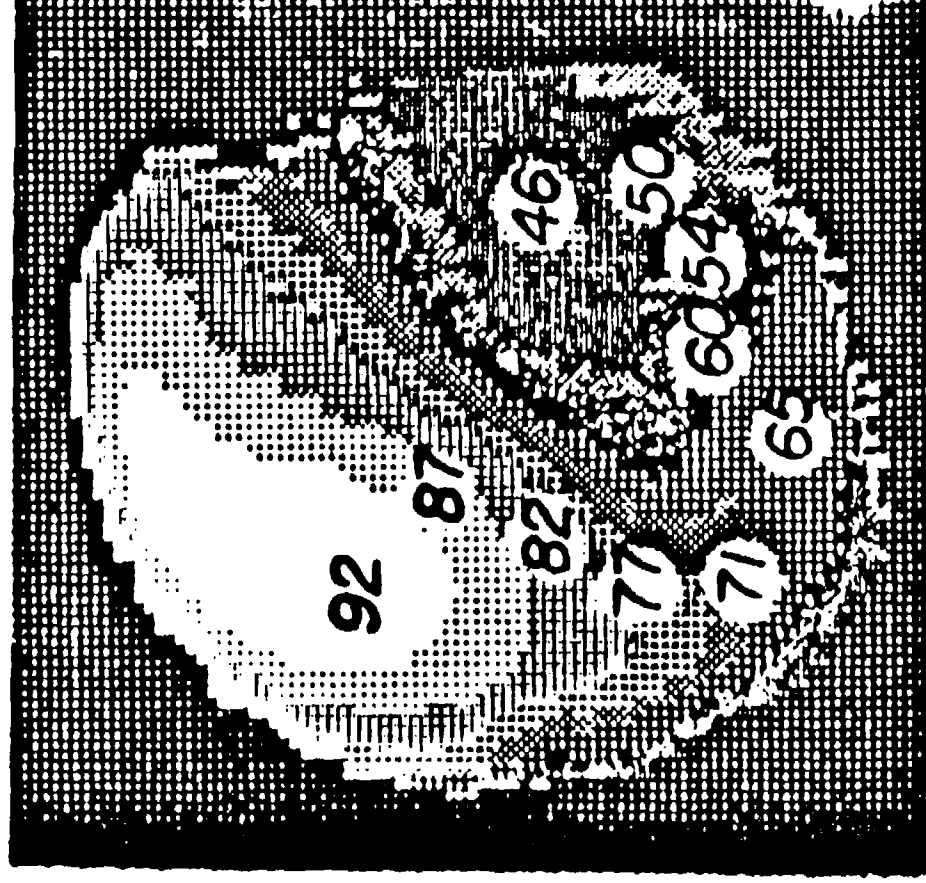


Fig. 10 Contour Plot of Phase Angle by which the Heat Release Oscillations Lead the Pressure Oscillations.

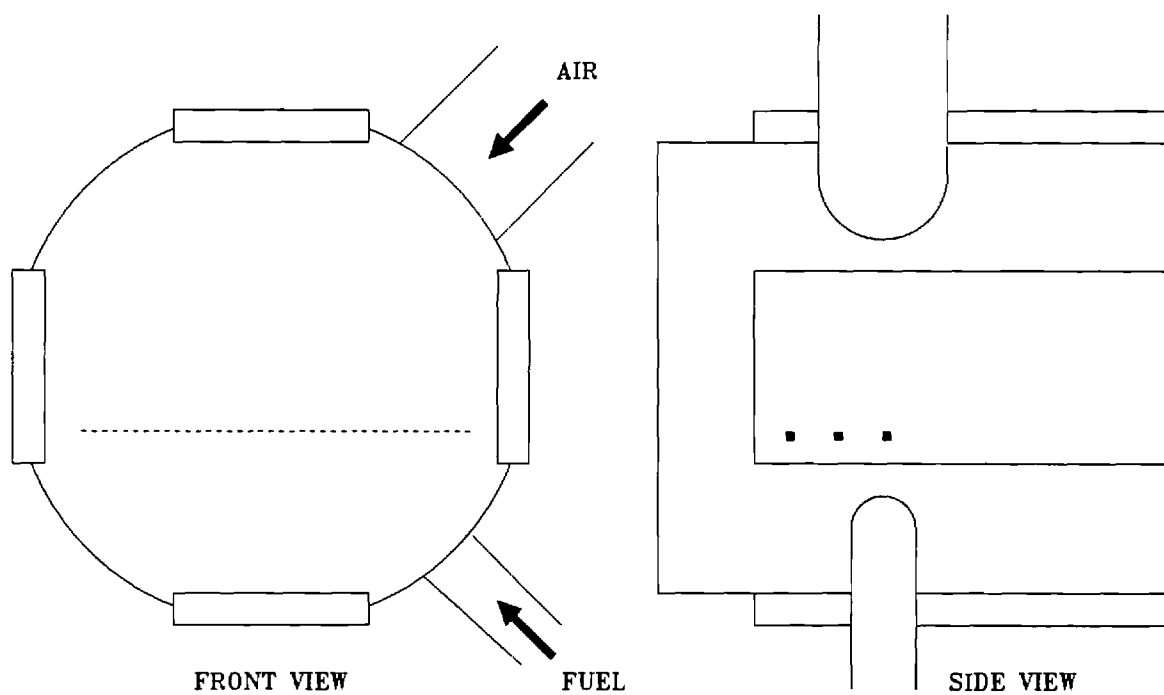
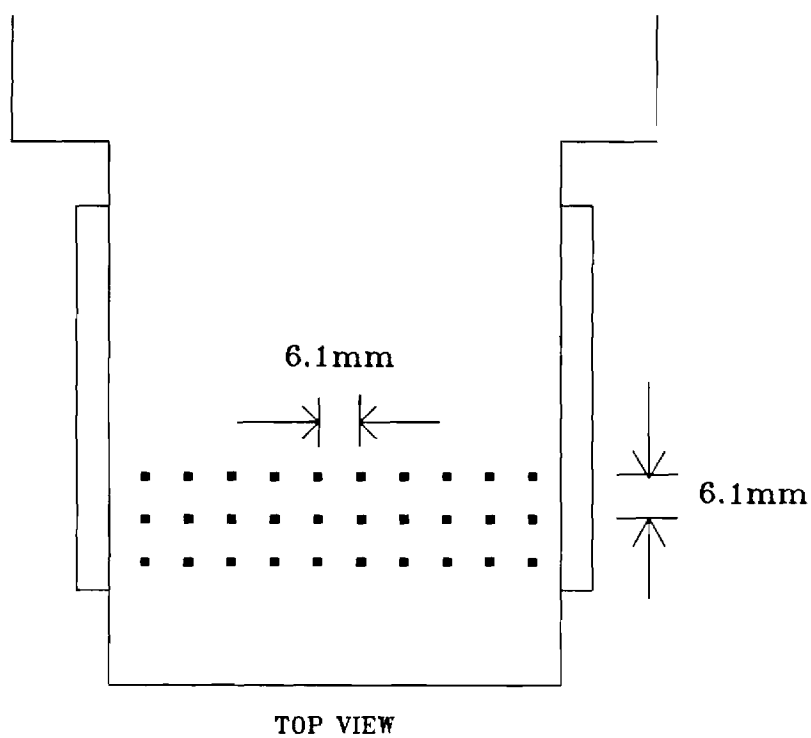


Fig. 11 Locations at which the Laser Doppler Velocimeter Results Shown in Figures 12 through 29 were Obtained. Each Location is Labeled (m,n).

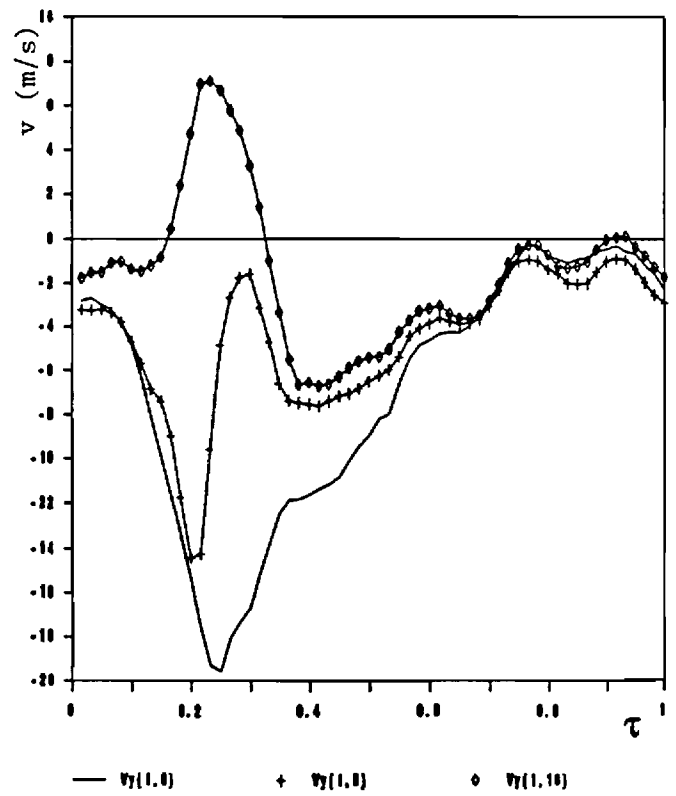
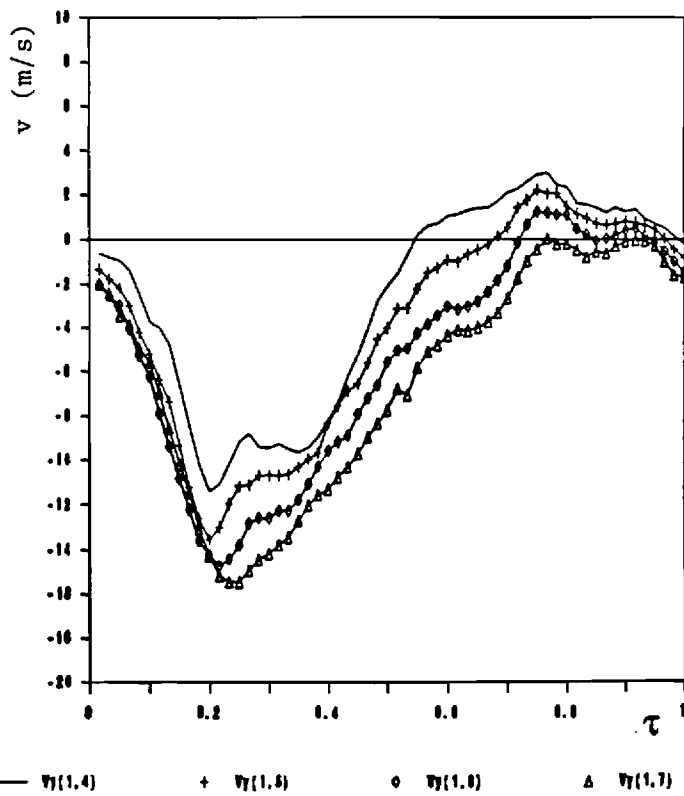
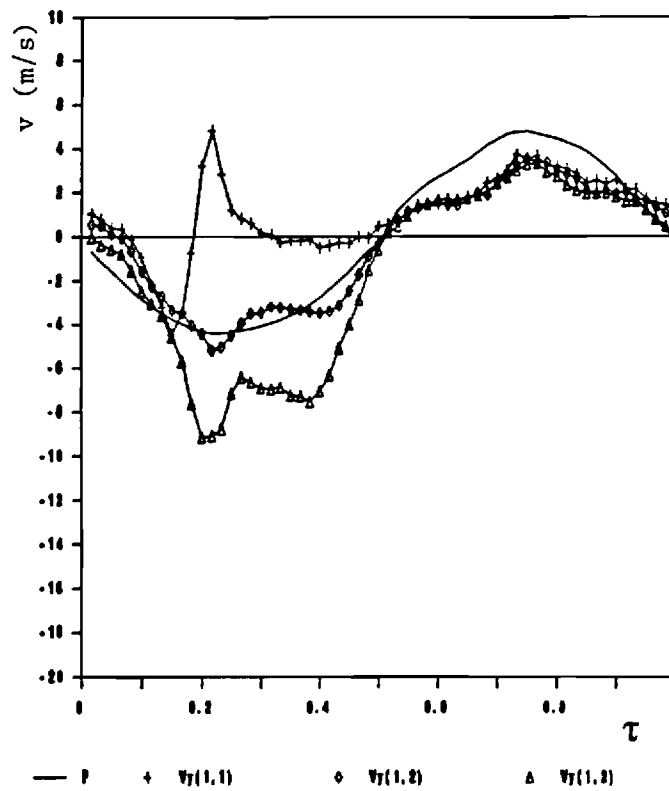


Fig. 12 Variation of the Vertical Mean Velocity (v) with Instant During a Cycle (τ) for Locations along the Line $m = 1$. The Top Plot includes the Pressure Trace for Reference.

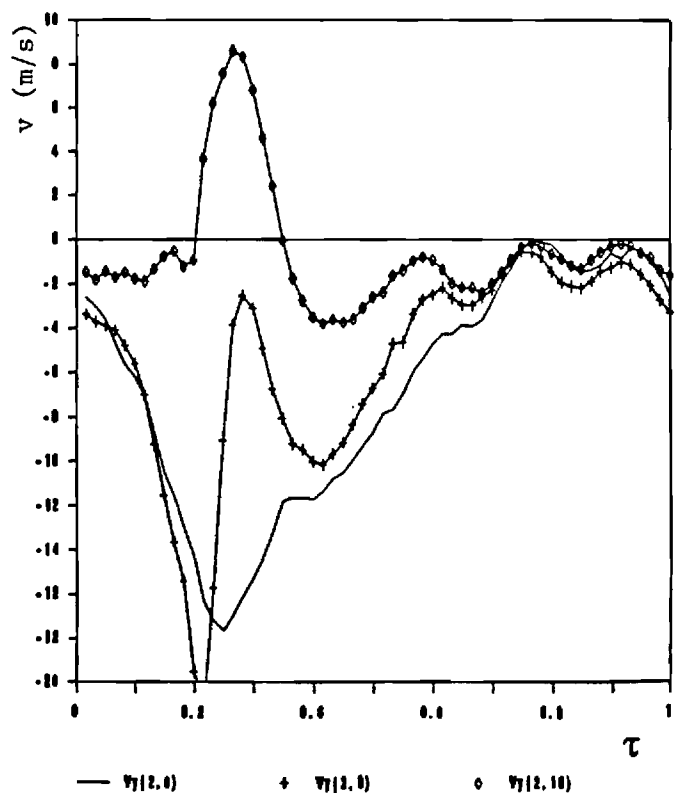
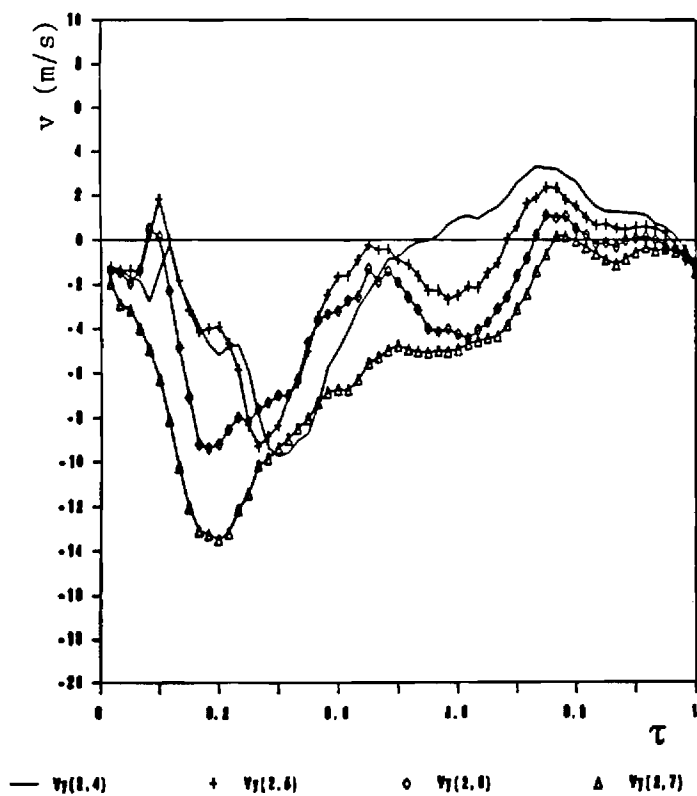
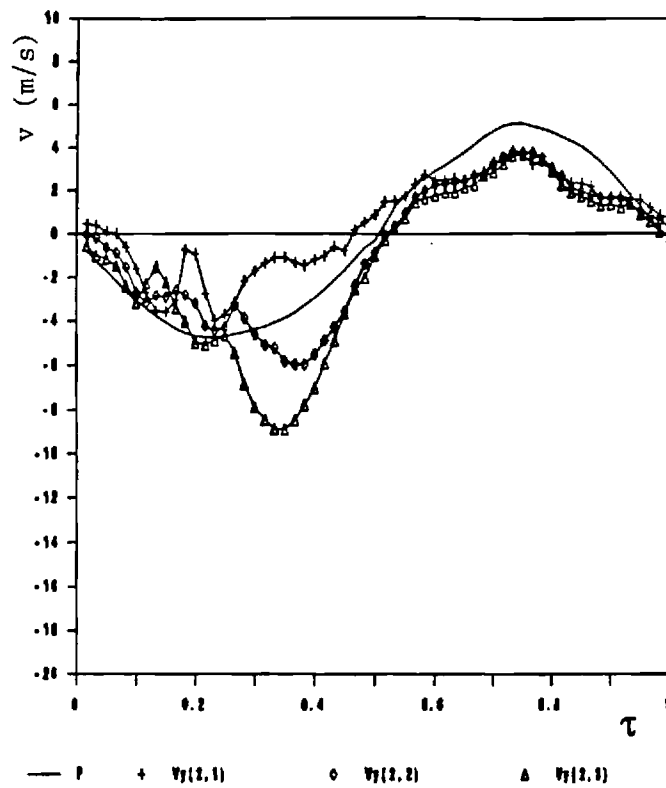


Fig. 13 Variation of the Vertical Mean Velocity (v) with Instant During a Cycle (τ) for Locations along the Line $m = 2$. The Top Plot includes the Pressure Trace for Reference.

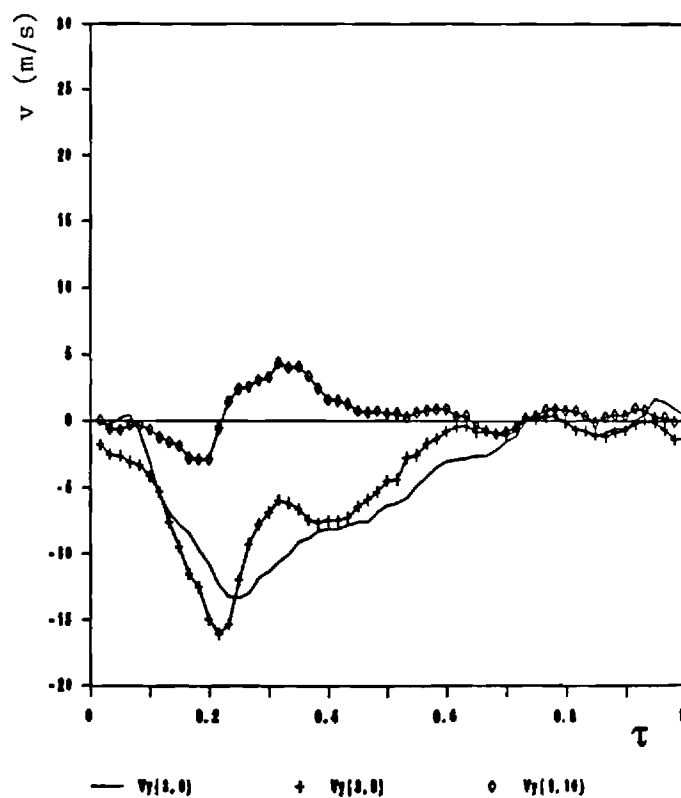
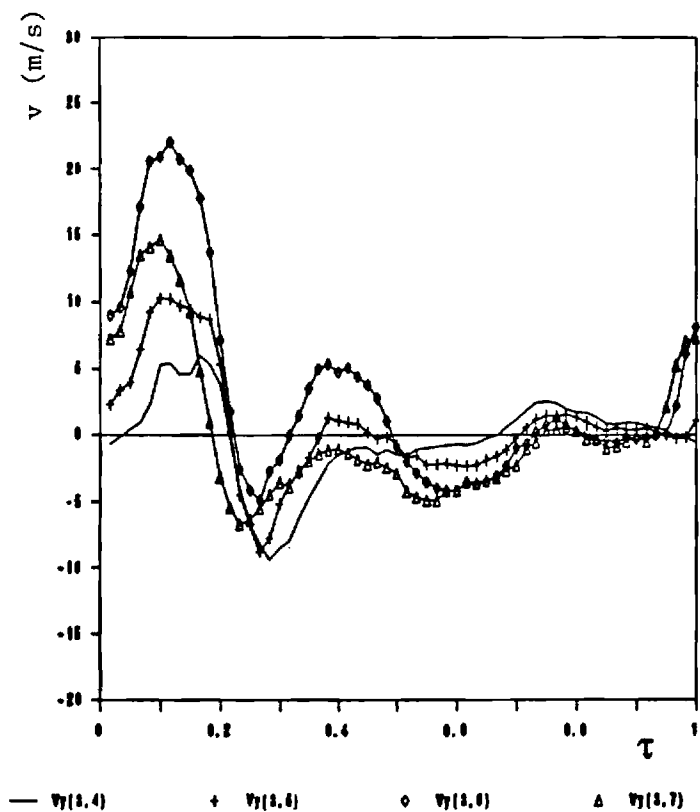
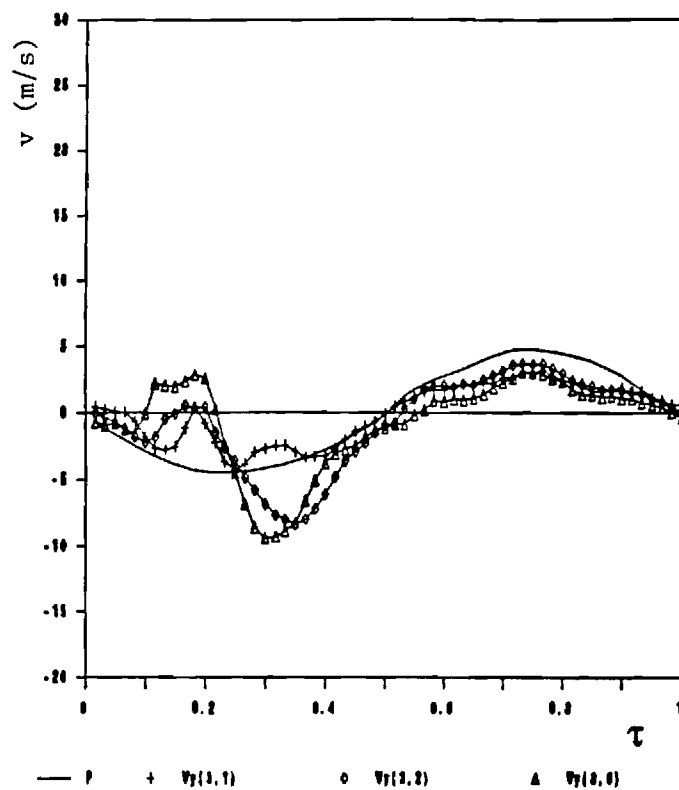


Fig. 14 Variation of the Vertical Mean Velocity (v) with Instant During a Cycle (τ) for Locations along the Line $m = 3$. The Top Plot includes the Pressure Trace for Reference.

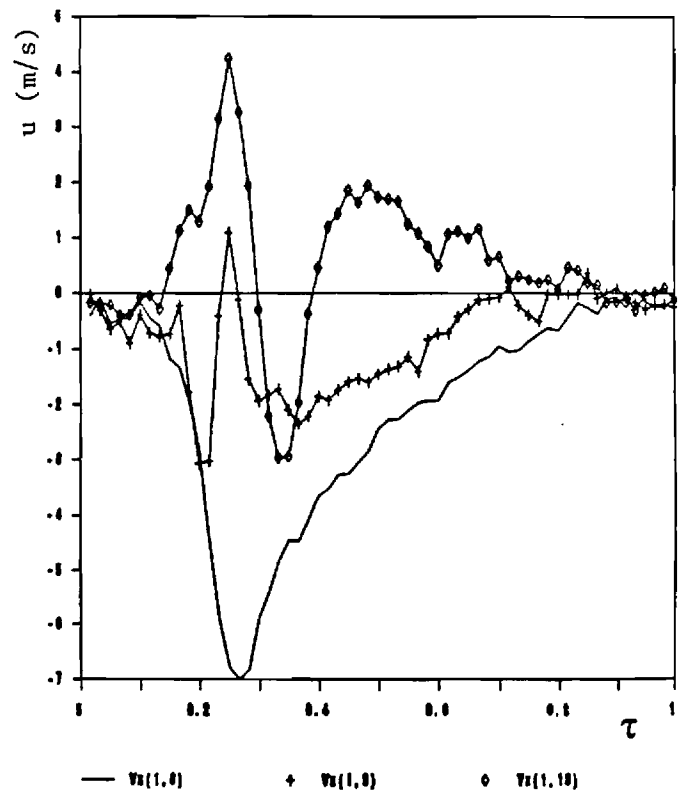
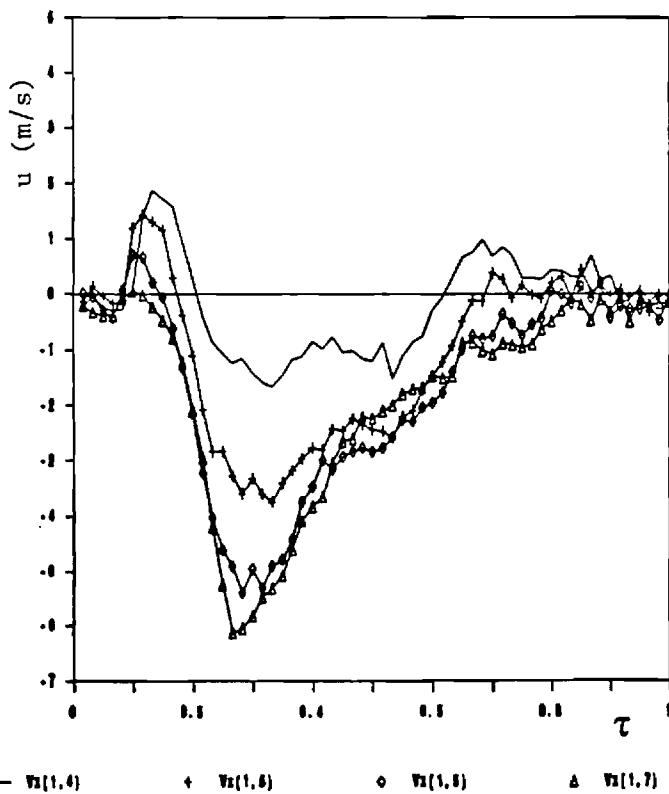
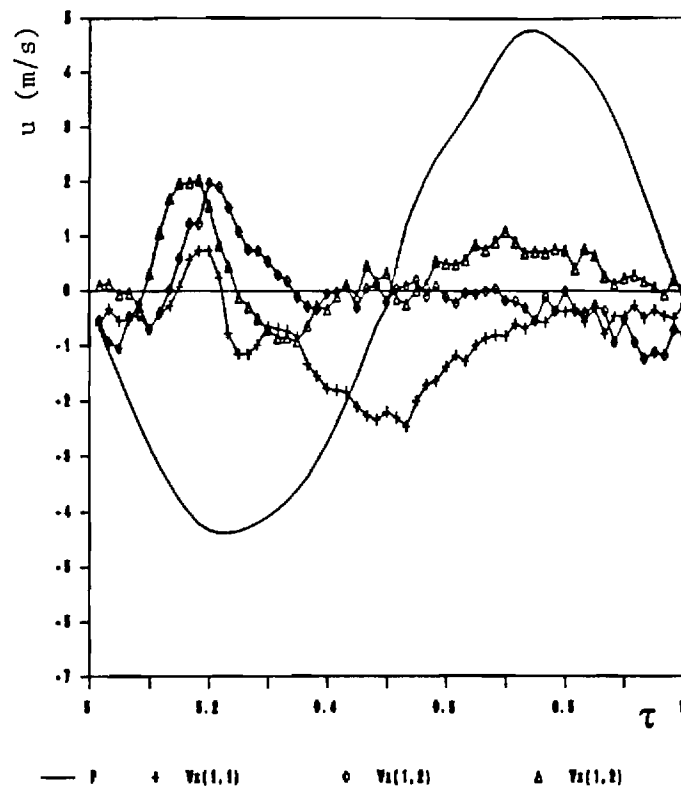


Fig. 15 Variation of the Axial Mean Velocity (u) with Instant During a Cycle (τ) for Locations along the Line $m = 1$. The Top Plot includes the Pressure Trace for Reference.

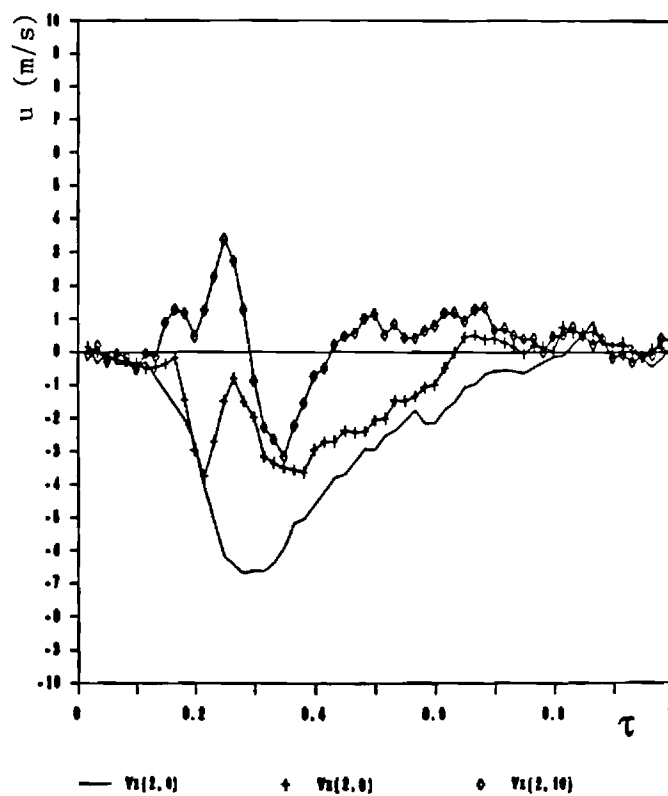
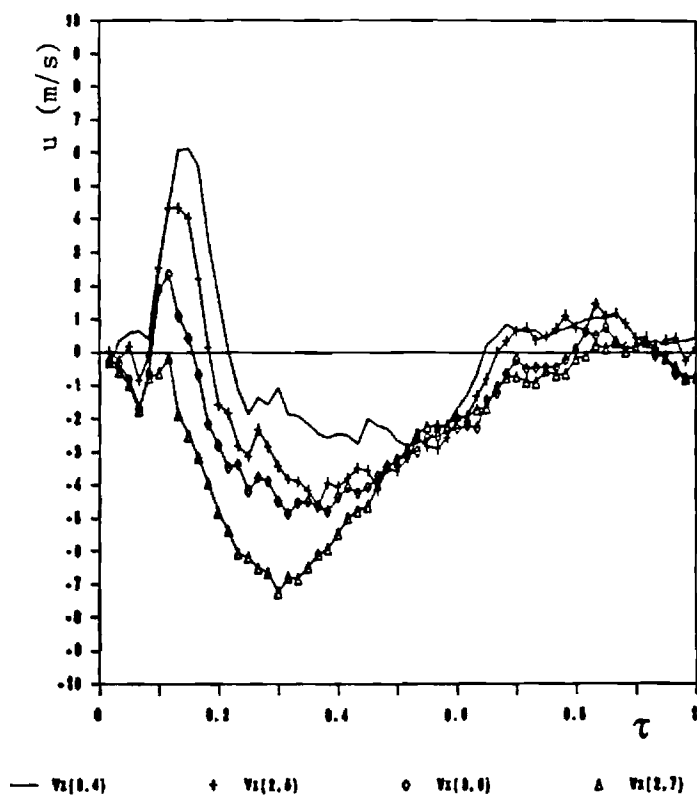
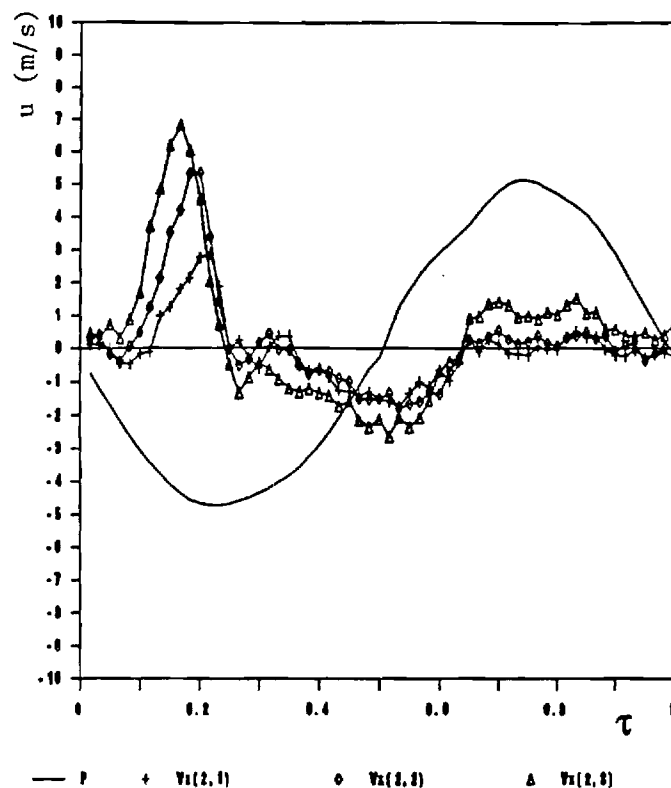


Fig. 16 Variation of the Axial Mean Velocity (u) with Instant During a Cycle (τ) for Locations along the Line $m = 2$. The Top Plot includes the Pressure Trace for Reference.

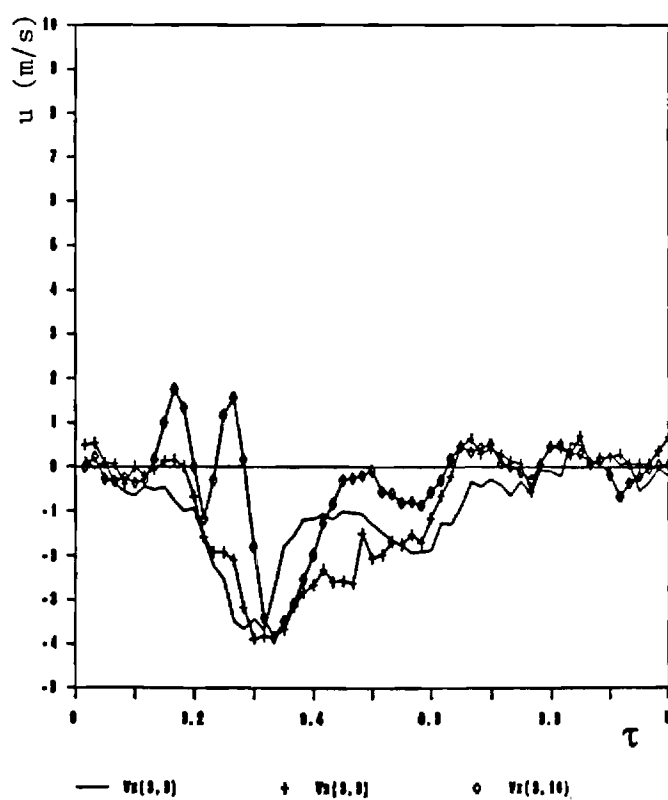
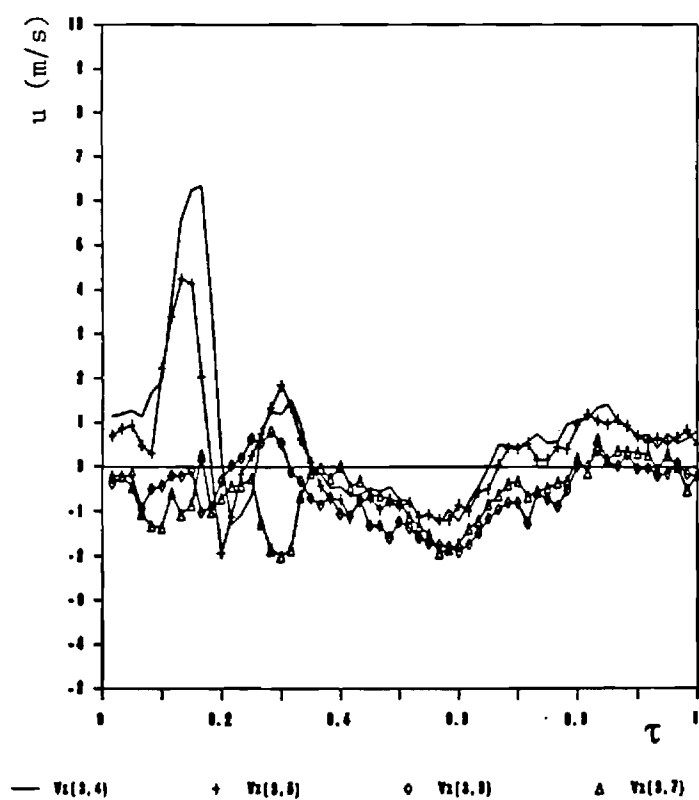
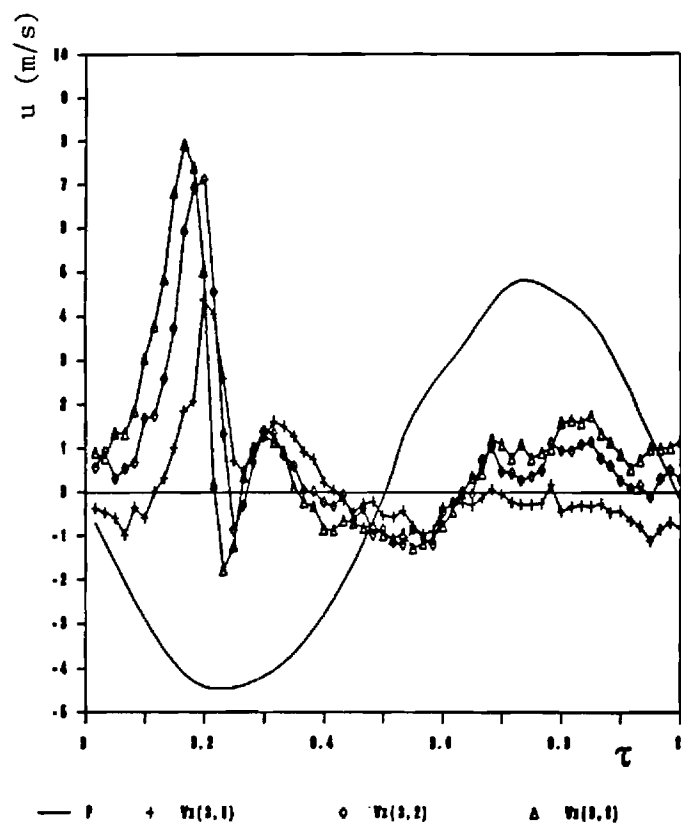


Fig. 17 Variation of the Axial Mean Velocity (u) with Instant During a Cycle (τ) for Locations along the Line $m = 3$. The Top Plot includes the Pressure Trace for Reference.

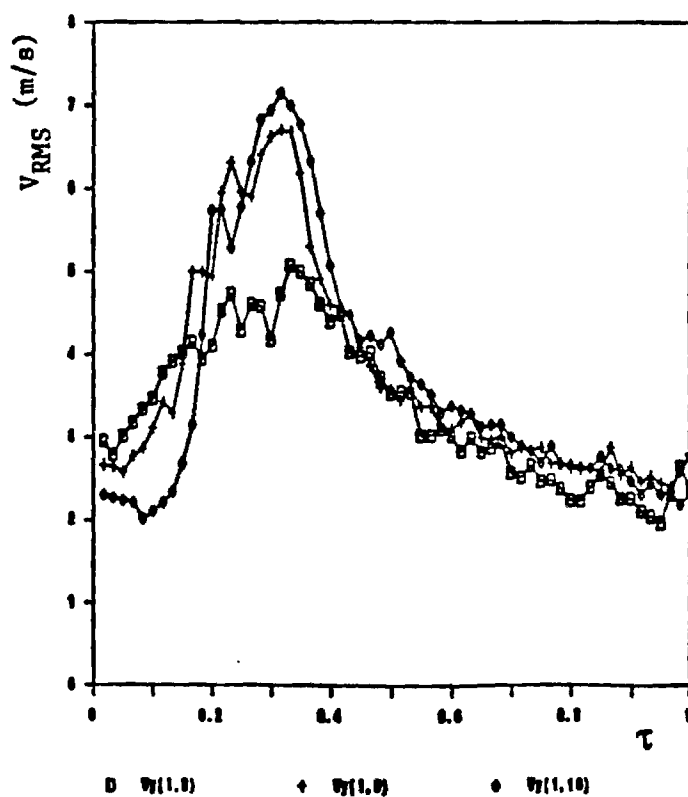
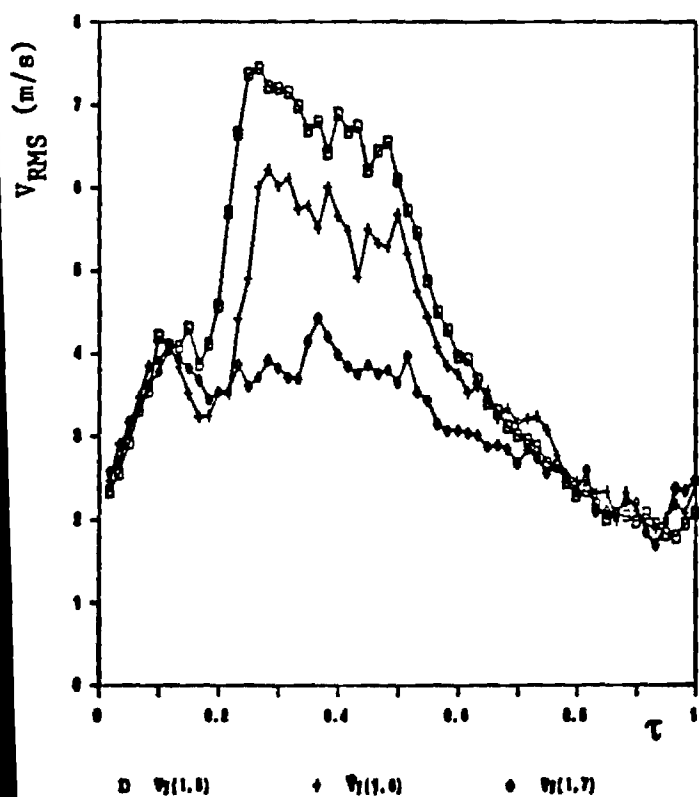
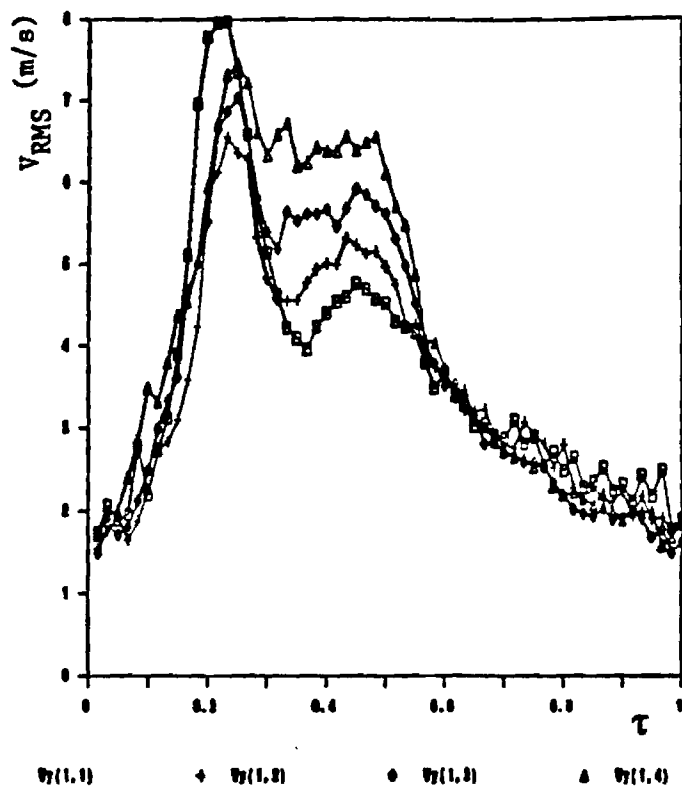


Fig. 18 Variation of the Vertical Turbulence Intensity (v_{RMS}) with Instant During a Cycle (τ) for Locations along the Line $m=1$.

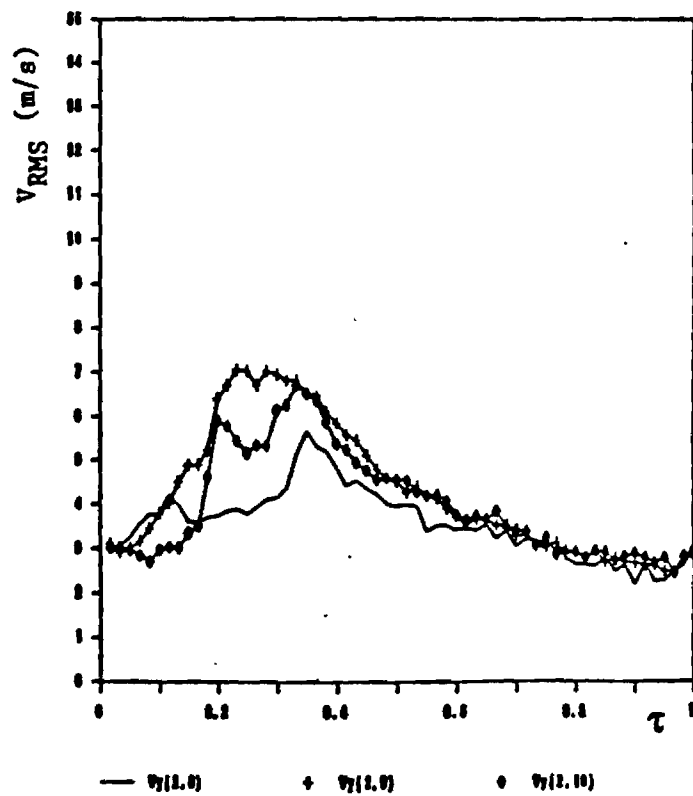
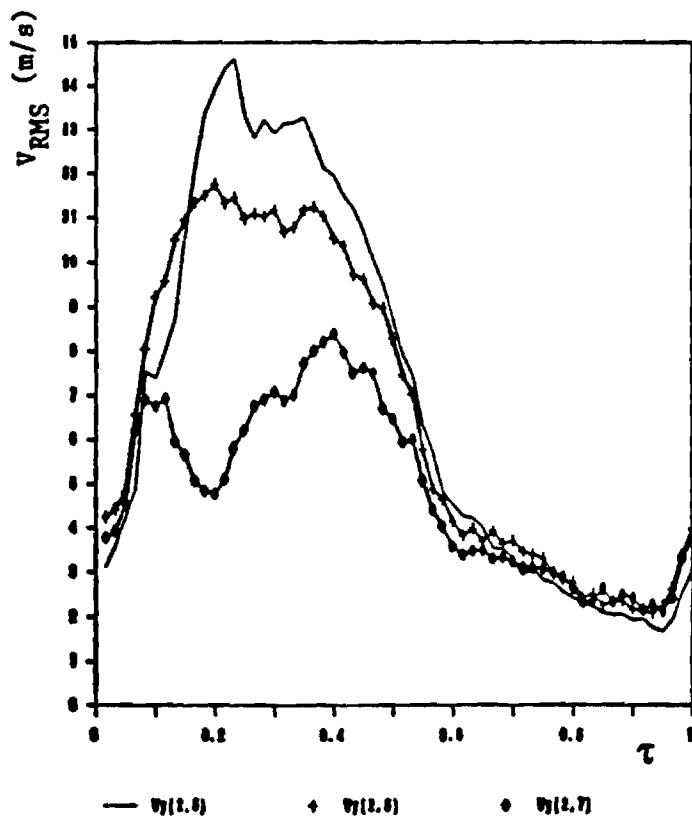
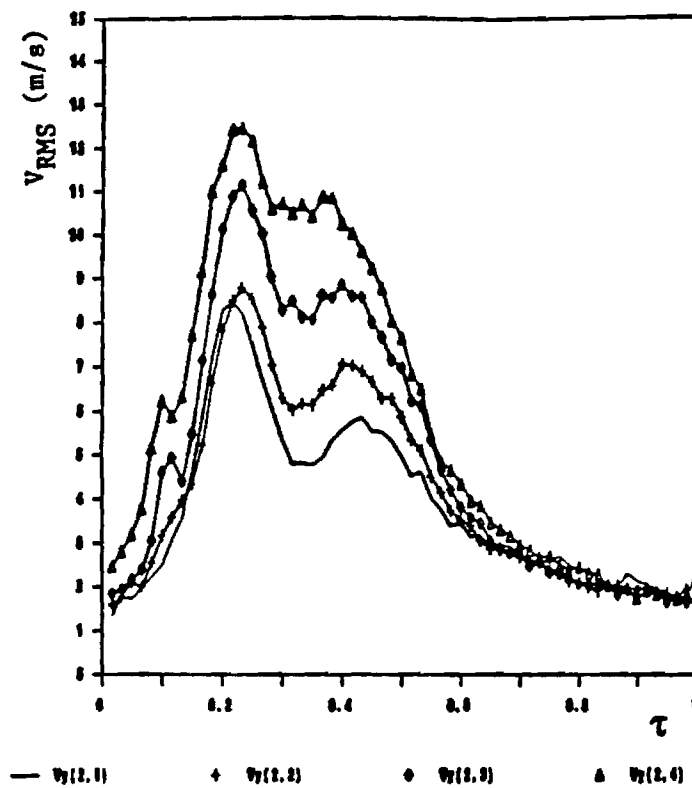


Fig. 19 Variation of the Vertical Turbulence Intensity (v_{RMS}) with Instant During a Cycle (τ) for Locations along the Line $m = 2$.

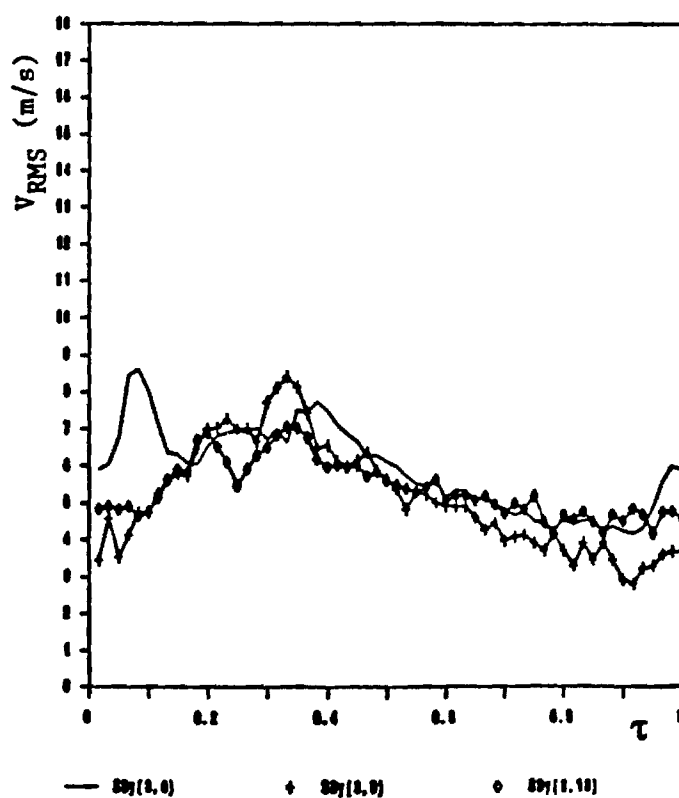
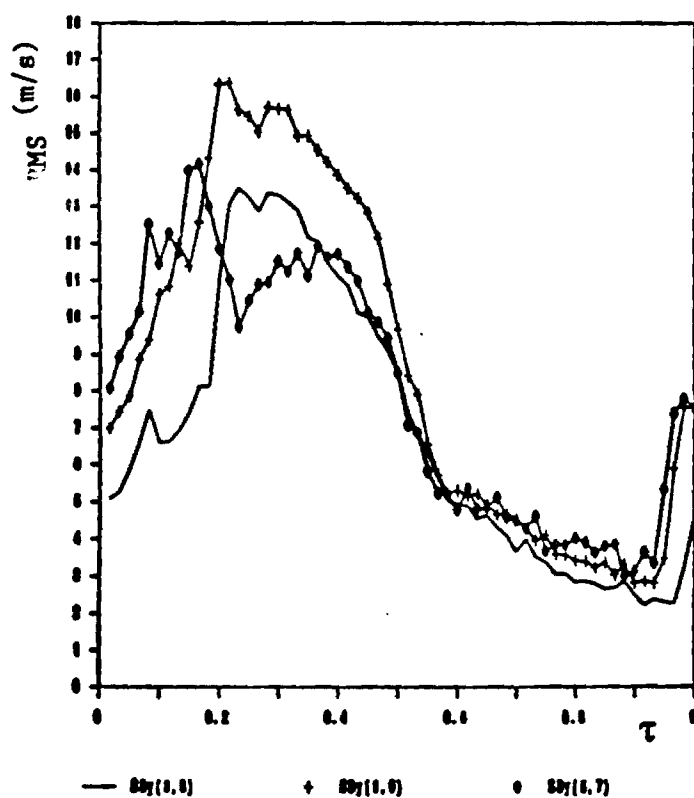
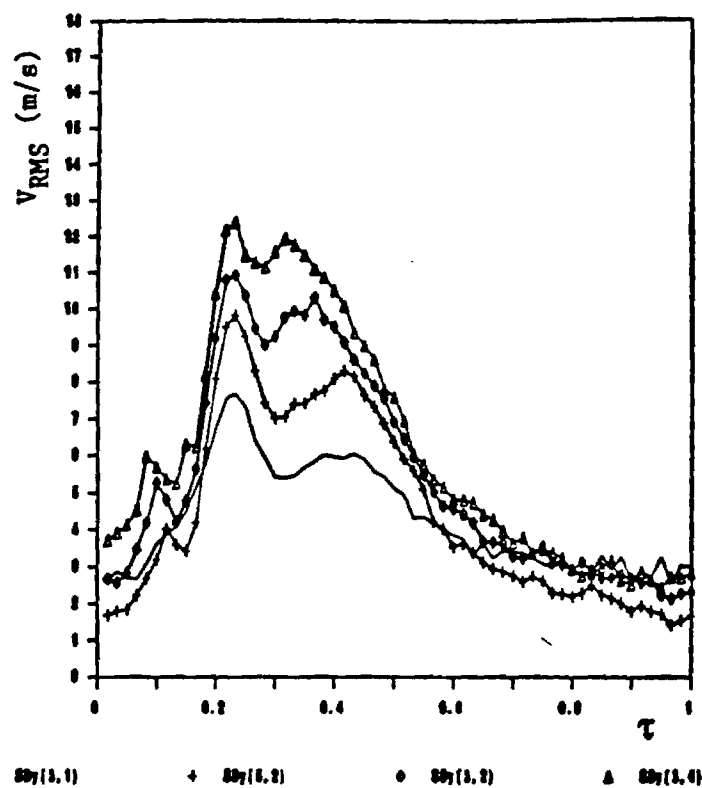


Fig. 20 Variation of the Vertical Turbulence Intensity (v_{RMS}) with Instant During a Cycle (τ) or Locations along the Line $m = 3$.

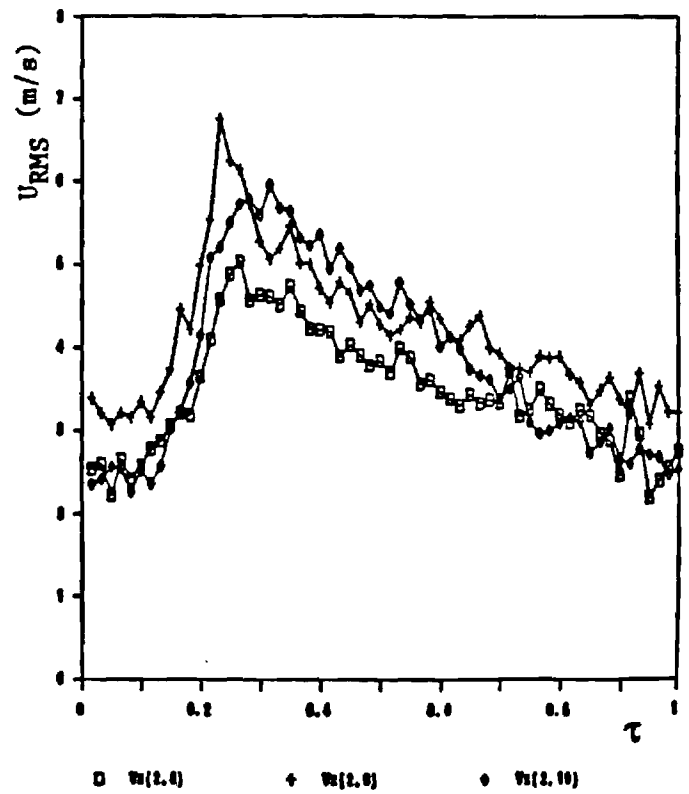
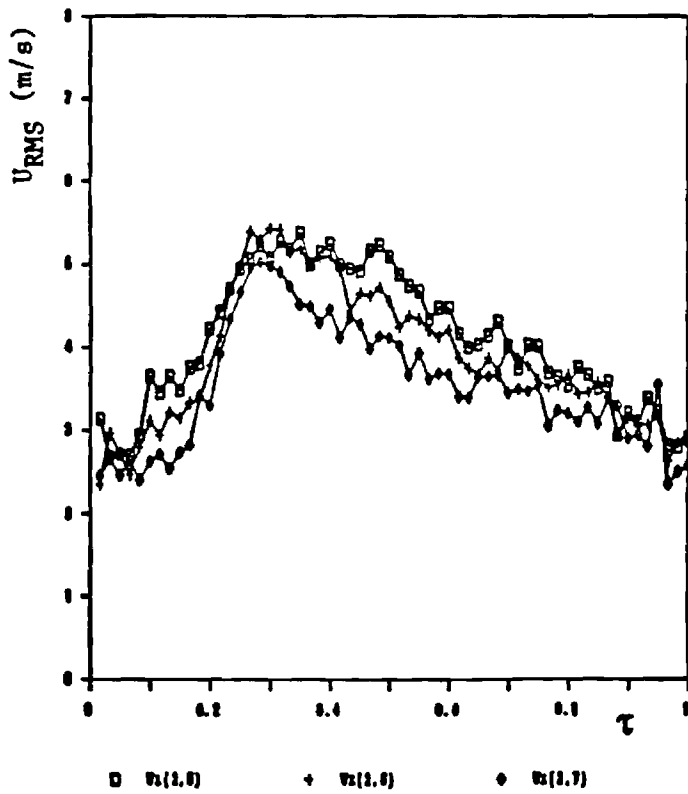
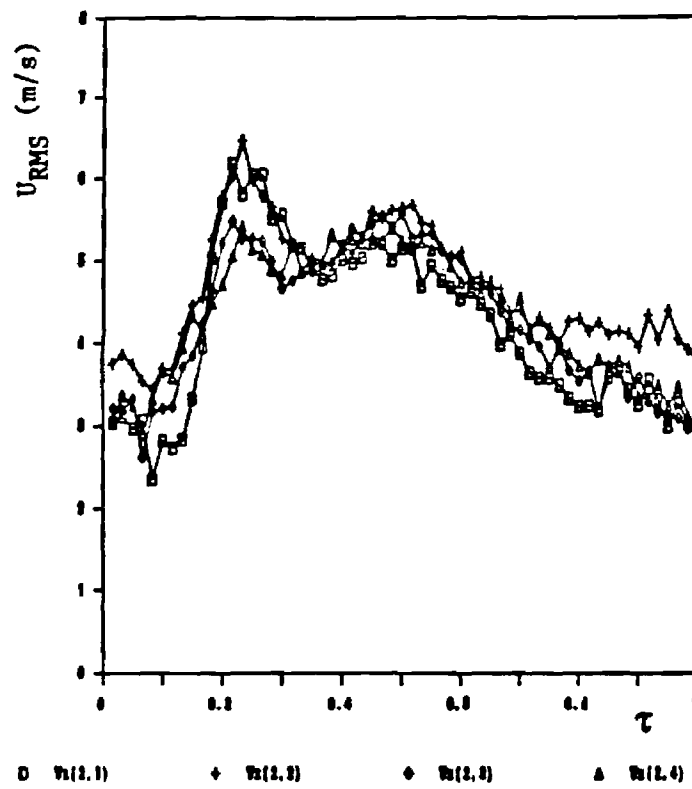


Fig. 21 Variation of the Axial Turbulence Intensity (u_{RMS}) with Instant During a Cycle (τ) for Locations along the Line $m = 1$.

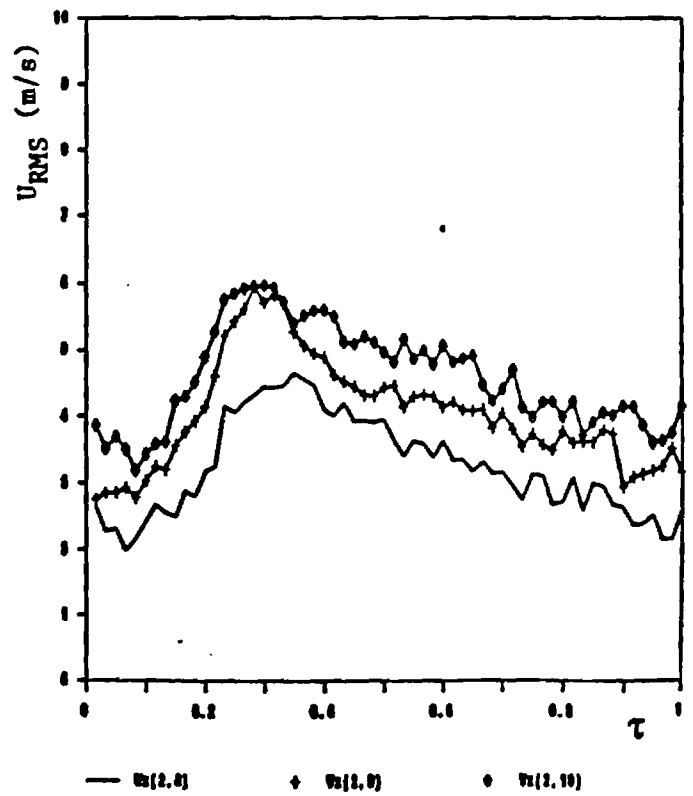
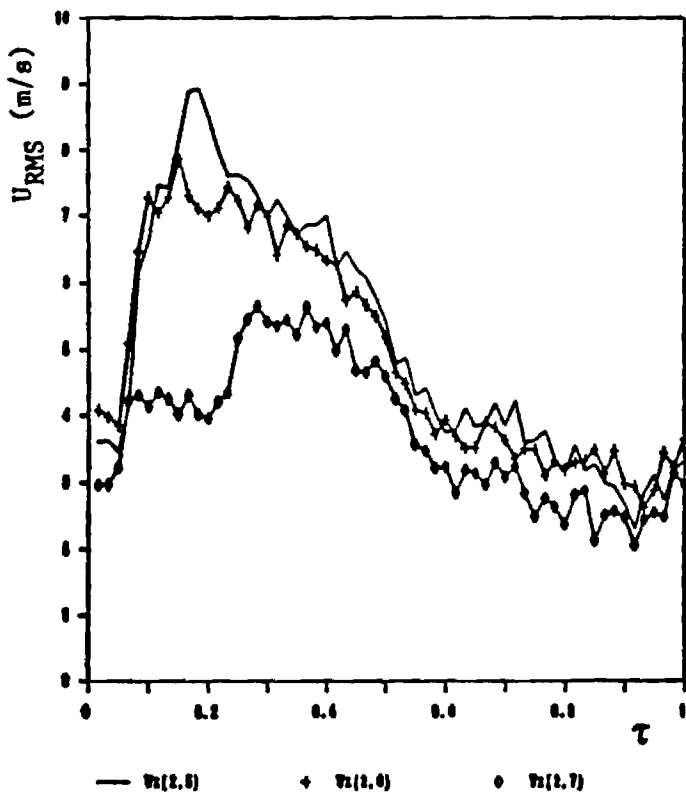
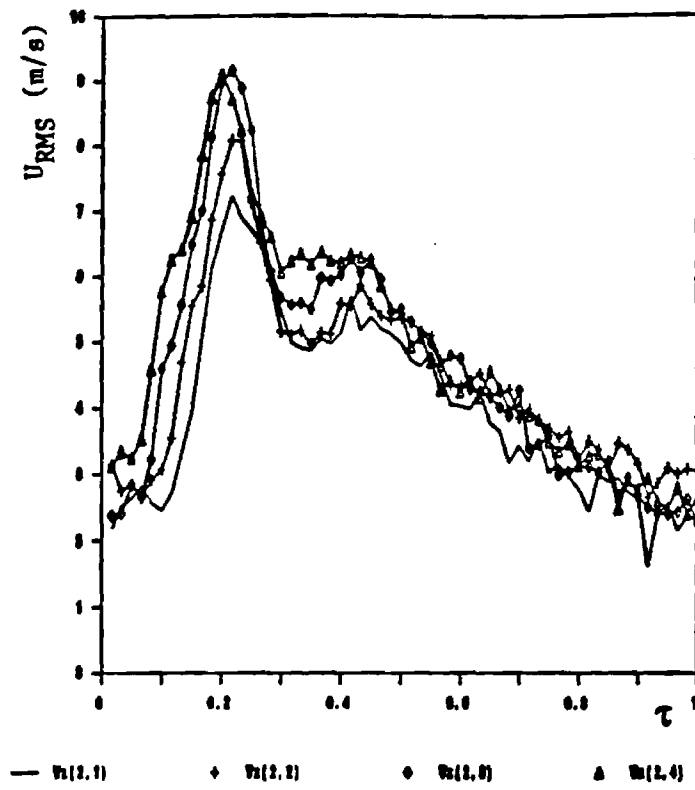


Fig. 22 Variation of the Axial Turbulence Intensity (u_{RMS}) with Instant During a Cycle (τ) for Locations along the Line $m = 2$.

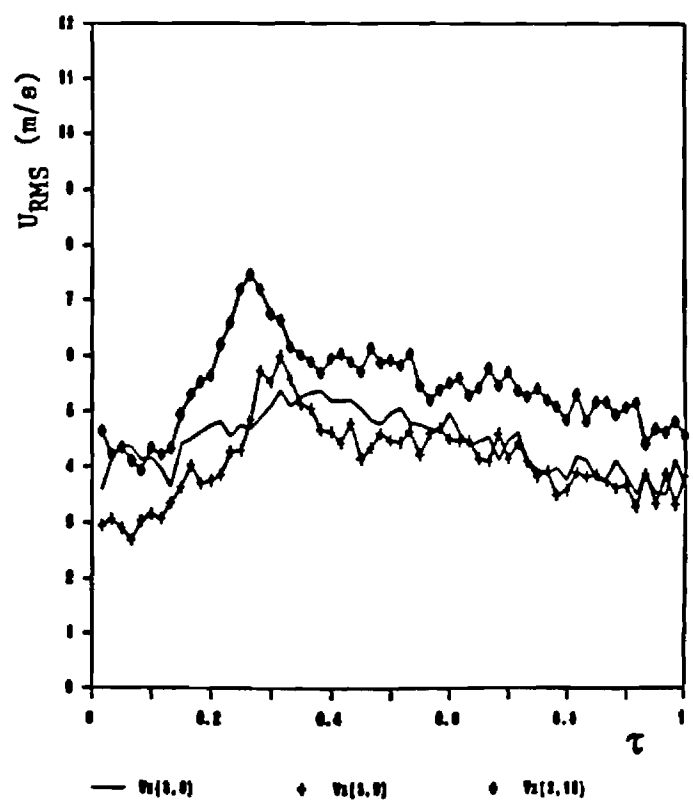
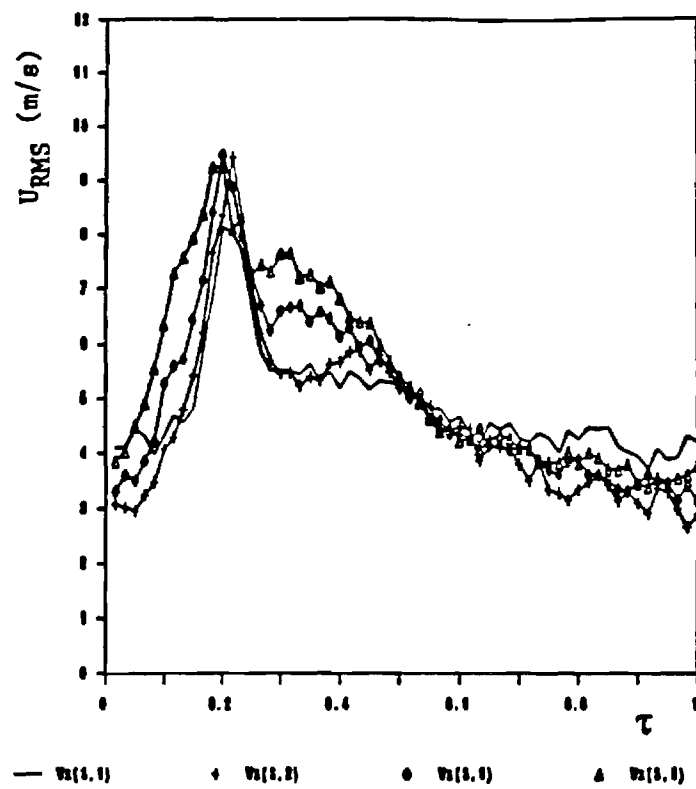


Fig. 23 Variation of the Axial Turbulence Intensity (u_{RMS}) with Instant During a Cycle (τ) for Locations along the Line $m = 3$.

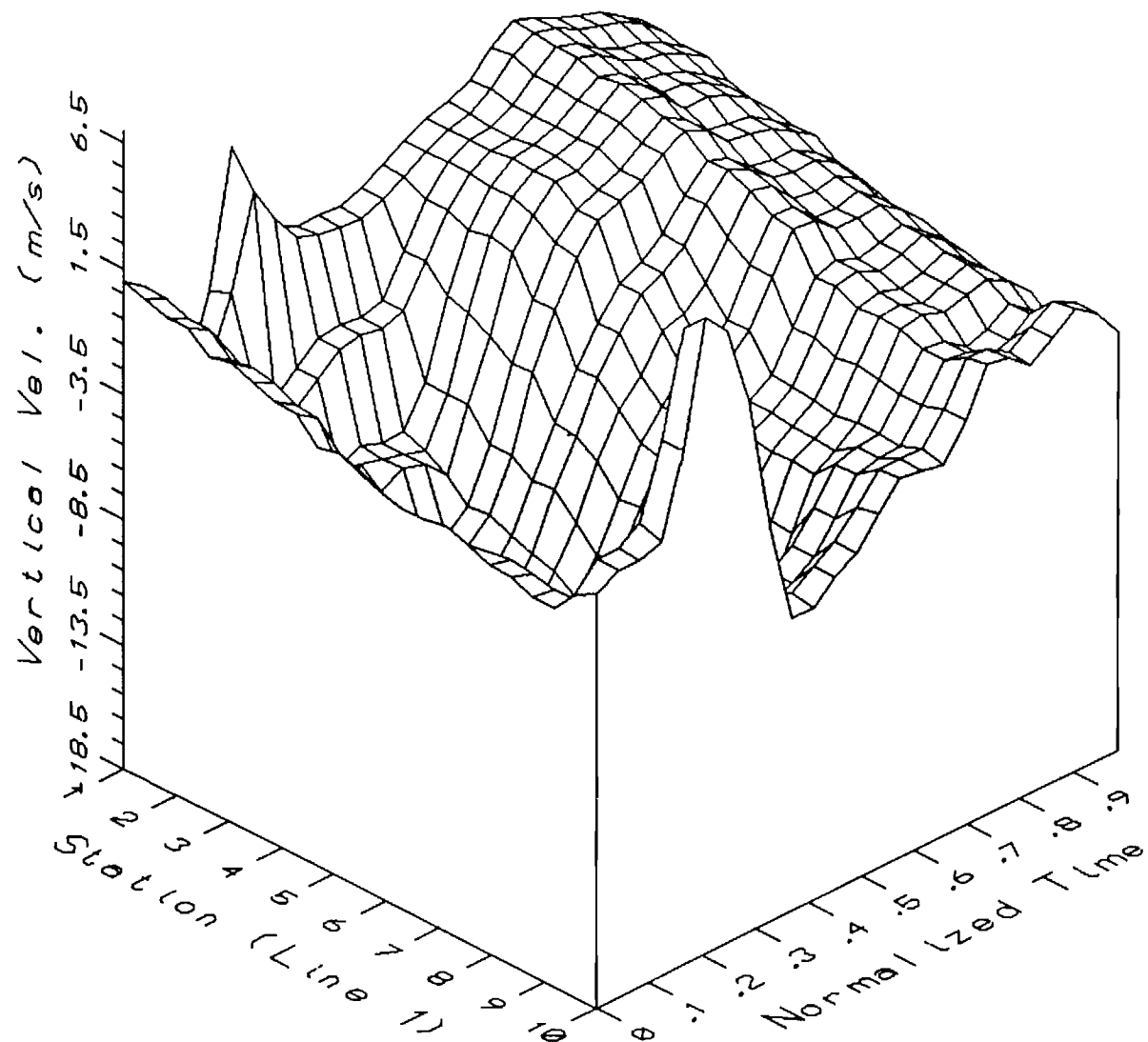


Fig. 24 Three Dimensional Plot of Vertical Mean Velocities during a Cycle for Locations along the Line $m = 1$.

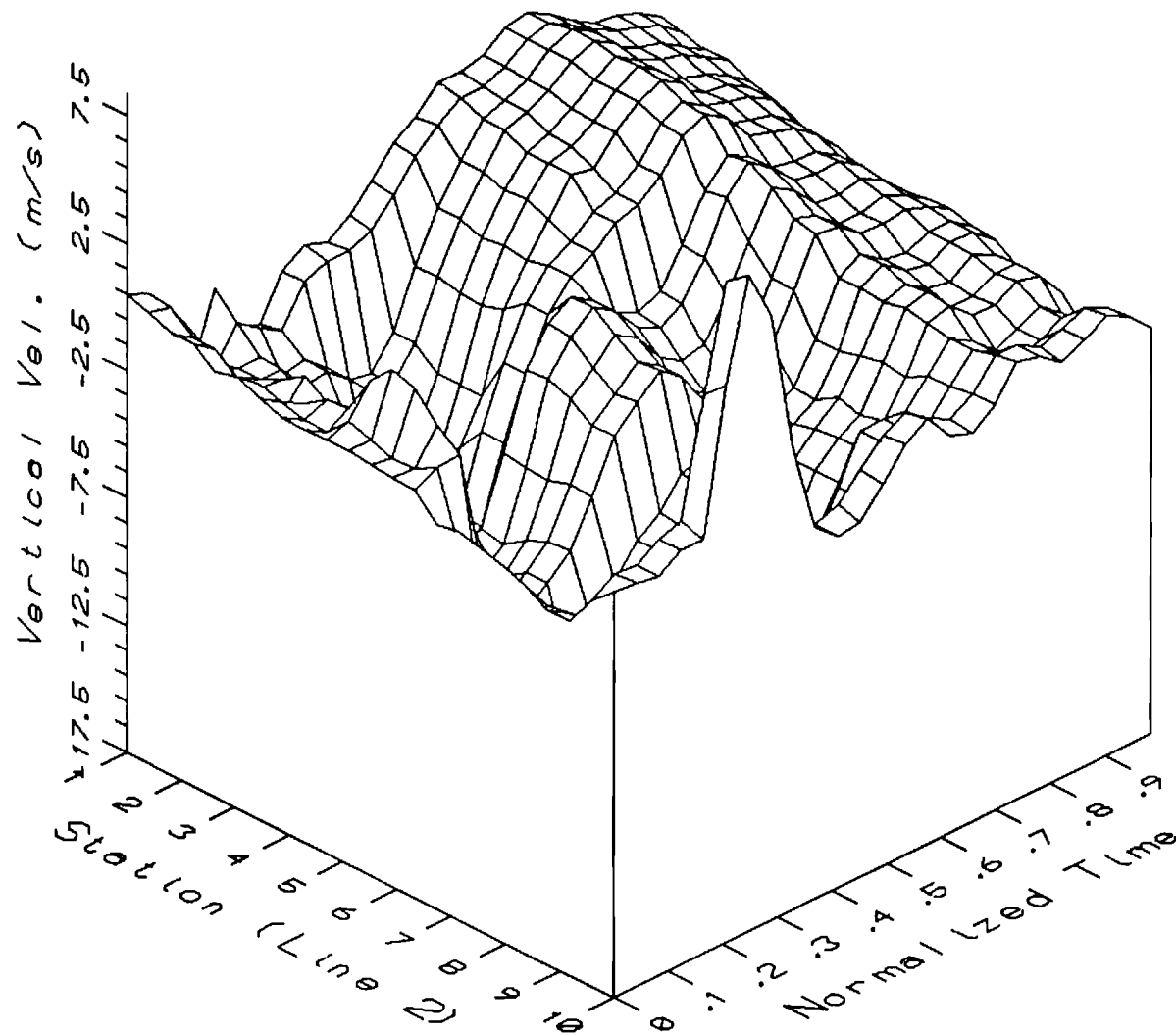


Fig. 25 Three Dimensional Plot of Vertical Mean Velocities during a Cycle for Locations along the Line $m = 2$.

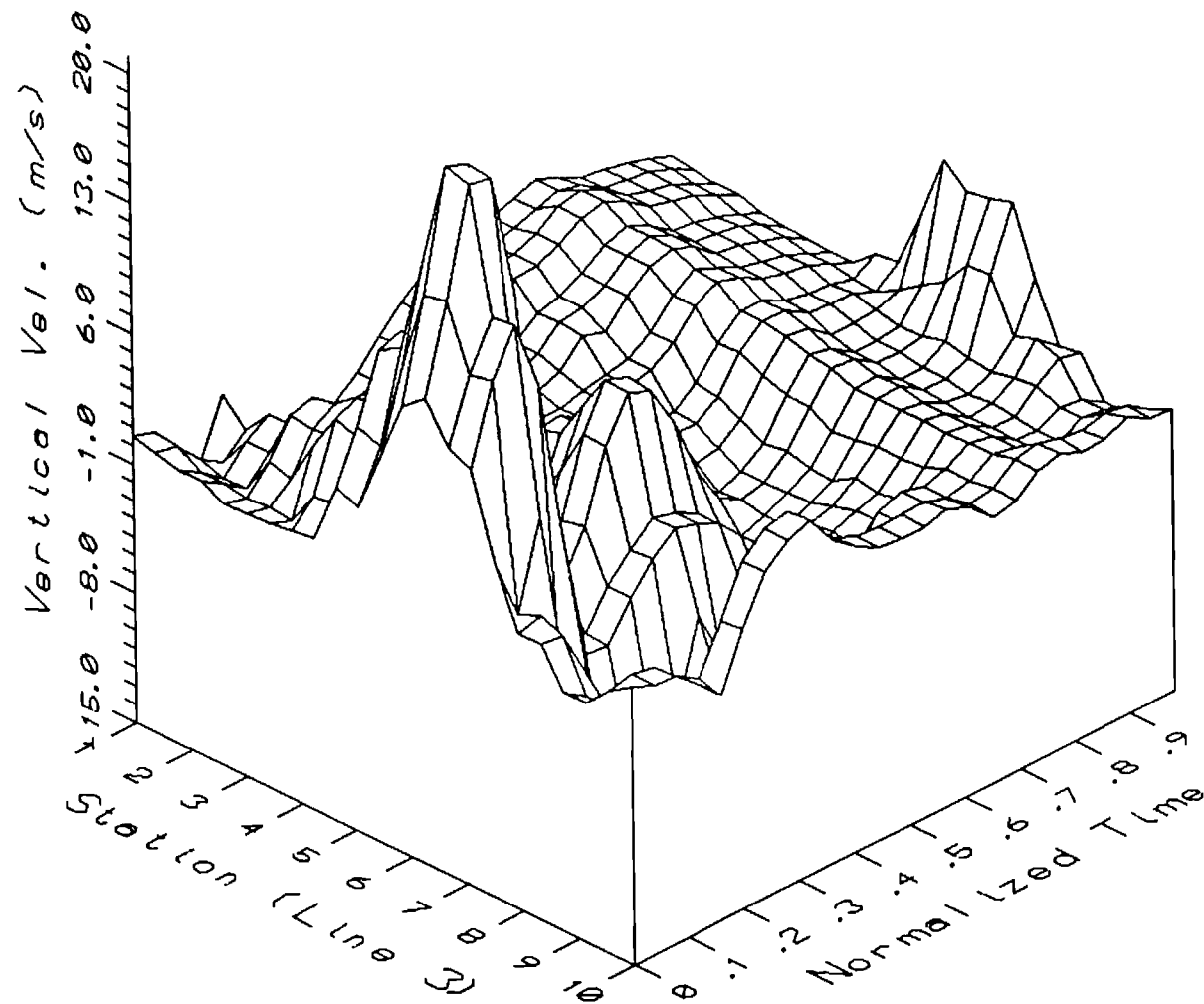


Fig. 26 Three Dimensional Plot of Vertical Mean Velocities during a Cycle for Locations along the Line $m = 3$.

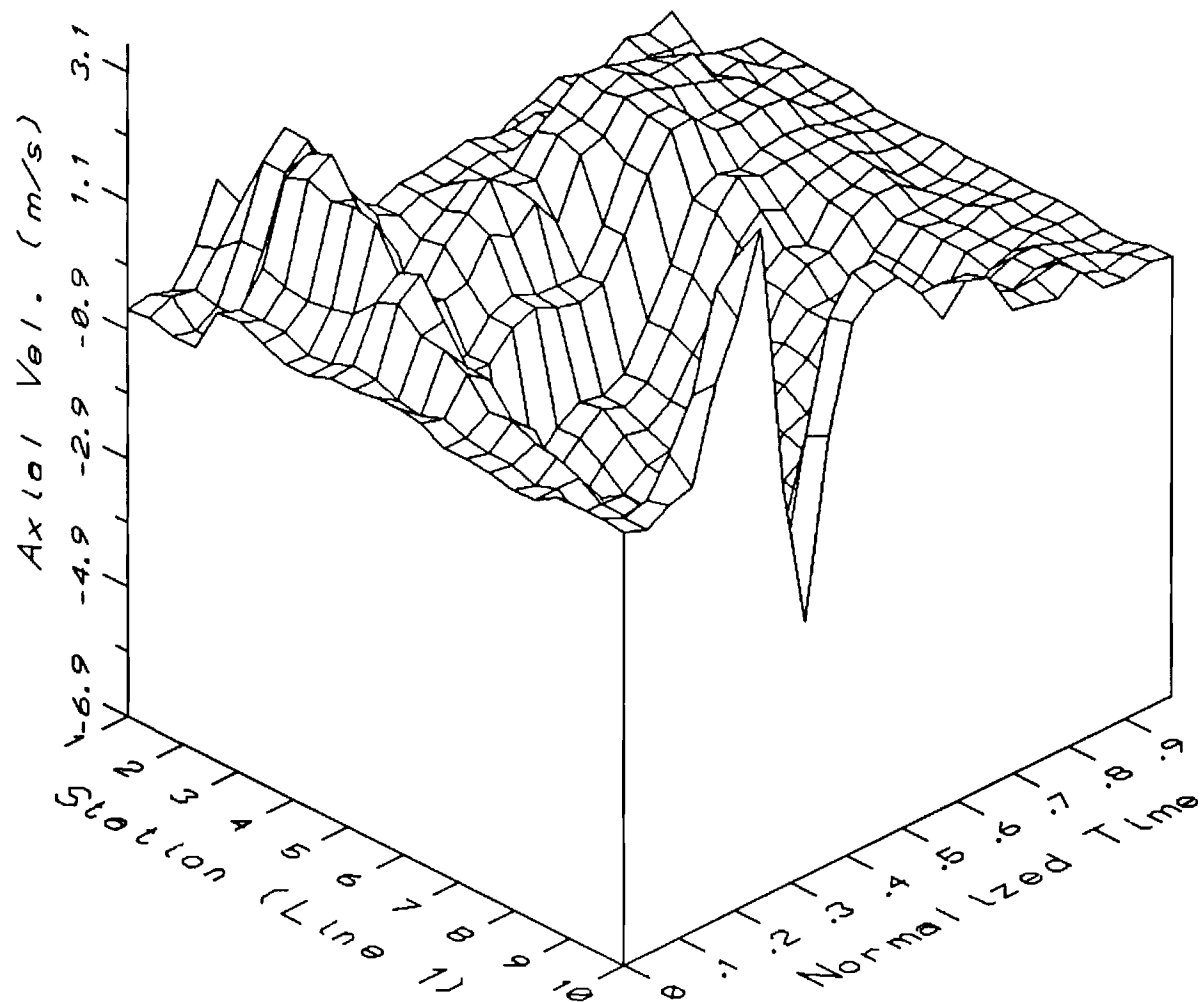


Fig. 27 Three Dimensional Plot of Axial Mean Velocities during a Cycle for Locations along the Line $m = 1$.

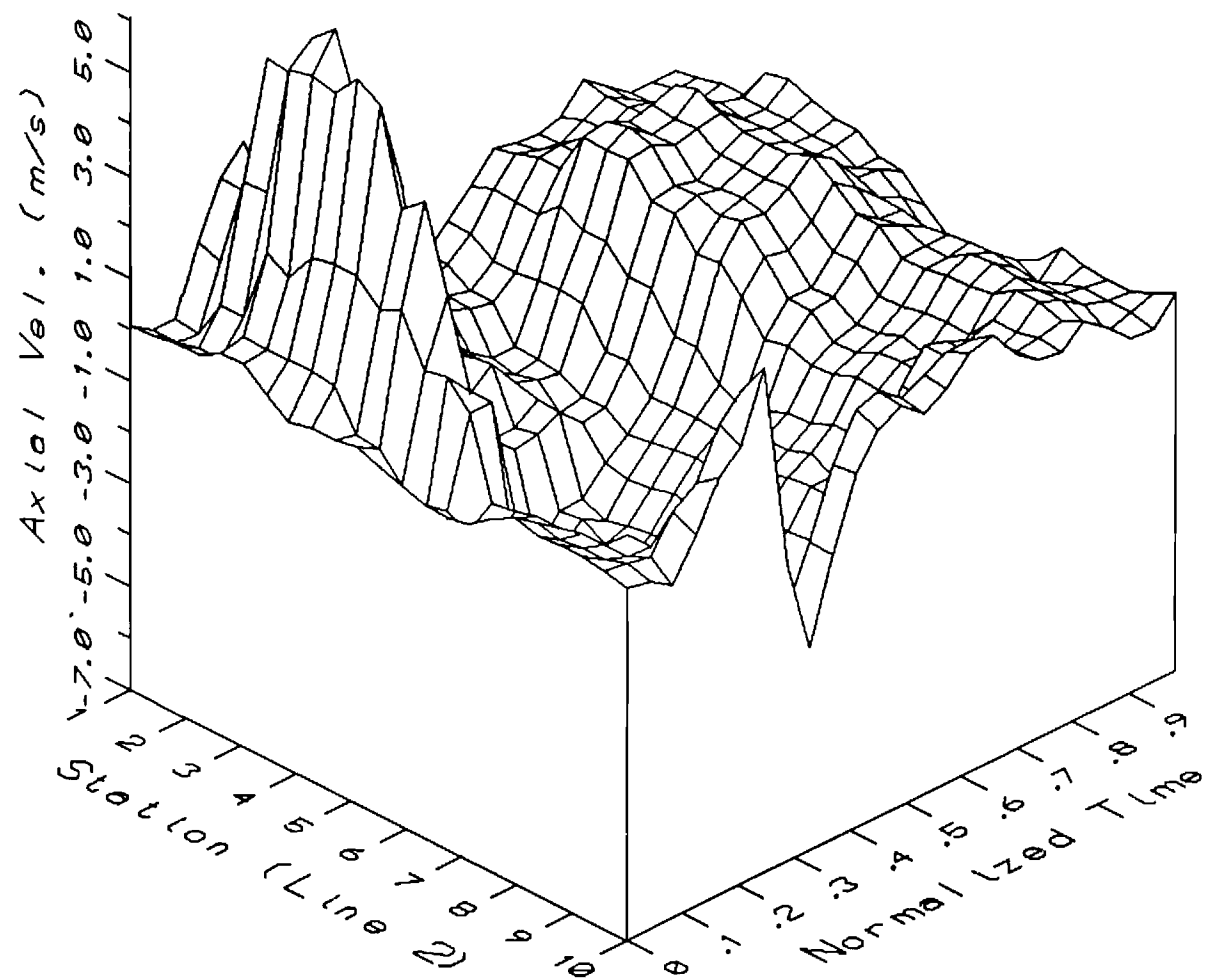


Fig. 28 Three Dimensional Plot of Axial Mean Velocities during a Cycle for Locations along the Line $m = 2$.

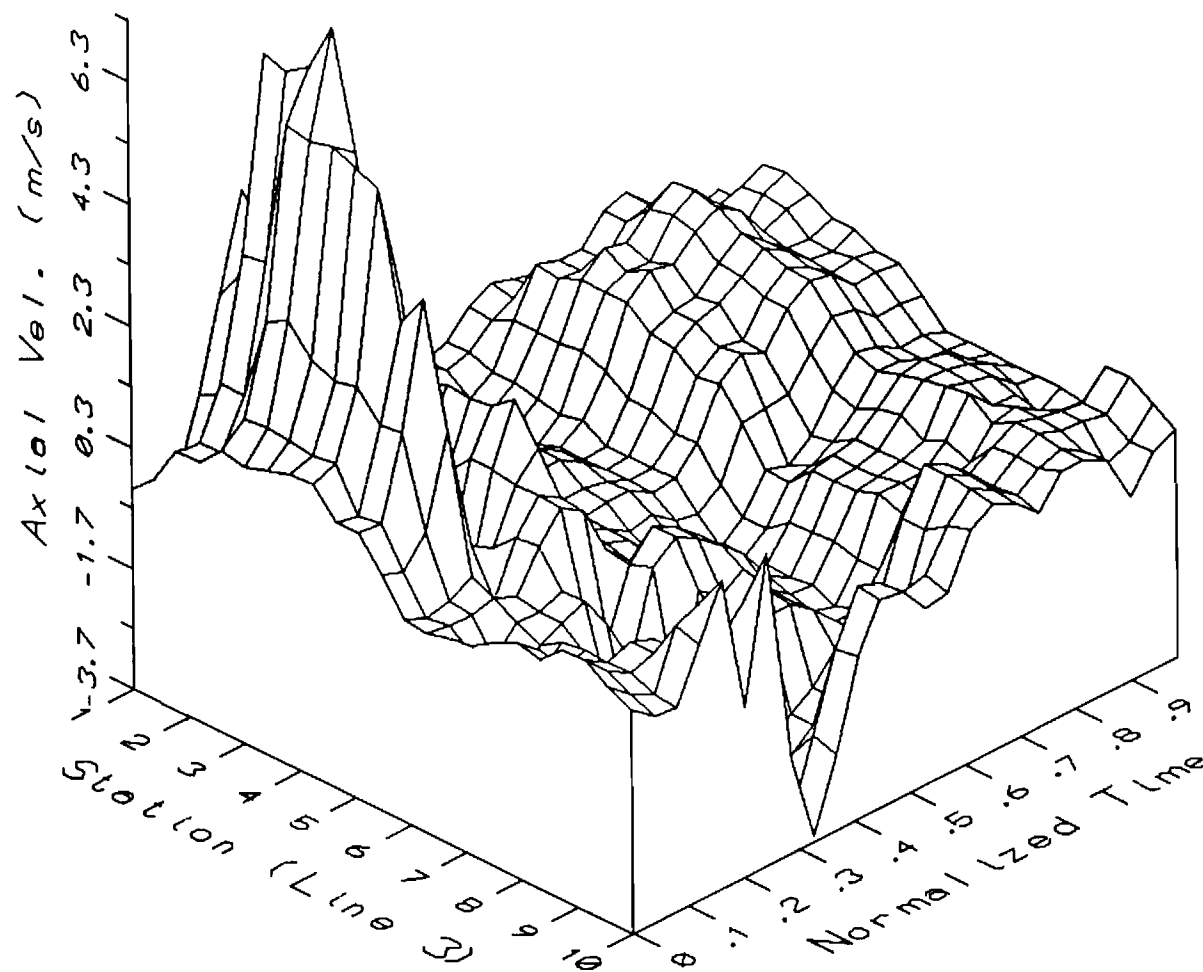


Fig. 29 Three Dimensional Plot of Axial Mean Velocities during a Cycle for Locations along the Line $m = 3$.

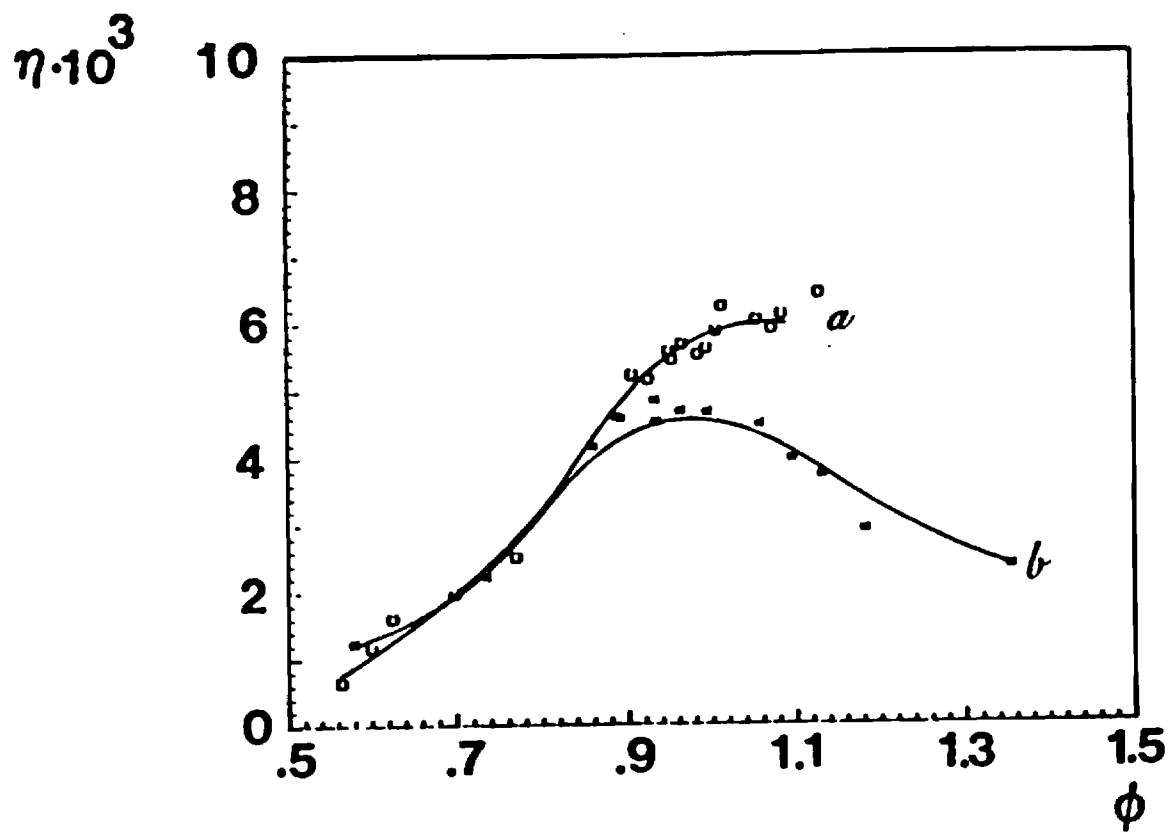


Fig. 30 Rayleigh Efficiency (η) as a Function of Equivalence Ratio (ϕ) for the Combustor Fitted with the a) Standard and b) Long Tailpipes.

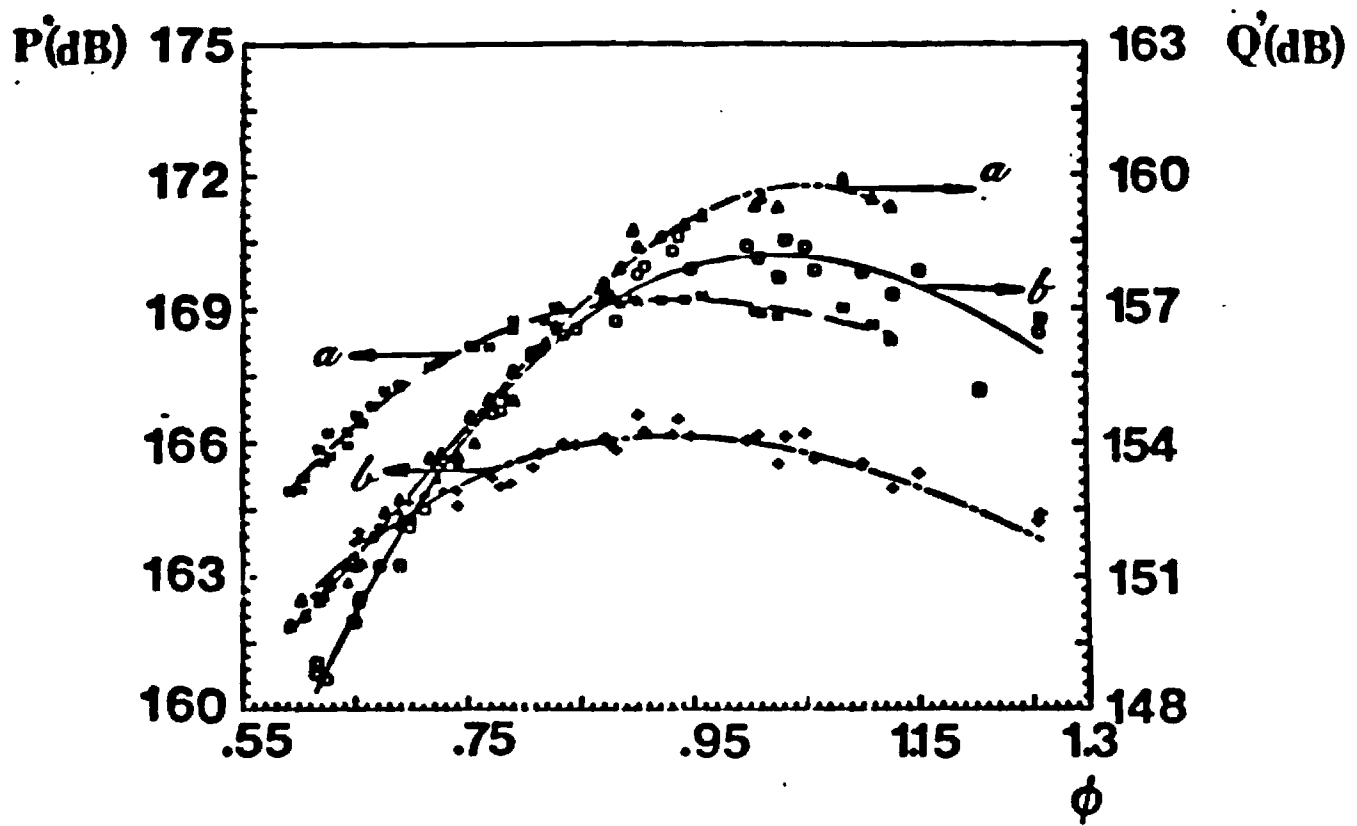


Fig. 31 Pressure (P') and Heat Release Fluctuations (Q') as a Function of Equivalence Ratio (ϕ) for the Combustor Fitted with the a) Standard and b) Long Tailpipes.

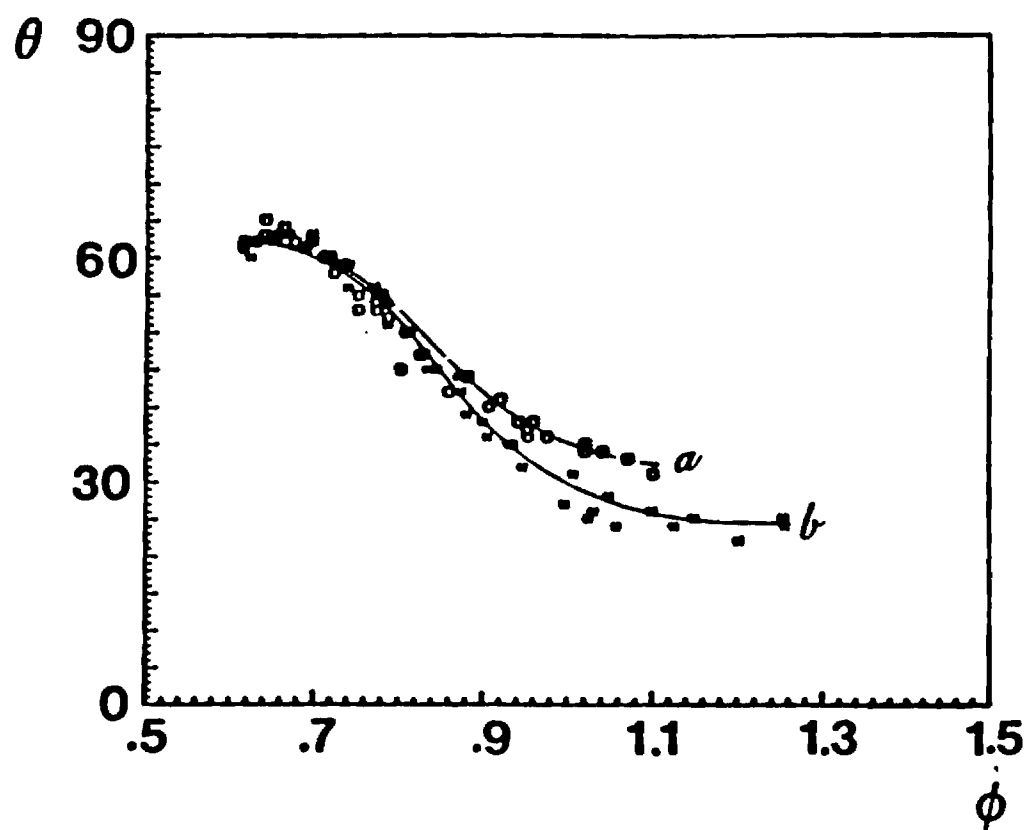


Fig. 32 Phase Angle (θ) by which the Heat Release Leads the Pressure as a Function of Equivalence Ratio (ϕ) for the Combustor Fitted with the a) Standard and b) Long Tailpipes.

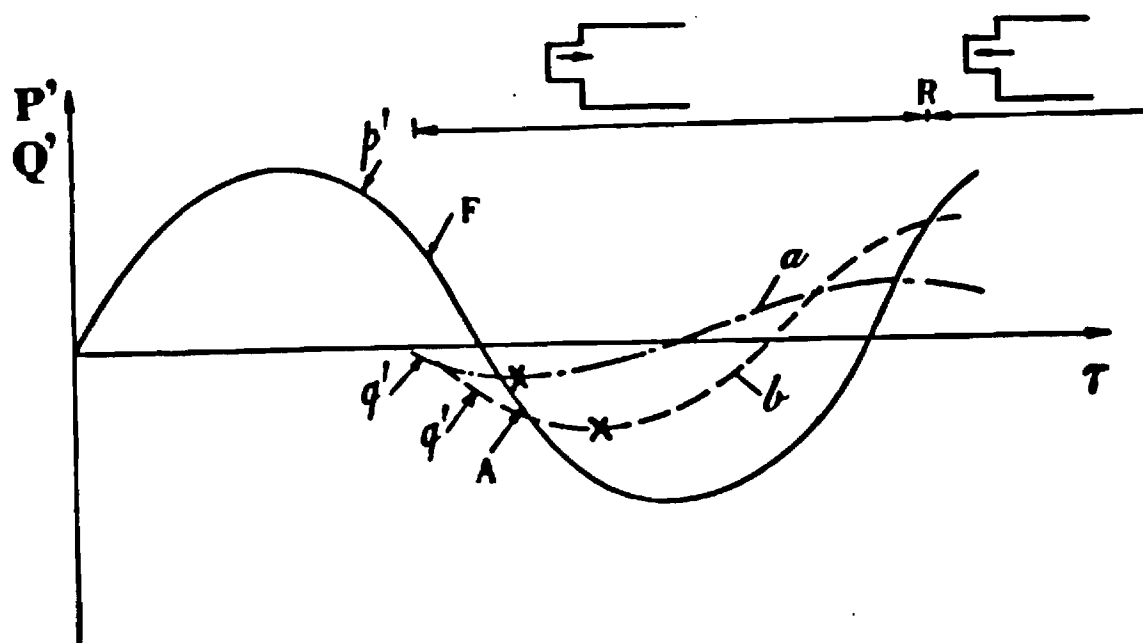


Fig. 33 Normalized Pressure (P') Cycle Showing the Timing of the Heat Release Oscillations (Q') for a) Lean and b) Rich Limits of Operation; Fuel Enters at "F", Air Enters at "A", Backflow into the Mixing Chamber Starts at "R"; the "X's" Denote the Instants of Reignition of the Fresh Fuel Charges.

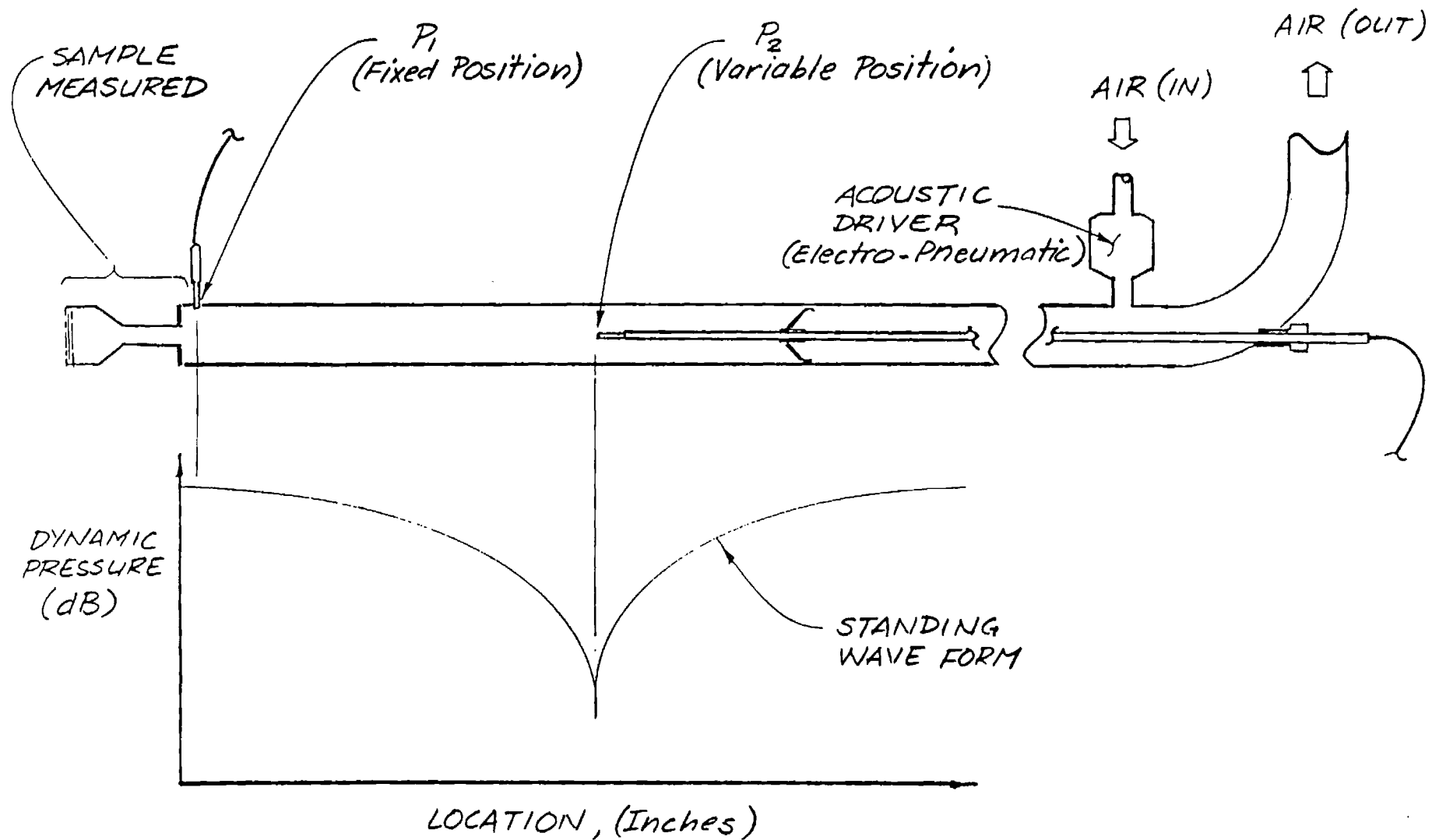


Fig. 34 Schematic of the Impedance Tube Experiment.

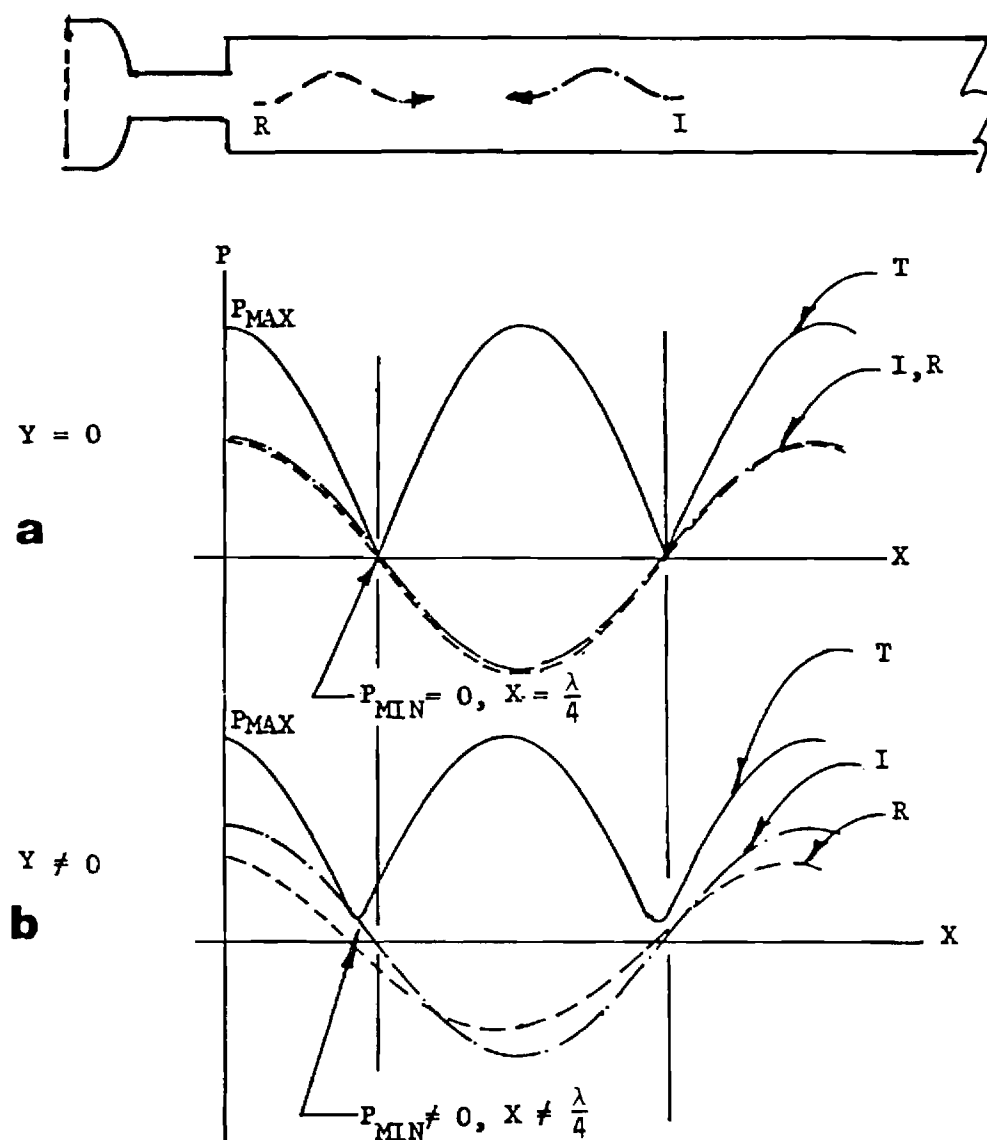


Fig. 35 Wave Form of the Incident (I), Reflected (R) and Total (T) Standing Wave for a) Hard Termination and b) Termination with Finite Admittance, as Shown by Plots of Pressure Amplitudes (P) versus Axial Distance along the Impedance Tube (X).

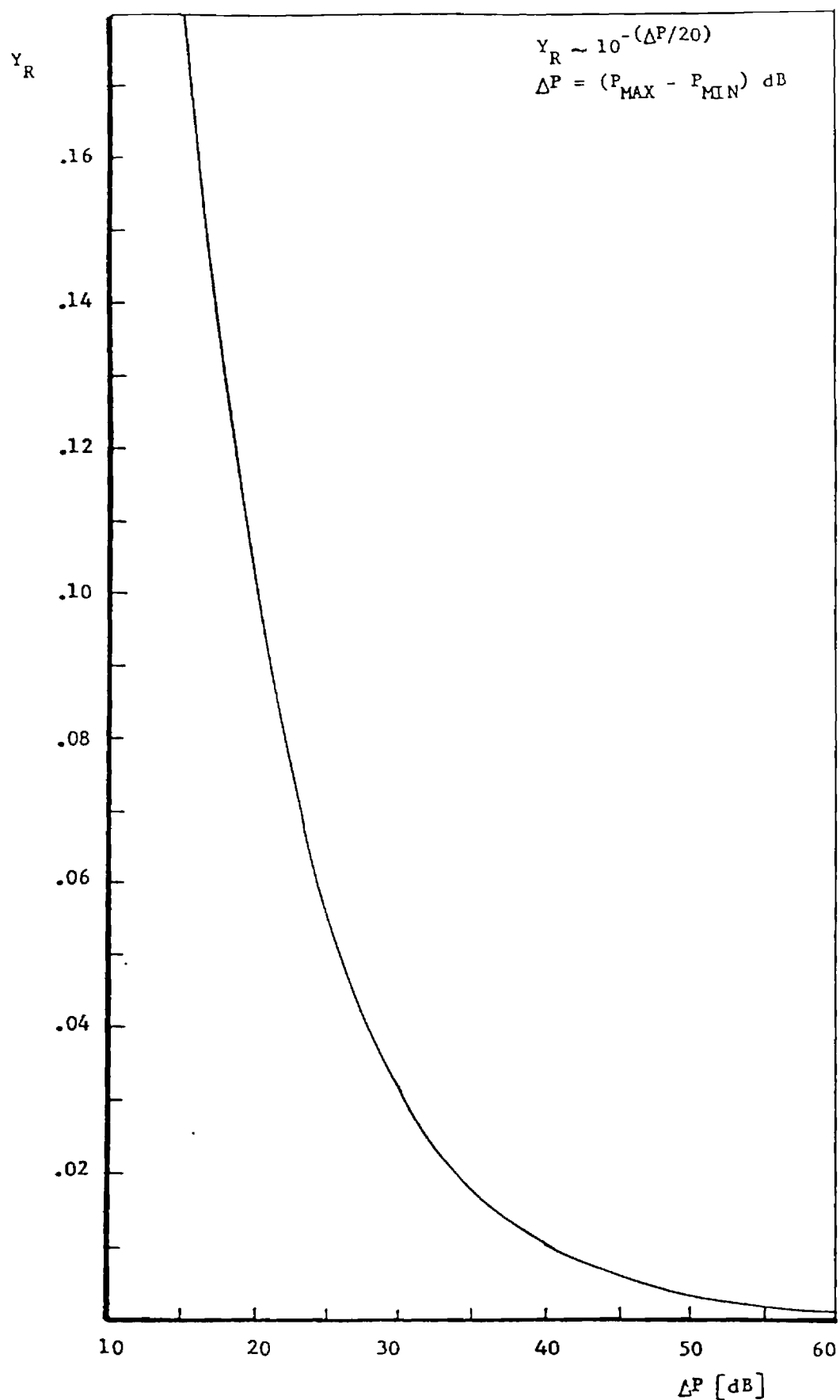


Fig. 36 Sensitivity of the Real Part of the Admittance (Y_R) to the Measured Pressure Difference between the Pressure Maximum and the Pressure Minimum (Δp).

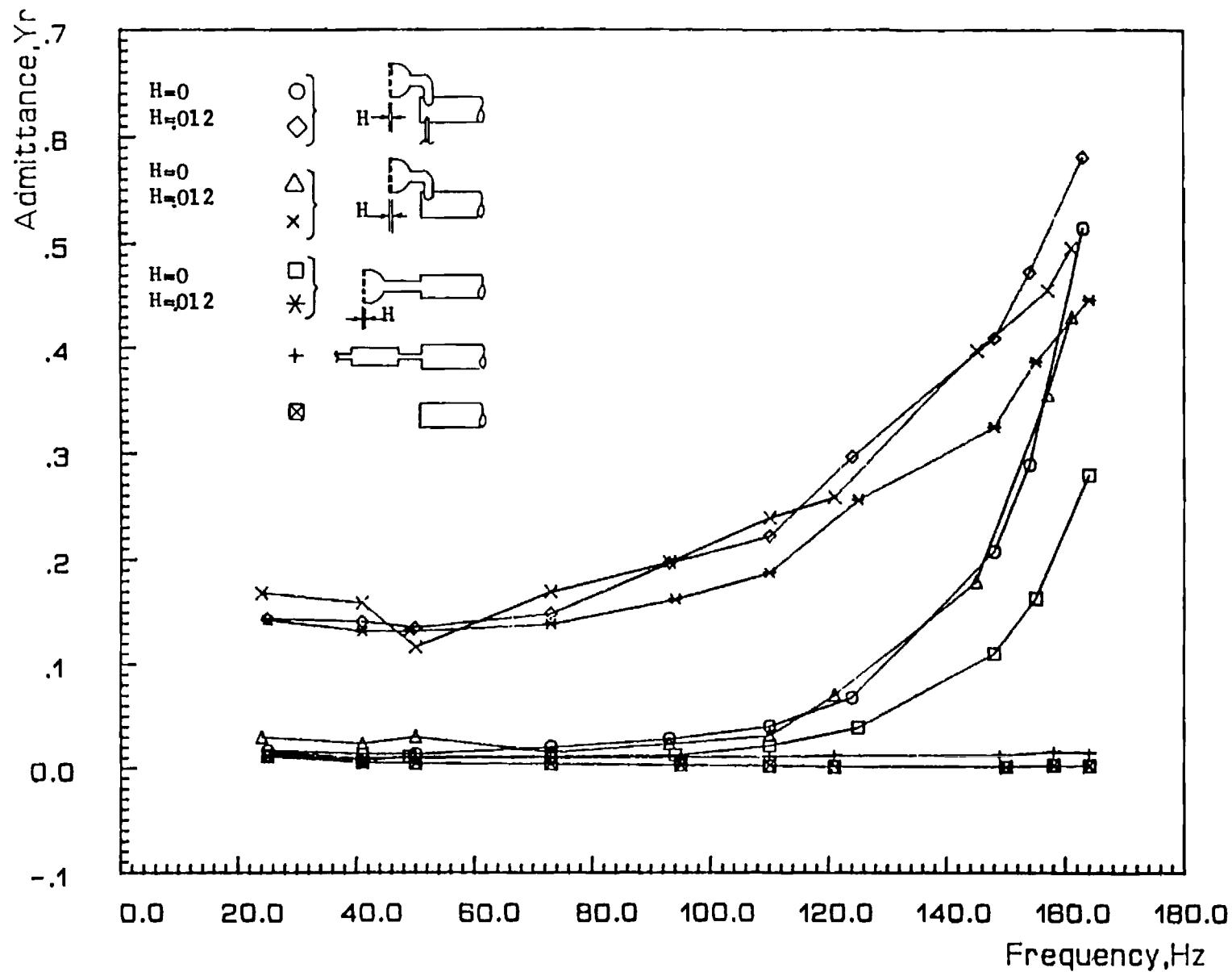


Fig. 37

Real Part of the Admittance (Y_r) as a Function of Frequency for Various Impedance Tube Terminations. H Denotes the Valve Gap Setting in Inches.

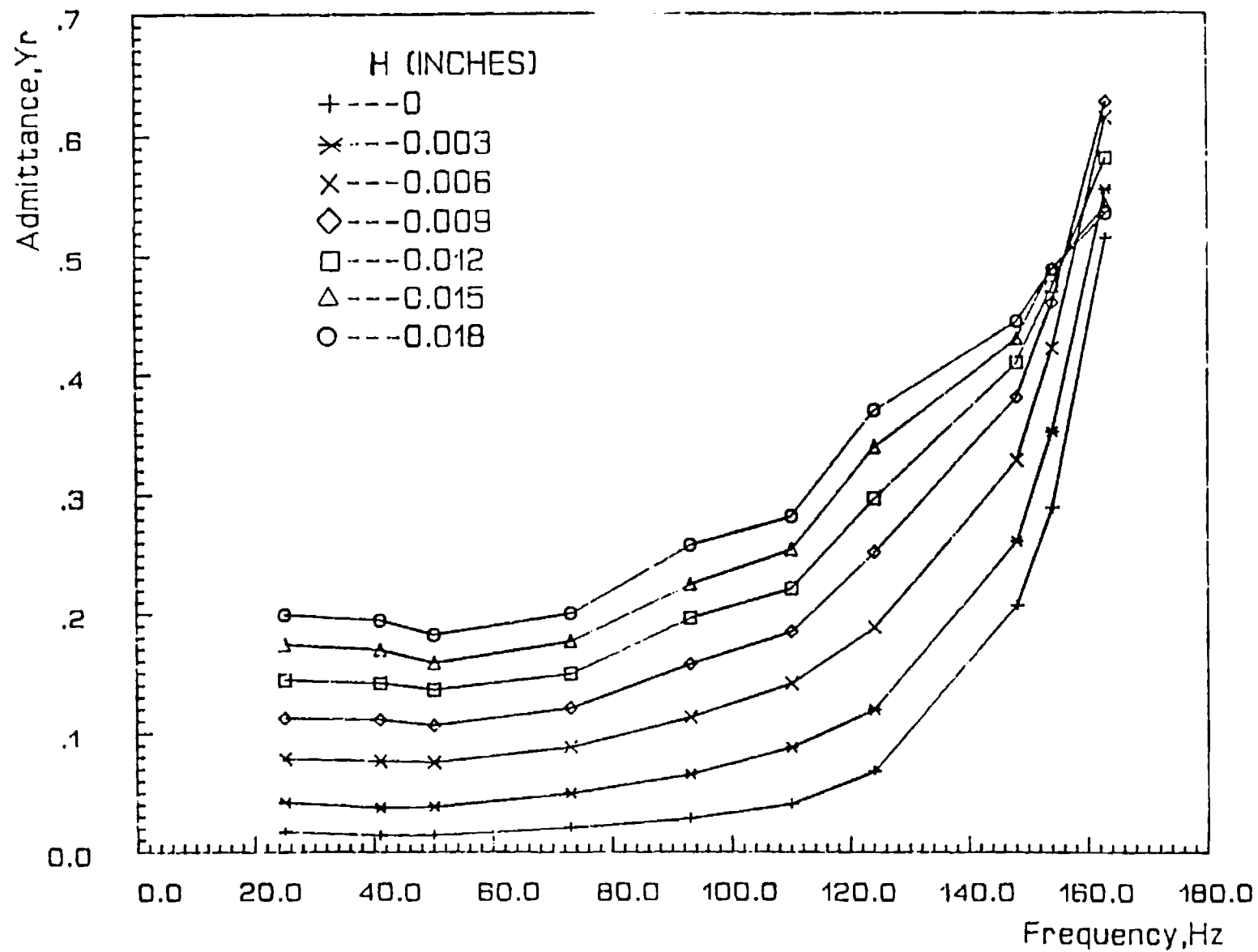


Fig. 38 Real Part of the Admittance (Y_r) of the Mixing Chamber as a Function of Frequency for Different Valve Gap Settings (H).

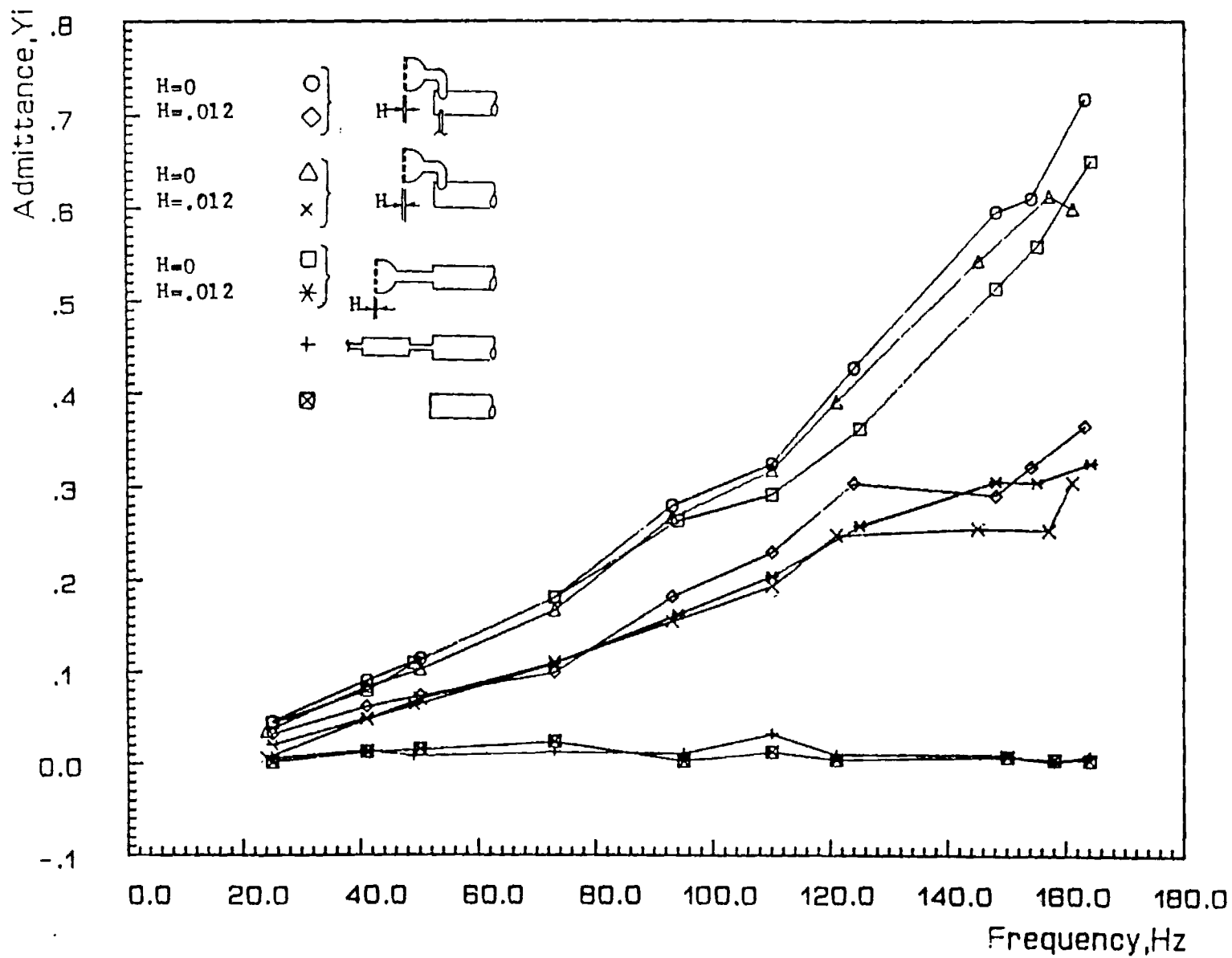


Fig. 39

Imaginary Part of the Admittance (Y_i) as a Function of Frequency for Various Impedance Tube Terminations. H Denotes the Valve Gap Setting in Inches.

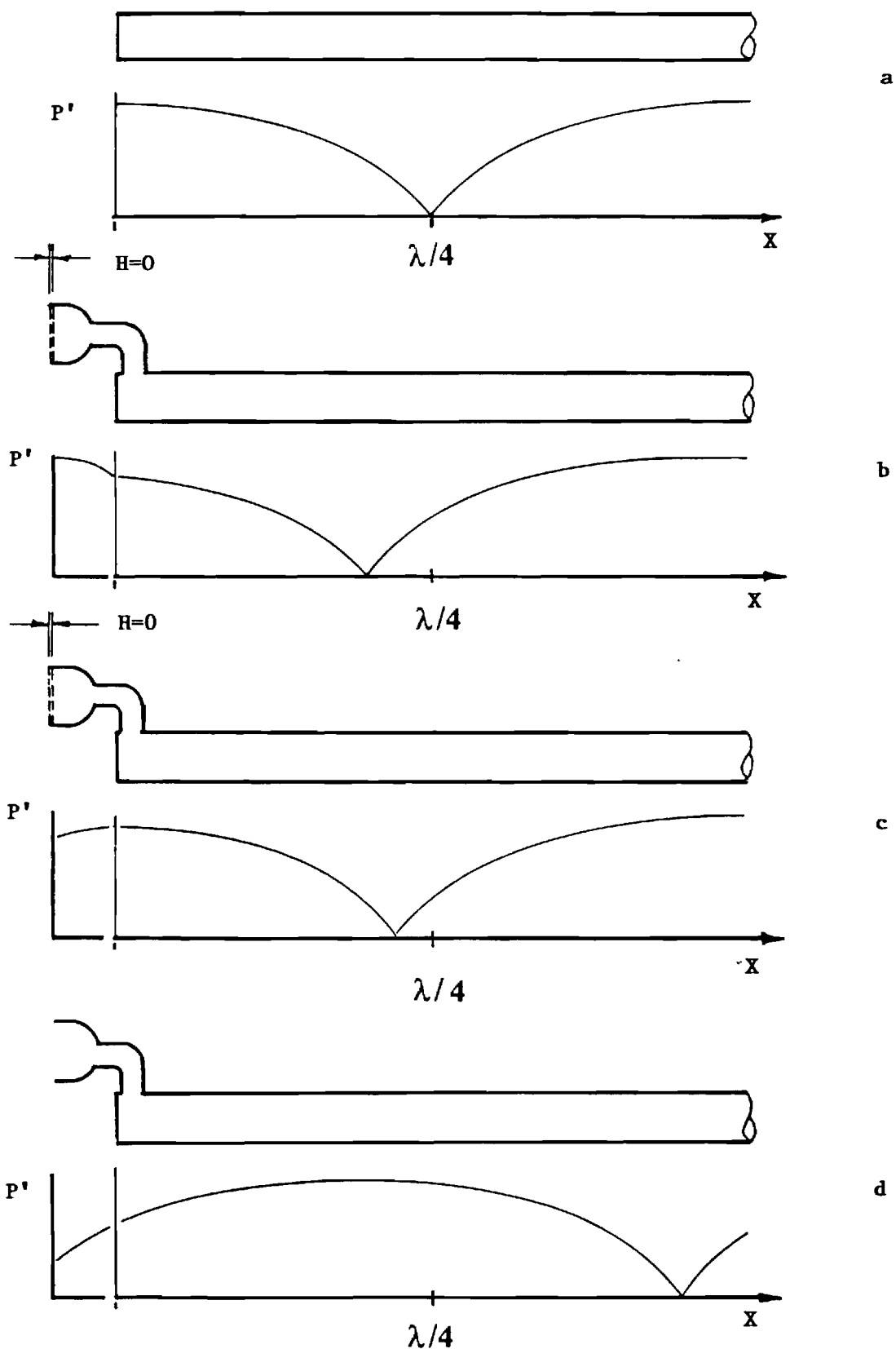


Fig. 40

Comparison of Pressure Amplitudes (P') along the Impedance Tube (X) Fitted with
a) Hard Termination, b) Closed Air Valve, c) Open Valve and d) Valve Housing
with Valve Plates Removed. The Actual Wave Pattern in the Valve Housing is More
Complex Due to the Geometry of the Housing. H Denotes the Valve Gap Setting.

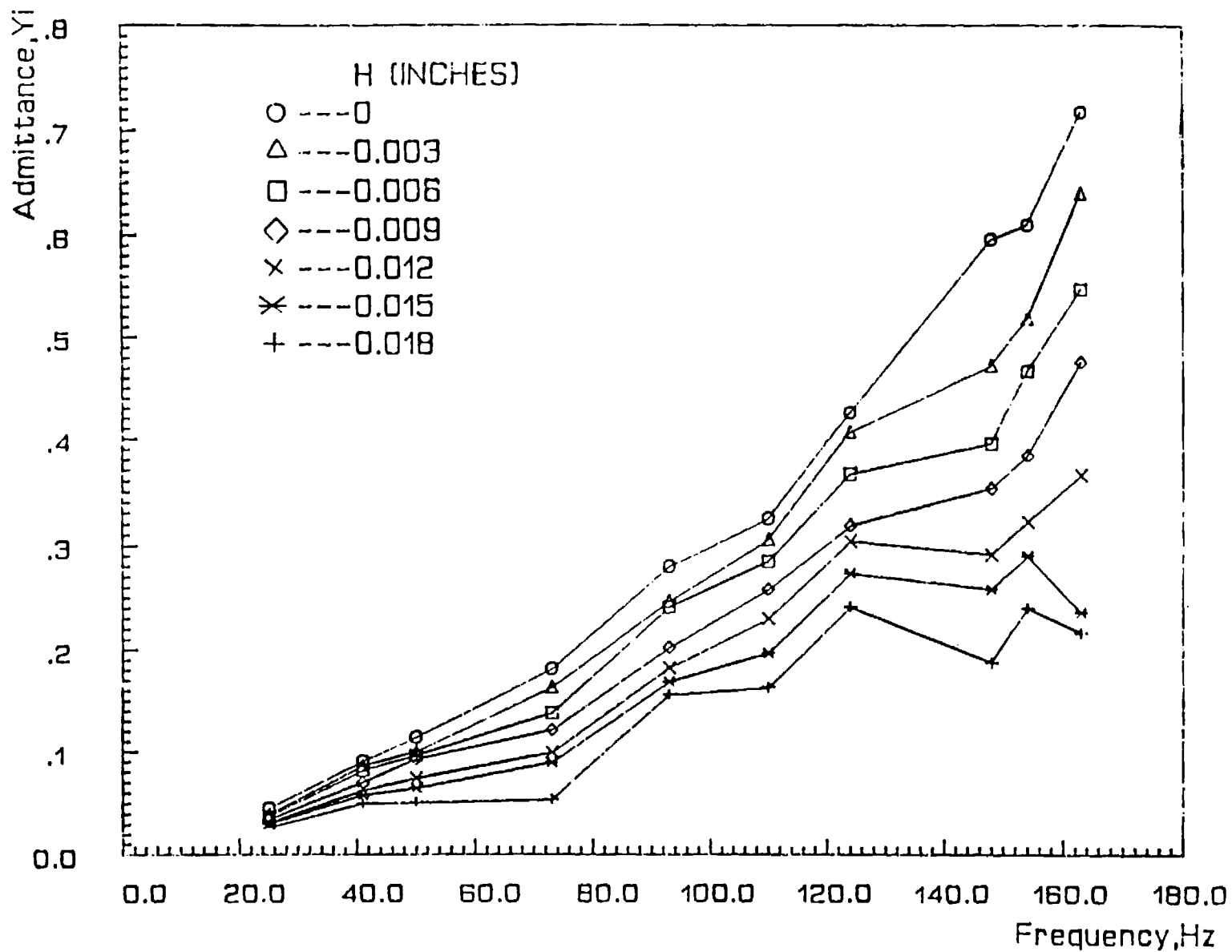


Fig. 41

Imaginary Part of the Admittance (Y_i) of the Mixing Chamber Assembly as a Function of Frequency for Different Air Valve Gap Settings (H).

Frequency = 38 Hz

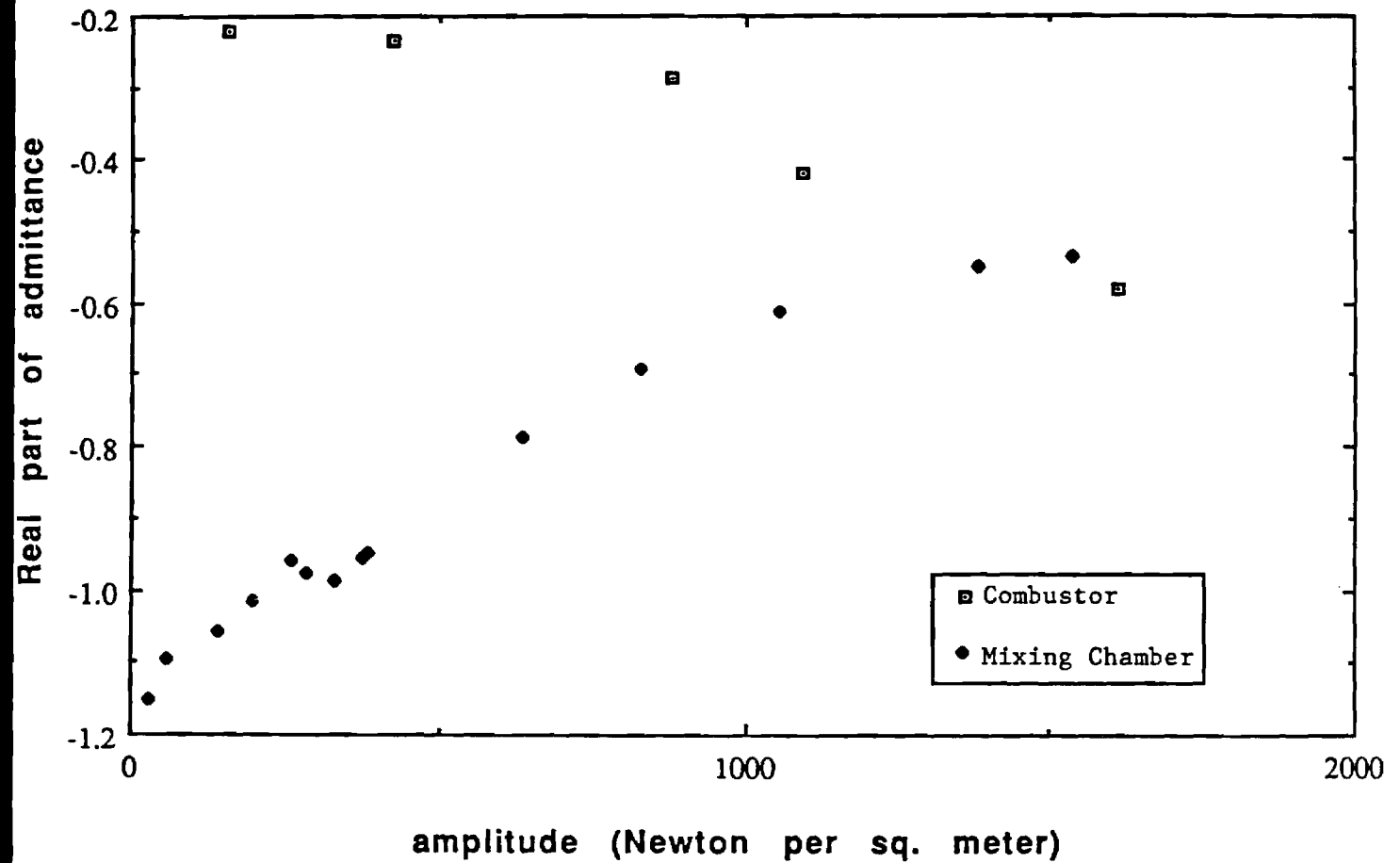


Fig. 42 Comparison of the Real Part of the Admittance as a Function of Pressure Amplitude for the Mixing Chamber Assembly only and for the Entire Helmholtz Combustor.
($1\text{N/m}^2 = 1.45 \times 10^{-4} \text{ psi}$)

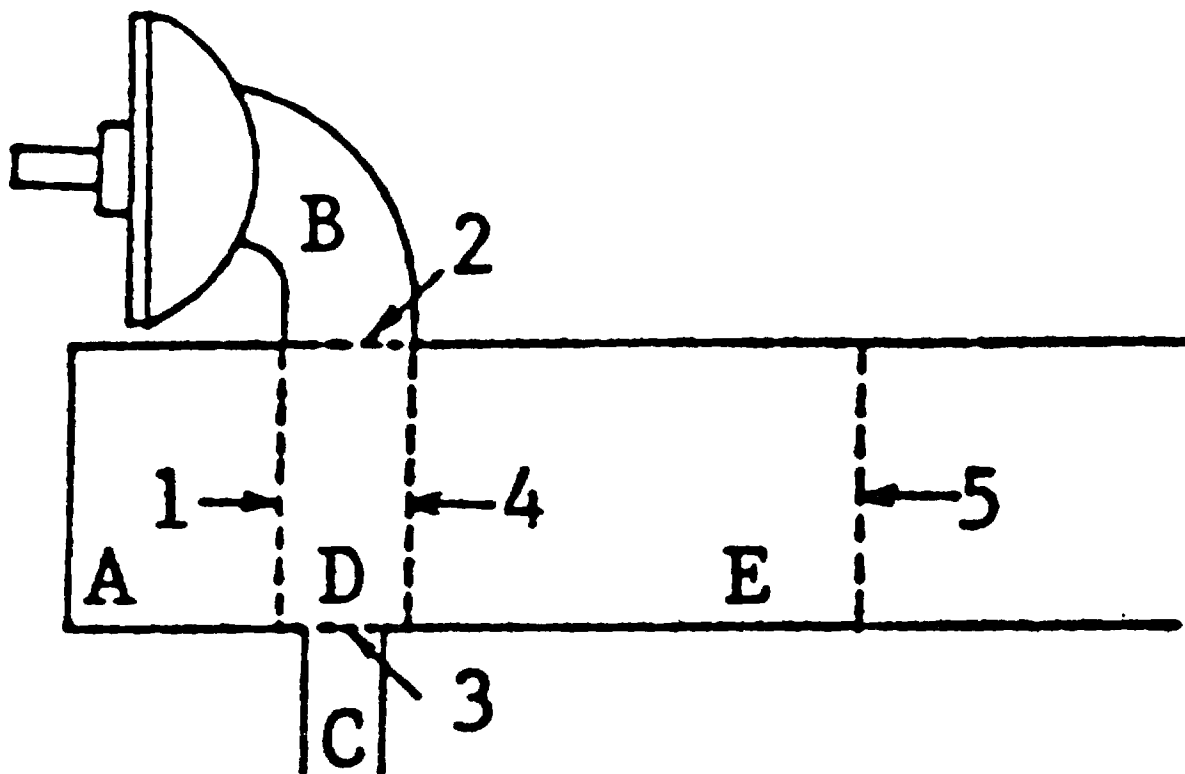


Fig. 43 Schematic Showing the Five Regions into which the Mixing Chamber Assembly has been Divided.

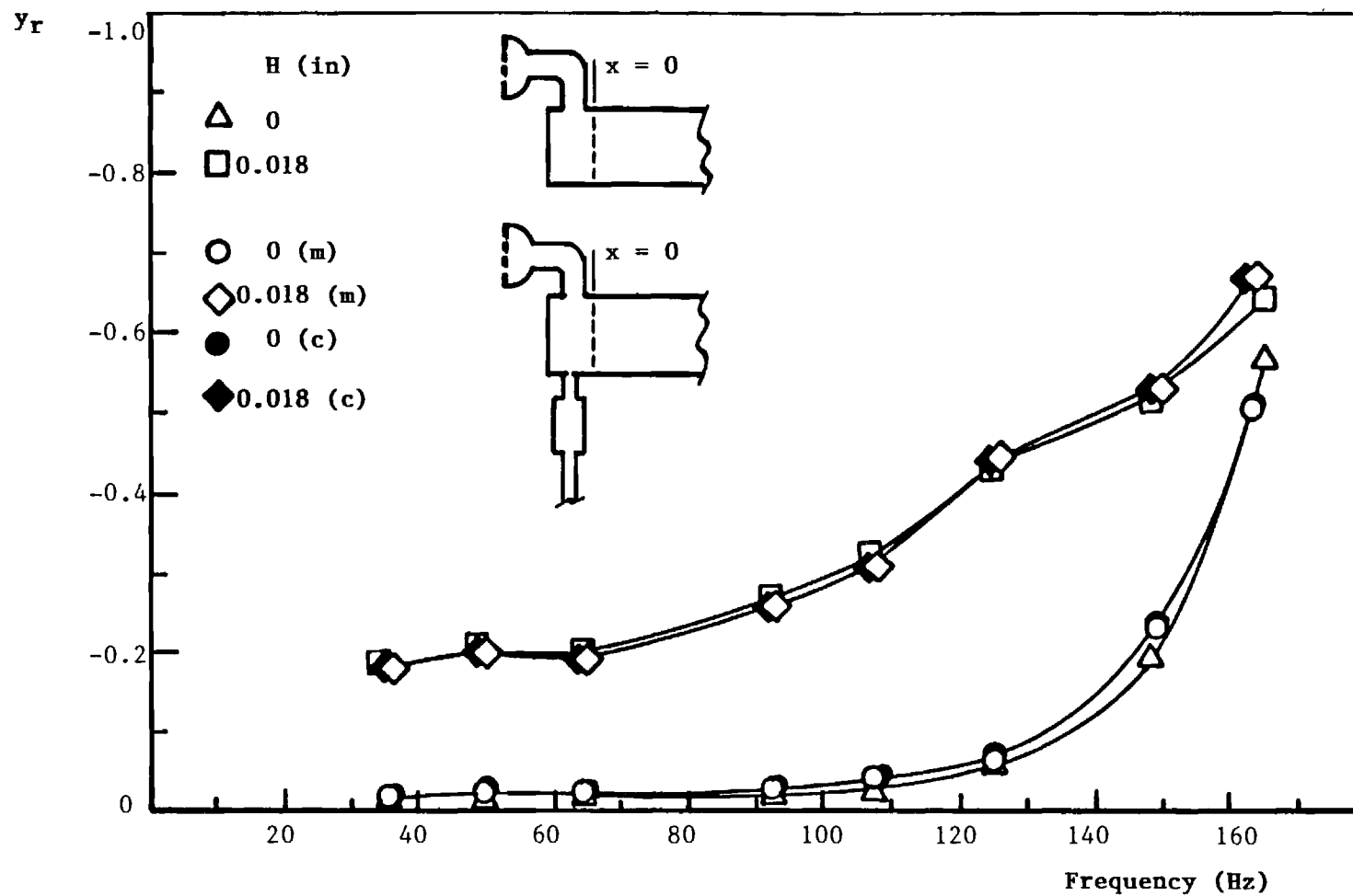


Fig. 44

Comparison between the Measured (m) and Calculated (c) Real Parts of the Admittance of the Mixing Chamber Assembly over a Range of Frequencies. H Denotes the Air Valve Gap Setting in Inches.

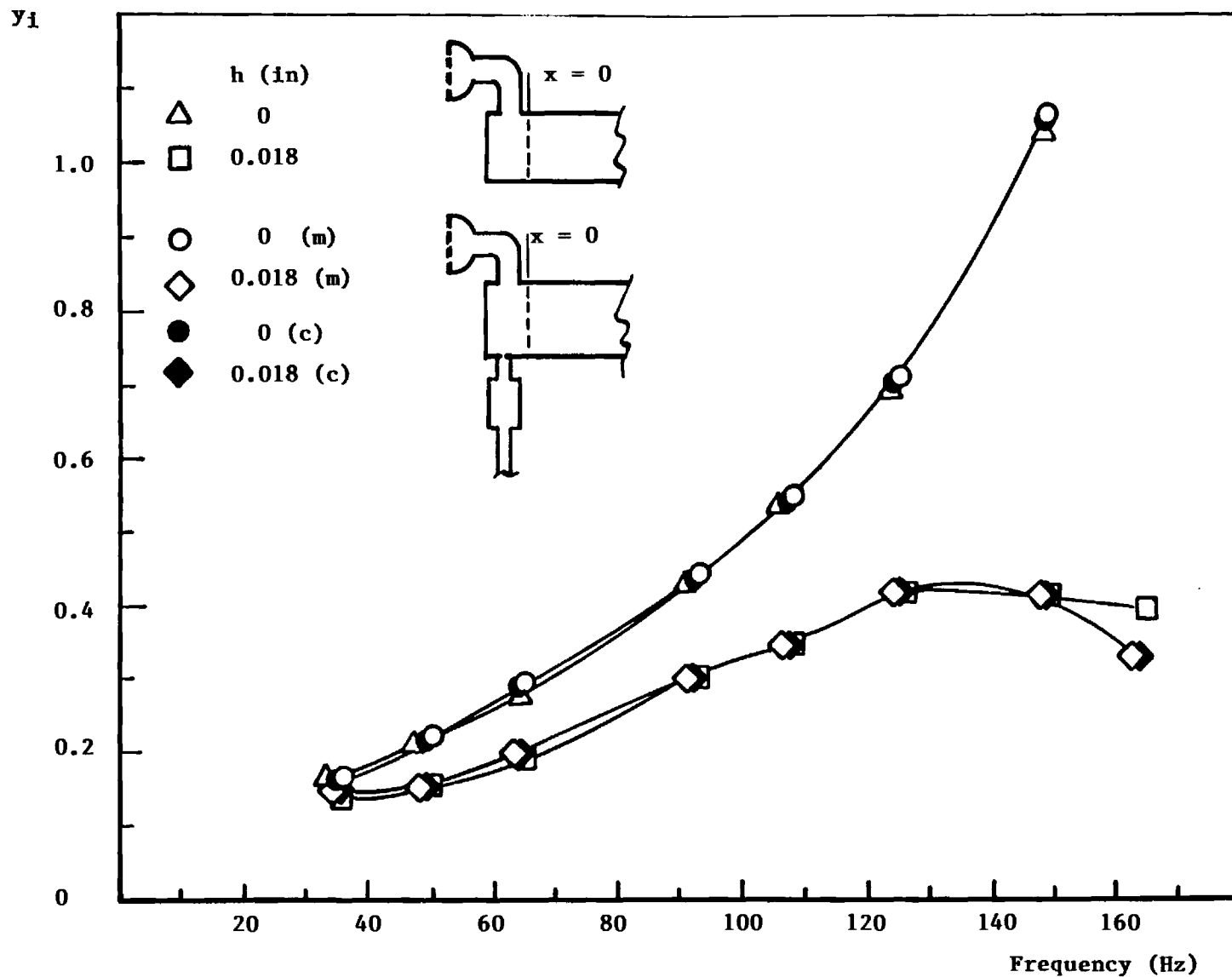


Fig. 45 Comparison between the Measured (m) and Calculated (c) Imaginary Parts of the Admittance of the Mixing Chamber Assembly over a Range of Frequencies. H Denotes the Air Valve Gap Setting in Inches.